frontiers | Research Topics

Rising stars in avian physiology 2024

Edited by
Sandra G. Velleman and Colin Guy Scanes

Coordinated by
Jiahui Xu

Published in
Frontiers in Physiology

ISSN 1664-8714
ISBN 978-2-8325-6874-3
DOI 10.3389/978-2-8325-6874-3

Generative AI statement
Any alternative text (Alt text) provided alongside figures in the articles in this ebook has been generated by Frontiers with the support of artificial intelligence and reasonable efforts have been made to ensure accuracy, including review by the authors wherever possible. If you identify any issues, please contact us.

About Frontiers

Frontiers is more than just an open access publisher of scholarly articles: it is a pioneering approach to the world of academia, radically improving the way scholarly research is managed. The grand vision of Frontiers is a world where all people have an equal opportunity to seek, share and generate knowledge. Frontiers provides immediate and permanent online open access to all its publications, but this alone is not enough to realize our grand goals.

Frontiers journal series

The Frontiers journal series is a multi-tier and interdisciplinary set of open-access, online journals, promising a paradigm shift from the current review, selection and dissemination processes in academic publishing. All Frontiers journals are driven by researchers for researchers; therefore, they constitute a service to the scholarly community. At the same time, the *Frontiers journal series* operates on a revolutionary invention, the tiered publishing system, initially addressing specific communities of scholars, and gradually climbing up to broader public understanding, thus serving the interests of the lay society, too.

Dedication to quality

Each Frontiers article is a landmark of the highest quality, thanks to genuinely collaborative interactions between authors and review editors, who include some of the world's best academicians. Research must be certified by peers before entering a stream of knowledge that may eventually reach the public - and shape society; therefore, Frontiers only applies the most rigorous and unbiased reviews. Frontiers revolutionizes research publishing by freely delivering the most outstanding research, evaluated with no bias from both the academic and social point of view. By applying the most advanced information technologies, Frontiers is catapulting scholarly publishing into a new generation.

What are Frontiers Research Topics?

Frontiers Research Topics are very popular trademarks of the *Frontiers journals series*: they are collections of at least ten articles, all centered on a particular subject. With their unique mix of varied contributions from Original Research to Review Articles, Frontiers Research Topics unify the most influential researchers, the latest key findings and historical advances in a hot research area.

Find out more on how to host your own Frontiers Research Topic or contribute to one as an author by contacting the Frontiers editorial office: frontiersin.org/about/contact

Rising stars in avian physiology: 2024

Topic editors
Sandra G. Velleman — The Ohio State University, United States
Colin Guy Scanes — University of Wisconsin–Milwaukee, United States

Topic coordinator
Jiahui Xu — University of California, Irvine, United States

Citation
Velleman, S. G., Scanes, C. G., Xu, J., eds. (2025). *Rising stars in avian physiology: 2024*. Lausanne: Frontiers Media SA. doi: 10.3389/978-2-8325-6874-3

Table of contents

frontiers | Frontiers in Physiology

TYPE Editorial
PUBLISHED 05 September 2025
DOI 10.3389/fphys.2025.1691951

OPEN ACCESS

EDITED AND REVIEWED BY:
Massimiliano Petracci,
University of Bologna, Italy

*CORRESPONDENCE
Sandra G. Velleman,
velleman.1@osu.edu

RECEIVED 24 August 2025
ACCEPTED 29 August 2025
PUBLISHED 05 September 2025

CITATION
Velleman SG and Scanes CG (2025) Editorial: Rising stars in avian physiology: 2024. *Front. Physiol.* 16:1691951. doi: 10.3389/fphys.2025.1691951

Editorial: Rising stars in avian physiology: 2024

Sandra G. Velleman[1]* and Colin G. Scanes[2]

[1]The Ohio State University, Columbus, OH, United States, [2]University of Wisconsin-Milwaukee, Milwaukee, WI, United States

KEYWORDS

broilers, early career, song birds, reproduction, thermal stress, satellite cells

Editorial on the Research Topic
Rising stars in avian physiology: 2024

In 2022, Frontiers in Avian Physiology published the initial Rising Stars Research Topic to aid in the development of researchers at early stages in their career with papers accepted from all disciplines in the area of Avian Physiology. The Research Topic was very successful with 46,508 article views and 16,272 article downloads. Thus, we viewed a Research Topic promoting those in the area of avian physiology to be critical to the sustainability of poultry and the poultry industry. As in the 2022 Rising Stars Research Topic, all areas of research in avian physiology were open for submission.

Bird reproduction was addressed by Singh et al., Bond et al., and Garcia-Meja et al. The timing and seasonal reproduction was studied by Singh et al. using dark-eyed Juncos. They found that gonadotropin releasing hormone was elevated in early breeding birds compared to migrating Juncos. With regard to commercial broilers, the presence of lipid biomarkers correlated with sperm mobility was reported on by Bond et al. The lipidome of the seminal plasma, sperm cell and whole semen was characterized in broilers with different sperm mobilities. Eight potential biomarkers of excellent sperm mobility were identified in this study. Although further evaluation is necessary, this may lead to screening strategies for fertility potential in roosters. On the hen side, Garcia-Meja et al. investigated physiological changes regulating calcium and phosphorus utilization which is essential for bone formation and eggshell mineralization. They found dietary supplementation with 1α-hydroxycholecalciferol increased medullary bone formation with increase bone mineral density in the humerus and tibia.

Birds are visual animals and have a complex system of vision. Bird vision was reported on by Seth et al., and Lingstädt et al. Seth et al. discussed how adeno-associated virus vectors are being used as gene therapy tools for the study and treatment of retinal disorders. These studies have been predominantly done using a murine model while retinal research in birds has been limited. In their novel study, adeno-associated virus serotypes were identified capable of transducing the avian retina. Lingstädt et al. reported on color perception in Jackdaws. They found that Jackdaws can discriminate colors based on their hue.

The effect of extrinsic stress on broilers was studied by Vaughn et al. and Harding et al. Extrinsic heat challenges from high ambient temperatures is a major factor affecting the poultry industry. Furthermore, the increase in temperature due to global warming

is likely to augment the current problem further causing both financial and food production impacts. In the study by Vaughn et al., broiler chickens were exposed to an acute heat challenge on day 4 posthatch after a period of embryonic heat conditioning commencing on embryonic day 7 where temperature was increased to 39.5 °C for 12 h and then maintained at 37.5 °C for 12 h through embryonic day 16. They found that embryonic heat conditioning reduced the severity of heat stress on the hypothalamic response. Harding et al. reported on how various ventilation shutdown procedures affect laying hens where rapid depopulation is required in situations like highly pathogenic avian influenza. The three treatments evaluated were ventilation shutdown plus heat, ventilation shutdown plus heat and relative humidity, and ventilation shutdown plus carbon dioxide. Their results found that ventilation shutdown with heat and relative humidity is a good method for the industry to use to rapidly depopulate laying hen facilities.

Yu et al. and Powell et al. investigated the adult myoblast population of cells, satellite cells, in the breast muscle. Satellite cells are responsible for all posthatch muscle growth and the repair and regeneration of muscle. Traditionally, it was thought that satellite cells were a homogenous population of cells. Although varying rates of proliferation and differentiation have been found in satellite cells isolated from the same muscle fiber. Yu et al. using transcriptome analysis of satellite cells isolated from the same pectoralis major muscle with different proliferation rates found 5,300 genes differentially expressed. Thus, providing proof of functional diversity of satellite cells. Powell et al. reported on the control of satellite cell gene expression and regulation of the translation of mRNAs into proteins by non-coding circular RNAs in satellite cells isolated from 2 different lines of turkeys and the effect of temperature. Circular RNA expression was found to be significantly affected by thermal treatment and genetic background of the satellite cells with 140 differentially expressed circular RNAs.

Cherenetsov and Utvenko published a review article on how avian migrants know where they are going on their first migration. The question remains how birds who fly individually like songbirds, navigate their migration route when they are not with experienced conspecifics. Recent research has found that first time migrants follow geomagnetic cues and perhaps other cues to help them navigate their migration path.

Author contributions

SV: Writing – original draft, Writing – review and editing. CS: Conceptualization, Writing – review and editing.

Funding

The author(s) declare that no financial support was received for the research and/or publication of this article.

Conflict of interest

The authors declare that the research was conducted in the absence of any commercial or financial relationships that could be construed as a potential conflict of interest.

The author(s) declared that they were an editorial board member of Frontiers, at the time of submission. This had no impact on the peer review process and the final decision.

Generative AI statement

The author(s) declare that no Generative AI was used in the creation of this manuscript.

Any alternative text (alt text) provided alongside figures in this article has been generated by Frontiers with the support of artificial intelligence and reasonable efforts have been made to ensure accuracy, including review by the authors wherever possible. If you identify any issues, please contact us.

Publisher's note

frontiers | Frontiers in Physiology

TYPE Original Research
PUBLISHED 18 September 2024
DOI 10.3389/fphys.2024.1476487

OPEN ACCESS

EDITED BY
Sami Dridi,
University of Arkansas, United States

REVIEWED BY
Elizabeth S. Greene,
University of Arkansas, United States
Paula Chen,
United States Department of Agriculture, United States

*CORRESPONDENCE
Kent M. Reed,
reedx054@umn.edu

RECEIVED 05 August 2024
ACCEPTED 28 August 2024
PUBLISHED 18 September 2024

CITATION
Powell AA, Velleman SG, Strasburg GM, Abrahante Lloréns JE and Reed KM (2024) Circular RNA expression in turkey skeletal muscle satellite cells is significantly altered by thermal challenge.
Front. Physiol. 15:1476487.
doi: 10.3389/fphys.2024.1476487

Circular RNA expression in turkey skeletal muscle satellite cells is significantly altered by thermal challenge

Ashley A. Powell[1], Sandra G. Velleman[2], Gale M. Strasburg[3], Juan E. Abrahante Lloréns[4] and Kent M. Reed[1]*

[1]Department of Veterinary and Biomedical Sciences, University of Minnesota, St. Paul, MN, United States, [2]Department of Animal Sciences, The Ohio State University, Wooster, OH, United States, [3]Department of Food Science and Human Nutrition, Michigan State University, East Lansing, MI, United States, [4]Minnesota Supercomputing Institute, University of Minnesota, Minneapolis, MN, United States

Introduction: Understanding the genetic mechanisms behind muscle growth and development is crucial for improving the efficiency of animal protein production. Recent poultry studies have identified genes related to muscle development and explored how environmental stressors, such as temperature extremes, affect protein production and meat quality. Non-coding RNAs, including circular RNAs (circRNAs), play crucial roles in modulating gene expression and regulating the translation of mRNAs into proteins. This study examined circRNA expression in turkey skeletal muscle stem cells under thermal stress. The objectives were to identify and quantify circRNAs, assess circRNA abundance following RNAse R depletion, identify differentially expressed circRNAs (DECs), and predict potential microRNA (miRNA) targets for DECs and their associated genes.

Materials and methods: Cultured cells from two genetic lines (Nicholas commercial turkey and The Ohio State Random Bred Control 2) under three thermal treatments: cold (33°C), control (38°C), and hot (43°C) were compared at both the proliferation and differentiation stages. CircRNA prediction and differential expression and splicing analyses were conducted using the CIRIquant pipeline for both the untreated and RNase R depletion treated libraries. Predicted interactions between DECs and miRNAs, as well as the potential impact of circRNA secondary structure on these interactions, were investigated.

Results: A total of 11,125 circRNAs were predicted within the treatment groups, between both untreated and RNase R treated libraries. Differential expression analyses indicated that circRNA expression was significantly altered by thermal treatments and the genetic background of the stem cells. A total of 140 DECs were identified across the treatment comparisons. In general, more DECs within temperature treatment comparisons were identified in the proliferation stage and more DECs within genetic line comparisons were identified in the differentiation stage.

Discussion: This study highlights the significant impact of environmental stressors on non-coding RNAs and their role in gene regulation. Elucidating the role of non-coding RNAs in gene regulation can help further our

understanding of muscle development and poultry production, underscoring the broader implications of this research for enhancing animal protein production efficiency.

KEYWORDS

non-coding RNA, circRNA, *Meleagris gallopavo*, *Pectoralis major*, differential splicing

1 Introduction

Animal agriculture plays an important role in meeting human nutritional needs, primarily by providing complex muscle proteins as meat. Currently, poultry is the largest sector of meat consumed in the US, with consumption levels continuing to rise. Turkey meat accounts for approximately 10% of the poultry meat revenue in the U.S. (United States Department of Agriculture- NASS, 2022). Sustainability in our food systems is crucial for ensuring long-term food security, reducing environmental impact, and promoting the health and wellbeing of current and future generations. Efficient production of animal protein is key to sustainable agriculture and successfully meeting meat consumption demands. Efficient *Pectoralis major* muscle (breast meat) production and growth performance has been and continues to be a focus of turkey breeding efforts (Duggan et al., 2023; Musselman, 2021).

Understanding the underlying genes involved in muscle meat growth and development can help further efforts towards increasing the efficiency of animal protein production. Recently, studies in poultry have identified genes and other factors related to muscle development and have begun to gather a better understanding of how environmental stressors can affect protein production and meat quality. Temperature extremes are one source of environmental stress that has detrimental effects on poultry production including increased fat deposition, compromised proteins, reduced growth rates, and even the death of young birds (Barnes et al., 2019; Henrikson et al., 2018; Lara and Rostagno, 2013; Nawab et al., 2018). Transcriptomics research has revealed genes (e.g., myostatin) and gene pathways (e.g., lipid deposition and growth hormone-boosting peptide pathways) involved in muscle development and meat quality (Dou et al., 2018; Ibrahim et al., 2021; Li et al., 2024). Identifying key genes and understanding their expression patterns reveals only part of the complex system that controls overall gene expression. Non-coding RNAs, such as long non-coding RNAs (lncRNAs) and micro RNAs (miRNAs), have been shown to play important roles in modulating gene expression through binding of DNA, mRNA, and proteins (O'Brien et al., 2018; Statello et al., 2021).

Growing evidence suggests that other classes of non-coding RNAs, such as circular RNAs (circRNAs), also play crucial roles in the regulation of gene expression (Lei et al., 2022; Reed et al., 2021; Tian et al., 2023; Wilusz, 2018). These single-stranded, closed-loop, non-coding RNAs are formed by a type of alternative splicing known as backsplicing, where the 3′ end of an exon covalently bonds to the 5′ end of an upstream exon. Several functions of circRNAs are hypothesized, including acting as molecular "sponges" that bind cellular miRNAs, serving as transcriptional regulators, and potentially acting as templates for translation into peptides (Barrett and Salzman, 2016; Tian et al., 2023; Wilusz, 2018; Zucko and Boris-Lawrie, 2020). Conservation of function of circRNAs is still being explored with many studies showing circRNA expression and function to be species specific (Santos-Rodriguez, Voineagu, and Weatheritt, 2021; Li and Wang, 2024) while other studies show conservation of circRNAs across species and even kingdoms (Gao et al., 2020; Huo et al., 2018), therefore predicting function of a circRNA can be limited by genome annotations within a given species. Previous studies have indicated that circRNAs may be crucial in muscle development and thermal stress responses (Ouyang et al., 2018; Reed et al., 2021).

Historically, circRNAs have been difficult to study due to a lack of bioinformatics resources. Until recently, distinguishing between linear and circular RNAs was difficult, but new tools have emerged for data-mining these specific RNA structures in RNAseq datasets (Barrett and Salzman, 2016; Gao, Wang, and Zhao, 2015; Wu et al., 2019). Multiple new tools utilizing different algorithms and identification approaches have been developed (Vromman et al., 2023), including the CIRI program and pipelines that accurately identify complementary backsplice junctions (Gao, Wang, and Zhao, 2015; Zhang et al., 2020).

In a previous study, we explored circRNAs as a novel facet of gene regulation and identified significant differential expression of circRNAs in thermally challenged turkey (*Meleagris gallopavo*) poults from different genetic lines (Reed et al., 2021). The first week post-hatch is critical for muscle development, as muscle stem cells (satellite cells, SCs) exhibit peak mitotic activity and are highly sensitive to temperature changes during this timeframe (Halevy et al., 2000; Mozdziak, Schultz, and Cassens, 1994; Patael et al., 2019; Piestun et al., 2017; Xu et al., 2021). Thermal stress during this period may alter the characteristics of SCs and result in changes in *Pectoralis major* muscle development.

In this study, we employed a data-mining approach to investigate differential expression of circRNAs in cultured turkey *Pectoralis major* muscle satellite cells (SCs) between and within SCs isolated from a modern commercial turkey and a historic slower growing turkey line under different thermal treatments. This investigation had four main objectives: 1) Identify and quantify circRNAs; 2) Test circRNA abundance in RNA following RNAse R depletion; 3) Identify differentially expressed circRNAs (DECs); and 4) Predict potential miRNA targets for DECs and their associated genes. Our long-term goal is to better understand the role of non-coding RNAs in gene regulation, specifically in the context of thermal stress responses during muscle development and its implications for poultry production.

2 Materials and methods

2.1 Materials

Transcript sequence data from the turkey SC libraries previously described in Reed et al. (2022) were used for circRNA analyses. Data

are accessioned as part of SRA BioProject PRJNA842679. For the purposes of this study, the experimental lines, thermal treatments, and data management are summarized below.

The control line (Randombred Control Line 2, RBC2), is a turkey line established in 1966 from commercial birds of that time and has been maintained at the Poultry Research Center at The Ohio State University (Nestor, 1977) without any conscious selection. The experimental line (Nicholas Commercial Turkeys, NCT), is a commercial meat-type turkey line selected for performance (yield, weight gain, feed conversion, etc.) in a modern turkey production system (Aviagen® Turkeys, Inc.). Cultured 1-week cells from both lines were subjected to proliferation and differentiation protocols to create four sets of SCs to be used in experimental treatments: RBC2-proliferation (RBC2-pro), RBC2-differentiation (RBC2-dif), NCT-proliferation (NCT-pro), and NCT-differentiation (NCT-dif). The satellite cell (SC) harvest, maintenance, differentiation and proliferation assays, and sequence data handling were previously described in detail in Reed et al. (2017), Reed et al. (2022), Reed et al. (2023). Three thermal treatments were assigned to each SC set: 33°C (cold), 38°C (control), and 43°C (hot). The RBC2-pro-cold treatment resulted in poor cell growth and RNA recovery and this treatment was excluded from sequencing. The remaining 11 experimental SC groups were replicated creating 22 SC libraries available for sequencing and analysis. Data from an analysis of small RNA (miRNA) sequencing from the same biosources (Reed et al., 2023) were also available for comparative analyses.

The reference turkey genome assembly and annotation (UMD5.1) from Ensembl (Meleagris_gallopavo.Turkey_5.1.dna.toplevel.fa genome; Meleagris_gallopavo.Turkey_5.1.109. gtf) were used to conduct these analyses.

2.2 Methods

2.2.1 circRNA predictions and quantifications

Prediction and quantification of circRNAs was performed with the python-based circRNA quantification and differential expression program: CIRIquant (Zhang et al., 2020). CircRNA identification was performed with the CIRI2 program that is embedded within CIRIquant. CIRI2 predicts circRNAs based on an algorithm that detects and differentiates between back-spliced junction (BSJ) reads and non-BSJ reads to reduce the number of false positives with a high level of sensitivity (Gao et al., 2015). Quantification was performed via CIRIquant and by re-alignment of RNA-seq reads against a pseudo-circular reference. Abundance of circRNA was estimated by comparison of BSJ reads and front-spliced reads (FSJ).

2.2.2 RNase depletion study

As a partial verification of circRNA prediction, and to assess depletion protocols for future circRNA studies, RNA of the SCs from the NCT control temperature group for both proliferation (NCT-pro-R) and differentiation (NCT-dif-R) was subjected to an RNase depletion protocol. Briefly, RNA samples were treated with RNase R enzyme to digest linear RNA molecules while retaining lariat or circular RNA structures. Digestion was performed on 4 ug of total DNAse-treated RNA using 10 units of RNase R exoribonuclease (Lucigen, Corp) following manufacturer's protocol (incubation reaction at 37°C for 20 min followed by 65°C for 20 min). The resulting RNAs were quantified and submitted to the University of Minnesota Genomics Center for library preparation and sequencing. The libraries were sequenced on the Illumina NovaSeq SP platform. Prediction of circRNAs in depleted samples was performed with CIRIquant utilizing the "RNase R effect correction" function. The "RNase R effect correction" function uses both the depleted and un-depleted expression to estimate the before-treatment expression levels of circRNAs detected in RNase R data (Zhang et al., 2020).

2.2.3 Differential expression analyses

2.2.3.1 Differential expression

Differential expression analyses were conducted with CIRIquant (Zhang et al., 2020) and differentially expressed circRNAs (DECs) in each comparison were identified as having FDR p-value <0.05 and log fold change (LogFC) > 1.0. DECs were predicted from the CIRIquant option that allowed for biological replicates (comparison was on treatment vs. treatment basis).

2.2.3.2 Differential circRNA splicing (circRNA vs. linear forms)

Differential splicing analyses were conducted with CIRIquant, using the option that did not allow for biological replicates (comparison was on a sample vs. sample basis). The likelihood of an RNA being found in its linear *versus* circular form is defined by the differential splicing (DS) score (Zhang et al., 2020). Splicing scores of DECs previously identified were averaged across sample comparisons for a final average DS score.

2.2.4 Functional prediction analyses

2.2.4.1 circRNA/miRNA interaction prediction

Potential interactions between the DECs and turkey micro-RNAs (miRNAs) were investigated through target binding site predictions. Targets were predicted by aligning miRNAs identified in turkey skeletal muscle satellite cells (Reed et al., 2023) with the sequences of the DECs with miRanda v3.3a (Enright et al., 2003) using position-weighted scoring, alignment score of >165, and |energy-kcal/mol| >7.0.

2.2.4.2 Secondary structure prediction

To investigate the effect of secondary structure on circRNAs, RNAfold (Lorenz et al., 2011) was used to examine a circRNA and its ability to bind with its associated miRNAs. Minimum free energy (MFE) and the thermodynamic ensemble (TE) structures were predicted at 37°C, 38°C [approximate temperature of newly hatched poults (Strasburg, unpublished) and control temperature for the cultured SC cells], and 39°C for circ09021. This circRNA was chosen based upon nucleotide (nt) length limits of RNAfold (10,000 nt) and had corresponding miRNA targets. This allowed assessment of TE structure at different temperatures and binding access of miRNAs to the targets predicted in the circRNA sequence. The associated miRNAs (alignment score of >150) were then aligned with the predicted secondary structure to assess if temperature affected binding ability.

3 Results

3.1 circRNA predictions and quantifications

A total of 10,679 unique circRNAs, mapping across 76 chromosomes and genome contigs, was identified across the

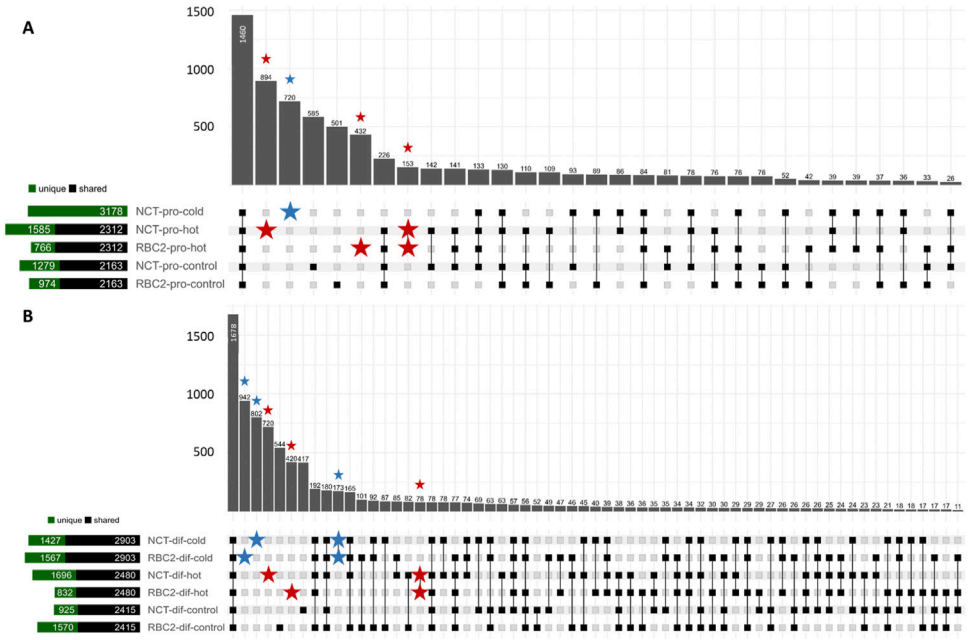

FIGURE 1
Upset plot depicting circRNAs predicted in the SCs in the proliferation stage **(A)** and the differentiation stage **(B)** by treatment. Set size bar plot shows circRNAs compared between RBC2 and NCT treatment equivalents (i.e., RBC2-pro-control vs. NCT-pro-control) to depict circRNAs shared between or unique to the treatments. circRNAs predicted only in cold treatments are marked with a blue star and circRNAs predicted only in hot treatments are marked with a red star.

TABLE 1 Comparison of circRNAs predicted in NCT control libraries, their RNase depleted counterpart libraries, and the CIRIquant RNase R effect correction output.

SC library	Total[a]	Unique[b]	Adjusted/Add/Loss[c]
NCT-pro-control	2,712	2,365	*NA*
NCT-pro-R	523	176	*NA*
NCT-pro-adjusted	2,888	0	14/176/0
NCT-dif-control	2,469	1920	*NA*
NCT-dif-R	1,216	667	*NA*
NCT-dif-adjusted	3,142	6	36/673/3

[a]total number of circRNAs, predicted in each library.
[b]number of circRNAs, that are unique to that library when compared to its counterpart or the adjusted library compared to both the un-depleted and depleted sample counterpart libraries.
[c]number of circRNAs, in the "adjusted" sample libraries that have predicted circRNA, scores corrected by CIRIquant, number of circRNAs, that are unique to the "adjusted" sample libraries as determined by CIRIquant, and the number of circRNAs, no longer detected in the "adjusted" libraries as determined by CIRIquant.

22 non-depleted SC libraries. In these non-depleted samples, 517 circRNAs were common and observed in all libraries, whereas 446 circRNAs were unique and only observed in single libraries (Figure 1; Supplementary Table S1). When combining libraries by treatment and sample type, 1,460 circRNAs were predicted to occur across all treatments and 3,132 circRNAs were unique to single treatments.

A total of 7,344 circRNAs was observed in the RBC2 SCs (non-depleted libraries), and 8,363 in the NCT SCs with 2,316 and 3,335 circRNAs unique to the RBC2 and NCT libraries, respectively. A greater number of circRNAs were predicted in SCs from the proliferating cells (6,779) than differentiating cells (5,198), with 4,847 and 3,266 circRNAs unique to SCs in proliferation and differentiation, respectively. When segregated by temperature treatment, 6,488 circRNAs were observed in the heat-treated SCs (43°C), 6,725 circRNAs were observed in the cold-treated SCs (33°C), and 6,334 were observed in the control treatment (38°C), with 1810, 2039, and 1,581 circRNAs unique to the hot, cold and control-treatment cells, respectively.

3.2 RNase depletion study

Analysis of sequences from the RNase depletion libraries revealed 792 circRNAs not previously detected in the non-depleted counterparts. In total, 446 novel circRNAs were predicted across the depleted

10.3389/fphys.2024.1476487

TABLE 2 Summary of differentially expressed circRNAs by treatment.

Treatment comparison[a]	Up[b]	Down[c]	Total	DS Up[d]	DS down[e]	# miRNA tbs[f]
Proliferation						
RBC2 vs. NCT (control)	6	9	15	0	0	465
RBC2 vs. NCT (hot)	13	16	29	0	0	715
RBC2 (control vs. hot)	8	3	11	0	0	352
NCT (control vs. hot)	11	5	16	0	0	433
NCT (control vs. cold)	18	6	24	0	0	554
Differentiation						
RBC2 vs. NCT (control)	4	4	8	0	0	176
RBC2 vs. NCT (cold)	11	21	32	0	0	698
RBC2 vs. NCT (hot)	5	8	13	0	0	190
RBC2 (control vs. hot)	17	9	26	1	2	574
NCT (control vs. hot)	20	15	35	3	0	673
RBC2 (control vs. cold)	12	17	29	0	0	674
NCT (control vs. cold)	6	18	24	2	0	570
Totals	131	128	262	6	2	

[a]treatment comparison name; the control group will always be either RBC2 in a genetic line comparison or control in a thermal comparison.
[b]number of circRNAs, upregulated in the experimental treatment.
[c]number of circRNAs, downregulated in the experimental treatment.
[d]number of circRNAs, differentially spliced towards an increase in circular form of the transcript.
[e]number of circRNAs, differentially spliced towards an increase in linear form of the transcript.
[f]number of predicted miRNA, target binding sites for DECs, within that treatment; miRNA, data used were from the same biosource that were collected in Reed et al., 2023.

proliferation and differentiation libraries (Supplementary Table S2). In the NCT-pro RNase comparison, 190 circRNAs underwent a quantification correction by CIRIquant when the RNase R effect correction was applied (Table 1). In the NCT-dif RNase R comparison, 712 circRNAs underwent a correction by CIRIquant with an additional 6 circRNAs being predicted in the CIRIquant adjusted library only and 3 circRNAs no longer being detected (Table 1).

3.3 Differential expression analyses

3.3.1 Differential expression

Twelve expression comparisons were made between SC lines and temperature treatments. Across all comparisons, a total of 292 instances of significant differential expression involving 140 circRNAs, were found with an average of 22 circRNAs (range: 8–35) differentially expressed in each treatment comparison. Length of these circRNAs ranged from 180 to 115,731 nt, with an average length of 31,280 nt. Results for each treatment comparison are summarized in Table 2 and Supplementary Table S3. A complete list of genes associated with each DEC can be found in Supplementary Table S4.

3.3.1.1 Proliferation cell stage

Five treatment comparisons were made with SC in the proliferation stage. Across all comparisons, 62 DECs were predicted (Table 2). Three comparisons were made between thermal treatments (control 38°C vs. hot 43°C; control 38°C vs. cold 33°C) within a genetic line (RBC2; NCT) and two comparisons were made between genetic lines (RBC2 vs. NCT) within thermal treatments (control 38°C; hot 43°C). Due to no survival of RBC2-cold treated SCs, no control 38°C vs. cold 33°C within the RBC2 line or cold 33°C RBC2 vs. NCT comparisons were conducted.

3.3.1.1.1 Proliferation: effects of temperature. Forty-two circRNAs were differentially expressed in comparisons between the thermal treatments within a genetic line (Figure 2A; Table 2; Supplementary Table S3) with eight circRNAs being differentially expressed in more than one treatment comparison (circ08490; circ09370; circ03849; circ01448; circ06785; circ08181; circ08945; circ10649). Two of these (circ08490, circ09370) had parent genes corresponding to known muscle protein genes, myosin light chain 10 and myogenin, respectively (Supplementary Table S4). The former being calcium binding and the latter a muscle-specific transcriptional activator that is required for skeletal muscle differentiation into multinucleated myotubes.

Heat treatment of the SCs resulted in differential expression of circRNAs in both the RBC2 and NCT cells. In the RBC2-control vs. hot comparison, 11 circRNAs were differentially expressed with three DECs being downregulated and eight upregulated at 43°C (Figure 2A; Table 2). Similarly, in the NCT-control vs. hot comparison, 26 circRNAs were differentially expressed with five DECs downregulated and 11 upregulated at 43°C. Three DECs were common to both the RBC2 and NCT control vs. hot treatment comparisons (circ08490, circ09370, and circ08945) and each were upregulated at 43°C.

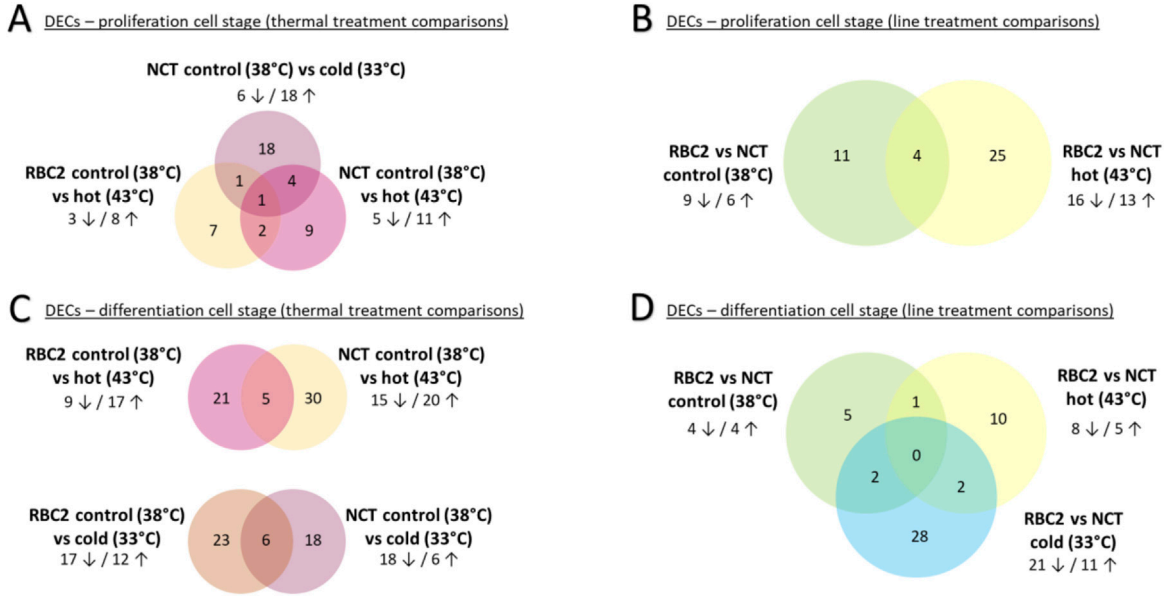

FIGURE 2
Venn diagram of DECS by treatment comparisons: **(A, C)** contain thermal treatment comparisons split by cell stages; **(B, D)** contain line treatment comparisons split by cell stages. Number of DECs given in venn diagram. Number of DECs up/downregulated within treatement comparisons are shown outside of the venn diagram.

In the NCT-control vs. cold comparison, 24 DECs were predicted, six being downregulated and 18 upregulated at 33˚C (Figure 2A; Table 2). Five of the DECs found in the NCT-cold treatment were also DECs in the NCT-hot treatment; four were upregulated (circ01448, circ06785, circ08181, and circ08945) and one downregulated (circ03849) in both comparisons. Two DECs were shared between the in NCT control vs. cold and RBC2 control vs. hot comparisons. One (circ10649 common to all comparisons) was upregulated in NCT SCs at 33˚C and downregulated in RBC2 SCs at 43˚C.

3.3.1.1.2 Proliferation: effects of genetic line. Forty circRNAs were differentially expressed in comparisons between the genetic lines within a thermal treatment (Figure 2B; Table 2; Supplementary Table S3). In the control temperature comparison (38˚C), 15 circRNAs were differentially expressed with six DECs being upregulated and nine downregulated in the NCT line relative to the RBC2 line (Table 2; Figure 2B). In the heat treatment comparison (43˚C), 29 circRNAs were differentially expressed with 13 DECs upregulated and 16 downregulated and in the NCT line relative to RBC2 line (Table 2; Figure 2B). Four DECs (circ09900, circ03853, circ03880, circ05033) were downregulated in both the control and heat treatment comparisons (Figure 2B).

3.3.1.2 Differentiation cell stage

Seven comparisons were made among treatment groups for SCs in the differentiation stage. Across all comparisons, 107 circRNAs were differentially expressed. Four comparisons were made between thermal treatments (control 38˚C vs. hot 43˚C; control 38˚C vs. cold 33˚C) within genetic line (RBC2; NCT) and three comparisons were made between genetic line (RBC2 vs. NCT) within a thermal treatment (control 38˚C; hot 43˚C; cold 33˚C).

3.3.1.2.1 Differentiation: effects of temperature. Eighty-three circRNAs were found to be differentially expressed between the thermal treatments within a genetic line comparisons with 29 circRNAs being differentially expressed in more than one treatment comparison (Figure 2C; Table 2; Supplementary Table S3). In the RBC2-control vs. hot comparison, 26 circRNAs were differentially expressed with nine DECs being downregulated and 17 DECs upregulated at 43˚C. In the NCT SCs, 35 circRNAs were differentially expressed with 15 DECs being downregulated and 20 upregulated at 43˚C in comparison to control. Five DECs were shared between the lines; two DECs (circ04456, circ04500) were downregulated in SCs of both lines, two (circ08896, circ09289) were upregulated in both comparisons, and one (circ09901) was upregulated in the NCT but downregulated in the RBC2 cells.

In the RBC2-control vs. cold comparison, 29 circRNAs were differentially expressed with 17 DECs being downregulated and 12 DECs upregulated at 33˚C (Figure 2C; Table 2; Supplementary Table S3). In the NCT-control vs. cold comparison, 24 circRNAs were differentially expressed with 18 DECs being downregulated and six upregulated in the cold treated cells in comparison to control. Six DECs were shared between the lines. Five DECs (circ06442, circ04456, circ04500, circ08492, circ08490) were downregulated at 33˚C in both the RBC2 and NCT comparisons. One DEC (circ07296) was downregulated at 33˚C in the NCT SCs but upregulated in the RBC2 SCs.

3.3.1.2.2 Differentiation: effects of genetic line. Forty-eight circRNAs were differentially expressed between the genetic lines within thermal treatment comparisons (Figure 2D; Table 2; Supplementary Table S3). In the NCT-RBC2 comparison at control temperature (38˚C) eight circRNAs were differentially expressed with four DECs being downregulated and four

upregulated in the NCT SCs compared to RBC2 (Figure 2D). In the heat temperature comparison (43°C), 13 circRNAs were differentially expressed with eight DECs being downregulated and five upregulated in the NCT line in comparison to the RBC2. In the cold temperature comparison (33°C), 32 circRNAs were differentially expressed with 21 DECs being downregulated and 11 upregulated in the NCT line in comparison to RBC2 (Table 2; Supplementary Table S3).

No DECs were shared across all genetic line comparisons but five DECs (circ0991, circ07152, circ07296, circ10074, circ08181) were shared between multiple within-line comparisons. Two DECs (circ07152, circ07296) were shared between the control and cold temperature comparison, and both were downregulated in the NCT line at 33°C but upregulated in the NCT at 38°C. A single DEC (circ09901) was shared between the hot and control temperature comparisons and was upregulated at 43°C but downregulated line at 38°C in the NCT SCs compared to RBC2 cells. Of the two DECs shared between the hot and cold temperature comparisons, circ10074 was upregulated at 43°C and downregulated at 33°C in the NCT line relative to RBC2 line and circ08181 was downregulate at 43°C and upregulated at 33°C in the NCT line relative to RBC2 line (Table 2).

3.3.2 Differential circRNA splicing (circRNA vs. linear forms)

Six DECs were found in three treatment comparisons to be differentially spliced (splice score > |.10|). All differentially spliced circRNAs (DSCs) occurred in the differentiating SCs and none were predicted in the proliferation SC comparisons (Table 2; Supplementary Table S3). Two circRNAs (circ04173; circ08492) were predicted to be down-spliced (increase in splicing towards the linear form) and one (circ01428) was up-spliced (increase in splicing towards the circular form) in the RBC2 control vs. hot treatment comparison. Three circRNAs (circ09737; circ06985; circ04168) were predicted to be up-spliced in the NCT control vs. hot treatment comparison and two circRNAs (circ04173; circ09737) were found to be predicted to be up-spliced in the NCT control vs. cold treatment comparisons (Table 2; Supplementary Table S3). Two DSCs (circ08492 and circ06985) have parent genes associated with known muscle genes, myosin light chain 10 and tropomyosin 1, respectively (Supplementary Table S4). The latter associated with actin-binding in contractile function. Three DSCs (circ04173, circ04168, circ04173) have the same parent gene, eukaryotic translation initiation factor 4 gamma 2 (eIF4G2, ENSMGAG00000005834). This gene employs various translational mechanisms to control gene expression involved in apoptosis, cell differentiation and survival, and embryonic development (Liu et al., 2023).

3.4 Functional prediction analyses

3.4.1 miRNA/circRNA interaction

A total of 3,396 miRNA target binding sites (alignment score >165) corresponding to 277 turkey miRNAs was predicted for the 136 DECs with miRanda (Supplementary Table S5). For each circRNA, the miRNA with the highest alignment score (average 177.63) is given in Supplementary Table S5. Four circRNAs (circ09737; circ09900; circ09901; circ01223) had no predicted miRNA target binding sites. The number of targets per DEC ranged from 1 to 115 with an average of 24.97/circRNA. In some cases, miRNAs were predicted to bind multiple times to a single circRNA. For example, mga-miR-103 had 54 predicted target binding sites. The highest overall alignment score (200) occurred for a target binding site in circ05242 corresponding to mga-miR-26a.

Of the 277 miRNAs with target binding sites in the DECs, 43 were differentially expressed microRNAs (DEMs) in either the SC proliferation or differentiation assays (Reed et al., 2023). Eight of these miRNAs (mga-miR-206, mga-miR-2954, mga-miR-3529, mga-miR-N54, mga-miR-N40, mga-miR-N72, mga-miR-N92, and mga-miR-N185) were differentially expressed in both proliferating and differentiating SCs and had binding sites within the differentially expressed circRNAs (DECs) observed in both of the SC developmental stages.

3.4.2 Secondary structure

RNAfold was used to demonstrate the potential effect of secondary structure on miRNA/circRNA interactions. Four secondary structures were predicted and examined for circ09021 (sequence data can be found in Supplementary Table S6). Included are the minimum free energy (MFE) structure, a predicted structure that does not take temperature into account and was predicted to be the same across all three temperature parameters, and three unique predicted thermodynamic ensemble (TE) structures corresponding to 37, 38°C and 39°C (TE_37, TE_38, TE_39; Supplementary Table S6; Figure 3). In general, the higher the temperature parameter, the greater the number of predicted unpaired nucleotides (Supplementary Table S6; Figure 3). Within circ09021, 11 miRNA target binding sites were predicted (alignment score >150) using miRanda. All of the predicted target binding locations were found to be unavailable for binding in the TE_37 and TE_38 structures due to loop formations. However, the TE_39 predicted secondary structure had two target binding sites exposed for mga-miR-N4 and mga-miR-N139 demonstrating the potential effect of slight temperature change on binding interactions. To investigate how slight the temperature change needed to induce a change in miRNA binding availability, RNAfold was reran to predict the secondary structure of circ09021 at 0.1°C increment changes from 38°C to 38.5°C (Supplementary Figure S1). At 38.4°C, mga-miR-N4 was able to first bind to circ09021. Three other binding sites were made available between 38°C and 38.5°C.

4 Discussion

CircRNAs are naturally occurring, single-stranded RNAs formed by altered transcript splicing and are extensively expressed in eukaryotes (Drula, Braicu, and Berindan-Neagoe, 2024). Phylogenetic sequence comparisons reveal circRNAs to be moderately conserved (Patop, Wüst, and Kadener, 2019) and expression analyses suggest tissue- and development-specific expression patterns (Misir et al., 2022). Studies hypothesize that circRNAs have diverse functions (Zhang et al., 2018) such as acting as miRNA sponges, binding endogenous competing RNAs, interacting with RNA binding proteins and/or mRNAs to

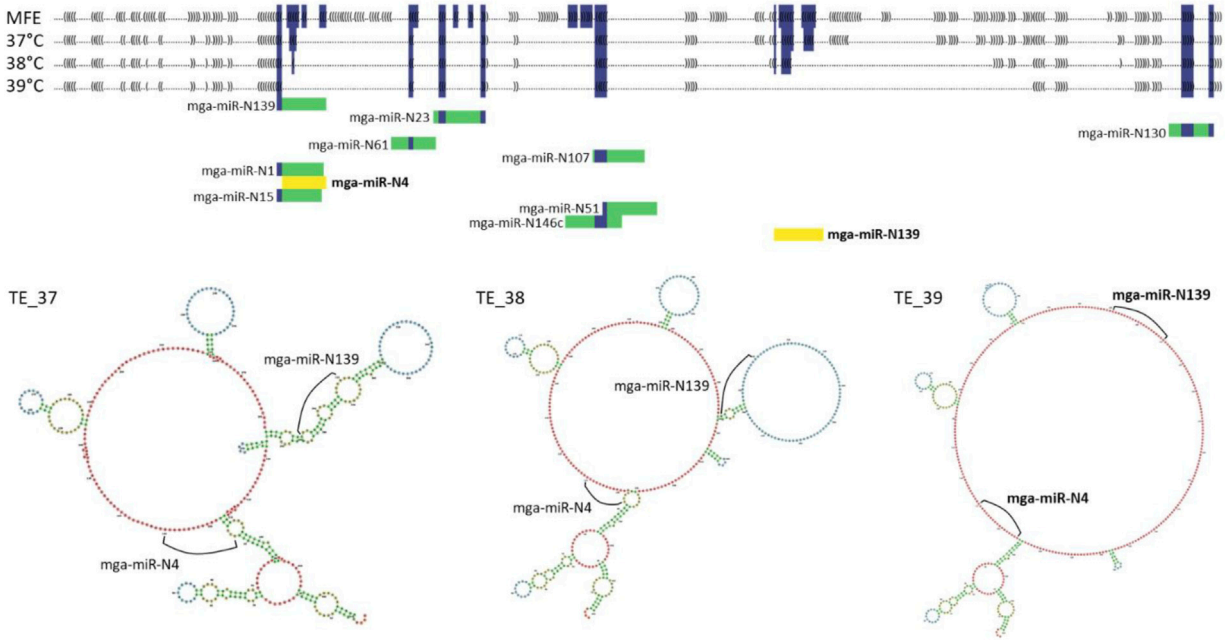

FIGURE 3
Dot-bracket secondary structure predictions for MFE and TE shown for circ09201 with miRNA target predcitions. miRNAs in yellow show target binding sites where the miRNA could bind. Folding structure predictions also shown by the 3 TE structures.3.

regulate transcription, or influencing alternative splicing (Huang Anqing et al., 2020). Several studies indicate that circRNAs play crucial roles in processes such as cell proliferation, differentiation, autophagy, apoptosis (Cao et al., 2018; Kulcheski et al., 2016; Liang et al., 2017; Panda et al., 2017), and influence gene expression during myogenesis (Das et al., 2020; Legnini et al., 2017). Results from this study further support the hypothesis that differential expression of circRNAs are impacted by genetic background and changes in temperature in turkey muscle SCs.

4.1 circRNA prediction and quantification

The number of unique circRNAs predicted from RNAseq analyses in poultry, varies greatly among studies. Analysis of breast muscle from embryonic chickens of multiple embryonic days, identified 4,226 circRNAs (Shen Xiaoxu et al., 2019) and over 13,000 unique circRNAs were identified from embryonic skeletal muscle (Ouyang et al., 2018). The circRNAs identified here in the turkey SCs (10,679) was greater than the number identified (8,924) in our analysis of skeletal muscle from thermally challenged turkey poults (Reed et al., 2021). The average length of circRNAs found in this study (average: 37,980 nt) exceeds those reported in circRNA studies conducted in chicken (average: 200–2,564 nt, range: <61–95985 nt; Chen et al., 2023; Huang Xuewei et al., 2020; Shen Manman et al., 2019; Wang et al., 2022), but falls within the range observed in our study of whole turkey muscle (average: ~36,200 nt, range: 134–~200,000 nt; Reed et al., 2021) and that of some mouse and human studies (average: 18,132 nt, range: 51–922930 nt; Vromman et al., 2023). The difference in average length could be a result of several factors including the use of CIRI2 compared to other prediction programs with different underlying prediction algorithms, variations in genome quality, differences in sequence read length, and alternative splicing events. A cursory analysis of the SC sequences with CIRI-AS, a program that detects alternative splicing of circRNAs, indicates occurrence of alternative splicing events. However, due to the limited sensitivity of read lengths <75 nt, further investigation was not pursued.

The circRNAs predicted in the turkey SCs were distributed across the genome. To investigate if there was a skewed distribution of circRNA prediction among chromosomes, a chi-square test between number of circRNAs predicted per chromosome and length of chromosome was conducted. A p-value of 0.24 indicates that the number of predicted circRNAs is most likely due to the chromosome length and no bias in chromosome representation was observed. The differential expression of circRNAs from muscle-related parent genes is not unexpected given that the source of the RNAseq data is muscle stem cells.

4.2 RNase depletion

Although most circRNAs occur at comparatively low levels, some surpass the expression levels of their linear RNA counterparts (Wilusz, 2018). Due to their resistance to degradation by RNA exonuclease, circRNAs are more stable than linear RNAs. RNase R treatments are commonly used to degrade linear RNA for circRNA enrichment. This enrichment allows for direct comparison of circRNA predictions from sequence data with and without enrichment. Although some characteristics such as genomic distribution were similar between the matched sources, RNase

depletion of the SC RNAs resulted in a 50%–80% reduction in the number of circRNAs predicted, and detection of 2,775 of previously undetected circRNAs in the non-depleted libraries. This highlights a potential weakness of data mining traditional mRNA data sets *versus* broader use of RNase depletion in library preparation and sequence generation.

4.3 Differential expression

This study of skeletal muscle SCs suggests that the production of circRNAs is significantly altered by thermal challenge as predicted in the muscle of thermally challenged turkey poults (Reed et al., 2021). Of the 140 DECs identified in the turkey SC's, 137 were also identified in our earlier study of muscle from turkey poults (Reed et al., 2021) suggesting conserved expression. Ten of these circRNAs (circ01223, circ01670, circ01781, circ01919, circ04932, circ05562, circ07670, circ08490, circ09289 and circ10481) were differentially expressed in both studies (Supplementary Table S7).

4.3.1 Thermal treatment comparisons

In all comparisons, the number of circRNAs showing increased expression was higher in cells incubated at the higher temperature. Temperature is a key regulatory factor for alternative mRNA splicing in both plants and animals (Shiina and Shimizu, 2020). Temperature-dependent alternative mRNA splicing has been demonstrated in mammals as a response to low body temperature during hibernation (Sano et al., 2015). Other effects on RNA splicing related to cellular temperature are changes in transcription rate of RNA polymerase II and RNA structure (Capovilla et al., 2015). Modifications of secondary RNA structure can affect the positioning of the spliceosomal complex which catalyzes backsplicing for the creation of circRNAs (Shi et al., 2021). These factors might contribute to the differences seen in circRNA expression in the cultured SCs. The differential expression of circRNAs with parent genes corresponding to known muscle protein genes demonstrates this potential impact. The cellular mechanisms of temperature-dependent alternative splicing continue to be the focus of ongoing research. Another potential cause to the differences in circRNA expression is that some of the circRNAs identified could simply be artifacts, though CIRIquant incorporates a multiple seed matching to help eliminate false positives (Drula et al., 2024; Gao et al., 2018)

The potential for shifts in gene expression due to thermal stress is important in poultry biology and ultimately meat production. Birds are homotherms but young birds have poor thermal regulation and they cannot maintain their body temperature when under even relatively mild thermal stress (Henrikson et al., 2018; Meltzer, 1983; Yahav, 2000). Thermal stress especially after hatch can in turn have long-term effects on the growth and structure of muscle (Patael et al., 2019; Piestun et al., 2017). Timing and degree of thermal stress are critical. Although development of satellite cells can be thermally stimulated during specific times in embryonic development, studies highlight changes in breast muscle histomorphology, metabolism, and physiology resulting from suboptimal incubation conditions (Oviedo-Rondón et al., 2020). For example, in broilers, mild thermal manipulation during early posthatch period can promote myogenic proliferation and differentiation (Halevy, 2020), whereas heat stress during the first 13 D posthatch can increase fat and collagen deposition and impair growth of the pectoralis muscle (Patael et al., 2019). Birds in production systems face potential new challenges due to climate change. These include not only higher mean temperatures, but also the increased frequency of extreme weather events, both hot and cold (Ruuskanen, Hsu, and Nord, 2021), which may in turn increase the incidence of adverse effects on muscle growth, development, and ultimately on meat quality.

4.3.2 Genetic line comparisons

Thermal comparisons within genetic lines (NCT and RBC2) found the majority of DECs were unique to genetic background with few DECs shared between lines in both proliferating and differentiating SCs (Supplementary Table S3). Differences in the DECs shared between the NCT and RBC2 lines can be attributed to underlying genetic differences from selection for commercial traits in the NCT birds. The RBC2 line been maintained at The Ohio State University, Poultry Research Center (Wooster, OH) without conscious selection for any trait since 1966 and has significantly different growth characteristics than the modern commercial bird (Lilburn and Nestor, 1991).

4.4 Functional predictions

4.4.1 circRNA/miRNA interactions

There is increasing evidence for the importance of RNA interactions in muscle biology. For example, our recent examination of miRNA expression in turkey muscles SCs in this same experimental system (Reed et al., 2023), detected significant expression differences among temperature treatments and between genetic lines. Including the eight miRNAs that had target binding sites with the DECs found in this study. In both proliferating and differentiating turkey SCs, significant differential expression of miRNAs important in muscle development (e.g., mga-miR-206) was found in response to thermal challenges in both turkey lines. Studies by Harding and Velleman (2016), and by Velleman and Harding (2017), suggest that miRNAs play roles in myogenic satellite cell migration. Interactions between miRNAs and circRNAs have the potential to alter these processes (Liang et al., 2017; Ouyang et al., 2018). These studies in turkey demonstrate how changes in non-coding RNAs could significantly affect cellular proliferation and differentiation, potentially affecting *Pectoralis major* muscle growth and development and subsequently breast meat quality.

Predictions of circRNA-miRNA interaction are often used support the hypothesis that circRNAs function as "molecular sponges". As demonstrated here, miRanda and related programs can identify thousands of potential miRNA target binding sites associated with circRNA sequences. However, identification of potential interactions does not translate directly to downstream function and detailed biochemical experiments are necessary to verify predicted interactions. The circRNAs identified in this study and the predicted miRNA interactions provide a framework for generating future hypotheses.

4.4.2 Secondary structures

Previous examinations of circRNAs have not considered how the cellular environment likely affects the function of these RNA molecules. As single stranded RNAs, circRNAs would create complex secondary and tertiary structures as a result of RNA folding. These dynamic structures respond to factors such as pH and temperature. As we have shown, a temperature increase of as little as 0.4°C induced changes in

predicted secondary structure and accessibility of miRNA target binding sites (Supplementary Figure S1). These predicted changes in binding ability due to RNA structures are likely what is happening biologically within cells suggesting that even slight changes in body temperature may increase or decrease miRNA binding or binding of circRNAs to proteins. While miRNA/circRNA interactions are important to understand modulation of gene expression, changes in secondary and tertiary structures from temperature changes should also be considered important (Somero, 2018). To the best of our knowledge, this is the first time miRNA/circRNA interactions have been viewed through the lens of secondary structure.

5 Conclusion

This investigation identified and quantified circRNAs expressed in turkey skeletal muscle stem cells cultured from the *Pectoralis major* muscle, under thermal challenge. The expression of circRNAs was significantly influenced by thermal treatments and the genetic background of the stem cells, with differentially expressed circRNAs (DECs) identified in each comparison. While the potential for these DECs to interact with miRNA targets is predicated to be significant, RNA secondary structure must be considered when evaluating these potential interactions. It is crucial to note that our circRNAs predictions and their interactions with miRNAs are theoretical and the circRNAs identified in this study were not experimentally verified. While these predictions offer hypotheses and a foundation for future research into the underlying cellular mechanisms, additional verification is required. The impact of environmental stressors on non-coding RNAs and their role in gene regulation remains a critical area of research, directly connected to muscle development and poultry production.

Data availability statement

Publicly available datasets were analyzed in this study. This data can be found here: SRA BioProject PRJNA842679.

Author contributions

AP: Conceptualization, Data curation, Formal Analysis, Investigation, Methodology, Visualization, Writing–original draft, Writing–review and editing. SV: Conceptualization, Resources, Writing–review and editing. GS: Conceptualization, Resources, Writing–review and editing. JA: Software, Writing–review and editing. KR: Conceptualization, Funding acquisition, Writing–original draft, Writing–review and editing.

Funding

The author(s) declare that financial support was received for the research, authorship, and/or publication of this article. This work was financially supported by the United States Department of Agriculture, National Institute of Food Agriculture, AFRI competitive grant no. 2020-67015-30827 to GS, KR, and SV.

Acknowledgments

We thank Kristelle Mendoza for performing the RNAse R depletion protocol for this project.

Conflict of interest

The authors declare that the research was conducted in the absence of any commercial or financial relationships that could be construed as a potential conflict of interest.

The author(s) declared that they were an editorial board member of Frontiers, at the time of submission. This had no impact on the peer review process and the final decision.

Publisher's note

Supplementary material

The Supplementary Material for this article can be found online at: https://www.frontiersin.org/articles/10.3389/fphys.2024.1476487/full#supplementary-material

References

Barnes, N. E., Mendoza, K. M., Strasburg, G. M., Velleman, S. G., and Reed, K. M. (2019). Thermal challenge alters the transcriptional profile of the breast muscle in Turkey poults. *Poult. Sci.* 98 (1), 74–91. doi:10.3382/ps/pey401

Barrett, S. P., and Salzman, J. (2016). Circular RNAs: analysis, expression and potential functions. *Development* 143 (11), 1838–1847. doi:10.1242/dev.128074

Cao, Y., You, S., Yao, Y., Liu, Z.-J., Hazi, W., Li, C.-Y., et al. (2018). Expression profiles of circular RNAs in sheep skeletal muscle. *Asian-Australasian J. Animal Sci.* 31 (10), 1550–1557. doi:10.5713/ajas.17.0563

Capovilla, G., Pajoro, A., Immink, R.Gh, and Schmid, M. (2015). Role of alternative pre-mRNA splicing in temperature signaling. *Curr. Opin. Plant Biol.* 27 (October), 97–103. doi:10.1016/j.pbi.2015.06.016

Chen, L., Ruan, J., Chen, Y., Deng, W., Lai, J., Fan, L., et al. (2023). RNA sequencing reveals CircRNA expression profiles in chicken embryo fibroblasts infected with velogenic newcastle disease virus. *Front. Veterinary Sci.* 10 (March), 1167444. doi:10.3389/fvets.2023.1167444

Das, A., Das, A., Das, D., Abdelmohsen, K., and Panda, A. C. (2020). Circular RNAs in myogenesis. *Biochimica Biophysica Acta (BBA) - Gene Regul. Mech.* 1863 (4), 194372. doi:10.1016/j.bbagrm.2019.02.011

Dou, T., Li, Z., Wang, K., Liu, L., Rong, H., Xu, Z., et al. (2018). Regulation of myostatin expression is associated with growth and muscle development in commercial broiler and DMC muscle. *Mol. Biol. Rep.* 45 (4), 511–522. doi:10.1007/s11033-018-4187-7

Drula, R., Braicu, C., and Berindan-Neagoe, I. (2024). Current advances in circular RNA detection and investigation methods: are we running in circles? *WIREs RNA* 15 (3), e1850. doi:10.1002/wrna.1850

Duggan, B., Ralph, J., Avendaño, S., Neeteson, A.-M., Burnside, T., and Koerhuis, A. (2023). Decades of breeding for welfare and sustainability. Available at: https://aviagen.com/assets/Welfare/AviagenDecades-of-WelfareReport_2023.pdf.

Enright, A. J., John, B., Gaul, U., Tuschl, T., Sander, C., and Marks, D. S. (2003). MicroRNA targets in Drosophila. *Genome Biol.* 5 (1), R1. doi:10.1186/gb-2003-5-1-r1

Gao, L., Chang, S., Xia, W., Wang, X., Zhang, C., Cheng, L., et al. (2020). Circular RNAs from *BOULE* play conserved roles in protection against stress-induced fertility decline. *Sci. Adv.* 6 (46), eabb7426. doi:10.1126/sciadv.abb7426

Gao, Y., Wang, J., and Zhao, F. (2015). CIRI: an efficient and unbiased algorithm for *de novo* circular RNA identification. *Genome Biol.* 16 (1), 4. doi:10.1186/s13059-014-0571-3

Gao, Y., Zhang, J., and Zhao, F. (2018). Circular RNA identification based on multiple seed matching. *Briefings Bioinforma.* 19 (5), 803–810. doi:10.1093/bib/bbx014

Halevy, O. (2020). Timing is everything—the high sensitivity of avian satellite cells to thermal conditions during embryonic and posthatch periods. *Front. Physiology* 11 (March), 235. doi:10.3389/fphys.2020.00235

Halevy, O., Geyra, A., Barak, M., Uni, Z., and Sklan, D. (2000). Early posthatch starvation decreases satellite cell proliferation and skeletal muscle growth in chicks. *J. Nutr.* 130 (4), 858–864. doi:10.1093/jn/130.4.858

Harding, R. L., and Velleman, S. G. (2016). MicroRNA regulation of myogenic satellite cell proliferation and differentiation. *Mol. Cell. Biochem.* 412 (1–2), 181–195. doi:10.1007/s11010-015-2625-6

Henrikson, Z. A., Vermette, C. J., Schwean-Lardner, K., and Crowe, T. G. (2018). Effects of cold exposure on physiology, meat quality, and behavior of Turkey hens and toms crated at transport density. *Poult. Sci.* 97 (2), 347–357. doi:10.3382/ps/pex227

Huang, A., Zheng, H., Wu, Z., Chen, M., and Huang, Y. (2020a). Circular RNA-protein interactions: functions, mechanisms, and identification. *Theranostics* 10 (8), 3503–3517. doi:10.7150/thno.42174

Huang, X., Zhang, J., Liu, Z., Wang, M., Fan, X., Wang, Li, et al. (2020b). Genome-wide analysis of differentially expressed mRNAs, lncRNAs, and circRNAs in chicken bursae of fabricius during infection with very virulent infectious bursal disease virus. *BMC Genomics* 21 (1), 724. doi:10.1186/s12864-020-07129-1

Huo, L., Zhang, P., Li, C., Rahim, K., Xiaoran, H., Xiang, B., et al. (2018). Genome-wide identification of circRNAs in pathogenic basidiomycetous yeast cryptococcus neoformans suggests conserved circRNA host genes over kingdoms. *Genes* 9 (3), 118. doi:10.3390/genes9030118

Ibrahim, D., Al-Khalaifah, H. S., Abdelfattah-Hassan, A., Eldoumani, H., Khater, S. I., Arisha, A. H., et al. (2021). Promising role of growth hormone-boosting peptide in regulating the expression of muscle-specific genes and related MicroRNAs in broiler chickens. *Animals* 11 (7), 1906. doi:10.3390/ani11071906

Kulcheski, F. R., Christoff, A. P., and Margis, R. (2016). Circular RNAs are miRNA sponges and can Be used as a new class of biomarker. *J. Biotechnol.* 238 (November), 42–51. doi:10.1016/j.jbiotec.2016.09.011

Lara, L., and Rostagno, M. (2013). Impact of heat stress on poultry production. *Animals* 3 (2), 356–369. doi:10.3390/ani3020356

Legnini, I., Di Timoteo, G., Rossi, F., Morlando, M., Briganti, F., Sthandier, O., et al. (2017). Circ-ZNF609 is a circular RNA that can Be translated and functions in myogenesis. *Mol. Cell* 66 (1), 22–37. doi:10.1016/j.molcel.2017.02.017

Lei, Q., Hu, X., Han, H., Wang, J., Liu, W., Zhou, Y., et al. (2022). Integrative analysis of circRNA, miRNA, and mRNA profiles to reveal ceRNA regulation in chicken muscle development from the embryonic to post-hatching periods. *BMC Genomics* 23 (1), 342. doi:10.1186/s12864-022-08525-5

Li, J., and Wang, X. (2024). Functional roles of conserved lncRNAs and circRNAs in eukaryotes. *Non-Coding RNA Res.* 9 (4), 1271–1279. doi:10.1016/j.ncrna.2024.06.014

Li, X., Zhao, X., Yu, M., Zhang, M., and Feng, J. (2024). Effects of heat stress on breast muscle metabolomics and lipid metabolism related genes in growing broilers. *Animals* 14 (3), 430. doi:10.3390/ani14030430

Liang, G., Yang, Y., Niu, G., Tang, Z., and Li, K. (2017). Genome-wide profiling of Sus scrofa circular RNAs across nine organs and three developmental stages. *DNA Res.* 24 (5), 523–535. doi:10.1093/dnares/dsx022

Lilburn, M. S., and Nestor, K. E. (1991). Body weight and carcass development in different lines of turkeys. *Poult. Sci.* 70 (11), 2223–2231. doi:10.3382/ps.0702223

Liu, Y., Cui, J., Hoffman, A. R., and Hu, J. F. (2023). Eukaryotic translation initiation factor eIF4G2 opens novel paths for protein synthesis in development, apoptosis and cell differentiation. *Cell Prolif.* 56 (3), e13367. doi:10.1111/cpr.13367

Lorenz, R., Bernhart, S. H., Siederdissen, C. H.Zu, Tafer, H., Flamm, C., Stadler, P. F., et al. (2011). ViennaRNA package 2.0. *Algorithms Mol. Biol.* 6 (1), 26. doi:10.1186/1748-7188-6-26

Meltzer, A. (1983). Thermoneutral zone and resting metabolic rate of broilers. *Br. Poult. Sci.* 24 (4), 471–476. doi:10.1080/00071668308416763

Misir, S., Wu, N., and Yang, B. B. (2022). Specific expression and functions of circular RNAs. *Cell Death and Differ.* 29 (3), 481–491. doi:10.1038/s41418-022-00948-7

Mozdziak, P. E., Schultz, E., and Cassens, R. G. (1994). Satellite cell mitotic activity in posthatch Turkey skeletal muscle growth. *Poult. Sci.* 73 (4), 547–555. doi:10.3382/ps.0730547

Musselman, M. (2021). The journey to sustainable breeding. Available at: https://www.hybridturkeys.com/en/news/journey-sustainable-breeding/(Accessed March 10, 2021).

Nawab, A., Ibtisham, F., Li, G., Kieser, B., Wu, J., Liu, W., et al. (2018). Heat stress in poultry production: mitigation strategies to overcome the future challenges facing the global poultry industry. *J. Therm. Biol.* 78 (December), 131–139. doi:10.1016/j.jtherbio.2018.08.010

Nestor, K. E. (1977). The stability of two randombred control populations of turkeys. *Poult. Sci.* 56 (1), 54–57. doi:10.3382/ps.0560054

O'Brien, J., Hayder, H., Zayed, Y., and Peng, C. (2018). Overview of MicroRNA biogenesis, mechanisms of actions, and circulation. *Front. Endocrinol.* 9 (August), 402. doi:10.3389/fendo.2018.00402

Ouyang, H., Chen, X., Wang, Z., Jiao, Yu, Jia, X., Li, Z., et al. (2018). Circular RNAs are abundant and dynamically expressed during embryonic muscle development in chickens. *DNA Res.* 25 (1), 71–86. doi:10.1093/dnares/dsx039

Oviedo-Rondón, E. O., Velleman, S. G., and Wineland, M. J. (2020). The role of incubation conditions in the onset of avian myopathies. *Front. Physiology* 11 (September), 545045. doi:10.3389/fphys.2020.545045

Panda, A. C., Grammatikakis, I., Munk, R., Gorospe, M., and Abdelmohsen, K. (2017). Emerging roles and context of circular RNAs. *WIREs RNA* 8 (2), e1386. doi:10.1002/wrna.1386

Patael, T., Piestun, Y., Soffer, A., Mordechay, S., Yahav, S., Velleman, S. G., et al. (2019). Early posthatch thermal stress causes long-term adverse effects on pectoralis muscle development in broilers. *Poult. Sci.* 98 (8), 3268–3277. doi:10.3382/ps/pez123

Patop, I. L., Wüst, S., and Kadener, S. (2019). Past, present, and future of circ RNA s. *EMBO J.* 38 (16), e100836. doi:10.15252/embj.2018100836

Piestun, Y., Patael, T., Yahav, S., Velleman, S. G., and Halevy, O. (2017). Early posthatch thermal stress affects breast muscle development and satellite cell growth and characteristics in broilers. *Poult. Sci.* 96 (8), 2877–2888. doi:10.3382/ps/pex065

Reed, K. M., Mendoza, K. M., Abrahante, J. E., Barnes, N. E., Velleman, S. G., and Strasburg, G. M. (2017). Response of Turkey muscle satellite cells to thermal challenge. I. Transcriptome effects in proliferating cells. *BMC Genomics* 18 (1), 352. doi:10.1186/s12864-017-3740-4

Reed, K. M., Mendoza, K. M., Abrahante, J. E., Velleman, S. G., and Strasburg, G. M. (2021). Data mining identifies differentially expressed circular RNAs in skeletal muscle of thermally challenged Turkey poults. *Front. Physiology* 12 (August), 732208. doi:10.3389/fphys.2021.732208

Reed, K. M., Mendoza, K. M., Kono, T., Powell, A. A., Strasburg, G. M., and Velleman, S. G. (2023). Expression of miRNAs in Turkey muscle satellite cells and differential response to thermal challenge. *Front. Physiology* 14 (November), 1293264. doi:10.3389/fphys.2023.1293264

Reed, K. M., Mendoza, K. M., Strasburg, G. M., and Velleman, S. G. (2022). Transcriptome response of proliferating muscle satellite cells to thermal challenge in commercial Turkey. *Front. Physiology* 13 (August), 970243. doi:10.3389/fphys.2022.970243

Ruuskanen, S., Hsu, B.-Y., and Nord, A. (2021). Endocrinology of thermoregulation in birds in a changing climate. *Mol. Cell. Endocrinol.* 519 (January), 111088. doi:10.1016/j.mce.2020.111088

Sano, Y., Shiina, T., Naitou, K., Nakamori, H., and Shimizu, Y. (2015). Hibernation-specific alternative splicing of the mRNA encoding cold-inducible RNA-binding protein in the hearts of hamsters. *Biochem. Biophysical Res. Commun.* 462 (4), 322–325. doi:10.1016/j.bbrc.2015.04.135

Santos-Rodriguez, G., Voineagu, I., and Weatheritt, R. J. (2021). Evolutionary dynamics of circular RNAs in primates. *eLife* 10 (September), e69148. doi:10.7554/eLife.69148

Shen, M., Li, T., Zhang, G., Wu, P., Chen, F., Lou, Q., et al. (2019a). Dynamic expression and functional analysis of circRNA in granulosa cells during follicular development in chicken. *BMC Genomics* 20 (1), 96. doi:10.1186/s12864-019-5462-2

Shen, X., Liu, Z., Cao, X., He, H., Han, S., Chen, Y., et al. (2019b). Circular RNA profiling identified an abundant circular RNA circTMTC1 that inhibits chicken skeletal muscle satellite cell differentiation by sponging miR-128-3p. *Int. J. Biol. Sci.* 15 (10), 2265–2281. doi:10.7150/ijbs.36412

Shi, S., Li, X., and Zhao, R. (2021). Detecting circRNA in purified spliceosomal P complex. *Methods* 196 (December), 30–35. doi:10.1016/j.ymeth.2021.02.002

Shiina, T., and Shimizu, Y. (2020). Temperature-dependent alternative splicing of precursor mRNAs and its biological significance: a review focused on post-transcriptional regulation of a cold shock protein gene in hibernating mammals. *Int. J. Mol. Sci.* 21 (20), 7599. doi:10.3390/ijms21207599

Somero, G. N. (2018). RNA thermosensors: how might animals exploit their regulatory potential? *J. Exp. Biol.* 221 (4), jeb162842. doi:10.1242/jeb.162842

Statello, L., Guo, C.-J., Chen, L.-L., and Huarte, M. (2021). Gene regulation by long non-coding RNAs and its biological functions. *Nat. Rev. Mol. Cell Biol.* 22 (2), 96–118. doi:10.1038/s41580-020-00315-9

Tian, Y., Shen, X., Zhao, J., Wei, Y., Han, S., and Yin, H. (2023). CircSUCO promotes proliferation and differentiation of chicken skeletal muscle satellite cells *via* sponging miR-15. *Br. Poult. Sci.* 64 (1), 90–99. doi:10.1080/00071668.2022.2124098

United States Department of Agriculture- NASS. 2022. "Poultry - production and value 2022 summary 04/27/2023."

Velleman, S. G., and Harding, R. L. (2017). Regulation of Turkey myogenic satellite cell migration by MicroRNAs miR-128 and miR-24. *Poult. Sci.* 96 (6), 1910–1917. doi:10.3382/ps/pew434

Vromman, M., Anckaert, J., Bortoluzzi, S., Buratin, A., Chen, C.-Y., Chu, Q., et al. (2023). Large-scale benchmarking of circRNA detection tools reveals large differences in sensitivity but not in precision. *Nat. Methods* 20 (8), 1159–1169. doi:10.1038/s41592-023-01944-6

Wang, Y., Guo, Z., Zi, C., Wu, P., Lv, X., Chen, L., et al. (2022). CircRNA expression in chicken granulosa cells illuminated with red light. *Poult. Sci.* 101 (4), 101734. doi:10.1016/j.psj.2022.101734

Wilusz, J. E. (2018). A 360° view of circular RNAs: from biogenesis to functions. *WIREs RNA* 9 (4), e1478. doi:10.1002/wrna.1478

Wu, J., Li, Y., Wang, C., Cui, Y., Xu, T., Wang, C., et al. (2019). CircAST: full-length assembly and quantification of alternatively spliced isoforms in circular RNAs. *Genomics, Proteomics and Bioinforma.* 17 (5), 522–534. doi:10.1016/j.gpb.2019.03.004

Xu, J., Strasburg, G. M., Reed, K. M., and Velleman, S. G. (2021). Response of Turkey pectoralis major muscle satellite cells to hot and cold thermal stress: effect of growth selection on satellite cell proliferation and differentiation. *Comp. Biochem. Physiology Part A Mol. and Integr. Physiology* 252 (February), 110823. doi:10.1016/j.cbpa.2020.110823

Yahav, S. (2000). Domestic fowl - strategies to confront environmental conditions. *Avian Poult. Biol. Rev.* 11 (2), 81–95. doi:10.1017/S004393390900049X

Zhang, J., Chen, S., Yang, J., and Zhao, F. (2020). Accurate quantification of circular RNAs identifies extensive circular isoform switching events. *Nat. Commun.* 11 (1), 90. doi:10.1038/s41467-019-13840-9

Zhang, Z., Yang, T., and Xiao, J. (2018). Circular RNAs: promising biomarkers for human diseases. *EBioMedicine* 34 (August), 267–274. doi:10.1016/j.ebiom.2018.07.036

Zucko, D., and Boris-Lawrie, K. (2020). Circular RNAs are regulators of diverse animal transcriptomes: one health perspective. *Front. Genet.* 11 (September), 999. doi:10.3389/fgene.2020.00999

Nomenclature

DEC(s)	differentially expressed circular RNA(s)
DEM(s)	differentially expressed microRNA(s)
DS	differential splicing
DSC(s)	differentially spliced circRNA(s)
SC(s)	satellite cell(s)
NCT	Nicholas Commercial Turkeys
RBC2	Randombred Control Line 2

frontiers | Frontiers in Physiology

TYPE Original Research
PUBLISHED 25 September 2024
DOI 10.3389/fphys.2024.1465817

OPEN ACCESS

EDITED BY
Sandra G. Velleman,
The Ohio State University, United States

REVIEWED BY
Jiahui Xu,
University of California, Irvine, United States
Nima Emami,
Novonesis NA, United States

*CORRESPONDENCE
Laura E. Ellestad,
lellestad@uga.edu

RECEIVED 16 July 2024
ACCEPTED 05 September 2024
PUBLISHED 25 September 2024

CITATION
Garcia-Mejia RA, Sinclair-Black M, Blair LR, Angel R, Jaramillo B, Regmi P, Neupane N, Proszkowiec-Weglarz M, Arbe X, Cavero D and Ellestad LE (2024) Physiological changes in the regulation of calcium and phosphorus utilization that occur after the onset of egg production in commercial laying hens. *Front. Physiol.* 15:1465817. doi: 10.3389/fphys.2024.1465817

Physiological changes in the regulation of calcium and phosphorus utilization that occur after the onset of egg production in commercial laying hens

R. Alejandra Garcia-Mejia[1], Micaela Sinclair-Black[1], Lyssa R. Blair[1], Roselina Angel[2], Bibiana Jaramillo[3], Prafulla Regmi[1], Nabin Neupane[1], Monika Proszkowiec-Weglarz[4], Xabier Arbe[5], David Cavero[5] and Laura E. Ellestad[1]*

[1]Department of Poultry Science, University of Georgia, Athens, GA, United States, [2]Department of Animal and Avian Sciences, University of Maryland, College Park, MD, United States, [3]Iluma Alliance, Durham, NC, United States, [4]Animal Biosciences and Biotechnology Laboratory, United States Department of Agriculture-Agricultural Research Service, Beltsville, MD, United States, [5]H&N International, Cuxhaven, Germany

At the onset of egg production, physiological changes governing calcium and phosphorus utilization must occur to meet demands for medullary bone formation and eggshell mineralization. The objective of this study was to identify these changes and determine if they are influenced by dietary supplementation with 1α-hydroxycholecalciferol (AlphaD3™, Iluma Alliance). Commercial laying hens fed either a control or AlphaD3-supplemented diet beginning at 18 weeks of age were sampled at 18 (n = 8) and 31 weeks (n = 8/diet) to evaluate mRNA expression associated with calcium and phosphorus utilization in kidney, shell gland, ileum, and liver, circulating vitamin D_3 metabolites, and bone quality parameters in humerus, tibia, and keel bone. Though diet did not heavily influence gene expression at 31 weeks, several significant differences were observed between 18- and 31-week-old hens. Heightened sensitivity to hormones regulating calcium and phosphorus homeostasis was observed at 31 weeks, indicated by increased parathyroid hormone receptor 1, calcium-sensing receptor, calcitonin receptor, and fibroblast growth factor 23 receptors in several tissues. Increased renal expression of 25-hydroxylase and vitamin D binding protein (***DBP***) at 31 weeks suggests kidney participates in local vitamin D_3 25-hydroxylation and DBP synthesis after egg production begins. Biologically active $1,25(OH)_2D_3$ was higher at 31 weeks, with correspondingly lower inactive $24,25(OH)_2D_3$. Increased expression of plasma membrane calcium ATPase 1 and calbindin in kidney, shell gland, and ileum suggests these are key facilitators of calcium uptake. Elevated renal inorganic phosphorus transporter 1 and 2 and sodium-dependent phosphate transporter IIa at 31 weeks suggests increased phosphorus excretion following hyperphosphatemia due to bone breakdown for eggshell formation. Diet did influence bone quality parameters. Bone mineral density in both humerus and tibia was higher in AlphaD3-supplemented hens at 31 weeks. Tibial bone mineral content increased between 18 and 31 weeks, with AlphaD3-supplemented hens increasing more than control hens. Moreover, control hens exhibited diminished tibial breaking strength at 31 weeks compared to hens at 18 weeks, while AlphaD3-

supplemented hens did not. Together, these results indicate supplementation with AlphaD3 enhanced bone mineralization during the medullary bone formation period and elucidate the adaptive pathways regulating calcium and phosphorus utilization after the onset of lay.

KEYWORDS

vitamin D_3, medullary bone, breaking strength, mineral homeostasis, shell gland, kidney, ileum

1 Introduction

At the onset of egg production, commercial laying hens adapt physiological mechanisms that facilitate the utilization of calcium and phosphorus, primarily for the purpose of eggshell mineralization and medullary bone formation (Nys et al., 1986b; Wu et al., 1994). These adaptive changes begin to occur at the onset of sexual maturity between 17 and 18 weeks (Lei et al., 2020; Bahry et al., 2023) and involve specific organs important for absorption, transport, and utilization of calcium and phosphorus that are necessary for egg production (Bar, 2008). Described changes that occur at the onset of lay include increased intestinal mineral absorption (Nys et al., 1992a), renal mineral reabsorption and excretion (Wideman, 1987), calcium uptake and utilization by the shell gland (Corradino et al., 1993; Samiullah and Roberts, 2014), and medullary bone formation (Dacke et al., 1993; Kerschnitzki et al., 2014). This study provides a holistic physiological approach to understanding changes in the molecular mechanisms associated with calcium and phosphorus utilization before and after the onset of egg production.

Hormonal regulation of calcium and phosphorus homeostasis is influenced by multiple factors throughout the 24-h egg formation cycle (Sinclair-Black et al., 2023). Eggshell formation causes fluctuations in plasma ionized calcium levels (Sinclair-Black et al., 2024) that are detected by the plasma membrane protein calcium-sensing receptor (**CASR**) (Diaz et al., 1997; Hui et al., 2021). A decrease in calcium triggers the release of parathyroid hormone (**PTH**) that binds to parathyroid hormone receptor 1 (**PTH1R**) in target tissues (Pinheiro et al., 2012), stimulating renal calcium reabsorption and phosphorus excretion (Elaroussi et al., 1993), renal production of biologically active $1,25(OH)_2D_3$ via 1α-hydroxylase (Fraser and Kodicek, 1973), intestinal calcium absorption (Nemere and Norman, 1986), and bone breakdown (Miller, 1978) releasing both calcium and phosphorus into the blood. As circulating calcium and phosphorus levels subsequently rise, calcitonin (**CALC**) opposes effects of PTH by acting through calcitonin receptor (**CALCR**), primarily by inhibiting bone remodeling (Warshawsky et al., 1980) and promoting renal calcium excretion (Cochran et al., 1970). Circulating levels of phosphorus are regulated by fibroblast growth factor 23 **(FGF23)**, a hormone produced by bone in response to hyperphosphatemia in chickens (Wang et al., 2018; Gloux et al., 2020a). Its action is mediated by fibroblast growth factor receptors 1–4 (**FGFR1, FGFR2, FGFR3,** and **FGFR4)** in conjunction with the co-receptor Klotho (**KL**). In mammals (Shimada et al., 2004b; Perwad et al., 2005) and chickens (Ren et al., 2017), FGF23 induces renal excretion of excess circulating phosphorus. It has also been shown to inhibit PTH secretion (Ben-Dov et al., 2007) and production of $1,25(OH)_2D_3$ (Shimada et al., 2004a) in mammals. Many of the hormonal mechanisms regulating calcium and phosphorus homeostasis during egg formation are not fully understood, particularly the roles of CALC and FGF23 (Yasuoka et al., 1998; Ogawa et al., 2003; Sinclair-Black et al., 2023).

The hormonal form of vitamin D_3, $1,25(OH)_2D_3$, plays a major role in regulating calcium and phosphorus homeostasis. It can induce transcription of membrane mineral transporters and intracellular chaperone proteins involved in calcium and phosphorus absorption and utilization in intestine and kidney (Bar et al., 1990). To become active, dietary vitamin D_3 is first constitutively hydroxylated by hepatic 25-hydroxylase to produce $25(OH)D_3$ (Tucker et al., 1973). These enzymes are encoded by the *CYP2R1* (Watanabe et al., 2013) or *CYP27A1* (Shang et al., 2023) genes. A second, rate-limiting hydroxylation is catalyzed by renal 1α-hydroxylase to produce biologically active $1,25(OH)_2D_3$. This enzyme is encoded by *CYP27B1* in mammals and fish (Monkawa et al., 1997; Shinki et al., 1997; Chun et al., 2014). However, this gene has not been identified in chickens to date, despite prior publications reporting measurements in its expression as reviewed in Sinclair-Black et al. (2023). Commercially available 1α-hydroxycholecalciferol is a pre-hydroxylated vitamin D_3 supplement (AlphaD3™, Iluma Alliance), requiring only the constitutive 25-hydroxylation referenced above. This could potentially improve the efficiency with which $1,25(OH)_2D_3$ is produced. The inactive vitamin D_3 metabolite, $24,25(OH)_2D_3$, is generated through an alternative hydroxylation step carried out by 24-hydroxylase, encoded by *CYP24A1* (Armbrecht et al., 1997; Nemere, 1999).

The period between medullary bone formation that begins at the onset of sexual maturity around 18 weeks of age (Hudson et al., 1993; Bahry et al., 2023) and peak egg production around 31 weeks of age assumes significance, as hens must develop and sustain the metabolic capacity to meet high mineral requirements throughout their productive life. Therefore, this study sought to elucidate physiological changes associated with calcium and phosphorus uptake and utilization that occur during the onset of lay between 18 and 31 weeks of age and determine if supplementation with AlphaD3 influenced these changes. The objectives were to measure 1) expression profiles of genes for hormone receptors mediating calcium and phosphorus homeostasis, enzymes involved in vitamin D_3 metabolism, and mineral transporters in kidney, shell gland, ileum, and liver; 2) circulating vitamin D_3 metabolites; and 3) parameters associated with skeletal integrity in hens fed control (18 and 31 weeks) or AlphaD3-supplemented (31 weeks) diets.

2 Materials and methods

2.1 Animals and experimental design

All animal procedures were approved by The Institutional Animal Care and Use Committee at the University of Georgia.

10.3389/fphys.2024.1465817

TABLE 1 Ingredients and nutrient composition of starter, grower, and developer diets.[a].

Ingredients, as-fed %	Starter	Grower	Developer
Corn	61.986	58.337	56.787
Soybean meal, 47%	25.937	21.237	16.500
Wheat bran	-	8.500	-
Fish meal, 60%	2.000	-	-
Alfalfa meal	-	2.364	4.200
Wheat middlings	5.000	5.000	16.600
Fine limestone	1.460	1.688	1.500
Soybean oil	1.000	1.000	0.800
Mono-dicalcium phosphate, 21%	0.767	0.320	0.080
Arbocel®[b]	-	0.500	1.111
Vitamin premix	0.500[c]	0.050[d]	0.050[d]
Sand	0.400	-	1.250
Sodium chloride	0.290	0.270	0.260
DL Methionine	0.187	0.151	0.129
L-Lysine HCL	0.147	0.108	0.111
Coban 90	0.090	0.090	0.090
Trace mineral premix[e]	0.080	0.080	0.080
Sodium bicarbonate	0.078	0.155	0.310
Choline chloride, 60%	-	0.073	0.040
Bacitracin methylene disalicylate (BMD)[f]	0.050	0.050	0.050
L-Threonine	0.023	0.022	0.025
L-Tryptophan	-	-	0.012
Axtra® PHY GOLD[g]	0.005	0.005	0.005
Formulated nutrient composition (analyzed)			
Crude Protein	19.185 (17.700)	17.700 (16.600)	15.900 (16.200)
Crude fiber	1.942 (2.400)	3.500 (4.000)	4.219 (4.600)
Calcium	1.050 (0.890)	1.000 (0.840)	1.000 (0.720)
Phosphorus	0.601 (0.660)	0.559 (0.620)	0.480 (0.500)

[a]The diets were fed as follows: starter (0–5 weeks of age), grower (6–10 weeks of age), developer (11–17 weeks of age). Hens sampled at 18 weeks (Baseline) continued to be fed developer diet through18 weeks.
[b]JRS, Pharma LP, patterson, NY.
[c]Provided the following per kilogram of diet: vitamin A, 11,022 IU; vitamin D_3, 2204 IU; vitamin E, 22.05 IU; vitamin B12, 0.02 mg; Menadione, 2.21 mg; riboflavin, 8.82 mg; d-pantothenic acid, 22.05 mg; thiamine, 4.41 mg; niacin, 88.19 mg; vitamin B6, 4.41 mg; folic acid, 1.10 mg; choline, 382 mg; biotin, 0.40 mg
[d]Provided the following per kilogram of diet: vitamin A, 10,019 IU; vitamin D_3, 4519 IU; vitamin E, 41.34 IU; vitamin B12, 0.02 mg; Menadione, 2.48 mg; riboflavin, 13.78 mg; d-pantothenic acid, 19.29 mg; thiamine, 3.44 mg; niacin, 55.11 mg; vitamin B6, 4.82 mg; folic acid, 1.65 mg; biotin, 0.55 mg.
[e]Provided the following per kilogram of diet: Calcium min, 25.6 mg; Calcium max, 33.6 mg; Manganese min, 107.2 mg; Zinc, 85.6 mg; Magnesium, 19.8 mg; Iron, 21 mg; Copper, 3.2 mg; Iodine, 0.8 mg; Selenium min, 0.3 mg.
[f]Zoetis, Parsipanny, NJ.
[g]Danisco Animal Nutrition & Health (IFF), cedar rapids, IA.

The commercial strain Nick Chick white-egg laying hens (H&N International, Cuxhaven, Germany) used in this experiment were part of a larger flock reared at the University of Georgia's Poultry Research Center according to the primary breeder's nutritional and management guidelines (H&N International, 2020). In brief, chicks were raised on the floor from day of hatch through 16 weeks of age, when they were transferred to individual layer cages in an environmentally-controlled poultry house. Beginning at 18 weeks of age, light intensity was increased from 0.6 to 1.6 foot-candle, and the photoperiod was increased by 1 h of light per week until a 16L:

TABLE 2 Ingredients and nutrient composition of basal onset and layer diets.[a].

Ingredients, as-fed %	Onset	Layer
Corn	49.444	45.923
Soybean meal, 47%	25.703	25.343
Wheat middlings	9.166	14.028
Coarse limestone	6.527	6.130
Fine limestone	2.798	3.306
Soybean oil	2.014	3.395
Alfalfa meal	2.000	-
Mono-dicalcium phosphate, 21%	1.358	0.770
Sodium chloride	0.300	0.260
DL Methionine	0.261	0.247
Sodium bicarbonate	0.116	0.128
Trace mineral premix[b]	0.080	0.076
L-Lysine HCL	0.045	0.028
Bacitracin methylene disalicylate (BMD)[c]	0.050	0.048
Arbocel®[d]	0.050	0.238
Choline chloride 60%	0.040	0.038
Vitamin premix[e,f]	0.025	0.025
L-Threonine	0.013	0.011
L-Tryptophan	0.010	0.009
Calculated nutrient content (analyzed)		
Crude Protein	17.890 (18.400)	17.203 (16.600)
Crude fiber	2.677 (4.000)	2.000 (4.100)
Calcium	4.000 (3.600)	3.990 (3.800)
Phosphorus	0.686 (0.730)	0.643 (0.550)

[a]Basal onset and layer diets were mixed with all ingredients except the vitamin premix, split in half, and remixed with either the control (no Alpha D3) or the AlphaD3-supplemented premix. Diets were fed as follows: onset (17–22 weeks), layer (22–31 weeks). The AlphaD3-supplemented diet had 3.5 μg 1α-hydroxycholecalciferol/kg. Analyzed 1α-hydroxycholecalciferol level was below detection limit for the control diet and 2.67 and 3.05 μg/kg for the AlphaD3 onset and layer diets, respectively.

[b]Provided the following per kilogram of diet: Calcium min, 25.6 mg; Calcium max, 33.6 mg; Manganese min, 107.2 mg; Zinc, 85.6 mg; Magnesium, 19.8 mg; Iron, 21 mg; Copper, 3.2 mg; Iodine, 0.8 mg; Selenium min, 0.3 mg.

[c]Zoetis, Parsipanny, NJ.

[d]JRS, Pharma LP, patterson, NY.

[e]Control premix provided the following per kilogram of diet: vitamin A, 10,000 IU; vitamin D_3 2000 IU, Vitamin B-12, 30 mg; vitamin E, 3 IU; vitamin K (menadione), 3.5 mg; riboflavin, 10 mg; pantothenic acid, 45 mg; thiamine, 20 mg; niacin, 4 mg; pyridoxine, 0.006 mg; folic acid, 0.03 mg; biotin, 1 mg.

[f]AlphaD3 premix provided the following per kilogram of diet: vitamin A, 10,000 IU; vitamin D_3 2000 IU, Vitamin B-12, 30 mg; vitamin E, 3 IU; vitamin K (menadione), 3.5 mg; riboflavin, 10 mg; pantothenic acid, 45 mg; thiamine, 20 mg; niacin, 4 mg; pyridoxine, 0.006 mg; folic acid, 0.03 mg; biotin, 1 mg; 1α-hydroxycholecalciferol, 3.5 μg.

8D program was achieved at 24 weeks of age. All birds had free access to water and were fed *ad libitum* with corn-soybean meal-based diets formulated to meet requirements of high-producing laying hens (Tables 1 and 2).

At 17 weeks of age, 24 hens were randomly allocated to one of three different experimental groups (n = 8 hens/group): (1) Baseline, which continued to be fed the developer diet and were sampled at 18 weeks of age prior to photostimulation and the onset of lay; (2) control, which were fed basal onset (17–22 weeks) and layer (22–31 weeks) diets and sampled at 31 weeks of age; and (3) AlphaD3, which were fed basal onset (17–22 weeks) and layer (22–31 weeks) diets supplemented with AlphaD3™ [1α-hydroxycholecalciferol (Iluma Alliance, Durham, NC)] and sampled at 31 weeks of age. Each hen was considered an experimental unit, so there were 8 biological replicates for all parameters measured. To make the experimental onset and layer diets, basal diets were mixed with all ingredients except the vitamin premix, split in half, and then re-mixed with one of two different vitamin pre-mixes for control (no AlphaD3) and AlphaD3 (3.5 μg/kg of feed) treatments. Vitamin D_3 inclusion for both diets was 2000 UI/kg, and AlphaD3 was supplemented on top of it.

2.2 Sample collection

Blood and tissues were collected from hens at 18 and 31 weeks of age. Hens sampled at 31 weeks of age were individually monitored, and blood and tissues were collected at 21 h post-oviposition when a hard-shelled egg was present in the shell gland to minimize variation associated with the daily laying cycle (Sinclair-Black et al., 2024). Whole blood (~4.5 mL) was collected from the brachial vein into S-monovette collection tubes containing lithium heparin (SARSTEDT, Inc., Newton, NC), centrifuged at 1,500 x *g* and 4°C for 15 min to isolate plasma, and plasma was stored at −20°C until analyzed for vitamin D_3 metabolites. Immediately following blood collection, hens were euthanized by intravenous administration of 1-mL pentobarbital sodium (Euthasol®, Virbac, Westlake, TX) into the brachial or medial metatarsal vein. The right lobe of the liver, central shell gland, caudal lobe of the right kidney (approximately 500 mg per tissue), and homogenized mucosal scrapings from the proximal 1/3 of the ileum (approximately 30 mg) were collected, immediately snap-frozen in liquid nitrogen, and stored at −80°C prior to total RNA isolation. Keel bone and right and left humerus and tibia were excised from each bird, cleaned of most of the muscle and connective tissue, and stored at −20°C until used for determination of bone parameters.

2.3 Vitamin D_3 metabolite determination

The vitamin D_3 metabolites 25-hydroxycholecalciferol, 24,25-dihydroxycholecalciferol, and 1,25-dihydroxycholecalciferol were analyzed by liquid chromatography-tandem mass spectrometry (Heartland Assays, Ames, IA). Each sample was analyzed in duplicate, and the average values of these duplicates were used for further analysis. The lower limits of detection (**LOD**) and quantification (**LOQ**) for each analyte are as follows: 25-hydroxycholecalciferol – 0.5 ng/mL (LOD) and 1.5 ng/mL (LOQ); 24,25-dihydroxycholecalciferol – 0.1 ng/mL (LOD) and 0.3 ng/mL (LOQ); and 1,25-dihydroxycholeaclcierol – 5.0 pg/mL (LOD) and 10 pg/mL (LOQ).

2.4 Total RNA isolation

Total RNA was isolated from approximately 30 mg of each tissue that was homogenized in QIAzol lysis reagent (Qiagen, Valencia, CA) following the manufacturer's instructions. Tissues were homogenized using a Mini-BeadBeater (Biospec Products, Bartlesville, OK) in bursts of 45 s and rested on ice between bursts, with total homogenization times of 90 s for kidney, ileum, and liver and 145 s for shell gland. Precipitated total RNA was reconstituted using 200 µL nuclease-free water. Total RNA quantification was determined using a Nanodrop ND1000 spectrophotometer (ThermoFisher Scientific, Waltham, MA). Evaluation of RNA integrity was performed via agarose gel electrophoresis using a UV imaging system (BioSpectrum, Upland, CA) and visualized with the Visionworks LS software (Wasserburg, Germany).

2.5 Reverse transcription-quantitative polymerase chain reaction (RT-qPCR)

One µg total RNA was reverse transcribed into cDNA using M-MuLV reverse transcriptase (200 U; New England Biolabs, Ipswich, MA), RNaseOUT inhibitor (8U; Invitrogen, Carlsbad, CA), and a mixture of anchored oligo-dT (TTTTTTTTTTTTTTTTTTTTTVN, Integrated DNA technologies, Coralville, IA) and random hexamer (ThermoFisher Scientific, Waltham, MA) primers in 20 µL reactions. As a control for genomic DNA contamination, equivalent amounts of total RNA from all samples were used to make a 1 µg pool that was then used to conduct a reaction with all components except the reverse transcriptase enzyme (**no RT**). The samples and no RT control were initially incubated with primers and dNTPs at 65°C for 5 min, then rested on ice for 1 min before addition of M-MuLV enzyme (except for the no RT reaction), M-MuLV buffer, and RNaseOUT. All samples and the no RT control were then incubated under the following conditions: 5 min at 25°C, 60 min at 42°C, and 20 min at 65°C. Each cDNA sample was diluted 10-fold upon the reaction's completion prior to analysis by qPCR. The cDNA used for 18s ribosomal RNA amplification was further diluted up to 1:500. Intron-spanning primers (Table 3; Integrated DNA Technologies) for each transcript were designed using Primer3 plus Software (Untergasser et al., 2012). Quantitative PCR thermal cycling was conducted using a StepOne Real-Time PCR System (Applied Biosystems, Foster City, CA). Duplicate reactions for each sample (10 µL) were run for all genes, with each reaction containing 2 µL of template cDNA, 5 µL 2X PowerUp™ SYBR Green Master Mix (ThermoFisher), and 400 nM of each primer. The average Ct value of duplicate reactions was used for further analysis. Target genes were normalized to glyceraldehyde-3-phosphate dehydrogenase (***GAPDH***) in kidney and ileum, *18S* ribosomal RNA in shell gland, and cyclophilin (***CYCLO***) in liver. These genes were demonstrated to be the most stable out of all the ones evaluated and were not affected by age or diet. To normalize and transform the data, the following equations were used: $\Delta Ct = Ct_{Target\ gene} - (Ct_{GAPDH}$ or Ct_{18S} or $Ct_{CYCLO})$ and $2^{-\Delta Ct}$ (Ellestad et al., 2009; Vaccaro et al., 2022). Expression levels of each gene were then calculated relative to the average value for that gene at 18 weeks (Baseline) using equation $(2^{-\Delta Ct})_{target}/(\text{average } 2^{-\Delta Ct})_{Baseline}$, making the value for 18 weeks (Baseline) equal to 1 in all cases.

2.6 Bone parameters

Bone mineral density (**BMD**; g/cm^3) and bone mineral content (**BMC**; g) were determined for keel, left humerus, and left tibia using a Lunar Prodigy dual-X-ray absorptiometry (**DEXA**) scanner (GE Healthcare, Chicago, IL). The orientation of the respective bones was the same in each scan for consistency. Bone-breaking strength was analyzed with a three-point bending test on the right tibia using a TA. HDplus Texture Analyser (Stable Micro Systems, Godalming, United Kingdom). Bones were thawed at room temperature, cleaned of any remaining surrounding soft tissue, wrapped in a damp paper towel to maintain moisture, and stored in a plastic bag at 4°C for 24 h before breaking. Each bone was positioned in the same orientation on two support points with a span of 40 mm between them. A load of

10.3389/fphys.2024.1465817

TABLE 3 Primers used for reverse transcription-quantitative PCR.

Gene symbol	Forward primer (5′ -3′)	Reverse primer (5′ -3′)	Transcript ID[a]
Hormonal signaling			
Calcium homeostasis			
CASR	CTGCTTCGAGTGTGTGGACT	GATGCAGGATGTGTGGTTCT	55,986
PTH1R	CCAAGCTACGGGAAACAAAT	ATGGCATAGCCATGAAAACA	08,796
CALCR	GCAGTTGCAAGAGCCAAATA	AGCTTTGTCACCAACACTCG	15,478
Phosphorus homeostasis			
FGFR1	GACAGACTTCAACAGCCAGC	CCAACATCACACCCGAGTTC	66,938
FGFR2	CAGGGGTCTCGGAATATGAA	GCTTCAGCCATCACCACTT	38,732
FGFR3	GGAGTACTTGGCGTCACAGA	TCTAGCAAGGCCAAAATCAG	01,712
FGFR4	CTTGCCCGTCAAGTGGAT	TGAAGATCTCCCACATCAGAA	25,332
KL[b]	CCAAGAGAGATGATGCCAAA	CATCCAGAAGGGACCAGACT	15,785[b]
Vitamin D_3 metabolism and action			
Vitamin D_3 hydroxylation			
CYP2R1	GGACAGCAATGGACAGTTTG	AGGAAAACGCAGGTGAAATC	09,745
CYP27A1	CTGTTATCAAGGAGACGCTGA	TTGGGGAAGAGGTAGTCTCC	03,899
CYP24A1	TGGTGACACCTGTGGAACTT	CTCCTGAGGGTTTGCAGAGT	59,161
Vitamin D_3 signaling			
DBP	GGAACTTCCTCTCCATGGTC	AGCAAGCTCTGTTCGACATC	18,962
VDR	CTGCAAAATCACCAAGGACA	CATCTCACGCTTCCTCTGC	96,121
RXRA	ACTGCCGCTACCAGAAGTGT	GACTCCACCTCGTTCTCGTT	59,924
RXRG	GAAGCCTACACGAAGCAGAA	CCGATCAGCTTGAAGAAGAA	49,224
Mineral uptake and utilization			
Calcium transport			
CALB1	AAGCAGATTGAAGACTCAAAGC	CTGGCCAGTTCAGTAAGCTC	74,265
SLC8A1	TCACTGCAGTCGTGTTTGTG	AAGAAAACGTTCACGGCATT	13,920
ATP2B1	TTAATGCCCGGAAAATTCAC	TCCACCAAACTGCACGATAA	80,355
TRPV6	TATGCTGGAACGAAAACTGC	TTGTGCTTGTTGGGATCAAT	23,779
Bicarbonate synthesis and transport			
CA2	CCTGACTACTCCACCACTGC	TCTCAGCACTGAAGCAAAGG	52,439
SLC26A9	TCCACGATGCTGTTTTGTTT	GAGCTGCTTTCATCCACAGA	01,070
Inorganic phosphorus transport			
SLC20A1	TATCCTCCTCATTTCGGCGG	CTCTTCTCCATCAGCGGACT	94,781
SLC20A2	CCATCCCCGTGTACCTTATG	AGACATGGCCATCACTCCTC	51,992
SLC34A1	AAGCCATCCAGAAGGTCATC	CAGTGGTGTGATGGCTGAG	58,978
SLC34A2	AAAGTGACGTGGACCATG	GAGACCGATGGCAAGATCAG	23,222
Reference genes			
GAPDH	AGCCATTCCTCCACCTTTGAT	AGTCCACAACACGGTTGCTGTAT	23,323
18S[c]	AGCCTGCGGCTTAATTTGAC	CAACTAAGAACGGCCATGCA	

(Continued on following page)

TABLE 3 (*Continued*) Primers used for reverse transcription-quantitative PCR.

Gene symbol	Forward primer (5′ -3′)	Reverse primer (5′ -3′)	Transcript ID[a]
CYCLO	GCTCATGAAATTGCCCCTGA	GCGTAAGCTGCCTTCTCTTTCTC	15,382

[a]Transcript identification from Ensembl chicken genome assembly GRCg6a http://www.ensembl.org/Gallus_gallus/Info/Index) preceded by ENSGALT000000 for all genes except *KL* and *18S* rRNA.
[b]Transcript identification from Ensembl chicken genome assembly GRCg7b preceded by ENSGALT000100.
[c]Sequence of 18S rRNA, is not on the assembled chicken genome, and primers were designed based on the sequence in GenBank (Accession Number AF173612).

25 kg with a test speed of 1 mm/s was applied to the midpoint section of the same plane of each bone. The peak force required to break the bone was obtained from the deformation curve to determine breaking strength (**N**), and the total energy required for fracture **(N.mm)** was determined. Cortical thickness was determined from a straight cut made halfway between the midpoint and the distal end of the tibia and measured at the anterior, posterior, medial, and lateral positions using a Small Point Jaw Digital Caliper (INSIZE, Loganville, GA) that has a resolution of 0.001 mm and accuracy of ±0.03 mm.

Keel deviation prevalence, keel deviation severity, and presence of keel fractures were determined. Presence of keel bone deviation and deviation severity were measured from images taken of the ventral side of the keel bone using the image processing software Fiji (Schindelin et al., 2012). A straight line was drawn from the carina apex to the caudal tip of the keel bone, and distance (cm) for each lateral deviation from the straight line was recorded. To score the presence or absence of deviations, keels without any deviation (<0.25 cm) were scored as "0" and those with a deviation (>0.25 cm) were scored as "1." For deviation severity, the maximum deviation distance was recorded and assessed with a 3-point scoring system adapted from that described in Heerkens et al. (2016): "0" for no deviations (<0.25 cm), "1" for mild deviations (0.25–0.75 cm), and "2" for severe deviations (>0.75 cm). To determine the presence of keel bone fracture, hens without any fractures were scored as "0" and hens with one or more fractures were scored as "1." Each variable was analyzed independently.

2.7 Statistical analysis

All data were analyzed with JMP Pro 16 software (SAS Institute, Cary, NC), with hen as the experimental unit (n = 8 hens/group). The Shapiro-Wilk normality test was used to determine normal distribution of all the data. Gene expression, vitamin D_3 metabolites, BMD, BMC, AUC, and cortical thickness were analyzed using a one-way analysis of variance (**ANOVA**), with experimental group as the model effect. Whenever the ANOVA indicated statistical significance ($p \leq 0.05$), *post hoc* means comparisons were performed using Fisher's test of least significant difference (**LSD**). A log transformation was applied to AUC data prior to analysis to achieve normality. Tibia breaking force was analyzed using Kruskal–Wallis test for non-parametric variables, and means comparison was performed using Fisher's LSD test. For keel bone deviation and fracture scoring, the Chi-square probability test was performed for the effect of experimental group. For all variables analyzed, a power level between 75%–100% was achieved and differences were considered significant at $p \leq 0.05$.

3 Results

3.1 Hormonal signaling

3.1.1 Calcium homeostasis

To evaluate changes in hormonal signaling associated with calcium homeostasis after the onset of lay, mRNA expression levels of *CASR, PTH1R,* and *CALCR* were measured in kidney, shell gland, ileum, and liver. Though no significant differences between diets were found at 31 weeks, there were several changes that occurred between 18 and 31 weeks in these tissues. Expression of all three genes was upregulated in kidney at 31 weeks ($p \leq 0.05$; Figure 1A). In shell gland, *CASR* expression did not change with age, but both *PTH1R* and *CALCR* were higher at 31 weeks ($p \leq 0.05$; Figure 1B). While expression of both *CASR* and *CALCR* did not differ between 18 and 31 weeks in ileum ($p > 0.05$), significant increases of approximately 60-fold were observed for *PTH1R* at 31 weeks in this tissue ($p \leq 0.05$; Figure 1C). In liver, levels of *CASR* and *PTH1R* were found to be increased at 31 weeks, with *CASR* exhibiting an almost 40-fold increase ($p \leq 0.05$; Figure 1D); however, *CALCR* was not detected in this tissue (Figure 1D).

3.1.2 Phosphorus homeostasis

To identify changes in FGF23 hormonal sensitivity after the onset of lay, expression of *FGFR1, FGFR2, FGFR3*, *FGFR4,* and the co-receptor *KL* were measured in kidney, a known target tissue for FGF23 signaling, and shell gland based on our previous findings associated with phosphorus utilization and signaling in this tissue (Sinclair-Black et al., 2024). Renal expression of *FGFR1, FGFR4*, and *KL* was found to be upregulated at 31 weeks ($p \leq 0.05$) but did not differ between diets ($p > 0.05$; Figure 2A). Interestingly, *FGFR2* was found to be significantly downregulated at 31 weeks only in the control hens, with AlphaD3 hens maintaining expression. This resulted in significant differences between hens fed different diets at 31 weeks ($p \leq 0.05$; Figure 2A). Renal expression of *FGFR3* did not exhibit changes after the onset of lay, nor was it influenced by diet ($p > 0.05$; Figure 2A). Though differences were not evident between control- and AlphaD3-fed hens at 31 weeks ($p > 0.05$), levels of *FGFR2, FGFR3, FGFR4,* and *KL* were found to be upregulated at 31 weeks in the shell gland, with *KL* exhibiting an increase of approximately 7-fold ($p \leq 0.05$; Figure 2B). However, no age- or diet-induced changes were detected for *FGFR1* in this tissue ($p > 0.05$; Figure 2B). These results indicate that hens acquire greater sensitivity to hormones responsible for regulating calcium and phosphorus homeostasis after the onset of lay, potentially as a mechanism to facilitate eggshell mineralization and medullary bone formation. Furthermore, upregulation of the expression of

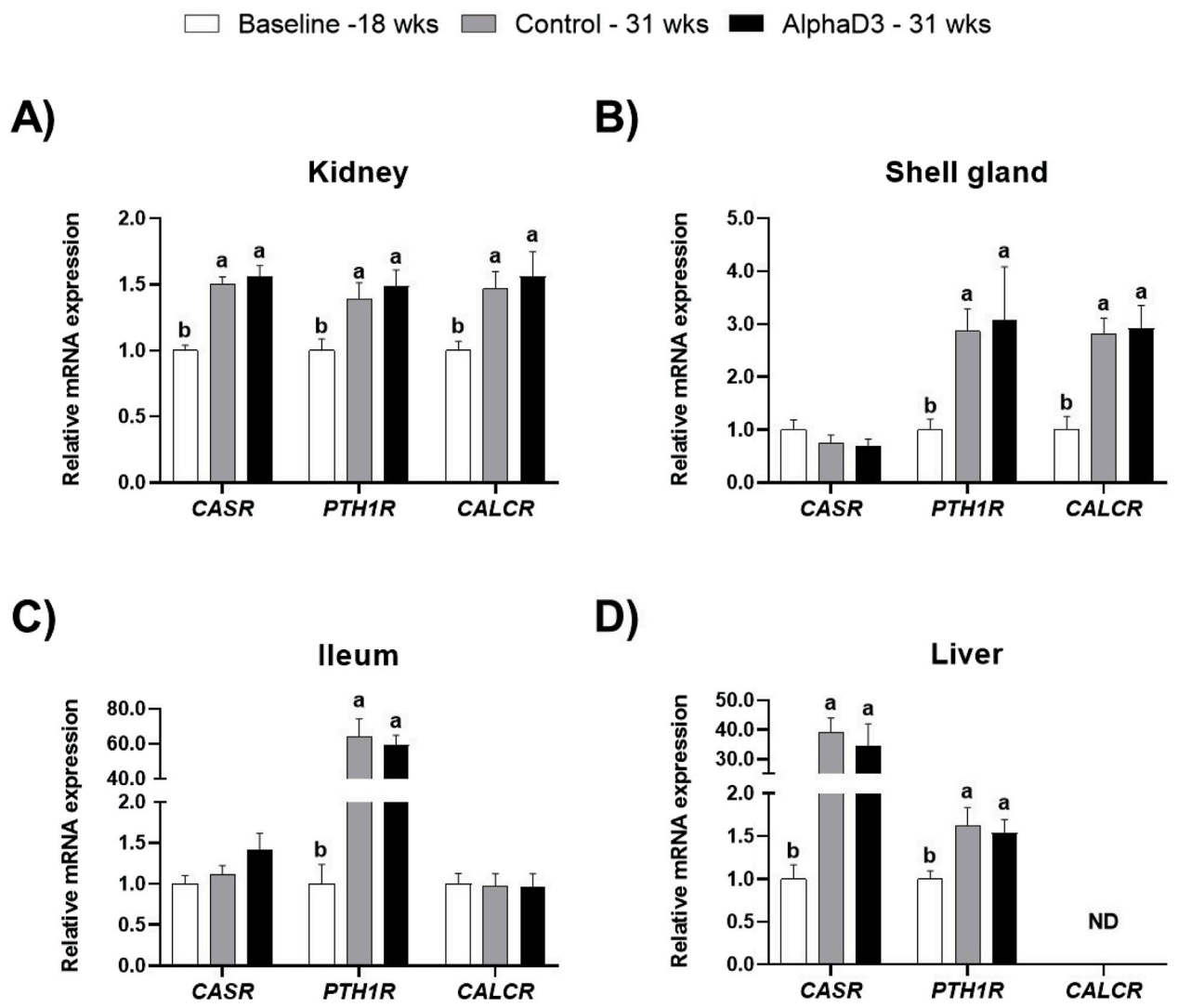

FIGURE 1
Expression profiles of receptors mediating hormonal regulation of calcium homeostasis. Levels of mRNA for *CASR*, *PTH1R*, and *CALCR* were determined in **(A)** kidney, **(B)** shell gland, **(C)** ileum, and **(D)** liver at 18 weeks (Baseline) in hens fed a single developer diet and 31 weeks in hens fed either a control or AlphaD3 (1α-hydroxycholecalciferol)- supplemented diet. Relative expression of mRNA was normalized to *GAPDH* mRNA in kidney and ileum, *18S* rRNA in shell gland, and *CYCLO* mRNA in liver. Values (mean +SEM) are expressed relative to the 18 weeks baseline group (equivalent to 1). Within each gene, different letters indicate values are significantly different between groups ($p \leq 0.05$; n = 8 hens/group). ND, not detected.

FGF23 receptors after the onset of lay in the shell gland suggests this tissue may be a novel target for FGF23 signaling.

3.2 Vitamin D_3 metabolism and action

3.2.1 Vitamin D_3 hydroxylation

To determine how the onset of lay may influence the synthesis of vitamin D_3 metabolites, expression of enzymes responsible for the conversion of cholecalciferol into its active or inactive forms was analyzed in kidney, shell gland, ileum, and liver. Expression of two 25-hydroxylase enzymes encoded by *CYP2R1* or *CYP27A1* were upregulated in kidney at 31 weeks compared to 18 weeks ($p \leq 0.05$), with no significant differences between diets at 31 weeks ($p > 0.05$; Figure 3A). The opposite age effect was observed for *CYP2R1* levels in the shell gland, where expression was downregulated after the onset of lay ($p \leq 0.05$), although no differences between diets were observed at 31 weeks ($p > 0.05$; Figure 3B). There were no significant changes observed for *CYP27A1* in shell gland ($p > 0.05$; Figure 3B). Although ileal expression of *CYP2R1* decreased after the onset of lay in both groups, AlphaD3-supplemented hens exhibited higher expression levels when compared to control hens at 31 weeks ($p \leq 0.05$; Figure 3C). Unlike the other tissues, hepatic *CYP2R1* was not significantly influenced by age or diet ($p > 0.05$), while levels of *CYP27A1* in liver were downregulated after the onset of lay ($p \leq 0.05$), with no differences between diets observed at 31 weeks ($p > 0.05$; Figure 3D). Inactivation of vitamin D_3 is mediated by the 24-hydroxylase enzyme encoded by *CYP24A1*, and no significant effects of age or diet were observed for any of the tissues where it was detected ($p > 0.05$; Figures 3A–D). Expression of *CYP27A1* and *CYP24A1* was not detected in ileum and liver, respectively. These results suggest that changes in expression of 25-hydroxylase genes

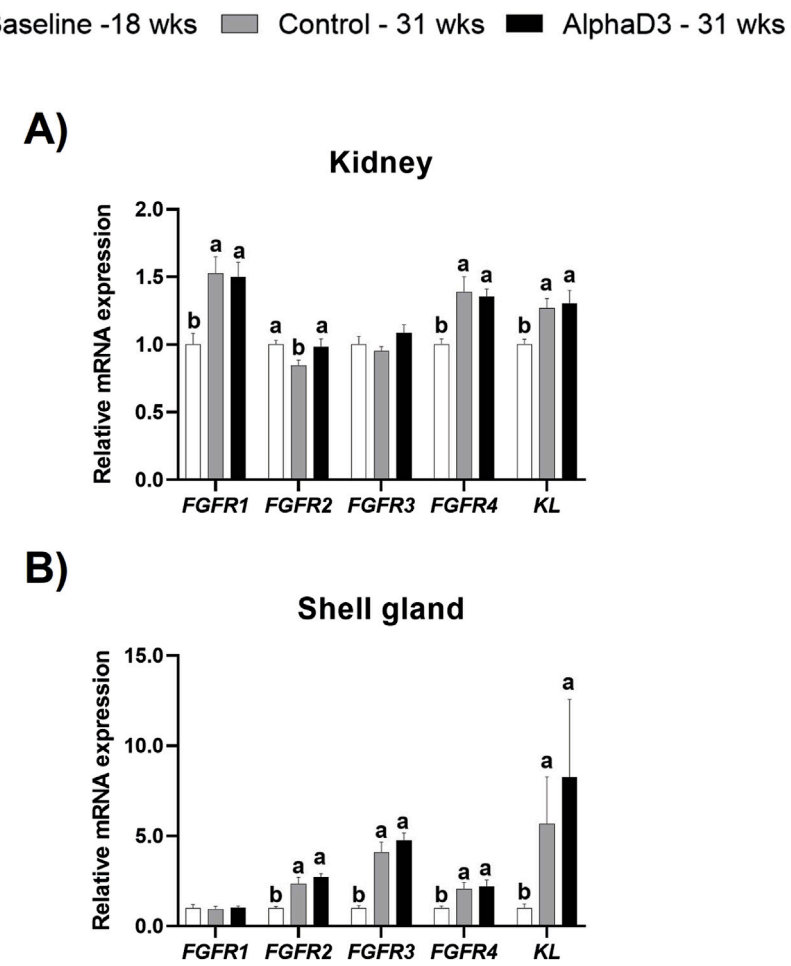

FIGURE 2
Expression profile of receptors mediating hormonal regulation of phosphorus homeostasis. Levels of mRNA for *FGFR1, FGFR2, FGFR3, FGFR4*, and *KL* were determined in **(A)** kidney and **(B)** shell gland at 18 weeks (Baseline) in hens fed a single developer diet and 31 weeks in hens fed either a control or AlphaD3 (1α-hydroxycholecalciferol)- supplemented diet. Relative expression of mRNA was normalized to *GAPDH* mRNA in kidney and *18S* rRNA in shell gland. Values (mean +SEM) are expressed relative to the baseline group (equivalent to 1). Within each gene, different letters indicate values are significantly different between groups ($p \leq 0.05$; n = 8 hens/group).

occur in several tissues after the onset of lay and indicate that, in addition to liver, kidney, shell gland, and ileum might also play a role in the 25-hydroxylation of dietary vitamin D_3.

3.2.2 Circulating vitamin D_3 metabolites

In addition to measuring mRNA expression, circulating levels of each vitamin D_3 metabolite were measured in plasma. Circulating $25(OH)D_3$ significantly decreased in both groups at 31 weeks when compared to 18 weeks ($p \leq 0.05$), with AlphaD3-supplemented hens exhibiting significantly lower plasma levels when compared to control hens ($p \leq 0.05$; Figure 4A). In contrast, plasma levels of $1,25(OH)_2D_3$ were higher at 31 weeks ($p \leq 0.05$), though no difference between diets was found ($p \leq 0.05$; Figure 4B). Circulating levels of $24,25(OH)_2D_3$ declined at 31 weeks ($p \leq 0.05$), again with no differences observed between diets at 31 weeks ($p \leq 0.05$; Figure 4C). Respective changes in these vitamin D_3 metabolites after the onset of lay indicate that higher levels of active $1,25(OH)_2D_3$ and lower levels of inactive $24,25(OH)_2D_3$ are likely important for the increased capacity to utilize calcium and phosphorus for egg production.

3.2.3 Vitamin D_3 signaling

In circulation, all three vitamin D_3 metabolites are bound by vitamin D binding protein (**DBP**), and genomic signaling initiated by $1,25(OH)_2D_3$ that regulates calcium and phosphorus homeostasis is mediated by vitamin D receptor (***VDR***) and its heterodimeric transcriptional partners, retinoid-X-receptor alpha (***RXRA***) or gamma (***RXRG***). Hence, mRNA levels of *DBP*, *VDR, RXR,* and *RXRG* were measured in kidney, shell gland, ileum, and liver to evaluate how vitamin D_3 transport and signaling change after the onset of lay. At 31 weeks, significant differences between diets were not detected for these genes in any tissue ($p > 0.05$); however, differences before and after the onset of lay were apparent (Figure 5). Although renal levels of *VDR* were not significantly affected by age ($p > 0.05$), expression of *DBP, RXRA*, and *RXRG* was found to be upregulated at 31 weeks ($p \leq 0.05$; Figure 5A). Unlike other

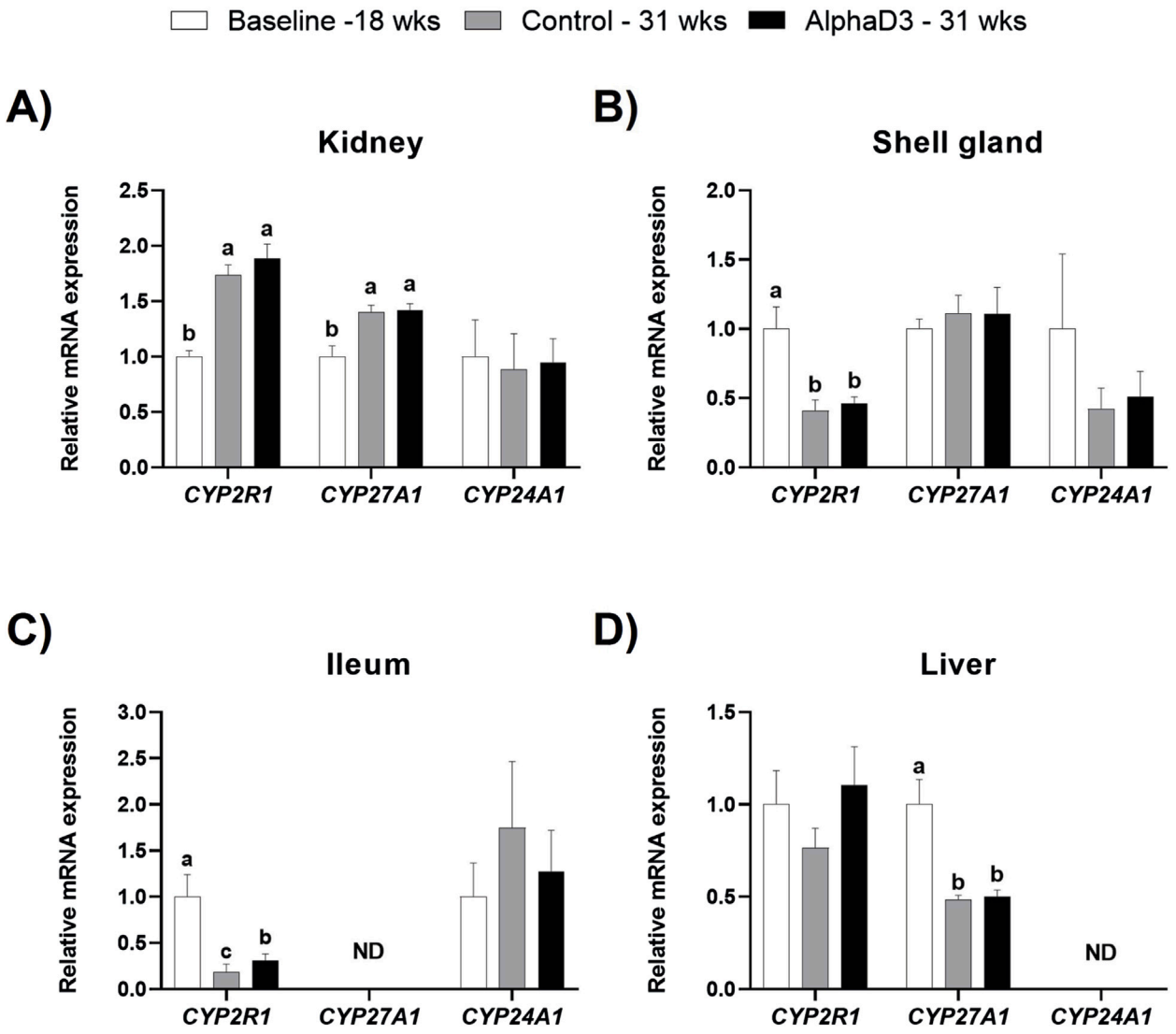

FIGURE 3
Expression profiles of enzymes regulating vitamin D_3 metabolism. Levels of mRNA for *CYP2R1, CYP27A1,* and *CYP24A1* were determined in **(A)** kidney, **(B)** shell gland, **(C)** ileum, and **(D)** liver at 18 weeks (Baseline) in hens fed a single developer diet and 31 weeks in hens fed either a control or AlphaD3 (1α-hydroxycholecalciferol)- supplemented diet. Relative expression of mRNA was normalized to *GAPDH* mRNA in kidney and ileum, *18S* rRNA in shell gland, and *CYCLO* mRNA in liver. Values (mean +SEM) are expressed relative to the baseline group (equivalent to 1). Within each gene, different letters indicate values are significantly different between groups ($p \leq 0.05$; n = 8 hens/group). ND, not detected.

tissues, *DBP* expression was not detected in the shell gland, and while levels of *VDR* were found to increase after the onset of lay ($p \leq 0.05$), no influence of age was observed for either *RXRA* or *RXRG* ($p > 0.05$; Figure 5B). In ileum, no significant differences were found for any of the genes ($p > 0.05$; Figure 5C). Furthermore, although no changes were observed for hepatic *DBP* and *RXRG* ($p > 0.05$), both *VDR* and *RXRA* were found to be downregulated in liver after the onset of lay ($p \leq 0.05$; Figure 5D). Taken together, it appears that kidney and shell gland become more responsive to $1,25(OH)_2D_3$ signaling after the onset of lay, while ileum seems to have a similar sensitivity before and after egg production begins. Furthermore, although DBP is mainly synthesized in the liver, upregulation of renal *DBP* after the onset of lay could facilitate an increase in local concentration of vitamin D_3 metabolites and $1,25(OH)_2D_3$ signaling.

3.3 Mineral uptake and utilization

3.3.1 Calcium and bicarbonate transport

In order to determine what genes might be involved in mediating calcium uptake and utilization associated with the onset of lay, plasma membrane calcium transporters sodium-calcium exchanger 1 (***NCX1***), ATPase plasma membrane calcium transporting 1 (***PMCA1***), and transient receptor potential cation channel subfamily V member 6 (***TRPV6***), as well as the intracellular calcium chaperone calbindin (***CALB1***), were measured in kidney, shell gland, ileum, and liver. Several transport proteins were found to be upregulated after the onset of lay; however, no differences were detected between diets at 31 weeks ($p > 0.05$; Figure 6). Although renal *NCX1* was not impacted by age ($p > 0.05$), expression of *PMCA1*, *TRPV6*, and *CALB1* increased at 31 weeks ($p \leq 0.05$;

10.3389/fphys.2024.1465817

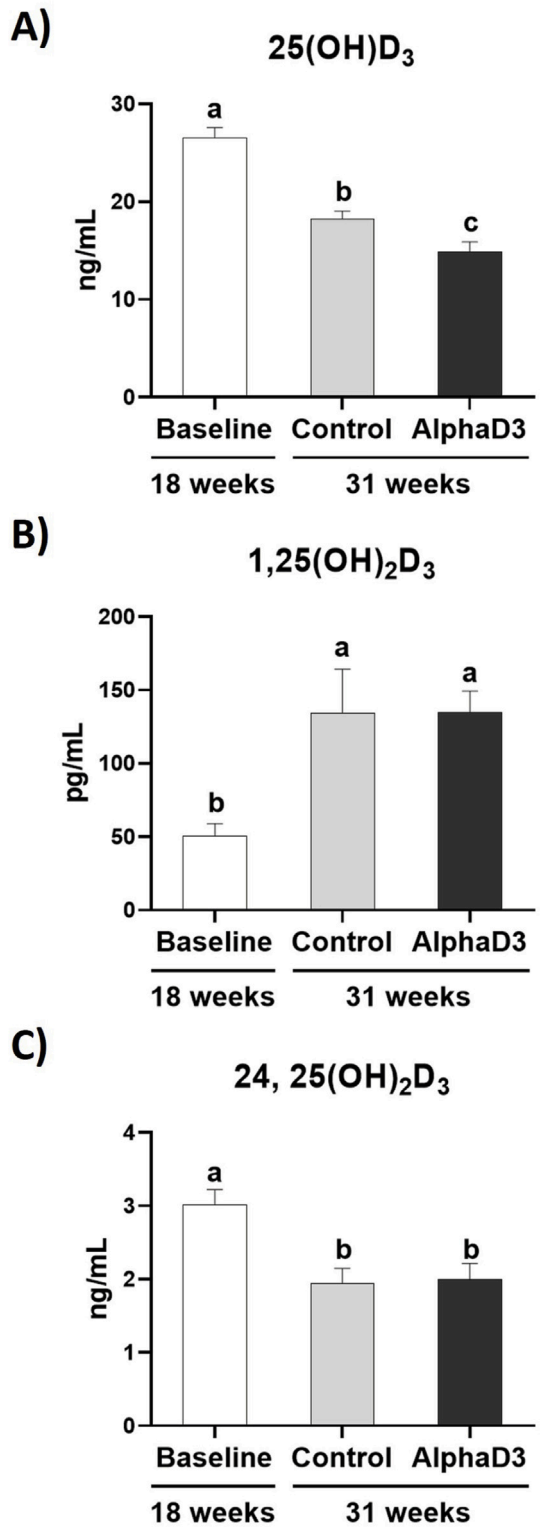

FIGURE 4
Circulating vitamin D3 metabolites. Levels of the circulating vitamin D3 metabolites **(A)** $25(OH)D_3$ (ng/mL), **(B)** $1,25(OH)_2D_3$, and **(C)** $24,25(OH)_2D_3$ were measured at 18 weeks (Baseline) in hens fed a single developer diet and 31 weeks in hens fed either a control or AlphaD3 (1α-hydroxycholecalciferol)- supplemented diet. Means (+SEM) with different letters are significantly different between groups ($p \leq 0.05$; n = 8 hens/group).

Figure 6A). In shell gland, *CALB1* was found to have the highest upregulation after the onset lay with a 40-fold increase ($p \leq 0.05$). Interestingly, *NCX1* was found to decrease after the onset of lay ($p \leq 0.05$), and *PMCA1* expression was not influenced by age ($p > 0.05$; Figure 6B). Similar to shell gland, ileal expression of *NCX1* was downregulated at 31 weeks; however, *PMCA1* and *CALB1* levels were found to increase, with *CALB1* exhibiting a 10-fold increase ($p \leq 0.05$; Figure 6C). No significant changes were observed in liver for *NCX1* or *PMCA1* ($p > 0.05$; Figure 6D). Expression of *TRPV6* was not detected in shell gland or ileum, and neither *TRPV6* or *CALB1* were detected in liver.

The structure of the eggshell is predominantly composed of calcium carbonate crystals, which requires the action of carbonic anhydrase (**CA2**), as well as the presence of bicarbonate ions, which are mobilized to the shell gland lumen by the solute carrier family 26 member 9 (***SLC26A9***). Hence, to evaluate the changes associated with eggshell formation in the shell gland after the onset of lay, mRNA expression levels of *CA2* and *SLC26A9* were evaluated. No differences were observed between diets at 31 weeks for either of the genes evaluated ($p > 0.05$); however, *CA2* exhibited an increase after the onset of lay, while *SLC26A9* was found to be downregulated at 31 weeks ($p \leq 0.05$; Figure 6B). These results indicate an acquired capacity to transfer calcium in kidney, shell gland, and intestine, as well as the ability to synthesize bicarbonate necessary for eggshell formation after the onset of lay.

3.3.2 Phosphorus transport

To evaluate changes in phosphorus uptake and utilization after the onset of lay, plasma membrane phosphorus transporters inorganic phosphorus transporter 1 (***P_iT-1***) and 2 (***P_iT-2***) and sodium-dependent phosphate transporter IIa (***NaP_iIIa***) and IIb (***NaP_iIIb***) were measured in kidney, shell gland, ileum, and liver. No differences were observed between diets at 31 weeks. Renal levels of *P_iT-1*, *P_iT-2*, and *NaP_iIIa* were upregulated in kidney at 31 weeks, with *P_iT-1* showing the largest increase with a 10-fold change ($p \leq 0.05$; Figure 7A). The phosphorus transporter *NaP_iIIb*, which was only detected in kidney, did not exhibit any changes ($p > 0.05$; Figure 7A). In the shell gland, expression of *P_iT-1*, *P_iT-2*, and *NaP_iIIb* was higher at 31 weeks, with *P_iT-1* and *NaP_iIIb* exhibiting increases of 12- and 40-fold, respectively ($p \leq 0.05$; Figure 7B). Ileal *NaP_iIIb* was the only phosphorus transporter with a significant increase of approximately 7-fold at 31 weeks ($p \leq 0.05$; Figure 7C). Liver did not exhibit any significant changes in these transporters after the onset of lay ($p > 0.05$; Figure 7D). Upregulation of select phosphorus transporters after the onset of lay likely indicates greater capacity of several tissues to transfer and utilize phosphorus. Specifically, *P_iT-1* appears to contribute largely to the renal excretion of phosphorus necessary after bone resorption to facilitate eggshell formation. In the shell gland, both *P_iT-1* and *NaP_iIIb* likely play a major role in phosphorus utilization during late eggshell formation, while *NaP_iIIb* seems to assist intestinal uptake in the ileum.

3.4 Changes in skeletal parameters after the onset of lay

To evaluate changes in bone mineralization and integrity in relation to medullary bone formation and the onset of lay, BMD and

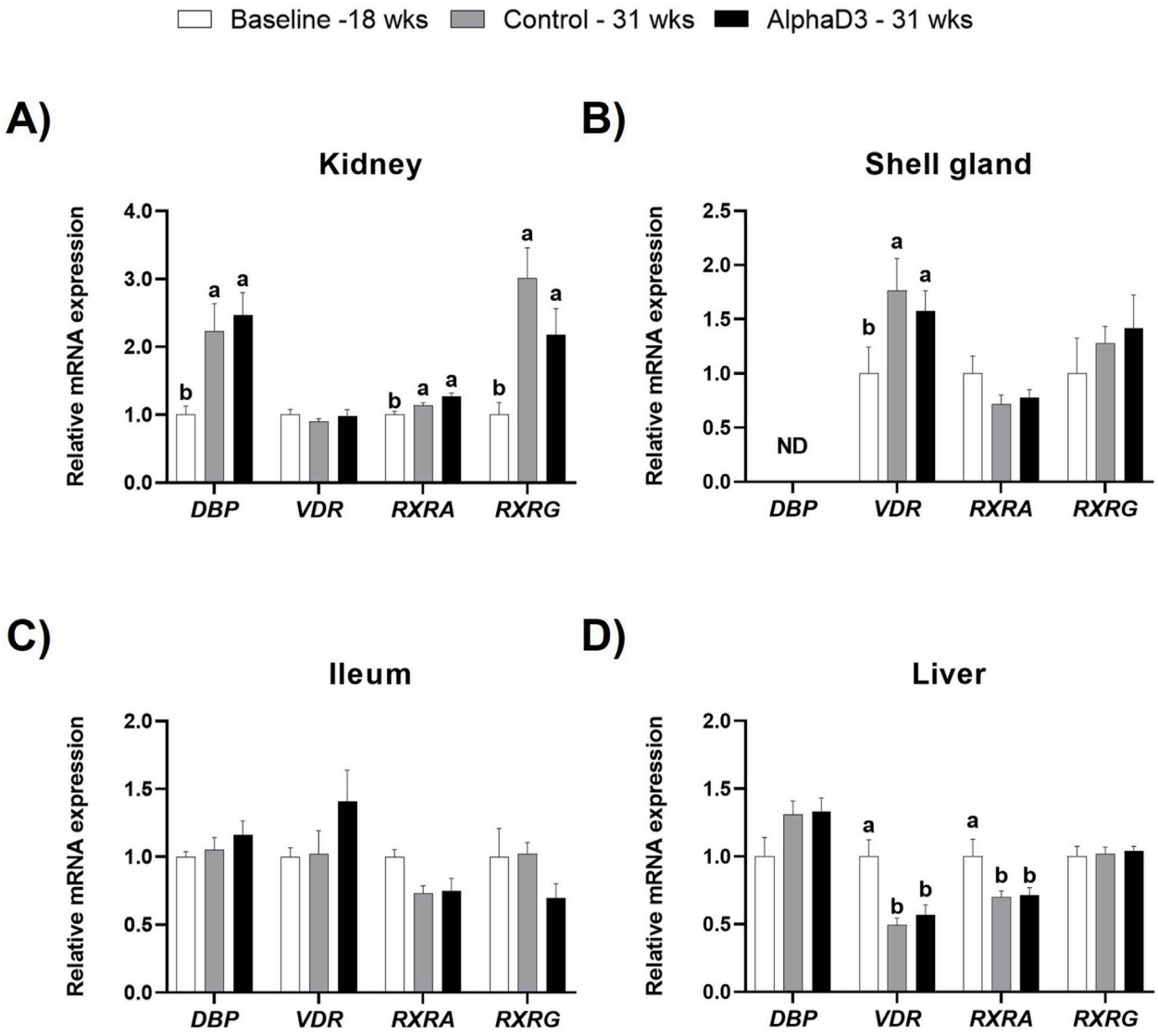

FIGURE 5
Expression profiles of vitamin D_3 genomic actions. Levels of mRNA for *DBP, VDR, RXRA,* and *RXRG* were determined in **(A)** kidney, **(B)** shell gland, **(C)** ileum, and **(D)** liver at 18 weeks (Baseline) in hens fed a single developer diet and 31 weeks in hens fed either a control or AlphaD3 (1α-hydroxycholecalciferol)- supplemented diet. Relative expression of mRNA was normalized to *GAPDH* mRNA in kidney and ileum, *18S* rRNA in shell gland, and *CYCLO* mRNA in liver. Values (mean +SEM) are expressed relative to the baseline group (equivalent to 1). Within each gene, different letters indicate values are significantly different between groups ($p \leq 0.05$; n = 8 hens/group). ND, not detected.

BMC were measured in humerus, keel bone, and tibia and breaking strength, cortical thickness, and AUC were determined for tibia. Keel bone BMD and BMC were not significantly impacted by age or diet ($p > 0.05$; Figures 8A,B). While humeral BMD was found to be lower in the control-fed hens at 31 weeks when compared to the other two groups, tibial BMD was higher for AlphaD3-supplemented hens when compared to both control-fed hens at 31 weeks and hens at 18 weeks ($p \leq 0.05$; Figure 8A). Similarly, although no changes were observed in humerus BMC ($p > 0.05$), onset of lay increased tibial BMC so that levels in both groups of 31-week-old hens were significantly higher than those at 18 weeks ($p \leq 0.05$), with hens fed the AlphaD3-supplemented diet having higher tibial BMC than control-fed hens ($p \leq 0.05$; Figure 8B). Furthermore, tibial breaking strength was found to decrease after the onset of lay for the control group, while AlphaD3-supplemented hens were able to maintain breaking strength at intermediate levels ($p \leq 0.05$; Figure 8C). No differences were found for tibial cortical thickness and AUC ($p > 0.05$; Figures 8D,E). Taken together, these results indicate that supplementation with AlphaD3 may improve bone mineral deposition during the critical period of medullary bone formation and help maintain bone strength after the onset of lay.

In order to determine changes in keel bone parameters associated with the onset of lay, variables indicatives of keel bone deformation and damage were scored. Prevalence and severity of keel bone deviation and fracture prevalence were measured. There were no statistically significant differences observed for any of the parameters evaluated ($p > 0.05$; Table 4). Interestingly, even hens prior to the onset of lay exhibited a deviation prevalence of 62.5%,

10.3389/fphys.2024.1465817

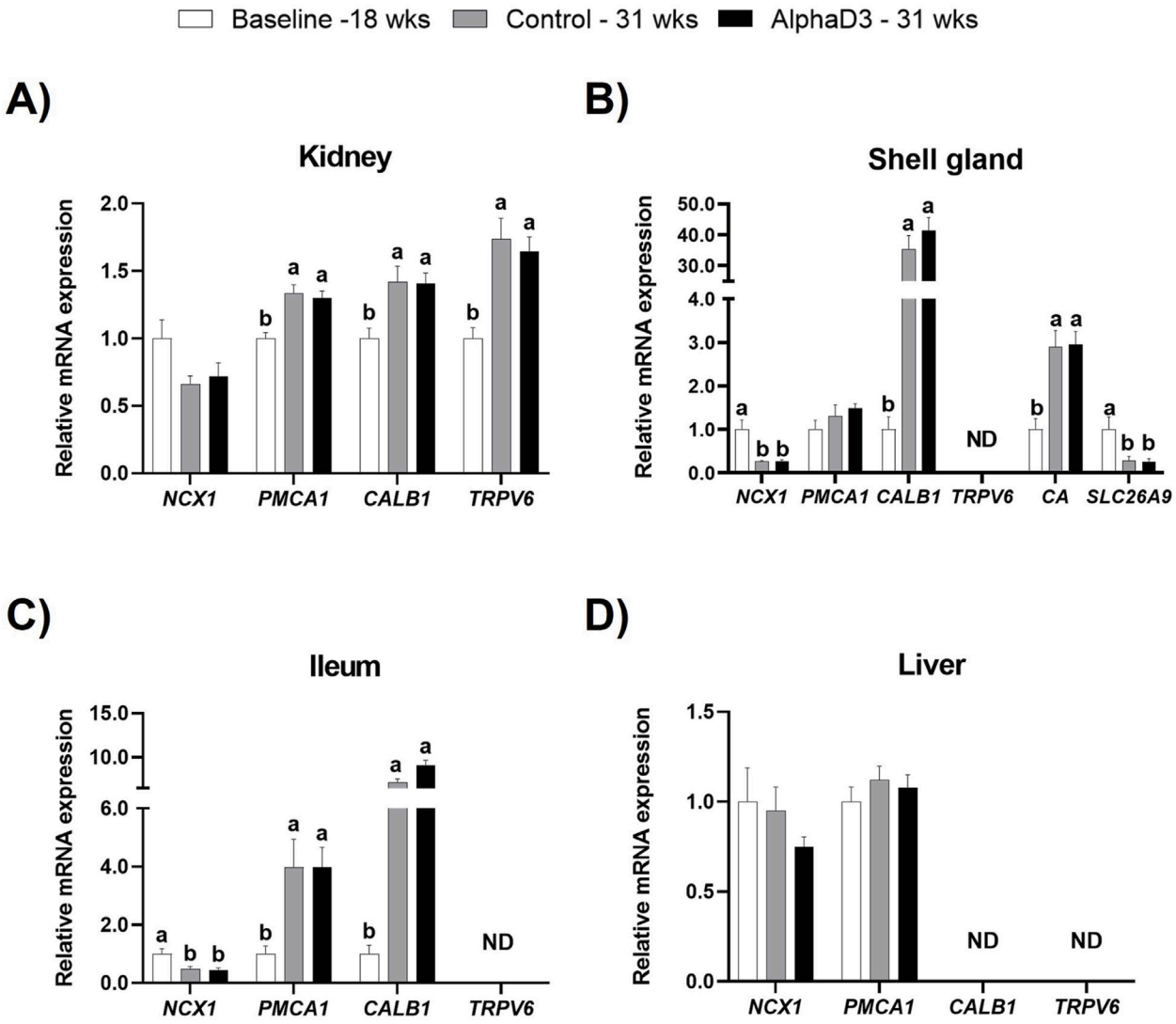

FIGURE 6
Expression profiles of calcium and bicarbonate uptake and utilization. Expression levels of mRNA for *NCX1, PMCA1, CALB1,* and *TRPV6* were determined in **(A)** kidney, **(B)** shell gland, **(C)** ileum, **(D)** liver, and *SLC26A9* and *CA2* in **(B)** shell gland at 18 weeks (Baseline) in hens fed a single developer diet and 31 weeks in hens fed either a control or AlphaD3 (1α-hydroxycholecalciferol)- supplemented diet. Relative expression of mRNA was normalized to *GAPDH* mRNA in kidney and ileum, *18S* rRNA in shell gland, and *CYCLO* mRNA in liver. Values (mean +SEM; n = 8 hens/group) are expressed relative to the baseline group (equivalent to 1). Within each gene, different letters indicate values are significantly different between groups ($p \leq 0.05$; n = 8 hens/group). ND, not detected.

and this increased at 31 weeks to 75% and 87.5% in control and AlphaD3-supplemented hens, respectively.

4 Discussion

At the onset of egg production, laying hens undergo many physiological changes necessary to facilitate uptake, storage, and utilization of large amounts of calcium for eggshell calcification. These start to occur around 2 weeks prior to the onset of lay and involve specialized tissues such as intestine, kidney, and shell gland that play major roles in calcium and phosphorus absorption, retention, and utilization (Bar, 2008). This study identified potential physiological mechanisms related to hormonal signaling and mineral transport in these tissues by measuring gene expression, as well as evaluated bone parameters prior to and after the onset of lay. The effect of dietary supplementation with AlphaD3 on these changes was also evaluated. Changes in gene expression were evaluated by measuring mRNA levels without further examination into whether protein levels of the same transcripts changed in a similar manner. Since variations in mRNA expression do not necessarily reflect functional modifications at the cellular level, caution should be exercised when interpreting the results. However, these data are useful at identifying systems and networks potentially involved in mediating changes that allow for enhanced handling of minerals necessary to support daily egg production. Transcriptional findings suggest PTH could be a major hormonal driver regulating calcium homeostasis across all tissues following the onset of lay, and this is particularly apparent in ileum and shell gland. Similarly, hormonal sensitivity to FGF23 appears to be

10.3389/fphys.2024.1465817

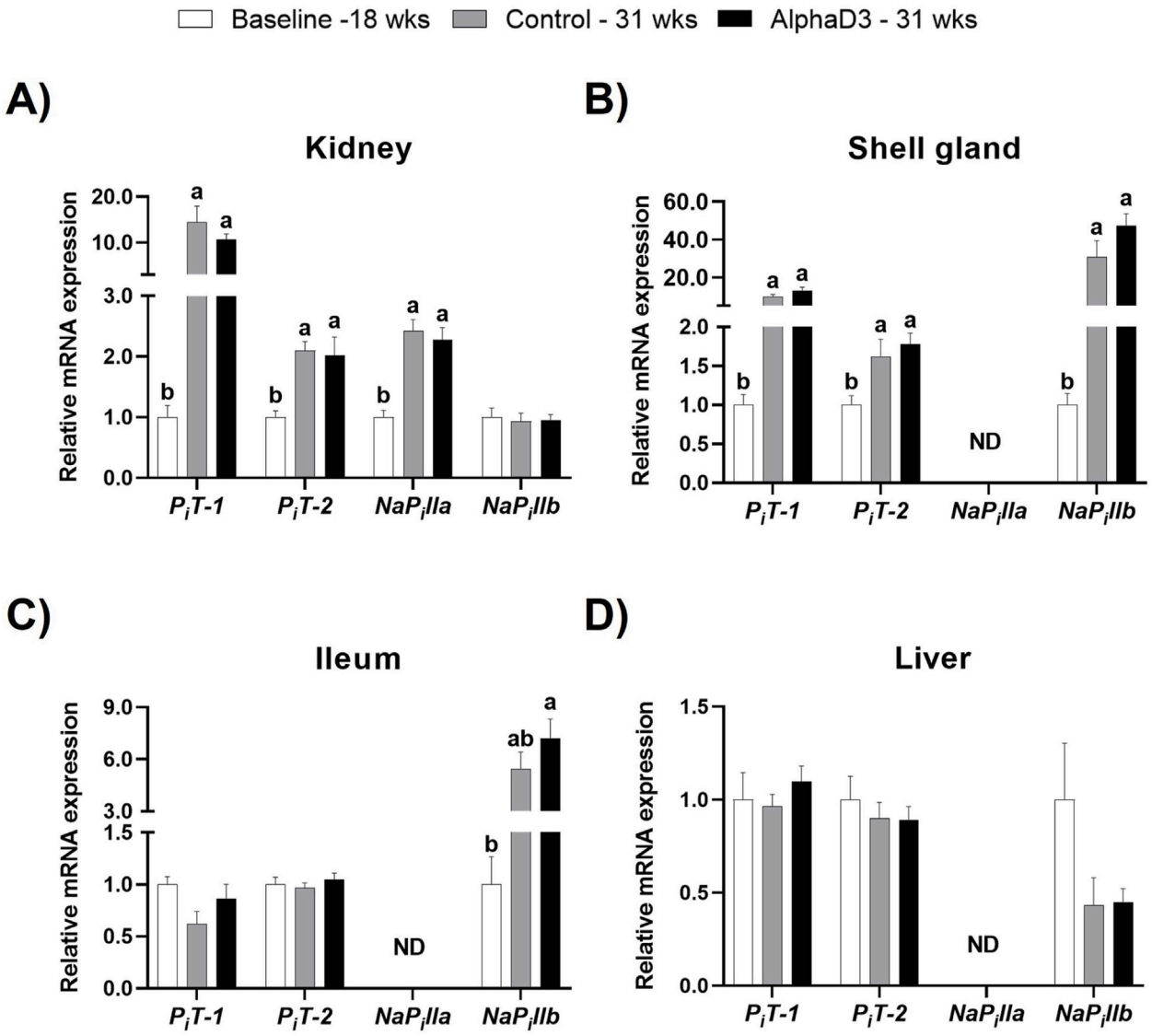

FIGURE 7
Expression profiles of phosphorus uptake and utilization. Expression levels of mRNA for *P_iT-1, P_iT-2, NaP$_i$IIa,* and *NaP$_i$IIb* were determined in **(A)** kidney, **(B)** shell gland, **(C)** ileum, and **(D)** liver at 18 weeks (Baseline) in hens fed a single developer diet and 31 weeks in hens fed either a control or AlphaD3 (1α-hydroxycholecalciferol)- supplemented diet. Relative expression of mRNA was normalized to *GAPDH* mRNA in kidney and ileum, *18S* rRNA in shell gland, and *CYCLO* mRNA in liver. Values (mean +SEM) are expressed relative to the baseline group (equivalent to 1). Within each gene, different letters indicate values are significantly different between groups ($p \leq 0.05$; n = 8 hens/group). ND, not detected.

upregulated after the onset of lay in kidney and shell gland, with the latter being identified as a novel target of this hormone. In addition to its role in mineral retention and excretion, kidney could be involved in the 25-hydroxylation of vitamin D_3 and DBP synthesis. Calbindin was demonstrated to have a primary role in assisting with calcium flux in all tissues, especially the shell gland, while calcium transporter *NCX1* does not seem to be influenced by these adaptative changes in any of the tissues examined. Phosphorus excretion and absorption appears to occur primarily through *P_iT-1* in kidney and *NaP$_i$IIb* in the ileum, respectively. Similarly, phosphorus utilization for hydroxyapatite and cuticle deposition within the eggshell seems to be mediated by *P_iT-1* and *NaP$_i$IIb* in the shell gland. The above findings related to hormonal signaling and mineral transport are depicted in Figure 9. It should be noted that hens were only sampled prior to lay at 18 weeks and during peak production at 31 weeks. Including ages between these would allow for a more comprehensive examination of the transition that occurs immediately around the onset of lay. Most mRNA expression profiles appeared unaffected by dietary supplementation with AlphaD3, a finding that could be result of the high efficiency with which hens at peak production are able handle the daily mineral turnover necessary for eggshell mineralization. Including intermediate ages during early lay may have revealed ways in which tissues other than bone were influenced by AlphaD3 in the diet. Despite few observable impacts on mRNA levels in the tissues examined, several bone mineralization parameters were improved by feeding hens AlphaD3 during the critical period of medullary bone formation between 18 and 31 weeks of age.

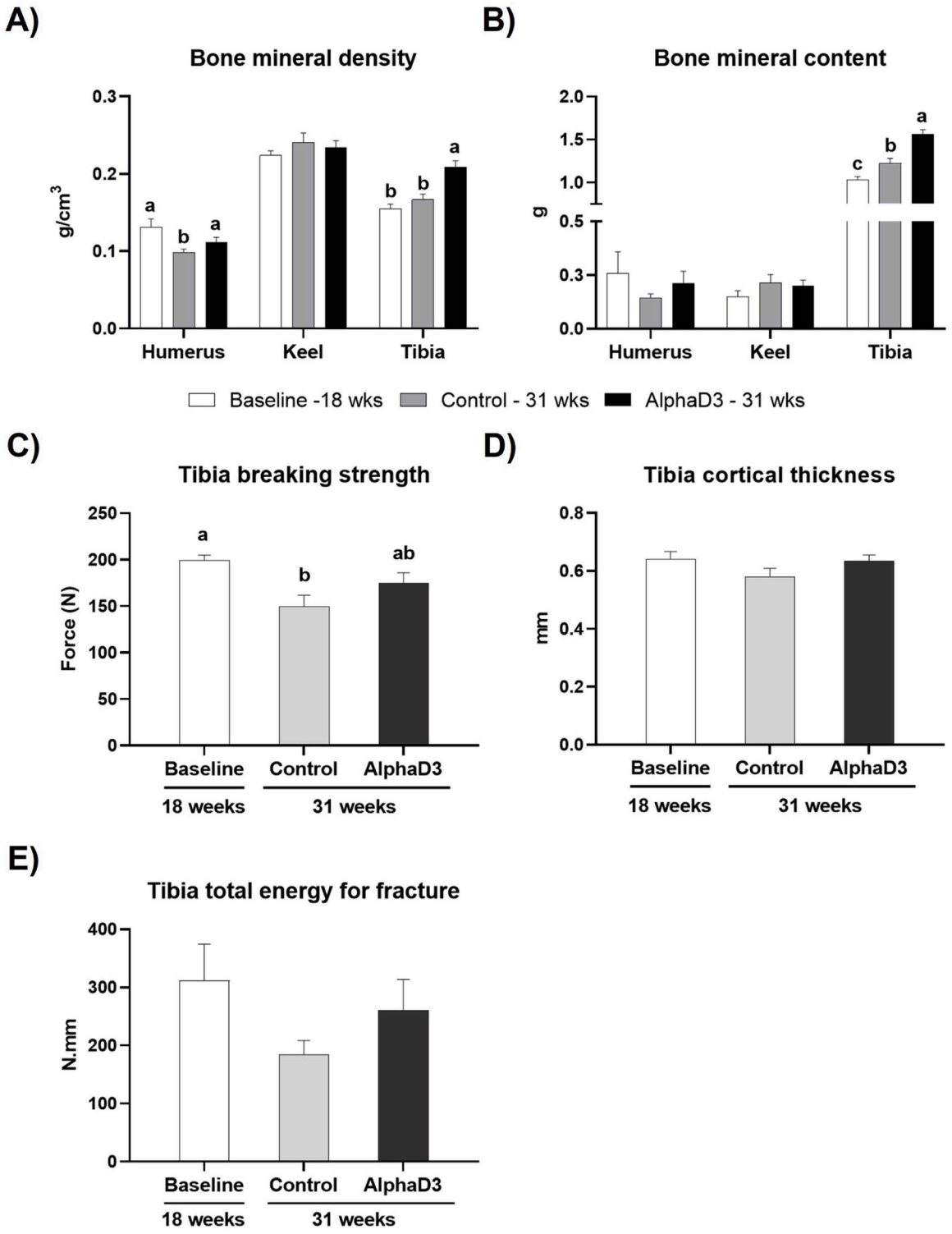

FIGURE 8
Changes in skeletal parameters after the onset of lay. **(A)** Bone mineral density (g/cm^3) and **(B)** bone mineral content (g) was determined for humerus, keel bone, and tibia, and **(C)** breaking strength (N), **(D)** cortical thickness (mm), and **(E)** Tibia total energy for fracture (N.mm) were determined in tibia. Each parameter was measured at 18 weeks (Baseline) in hens fed a single developer diet and 31 weeks in hens fed either a control or AlphaD3 (1α-hydroxycholecalciferol)- supplemented diet. Within each bone **(A, B)** or graph **(C, D, E)**, values (mean +SEM) with different letters are significantly different between groups ($p \leq 0.05$; n = 8 hens/group).

TABLE 4 Keel bone deviation and fracture score distributions across experimental groups.

	Baseline		Control		AlphaD3		
	18 weeks		31 weeks		31 weeks		
	n	%	n	%	n	%	*p*-value
Deviation prevalence	5/8	62.5 ± 6.05	6/8	75.0 ± 5.41	7/8	87.5 ± 4.13	0.5279
Deviation severity							0.4079
0 (Straight)	3/8	37.5 ± 6.05	2/8	25.0 ± 5.41	1/8	12.5 ± 4.13	
1 (Mild)	5/8	62.5 + 6.05	5/8	62.5 ± 6.05	6/8	75.0 ± 5.41	
2 (Severe)	0/8	0.0 ± 0.0	1/8	12.5 ± 4.13	1/8	12.5 ± 4.13	
Fracture prevalence	0/8	0.0 ± 0.0	1/8	12.5 ± 4.13	0/8	0.0 ± 0.0	0.3679

Hormonal regulation of calcium homeostasis is primarily mediated by the synchronized activity of CASR, PTH, and CALC, though specific involvement of each of these during the onset of lay is not fully understood. Observations from this study found expression of *CASR* to change between 18- and 31-week in kidney and liver, with liver exhibiting a pronounced 60-fold increase. Although renal involvement in calcium homeostasis has been widely described (Sommerville and Fox, 1987; Wideman, 1987), liver is not canonically associated in this process beyond 25-hydroxylation of vitamin D_3 (Shang et al., 2023). CASR is not specific to calcium and has been demonstrated to contain binding sites for other divalent ions including magnesium (Quinn et al., 2013), zinc, and iron (Chanpaisaeng et al., 2021), as well as phosphate (Centeno et al., 2019) and aromatic amino acids (Conigrave et al., 2000). Hence, it is possible that hepatic expression of this gene may be related to the vitellogenesis and influenced by estrogen levels (Gloux et al., 2019; Cui et al., 2020). There are very few studies in chickens related to hepatic expression of CASR and, in contrast to this study, Deng et al. (2010) reported that this gene was not detected in liver or other tissues such as heart, spleen, lungs, pancreas, or stomach of laying hens. However, hepatic expression of this gene has been shown in mammals, and studies with mouse hepatocytes demonstrated CASR's capability to sense and mobilize calcium associated with bile secretion (Canaff et al., 2001) and induce intracellular calcium elevation (Xing et al., 2010).

The influence of PTH on regulation of calcium and phosphorus uptake and utilization was demonstrated in this study, where all tissues evaluated had heightened *PTH1R* mRNA expression after the onset of lay, an event that was only observed for this gene. Although function of PTH have been well described in kidney (Wideman, 1987; Elaroussi et al., 1993), the most apparent upregulation in this study was observed in ileum. For decades, the influence of PTH on intestinal calcium and phosphorus absorption has been described as indirect, as it occurs primarily via activation of $1,25(OH)_2D_3$ (Tanaka et al., 1971; Bar et al., 1990). However, other authors have suggested that PTH may directly stimulate calcium absorption in mice (Picotto et al., 1997), fish (Rotllant et al., 2006), and chickens (Nemere and Norman, 1986). Thus, ileal upregulation of *PTH1R* in this study could indicate a direct effect of PTH on the intestine to meet increasing calcium demands after the onset of lay.

In the case of shell gland, fewer studies into the role of PTH signaling have been conducted. In the research presented here, *PTH1R* was found to be upregulated in the shell gland of hens at 31 weeks. Consistent with this, Thiede et al. (1991) measured *PTH1R* mRNA levels in the laying hen oviduct and found greatest expression in the shell gland. A possible role for PTH in oviduct differentiation and development as well as regulation of smooth muscle activity in this tissue was hypothesized in the aforementioned study. Furthermore, receptor binding affinity for PTH in the shell gland of laying hens (Ieda et al., 2000) and guinea fowl (Ogawa et al., 2000) was found to increase during periods of eggshell calcification, while no variations were observed in non-laying birds. This indicates a strong association of PTH with the oviposition cycle that was also evidenced by Sinclair-Black et al. (2024), where upregulation of *PTH1R* in the shell gland was observed between 21 and 24 HPOP. This correlates with findings from the present study, where tissue collection occurred at 21 HPOP and upregulation of *PTH1R* was observed. Together, this suggests that PTH signaling through PTH1R may play an important role in providing shell gland with the capacity to transfer minerals for eggshell formation.

Of the tissues examined, *CALCR* was found to only increase in kidney and shell gland after the onset of egg production, the two tissues found to have the most capacity for mineral transport in this study. Tissue collection from this study occurred when a hard-shelled egg was present in the shell gland; thus, increased *CALCR* expression in kidney and shell gland observed here are likely to ensure sensitivity to the regulatory response by calcitonin at the end of the oviposition cycle, when eggshell formation is almost complete and calcium demands for this process decrease. Yasuoka et al. (1998) demonstrated increased binding affinity of calcitonin to its receptor in the laying hen kidney between 3 h before oviposition and 2 h post-oviposition, consistent with times of lower calcium demands and when tissues were collected in the present study. Similar findings were observed in the shell gland of laying hens by Ieda et al. (2001) and guineafowl by Ogawa et al. (2003), where calcitonin binding affinity increased at later stages of eggshell formation. These results correlate with observations from Sinclair-Black et al. (2024), where mRNA levels of shell gland *CALCR* in laying hens had greater expression between 2 h before oviposition and 1 h post-oviposition. During this time, mineral requirements in the shell gland switch from high amounts of calcium to phosphorus for hydroxyapatite

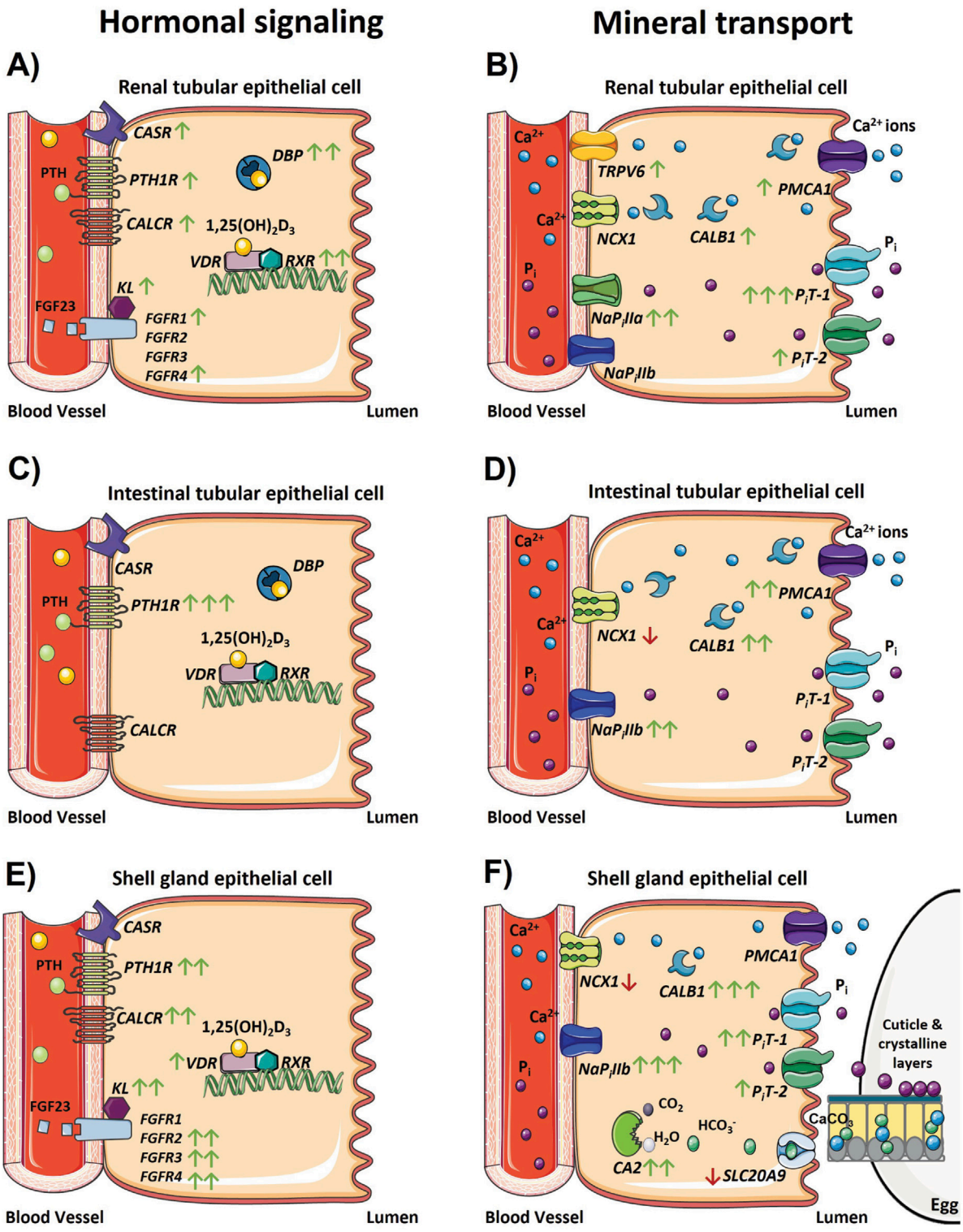

FIGURE 9
Changes in the physiological regulation of calcium and phosphorus homeostasis after the onset of egg production. Models depicting changes in gene expression associated with hormonal signaling regulating calcium and phosphorus homeostasis and transport that occur in the **(A, B)** kidney, **(C, D)** ileum, and **(E, F)** shell gland during the onset of lay. Green and red arrows indicate genes that were significantly increased or decreased in expression between 18 and 31 weeks, respectively, and the number of arrows represents the magnitude of the changes. One arrow indicates a fold change between 1 and 2; two arrows indicate a fold change between 2 and 10; and three arrows indicate a fold change greater than 10. The absence of any arrow indicates no significant changes were detected between 18 and 31 weeks. The absence of a gene depicted in each model indicates its expression was not detected in that tissue, with the exception of *FGFR1 – 4* and *KL* in the ileum because these genes were not analyzed in that tissue. Parts of the figure were created using pictures from Servier Medical Art (https://smart.servier.com/), licensed under a Creative Commons Attribution 4.0 Unported License (https://creativecommons.org/licenses/by/4.0/).

and cuticle deposition within the eggshell, and CALC might play an important role in this process.

Hormonal regulation of phosphorus homeostasis exerted by FGF23 signaling also appears to be upregulated in kidney and shell gland after the onset of lay, specifically observed through increased expression of *FGF* receptors and *KL*, their co-receptor. In mammals (Shimada et al., 2004b; Perwad et al., 2005) and chickens (Ren et al., 2017), FGF23 has been associated with renal excretion of excess circulating phosphorus. In the current study, renal expression of *FGFR1, FGFR4,* and *KL* was upregulated at 31 weeks. When measured throughout the 24-h oviposition cycle in Sinclair-Black et al. (2024), renal expression of *FGFR1* and *KL* had no variation, while *FGFR2*,*FGFR3*, *FGFR4* were influenced by time. In that study, a decrease in *FGFR3* was observed after 21 HPOP, so it is likely that *FGFR3* did not change here due to the time of tissue collection; however, these and other findings support the role of FGF23 signaling in this tissue to promote renal excretion of phosphorus (Kerschnitzki et al., 2014; Gloux et al., 2020a).

Findings presented here suggest that shell gland is a novel target for FGF23 signaling, as indicated by increased expression of *FGFR2 - 4* and *KL* after the onset of egg production. Signaling of FGF23 in this tissue may be associated with phosphorus uptake and utilization at the later stages of eggshell formation, as it was observed in Sinclair-Black et al. (2024) that upregulated expression of these genes occurred between 18 and 24 HPOP. Signaling by FGF23 could regulate expression of specific phosphorus transporters. Its pattern in the shell gland was followed by increased expression of *P_iT-1* (Sinclair-Black et al., 2024), and our findings also indicated upregulation of *P_iT-1, P_iT-2,* and *NaP_iIIb* in the shell gland concurrently with mediators of FGF23 signaling. These changes support that FGF23 could be involved in mediating phosphorus deposition within the hydroxyapatite layer of the eggshell immediately below the cuticle that has been suggested to be required for halting calcification of the shell (Cusack et al., 2003) or formation of the cuticle itself. Taken together, these findings suggest that after the onset of lay, hens acquire greater sensitivity to hormones regulating calcium and phosphorus homeostasis in target tissues involved in mediating increased demands of these minerals for bone remodeling and eggshell formation.

Vitamin D_3 metabolism by 25-hydroxylase, encoded by *CYP2R1* or *CYP27A1*, was found to be either downregulated or not influenced by the onset of lay in all tissues examined except kidney, which exhibited a fold increase of approximately 1.5 or higher after the onset of lay for both genes. It was only recently that *CYP27A1* was confirmed to encode for an alternative 25-hydroxylase (Shang et al., 2023), and *CYP2R1* has been catalogued as highly conserved between avian and mammalian species (Watanabe et al., 2013). Liver has been identified to be the major tissue responsible for conversion of circulating vitamin D_3 into 25(OH)D_3 in mammals (Ponchon et al., 1969). In avian species, early studies demonstrated *in vitro* 25-hyroxylase activity in liver homogenates (Tucker et al., 1973), as well as identified liver as an important tissue in this process through *in vivo* studies (Bhattacharyya and Deluca, 1974). However, it appears that liver is not the exclusive tissue with 25-hydroxylase activity in chickens. Tucker et al. (1973) first demonstrated that renal 25-hydroxylase from white Leghorn hens can play this role *in vitro*, which would give kidney the ability to perform the full two-step transformation of vitamin D_3 into its active form. Similar to results presented here, Sinclair-Black et al. (2024) observed minor changes in hepatic *CYP2R1* mRNA expression over the oviposition cycle, while renal expression of this gene was noted to increase towards periods of peak eggshell calcification. Furthermore, Bhattacharyya and Deluca (1974) evaluated regulation of liver 25-hydroxylase in chickens and discussed the possibility that, although kidney may have the capacity to convert dietary vitamin D_3 into 25(OH)D_3, it may not necessarily contribute to circulating levels of this metabolite. This is likely associated with the fact that when synthesized in the kidney, 25(OH)D_3 can be immediately hydroxylated into 1,25$(OH)_2D_3$ by renal 1α-hydroxylase and utilized for renal calcium reabsorption. Investigation into tissue distribution of *CYP27A1* in both male and female 8-week-old broiler chickens demonstrated an approximate 20-fold difference between liver and kidney, with liver levels being the highest amongst all tissues examined (Shang et al., 2023). This would suggest that liver remains the primary site of CYP27A1 25-hydroxylase activity, while the kidney may exhibit 25-hydroxylase activity by both enzymes for local production of 25(OH)D_3 and, ultimately, 1,25$(OH)_2D_3$. Thus, results presented in the current study provide support for the notion that the conversion of dietary vitamin D_3 into 25(OH)D_3 can take place at the renal level, particularly during periods characterized by elevated calcium demands such as eggshell formation and medullary bone replenishment. Furthermore, it was observed that, although expression of genes encoding 25-hydroxylase in kidney were upregulated, circulating levels of 25(OH)D_3 decreased at 31 weeks. This is presumably a result of greater conversion of this metabolite to 1,25$(OH)_2D_3$ in the kidney, as is evidenced by an increase in circulating 1,25$(OH)_2D_3$ and an accompanying decrease in the inactive 24,25$(OH)_2D_3$ metabolite. Collectively, activation of dietary vitamin D_3 is upregulated by the onset of lay as a responsive mechanism to escalating calcium and phosphorus demands. Additionally, the kidney may undertake a local role in both activating hydroxylation steps that ultimately facilitate calcium reabsorption and phosphorus excretion in this tissue.

Both 25(OH)D_3 and 1,25$(OH)_2D_3$ bind to circulating DBP to be transported to target tissues (White and Cooke, 2000). In mammals, the major synthesis site of this binding protein is the liver (Cooke et al., 1991), although expression of the gene encoding for this protein is present in several other tissues, including kidney, testis, placenta, and adipose, but it has not been detected in either intestine or uterus (McLeod and Cooke, 1989). However, to the authors' best knowledge, no literature has been published elucidating *DBP* mRNA tissue distribution in chickens, though the protein has been detected in chicken serum (Bouillon et al., 1980). Findings from the current study confirm expression of *DBP* in laying hen kidney and liver, and unpublished data revealed levels in liver to be over 600-fold higher than those in other tissues (R.A. Garcia-Mejia, M. Sinclair-Black, and L.E. Ellestad). Similar to lack of detection in mammalian uterus, DBP was not detected in the shell gland in this study; however, it was found to be expressed in the ileum. As with 25-hydroxylase expression, kidney was found to be the only tissue where *DBP* was influenced by sexual maturation, with a 2-fold increase after the onset of lay. Research from Nys et al. (1986a) first demonstrated a marked increase in circulating DBP and 1,25$(OH)_2D_3$ in hens between 8 and 24 weeks as they approached the onset of egg production, specifically starting 2 weeks prior to the first

oviposition. Further research by Nys et al. (1989) evaluated the effect of the onset of lay on plasma DBP levels by inducing sexual maturity in 12 weeks old pullets via administration of estrogen alone or in combination with testosterone, which induced an increase in DBP levels after treatment. In addition, circulating DPB levels were analyzed in mature laying hens and these were found to be even higher than those of induced immature pullets. These findings suggest a close relationship between the onset of lay and both DBP and $1,25(OH)_2D_3$ in circulation. From the present study, the upregulation of renal *DBP* could indicate that the kidney plays a role in production of this protein following the onset of lay, which might allow this tissue to respond to $1,25(OH)_2D_3$ more efficiently.

The expression of genes associated with calcium uptake and utilization exhibited a discernible increase following the onset of egg production, particularly in kidney, shell gland, and ileum that are all actively engaged in mineral transport. These included upregulated expression of *PMCA1* and *CALB1* in kidney, shell gland, and ileum, as well as increased *TRPV6* in the kidney. However, the calcium transporter *NCX1* was found to be downregulated in all tissues examined. Renal *NCX1* was found to be unaffected by time within the oviposition cycle in laying hens (Sinclair-Black et al., 2024) or throughout different production stages (San et al., 2021). In addition, expression of *TRPV6* in this study was only detected in the kidney, which is consistent with findings from other authors where *TRPV6* was not detected in shell gland (Sinclair-Black et al., 2024) or ileum (Proszkowiec-Weglarz and Angel, 2013). There are no reports to date for liver that the authors are aware of, though unpublished data in our lab indicated it is not detected in this tissue (R.A. Garcia-Mejia, M. Sinclair-Black, and L.E. Ellestad). In the intestine, the calcium chaperone *CALB1* has been previously reported to increase 5-fold after sexual maturity in the intestine of laying hens (Nys et al., 1992a) and 12-fold in the intestine after an intramuscular dose of $1,25(OH)_2D_3$ (Theofan et al., 1986). The increase observed in the present study is consistent with those findings.

In the shell gland, Jonchère et al. (2012) measured ion transporter expression during the presence or absence of a calcifying egg and observed downregulation of *NCX1* and upregulation of *PMCA1* and *CALB1* during eggshell calcification, which correlates with findings from the current study. Ieda et al. (1995) reported an increase in both *VDR* and *CALB1* in the shell gland with the presence of a calcifying egg, and increased mRNA expression of *CALB1* after the onset of lay has been demonstrated in prior studies (Nys et al., 1989; Bar et al., 1990), as observed here. Furthermore, findings presented in the current study exhibited upregulation of *VDR* in shell gland following the onset of egg production, which is supported by previous research (Ieda et al., 1995; Yoshimura et al., 1997). Similarly, findings from Sinclair-Black et al. (2024) described expression of shell gland *VDR* to increase towards times of peak eggshell calcification and decline around oviposition and ovulation. However, whether shell gland *CALB1* expression is vitamin D_3-dependent is not clear (Corradino, 1993; Yoshimura et al., 1997; Ohira et al., 1998), and it appears its expression could be driven by estrogen (Navickis et al., 1979; Corradino et al., 1993) or calcium flux (Bar et al., 1992; Nys et al., 1992b; Bar et al., 1996). Required for $CaCO_3$ synthesis, expression of *CA* in the shell gland was upregulated after the onset of egg production; however, the bicarbonate transporter *SLC26A9* was found to be downregulated. This is contradictory to findings from other authors that suggest eggshell formation induces upregulation of this gene (Jonchère et al., 2012). However, the difference between results presented here and findings from the aforementioned study are likely related to the fact that tissues were collected in this study at 21 HPOP, when calcification is complete. This is supported by observations in Sinclair-Black et al. (2024), where expression of *SLC26A9* increased between ovulation and late calcification but was downregulated between 21 and 24 HPOP.

Phosphorus metabolism in laying hens is also heavily influenced by egg production, as the mechanisms required for eggshell formation involve medullary bone breakdown. The kidney has been demonstrated to play major role in regulation of calcium and phosphorus homeostasis (Wideman, 1987), and excretion of phosphorus has been shown to increase during periods of peak eggshell calcification associated with medullary bone remodeling for eggshell formation (Nys et al., 1986b; Kerschnitzki et al., 2014). In the kidney, *P_iT-I* appears to be the primary transporter mediating phosphorus flux during egg production, as demonstrated by a 15-fold increase in expression between 18 and 31 weeks. This finding correlates with increased renal *P_iT-1* and *P_iT-2* expression during times of peak (Sinclair-Black et al., 2024) or late (Gloux et al., 2020b) eggshell formation, probably to support renal phosphorus excretion. A similar increase was observed for shell gland *P_iT-I* levels; however, this tissue seemed to have an even greater increase in *NaP_illb* expression, with a near 40-fold increase in at 31 weeks compared to 18 weeks. Phosphorus transport in the shell gland could increase in order to synthesize the eggshell cuticle (Sinclair-Black et al., 2024), composed of a large concentration of phosphorus (Cusack et al., 2003), as well as a thin layer of hydroxyapatite crystals beneath the cuticle, known as vertical crystal layer (Dennis et al., 1996; Kulshreshtha et al., 2022). Furthermore, as indicated previously, upregulation of phosphorus transporters in the shell gland could be mediated by FGF23 signaling. In general, hens at 31 weeks exhibited greater capacity for mineral transport, utilization, and uptake in kidney, ileum, and shell gland as calcium and phosphorus demands escalate to fulfill eggshell formation requirements.

Dietary supplementation with AlphaD3 maintained bone mineralization and breaking strength after the onset of egg production. Hens fed AlphaD3 exhibited conservation of humerus BMD and tibia breaking strength at 31 weeks, as well as higher tibia BMD and BMC at this age. Changes in bone mineralization in this study may be correlated with improved medullary bone formation in AlphaD3-fed hens compared to control-fed hens. Although medullary bone was not measured in this study and further investigation would be needed to confirm this, DEXA is considered a reliable tool to measure bone density, which is indirectly associated with medullary bone (Hester et al., 2004). The increase in BMD and BMC that was observed between 18 and 31 weeks could be attributed to changes in medullary bone, considering that cortical bone formation is limited following the onset of sexual maturity (Hudson et al., 1993; Whitehead, 2004). Given that medullary bone formation induced by the onset of sexual maturity acts as one of the major calcium reservoirs in laying hens, enhancement in this process would hold significant importance. Frost et al. (1990) reported increased tibia weight in 53-week-old laying hens after supplementation with 1α-hydroxycholecalciferol. Similar findings have been observed in broiler chickens, where increased tibia ash (Biehl et al., 1995) and strength (Han et al., 2009) were reported with 1α-hydroxycholecalciferol in the diet.

Thus, our findings suggest that supplementation with AlphaD3 may facilitate medullary bone formation during early stages of the production cycle. As such, it has the potential to reduce fracture incidences as hens age, thereby countering skeletal health issues associated with high mineral demands during extended production and improving animal welfare. As AlphaD3 did not have any other major effects in this study, mechanisms by which it improved skeletal parameters are unknown but could involve direct actions on bone itself. Elucidation of AlphaD3 effects on bone could be uncovered by investigation into gene expression at the mRNA or protein level, biochemical markers for remodeling, and high-resolution structural analyses.

In conclusion, findings from this study revealed tissue-specific involvement of select transporters and hormonal signaling mechanisms potentially influencing functional changes associated with eggshell formation and bone mineralization in laying hens following the onset of egg production. The tissues evaluated exhibited a remarkable capacity to alternate between highly demanding states of increased mineral absorption, retention, or excretion in order to maintain homeostasis between eggshell formation and bone mineralization. Key regulators of mineral homeostasis in kidney and shell gland that were identified represent potential targets for strategies aimed at enhancing mineral utilization by laying hens. In addition, targeted nutritional approaches that improve efficiency of utilization and activation of dietary vitamin D_3 could be used to optimize development of medullary bone, ultimately improving skeletal integrity and hen welfare at all stages of production.

Five Future studies that expand on the current findings should incorporate additional methods such as transcriptomics and metabolomics that allow for a more robust identification of the broader physiological pathways and processes involved. Functional validation of pathways and genes identified by analysis of protein expression and activity, as well as the use of *in vitro* methods that allow a detailed investigation into molecular and cellular processes, will ultimately provide fundamental information necessary to develop successful strategies allowing hens to efficiently utilize minerals for skeletal remodeling and eggshell deposition throughout all stages of egg production. CONFLICT OF INTEREST

The authors declare that the research was conducted in the absence of any commercial or financial relationships that could be construed as a potential conflict of interest.

Data availability statement

The raw data supporting the conclusions of this article will be made available by the authors, without undue reservation.

Ethics statement

The animal study was approved by the University of Georgia Institutional Animal Care and Use Committee. The study was conducted in accordance with the local legislation and institutional requirements.

Author contributions

RG-M: Conceptualization, Data curation, Formal Analysis, Investigation, Methodology, Writing–original draft. MS-B: Investigation, Methodology, Writing–review and editing. LB: Investigation, Writing–review and editing. RA: Conceptualization, Methodology, Writing–review and editing. BJ: Conceptualization, Writing–review and editing. PR: Investigation, Methodology, Supervision, Writing–review and editing. NN: Methodology, Writing–review and editing. MP-W: Investigation, Methodology, Writing–review and editing. XA: Conceptualization, Writing–review and editing. DC: Conceptualization, Writing–review and editing. LE: Conceptualization, Data curation, Formal Analysis, Funding acquisition, Investigation, Methodology, Supervision, Writing–review and editing.

Funding

The author(s) declare that financial support was received for the research, authorship, and/or publication of this article. Funding for this project was provided to LE by USDA National Institute of Food and Agriculture competitive grant #2024-67015-42326 and Faculty Seed Grant in the Sciences and Engineering grant #000338 from the Office of Research at the University of Georgia.

Acknowledgments

The authors would like to thank Brett Marshall, Ky Meeks, Manuel Arango, Shailes Bhattrai, Lauren Vaccaro, and Grant Bennett for their assistance with sample collection and initial editing of this manuscript.

Conflict of interest

Author BJ was employed by Iluma Alliance. Authors XA and DC were employed by H&N International GmbH.

The remaining authors declare that the research was conducted in the absence of any commercial or financial relationships that could be construed as a potential conflict of interest.

The author(s) declared that they were an editorial board member of Frontiers, at the time of submission. This had no impact on the peer review process and the final decision.

Publisher's note

References

Armbrecht, H. J., Chen, M. L., Hodam, T. L., and Boltz, M. A. (1997). Induction of 24-hydroxylase cytochrome P450 mRNA by 1,25-dihydroxyvitamin D and phorbol esters in normal rat kidney (NRK-52E) cells. *J. Endocrinol.* 153 (2), 199–205. doi:10.1677/joe.0.1530199

Bahry, M. A., Hanlon, C., Ziezold, S. S., Bédécarrats, G. Y., and Bédécarrats, G. Y. (2023). Impact of growth trajectory on sexual maturation in layer chickens. *Front. Physiol.* 14, 1174238. doi:10.3389/fphys.2023.1174238

Bar, A. (2008). Calcium homeostasis and vitamin D metabolism and expression in strongly calcifying laying birds. *Comp. Biochem. Physiol. A. Mol. Int. Physiol.* 151 (4), 477–490. doi:10.1016/j.cbpa.2008.07.006

Bar, A., Shani, M., Fullmer, C. S., Brindak, M. E., and Striem, S. (1990). Modulation of chick intestinal and renal calbindin gene expression by dietary vitamin D3, 1,25-dihydroxyvitamin D3, calcium and phosphorus. *Mol. Cell. Endocrinol.* 72 (1), 23–31. doi:10.1016/0303-7207(90)90236-2

Bar, A., Vax, E., Hunziker, W., Halevy, O., and Striem, S. (1996). The role of gonadal hormones in gene expression of calbindin (Mr28,000) in the laying hen. *Gen. Comp. Endocrinol.* 103 (1), 115–122. doi:10.1006/gcen.1996.0100

Bar, A., Vax, E., and Striem, S. (1992). Relationships between calbindin (Mr 28,000) and calcium transport by the eggshell gland. *Comp. Biochem. Physiol. A. Physiol.* 101 (4), 845–848. doi:10.1016/0300-9629(92)90367-Y

Ben-Dov, I. Z., Galitzer, H., Lavi-Moshayoff, V., Goetz, R., Kuro-o, M., Mohammadi, M., et al. (2007). The parathyroid is a target organ for FGF23 in rats. *J. Clin. Invest.* 117 (12), 4003–4008. doi:10.1172/JCI32409

Bhattacharyya, M. H., and Deluca, H. F. (1974). The regulation of calciferol-25-hydroxylase in the chick. *Biochem. Biophys. Res. Comm.* 59 (2), 734–741. doi:10.1016/S0006-291X(74)80041-0

Biehl, R. R., Baker, D. H., and DeLuca, H. F. (1995). 1 alpha-hydroxylated cholecalciferol compounds act additively with microbial phytase to improve phosphorus, zinc and manganese utilization in chicks fed soy-based diets. *J. Nutr.* 125 (9), 2407–2416. doi:10.1093/jn/125.9.2407

Bouillon, R., Van Baelen, H., Tan, B. K., and De Moor, P. (1980). The isolation and characterization of the 25-hydroxyvitamin D-binding protein from chick serum. *J. Biol. Chem.* 225 (22), 10925–10930. doi:10.1016/S0021-9258(19)70395-0

Canaff, L., Petit, J. L., Kisiel, M., Watson, P. H., Gascon-Barre, M., and Hendy, G. N. (2001). Extracellular calcium-sensing receptor is expressed in rat hepatocytes: coupling to intracellular calcium mobilization and stimulation of bile flow. *J. Biol. Chem.* 276 (6), 4070–4079. doi:10.1074/jbc.M009317200

Centeno, P. P., Herberger, A., Mun, H. C., Tu, C., Nemeth, E. F., Chang, W., et al. (2019). Phosphate acts directly on the calcium-sensing receptor to stimulate parathyroid hormone secretion. *Nat. Commun.* 10 (4693), 4693. doi:10.1038/s41467-019-12399-9

Chanpaisaeng, K., Teerapornpuntakit, J., Wongdee, K., and Charoenphandhu, N. (2021). Emerging roles of calcium-sensing receptor in the local regulation of intestinal transport of ions and calcium. *Am. J. Physiol-Cell Ph.* 320 (3), C270–C278. doi:10.1152/ajpcell.00485.2020

Chun, R. F., Blatter, E., Elliott, S., Fitz-Gibbon, S., Rieger, S., Sagasti, A., et al. (2014). Cloning of a functional 25-hydroxyvitamin D-1α-hydroxylase in zebrafish (*Danio rerio*). *Cell. biochem. Funct.* 32 (8), 675–682. doi:10.1002/cbf.3071

Cochran, M., Peacock, M., Sachs, G., and Nordin, B. E. (1970). Renal effects of calcitonin. *Br. Med. J.* 1, 135–137. doi:10.1136/bmj.1.5689.135

Conigrave, A. D., Quinn, S. J., and Brown, E. M. (2000). L-Amino acid sensing by the extracellular Ca2+-sensing receptor. *PNAS* 97 (9), 4814–4819. doi:10.1073/pnas.97.9.4814

Cooke, N. E., McLeod, J. F., Wang, X. K., and Ray, K. (1991). Vitamin D binding protein: genomic structure, functional domains, and mRNA expression in tissues. *J. Steroid. Biochem. Mol. Biol.* 40 (4-6), 787–793. doi:10.1016/0960-0760(91)90304-n

Corradino, R. A. (1993). Calbindin D28K regulation in precociously matured chick egg shell gland *in vitro*. *Gen. Comp. Endocrinol.* 91 (2), 158–166. doi:10.1006/gcen.1993.1115

Corradino, R. A., Smith, C. A., Krook, L. P., and Fullmer, C. S. (1993). Tissue-specific regulation of shell gland calbindin D28K biosynthesis by estradiol in precociously matured, vitamin D-depleted chicks. *Endocrinology* 132 (1), 193–198. doi:10.1210/endo.132.1.8419123

Cui, Z., Amevor, F. K., Feng, Q., Kang, X., Song, W., Zhu, Q., et al. (2020). Sexual maturity promotes yolk precursor synthesis and follicle development in hens via liver-blood-ovary signal axis. *Animals* 10 (12), 2348. doi:10.3390/ani10122348

Cusack, M., Fraser, A. C., and Stachel, T. (2003). Magnesium and phosphorus distribution in the avian eggshell. *Comp. Biochem. Physiol. B. Biochem. Mol. Biol.* 134 (1), 63–69. doi:10.1016/s1096-4959(02)00185-9

Dacke, C. G., Arkle, S., Cook, D. J., Wormstone, I. M., Jones, S., Zaidi, M., et al. (1993). Medullary bone and avian calcium regulation. *J. Exp. Biol.* 184 (1), 63–88. doi:10.1242/jeb.184.1.63

Deng, G. C., Bi, J. M., Qiao, J. A., He, G. E., Wu, B. N., Zhang, M. J., et al. (2010). Expression and tissue distribution of extracellular calcium-sensing receptor (CaSR) mRNA in chickens. *Turk. J. Vet. Anim. Sci.* 34 (3), 249–254. doi:10.3906/vet-0809-27

Dennis, J. E., Xiao, S. Q., Agarwal, M., Fink, D. J., Heuer, A. H., and Caplan, A. I. (1996). Microstructure of matrix and mineral components of eggshells from White Leghorn chickens (Gallus gallus). *J. Morphol.* 228 (3), 287–306. doi:10.1002/(SICI)1097-4687(199606)228:3<287::AID-JMOR2>3.0.CO;2-#

Diaz, R., Hurwitz, S., Chattopadhyay, N., Pines, M., Yang, Y., Kifor, O., et al. (1997). Cloning, expression, and tissue localization of the calcium-sensing receptor in chicken (*Gallus domesticus*). *Am. J. Physiol.* 273 (3), R1008–R1016. doi:10.1152/ajpregu.1997.273.3.R1008

Elaroussi, M. A., Forte, L. R., Eber, S. L., and Biellier, H. V. (1993). Adaptation of the kidney during reproduction: role of estrogen in the regulation of responsiveness to parathyroid hormone. *Poult. Sci.* 72 (8), 1548–1556. doi:10.3382/ps.0721548

Ellestad, L. E., Malkiewicz, S. A., Guthrie, H. D., Welch, G. R., and Porter, T. E. (2009). Expression and regulation of glucocorticoid-induced leucine zipper in the developing anterior pituitary gland. *J. Mol. Endcrinol.* 42 (2), 171–183. doi:10.1677/JME-08-0066

Fraser, D. R., and Kodicek, E. (1973). Regulation of 25-hydroxycholecalciferol-1-hydroxylase activity in kidney by parathyroid hormone. *Nat. New. Biol.* 241 (110), 163–166. doi:10.1038/newbio241163a0

Frost, T. J., Roland, D. A., and Untawale, G. G. (1990). Influence of vitamin D3, 1 alpha-hydroxyvitamin D3, and 1,25-dihydroxyvitamin D3 on eggshell quality, tibia strength, and various production parameters in commercial laying hens. *Poult. Sci.* 69 (11), 2008–2016. doi:10.3382/ps.0692008

Gloux, A., Duclos, M. J., Brionne, A., Bourin, M., Nys, Y., and Rehault-Godbert, S. (2019). Integrative analysis of transcriptomic data related to the liver of laying hens: from physiological basics to newly identified functions. *BMC Genom* 20, 821. doi:10.1186/s12864-019-6185-0

Gloux, A., Le Roy, N., Ezagal, J., Même, N., Hennequet-Antier, C., Piketty, M. L., et al. (2020a). Possible roles of parathyroid hormone, 1,25(OH)2D3, and fibroblast growth factor 23 on genes controlling calcium metabolism across different tissues of the laying hen. *Domest. Anim. Endocrinol.* 72, 106407–106412. doi:10.1016/j.domaniend.2019.106407

Gloux, A., Le Roy, N., Même, N., Piketty, M. L., Prié, D., Benzoni, G., et al. (2020b). Increased expression of fibroblast growth factor 23 is the signature of a deteriorated Ca/P balance in ageing laying hens. *Sci. Rep.* 10, 21124. doi:10.1038/s41598-020-78106-7

Han, J. C., Yang, X. D., Zhang, T., Li, H., Li, W. L., Zhang, Z. Y., et al. (2009). Effects of 1alpha-hydroxycholecalciferol on growth performance, parameters of tibia and plasma, meat quality, and type IIb sodium phosphate cotransporter gene expression of one-to twenty-one-day-old broilers. *Poult. Sci.* 88 (2), 323–329. doi:10.3382/ps.2008-00252

Heerkens, J. L., Delezie, E., Rodenburg, T. B., Kempen, I., Zoons, J., Ampe, B., et al. (2016). Risk factors associated with keel bone and foot pad disorders in laying hens housed in aviary systems. *Poult. Sci.* 95 (3), 482–488. doi:10.3382/ps/pev339

Hester, P. Y., Schreiweis, M. A., Orban, J. I., Mazzuco, H., Kopka, M. N., Ledur, M. C., et al. (2004). Assessing bone mineral density *in vivo*: dual energy X-ray absorptiometry. *Poult. Sci.* 83 (2), 215–221. doi:10.1093/ps/83.2.215

H&N International (2020). "Nick Chick white egg layers new management guide," in *H&N international gmbh*. (Cuxhaven, Germany: H&N International).

Hudson, H. A., Britton, W. M., Rowland, G. N., and Buhr, R. J. (1993). Histomorphometric bone properties of sexually immature and mature white leghorn hens with evaluation of fluorochrome injection on egg production traits. *Poult. Sci.* 72 (8), 1537–1547. doi:10.3382/ps.0721537

Hui, Q., Zhao, X., Lu, P., Liu, S., Nyachoti, M., O, K., et al. (2021). Molecular distribution and localization of extracellular calcium-sensing receptor (CaSR) and vitamin D receptor (VDR) at three different laying stages in laying hens (Gallus gallus domesticus). *Poult. Sci.* 100 (5), 101060. doi:10.1016/j.psj.2021.101060

Ieda, T., Saito, N., Ono, T., and Shimada, K. (1995). Effects of presence of an egg and calcium deposition in the shell gland on levels of messenger ribonucleic acid of CaBP-D28K and of vitamin D3 receptor in the shell gland of the laying hen. *Gen. Comp. Endocrinol.* 99 (2), 145–151. doi:10.1006/gcen.1995.1095

Ieda, T., Takahashi, T., Saito, N., Yasuoka, T., Kawashima, M., Izumi, T., et al. (2001). Changes in calcitonin receptor bidning in the shell gland of laying hens (*Gallus domesticus*) during the oviposition cycle. *J. Poult. Sci.* 38 (3), 203–212. doi:10.2141/jpsa.38.203

Ieda, T., Takahashi, T., Saito, N., Yasuoka, T., Kawashima, M., and Shimada, K. (2000). Changes in parathyroid hormone-related peptide receptor binding in the shell gland of laying hens (*Gallus domesticus*) during the oviposition cycle. *Gen. Comp. Endocrinol.* 117 (2), 182–188. doi:10.1006/gcen.1999.7395

Jonchère, V., Brionne, A., Gautron, J., and Nys, Y. (2012). Identification of uterine ion transporters for mineralisation precursors of the avian eggshell. *BMC Physiol.* 12, 10–17. doi:10.1186/1472-6793-12-10

Kerschnitzki, M., Zander, T., Zaslansky, P., Fratzl, P., Shahar, R., and Wagermaier, W. (2014). Rapid alterations of avian medullary bone material during the daily egg-laying cycle. *Bone* 69, 109–117. doi:10.1016/j.bone.2014.08.019

Kulshreshtha, G., D'Alba, L., Dunn, I. C., Rehault-Godbert, S., Rodriguez-Navarro, A. B., and Hincke, M. T. (2022). Properties, genetics and innate immune function of the cuticle in egg-laying species. *Front. Immunol.* 13, 838525. doi:10.3389/fimmu.2022.838525

Lei, S., Yanyan, S., Hong, X., Yifan, L., Yunlei, L., Ziyan, H., et al. (2020). Effect of age at photostimulation on sexual maturation and egg-laying performance of layer breeders. *Poult. Sci.* 99 (2), 812–819. doi:10.1016/j.psj.2019.12.027

McLeod, J. F., and Cooke, N. E. (1989). The vitamin D-binding protein, α-fetoprotein, albumin multigene family: detection of transcripts in multiple tissues. *J. Biol. Chem.* 264 (36), 21760–21769. doi:10.1016/S0021-9258(20)88249-0

Miller, S. C. (1978). Rapid activation of the medullary bone osteoclast cell surface by parathyroid hormone. *J. Cell. Bio.* 76 (3), 615–618. doi:10.1083/jcb.76.3.615

Monkawa, T., Yoshida, T., Wakino, S., Shinki, T., Anazawa, H., Deluca, H. F., et al. (1997). Molecular cloning of cDNA and genomic DNA for human 25-hydroxyvitamin D3 1 alpha-hydroxylase. *Biochem. Biophys. Res. Comm.* 239 (2), 527–533. doi:10.1006/bbrc.1997.7508

Navickis, R. J., Katzenellenbogen, B. S., and Nalbandov, A. V. (1979). Effects of the sex steroid hormones and vitamin D3 on calcium-binding proteins in the chick shell gland. *Biol. Repro.* 21 (5), 1153–1162. doi:10.1095/biolreprod21.5.1153

Nemere, I. (1999). 24,25-Dihydroxyvitamin D3 suppresses the rapid actions of 1,25-Dihydroxyvitamin D3 and parathyroid hormone on calcium transport in chick intestine. *J. Bone Min. Res.* 14 (9), 1543–1549. doi:10.1359/jbmr.1999.14.9.1543

Nemere, I., and Norman, A. W. (1986). Parathyroid hormone stimulates calcium transport in perfused duodena from normal chicks: comparison with the rapid (transcaltachic) effect of 1,25-dihydroxyvitamin D3. *Endocrinology* 119 (3), 1406–1408. doi:10.1210/endo-119-3-1406

Nys, Y., Baker, K., Bouillon, R., Van Baelen, H., and Lawson, D. E. (1992a). Regulation of calbindin D 28K and its mRNA in the intestine of the domestic hen. *Gen. Comp. Endocrinol.* 86 (3), 460–468. doi:10.1016/0016-6480(92)90071-Q

Nys, Y., Baker, K., and Lawson, D. E. (1992b). Estrogen and a calcium flux dependent factor modulate the calbindin gene expression in the uterus of laying hens. *Gen. Comp. Endocrinol.* 87 (1), 87–94. doi:10.1016/0016-6480(92)90153-B

Nys, Y., Bouillon, R., Van Baelen, H., and Williams, J. (1986a). Ontogeny and oestradiol dependence of vitamin D-binding protein blood levels in chickens. *J. Endocrinol.* 108 (1), 81–87. doi:10.1677/joe.0.1080081

Nys, Y., Mayel-Afshar, S., Bouillon, R., Van Baelen, H., and Lawson, D. E. (1989). Increases in calbindin D 28K mRNA in the uterus of the domestic fowl induced by sexual maturity and shell formation. *Gen. Comp. Endocrinol.* 76 (2), 322–329. doi:10.1016/0016-6480(89)90164-0

Nys, Y., N'Guyen, T. M., Williams, J., and Etches, R. J. (1986b). Blood levels of ionized calcium, inorganic phosphorus, 1,25-dihydroxycholecalciferol and gonadal hormones in hens laying hard-shelled or shell-less eggs. *J. Endocrinol.* 111 (1), 151–157. doi:10.1677/joe.0.1110151

Ogawa, H., Takahashi, T., Kuwayama, T., and Kawashima, M. (2003). Presence of calcitonin receptors in shell gland of the guineafowl and changes in binding property during an oviposition cycle. *Poult. Sci.* 82 (8), 1302–1306. doi:10.1093/ps/82.8.1302

Ogawa, H., Takahashi, T., Yasuoka, T., Kuwayama, T., Tanaka, K., and Kawashima, M. (2000). Parathyroid hormone receptor binding property in the shell gland of oviduct of the guineafowl during an oviposition cycle. *Poult. Sci.* 79 (4), 575–579. doi:10.1093/ps/79.4.575

Ohira, H., Yoshimura, Y., and Tamura, T. (1998). Increase in calcium binding protein-D28K contents in the shell gland by an injection of 1, 25-Dihydroxyvitamin D3 into the shell gland lumen in laying hens. *J. Poult. Sci.* 35 (2), 99–107. doi:10.2141/jpsa.35.99

Perwad, F., Azam, N., Zhang, M. Y., Yamashita, T., Tenenhouse, H. S., and Portale, A. A. (2005). Dietary and serum phosphorus regulate fibroblast growth factor 23 expression and 1,25-dihydroxyvitamin D metabolism in mice. *Endocrinology* 146 (12), 5358–5364. doi:10.1210/en.2005-0777

Picotto, G., Massheimer, V., and Boland, R. (1997). Parathyroid hormone stimulates calcium influx and the cAMP messenger system in rat enterocytes. *Am. J. Physiol-Cell Ph.* 273 (4), C1349–C1353. doi:10.1152/ajpcell.1997.273.4.C1349

Pinheiro, P. L., Cardoso, J. C., Power, D. M., and Canario, A. V. (2012). Functional characterization and evolution of PTH/PTHrP receptors: insights from the chicken. *BMC Ecol. Evol.* 12, 110–125. doi:10.1186/1471-2148-12-110

Ponchon, G., Kennan, A. L., and DeLuca, H. F. (1969). Activation of vitamin D by the liver. *J. Clin. Invest.* 48 (11), 2032–2037. doi:10.1172/JCI106168

Proszkowiec-Weglarz, M., and Angel, R. (2013). Calcium and phosphorus metabolism in broilers: effect of homeostatic mechanism on calcium and phosphorus digestibility. *J. Appl. Poult. Res.* 22 (3), 609–627. doi:10.3382/japr.2012-00743

Quinn, S. J., Thomsen, A. R. B., Egbuna, O., Pang, J., Baxi, K., Goltzman, D., et al. (2013). CaSR-mediated interactions between calcium and magnesium homeostasis in mice. *Am. J. Physiol-Cell Ph.* 304 (7), E724–E733. doi:10.1152/ajpendo.00557.2012

Ren, Z., Ebrahimi, M., Bütz, D. E., Sand, J. M., Zhang, K., and Cook, M. E. (2017). Antibody to fibroblast growth factor 23-peptide reduces excreta phosphorus of laying hens. *Poult. Sci.* 96 (1), 127–134. doi:10.3382/ps/pew189

Rotllant, J., Guerreiro, P. M., Redruello, B., Fernandes, H., Apolónia, L., Anjos, L., et al. (2006). Ligand binding and signalling pathways of PTH receptors in sea bream (Sparus auratus) enterocytes. *Cell. Tissue. Res.* 323 (2), 333–341. doi:10.1007/s00441-005-0070-7

Samiullah, S., and Roberts, J. R. (2014). The eggshell cuticle of the laying hen. *J. Word's Poult. Sci.* 70 (4), 693–708. doi:10.1017/S0043933914000786

San, J., Zhang, Z., Bu, S., Zhang, M., Hu, J., Yang, J., et al. (2021). Changes in duodenal and nephritic Ca and P absorption in hens during different egg-laying periods. *Heliyon* 7, e06081–e06086. doi:10.1016/j.heliyon.2021.e06081

Schindelin, J., Arganda-Carreras, I., Frise, E., Kaynig, V., Longair, M., Pietzsch, T., et al. (2012). Fiji: an open-source platform for biological-image analysis. *Nat. Methods* 9 (7), 676–682. doi:10.1038/nmeth.2019

Shang, S., He, Z., Hou, W., Chen, X., Zhao, X., Han, H., et al. (2023). Molecular cloning, expression analysis and functional characterization of chicken cytochrome P450 27A1: a novel mitochondrial vitamin D3 25-hydroxylase. *Poult. Sci.* 102 (8), 102747. doi:10.1016/j.psj.2023.102747

Shimada, T., Hasegawa, H., Yamazaki, Y., Muto, T., Hino, R., Takeuchi, Y., et al. (2004a). FGF-23 is a potent regulator of vitamin D metabolism and phosphate homeostasis. *J. Bone Min. Res.* 19 (3), 429–435. doi:10.1359/JBMR.0301264

Shimada, T., Kakitani, M., Yamazaki, Y., Hasegawa, H., Takeuchi, Y., Fujita, T., et al. (2004b). Targeted ablation of Fgf23 demonstrates an essential physiological role of FGF23 in phosphate and vitamin D metabolism. *J. Clin. Invest.* 113 (4), 561–568. doi:10.1172/JCI19081

Shinki, T., Shimada, H., Wakino, S., Anazawa, H., Hayashi, M., Saruta, T., et al. (1997). Cloning and expression of rat 25-hydroxyvitamin D3-1alpha-hydroxylase cDNA. *Proc. Natl. Acad. Sci. U. S. A* 94 (24), 12920–12925. doi:10.1073/pnas.94.24.12920

Sinclair-Black, M., Garcia-Mejia, R. A., Blair, L. R., Angel, R., Arbe, X., Cavero, D., et al. (2024). Circadian regulation of calcium and phosphorus homeostasis during the oviposition cycle in laying hens. *Poult. Sci.* 103 (2), 103209. doi:10.1016/j.psj.2023.103209

Sinclair-Black, M., Garcia-Mejia, R. A., and Ellestad, L. E. (2023). Physiological regulation of calcium and phosphorus utilization in laying hens. *Front. Physiol.* 14, 1112499. doi:10.3389/fphys.2023.1112499

Sommerville, B. A., and Fox, J. (1987). Changes in renal function of the chicken associated with calcitonin and parathyroid hormone. *Gen. Comp. Endocrinol.* 66 (3), 381–386. doi:10.1016/0016-6480(87)90248-6

Tanaka, Y., DeLuca, H. F., Omdahl, J., and Holick, M. F. (1971). Mechanism of action of 1,25-dihydroxycholecalciferol on intestinal calcium transport. *Proc. Natl. Acad. Sci. U. S. A* 68 (6), 1286–1288. doi:10.1073/pnas.68.6.1286

Theofan, G., Nguyen, A. P., and Norman, A. W. (1986). Regulation of calbindin-D28K gene expression by 1,25-dihydroxyvitamin D3 is correlated to receptor occupancy. *J. Biol. Chem.* 261 (36), 16943–16947. doi:10.1016/S0021-9258(19)75981-X

Thiede, M. A., Harm, S. C., McKee, R. L., Grasser, W. A., Duong, L. T., and Leach, R. M. (1991). Expression of the parathyroid hormone-related protein gene in the avian oviduct: potential role as a local modulator of vascular smooth muscle tension and shell gland motility during the egg-laying cycle. *Endocrinology* 129 (4), 1958–1966. doi:10.1210/endo-129-4-1958

Tucker, G., Gagnon, R. E., and Haussler, M. R. (1973). Vitamin D3-25 hydroxylase: tissue occurrence and apparent lack of regulation. *Arch. Biochem. Biophys.* 155 (1), 47–57. doi:10.1016/S0003-9861(73)80008-6

Untergasser, A., Cutcutache, I., Koressaar, T., Ye, J., Faircloth, B. C., Remm, M., et al. (2012). Primer3—new capabilities and interfaces. *Nucleic acids. Res.* 40 (15), e115. doi:10.1093/nar/gks596

Vaccaro, L. A., Porter, T. E., and Ellestad, L. E. (2022). The effect of commercial genetic selection on somatotropic gene expression in broilers: a potential role for insulin-like growth factor binding proteins in regulating broiler growth and body composition. *Front. Physiol.* 13, 935311–935317. doi:10.3389/fphys.2022.935311

Wang, R. M., Zhao, J. P., Wang, X. J., Jiao, H. C., Wu, J. M., and Lin, H. (2018). Fibroblast growth factor 23 mRNA expression profile in chickens and its response to dietary phosphorus. *Poult. Sci.* 97 (7), 2258–2266. doi:10.3382/ps/pey092

Warshawsky, H., Glotzman, D., Rouleau, M. F., and Bergeron, J. J. (1980). Direct *in vivo* demonstration by radioautography of specific binding sites for calcitonin in skeletal and renal tissues of the rat. *J. Cell. Bio.* 85 (3), 682–694. doi:10.1083/jcb.85.3.682

Watanabe, K. P., Kawai, Y. K., Ikenaka, Y., Kawata, M., Ikushiro, S., Sakaki, T., et al. (2013). Avian cytochrome P450 (CYP) 1-3 family genes: isoforms, evolutionary relationships, and mRNA expression in chicken liver. *PLoS ONE* 8 (9), e75689. doi:10.1371/journal.pone.0075689

White, P., and Cooke, N. (2000). The multifunctional properties and characteristics of vitamin D-binding protein. *Trends Endocrinol. Metab.* 11 (8), 320–327. doi:10.1016/S1043-2760(00)00317-9

Whitehead, C. C. (2004). Overview of bone biology in the egg-laying hen. *Poult. Sci.* 83 (2), 193–199. doi:10.1093/ps/83.2.193

Wideman, R. F. (1987). Renal regulation of avian calcium and phosphorus metabolism. *J. Nutr.* 117 (4), 808–815. doi:10.1093/jn/117.4.808

Wu, J. C., Smith, M. W., Turvey, A., Keable, S. J., and Colston, K. W. (1994). Differential regulation of vitamin D receptor and intestinal calcium transport occurring during sexual maturation in the fowl (*Gallus domesticus*). *Comp. Biochem. Physiol. A. Physiol.* 109 (3), 713–720. doi:10.1016/0300-9629(94)90214-3

Xing, W., Li, G., Xi, Y., Guo, J., Li, H., Li, H., et al. (2010). The functional expression of calcium-sensing receptors in BRL cells and related signal transduction pathway responsible for intracellular calcium elevation. *Mol. Cell. Biochem.* 343, 13–19. doi:10.1007/s11010-010-0493-7

Yasuoka, T., Kawashima, M., Takahashi, T., Tatematsu, N., and Tanaka, K. (1998). Calcitonin receptor binding properties in bone and kidney of the chicken during the oviposition cycle. *J. Bone Min. Res.* 13 (9), 1412–1419. doi:10.1359/jbmr.1998.13.9.1412

Yoshimura, Y., Ohira, H., and Tamura, T. (1997). Immunocytochemical localization of vitamin D receptors in the shell gland of immature, laying, and molting hens. *Gen. Comp. Endocrinol.* 108 (2), 282–289. doi:10.1006/gcen.1997.6972

frontiers | Frontiers in Physiology

TYPE Original Research
PUBLISHED 15 November 2024
DOI 10.3389/fphys.2024.1504557

OPEN ACCESS

EDITED BY
Sandra G. Velleman,
The Ohio State University, United States

REVIEWED BY
Yuwares Malila,
National Center for Genetic Engineering and Biotechnology (BIOTEC), Thailand
Young-Joo Yi,
Sunchon National University,
Republic of Korea

*CORRESPONDENCE
K. Diehl,
Kristen.Diehl@usda.gov

†These authors have contributed equally to this work

RECEIVED 30 September 2024
ACCEPTED 30 October 2024
PUBLISHED 15 November 2024

CITATION
Bond A, Mills KM, Ferreira CR, Harford I, Flack B, Long JA and Diehl K (2024) Broiler breeder putative lipid biomarkers associated with sperm mobility.
Front. Physiol. 15:1504557.
doi: 10.3389/fphys.2024.1504557

Broiler breeder putative lipid biomarkers associated with sperm mobility

A. Bond[1†], K. M. Mills[2†], C. R. Ferreira[3], I. Harford[4], B. Flack[4], J. A. Long[2] and K. Diehl[2*]

[1]Department of Animal and Avian Sciences, University of Maryland, College Park, MD, United States, [2]Agricultural Research Service, Beltsville Agricultural Research Center, United States Department of Agriculture, Beltsville, MD, United States, [3]Bindley Bioscience Center, Purdue University, West Lafayette, IN, United States, [4]Cobb-Vantress Inc., Siloam Springs, AR, United States

Introduction: Biomarkers indicative of sperm mobility in broiler breeders would provide the ability to screen for fertility potential, with a positive correlation established between sperm mobility and fertilization potential. This study characterized the lipidome of seminal plasma (SP), sperm cell (SC), and whole semen (WS) isolated from broiler breeder roosters with different sperm mobility phenotypes across key timepoints of the semen production cycle.

Methods: WS samples were collected from five high mobility roosters and five low mobility roosters during early, mid, and late semen production, with SP separated from SC by centrifugation. Using multiple reaction monitoring (MRM) profiling, a total of 3241 lipid species were identified in rooster semen across ten lipid classes. Metaboanalyst 6.0 was used to analyze the relative ion intensity for each lipid species due to sperm mobility phenotype through a t-test and due to timepoint through a one-way ANOVA, with lipid ontology enrichment analysis performed using LION. Metaboanalyst 6.0 was also used to perform biomarker analysis for the sperm mobility phenotype in WS samples.

Results: Lipid class total abundance differed with sample type, sperm mobility phenotype, and timepoint. A total of 31, 99, and 112 lipid species were found to be different between low and high mobility males across timepoints in the SP, SC, and WS samples, respectively. Lipid ontology enrichment analysis revealed stark contrasts in lipid-based functions key to sperm survival, storage, and productivity between low and high sperm mobility phenotypes. Through biomarker analysis, 8 lipid species were identified as excellent sperm mobility biomarkers that could be detected in early and mid-semen production.

Discussion: Timepoint based changes in lipid species were unique to each sperm mobility phenotype, with low sperm mobility roosters exhibiting a larger number of lipid species changes over the semen production cycle in the SP and SC when compared to high sperm mobility roosters. This is the first study to characterize poultry semen lipidome using MRM profiling. The lipid species identified between low and high sperm mobility roosters could be utilized in the poultry industry as potential biomarkers of fertility potential, with the ability to screen for the economical trait of fertility potential early in semen production.

KEYWORDS

broiler breeder, semen, sperm mobility, lipidome, age

1 Introduction

Semen biomarkers indicative of sperm mobility in broiler breeders would provide the ability to screen for fertility potential, with a positive correlation previously established between mobility and fertilization potential. Poor broiler breeder semen quality has many negative impacts on the poultry industry, including reduced fertility rates and increased housing costs to accommodate the number of roosters required to meet fertility requirements (Xue et al., 2022). Traditionally, poultry semen quality can be assessed through semen volume, sperm concentration, sperm viability, and subjective motility assessment, but these methods cannot be directly correlated to fertility potential (Donoghue et al., 1995). Methods that quantify poultry sperm function, such as sperm mobility assessment, and that provide potential biomarkers of fertility potential that can be utilized in the poultry industry, such as omic-based assessment, can improve overall flock male fertility at a faster rate than traditional methodology. The increase in the demand for broiler production has enhanced the need for efficient flock fertility rates. In a commercial setting, a single male will breed multiple females, making the impact of the rooster contribution on fertility rates greater than that of the hen.

The sperm mobility assay is an *in vitro* test that requires sperm to swim in a directional manner against resistance, which parallels the requirements *in vivo* for sperm to swim to sperm storage tubule (SST) temporary storage as well as from the SSTs to the ovum for fertilization. Sperm mobility is currently the only semen quality parameter directly associated with fertility potential in poultry. Further, roosters with low or high sperm mobility stay consistent in flock rankings through early and mid-timepoints of the semen production cycle. While the sperm mobility assay is informative, it is labor intensive and requires specialized equipment, which is not feasible in an industry setting. For seamless industry adoption, automated mid-high throughput methods are necessary to detect sperm mobility phenotypes, ideally during early semen production. Lipidomics is an emerging omic-based technology that could allow the poultry industry to economically screen for sperm mobility phenotypes if reliable biomarkers could be identified. Lipids were selected as the basis for this research as sperm cell and seminal plasma lipids are integral to proper sperm function, including processes involving viability, SST storage, and ovum fertilization.

Sperm cell lipids contribute to membrane composition, signaling, metabolism, and a myriad of other functions that aid in sperm mobility. These include sperm cell membrane integrity and fluidity, lipid based signaling mechanisms, and energy sources that can be utilized through lipid metabolism mechanisms. Lipids are available in poultry sperm in the form of polyunsaturated fatty acids (PUFAs), playing key roles in sperm membrane integrity and function. In particular, arachidonic acid, docosatetraenoic acid, and the other members of the n-6 family contribute to membrane sperm fluidity and flexibility for sperm functions during *in vitro* storage (Cerolini et al., 2003). Also, docosahexaenoic acid and its respective n-3 family facilitate sperm development, motility, and viability (Khoshvaght et al., 2016). Sperm plasma membrane lipids also impact sperm cryotolerance during cryopreservation procedures (Musa et al., 2021). Phospholipid class abundances in spermatozoa throughout the reproductive period of male chickens has been previously correlated with *in vivo* fertility rates, with phosphatidylserine and phosphatidylcholine displaying a pattern of changes with age positively and negatively, respectively, in relation to the changes of fertility (Cerolini et al., 1997). Shifts in sperm cell lipid composition impact sperm membrane fluidity and diffusion, directly influencing sperm nutrient uptake from the seminal plasma and/or oviductal fluids.

The biochemical characteristics and physiological roles of the various seminal plasma components in birds (carbohydrates, lipids, amino acids, hormones, and proteins) are poorly understood (Blesbois et al., 2004). The total lipid content of seminal plasma is lower than the total lipid content seen in sperm cells, with a lower proportion of phosphatidylcholine and high levels of cholesterol esters and triglycerides (Longo, 2014; Zaniboni and Cerolini, 2009; Douard et al., 2000). Though lipid functions in the seminal plasma have not been fully elucidated, poultry seminal plasma lipid content has been previously associated with fertility rates and has been shown to change with age. Shifts in seminal plasma lipid composition through dietary intervention has been utilized to increase semen fertilizing ability (Blesbois et al., 1997; Blesbois et al., 2004). However, seminal plasma lipid concentrations are impacted by age, with concentrations higher in seminal plasma of older roosters than in younger roosters (Kelso et al., 1996). Additionally, the presence of seminal plasma greatly impacts the success of bird sperm fertilizing capacity during *in vitro* semen biotechnologies, indicating potential impacts on sperm mobility (Blesbois et al., 2004).

Early semen screening for sperm mobility would allow the poultry industry to minimize costs associated with males exhibiting low fertility potential. The focus of this study is to characterize the lipidome of seminal plasma (SP), sperm cells (SC), and whole semen (WS) in broiler breeders with different sperm mobility phenotypes. In addition, this study assessed how the lipidome changes across the male production cycle in these sample types for low and high mobility phenotypes. This is the first study to characterize the lipidome of poultry semen fractions using multiple reaction monitoring (MRM) profiling. Through this analysis, potential lipid biomarkers of sperm mobility will also be identified, which could be utilized in the broiler breeder industry for selecting rooster with improved sperm mobility and, consequently, improved fertility potential.

2 Materials and methods

All procedures in this study were approved by the Institutional Animal Care and Use Committee of the Beltsville Animal Research Center (BARC), United States Department of Agriculture. Forty Cobb broiler breeder roosters were obtained at 22 weeks of age and used for this study. Roosters were housed individually at BARC from 22 to 55 weeks of age. Throughout the study duration, roosters had *ad libitum* access to water and were fed based on Cobb broiler breeder management guidelines. At 22 weeks of age, rooster photoperiod was increased to 10L:14D with weekly increases of 1 h of light until 16 h of light was reached to encourage the initiation of sexual maturation, inducing semen production. Semen was collected twice weekly from each rooster from 25 to 55 weeks of age, using the abdominal massage method to collect semen (Burrows and Quinn, 1935).

At 27–29 weeks of age, semen was collected and examined using the sperm mobility assay (Manier et al., 2019). Briefly, 10 µL of the collected semen sample is diluted with 3% sodium nitrate and a single wavelength photometer IMV Micro-Reader is used to measure absorbance to determine concentration. Mobility buffer is used to dilute the semen to 1×10^9 sperm/mL prior to overlay of 300 µL of the diluted semen sample on a 6% Accudenz solution preheated to 41°C. Finally, absorbance is measured following a 5-minute cuvette incubation at 41°C to obtain a sperm mobility score. A total 4 sperm mobility screenings were performed during this period and the scores obtained for each screening was averaged for individual roosters. Roosters were classified as having low, average, and high sperm mobility, with the top 5 roosters used as the high mobility samples for this study and the bottom 5 roosters used as the low mobility samples for this study. Low, average, and high sperm mobility cutoffs were previously established. Low sperm mobility roosters used in this study had an average sperm mobility score of 0.256, while high sperm mobility roosters used in this study had an average sperm mobility score of 0.659.

Semen samples utilized in this study were collected from low and high sperm mobility roosters at 30, 42, and 55 weeks of age, corresponding to early, mid, and late timepoints during the semen production cycle. At each collection timepoint, a subset of the collected semen sample was snap frozen in liquid nitrogen and utilized as the WS samples described in this study. The remaining semen was separated by centrifugation to produce SC and SP samples described in this study. Briefly, semen samples were centrifuged at 2000 × g for 5 min at 4°C. The SP was removed as the supernatant and placed into a clean microcentrifuge tube, leaving behind the SC sample to be snap frozen in liquid nitrogen. The SP sample was centrifuged at 12,000 × g for 20 min at 4°C twice to remove remaining SC, prior to being snap frozen in liquid nitrogen. All samples were stored at −80°C until analysis.

Lipidomic analysis was performed using methods previously described (Reis et al., 2023). Briefly, lipids were extracted from samples using the Bligh and Dyer method (Bligh and Dyer, 1959), involving a methanol and chloroform extraction leading to sample separation into three phases consisting of the polar, protein, and organic (lipid) phase. The lipid phase was isolated and dried in a vacuum concentrator for 8 h, with dried pellets resuspended in 200 µL of acetonitrile, methanol, and ammonium acetate 3:6.65:0.35 (v/v/v) prior to a further 10X dilution of sample in solvent before direct injection. Multiple reaction monitoring (MRM) profiling was performed using a discovery phase followed by a screening phase. During the discovery phase, pooled samples were screened for the chemical classes of acylcarnitine (AC), cholesteryl ester (CE), ceramide (CER), phosphatidylcholine (PC), phosphatidylethanolamine (PE), phosphatidylinositol (PI), phosphatidylglycerol (PG), phosphatidylserine (PS), diacylglycerol (DG), and triacylglycerol (TG) lipids. DG and TG lipids were profiled using one fatty acyl neutral loss as a product ion for the MRM scan. The specific fatty acyl chain will be indicated next to the name of the class. For example, DG 16:0 means DG with a product ion compatible with palmitic acid. For the discovery phase, samples were pooled by sperm mobility phenotype, dried by nitrogen flow for 8 h prior, diluted in 200 µL of acetonitrile/methanol/ammonium acetate 300 mM 3:6.65:0.35 (v/v/v). Pooled samples were injected into the microautosampler (G1377A) in a QQQ6410 triple quadrupole mass spectrometer (Agilent Technologies, San Jose, CA) equipped with an ESI ion source. Initial chemical class data was processed using MSConvert 20 to convert profiling method data into mzML format. Unidentified MRM ion pairs were assigned tentative lipid class attributions based on associated functional group and biological information using Lipid Maps (http://www.lipidmaps.org/). A one-way ANOVA was used to compare lipid class total abundance across semen fractions using data generated through the discovery phase. Ions with values >30% in at least one of the samples compared to a blank within each profiling method were selected to be further analyzed in the screening phase.

Due to the large number of MRMs selected to be screened, individual samples were interrogated using three lists of MRMs, referred to as methods: M1 (CER, PC, and PE lipid species), M2 (TG lipid species), and M3 (AC, DG, CE, PS, PI, and PG lipid species). For screening phase data analysis, the relative ion intensity of a given MRM in each sample was calculated and analyzed by individual method. A two-way ANOVA was used to compare lipid class total abundance due to sperm mobility phenotype and timepoint using data generated through the screening phase. For both analyses, means were separated using the LSMeans statement in SAS. Relative intensity of MRM ion pairs was analyzed using MetaboAnalyst 6.0, with autoscaling data normalization. Student's t-test analysis was used to identify MRMs that distinguish between low sperm mobility and high sperm mobility phenotypes, using an alpha of 0.05 of nominal *P*-value to identify differentially distributed lipids. Differentiating lipids were also subjected to biomarker analysis using classical univariate receiver operating characteristic (ROC) curve analysis with area-under-the-curve (AUC) value representative of biomarker potential. The following AUC scale was used to evaluate lipids as potential biomarkers: greater than or equal to 0.9 scored as excellent; greater than or equal to 0.8 but less than 0.9 scored as good; greater than or equal to 0.7 but less than 0.8 scored as fair; greater than or equal to 0.6 but less than 0.7 scored as poor; and less than 0.6 scored as fail (Xia et al., 2013). MRMs were also compared across timepoints by one-way ANOVA followed by Fisher *post hoc* analysis using Metaboanalyst 6.0. Differentiating lipid species identified between low and high sperm mobility samples as well as across timepoints within a given sperm mobility phenotype were subjected to functional annotation analysis using the target list mode of Lipid Ontology Enrichment Analysis (LION, http://lipidontology.com) (Molenaar et al., 2019; Molenaar et al., 2023). All lipid species detected within the appropriate fraction were inputted as the lipid background list for analysis.

3 Results

3.1 Lipid class distribution in semen fractions

SP and SC samples exhibited unique lipid class total abundance profiles, with WS samples displaying aspects of both fractions (Figure 1). Overall, CER and PC lipid classes were most prevalent while PG and PI lipid classes were least prevalent. One-way ANOVA results examining lipid class total abundance differences due to fraction revealed significant differences in 8 out of the 10 lipid classes. The lipid classes that displayed significant differences

10.3389/fphys.2024.1504557

are as follows: AC, CER, DG containing a 18:0 fatty acyl chain (DG 18:0) DG 18:0, DG 18:1, PC, PE, PG, PI, and PS. Total abundance differences due to fraction were not observed in a subset of the DG lipid classes as well as the CE and TG lipid classes. Post-hoc comparisons between SP and WS as well as SC and SP were significant for AC, CER, DG 18:0, DG 18:1, PC, PE, PG, and PS lipid classes, with total abundance greater in WS and SC samples when compared to SP samples. The PI lipid class showed significance in the *post hoc* comparison between SP and WS as well as SC and WS, with total abundance greatest in WS and total abundance lower in SC and SP samples. Five lipid classes were most prevalent in SC samples compared with WS and SP samples: AC, CER, DG 18:0, DG 18:1, PC, and PE. Three lipid classes were most prevalent in WS samples compared with SC and SP samples: PG, PI, and PS. None of the lipid classes were most prevalent in SP samples when compared to SC and WS samples, indicating the SP fraction contained lower lipid levels than the WS and SC fractions.

3.2 Lipid class distribution across sperm mobility phenotypes and timepoints

Two-way ANOVA results examining lipid class total abundance differences due to sperm mobility phenotype and timepoint showed total abundance of 7 and 10 lipid classes differed with the main effects of sperm mobility phenotype and timepoint, respectively, in SP, SC, and WS samples, with significant interactions identified in 2 lipid classes from the WS samples. Within WS samples, total abundance of CER, DG 18:0, PC, and TG 14:0 lipid classes were higher in low sperm mobility samples while total abundance of DG 16:1 lipid class was higher in high sperm mobility samples. Additionally, in WS samples, total abundance of CE, DG 16:1, PG, TG 16:0, and TG 18:1 lipid classes peaked at the late timepoint, while total abundance of TG 18:0 and DG 18:2 lipid classes peaked at the early timepoint (Figure 2). Within SC samples, total abundance of AC and TG 14:0 lipid classes were higher in high and low sperm mobility samples, respectively. In terms of timepoint, SC total abundance of CER, DG 18:0, DG 18:1, DG 18:2, PC, PE, PI, TG 18:0, and TG 18:1 lipid classes increased with time, while SC total abundance of the TG 16:0 lipid class peaked at the mid timepoint (Figure 3). In SP samples, total abundance of PI and PS lipid classes was higher in high sperm mobility samples compared to low sperm mobility samples. SP total abundance of DG 18:1, PE, TG 16:0, TG 18:0 and TG 18:1 lipid classes peaked at the early timepoint, PI and PS lipid classes peaked at the mid timepoint, and the AC lipid class while peaked at the late timepoint (Figure 4). Total abundance levels of lipid classes not mentioned above were not different among sperm mobility phenotypes or timepoints.

3.3 Differentially abundant lipid species due to mobility

T-test comparison of screening phase lipid species in sperm cell, seminal plasma, and whole semen samples at each timepoint revealed a total of 198 individual lipid species that differed between sperm mobility phenotypes, with overlap of significant lipid species across the semen fractions and timepoints. The largest

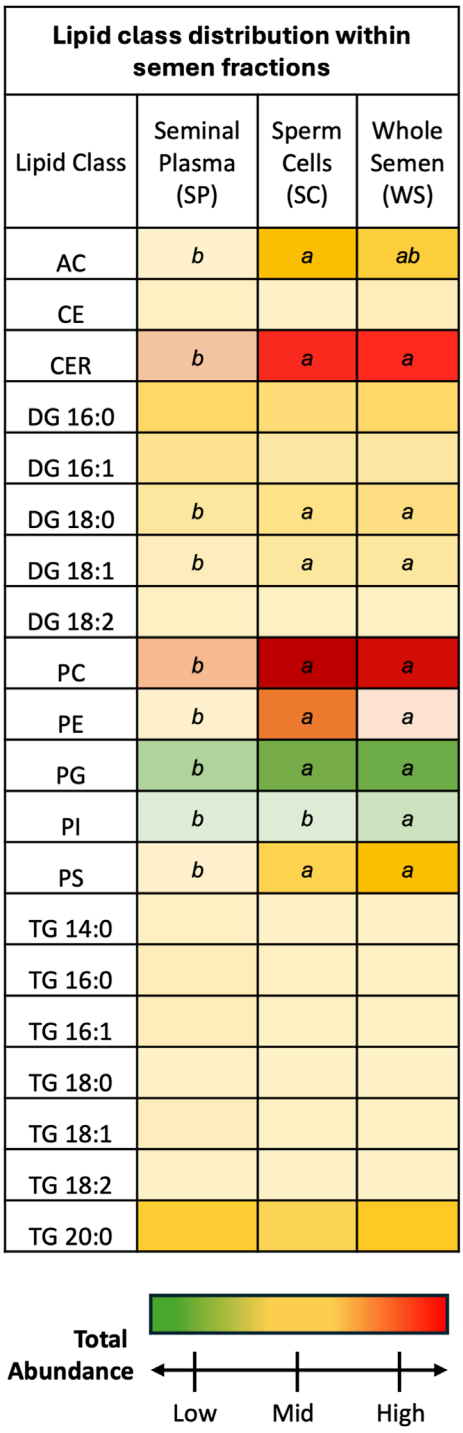

FIGURE 1
Discovery phase total abundance of lipids from 20 lipid classes. Ceramides and phosphatidyl cholines were most prevalent. Phosphatidyl glycerols and phosphatidylinositols were least prevalent. Fraction comparisons with statistically significant differences are indicated by different letters: ab $p < 0.05$. The following lipid classes were analyzed during the discovery phase: acylcarnitine (AC), cholesteryl ester (CE), ceramides (CER), diacylglycerol containing a 16:0 fatty acyl chain (DG 16:0), 16:1 (DG 16:1), 18:0 (DG 18:0), 18:1 (DG 18:1), and 18:2 (DG 18:2), phosphatidylcholine (PC), phosphatidylethanolamine (PE), phosphatidylglycerol (PG), phosphatidylinositol (PI), phosphatidylserine (PS), and triacylglycerol containing a 14:0 fatty acyl chain (TG 14:0), 16:0 (TG 16:0), 16:1 (TG 16:1), 18:0 (TG 18:0), 18:1 (TG 18:1), 18:2 (TG 18:2), and 20:0 (TG 20:0).

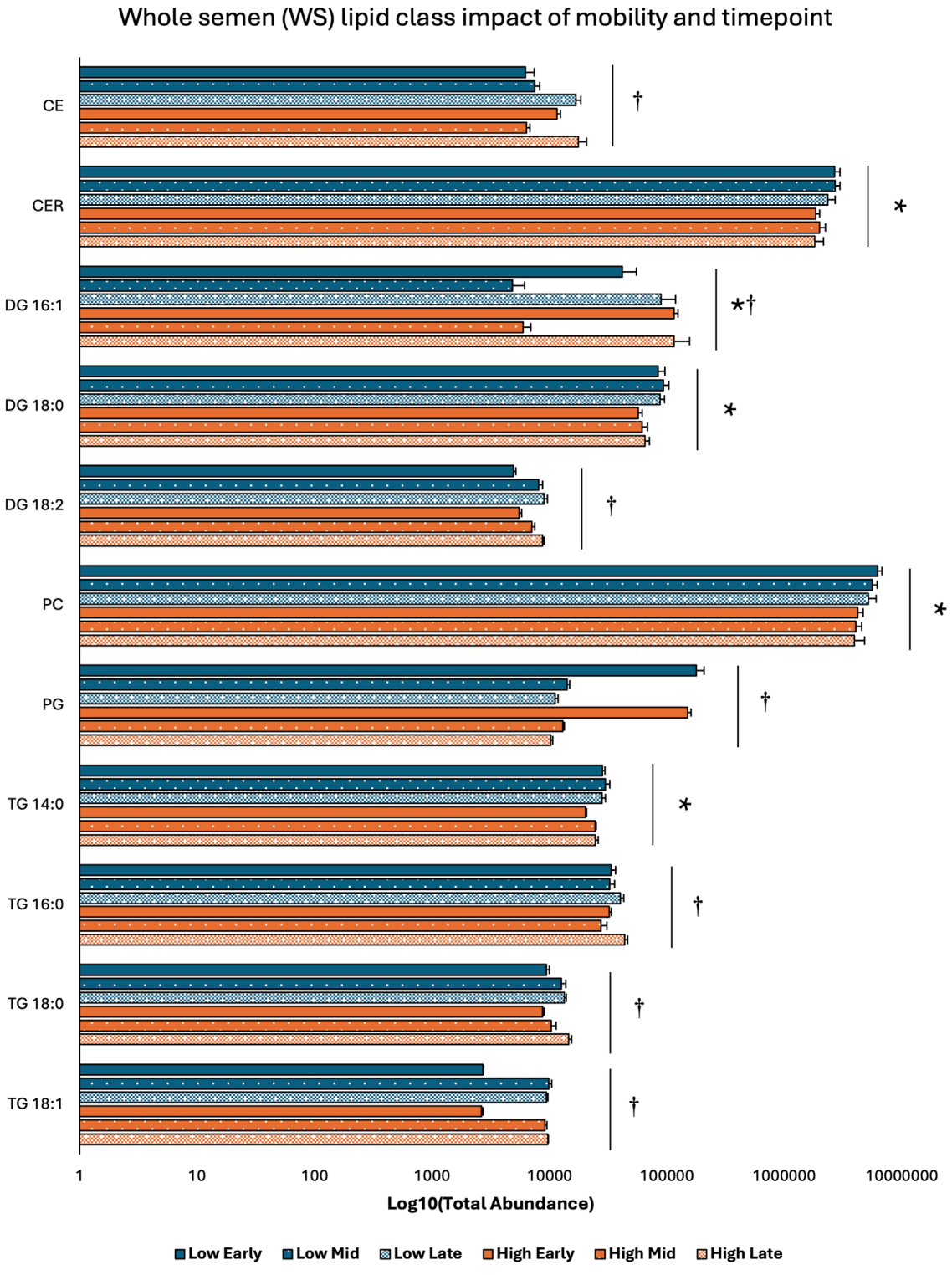

FIGURE 2
Impacts of sperm mobility phenotype and timepoint on lipid class total abundance in whole semen (WS). Lipid class total abundance differences among sperm mobility phenotypes and semen production timepoints in whole semen (WS) samples. The following lipid classes were analyzed during the screening phase: acylcarnitine (AC), cholesteryl ester (CE), ceramides (CER), diacylglycerol containing a 16:0 fatty acyl chain (DG 16:0), 16:1 (DG 16:1), 18:0 (DG 18:0), 18:1 (DG 18:1), and 18:2 (DG 18:2), phosphatidylcholine (PC), phosphatidylethanolamine (PE), phosphatidylglycerol (PG), phosphatidylinositol (PI), phosphatidylserine (PS), and triacylglycerol containing a 14:0 fatty acyl chain (TG 14:0), 16:0 (TG 16:0), 16:1 (TG 16:1), 18:0 (TG 18:0), 18:1 (TG 18:1), 18:2 (TG 18:2), and 20:0 (TG 20:0). Asterisk symbols denote significant differences due to sperm mobility phenotype while dagger symbols denote significant differences due to timepoint.

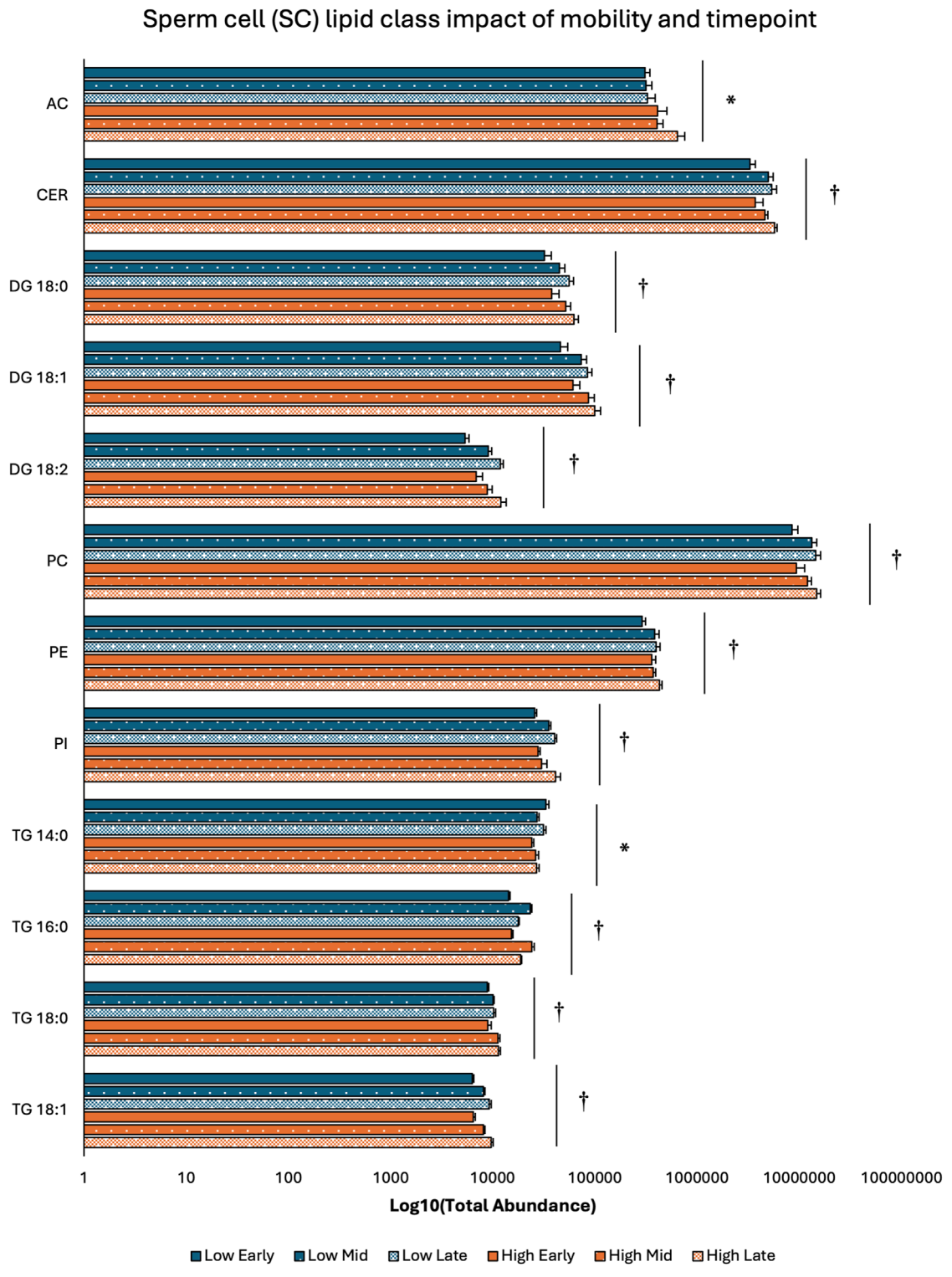

FIGURE 3
Impacts of sperm mobility phenotype and timepoint on lipid class total abundance in sperm cells (SC). Lipid class total abundance differences among sperm mobility phenotypes and semen production timepoints in sperm cell (SC) samples. The following lipid classes were analyzed during the screening phase: acylcarnitine (AC), cholesteryl ester (CE), ceramides (CER), diacylglycerol containing a 16:0 fatty acyl chain (DG 16:0), 16:1 (DG 16:1), 18:0 (DG 18:0), 18:1 (DG 18:1), and 18:2 (DG 18:2), phosphatidylcholine (PC), phosphatidylethanolamine (PE), phosphatidylglycerol (PG), phosphatidylinositol (PI), phosphatidylserine (PS), and triacylglycerol containing a 14:0 fatty acyl chain (TG 14:0), 16:0 (TG 16:0), 16:1 (TG 16:1), 18:0 (TG 18:0), 18:1 (TG 18:1), 18:2 (TG 18:2), and 20:0 (TG 20:0). Asterisk symbols denote significant differences due to sperm mobility phenotype while dagger symbols denote significant differences due to timepoint.

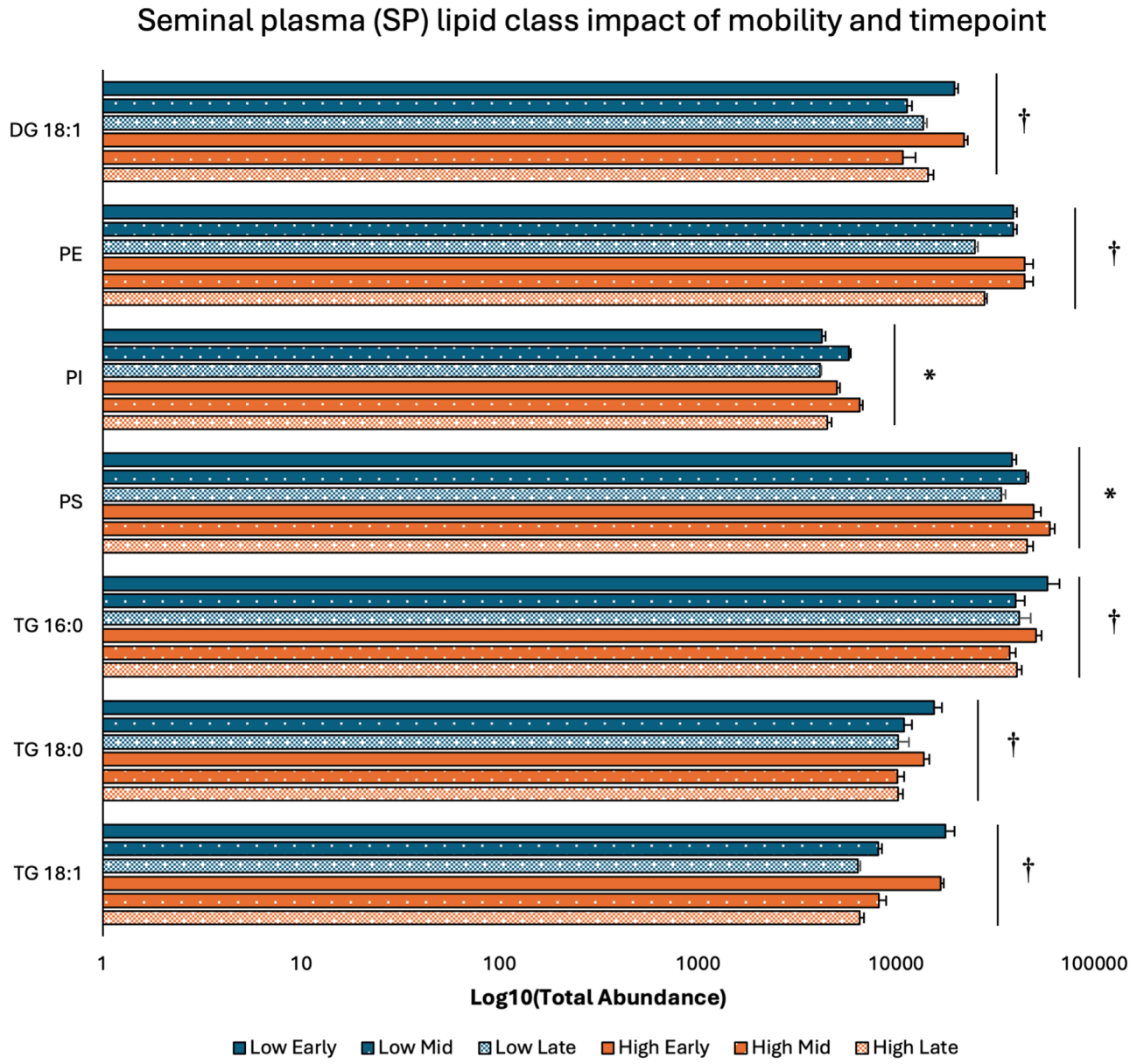

FIGURE 4
Impacts of sperm mobility phenotype and timepoint on lipid class total abundance in seminal plasma (SP). Lipid class total abundance differences among sperm mobility phenotypes and semen production timepoints in seminal plasma (SP) samples. The following lipid classes were analyzed during the screening phase: acylcarnitine (AC), cholesteryl ester (CE), ceramides (CER), diacylglycerol containing a 16:0 fatty acyl chain (DG 16:0), 16:1 (DG 16:1), 18:0 (DG 18:0), 18:1 (DG 18:1), and 18:2 (DG 18:2), phosphatidylcholine (PC), phosphatidylethanolamine (PE), phosphatidylglycerol (PG), phosphatidylinositol (PI), phosphatidylserine (PS), and triacylglycerol containing a 14:0 fatty acyl chain (TG 14:0), 16:0 (TG 16:0), 16:1 (TG 16:1), 18:0 (TG 18:0), 18:1 (TG 18:1), 18:2 (TG 18:2), and 20:0 (TG 20:0). Asterisk symbols denote significant differences due to sperm mobility phenotype while dagger symbols denote significant differences due to timepoint.

number of lipid species differences between low mobility and high mobility samples were observed in whole semen samples, with 77, 34, and 1 lipid species determined at the early, mid, and late sampling timepoints, respectively (Supplementary File S1). Sperm cell samples showed minimal lipid species differences between low and high mobility samples at the early and mid-sampling timepoints, with only 11 lipid species at each timepoint, but 77 lipid species differences at the late timepoint (Supplementary File S1). The least number of lipid species differences between low mobility and high mobility samples were observed in seminal plasma samples with 8, 12, and 11 lipid species determined at the early, mid, and late sampling timepoints, respectively (Supplementary File S1).

Lipid ontology enrichment analysis (LION) revealed lipid species with increased abundance in low sperm mobility WS and SC samples showed enrichment for diacylglycerols, lipid-mediated signaling, and negative or neutral charge headgroups. On the other hand, lipid species with increased abundance in high sperm mobility WS and SC samples showed enrichment for

triacylglycerols, sphingolipids, and positive charge headgroups (Figures 5A, 6A). LION analysis of lipid species that differed in SP samples from low and high sperm mobility roosters revealed unique lipid ontology terms when compared to those obtained through analysis of SC and WS samples. LION analysis showed abundant lipid species in low sperm mobility SP samples were enriched for lysoglycerophospholipids, very low transition temperature, polyunsaturated fatty acids, and below average bilayer thickness. Conversely, abundant lipid species in high sperm mobility SP samples were enriched for very high transition temperature, very low lateral diffusion, very high bilayer thickness, and positive charge headgroups. SP lipid species differentiating between sperm mobility phenotypes were enriched for derivatives of glycerophosphoethanolamines, with low and high sperm mobility samples showing enrichment for monoacylglycerophosphoethanolamines and 1-alkyl,2-acylglycerophosphoethanolamines, respectively (Figure 7A).

3.4 Differentially abundant lipid species due to timepoint

A total of 249 individual lipid species differed among timepoints, with 146 lipid species uniquely identified in low sperm mobility rooster samples, 51 lipid species uniquely identified in high sperm mobility rooster samples and 52 lipid species overlapping between the two sperm mobility phenotypes. Samples originating from low and high sperm mobility roosters showed unique changes in lipid species over time, with a degree of overlap observed in SC samples and minimal overlap in WS and SP samples. For high sperm mobility roosters, 20, 81, and 3 lipid species differed among timepoints in WS, SC, and SP samples, respectively (Supplementary File S2). On the other hand, in low sperm mobility roosters, 18, 144, and 75 lipid species differed among timepoints in WS, SC, and SP samples, respectively (Supplementary File S2). Within WS samples, no overlap was observed between low and high sperm mobility samples. Additionally, *post hoc* comparison showed WS lipid species changes were primarily observed in early to mid-timepoint comparisons in high sperm mobility samples while lipid species changes were primarily observed in early to late-timepoint comparisons in low sperm mobility samples. In SC samples, 41 lipid species overlapped between low and high sperm mobility samples timepoint analyses. Post-hoc comparison of SC lipid species changes over time revealed observed changes were primarily localized to the early to late timepoint comparisons in both low and high sperm mobility samples. Only 1 lipid overlapped between low and high sperm mobility samples timepoint analyses of SP samples. In both low and high sperm mobility SP samples, *post hoc* comparison revealed observed changes were primarily localized to the early to mid-timepoint comparisons.

In low sperm mobility WS samples, high lateral diffusion and 1-alkyl,2-acylglycerols were among the enriched LION terms associated with time, while in high sperm mobility WS samples, diacylglycerols, membrane components, lipid mediated signaling, and plasmalogens were among the enriched LION terms associated with time (Figure 5B). In SC samples, low and high sperm mobility rooster lipid species associated with time exhibited enrichment for the following terms: DG (34:1) and (34:2), negative intrinsic curvature, membrane components, 1-alkyl,2-acylglycerols, lipid-mediated signaling, and headgroup with positive charge. Unique terms enriched in low sperm mobility SC samples included diacylglycerophosphocholines, diacylglycerophosphoethanolamines, sphingolipids such as ceramides, and endoplasmic reticulum. On the other hand, unique terms enriched in high sperm mobility SC samples included monoacylglycerophosphocholines, lysoglycerophospholipids, and headgroup with neutral charge (Figure 6B). Lastly, in SP samples, overlap was observed in very low transition temperature and glycerophosphocholines LION terms between lipid species associated with time in low and high sperm mobility samples. Conversely, LION terms involving lateral diffusion and bilayer thickness contrasted in low and high sperm mobility SP samples. In addition, low sperm mobility SP samples showed enrichment of membrane components, glycerophosphoethanolamines such as diacylglycerophosphocholines, mitochondrion, endoplasmic reticulum, and headgroup with positive charge LION terms, which were not observed in high sperm mobility SP samples (Figure 7B).

3.5 Biomarker analysis

ROC curve analysis was performed to determine the potential of lipid species signatures in whole semen as biomarkers of sperm mobility. There were 8 lipid species identified as excellent biomarkers (AUC >0.9) during the early timepoint that could be tested through the mid timepoint, with these lipid species maintaining an AUC greater than 0.8 in the mid timepoint as well (Table 1). Lysophosphatidylethanolamine (20:3), eicoseneoylcarnitine, and phosphatidylserine (42:6) maintained their status as excellent biomarkers through the mid timepoint. Further, all lipids during the late timepoint either became poor or failed biomarkers. Two of the eight lipids, sphingomyelin (d18:1/19:0) and phosphatidylserine (42:6), were higher in abundance and indicative of low mobility during the early period. The remainder of the potential biomarkers of sperm mobility were predictive of high mobility (Figure 8).

4 Discussion

The overall goal of this study was to examine the lipidome of poultry semen fractions using MRM profiling, with special focus on lipid shifts due to sperm mobility phenotype and timing in the semen production cycle. This study is the first to characterize the lipidome of WS, SC, and SP in broiler breeder roosters. Further, this study identified and biologically analyzed 198 lipid species associated with sperm mobility phenotype and 249 lipid species associated with timing in the semen production cycle. Lastly, this study determined 8 potential biomarkers that scored as excellent biomarkers of the sperm mobility phenotype in early semen production, with these biomarkers remaining excellent or good throughout mid-semen production as well. Results from this study are imperative for determining how semen lipid composition intersects with sperm mobility as well as how this lipid composition

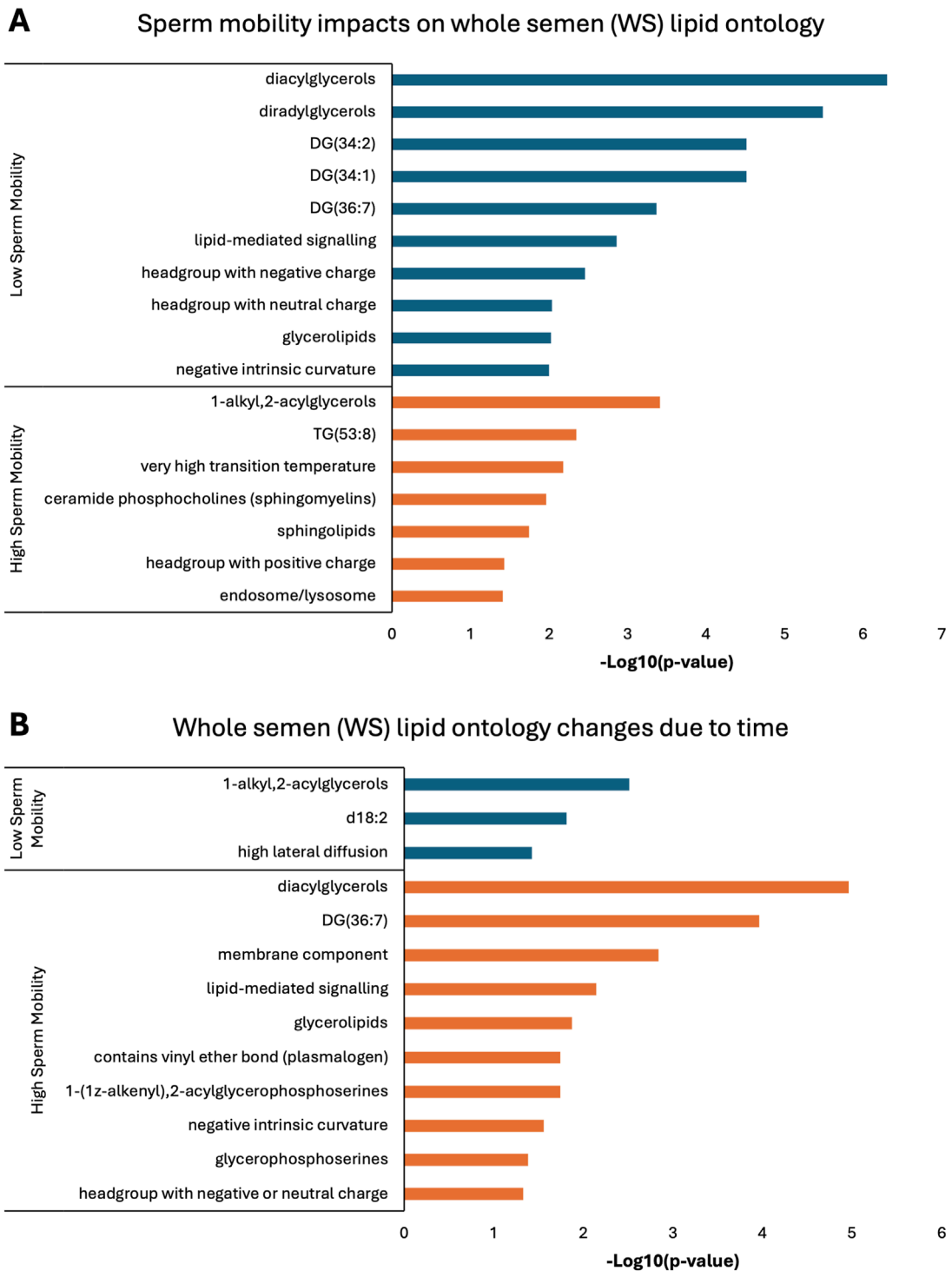

FIGURE 5
Biological functions of lipid species in whole semen (WS). Enriched lipid ontology terms generated from lipid ontology enrichment analysis (LION) of lipid species significant due to **(A)** sperm mobility phenotype and **(B)** timepoint in the semen production cycle.

changes throughout the sperm production cycle, ultimately leading to reduced sperm mobility with rooster age. Biomarkers identified will require further evaluation but are an important milestone moving the broiler breeder industry closer to mid-high throughput options for fertility potential screening in roosters.

Unique lipid class total abundances were found in the SP and SC, with WS integrating aspects of both fractions. The most prevalent lipid classes identified in poultry semen were CER, PC, and PE, with increased abundance in SC and WS fractions compared to the SP fraction. Ceramides are known to increase membrane rigidity and

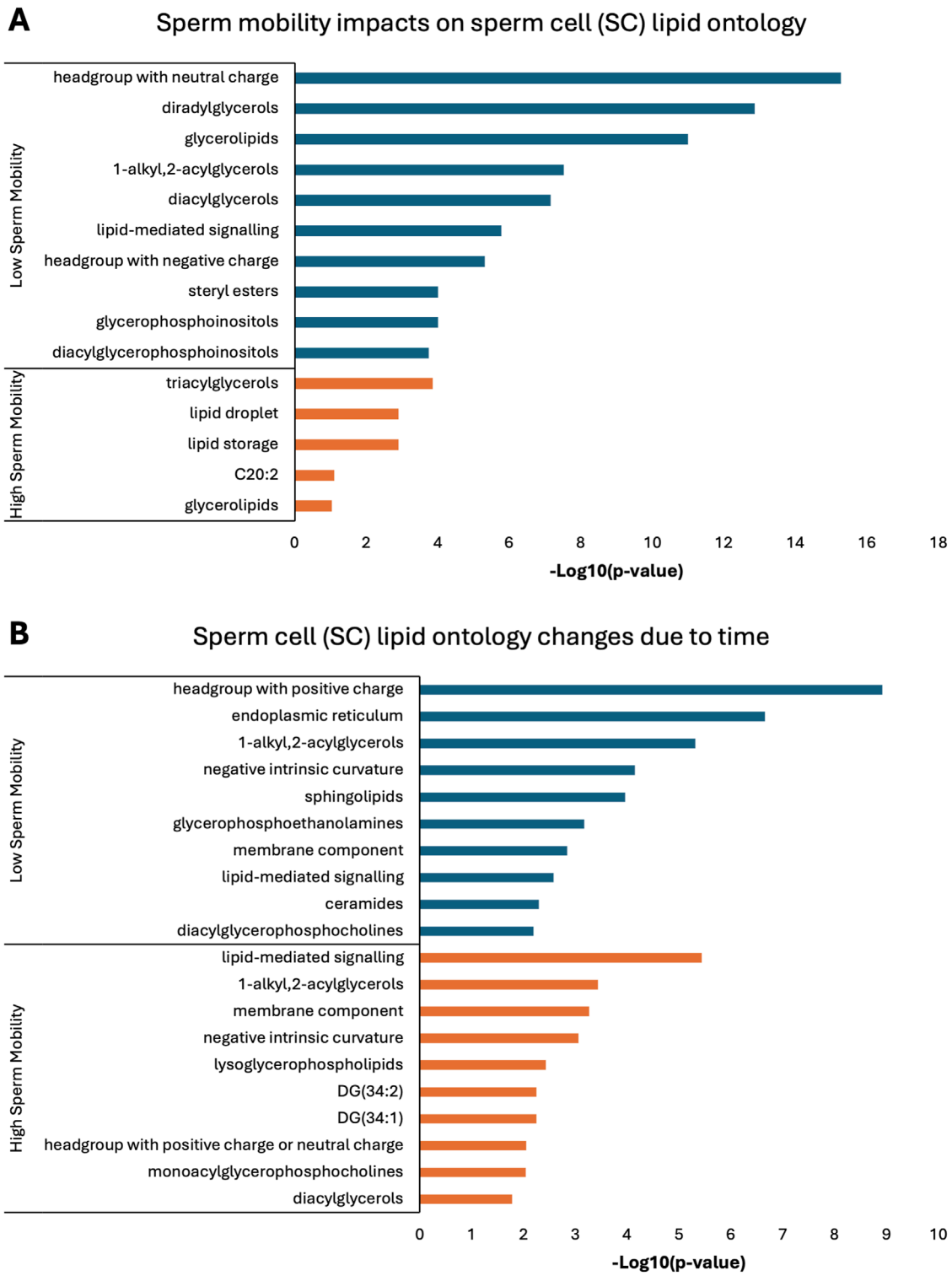

FIGURE 6
Biological functions of lipid species in sperm cells (SC). Enriched lipid ontology terms generated from lipid ontology enrichment analysis (LION) of lipid species significant due to **(A)** sperm mobility phenotype and **(B)** timepoint in the semen production cycle.

participate in membrane diffusion of small solutes, such as proteins (Alonso and Goñi, 2018; Farrani and Maggio, 2017; Alonso and Goñi, 2018). Additionally, ceramides contribute to lipid traffic across membranes through their participation in lipid rafts (Pinto et al., 2011). Phosphatidylcholine and phosphatidylethanolamine are the most important components of the sperm plasma membrane,

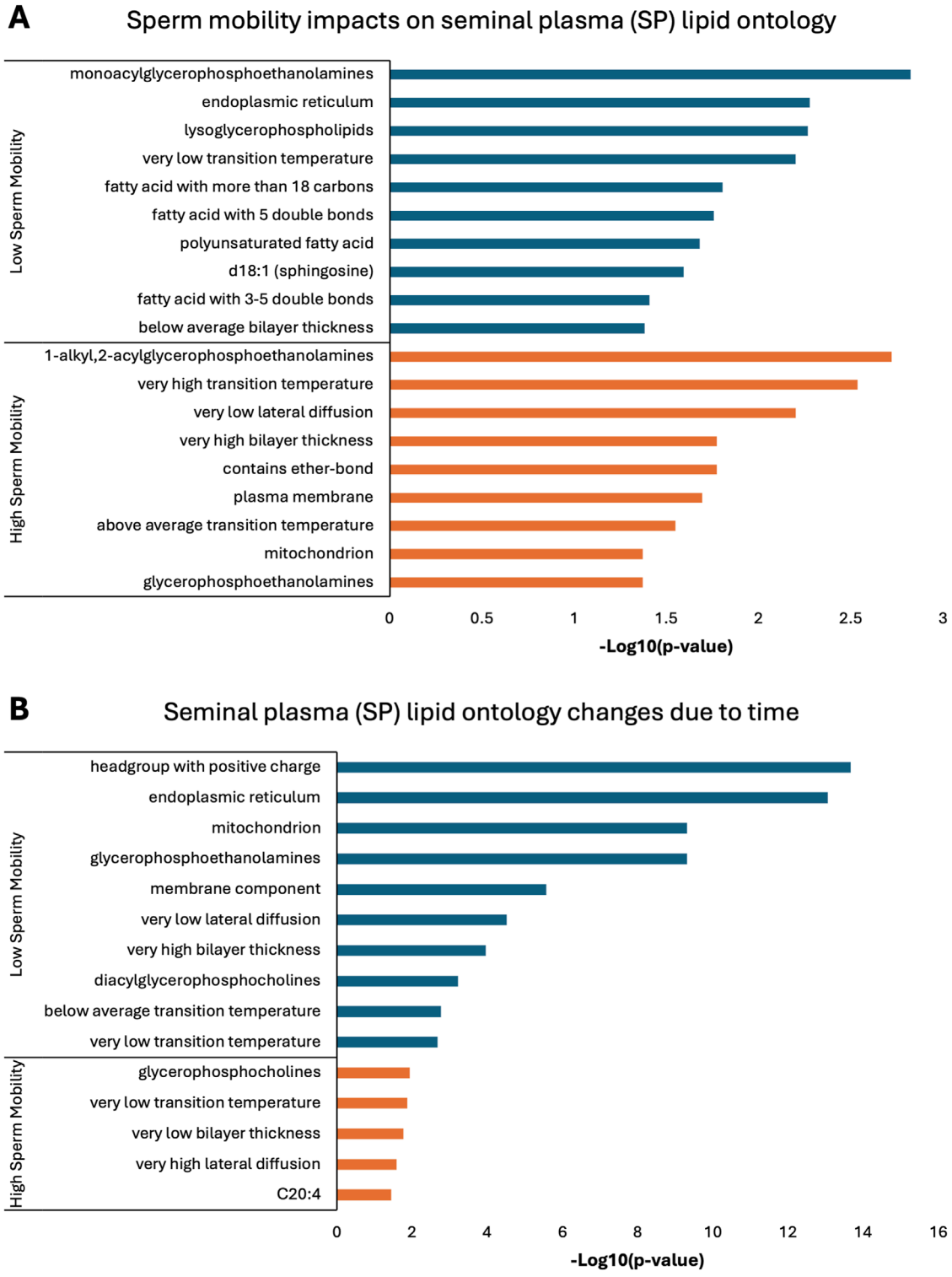

FIGURE 7
Biological functions of lipid species in seminal plasma (SP). Enriched lipid ontology terms generated from lipid ontology enrichment analysis (LION) of lipid species significant due to **(A)** sperm mobility phenotype and **(B)** timepoint in the semen production cycle.

with abundance levels and ratios serving as indicators of sperm fertilization potential (Shan et al., 2020). The high total abundance of ceramide, phosphatidylcholine, and phosphatidylethanolamine lipid classes in poultry semen, all of which play key roles in the sperm membrane composition and function, is consistent with the high density of sperm cells in poultry when compared to mammalian

TABLE 1 Relative difference and biomarker analysis between high and low mobility phenotype in lipid abundance from whole semen collected at different timepoints.

Method	Tentative ID attribution/MRM ID	Lipid class	Common name	High--low FC[a] (log_2)	*p*-value	AUC[b]	Timepoint[c]
M1	LPE (20:3)	Glycerophosphoethanolamine	Lysophosphatidylethanolamine (20:3)	0.68	0.02	0.92	Early
				0.42	0.03	0.96	Mid
	PC(20:0),LPC(21:0),PC(O-21:0)	Glycerophosphocholine	PC(20:0),LPC(21:0),PC(O-21:0)	0.44	0.02	0.92	Early
				0.36	0.04	0.84	Mid
	PC(35:6),PC(P-36:5)	Glycerophosphocholine	PC(35:6),PC(P-36:5)	0.60	<0.01	1.00	Early
				0.51	0.03	0.88	Mid
	PC(38:7),PC(37:0),PC(O-38:0)	Glycerophosphocholine	PC(38:7),PC(37:0),PC(O-38:0)	0.25	0.04	0.92	Early
				0.18	0.11	0.84	Mid
	SM(d16:0/20:0)	Sphingomyelin	Sphingomyelin (d16:0/20:0)	0.50	0.03	0.92	Early
				0.50	0.06	0.84	Mid
	SM(d18:1/19:0)	Sphingomyelin	Sphingomyelin (d18:1/19:0)	−0.15	0.04	0.92	Early
				0.22	0.05	0.84	Mid
M3	CAR(20:1)	Acylcarnitine	(11Z)-eicoseneoylcarnitine	1.99	<0.01	1.00	Early
				0.27	0.01	0.92	Mid
	PS(42:6)	Glycerophosphoserine	Phosphatidylserine (42:6)	−0.34	0.02	0.92	Early
				0.22	0.01	1.00	Mid

[a]Fold Change.

[b]Area under the curve (AUC) from ROC, curve analysis to evaluate potential mobility biomarkers within whole semen.

[c]Males were collected at three different timepoints: Early, Mid, and Late. all lipids within this table lost their biomarker potential by the late timepoint.

10.3389/fphys.2024.1504557

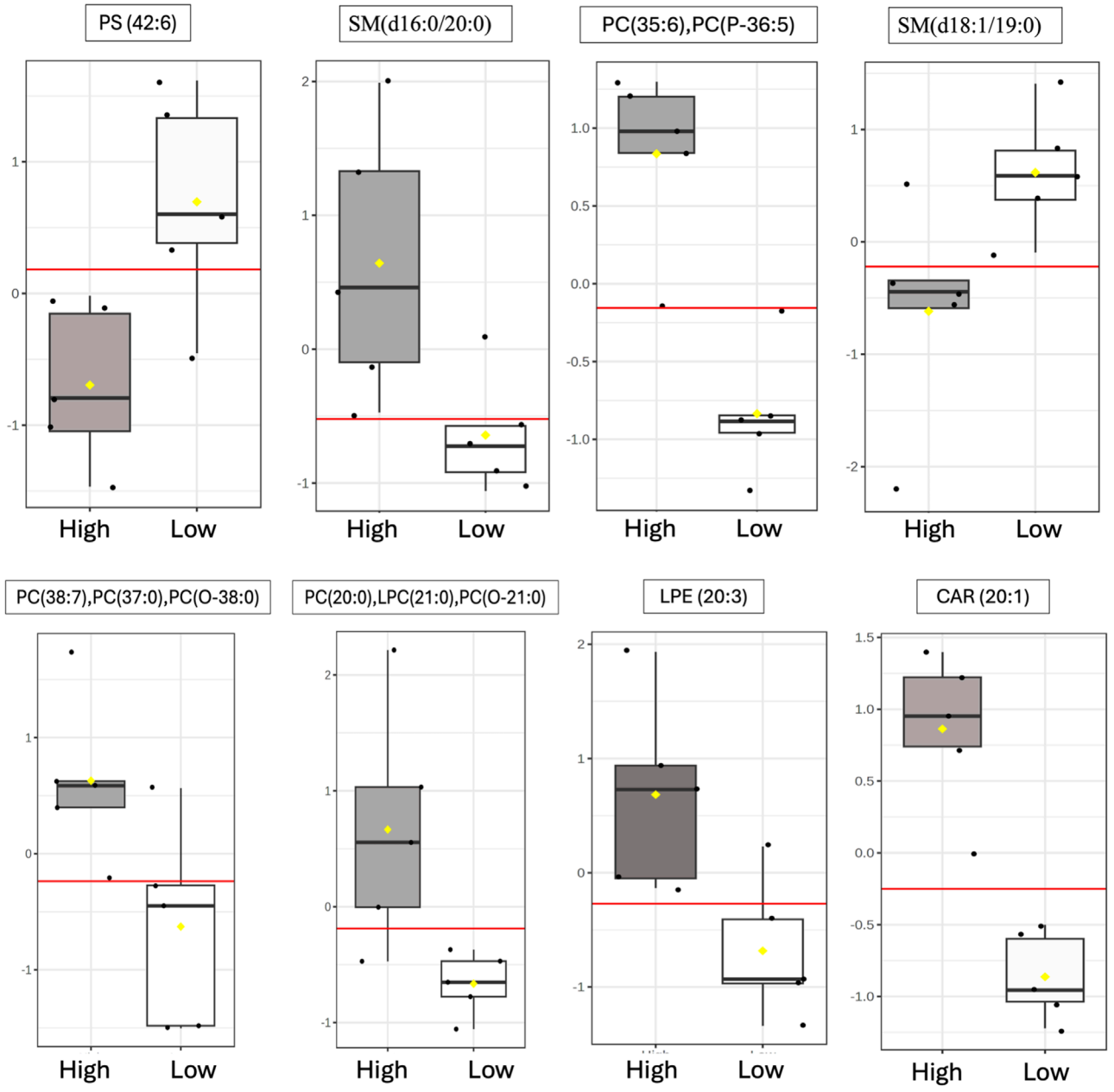

FIGURE 8
Identification of putative sperm mobility biomarkers in whole semen. Distribution during the early timepoint of differentially abundant lipids within high vs low mobility males following ROC curve analysis that maintained excellent biomarker status through the Mid timepoints. The following AUC scale was used to evaluate lipids as potential biomarkers: greater than or equal to 0.9 scored as excellent; greater than or equal to 0.8 but less than 0.9 scored as good; greater than or equal to 0.7 but less than 0.8 scored as fair; greater than or equal to 0.6 but less than 0.7 scored as poor; and less than 0.6 scored as fail. The yellow notches within the distribution plots represent the 95% confidence interval around the median for each group. If the notches do not line up, the medians are likely different. The red line represents the median. The *y*-axis for box plots represents the relative ion intensity of lipids within each sample.

semen. Further, similar lipid class proportions have been previously reported for poultry semen, confirming that MRM profiling results are consistent with less robust technologies that are unable to resolve down to the lipid species level.

Low sperm mobility roosters exhibited increased total abundance of CER, PC, DG 18:0, and TG 14:0 lipids, while high sperm mobility roosters exhibited increased total abundance of DG 16:1, AC, PI, and PS lipids. Several studies in mammals have identified key CER and PC lipids in semen associated with reduced male performance, while increased TG 14:0 lipids were associated with morphological defects in swine semen (Chen et al., 2021; Shan et al., 2020; Mills et al., 2024). Additionally, PC and AC lipid levels were negatively associated with poultry sperm motility/mobility while PS lipid levels were positively associated

(Cerolini et al., 1997; Froman and Kirby, 2005). Interestingly, the identified lipid classes play diverse roles in sperm physiological functions, from sperm cell membrane integrity/fluidity to lipid based signaling to sperm energy sources. This could indicate that sperm mobility phenotypes result from a culmination of several physiological mechanisms. Though PI lipids display low abundance in poultry semen, phosphoinositide signaling has been identified as imperative for sperm motility as well as SST metabolic processes in poultry, indicating potential mechanistic links between increased SP PI levels and increased sperm mobility (Lemoine et al., 2009; Yang et al., 2021). Diglycerides play vast roles in sperm function, including key roles in the acrosome reaction and sperm metabolism. Mammalian research results on diglyceride impacts on sperm fertility potential are mixed, with reports of increased diglyceride levels in high fertility and low fertility males, similar to the results from this study (Shan et al., 2020; Sebastian et al., 1987). In addition to sperm mobility-based differences, each lipid class examined differed among semen production cycle timepoints, indicating that the lipidome of broiler breeder rooster semen is dynamic. In WS and SC samples, a majority of the lipid classes were most abundant at the late timepoint, while in SP samples, 5 lipid class abundances peaked at the early timepoint. Early SP lipid changes could serve to drive later changes in SC/WS, ultimately influencing sperm mobility. The lipid class changes due to age indicated in this study do not completely align with previous broiler breeder reports from 2 decades ago (Kelso et al., 1996). This could be due to line-based differences and/or that intensive genetic selection has shifted the lipid composition of broiler breeder semen.

LION analysis of lipid species that differed between low and high sperm mobility phenotypes revealed stark contrasts in transition temperature, lateral diffusion, and bilayer thickness. Transition temperature, bilayer thickness, and lateral diffusion are tightly linked to lipid bilayer membrane fluidity and integrity, which regulate nutrient availability, trans-membrane transport proteins activity, and intracellular signaling. Semen transition temperature has been showed to be reduced in species less resistant to temperature changes (Drobnis et al., 1993). Increased bilayer thickness increased trans-membrane transport proteins activity, for ions such as calcium which impacts sperm mobility, up to a peak prior to decreasing activity once the bilayer threshold has been obtained (Johannsson et al., 1981). High sperm mobility samples exhibited increased transition temperature and bilayer thickness, potentially increasing temperature stability and calcium trans-membrane transport in semen obtained from these roosters. Additionally, low sperm mobility samples exhibited enrichment of lateral diffusion, a process increasing membrane fluidity that is required during later stages of sperm-ovum interaction (Wolfe et al., 1998). This premature shift may leave low mobility semen incapable of membrane fluidity changes at later stages of fertilization. Overall, low sperm mobility semen fractions exhibited changes in a larger number of lipid species due to timing in the semen production cycle than high sperm mobility semen fractions, particularly in SC and SP samples. In SC samples, LION terms related to lipid signaling and membrane components appear enriched due to timepoint in both low and high sperm mobility phenotypes, implying similar time-based shifts unrelated to sperm mobility. In SP samples, LION terms related to bilayer thickness and lateral diffusion appear again, with high sperm mobility samples shifting with time toward lower bilayer thickness and higher lateral diffusion as was previously observed in low sperm mobility samples. Through lipid species changes during the semen production cycle, high and low sperm mobility samples appear to converge and become more similar at later timepoints. This is also supported by the apparent reduction in the number of lipid species differing between the two sperm mobility phenotypes, with the largest differences observed during the early timepoint and nearly no differences observed by the late timepoint. A trend toward convergence in also observed in broiler breeder sperm mobility scores over time, with low sperm mobility roosters improving sperm mobility scores with time while high sperm mobility roosters remain constant (Bowling et al., 2003).

ROC curve analysis identified three excellent biomarkers associated with mobility that can be tested beginning at 30 weeks (early) through 42 weeks of age (mid). LPE (20:3) and CAR (20:1) were associated with high mobility and PS (42:6) with low mobility at 30 weeks of age. CAR (20:1), also known as eicoseneoylcarnitine, is a structural derivative of carnitine that acts as a metabolite for cellular energy and metabolism (Degtyarenko et al., 2007). Carnitines are naturally occurring antioxidants and have been documented to be important for sperm maturation, with L-carnitine levels high within the epididymis, as well as sperm metabolism, with sperm cells utilizing fatty acid oxidation for energy supply (Soufir et al., 1981; Jeulin et al., 1987). In young broiler breeder roosters aged 24–34 weeks, increasing levels of supplemented L-carnitine resulted in an increase in sperm concentration, live sperm, and sperm quality factor—another fertility index for male poultry (Mohammadi et al., 2021). This data agrees with other work done in aging roosters where increased L-carnitine supplementation improved overall semen quality and sperm quality factor (Elokil et al., 2019). CAR (20:1) may serve to improve energy availability for sperm metabolism and may support sperm maturation at the level of the epididymis. In birds, successful fertilization can only occur when the sperm cells enter or be stored within SST (Alexander et al., 1993). Modifications of carbohydrates and phospholipids within the sperm plasma membrane decreases the capacity to survive selection and storage within SSTs, thus reducing fertility (Froman and Thurston, 1984; Donoghue et al., 1995). In the rooster sperm cell head and body membranes, PC and PE lipids are prevalent, with PS being the smallest lipid class (Bongalhardo et al., 2002). LPE (20:3) and PS (42:6) are both sperm plasma membrane lipids and their modifications or ratios within individual rooster could lead to downstream sperm mobility phenotype differences. With PS established as a less prevalent lipid class in poultry semen, the higher abundance of PS (42:6) in low mobility males may result in decreased mobility.

Historically, low sperm mobility leading to decreased fertility potential has been a detriment to the broiler breeder industry. From the standpoint of the producer, fertility prediction as early as possible is advantageous as this reduces economic losses incurred by male fertility challenges. Thus, having an early-detectable biomarker or biomarker panel indicative of fertility potential would be highly valuable to the broiler breeder industry. The ability to perform early semen lipidome biomarker screening to detect sperm mobility phenotypes would assist in mitigating the financial disparities stemming from low sperm mobility roosters. Results from this

study determined differences in lipid class abundance and individual lipid species between low and high sperm mobility rooster semen fractions. Eight of the lipid species identified in WS also scored highly as putative biomarkers of the sperm mobility phenotype. However, this study also indicated age-based associations on the lipid composition of poultry semen fractions, which is important to consider when determining when biomarker screening can be performed. Additional research is needed to validate putative biomarkers of the sperm mobility phenotype and to determine acceptable screening timelines that allow reliable results, ultimately allowing for industry-based selection strategies to improve broiler breeder rooster fertility potential.

Data availability statement

The original contributions presented in the study are included in the article/Supplementary Material, further inquiries can be directed to the corresponding author.

Ethics statement

The animal study was approved by the Institutional Animal Care and Use Committee of the Beltsville Animal Research Center (BARC), United States Department of Agriculture. The study was conducted in accordance with the local legislation and institutional requirements.

Author contributions

AB: Data curation, Formal Analysis, Writing–original draft, Writing–review and editing. KM: Data curation, Formal Analysis, Software, Writing–original draft, Writing–review and editing. CF: Investigation, Methodology, Writing–review and editing. IH: Conceptualization, Funding acquisition, Investigation, Writing–review and editing. BF: Conceptualization, Funding acquisition, Investigation, Writing–review and editing. JL: Conceptualization, Funding acquisition, Investigation, Writing–review and editing. KD: Data curation, Formal Analysis, Investigation, Methodology, Project administration, Supervision, Visualization, Writing–original draft, Writing–review and editing.

Funding

The author(s) declare that financial support was received for the research, authorship, and/or publication of this article. Funding was provided by Cobb Genetics Inc. to JL through a Cobb Research Initiative grant.

Acknowledgments

The contributions of Diane Hildenberger, Amy Shannon, and the BARC Poultry Care Crew to sample collection are greatly appreciated.

Conflict of interest

Authors IH and BF were employed by the company Cobb-Vantress Inc.

The remaining authors declare that the research was conducted in the absence of any commercial or financial relationships that could be construed as a potential conflict of interest.

The authors declare that this study received funding from Cobb-Vantress Inc. The funder had the following involvement in the study: conceptualization, funding acquisition, investigation, writing-review and editing.

Publisher's note

All claims expressed in this article are solely those of the authors and do not necessarily represent those of their affiliated organizations, or those of the publisher, the editors and the reviewers. Any product that may be evaluated in this article, or claim that may be made by its manufacturer, is not guaranteed or endorsed by the publisher.

Supplementary material

The Supplementary Material for this article can be found online at: https://www.frontiersin.org/articles/10.3389/fphys.2024.1504557/full#supplementary-material

References

Alexander, A., Graham, J., Hammerstedt, R., and Barbato, G. (1993). Effects of genotype and cryopreservation of avian semen on fertility and number of perivitelline spermatozoa. *Br. Poult. Sci.* 34, 757–764. doi:10.1080/00071669308417634

Alonso, A., and Goñi, F. M. (2018). The physical properties of ceramides in membranes. *Annu. Rev. Biophys.* 47, 633–654. doi:10.1146/annurev-biophys-070317-033309

Blesbois, E., Douard, V., Germain, M., Boniface, P., and Pellet, F. (2004). Effects of n-3 polyunsaturated dietary supplementation on the reproductive capacity of male turkeys. *Theriogenology* 61, 537–549. doi:10.1016/S0093-691X(03)00207-3

Blesbois, E., Lessire, M., Grasseau, I., Hallouis, J. M., and Hermier, D. (1997). Effect of dietary fat on the fatty acid composition and on fertilizing ability of fowl semen. *Biol. Reprod.* 56, 5. doi:10.1095/biolreprod56.5.1216

Bligh, E. G., and Dyer, W. J. (1959). A rapid method of total lipid extraction and purification. *Can. J. Biochem. Physiol.* 37, 911–917. doi:10.1139/o59-099

Bongalhardo, D., Somnapan-Kakuda, N., and Buhr, M. (2002). Isolation and unique composition of purified head plasma membrane from rooster sperm. *Poult. Sci.* 81, 1877–1883. doi:10.1093/ps/81.12.1877

Bowling, E. R., Froman, D. P., Davis, A. J., and Wilson, J. L. (2003). Attributes of broiler breeder males characterized by low and high sperm mobility. *Poult. Sci.* 82, 1796–1801. doi:10.1093/ps/82.11.1796

Burrows, W. H., and Quinn, J. P. (1935). A method of obtaining spermatozoa from the domestic fowl. *Poult. Sci.* 14, 251–253. doi:10.3382/ps.0140251

Cerolini, S., Kelso, K. A., Noble, R. C., Speake, B. K., Pizzi, F., and Cavalchini, L. G. (1997). Relationship between spermatozoan lipid composition and

fertility during aging of chickens. *Biol. Reprod.* 57, 976–980. doi:10.1095/biolreprod57.5.976

Cerolini, S., Pizzi, F., Gliozzi, T., Maldjiani, A., Zaniboni, L., and Parodi, L. (2003). Lipid manipulation of chicken semen by dietary means and its relation to fertility: a review. *World's Poult. Sci. J.* 59, 65–75. doi:10.1079/wps20030003

Chen, S., Wang, M., Li, L., Wang, J., Ma, X., Zhang, H., et al. (2021). High-coverage targeted lipidomics revealed dramatic lipid compositional changes in asthenozoospermic spermatozoa and inverse correlation of ganglioside GM3 with sperm motility. *Reprod. Biol. Endocrinol.* 19, 105. doi:10.1186/s12958-021-00792-3

Degtyarenko, K., De Matos, P., Ennis, M., Hastings, J., Zbinden, M., McNaught, A., et al. (2007). ChEBI: a database and ontology for chemical entities of biological interest. *Nucleic Acids Res.* 36, D344–D350. doi:10.1093/nar/gkm791

Donoghue, A., Bakst, M., Holsberger, D., and Donoghue, D. (1995). Effect of semen storage on the number of spermatozoa in the perivitelline layer of laid Turkey eggs. *Reproduction* 105, 221–225. doi:10.1530/jrf.0.1050221

Douard, V., Hermier, D., and Blesbois, E. (2000). Changes in Turkey semen lipids during liquid *in vitro* storage. *Biol. Reprod.* 63, 1450–1456. doi:10.1095/biolreprod63.5.1450

Drobnis, E. Z., Crowe, L. M., Berger, T., Anchordoguy, T. J., Overstreet, J. W., and Crowe, J. H. (1993). Cold shock damage is due to lipid phase transitions in cell membranes: a demonstration using sperm as a model. *J. Exp. Zool.* 265, 432–437. doi:10.1002/jez.1402650413

Elokil, A. A., Bhuiyan, A. A., Liu, H.-Z., Hussein, M. N., Ahmed, H. I., Azmal, S. A., et al. (2019). The capability of L-carnitine-mediated antioxidant on cock during aging: evidence for the improved semen quality and enhanced testicular expressions of GnRH1, GnRHR, and melatonin receptors MT 1/2. *Poult. Sci.* 98, 4172–4181. doi:10.3382/ps/pez201

Fanani, M. L., and Maggio, B. (2017). The many faces (and phases) of ceramide and sphingomyelin I—single lipids. *Biophys. Rev.* 9, 589–600. doi:10.1007/s12551-017-0297-z

Froman, D., and Thurston, R. (1984). Decreased fertility resulting from treatment of fowl spermatozoa with neuraminidase or phospholipase C. *Poult. Sci.* 63, 2479–2482. doi:10.3382/ps.0632479

Froman, D. P., and Kirby, J. D. (2005). Sperm mobility: phenotype in roosters (*Gallus domesticus*) determined by mitochondrial function. *Biol. Reprod.* 72, 562–567. doi:10.1095/biolreprod.104.035113

Hagiuda, J., Ishikawa, H., Furuuchi, T., Hanawa, Y., and Marumo, K. (2014). Relationship between dyslipidaemia and semen quality and serum sex hormone levels: an infertility study of 167 Japanese patients. *Andrologia* 46, 131–135. doi:10.1111/and.12057

Jeulin, C., Soufir, J., Marson, J., Paquignon, M., and Dacheux, J. (1987). The distribution of carnitine and acetylcarnitine in the epididymis and epididymal spermatozoa of the boar. *Reproduction* 79, 523–529. doi:10.1530/jrf.0.0790523

Johannsson, A., Smith, G. A., and Metcalfe, J. C. (1981). The effect of bilayer thickness on the activity of (Na+, K+)-ATPase. *Biochim. Biophys. Acta* 641, 2. doi:10.1016/0005-2736(81)90498-3

Kelso, K. A., Cerolini, S., Noble, R. C., Sparks, N. H., and Speake, B. K. (1996). Lipid and antioxidant changes in semen of broiler fowl from 25 to 60 weeks of age. *J. Reprod. Fert.* 106, 201–206. doi:10.1530/jrf.0.1060201

Khoshvaght, A., Towhidi, A., Zare-shahneh, A., Noruozi, M., Zhandi, M., Dadashpour Davachi, N., et al. (2016). Dietary n-3 PUFAs improve fresh and post-thaw semen quality in Holstein bulls via alteration of sperm fatty acid composition. *Theriogenology* 85, 807–812. doi:10.1016/j.theriogenology.2015.10.023

Lemoine, M., Dupont, J., Guillory, V., Tesseraud, S., and Blesbois, E. (2009). Potential involvement of several signaling pathways in initiation of the chicken acrosome reaction. *Biol. Reprod.* 81, 657–665. doi:10.1095/biolreprod.108.072660

Long, J. A. (2014). "Applied andrology in chickens and turkeys," in *Anim. Ando: theories and applications*. Editors P. J. Chenoweth, and S. P. Lorton (CABI), 197–225.

Mills, K. M., Minton, A. M., and Ferreira, C. R. (2024). Adapting lipidomic sample processing methods for boars housed in commercial settings. *Transl. Anim. Sci.* 8, txae139. doi:10.1093/tas/txae139

Manier, M. K., Welch, G., Van Nispen, C., Bakst, M. R., and Long, J. (2019). Low-mobility sperm phenotype in the domestic turkey: Impact on sperm morphometry and early embryonic death. *Reprod. Dom. Anim.* 54, 3.

Mohammadi, V., Sharifi, S. D., Sharafi, M., Mohammadi-Sangcheshmeh, A., Shahverdi, A., and Alizadeh, A. (2021). Manipulation of fatty acid profiles in roosters' testes, alteration in sexual hormones, improvements in testicular histology characteristics and elevation sperm quality factor by L-carnitine. *Theriogenology* 161, 8–15. doi:10.1016/j.theriogenology.2020.10.005

Molenaar, M. R., Haaker, M. W., Vaandrager, A. B., Houweling, M., and Helms, J. B. (2023). Lipidomic profiling of rat hepatic stellate cells during activation reveals a two-stage process accompanied by increased levels of lysosomal lipids. *J. Biol. Chem.* 299, 103042. doi:10.1016/j.jbc.2023.103042

Molenaar, M. R., Jeucken, A., Wassenaar, T. A., van de Lest, C. H. A., Brouwers, J. F., and Helms, J. B. (2019). LION/web: a web-based ontology enrichment tool for lipidomic data analysis. *GigaScience* 8, giz061. doi:10.1093/gigascience/giz061

Musa, N. J., Ratchamak, R., Ratsiri, T., Vongpralub, T., Boonkum, W., Semaming, Y., et al. (2021). Lipid profile of sperm cells in Thai native and commercial roosters and its impact on cryopreserved semen quality. *Trop. Anim. Health Prod.* 53, 1.

Pinto, S. N., Silva, L. C., Futerman, A. H., and Prieto, M. (2011). Effect of ceramide structure on membrane biophysical properties: the role of acyl chain length and unsaturation. *BBA. Biomembr.* 1808, 2753–2760. doi:10.1016/j.bbamem.2011.07.023

Reddy, R. P. (1995). *Artificial insemination of broilers: economic and management implications*.

Reis, L. G., Casey, T. M., Sobreira, T. J. P., Cooper, B. R., and Ferreira, C. R. (2023). Step-by-step approach to build multiple reaction monitoring (MRM) profiling instrument acquisition methods for class-based lipid exploratory analysis by mass spectrometry. *J. Biomol. Tech.* 34, 3fc1f5fe.1972c438. doi:10.7171/3fc1f5fe.1972c438

Sebastian, S. M., Selvaraj, S., Aruldhas, M. M., and Govindarajulu, P. (1987). Pattern of neutral and phospholipids in the semen of normothermic, oligospermic and azoospermic men. *J. Reprod. Fert.* 79, 373–378. doi:10.1530/jrf.0.0790373

Shan, S., Xu, F., Bleyer, M., Becker, S., Melbaum, T., Wemheuer, W., et al. (2020). Association of α/β-Hydrolase D16B with bovine conception rate and sperm plasma membrane lipid composition. *Int. J. Mol. Sci.* 21 (2), 627. doi:10.3390/ijms21020627

Soufir, J. C., Marson, J., and Jouannet, P. (1981). Free L-carnitine in human seminal plasma. *Int. J. Androl.* 4, 388–397. doi:10.1111/j.1365-2605.1981.tb00723.x

Wolfe, C. A., James, P. S., Mackie, A. R., Ladha, S., and Jones, R. (1998). Regionalized lipid diffusion in the plasma membrane of mammalian spermatozoa. *Biol. Reprod.* 59, 1506–1514. doi:10.1095/biolreprod59.6.1506

Xia, J., Broadhurst, D. I., Wilson, M., and Wishart, D. S. (2013). Translational biomarker discovery in clinical metabolomics: an introductory tutorial. *Metabolomics* 9 (3), 280–299. doi:10.1007/s11306-012-0482-9

Xue, F., Liu, Y., Lv, Z., Zhang, J., Xiong, S., Zha, L., et al. (2022). Regulatory effects of differential dietary energy levels on spermatogenesis and sperm motility of yellow-feathered breeder cocks. *Front. Vet. Sci.* 9, 1.

Yang, G., Li, S., Zhao, Q., Chu, J., Zhou, B., Fan, S., et al. (2021). Transcriptomic and metabolomic insights into the variety of sperm storage in the oviduct of egg layers. *Poult. Sci.* 100, 6. doi:10.1016/j.psj.2021.101087

Zaniboni, L., and Cerolini, S. (2009). Liquid storage of Turkey semen: changes in quality parameters, lipid composition and susceptibility to induced *in vitro* peroxidation in control, n-3 fatty acids and alpha-tocopherol rich spermatozoa. *Anim. Reprod. Sci.* 112, 51–65. doi:10.1016/j.anireprosci.2008.04.002

frontiers | Frontiers in Physiology

TYPE Original Research
PUBLISHED 20 February 2025
DOI 10.3389/fphys.2025.1547188

OPEN ACCESS

EDITED BY
Krystyna Pierzchała-Koziec,
University of Agriculture in Krakow, Poland

REVIEWED BY
Kate Kosmac,
Augusta University, United States
Małgorzata Gumułka,
University of Agriculture in Krakow, Poland
Paul Siegel,
Virginia Tech, United States

*CORRESPONDENCE
Hui Yu,
yu.3859@osu.edu

RECEIVED 17 December 2024
ACCEPTED 03 February 2025
PUBLISHED 20 February 2025

CITATION
Yu H, Li Z, Yimiletey J, Wan C and Velleman S (2025) Molecular characterization of the heterogeneity of satellite cell populations isolated from an individual Turkey pectoralis major muscle.
Front. Physiol. 16:1547188.
doi: 10.3389/fphys.2025.1547188

Molecular characterization of the heterogeneity of satellite cell populations isolated from an individual Turkey pectoralis major muscle

Hui Yu*, Zhenyang Li, Joseph Yimiletey, Chunmei Wan and Sandra Velleman

Department of Animal Sciences, The Ohio State University, Columbus, OH, United States

Satellite cells (SCs) are myogenic stem cells responsible for post hatch muscle growth and the regeneration of muscle fibers. Satellite cells are not a homogenous population of cells within a muscle and have variable rates of proliferation and differentiation even within a single fiber type muscle like the turkey pectoralis major muscle. In this study, the single satellite cell clones derived from the same turkey pectoralis major muscle with different proliferation rates were compared. The clones were classified as either fast-growing (early clone) or slow-growing (late clone) SCs. To thoroughly examine the molecular differences between these two groups, RNA sequencing was conducted to compare their transcriptomes following 72 h of proliferation. Principal Component Analysis confirmed that the transcriptomic profiles of early- and late-clones are markedly distinct. Differential gene expression analysis identified over 5,300 genes that were significantly differentially expressed between the two groups of cells. Gene ontology analysis showed that genes highly expressed in early clones are responsible for the fundamental aspects of muscle biology, including muscle tissue development and structural maturation. Conversely, genes upregulated in late clones are involved in cell-cell communication, extracellular matrix interactions, signal ligand activity, and cytokine activity—key components for forming an extracellular niche essential for functional satellite cells maintenance. Further examination of specific gene ontology categories such as muscle structure development and extracellular matrix components indicated significant differences in gene expression patterns between early- and late-clones. These findings highlight the genetic and functional diversity of SCs in turkeys. The distinct roles of these satellite cell populations indicate that a balance between them is necessary for preserving the normal physiological functions of SCs.

KEYWORDS

satellite cells, heterogeneity, Turkey, pectoralis major muscle, RNAsequencing

1 Introduction

In food animal agriculture, it is crucial to identify mechanisms that can enhance the efficiency of muscle growth to meet human nutritional needs. In the United States, poultry is the most consumed type of meat, with consumption rates steadily increasing. Turkey meat, valued at approximately $6.57 billion, accounts for 10% of the poultry meat revenue, according to the United States Department of Agriculture (Poultry - Production and Value 2023 Summary) (NASS, 2023). Maintaining sustainability in our food supply chains is necessary for ensuring continuous food availability and improving the health and wellbeing of current and future populations. Sustainable production of animal protein is vital for meeting meat consumption demands (Duggan et al., 2023). In the commercial turkey industry, the breast muscle (pectoralis major muscle; p. major) is the most economically valuable muscle. Efficient development of the *p. major* muscle remains a primary focus in turkey breeding strategies.

In poultry, the mechanism that drive skeletal muscle development differ between the embryonic and post-hatch stages. During the embryonic stage, skeletal muscle develops through the proliferation and differentiation of myoblasts, which fuse to develop multinucleated myotubes. These myotubes then differentiate into mature muscle fibers, producing muscle-specific contractile proteins. Myofiber formation is complete at hatch (Smith, 1963), and further growth occurs through the addition of nuclei to existing fibers from satellite cells (SCs), the adult myoblasts, leading to the enlargement of fibers via hypertrophic growth (Moss and Leblond, 1971; Cardasis and Cooper, 1975). Once growth is complete, SCs enter a quiescent state (Schultz et al., 1978), remaining in their niche until they are activated to repair and regenerate damaged muscle fibers (Yin et al., 2013).

Initially identified by Mauro (1961), SCs are located between the sarcolemma and the basal lamina of myofibers and comprise a heterogenous population of muscle stem cells (Schultz, 1974; Biressi and Rando, 2010; Tierney and Sacco, 2016). Khodabukus and Baar (Khodabukus and Baar, 2015) observed that SCs originating from slow and fast myofibers express corresponding slow and fast contractile proteins and retain the metabolic characteristics of their original myofibers. Even within the same regenerating muscle fiber, SCs divide asymmetrically, producing two distinct daughter cells—one that retains the capacity for stem cell self-renewal and another that commits to proliferation and differentiation (Kuang et al., 2007; Ono et al., 2010). SCs isolated from turkey lines with different growth rates show distinct responses to thermal stress and exhibit altered transcriptomic profiles (Reed et al., 2022a; Reed et al., 2022b). Notably, selective breeding for enhanced growth and increased breast muscle yield in turkeys has transformed the satellite cell (SC) population in the p.major muscle into cells with higher proliferation and differentiation rates, along with an elevated adipogenic potential (Clark et al., 2017; Velleman and Coy, 2020; Xu et al., 2021b).

The turkey p.major muscle consists homogeneous Type IIb fibers; however, even within this single fiber-type muscle, McFarland et al. (1995). identified significant heterogeneity among SCs. In this study, 73 distinct SCs were isolated from the *p. major* muscle of a 6-week-old Nicholas tom turkey. Each single-cell clone was cultured, expanded, and categorized based on its proliferation rate. The fastest-growing cells reached 65% confluency within 17 days (early clones), whereas the slowest-growing cells required 30 days to reach the same confluency level (slow clones), highlighting substantial variability in growth rates among the isolated cells. Subsequent biological analyses revealed that the early clones exhibited greater responsiveness to fibroblast growth factor 2 stimulation and expressed higher levels of *fibroblast growth factor receptor 1* at the onset of proliferation. During differentiation, these cells also showed elevated production of heparan sulfate proteoglycan (McFarland et al., 2003). Furthermore, a follow-up study demonstrated that the early clones were more sensitive to the inhibitory effects of transforming growth factor beta on both proliferation and differentiation compared to the slower-growing late cells (Yun et al., 1997). Based on these previous findings, we hypothesized that early and late clones represent two genetically distinct populations characterized by fundamentally different transcriptomic profiles. These intrinsic genetic differences likely drive their varied responses to biological stimuli, influencing key processes such as proliferation, differentiation, and responsiveness to growth factors and signaling molecules. To test this hypothesis, we compared the transcriptional differences between the early and late clones after 72 h proliferation. Gene functional analysis was conducted to characterize the key molecular pathways and mechanisms that differentiate the 2 cell populations. Uncovering the satellite cell-mediated mechanisms involved in the development of the *p. major* muscle will facilitate the development of strategies to promote animal growth and meat production.

2 Materials and methods

2.1 Turkey myogenic satellite cells

The satellite cell clones utilized in the current study were previously developed by McFarland et al. (1995). Briefly, SCs were isolated from the pectoralis major muscle of a 6-week-old Nicholas tom turkey, sourced from a local producer raising them for consumption purposes. These SCs were suspended in McCoy's 5A medium, and individual cells were selected and transferred to a 96-well cell culture plate using the Quixell cell manipulator robotic system (Stoelting Co., Wood Dale, IL). This instrument utilizes a micropipette to isolate individual suspended SCs and place them into wells to growth cell clones. These clones were categorized based on their proliferation rates. Clones that reached confluency within 17–19 days in a 25 cm^2 tissue culture flask were considered as early clones, reflecting their fast growth/proliferation rates. In contrast, clones requiring 28–29 days to achieve confluency were classified as slow clones, indicative of slower growth/proliferation rates. All clones were preserved in liquid nitrogen for future use.

The early and late clones were cultured as described previously (Reed et al., 2017; Xu et al., 2021b). Briefly, the same number of cells were plated and incubated at 38°C for 24 h in plating medium consisting of Dulbecco's Modified Eagle's Medium (D5523, Sigma Aldrich, St. Louis, MO), 10% chicken serum (C5405, Sigma Aldrich, St. Louis, MO), 5% horse serum (H1270, Sigma Aldrich, St. Louis, MO), 1% antibiotics-antimycotics (30004CI, Corning, New York, NY), and 0.1% gentamicin (GT-10, Omega Scientific, Tarzana, CA). After 24 h, the cells were changed to a feeding medium consisting of

McCoy's 5A Medium (M4892, Sigma Aldrich, St. Louis, MO), 10% chicken serum, 5% horse serum, 1% antibiotics-antimycotics, and 0.1% gentamicin, and cultured at 38°C for an additional 72 h. The growth medium was refreshed every 24 h during this 72-h proliferation period. At harvest, the cell medium was removed, and the cells were washed twice with phosphate-buffered saline before being collected into TRIzol Reagent (15596018, ThermoFisher, Waltham, WA) and stored at −80°C until RNA isolation.

2.2 RNA isolation and sequencing

Total RNA was isolated from each sample using TRIzol Reagent, following the manufacturer's instructions. RNA integrity and quantification were assessed at The Genomics Shared Resource, The Ohio State University, using the Agilent 2,100 Bioanalyzer. Only RNA samples with an RNA Integrity Number (RIN) greater than 9 were sent to Innomics Inc. (Sunnyvale, CA). for sequencing. Sequencing was performed on the DNBSEQ platform with stranded paired-end 150 bp reads. Four replicates were included for each cell line.

2.3 RNAseq data analysis

Quality control checks on raw sequence data from each sample were performed with FastQC (v0.12.1) (Andrews, 2010). Reads were aligned to reference turkey genome (UMD 5.1, ENSEMBL Annotation 111) using STAR (v2.7.11b) with default parameters (Dobin et al., 2013). All samples passed the post-alignment quality check (QualiMap v.2.3) (Okonechnikov et al., 2016). The DEseq2 (Love et al., 2014) method was used for differential expression analysis comparing early and late clones. The adjusted p-value was calculated using the default "BH" setting in DESeq2, which controls the false discovery rate (FDR)—the expected proportion of false discoveries among the rejected hypotheses. The FDR is a less stringent condition than the family-wise error rate, making these methods more powerful compared to others (Benjamini and Hochberg, 1995).

Gene identifiers for annotated genes were obtained through an iterative process from multiple sources. Primarily, these identifiers were sourced directly from the ENSEMBL annotations. For genes lacking corresponding ENSEMBL IDs, annotations were obtained from Dr. Kent M. Reed and relevant publications from his research group (Reed et al., 2017; Barnes et al., 2019; Reed et al., 2022a; Reed et al., 2022b). Gene ontology analysis was performed using g: Profiler (available at https://biit.cs.ut.ee/gprofiler/gost) (Kolberg et al., 2023). The input consisted of genes with a log fold change (logFC) greater than 2 and a $P < 0.01$. *Meleagris gallopavo* (Turkey) was selected as the reference genome for the analysis. The g: SCS algorithm was used for computing multiple testing correction for p-values gained from GO and pathway enrichment analysis. The top five Gene Ontology (GO) terms were presented in Figure 3. The specific gene ontology terms related to muscle structure development, extracellular matrix, signaling receptor activator activity, and cytoskeletal protein binding were retrieved from EBI QuickGO database (https://www.ebi.ac.uk/QuickGO/). The PANTHER Overrepresentation Test (Protein Analysis Through Evolutionary Relationships, Version 19.0, released on 2024–06–20) was conducted using the PANTHER database (https://pantherdb.org/). *Gallus gallus* was selected as the reference organism and reference gene list. The analysis employed Fisher's Exact Test with Bonferroni correction for multiple testing. The top five GO terms identified are presented in Tables 1, 2. The input genes were selected based on a Log_2FC greater than 2 and a $P < 0.05$.

3 Results

3.1 Summary of overall gene expression

Total RNA was extracted from both early clones (n = 4) and late clones (n = 4), with each sample comprising pooled material from 3 wells to construct individual barcoded libraries. Sequencing generated over 257 million 150 bp paired-end reads (SRA BioProject: PRJNA1196520). The number of reads per library ranged from 28.6 to 35.3 million, with an average of 32.2 million (Table 1). The average proportion of nucleotides with a quality score above 20 (Q20) was over 98.5%, and those with a quality score above 30 (Q30) averaged 95.5%. The results from replicate libraries were consistent.

Evidence of expression (at least one mapped read per library) was observed for an average of 13,565 genes, with a nearly equal distribution between early clones (13,581) and late clones (13,549). Over 82% of the reads uniquely mapped to the turkey genome (Table 1). We conducted Bartlett's test of sphericity, with a result of $p < 0.0001$, and the Kaiser-Meyer-Olkin (KMO) test, with an overall KMO of 0.91. These results suggest that the data is suitable for factor analysis. Subsequently, we carried out principal component analysis (PCA), which revealed distinct clustering of early and late clones along the first two principal components based on normalized read counts, as visualized in Figure 1A. This analysis highlights the substantial variations between the 2 cell populations. Technical replicates clustered closely as nearest neighbors within the PCA space, confirming the validity of pooling replicates for expression analysis. Heatmaps, organized by early and late clones, revealed a distinct separation between the two groups while preserving the relationships within each group of cells (Figure 1B), further supporting the significant differences between early and late clones.

3.2 Differential gene expression

Differences in gene expression between the 2 cell populations are illustrated by the distribution of unique and shared expressed genes, as shown in the Bland-Altman plot (MA plot) in Figure 2A. The MA plot displays the log ratio (M) of gene expression against the average expression (A) to visualize differences between the two groups. A total of 5,347 genes were identified as differentially expressed genes (DEGs) with an adjusted $p < 0.05$; of these, 2,675 genes were upregulated in late clones and 2,672 genes were upregulated in early clones. A more detailed analysis of these DEGs, using a stringent fold change threshold of $|Log_2FC| > 2$ and an adjusted $p < 0.001$, identified 181 genes upregulated in late clones and 199 genes upregulated in early clones. This finding highlights the

TABLE 1 Summary of RNAseq data for 72 h proliferation experiment. For each library the total number of raw reads, Q20 (%), Q30 (%), the number of observed genes (mapped reads >1) by library and the percentage of uniquely mapped reads are given.

Cell line	Replicates	PE reads	Q20 (%)	Q30 (%)	GC content (%)	Observed genes	Uniquely mapped reads %
Early Clones	1	28,649,147	98.74	96.53	48.51	13,431	82.11%
	2	28,867,578	98.77	96.62	48.35	13,500	83.28%
	3	32,174,596	98.67	96.26	48.27	13,679	83.42%
	4	35,349,407	98.81	96.71	48.30	13,712	83.35%
Late Clones	1	34,603,174	98.74	96.50	48.03	13,611	86.44%
	2	33,454,390	98.69	96.39	48.19	13,545	86.35%
	3	33,739,352	98.74	96.49	48.14	13,541	86.03%
	4	30,894,176	98.74	96.55	48.95	13,497	84.48%

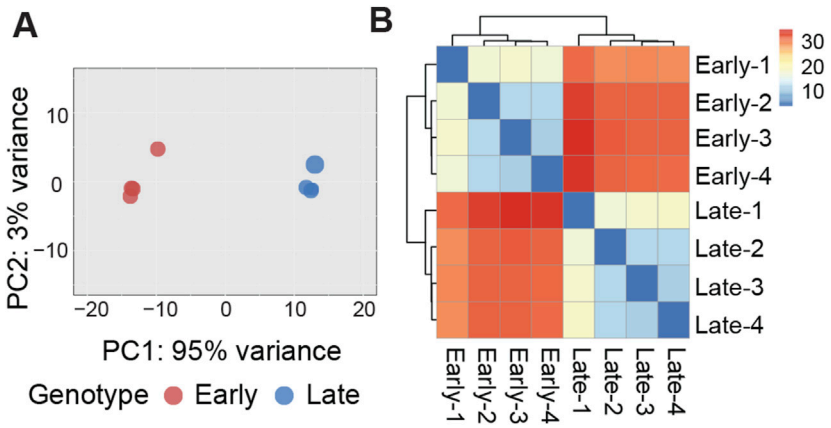

FIGURE 1
(A) Graphical representation of the first (PC1) and second (PC2) principal components (PC) affecting gene expression patterns in early and late cell clones. **(B)** Heatmap of sample-to-sample distance matrix showing the dissimilarities between early clones and late clones and the similarity between samples within each clone.

substantial differences between early and late clones, despite both exhibiting a similar number of differentially expressed genes (Figure 2B).

3.3 Gene functional analysis

Gene functional enrichment analysis was conducted on differentially expressed genes using two resources: the PATHER (Protein Analysis Through Evolutionary Relationships) knowledgebase and g:Profiler (g: GOSt Functional Profiling). The PATHER overrepresentation test applied genes mapped to chicken (*Gallus gallus*) gene sets, while g:Profiler analysis used turkey (*M. gallopavo*) as the input organism. The use of both resources ensured that the functional analysis results were validated against orthologous chicken gene sets, providing consistency and robust validation of the findings. For the analysis, DEGs with a fold change threshold of $|Log_2FC| > 2$ and an adjusted $p < 0.05$ were included in the PATHER analysis, while a more stringent adjusted $p < 0.01$ with the same fold change threshold was applied in the g:Profiler analysis.

The analysis of upregulated genes in late clones using g:Profiler (Figure 3A) revealed significant enrichment across various categories. In the GO Molecular Functions category, the most significant enrichments were observed for cell receptor ligand activity ($-\log_{10}$ (adjusted p-value) = 5.38), signaling receptor activator activity ($-\log_{10}$ (adjusted p-value) = 5.35), cytokine activity ($-\log_{10}$ (adjusted p-value) = 4.72), and molecular function activator activity ($-\log_{10}$ (adjusted p-value) = 3.04). For the GO Cellular Components category, the highest enrichment scores were found for the extracellular region ($-\log_{10}$ (adjusted p-value) = 15.04), extracellular space ($-\log_{10}$ (adjusted p-value) = 5.28), and cellular anatomical entity ($-\log_{10}$ (adjusted p-value) = 1.64). These findings align with results from the KEGG pathways, where extracellular-receptor interaction featured prominently ($-\log_{10}$ (adjusted p-value) = 5.79). In the GO Biological Processes category, notable enrichments were linked to functions such as cell communication ($-\log_{10}$ (adjusted p-value) = 5.29), signaling ($-\log_{10}$ (adjusted p-value) = 5.10), tube development ($-\log_{10}$ (adjusted p-value) = 4.68), and vasculature development ($-\log_{10}$ (adjusted p-value) = 4.50).

In contrast to the gene enrichment profile observed in late clones, the early clones exhibit a distinct pattern of enrichment

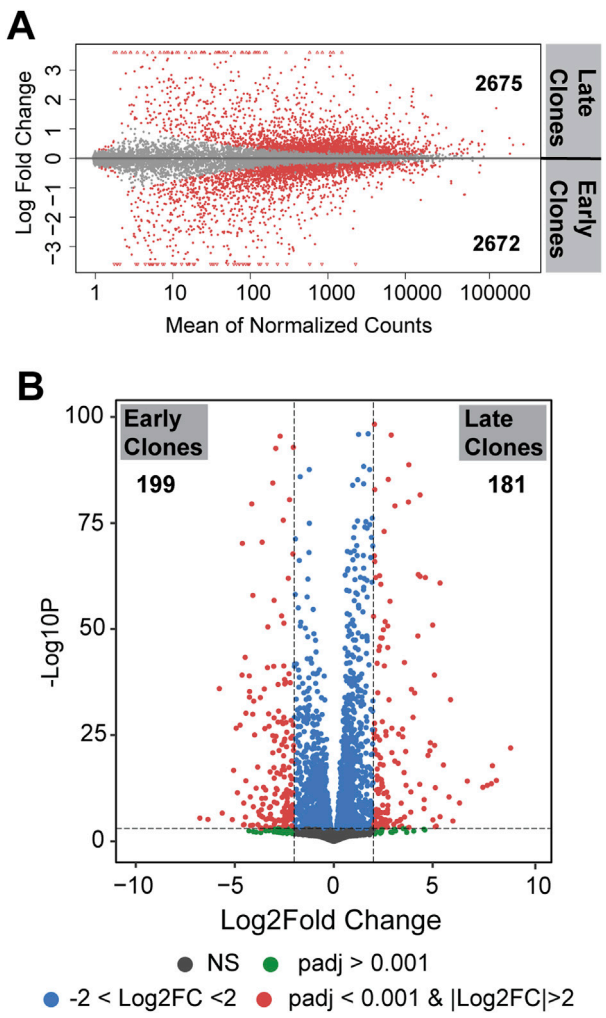

FIGURE 2
(A) MA plot (Bland-Altman plot) depicting differentially expressed genes on a logarithmic scale. Genes with $p < 0.05$ are labeled in red. The number indicated the upregulated genes in each clones. **(B)** Volcano plot presenting differentially expressed genes. Genes with $p < 0.001$ and $|Log_2FC| > 2$ are labeled in red.

(Figure 3B). The top enrichments in the GO Biological Processes category are primarily associated with muscle cell function and development, including muscle cell differentiation ($-log_{10}$ (adjusted p-value) = 1.76), muscle structure development ($-log_{10}$ (adjusted p-value) = 1.54), and skeletal muscle organ development ($-log_{10}$ (adjusted p-value) = 1.47). In the GO Molecular Function category, notable enrichments include cytoskeletal protein binding ($-log_{10}$ (adjusted p-value) = 2.32) and axon guidance receptor activity ($-log_{10}$ (adjusted p-value) = 1.30). Meanwhile, the GO Cellular Components category shows significant enrichment in cell periphery ($-log_{10}$ (adjusted p-value) = 1.51), plasma membrane ($-log_{10}$ (adjusted p-value) = 1.47), and receptor complex ($-log_{10}$ (adjusted p-value) = 1.39).

The examination of upregulated genes in late clones (146 IDs mapped to the *G. gallus* gene set, Table 2) using PATHER revealed significant enrichments in the GO Molecular Function category. The top enrichments included extracellular matrix structural constituent conferring tensile strength (27.33-fold, p = 9.13E-06), extracellular matrix structural constituent (17.49-fold, p = 3.08E-05), growth factor activity (12.58-fold, p = 6.56E-08), integrin binding (12.34-fold, p = 2.92E-03), and cytokine activity (8.97-fold, p = 8.06E-05). Within the GO Biological Processes category, extracellular matrix organization (9.70-fold, p = 8.30E-05) and skeletal system development (6.25-fold, p = 2.17E-02) emerged as the top two most highly expressed terms. For the GO Cellular Components category, significant enrichments were observed in the basement membrane (11.93-fold, p = 1.07E-02) and extracellular space (5.36-fold, p = 3.79E-16).

The analysis of upregulated genes in early clones (133 IDs mapped to the *G. gallus* gene set, Table 3) using PATHER revealed a different pattern compared to late clones. In the GO Cellular Components category, the top enrichments were associated with muscle structure, specifically myofilament (26.33-fold, p = 1.36E-02) and sarcomere (8.13-fold, p = 2.50E-02). These findings align with the muscle development functions identified in the g:Profiler analysis (Figure 3B). However, the GO Molecular Function and Biological Process categories in PATHER highlighted a unique emphasis on nervous system establishment. In the GO Molecular Function category, the top enrichments included axon guidance receptor activity (71.09-fold, p = 1.12E-02) and acetylcholine-gated monoatomic cation-selective channel activity (25.39-fold, p = 2.03E-04). Similarly, in the GO Biological Processes category, the terms with the highest expression were excitatory postsynaptic potential (18.85-fold, p = 3.48E-04) and chemical synaptic transmission (18.03-fold, p = 4.79E-04).

Given the significant differences observed in the functional annotation of DEGs between early and late clones, we conducted a detailed analysis of individual gene ontology terms to further validate our findings. Using results from g:Profiler, we focused on gene ontology categories associated with upregulated genes in late clones, including the extracellular matrix (GO:0031012) and signaling receptor pathway (GO:0030546). Among the 1,502 genes associated with the extracellular matrix, 291 were identified in our dataset, and their expression patterns, as visualized in a heatmap, revealed clear distinctions between early and late clones (Supplementary Figure S1A). Similarly, of the 1,530 genes related to the signaling receptor pathway, 163 were mapped in our dataset, with their heatmap also showing distinct patterns between the two groups (Supplementary Figure S1B). In parallel, we examined two gene ontology terms associated with upregulated genes in early clones: muscle structure development (GO:0061061) and cytoskeletal protein binding (GO:008092). From the muscle structure development category, 229 out of 1,793 genes were detected in our dataset. The corresponding heatmap (Supplementary Figure S2A) highlighted distinct expression differences between early and late clones (Supplementary Figure S2A). Likewise, of the 2,484 genes associated with cytoskeletal protein binding, 665 were mapped in our dataset. The heatmap for these genes (Supplementary Figure S2B) further highlighted the divergent expression patterns between the two clones.

3.4 Top expressed genes in the 2 cell populations

The 40 most significant differentially expressed genes with the greatest expression differences between the 2 cell populations are

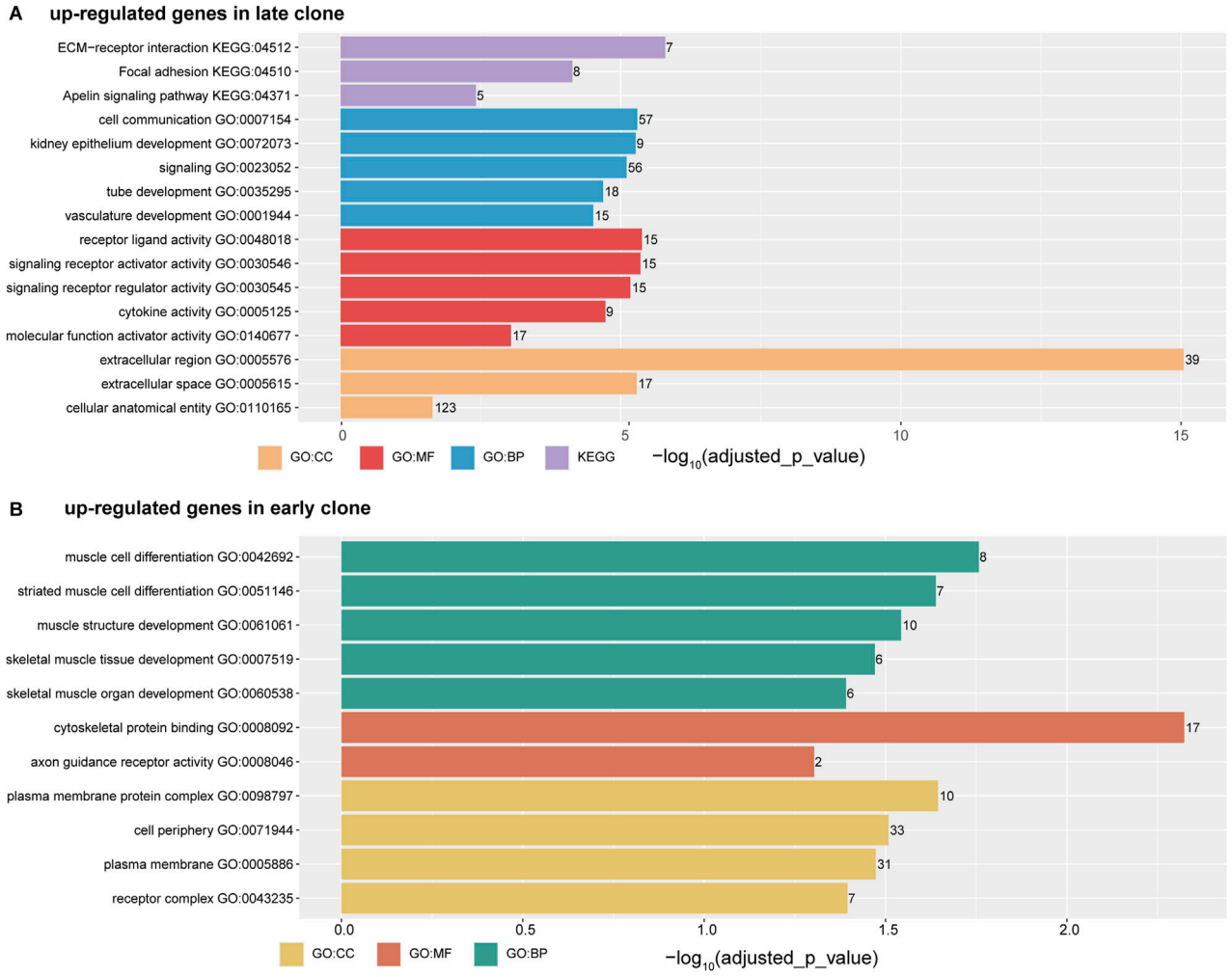

FIGURE 3
The horizontal bar chart illustrates the top five ontology terms, categorized into CC (Cellular Components), MF (Molecular Functions), BP (Biological Processes), and KEGG (Kyoto Encyclopedia of Genes and Genomes) pathways. The x-axis represents the -$\log_{10}$ (adjusted *p*-value), while the numbers displayed on each bar indicate the number of genes associated with each term. **(A)** Functional analysis of genes upregulated in late clones. **(B)** Functional analysis of genes upregulated in early clones.

presented in Figure 4. Among these, the most highly upregulated gene in late clones ($Log_2FC = 8.60$) was identified as an ortholog of *avian beta-defensin 4* (*AvBD4*). In chickens, this gene is part of a 14-member family of antimicrobial peptides known for their broad-spectrum activity and critical role in the innate immune system (Sugiarto and Yu, 2004). Also upregulated was *homeobox B3* (*HOXB3*, $Log_2FC = 7.88$), a member of the HOX gene family, which is linked to embryonic development, as well as the progression of diseases and cancers (Chan et al., 2005; Alharbi et al., 2013; Chen et al., 2013). Another upregulated gene, *Platelet-Derived Growth Factor C* (*PDGFC*, $Log_2FC = 7.68$), plays a key role in tissue remodeling, angiogenesis, and embryonic development (Reigstad et al., 2005). The *Prostaglandin Endoperoxide Synthase 2*, also known as *Cyclooxygenase 2* (*PTGS2/COX2*, $Log_2FC = 5.37$), plays a crucial role in inflammatory signaling pathologies. Its induction leads to the production of Prostaglandin E2, essential for effective skeletal muscle stem cell function, enhancing regeneration and muscle strength (Ho et al., 2017; Martin-Vazquez et al., 2023).

The top upregulated gene in early clones is an ortholog of *Von Willebrand Factor D and EGF Domain-Containing Protein* (*VWDE*, $Log_2FC = -6.77$), which is predicted to facilitate signaling receptor binding activity and play a role in anatomical structure development (Alliance of Genome Resources, 2024). Additionally, several upregulated genes in early clones are linked to neuronal excitability and synaptic function. These include *Potassium Calcium-Activated Channel Subfamily N Member 1* (*KCNN1*, $Log_2FC = -5.78$), *Potassium Voltage-Gated Channel Interacting Protein 1* (*KCNIP1*, $Log_2FC = -5.12$), and *Potassium Sodium-Activated Channel Subfamily T Member 1* (*KCNT1*, $Log_2FC = -4.55$). The upregulation of the muscle-specific gene *Myosin 18B* (*MYO18B*, $Log_2FC = -4.93$) suggests a role for early clones in sarcomere integrity and assembly (Berger et al., 2017). Furthermore, the association of *MYO18B* with certain myopathies highlights the potential involvement of early clones in both normal muscle function and disease (Alazami et al., 2015; Malfatti et al., 2015).

10.3389/fphys.2025.1547188

TABLE 2 PANTHER Overrepresentation test of upregulated DEGs in the late clones after 72 h of proliferation. Shown are the gene ontology categories with the greatest fold enrichment in the GO biological process category.

Upregulated gene ontology terms in late clones					
	Gallus gallus (18366)	Turkey DEG (146 out of 168)	Expected	Fold enrichment	*p*-value
GO molecular function					
Extracellular matrix structural constituent conferring tensile strength (GO:0030020)	28	7	0.26	27.33	0.000
Extracellular matrix structural constituent (GO:0005201)	50	8	0.46	17.49	0.000
Growth factor activity (GO:0008083)	113	13	1.03	12.58	0.000
Integrin binding (GO:0005178)	62	7	0.57	12.34	0.003
Cytokine activity (GO:0005125)	134	11	1.23	8.97	0.000
GO Biological Process					
Extracellular matrix organization (GO:0030198)	124	11	1.13	9.70	0.000
Skeletal system development (GO:0001501)	175	10	1.60	6.25	0.022
Cell adhesion (GO:0007155)	474	19	4.34	4.38	0.000
Animal organ development (GO:0048513)	856	27	7.83	3.45	0.000
Cell surface receptor signaling pathway (GO:0007166)	1,027	28	9.39	2.98	0.001
GO Cellular Component					
Basement membrane (GO:0005604)	55	6	0.50	11.93	0.011
Extracellular space (GO:0005615)	831	41	7.65	5.36	0.000

3.5 Expression of genes associated with muscle growth and SC function

Since the two SC populations were categorized by distinct cell proliferation rates, and McFarland et al. (2003) reported that early clones are more responsive to fibroblast growth factor 2 (FGF2), showing higher gene expression levels of *FGF2* and *FGF receptor-1* (*FGFR1*) at the onset of proliferation compared to slower-growing cells, we specifically examined the expression of *FGF2* and *FGFR1*. While there was no significant difference in *FGF2* expression ($Log_2FC = 0.12$), fast-growing SCs exhibited marked higher expression of *FGFR1* ($Log_2FC = -1.74$), consistent with the earlier report. Additionally, we analyzed the expression of other FGF family genes, including *FGF10, FGF12, FGF13, FGF16, FGF19,* and *FGF22*, and found no significant differences between the 2 cell populations. Intriguingly, *FGFBP1*, a secreted molecule that functions to chaperone FGF ligands from the extracellular matrix to cognate receptors—thereby enhancing the biological activity of FGF ligands—was significantly elevated in slow-growing SCs ($Log_2FC = 4.45$), suggesting a possible alternative pathway in slow-growing cells to mediate FGF signaling (Abuharbeid et al., 2006; Briones et al., 2006).

In addition to the FGF gene family, we also explored the expression of receptors associated with insulin-like growth factors (IGFs), including the IGF1 receptor (IGF1R) and the IGF-binding protein (IGFBP) family. IGFs are known for their diverse roles as endocrine, paracrine, and autocrine factors that are crucial for cell growth, proliferation, differentiation, and survival (Allard and Duan, 2018). Although the changes were statistically significant, late clones exhibited an increase in *IGF1R* expression ($Log_2FC = 0.29$) and a more pronounced upregulation of *IGFBP5* ($Log_2FC = 1.69$). Notably, overexpression of *Igfbp5* has been shown to induce delayed muscle development in mice (Salih et al., 2004), suggesting that the significant elevation of *IGFBP5* in slow-growing SCs may play a role in their reduced proliferation rates.

Notch signaling is crucial for regulating SC functions such as proliferation, differentiation, and self-renewal. Activation of HES1 through this pathway modulates the transcription of the myogenic transcription factor *MYOD1* and the Notch ligand *DLL1*, thereby modulating the activation state of SCs (Gioftsidi et al., 2022; Vargas-Franco et al., 2022). Our analysis of key genes involved in Notch signaling revealed increased levels of *HES1* ($Log_2FC = -2.19$), *MYOD1* ($Log_2FC = -0.64$), and *DLL1* ($Log_2FC = -2.10$) in fast-growing SCs, indicating constitutive activation of the Notch signaling pathway in these cells. Additionally, an elevated expression of the *MYOG* (myogenin, $Log_2FC = -1.51$) gene, one of the key factors regulating myogenesis, was observed in the fast-growing SCs. However, the expression of the transcription factor *PAX7* ($Log_2FC = 0.04$), a marker associated with SC proliferation, remained similar between the two SC populations. Taken together, the activation of Notch signaling and the increased expression of *MYOD1* and *MYOG* likely contribute to the enhanced proliferation and differentiation capabilities of fast-growing satellite cells.

4 Discussion

Over the past several decades, selective breeding for accelerated growth performance in poultry has produced faster-growing lines

TABLE 3 PANTHER Overrepresentation test of upregulated DEGs in the early clones after 72 h of proliferation. Shown are the gene ontology categories with the greatest fold enrichment in the GO biological process category.

Upregulated gene ontology terms in early clones					
	Gallus gallus (18366)	Turkey DEG (133 out of 155)	Expected	Fold enrichment	*p*-value
GO molecular function					
Axon guidance receptor activity (GO:0008046)	5	3	0.04	71.09	0.011
Acetylcholine-gated monoatomic cation-selective channel activity (GO:0022848)	28	6	0.24	25.39	0.000
Semaphorin receptor binding (GO:0030215)	25	5	0.21	23.70	0.004
Transmitter-gated monoatomic ion channel activity involved in regulation of postsynaptic membrane potential (GO: 1904315)	49	8	0.41	19.35	0.000
Excitatory extracellular ligand-gated monoatomic ion channel activity (GO:0005231)	43	6	0.36	16.53	0.003
GO biological process					
Excitatory postsynaptic potential (GO:0060079)	44	7	0.37	18.85	0.000
Chemical synaptic transmission, postsynaptic (GO:0099565)	46	7	0.39	18.03	0.000
Neural crest cell development (GO:0014032)	54	6	0.46	13.17	0.027
Regulation of postsynaptic membrane potential (GO:0060078)	65	7	0.55	12.76	0.005
Stem cell development (GO:0048864)	56	6	0.47	12.70	0.033
GO cellular component					
Myofilament (GO:0036379)	18	4	0.15	26.33	0.014
Sarcomere (GO:0030017)	102	7	0.86	8.13	0.025
Postsynaptic membrane (GO:0045211)	156	9	1.32	6.84	0.007
Plasma membrane region (GO:0098590)	511	16	4.31	3.71	0.007
Neuron projection (GO:0043005)	620	17	5.23	3.252	0.020

with enhanced breast muscle development compared to non-selected slow-growing lines (Havenstein et al., 2007). Growth-selected turkeys exhibit increased myofiber diameter and reduced connective tissue spacing in the p.major muscle compared to non-selected counterparts (Velleman et al., 2003). However, alongside this selection, reports of undesirable muscle fiber damages, such as deep pectoral myopathy and focal myopathy (Siller, 1985; Wilson et al., 1990), have emerged. These observed alterations in p.major muscle development, growth trajectory and morphological characteristics possibly correlate with changes in the SC populations intrinsic to the p.major muscle (Ferreira et al., 2020; Pejskova et al., 2024). Indeed, previous comparative investigations between faster-growing Nicholas Commercial (NC) turkeys and random-bred populations demonstrated that SCs derived from NC turkeys exhibit enhanced proliferative and differentiation capacities, elevated intracellular lipid content, and increased susceptibility to thermal stress (Xu et al., 2021a; Xu et al., 2021b).

Satellite cells are not a homogenous population of cells (Feldman and Stockdale, 1991; Kuang et al., 2007; Ono et al., 2010). McFarland et al. (1995) identified substantial intrinsic heterogeneity among SC populations derived from the same p.major muscle, demonstrating variability in proliferative and differentiative rates as well as differential growth factor responsiveness. Building on the SCs isolated in McFarland et al. (1995) study, the current research investigated the transcriptomic differences between the SC populations with different proliferation rate. The results indicated substantial transcriptomic differences between the 2 cell populations. Specifically, over 5,000 genes exhibited differential expression, with 2,675 genes upregulated in late clones and 2,672 genes upregulated in early clones. Gene ontology analysis from two independent sources highlighted substantial differences. Pathways prevalent in early clones were primarily associated with the establishment of fundamental muscle structure and cytoskeletal development. Conversely, the functional analysis of late clones revealed pathways involved in extracellular receptor interactions, cell communication, signaling, and cytokine activity. These functional annotations suggest that SCs exhibit considerable functional diversity. The maintenance of normal muscle homeostasis depends on a balance between these distinct SC populations. The current study is the first to genetically characterize two distinct SC populations from the same turkey p. major muscle.

Nutrient availability influences SC activity, which in turn affects muscle development and structural changes. Studies have

FIGURE 4
Expression levels of the top 20 genes with the most significant differences between early and late clones. The Log_2FC for each gene is shown (adjusted *p*-value <0.05).

demonstrated that reduced nutrient availability diminishes SC proliferation and differentiation, resulting in lower body weight and *p. major* muscle mass (Halevy et al., 2000; Mozdziak et al., 2002; Halevy et al., 2003; Powell et al., 2013; Harthan et al., 2014). Furthermore, the *p. major* muscles from chicks subjected to feed restriction during the first week post-hatch exhibit increased muscle fiber necrosis and adipose deposition, along with altered expression of myogenic transcriptional regulatory factors that control SC proliferation and differentiation (Velleman et al., 2010; Velleman et al., 2014a). Interestingly, if nutrient restriction is initiated in the second week post-hatch, these adverse effects on myogenic gene expression, muscle fat content, and morphological structure are not observed (Velleman et al., 2014a; Velleman et al., 2014b). These findings suggested that nutrition affects SC biology and that this effect is time sensitive. Therefore, a future direction of the current study is to investigate whether nutrition could affect early and late clones differently. While the current studies have genetically characterized two populations of SCs, we believe there are additional distinct populations of SCs, as suggested by numerous publications from human biomedical research (Dell'Orso et al., 2019; Barruet et al., 2020; Sousa-Victor et al., 2022). Consequently, it is crucial to identify and characterize more SC populations in turkey *p. major* muscles. A further step is to explore whether specific nutritional supplements can enhance the growth of particular SC populations. Moreover, it is important to assess the overall contribution of SC heterogeneity to muscle growth and development. By understanding these dynamics, we can potentially develop nutritional strategies to optimize muscle growth in livestock, thereby improving meat quality and production efficiency.

The Organization for Economic Co-operation and Development (OECD) and the Food and Agricultural Organization (FAO) of the United Nations, (2023) predicts that the global population will grow by 11% from 7.9 billion in 2022 to 8.6 billion in 2032. Concurrently, global meat production is projected to increase by 15% by 2032, with poultry meat anticipated to represent 48% of this growth over the next decade (OECD/FAO, 2023). This underscores the poultry industry's need to enhance animal growth and meat production. Given the critical role of SCs in driving muscle growth, future nutrition and breeding strategies should incorporate considerations of SC dynamics to optimize these processes effectively.

5 Conclusion

This study has identified specific genes and gene pathways that differentiate fast-growing and slow-growing satellite cells, isolated from single-cell colony expansions. Our RNA-seq analysis offers a snapshot of gene expression changes along a continuum, which may correspond to functional variations in gene products. The transcriptomic profiles of early and late clones show significant differences, associated with distinct functional annotations. We hypothesize that normal muscle function and homeostasis are sustained by delicate balances among different SC populations. Disruption of this equilibrium could hamper muscle growth and may lead to reduced meat production. Further research is needed to definitively determine how SC heterogeneity contributes to the overall muscle growth.

Data availability statement

The data presented in the study are deposited in BioProject repository, accession number PRJNA1196520. The data has released to public and can be accessed at https://www.ncbi.nlm.nih.gov/bioproject/PRJNA1196520.

Ethics statement

The animal study was approved by the South Dakota State University Animal Care and Use Committee. The study was conducted in accordance with the local legislation and institutional requirements.

Author contributions

HY: Conceptualization, Formal Analysis, Funding acquisition, Investigation, Methodology, Project administration, Resources, Software, Supervision, Validation, Visualization, Writing–original draft, Writing–review and editing. ZL: Data curation, Writing–original draft. JY: Data curation, Resources,

Writing–original draft. CW: Data curation, Resources, Writing–original draft. SV: Conceptualization, Resources, Writing–review and editing.

Funding

The author(s) declare that financial support was received for the research, authorship, and/or publication of this article. This research was supported through Start-Up funding provided by The Ohio State University (Department of Animal Sciences) to HY

Acknowledgments

The authors thank Cindy Coy for technical assistance in culturing the satellite cells used in this study. The authors thank Kent M. Reed for help with gene annotation.

Conflict of interest

The authors declare that the research was conducted in the absence of any commercial or financial relationships that could be construed as a potential conflict of interest.

The author(s) declared that they were an editorial board member of Frontiers, at the time of submission. This had no impact on the peer review process and the final decision.

Generative AI statement

The authors declare that no Generative AI was used in the creation of this manuscript.

Publisher's note

Supplementary material

The Supplementary Material for this article can be found online at: https://www.frontiersin.org/articles/10.3389/fphys.2025.1547188/full#supplementary-material

References

Abuharbeid, S., Czubayko, F., and Aigner, A. (2006). The fibroblast growth factor-binding protein FGF-BP. *Int. J. Biochem. Cell Biol.* 38 (9), 1463–1468. doi:10.1016/j.biocel.2005.10.017

Alazami, A. M., Kentab, A. Y., Faqeih, E., Mohamed, J. Y., Alkhalidi, H., Hijazi, H., et al. (2015). A novel syndrome of Klippel-Feil anomaly, myopathy, and characteristic facies is linked to a null mutation in MYO18B. *J. Med. Genet.* 52 (6), 400–404. doi:10.1136/jmedgenet-2014-102964

Alharbi, R. A., Pettengell, R., Pandha, H. S., and Morgan, R. (2013). The role of HOX genes in normal hematopoiesis and acute leukemia. *Leukemia* 27 (5), 1000–1008. doi:10.1038/leu.2012.356

Allard, J. B., and Duan, C. (2018). IGF-binding proteins: why do they exist and why are there so many? *Front. Endocrinol. (Lausanne)* 9, 117. doi:10.3389/fendo.2018.00117

Alliance of Genome Resources, C (2024). Updates to the alliance of genome resources central infrastructure. *Genetics* 227 (1), iyae049. doi:10.1093/genetics/iyae049

Andrews, S. (2010). FASTQC. A quality control tool for high throughput sequence data.

Barnes, N. E., Mendoza, K. M., Strasburg, G. M., Velleman, S. G., and Reed, K. M. (2019). Thermal challenge alters the transcriptional profile of the breast muscle in Turkey poults. *Poult. Sci.* 98 (1), 74–91. doi:10.3382/ps/pey401

Barruet, E., Garcia, S. M., Striedinger, K., Wu, J., Lee, S., Byrnes, L., et al. (2020). Functionally heterogeneous human satellite cells identified by single cell RNA sequencing. *Elife* 9, e51576. doi:10.7554/eLife.51576

Benjamini, Y., and Hochberg, Y. (1995). Controlling the false discovery rate: a practical and powerful approach to multiple testing. *J. R. Stat. Soc. Ser. B Methodol.* 57 (1), 289–300. doi:10.1111/j.2517-6161.1995.tb02031.x

Berger, J., Berger, S., Li, M., and Currie, P. D. (2017). Myo18b is essential for sarcomere assembly in fast skeletal muscle. *Hum. Mol. Genet.* 26 (6), 1146–1156. doi:10.1093/hmg/ddx025

Biressi, S., and Rando, T. A. (2010). Heterogeneity in the muscle satellite cell population. *Semin. Cell Dev. Biol.* 21 (8), 845–854. doi:10.1016/j.semcdb.2010.09.003

Briones, V. R., Chen, S., Riegel, A. T., and Lechleider, R. J. (2006). Mechanism of fibroblast growth factor-binding protein 1 repression by TGF-beta. *Biochem. Biophys. Res. Commun.* 345 (2), 595–601. doi:10.1016/j.bbrc.2006.04.052

Cardasis, C. A., and Cooper, G. W. (1975). An analysis of nuclear numbers in individual muscle fibers during differentiation and growth: a satellite cell-muscle fiber growth unit. *J. Exp. Zool.* 191 (3), 347–358. doi:10.1002/jez.1401910305

Chan, K. K., Chen, Y. S., Yau, T. O., Fu, M., Lui, V. C., Tam, P. K., et al. (2005). Hoxb3 vagal neural crest-specific enhancer element for controlling enteric nervous system development. *Dev. Dyn.* 233 (2), 473–483. doi:10.1002/dvdy.20347

Chen, J., Zhu, S., Jiang, N., Shang, Z., Quan, C., and Niu, Y. (2013). HoxB3 promotes prostate cancer cell progression by transactivating CDCA3. *Cancer Lett.* 330 (2), 217–224. doi:10.1016/j.canlet.2012.11.051

Clark, D. L., Strasburg, G. M., Reed, K. M., and Velleman, S. G. (2017). Influence of temperature and growth selection on Turkey pectoralis major muscle satellite cell adipogenic gene expression and lipid accumulation. *Poult. Sci.* 96 (4), 1015–1027. doi:10.3382/ps/pew374

Dell'Orso, S., Juan, A. H., Ko, K. D., Naz, F., Perovanovic, J., Gutierrez-Cruz, G., et al. (2019). Single cell analysis of adult mouse skeletal muscle stem cells in homeostatic and regenerative conditions. *Development* 146 (12), dev174177. doi:10.1242/dev.174177

Dobin, A., Davis, C. A., Schlesinger, F., Drenkow, J., Zaleski, C., Jha, S., et al. (2013). STAR: ultrafast universal RNA-seq aligner. *Bioinformatics* 29 (1), 15–21. doi:10.1093/bioinformatics/bts635

Duggan, B. R. J., Avendaño, S., Neeteson, A.-M., Burnside, T., and Koerhuis, A. (2023). Decades of breeding for welfare and sustainability,.).

Feldman, J. L., and Stockdale, F. E. (1991). Skeletal muscle satellite cell diversity: satellite cells form fibers of different types in cell culture. *Dev. Biol.* 143 (2), 320–334. doi:10.1016/0012-1606(91)90083-f

Ferreira, T. Z., Kindlein, L., Flees, J. J., Shortnacy, L. K., Vieira, S. L., Nascimento, V. P., et al. (2020). Characterization of pectoralis major muscle satellite cell population heterogeneity, macrophage density, and collagen infiltration in broiler chickens affected by wooden breast. *Front. Physiol.* 11, 529. doi:10.3389/fphys.2020.00529

Gioftsidi, S., Relaix, F., and Mourikis, P. (2022). The Notch signaling network in muscle stem cells during development, homeostasis, and disease. *Skelet. Muscle* 12 (1), 9. doi:10.1186/s13395-022-00293-w

Halevy, O., Geyra, A., Barak, M., Uni, Z., and Sklan, D. (2000). Early posthatch starvation decreases satellite cell proliferation and skeletal muscle growth in chicks. *J. Nutr.* 130 (4), 858–864. doi:10.1093/jn/130.4.858

Halevy, O., Nadel, Y., Barak, M., Rozenboim, I., and Sklan, D. (2003). Early posthatch feeding stimulates satellite cell proliferation and skeletal muscle growth in Turkey poults. *J. Nutr.* 133 (5), 1376–1382. doi:10.1093/jn/133.5.1376

Harthan, L. B., McFarland, D. C., and Velleman, S. G. (2014). The effect of nutritional status and myogenic satellite cell age on Turkey satellite cell proliferation, differentiation, and expression of myogenic transcriptional regulatory factors and

heparan sulfate proteoglycans syndecan-4 and glypican-1. *Poult. Sci.* 93 (1), 174–186. doi:10.3382/ps.2013-03570

Havenstein, G. B., Ferket, P. R., Grimes, J. L., Qureshi, M. A., and Nestor, K. E. (2007). Comparison of the performance of 1966- versus 2003-type turkeys when fed representative 1966 and 2003 Turkey diets: growth rate, livability, and feed conversion. *Poult. Sci.* 86 (2), 232–240. doi:10.1093/ps/86.2.232

Ho, A. T. V., Palla, A. R., Blake, M. R., Yucel, N. D., Wang, Y. X., Magnusson, K. E. G., et al. (2017). Prostaglandin E2 is essential for efficacious skeletal muscle stem-cell function, augmenting regeneration and strength. *Proc. Natl. Acad. Sci. U. S. A.* 114 (26), 6675–6684. doi:10.1073/pnas.1705420114

Khodabukus, A., and Baar, K. (2015). Contractile and metabolic properties of engineered skeletal muscle derived from slow and fast phenotype mouse muscle. *J. Cell Physiol.* 230 (8), 1750–1757. doi:10.1002/jcp.24848

Kolberg, L., Raudvere, U., Kuzmin, I., Adler, P., Vilo, J., and Peterson, H. (2023). g: Profiler-interoperable web service for functional enrichment analysis and gene identifier mapping (2023 update). *Nucleic Acids Res.* 51 (W1), W207–W212. doi:10.1093/nar/gkad347

Kuang, S., Kuroda, K., Le Grand, F., and Rudnicki, M. A. (2007). Asymmetric self-renewal and commitment of satellite stem cells in muscle. *Cell* 129 (5), 999–1010. doi:10.1016/j.cell.2007.03.044

Love, M. I., Huber, W., and Anders, S. (2014). Moderated estimation of fold change and dispersion for RNA-seq data with DESeq2. *Genome Biol.* 15 (12), 550. doi:10.1186/s13059-014-0550-8

Malfatti, E., Bohm, J., Lacene, E., Beuvin, M., Romero, N. B., and Laporte, J. (2015). A premature stop codon in MYO18B is associated with severe nemaline myopathy with cardiomyopathy. *J. Neuromuscul. Dis.* 2 (3), 219–227. doi:10.3233/JND-150085

Martin-Vazquez, E., Cobo-Vuilleumier, N., Lopez-Noriega, L., Lorenzo, P. I., and Gauthier, B. R. (2023). The PTGS2/COX2-PGE(2) signaling cascade in inflammation: pro or anti? A case study with type 1 diabetes mellitus. *Int. J. Biol. Sci.* 19 (13), 4157–4165. doi:10.7150/ijbs.86492

Mauro, A. (1961). Satellite cell of skeletal muscle fibers. *J. Biophys. Biochem. Cytol.* 9 (2), 493–495. doi:10.1083/jcb.9.2.493

McFarland, D., Gilkerson, K., Pesall, J., Walker, J., and Yun, Y. (1995). Heterogeneity in growth characteristics of satellite cell populations. *Cytobios* 82 (328), 21–27.

McFarland, D. C., Liu, X., Velleman, S. G., Zeng, C., Coy, C. S., and Pesall, J. E. (2003). Variation in fibroblast growth factor response and heparan sulfate proteoglycan production in satellite cell populations. *Comp. Biochem. Physiol. C Toxicol. Pharmacol.* 134 (3), 341–351. doi:10.1016/s1532-0456(02)00272-7

Moss, F. P., and Leblond, C. P. (1971). Satellite cells as the source of nuclei in muscles of growing rats. *Anat. Rec.* 170 (4), 421–435. doi:10.1002/ar.1091700405

Mozdziak, P. E., Walsh, T. J., and McCoy, D. W. (2002). The effect of early posthatch nutrition on satellite cell mitotic activity. *Poult. Sci.* 81 (11), 1703–1708. doi:10.1093/ps/81.11.1703

Nass, U. S. D. o.A. (2023). Poultry - production and value 2023 summary

OECD/FAO (2023). *OECD-FAO agricultural outlook 2023–2032*. Paris, France: OECD Publishing, 20–76+184–201.

Okonechnikov, K., Conesa, A., and Garcia-Alcalde, F. (2016). Qualimap 2: advanced multi-sample quality control for high-throughput sequencing data. *Bioinformatics* 32 (2), 292–294. doi:10.1093/bioinformatics/btv566

Ono, Y., Boldrin, L., Knopp, P., Morgan, J. E., and Zammit, P. S. (2010). Muscle satellite cells are a functionally heterogeneous population in both somite-derived and branchiomeric muscles. *Dev. Biol.* 337 (1), 29–41. doi:10.1016/j.ydbio.2009.10.005

Pejskova, L., Pisconti, A., Lunde, M., Ho, K. Y., Solberg, N. T., Koga, S., et al. (2024). Wooden breast myopathy is characterized by satellite cell dysfunction and syndecan-4 shedding. *Front. Physiol.* 15, 1513311. doi:10.3389/fphys.2024.1513311

Powell, D. J., McFarland, D. C., Cowieson, A. J., Muir, W. I., and Velleman, S. G. (2013). The effect of nutritional status on myogenic satellite cell proliferation and differentiation. *Poult. Sci.* 92 (8), 2163–2173. doi:10.3382/ps.2013-03107

Reed, K. M., Mendoza, K. M., Abrahante, J. E., Barnes, N. E., Velleman, S. G., and Strasburg, G. M. (2017). Response of Turkey muscle satellite cells to thermal challenge. I. transcriptome effects in proliferating cells. *BMC Genomics* 18 (1), 352. doi:10.1186/s12864-017-3740-4

Reed, K. M., Mendoza, K. M., Strasburg, G. M., and Velleman, S. G. (2022a). Transcriptome response of proliferating muscle satellite cells to thermal challenge in commercial Turkey. *Front. Physiol.* 13, 970243. doi:10.3389/fphys.2022.970243

Reed, K. M., Mendoza, K. M., Xu, J., Strasburg, G. M., and Velleman, S. G. (2022b). Transcriptome response of differentiating muscle satellite cells to thermal challenge in commercial Turkey. *Genes (Basel)* 13 (10), 1857. doi:10.3390/genes13101857

Reigstad, L. J., Varhaug, J. E., and Lillehaug, J. R. (2005). Structural and functional specificities of PDGF-C and PDGF-D, the novel members of the platelet-derived growth factors family. *FEBS J.* 272 (22), 5723–5741. doi:10.1111/j.1742-4658.2005.04989.x

Salih, D. A., Tripathi, G., Holding, C., Szestak, T. A., Gonzalez, M. I., Carter, E. J., et al. (2004). Insulin-like growth factor-binding protein 5 (Igfbp5) compromises survival, growth, muscle development, and fertility in mice. *Proc. Natl. Acad. Sci. U. S. A.* 101 (12), 4314–4319. doi:10.1073/pnas.0400230101

Schultz, E. (1974). A quantitative study of the satellite cell population in postnatal mouse lumbrical muscle. *Anat. Rec.* 180 (4), 589–595. doi:10.1002/ar.1091800405

Schultz, E., Gibson, M. C., and Champion, T. (1978). Satellite cells are mitotically quiescent in mature mouse muscle: an EM and radioautographic study. *J. Exp. Zool.* 206 (3), 451–456. doi:10.1002/jez.1402060314

Siller, W. G. (1985). Deep pectoral myopathy: a penalty of successful selection for muscle growth. *Poult. Sci.* 64 (8), 1591–1595. doi:10.3382/ps.0641591

Smith, J. H. (1963). Relation of body size to muscle cell size and number in the chicken,. *Poult. Sci.* 42 (2), 283–290. doi:10.3382/ps.0420283

Sousa-Victor, P., Garcia-Prat, L., and Munoz-Canoves, P. (2022). Control of satellite cell function in muscle regeneration and its disruption in ageing. *Nat. Rev. Mol. Cell Biol.* 23 (3), 204–226. doi:10.1038/s41580-021-00421-2

Sugiarto, H., and Yu, P. L. (2004). Avian antimicrobial peptides: the defense role of beta-defensins. *Biochem. Biophys. Res. Commun.* 323 (3), 721–727. doi:10.1016/j.bbrc.2004.08.162

Tierney, M. T., and Sacco, A. (2016). Satellite cell heterogeneity in skeletal muscle homeostasis. *Trends Cell Biol.* 26 (6), 434–444. doi:10.1016/j.tcb.2016.02.004

Vargas-Franco, D., Kalra, R., Draper, I., Pacak, C. A., Asakura, A., and Kang, P. B. (2022). The Notch signaling pathway in skeletal muscle health and disease. *Muscle Nerve* 66 (5), 530–544. doi:10.1002/mus.27684

Velleman, S. G., Anderson, J. W., Coy, C. S., and Nestor, K. E. (2003). Effect of selection for growth rate on muscle damage during Turkey breast muscle development. *Poult. Sci.* 82 (7), 1069–1074. doi:10.1093/ps/82.7.1069

Velleman, S. G., and Coy, C. S. (2020). Research Note: effect of selection for body weight on the adipogenic conversion of Turkey myogenic satellite cells by Syndecan-4 and its covalently attached N-glycosylation chains. *Poult. Sci.* 99 (2), 1209–1215. doi:10.1016/j.psj.2019.12.029

Velleman, S. G., Coy, C. S., and Emmerson, D. A. (2014a). Effect of the timing of posthatch feed restrictions on broiler breast muscle development and muscle transcriptional regulatory factor gene expression. *Poult. Sci.* 93 (6), 1484–1494. doi:10.3382/ps.2013-03813

Velleman, S. G., Coy, C. S., and Emmerson, D. A. (2014b). Effect of the timing of posthatch feed restrictions on the deposition of fat during broiler breast muscle development. *Poult. Sci.* 93 (10), 2622–2627. doi:10.3382/ps.2014-04206

Velleman, S. G. N. K. E. C. C. S., Harford, I., and Anthony, N. B. (2010). Effect of posthatch feed restriction on broiler breast muscle development and muscle transcriptional regulatory factor gene and heparan sulfate proteoglycan expression. *Int. J. Poult. Sci.* 9 (5), 417–425. doi:10.3923/ijps.2010.417.425

Wilson, B. W., Nieberg, P. S., Buhr, R. J., Kelly, B. J., and Shultz, F. T. (1990). Turkey muscle growth and focal myopathy. *Poult. Sci.* 69 (9), 1553–1562. doi:10.3382/ps.0691553

Xu, J., Strasburg, G. M., Reed, K. M., and Velleman, S. G. (2021a). Effect of temperature and selection for growth on intracellular lipid accumulation and adipogenic gene expression in Turkey pectoralis major muscle satellite cells. *Front. Physiol.* 12, 667814. doi:10.3389/fphys.2021.667814

Xu, J., Strasburg, G. M., Reed, K. M., and Velleman, S. G. (2021b). Response of Turkey pectoralis major muscle satellite cells to hot and cold thermal stress: effect of growth selection on satellite cell proliferation and differentiation. *Comp. Biochem. Physiol. A Mol. Integr. Physiol.* 252, 110823. doi:10.1016/j.cbpa.2020.110823

Yin, H., Price, F., and Rudnicki, M. A. (2013). Satellite cells and the muscle stem cell niche. *Physiol. Rev.* 93 (1), 23–67. doi:10.1152/physrev.00043.2011

Yun, Y., McFarland, D. C., Pesall, J. E., Gilkerson, K. K., Vander Wal, L. S., and Ferrin, N. H. (1997). Variation in response to growth factor stimuli in satellite cell populations. *Comp. Biochem. Physiol. A Physiol.* 117 (4), 463–470. doi:10.1016/s0300-9629(96)00404-5

frontiers | Frontiers in Physiology

TYPE Original Research
PUBLISHED 20 February 2025
DOI 10.3389/fphys.2025.1543469

OPEN ACCESS

EDITED BY
Sandra G. Velleman,
The Ohio State University, United States

REVIEWED BY
Koichi J. Homma,
Teikyo University, Japan
Thomas Pike,
University of Lincoln, United Kingdom

*CORRESPONDENCE
Farina Lingstädt,
farina.lingstaedt@ruhr-uni-bochum.de
Jonas Rose,
jonas.rose@ruhr-uni-bochum.de

RECEIVED 11 December 2024
ACCEPTED 29 January 2025
PUBLISHED 20 February 2025

CITATION
Lingstädt F, Apostel A and Rose J (2025) "Distribution of dominant wavelengths predicts jackdaw (*Corvus monedula*) color discrimination performance". *Front. Physiol.* 16:1543469. doi: 10.3389/fphys.2025.1543469

"Distribution of dominant wavelengths predicts jackdaw (*Corvus monedula*) color discrimination performance"

Farina Lingstädt*, Aylin Apostel and Jonas Rose*

Neural Basis of Learning, Department of Psychology, Ruhr University Bochum, Bochum, Germany

Color vision is an important perceptual ability in most species and a crucial capacity underlying any cognitive task working with color stimuli. Birds are known for their outstanding vision and tetrachromacy. Two jackdaws were trained to indicate whether they perceive two colors as same or different. The dominant wavelengths of the experimental colors were assessed to relate the birds' performance to the physical qualities of the stimuli. The results indicate that the differences or similarities in dominant wavelengths of the colors had a strong influence on the behavioral data. Colors related to a reduced discriminatory performance were colors of particularly close wavelengths, whereas differences in saturation or brightness were less relevant. Overall, jackdaws mostly relied on hue to discriminate color pairs, and their behavior strongly reflected the physical composition of the color set. These findings show that when working with color stimuli, not only the perceptual abilities of the particular species, but also the technical aspects concerning the color presentation have to be considered carefully.

KEYWORDS

color discrimination, jackdaws (*Corvus monedula*), color vision, psychophysics, dominant wavelength, color stimuli

Introduction

Birds are highly visual animals (even caricatured as "eyes with wings", see Jones et al., 2007; Martin, 2012) and possess a complex visual system comprising not only three (as in humans and some other primate species; Jacobs, 2009), but four distinct photoreceptor pigments, which in some bird species has already been shown to enable tetrachromatic vision (Kelber et al., 2003). In modern cognitive neuroscience, various avian species are used in a wide range of studies probing cognitive abilities such as working memory (e.g., Diekamp et al., 2002 with pigeons and Hahn et al., 2021 with crows), categorization (e.g., Apostel et al., 2023a with jackdaws and Wasserman et al., 2023 with pigeons), and numerosity (e.g., Kobylkov et al., 2022 with chicks and Wagener et al., 2018 with crows). Almost all these studies use colorful visual stimuli displayed on computer monitors. For us as humans, this represents a clear and vivid illustration of the experimental approach. However, it is fundamental to also consider the specific visual capabilities of each bird species and general differences from trichromats (Hart and Hunt, 2007). We propose that objective measures of physical stimulus properties and psychophysical assessments of color discrimination are needed to more accurately interpret and understand experimental results in the work with avian subjects.

Corvids in particular show remarkable abilities in higher cognitive functions, such as working memory (Hahn et al., 2021; Veit et al., 2014), categorization (Apostel et al., 2023a; Vernouillet et al., 2021), rule-guided behavior (Veit and Nieder, 2013; Wilson et al., 1985), episodic-like memory (Clayton and Dickinson, 1998; Emery and Clayton, 2004), and tool use (Rutz and St. Clair, 2013; Rutz et al., 2016). Despite their focus on higher cognition, studies researching cognitive abilities such as working memory capacity also need to consider the perceptual abilities of their research subjects. This is especially relevant for studies targeting working memory, since change-detection paradigms use color among the items' properties to probe capacity limitations (e.g., Balakhonov and Rose, 2017). A recent study on working memory in jackdaws, members of the corvid family, investigated the effects of enhanced memory demands on the accuracy of color working memory representations (Apostel et al., 2023b). Not only have the authors demonstrated similar biases towards categorical representations of color between corvids and primates, but they also discussed differences in color perception and the importance of avian calibrated experimental conditions. We intend to build up on this discussion, by assessing the color discrimination performance of jackdaws and its relationship to the physical properties of the experimental colors.

It is well established that the visual spectrum of several bird species includes ultraviolet light (Hart and Hunt, 2007; Kelber, 2019). However, an assessment of how this influences the perception of the remaining colors is mostly lacking (with the exception of hummingbird color vision, see Herrera et al., 2008; Stoddard et al., 2020). So far, only few attempts of an actual psychometric assessment of color discrimination abilities in birds were made that span only a small range of species (see Wright, 1972 for pigeons; Stoddard et al., 2020 for hummingbirds and Olsson et al., 2015 for chickens). The results obtained so far make it apparent that psychometric functions of color discrimination obtained in one bird species are not necessarily transferable to others. Additionally, avian species most used in higher cognitive tasks, such as parrots and corvids, have not been properly assessed in this regard. In order to accurately assess the performance of corvids in cognitive tasks involving colored stimulation, the current study investigated the color discrimination abilities of jackdaws using methods of color generation and presentation that were also used in other studies (see, e.g., Apostel et al., 2023b). To better interpret the performance of the birds with respect to the specific stimulus set, the main physical characteristics of the colors, dominant wavelength, luminance, and saturation, were assessed and correlated with the discrimination curve obtained from the behavioral data.

We found that the performance of the birds in the color discrimination task was mostly dependent on hue, with luminance and saturation only accounting for a small part of the variance in the data. Additionally, we confirmed previously reported challenges in color display (Bae et al., 2014) – color stimuli created to be isoluminant and with equidistant hues deviated significantly from the actual colors rendered on a PC screen, even though this screen was specifically chosen for its distinctive color rendering and display quality. This study highlights both the need for species-specific evaluations of color discrimination as well as thorough assessments of the physical characteristics of the color stimuli to better interpret experimental data.

Methods

Subjects

The subjects of this study were two jackdaws, approximately 3.5 years of age. They came from the same hand-raised colony and were thus exposed to the same environment while growing up. The subjects were randomly chosen from a larger social group housed in a spacious indoor aviary with a 12-h day and night cycle and unrestricted access to water and grit. During the behavioral training and experimental sessions, access to food was restricted according to a food protocol that allowed food-pellets (BEO special, Vitrakraft) to be used as reward. On days without training or testing, food was given *ad libitum*. All experimental procedures and housing conditions were carried out in accordance with the National Institutes of Health Guide for Care and Use of Laboratory Animals and were authorized by the national authority (LANUV).

Behavioral setup

The behavioral experiments were performed in a Skinner box with a size of 71 cm (width), by 48 cm (depth) by 80 cm (height). The box was equipped with a 27″ monitor (AW2720HF, dell Alienware) and a 29 cm (width) by 49 cm (height) infrared touch frame (PQ Labs G4). The experiments were conducted in completely dark conditions within the Skinner box, illuminated only by the visual display from the monitor. The birds were positioned on a perch 14 cm away from the monitor, their behavior was remotely monitored with an IP camera (Edimax), and correct responses were rewarded with a custom-made automatic pellet feeder (https://www.ngl.psy.ruhr-uni-bochum.de/ngl/shareware/pellet-feeder.html.en). All experiments were controlled by custom MATLAB code, using the OTBR (Otto and Rose, 2023) and Psychophysics (Brainard and Vision, 1997) toolboxes. The digital input and output to and from the controlling PC were handled by a custom-built microcontroller (ODROID).

Color stimuli

The experimental colors used in this study were generated using MATLAB, where they were defined in the HSV color space. Saturation and value were set to 1, because only clear spectral colors were needed (Figure 1A). Hue was split into 64 equally spaced colors using the full range to create a gamut (full circular color range, Figure 1B). HSV values were then transformed into RGB values (for display purposes) using built-in MATLAB functions, and further into the CIE-XYZ values to calculate the theoretical dominant wavelength of each color (CIE, 1932). CIE, short for 'international commission of illumination', represents efforts made to develop a color space that is standardized to human perception. By matching a given light source with three independent red, green and blue lights, color matching functions were obtained that represent the standard observer's perceived proportions of each light in any given color. By doing so, a color space that matches the physical properties of a color to the human psychophysical perception was created (Shaw and Fairchild, 2002). For the present study, calculations of dominant wavelengths were

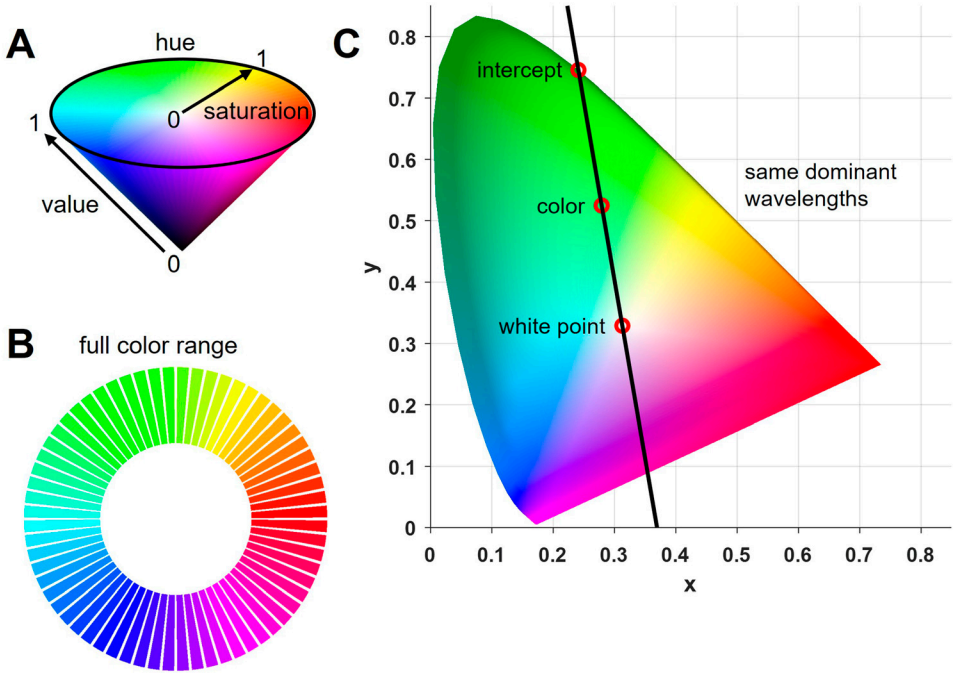

FIGURE 1
Experimental colors. **(A)** A full range of colors, or gamut, was obtained by diving hue in the HSV color space into 64 equidistant angles and setting saturation and value to 1, thereby creating full spectral colors. **(B)** Full color range (gamut) used in the experiment (64 colors). **(C)** CIE chromaticity diagram including the white point D65 and an example color (derived from converting the RGB values into CIE-XYZ values) from the full gamut. A linear function was fitted through both to create an intercept with the outer spectral color line. All colors on this line have the same dominant wavelength which can be obtained by identifying the intercept and its corresponding wavelength in standardized tables.

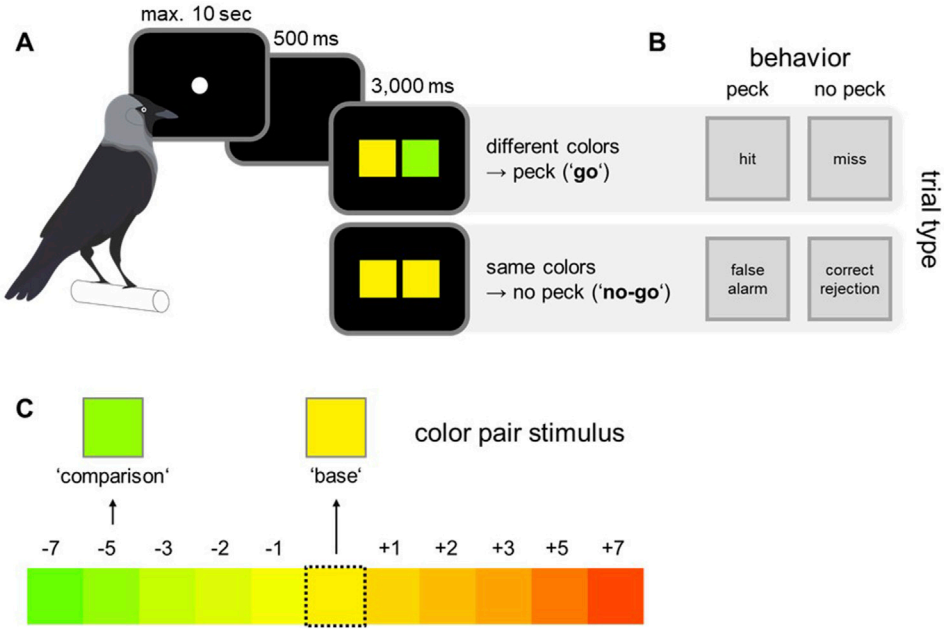

FIGURE 2
Experimental paradigm, overview of behavioral responses and color pair selection. **(A)** The birds were trained on a go/no-go paradigm. To start a trial, the birds pecked the initialization stimulus. In "go" trials the correct behavior was to directly peck on the monitor, whereas in "no-go" trials the birds had to wait for a second test array before responding. **(B)** Depending on experimental condition and behavioral response, four distinct response types could be differentiated: hit, miss, false alarm, and correct rejections. **(C)** Out of the whole gamut, one color was randomly selected as base color. The corresponding comparison color was randomly selected within a range of 7 adjacent colors in both directions of the color wheel, resulting in 10 distinct color steps, representing distinct color pair differences.

based on the D65 white point (for stimuli displayed on a computer monitor) and x and y coordinates of each experimental color (derived from CIE-XYZ values). By fitting a linear function to all experimental colors (going through both, the respective color and D65), the dominant wavelength could be determined from the intercept of the resulting line and the spectral color line (Figure 1C; see Malacara, 2002). The normative data about which wavelength corresponds to which exact point on the spectral color line was obtained from standardized tables (Stockman and Sharpe, 2000).

To compare the values of calculated dominant wavelengths with the actual colors displayed on the monitor, post-hoc measurements were conducted using a spectroradiometer (Konica Minolta Chroma Meter CS-150). For these measurements, color stimuli were presented on the monitor in the same way as they were presented as sample stimulus in the behavioral paradigm (the same color shown twice as in the 'no go' condition, Figure 2A). For each color, 10 measurements of wavelength, luminance and saturation were taken in darkness, and averaged.

Behavioral paradigm

The birds were trained on a go/no-go paradigm with specific color pairs. The task was to indicate whether two simultaneously presented colors were perceived as same or different. To obtain a food reward, the birds had to respond to color arrays showing different color hues or withhold from pecking until a second test array appeared if the two presented colors were different (Figure 2A).

To initiate each trial, the birds had to peck on a small white circle (initialization stimulus, Figure 2A). After a delay of 500 ms, two colored squares were displayed for 3,000 ms (size: five by 5 cm, left: base color; right: comparison color). In such a go/no go paradigm, four response types could be distinguished (Figure 2B). If both squares were of different color (go trials), the correct response was to peck anywhere on the monitor (hit). In no-go trials, the birds had to wait for a second test array to be presented (correct rejection) before pecking (color squares of test 2 were always different). The birds were rewarded for correct pecks and received a brief monitor flash and short time-out as error signal if they pecked in no-go trials (false alarm) or missed to respond in go trials (miss). Since the second test array in no-go trials always contained different colors, the birds could receive a reward in these trials as well, which ensured that the birds did not simply stop responding in no-go trials.

The number of go and no-go trials was balanced in each experimental session and the order of trial types was pseudo-randomized. Further, the color pairs for each trial were chosen pseudo-randomly. Pseudo-randomization was done to ensure that the same trial type or color combination did not occur more than three times consecutively. Every color pair consisted of a base color, which was chosen out of the whole range of all 64 colors, and a comparison color (Figure 2C). The comparison color was chosen out of a defined set of 10 colors for every base color (resulting in 10 distinct color steps, representing distinct color pair differences). This set was defined by the relative distance of all comparison colors to the respective base color. Each comparison color was either 1, 2, 3, 5 or 7 steps away from the base color in both directions of the color wheel (Figure 2C).

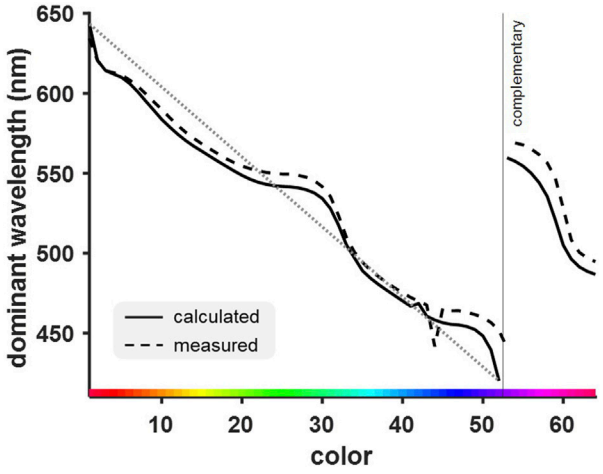

FIGURE 3
Calculated and measured dominant (and complementary) wavelengths of the experimental colors deviated from an ideal linear relationship (grey dotted line) between wavelength and color. This deviation was more pronounced for measured wavelengths, which further included the color distortion of the computer monitor. Reduced slopes for certain green and blue hues indicate a higher similarity of colors within these wavelength ranges (color ID 22-34, and 41-52, respectively).

Data collection and analysis

A period of training was done in the beginning to ensure that the birds perform the go/no go task. They were only presented with three colors that were chosen out of the full range of 64 colors with a maximum distance in hue. The training period ended, once the birds performed on this above 60% correct responses (overall, hits and correct rejections). For the final collection of data, the whole gamut of colors was used as base color from the beginning. The comparison color steps were introduced sequentially; first the comparison colors being ±7 steps away (bidirectional), then those ±5 steps from the base color and finally the color steps ±1, ±2, and ±3 steps were introduced together. While new color steps were introduced, the former color steps were still probed in a randomized fashion to keep the animals engaged in the task.

All analyses were performed with MATLAB, using custom code and the Curve Fitting Toolbox. If not indicated otherwise, performance was calculated as mean percent correct responses, with chance level being at 50%. Receiver operating characteristic curves (ROC) were modeled to quantify the deviation of the birds' performance from chance by calculating the area under the curve. ROC curves were based on logistic regression of the data. Cochran's Q-Test was used to test for differences in distribution of correct responses per color. Discrimination curve modelling was done by fitting a non-linear regression to the performance data using the Curve Fitting Toolbox. Post hoc power analysis was done using G*Power 3.1. To quantify the contribution of each of the measured physical parameters (wavelength, luminance, saturation) to the discrimination performance of the birds, coefficients of multiple correlation and the corresponding R^2 values were calculated. In other words, the performance of the birds was correlated with each

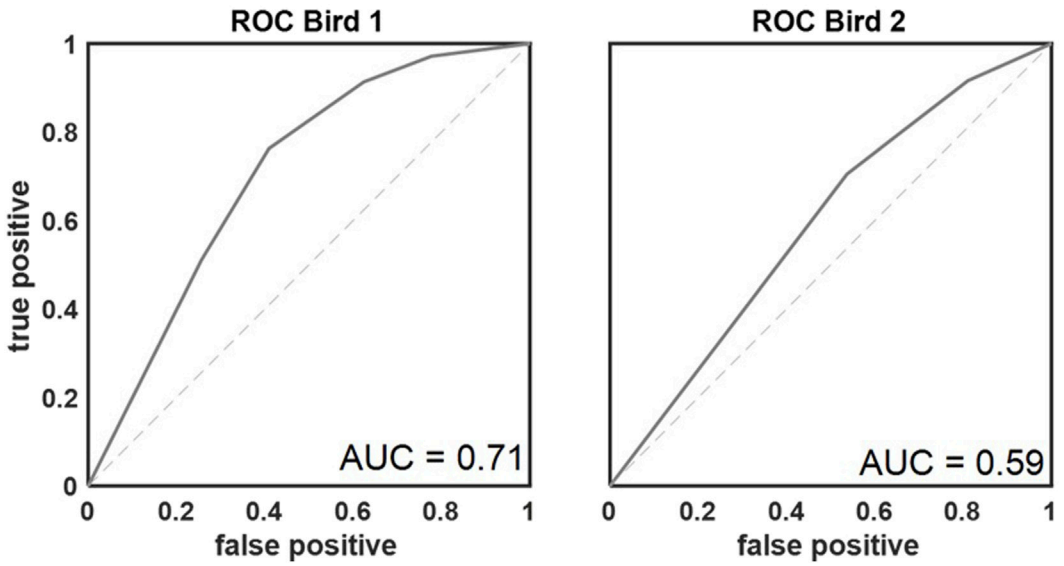

FIGURE 4
Receiver operating characteristic curves for both birds. AUROC values of 0.71 and 0.59 respectively demonstrated that the discriminatory performance of the birds was above chance (AUC = 0.5; indicated with dashed line).

of the color stimulus parameters, corrected for the intercorrelations between those parameters.

Results

Calculated and measured dominant wavelengths deviated similarly from a linear color distribution

The dominant wavelength of each color used in this study was calculated and compared to the wavelength obtained from measurements in the experimental setup (see Supplementary Table S2). This enabled a comparison between calculated and actual dominant wavelength to assess in which ways the experimental monitor distorted the originally intended presentation of the colors. A dominant wavelength could be calculated for most experimental colors (solid curve, Figure 3) except some purple hues for which only complementary instead of dominant wavelengths could be calculated (indicated via the vertical line in Figure 3; see Burger and Burge, 2015). The solid black curve in Figure 3 clearly shows that dominant wavelengths of almost all colors deviated from the ideal linear wavelength distribution shown by the dotted grey line. The dashed black curve represents the measured dominant wavelengths, which generally followed the same pattern but did not overlap with the calculated values. Thus, the color rendering of the monitor was not precise enough to produce the intended color according its RGB values. The largest deviation between both the measured and calculated wavelengths and the linear course was obvious for some green and blue hues (Figure 3 color IDs 22-34 and 41-52; see Supplementary Table S2). The reduced slope indicates that these colors were much more similar to one another than other colors, even though they were created aiming for identical wavelength differences.

Birds showed color-dependent discrimination performance

In total, 82 sessions were analyzed in which the birds completed 24,426 color comparisons (bird 1, n = 20,365; bird 2, n = 4,061). The number of completed trials was similar across all base colors ($Q(63) = 20.994$, $p = 1.00$; average number of presentations per color ±standard deviation = 381.66 ± 11.28). Overall, both birds performed well above the chance level of 50% correct (Figure 4). As explained above, four different response types could be differentiated (Figure 2B). Performance of the birds referred to the percentage of correct responses (hits and correct rejections; mean ± standard deviation in %: hit_{bird1} = 72.47 ± 10.68, hit_{bird2} = 76.11 ± 8.62, correct $rejection_{bird1}$ = 81.32 ± 8.46, correct $rejection_{bird2}$ = 72.99 ± 5.64), which was higher than the percentage of incorrect responses (misses and false alarm; mean ± standard deviation in %: $miss_{bird1}$ = 27.52 ± 10.68, $miss_{bird2}$ = 5.8 ± 11.11, false $alarm_{bird1}$ = 18.68 ± 8.46, false $alarm_{bird2}$ = 6.5 ± 11.84). In total, correct responses (hit and correct rejection) were most frequent (76.77% of all responses). The proportion of correct responses was further quantified by calculating the area under the receiver operating characteristics curves (Figure 4) resulting in values of 0.71 (bird 1) and 0.59 (bird 2).

Behavioral performance was color-dependent and decreased with color pair difference

As explained above, each base color was combined with 10 different comparison colors. Due to the training history (color steps were introduced successively starting with the largest color steps of ±7) the number of trials per color step differed. The final data set included all trials with the whole gamut used as base colors

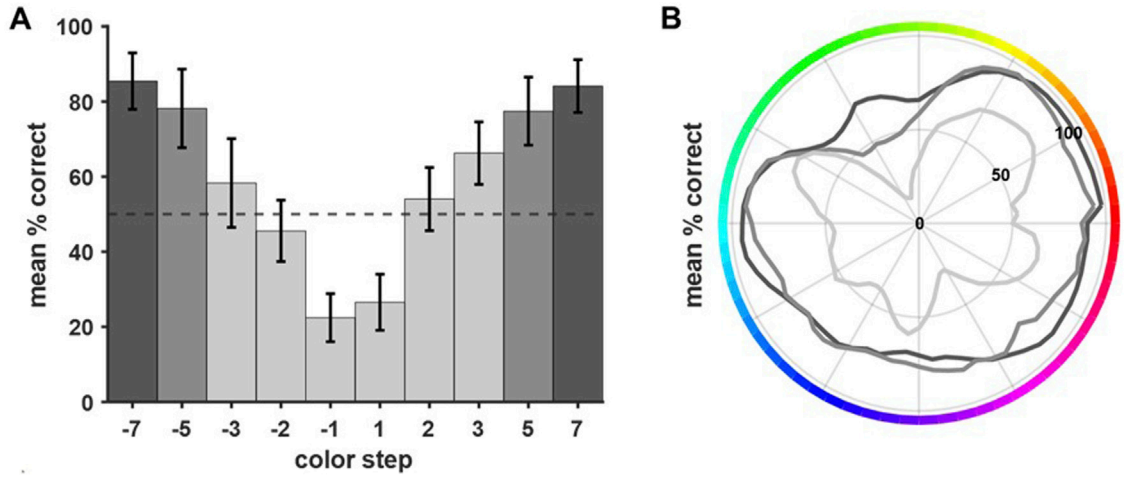

FIGURE 5
Performance differed depending on the distance between base and comparison color and the base color itself. **(A)** The average performance was calculated per color step (pooled across all colors, error bars show SEM). Performance decreased the closer base color and comparison color were (irrespective of the direction of shift). For color comparisons closer than three steps, the performance dropped below chance level. **(B)** In general, the performance per base color decreased with decreasing difference between base and comparison color (grey shading indicates color steps, dark grey = ±7, grey = ±5, and light grey = ±3, ±2, ±1). Clear differences in performance per base color became apparent for the more difficult comparisons (i.e., color steps ±3, ±2, ±1). Here, the birds showed clear drops in performance for close comparisons within the green, the blue, and the purple range.

(see Supplementary Table S1). The average performance decreased as the distance between base and comparison color became smaller (Figure 5A). For comparison colors closer than 3 steps, the performance dropped below chance level (light grey, Figure 5). The symmetrical distribution of performance levels argued against different levels of difficulty due to clockwise or counterclockwise comparison color shifts. Behavioral performance differed not only per color step but also as a function of specific base colors. Figure 5B shows the performance per base color pooled across specific comparison color steps (light grey: ±1/2/3; grey: ±5; dark grey: ±7). Overall, performance differed significantly between the different target colors (all data pooled, $Q(63) = 834.4025$, $p < 0.001$). The outer, dark grey line contains all trials with color steps of ±7. The performance was quite similar for different base colors, showing only slightly reduced performance in the green and blue range. The middle grey line visualizes the performance in trials with intermediate color steps (±5). Overall performance was reduced but again showed only minor differences between specific base colors. Clear color-dependent differences became apparent for the closest color comparisons (color steps ±3, ±2 and ±1, inner light grey line). Clear drops in performance could be seen for green, blue, and purple hues.

Discrimination curve modelling revealed discrimination abilities depended on base color

A discrimination curve was modeled to fit the behavioral data of all completed color comparisons. A post-hoc analysis revealed that a discrimination curve fitted to the present data set can reveal differences in color discrimination performance with a power of $(1-\beta) = 0.93$. A three peaked curve was found to fit the data best ($R^2 = 0.91$, RMSE = 4.25, df = 49.57). The peaks were found in the orange, cyan, and purple spectra (Figure 6). Lowest performance was found for green and blue hues. These colors correspond to those found to be much more similar to one another based on their dominant wavelengths (see Figure 3).

Dominant wavelength represented the physical parameter most predictive of the behavioral performance

Finally, to confirm that the obtained discrimination curve was indeed a function of the birds' abilities to distinguish the presented wavelengths rather than their luminance or saturation, correlation and analysis of shared variance were conducted. Figure 7 shows the distribution of all three measured characteristics of presented colors (luminance, wavelength and saturation) across the entire stimulus set.

Standard correlation analysis showed a high positive correlation between performance and dominant wavelength ($r = 0.402$, $p = 0.001$). The other two variables failed to reach significance in their correlation with performance and were comparatively small, with saturation ($r = -0.064$, $p = 0.614$) being slightly more relevant than luminance ($r = -0.044$, $p = 0.729$). This showed that with 16% shared variance ($R^2_{wavelength} = 0.16$), the wavelengths of the presented colors had the biggest influence on discrimination performance ($R^2_{saturation} = 0.004$, $R^2_{luminance} = 0.002$).

Since the physical measures of color represent integral stimulus properties that are related with each other, a partial correlation was calculated in addition. This changed the absolute values of the correlations, but not the pattern. With a shared variance of now 26%, wavelength remained the most influential ($r = 0.512$, $p < 0.0001$, $R^2 = 0.26$). The negative correlations of saturation ($r = -0.331$, $p = 0.009$, $R^2 = 0.11$) and luminance ($r = -0.306$, $p = 0.01$, $R^2 = 0.09$) were bigger as well and reached significance, but

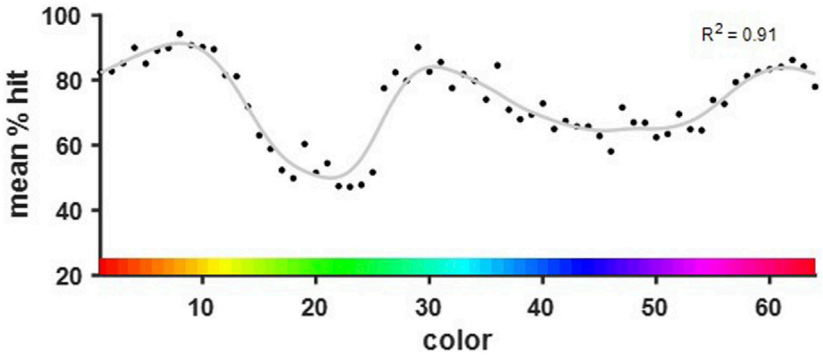

FIGURE 6
Discrimination curve fitted to the performance per base color over all color steps. The three peaks of the curve were found in the orange, cyan, and purple spectra. The local minima corresponded with the green and blue hues that were shown to differ the least in their dominant wavelengths.

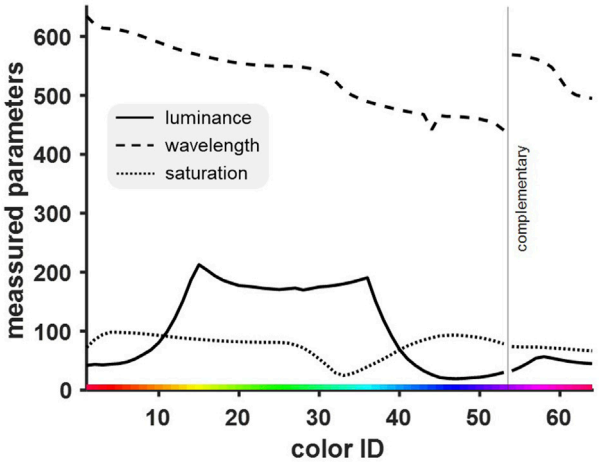

FIGURE 7
Distribution of three different physical measures of color [luminance (cd/m^2), wavelength (nm), saturation (%)]. The three measured parameters differed in their course and from the intended linear color display. We expected to find an equidistant distribution of wavelengths (see Figure 3) and both saturation and luminance to be constant at their respective maximum value. While saturation was relatively constant, luminance was relatively high for one-half of the colors and relatively low for the others.

these variables were still not as influential as the wavelengths of the colors.

Discussion

Our study aimed to find a psychometric color discrimination curve for jackdaws to better interpret behavioral results obtained from various experimental paradigms (using color stimuli). In addition, we performed detailed measurements of rendered colors to evaluate color accuracy of stimulus generation and computer monitor display (i.e., dominant wavelength, luminance, saturation). We found that the rendered colors deviated from the intended linear color range, resulting in color ranges comprising more similar or more distinct color hues. The birds were able to perform above chance level and, as expected, performance dropped when hues became more similar to each other. Overall, birds mostly relied on hue to differentiate color pairs. Drops in discrimination performance mostly correlated with physical stimulus properties, which again highlights the importance to also include detailed stimulus information when interpreting behavioral findings (also see Bae et al., 2014).

Overall, the birds performed well at the task and were able to discriminate the colors above chance level. For distant comparison colors (color steps ±5, ±7), performance was very similar across all colors, with about 80 percent correct responses. When looking at the closest color steps (±1, ±2, ±3), performance dropped below chance level. A closer look at the performance revealed a color dependency for the discrimination ability of adjacent color pairs (Figure 5B). Here, behavioral performance correlated strongly with the physical stimulus properties, namely, dominant wavelength. Thus, irregularities of the hue distribution had a strong effect on discrimination ability which became more pronounced for close and especially adjacent color pairs. In general, birds mostly relied on wavelength to discriminate color pairs and were less affected by the other physical stimulus properties, i.e., luminance and brightness. This supports earlier findings, such as in budgerigars, where it has been shown that the birds are able to discriminate colors regardless of their brightness level (Goldsmith and Butler, 2005). For saturation previous findings indicate that chicks generalize across hues and saturations in the same way (Scholtyssek et al., 2016). Thus, those seem to be related qualities of color that can independently but similarly contribute to bird color discrimination. In our study, the birds seemed to have identified hue as the defining characteristic of the color and thus used this chromatic dimension to base their responses on rather than saturation. Of course, as 'integral stimulus parameters' (as described in CIE, 1932), hue, saturation and brightness are highly correlated and cannot easily be investigated individually (Burns and Shepp, 1988; Xie and Fairchild, 2023). Interestingly, while wavelength and discrimination performance had a positive correlation, the correlation of both luminance and saturation with performance was negative, which shows, that the pattern of performance did not coincide with the pattern of either of

those parameters. This indicates even further that mostly the wavelength of the colors was informative to the birds.

We fitted a discrimination curve to the data, which revealed three peaks of increased discrimination ability in jackdaws. Although this would generally align with peaks of receptor sensitivity in the visual system as shown in previous work (Hart and Hunt, 2007), our non-linear stimulus distribution complicates this interpretation. We found that the minima of the discrimination curve map onto those wavelengths with a reduced distance (between them). Thus, this can most likely be explained by a higher physical similarity of the color pairs tested instead of reduced sensitivity in the specific color range. This interpretation was supported by findings from a small side study with humans, in which a small sample of human participants was tested in the same experimental setup under the exact same conditions and the pattern of performance we found was very similar to the birds. A detailed description of this preliminary study goes beyond the scope of this paper; however, it can be mentioned that the human subjects showed a very similar discrimination curve despite profound differences in both visual systems (see Supplementary Figure S1). Both birds and humans were thus equally affected in their color discrimination by the non-linear distribution of wavelengths.

Normally, differences in color perception between human and avian subjects must be expected given the differences in the visual systems of birds and humans (tetrachromatic vs trichromatic vision, Kelber, 2019; Kelber et al., 2003). However, in terms of perceptual ability, humans and birds seem to have evolved similarly. Both birds and humans are highly visual animals (Hutmacher, 2019; Jones et al., 2007; Martin, 2012). Being able to discriminate a wide range of colors allowed them to be successful in their respective environments. For instance, heightened color discrimination through tri- and tetrachromacy was relevant in finding the ripest food containing the most calories (Smith et al., 2003; Stoddard et al., 2020). This put similar pressure on birds and early humans, with which a similar color discrimination ability evolved, even though their brains are vastly different (Lefebvre et al., 2004; Osorio and Vorobyev, 2008). Not only in color perception, but also in many cognitive tasks some bird families, such as corvids, show similar abilities to primates and monkeys, despite their different brains. We can see, for example, similarities in cognitive control (Balakhonov and Rose, 2017) and working memory capacity limitations (Hahn et al., 2021).

Still, even though birds and humans are similar in color perception abilities, the underlying physiology differs. One major difference is the presence of a fourth receptor type in the avian retina, sensitive to ultraviolet wavelengths (Kelber, 2019), which adds another dimension to the bird color space (Stoddard et al., 2020) and might even influence perception of other colors (Emmerton and Delius, 1980). Consequently, to examine pure perceptual color discrimination, adapted experimental hardware (e.g., monitors capable of rendering UV with precise color display) and a better knowledge of the specific avian photoreceptor pigment sensitivity (e.g., as for pigeons in Bowmaker et al., 1997, hummingbirds in Huth and Burkhardt, 1972 or Bennet et al., 1996 in zebra finches) would be necessary. A previous study on hummingbird color vision established an innovative tetrachromatic color space, adapted to hummingbird cone sensitivities and their ability to discriminate non-spectral colors containing a UV component (Stoddard et al., 2020). An approach like this allows to fully map the color discrimination ability of an avian species and should be obtained for other bird species as well. However, up to now color cone sensitivities are only known for few bird species such as pigeons (Bowmaker et al., 1997), chickens (Osorio et al., 1999), and hummingbirds (Herrera et al., 2008) and in most experimental setups the UV component of color stimuli cannot easily be incorporated. An advantage of the hummingbird study by Stoddard et al. (2020) was their use of innovative light sources displaying the color stimuli. In their 'TetraColorTubes' individual LEDs of red, green, blue and UV could be illuminated to create a unique color comprised of different proportions of those colors, adapted to the specific spectral sensitivities of the hummingbirds (Stoddard et al., 2020). So far, to our knowledge, no commercially available PC screen can display UV components. Further developing such systems to then gain better understanding of other bird species', including jackdaws, color discrimination abilities, would be an interesting avenue for the future.

To examine our color stimuli, we used the CIE color space, even though it originally was made for humans. We found that it is beneficial for a characterization of colors because it allows to connect a RGB color with its underlying physical wavelength. CIE-XYZ, as a device independent standard observer model, allows to draw conclusions about colors regardless of their medium of presentation. From the three-dimensional CIE-XYZ space, the two-dimensional chromaticity of all colors was calculated as a luminance-independent measure (Shaw and Fairchild, 2002). Further transformation of the data allowed us to calculate the corresponding dominant wavelength for each experimental color (Malacara, 2002). This approach revealed an already non-uniform distribution of wavelengths despite the uniform hue distribution within the HSV color space for our intended colors. Thus, the strongest deviation from the ideal linear color range was due to the transformation of HSV colors into their corresponding RGB values instead of imprecise color rendering. Calculated and measured wavelengths coincided largely, which again emphasizes the need for better controlled color generation procedures and additional post-hoc measurements of experimental colors.

Our findings are crucial for future studies on color perception and highlight once again that precise stimulus control and even the examination of physical stimulus parameter are necessary (Bae et al., 2014; Hardman et al., 2017). However, as mentioned in the introduction, more detailed knowledge on color discrimination abilities is also of relevance for work related to cognition. For example, change detection paradigms need to consider that certain color pairs might be easier to differentiate. Consequently, the specific color pair could affect the number of items for which color changes can be correctly identified. Similarly, a recent study in jackdaws revealed that certain colors seem to be memorized more precisely and more easily than others (Apostel et al., 2023b) – a finding also known for primates and humans (Bae et al., 2015; Panichello et al., 2019) and potentially of consequence for future studies. Although this seems to represent a behavioral strategy to balance memory precision and capacity limitations, the precise

position of attractor colors could be related to color rendering details and or cone sensitivity peaks (Apostel et al., 2023b).

In conclusion, using colorful stimuli in a neuroscience experiment allows for a rich and naturalistic stimulus set. Jackdaws can readily discriminate different colors based on their hue. Yet, one needs to examine physical stimulus parameter and to consider the specific distribution of wavelengths when interpreting the results of a study involving colorful stimuli.

Data availability statement

The original contributions presented in the study are included in the article/Supplementary Material, further inquiries can be directed to the corresponding authors.

Ethics statement

The studies involving humans were approved by Ethik-Kommission der Fakultät für Psychologie an der Ruhr-Universität Bochum. The studies were conducted in accordance with the local legislation and institutional requirements. Written informed consent for participation was not required from the participants or the participants' legal guardians/next of kin in accordance with the national legislation and institutional requirements. The animal study was approved by Landesamt für Natur, Umwelt und Verbraucherschutz Nordrhein-Westfahlen (LANUV). The study was conducted in accordance with the local legislation and institutional requirements.

Author contributions

FL: Conceptualization, Formal Analysis, Investigation, Methodology, Software, Visualization, Writing–original draft. AA: Conceptualization, Methodology, Project administration, Software, Supervision, Visualization, Writing–review and editing. JR: Conceptualization, Funding acquisition, Project administration, Supervision, Writing–review and editing.

Funding

The author(s) declare that financial support was received for the research, authorship, and/or publication of this article. This work was supported by a Volkswagen Foundation Freigeist Fellowship to JR and the German Research Foundation (Deutsche Forschungsgemeinschaft, DFG) to JR(SFB 874/B13, project number: 122679504 and SFB 1280/A19 project number: 316803389).

Conflict of interest

The authors declare that the research was conducted in the absence of any commercial or financial relationships that could be construed as a potential conflict of interest.

Generative AI statement

The author(s) declare that no Generative AI was used in the creation of this manuscript.

Publisher's note

All claims expressed in this article are solely those of the authors and do not necessarily represent those of their affiliated organizations, or those of the publisher, the editors and the reviewers. Any product that may be evaluated in this article, or claim that may be made by its manufacturer, is not guaranteed or endorsed by the publisher.

Supplementary material

The Supplementary Material for this article can be found online at: https://www.frontiersin.org/articles/10.3389/fphys.2025.1543469/full#supplementary-material

References

Apostel, A., Hahn, L. A., and Rose, J. (2023a). Jackdaws form categorical prototypes based on experience with category exemplars on experience with category exemplars. *Brain Struct. Funct.*, 229(3), 593–608. doi:10.1007/s00429-023-02651-w

Apostel, A., Panichello, M., Buschman, T. J., and Rose, J. (2023b). Corvids optimize working memory by categorizing continuous stimuli working memory by categorizing continuous stimuli. *Commun. Biol.*, 6, 1122. doi:10.1038/s42003-023-05442-5

Bae, G. Y., Olkkonen, M., Allred, S. R., and Flombaum, J. I. (2015). Why some colors appear more memorable than others: a model combining categories and particulars in color working memory memorable than others: a model combining categories and particulars in color working memory. *J. Exp. Psychol. General*, 144(4), 744–763. doi:10.1037/xge0000076

Bae, G. Y., Olkkonen, M., Allred, S. R., Wilson, C., and Flombaum, J. I. (2014). Stimulus-specific variability in color working memory with delayed estimation. *J. Vis.* 14 (4), 7–23. doi:10.1167/14.4.7

Balakhonov, D., and Rose, J. (2017). Crows rival monkeys in cognitive capacity. *Sci. Rep.* 7 (1), 8809. doi:10.1038/s41598-017-09400-0

Bennet, A. T. D., Cuthill, I. C., Partidge, J. C., and Maier, E. J. (1996). Ultraviolet vision and mate choice in zebra finches. *Nature* 380, 433–435. doi:10.1038/380433a0

Bowmaker, J. K., Heath, L. A., Wilkie, S. E., and Hunt, D. M. (1997). Visual pigments and oil droplets from six classes of photoreceptor in the retinas of birds. *Vis. Res.* 37 (16), 2183–2194. doi:10.1016/s0042-6989(97)00026-6

Brainard, D. H., and Vision, S. (1997). The psychophysics toolbox. *Spat. Vis.* 10 (4), 433–436. doi:10.1163/156856897x00357

Burger, W., and Burge, M. J. (2015). *Digitale bildverarbeitung*. Springer, 363–370.

Burns, B., and Shepp, B. E. (1988). Dimensional interactions and the structure of psychological space: the representation of hue, saturation, and brightness space: the representation of hue, saturation, and brightness. *Percept. and Psychophys.*, 43(5), 494–507. doi:10.3758/bf03207885

CIE (1932). *Commission internationale de l'Eclairage proceedings, 1931*. Cambridge: University Press.

Clayton, N. S., and Dickinson, A. (1998). Episodic-like memory during cache recovery by scrub jays jays. *Nature*, 395(6699), 272–274. doi:10.1038/26216

Diekamp, B., Kalt, T., and Güntürkün, O. (2002). Working memory neurons in pigeons. *J. Neurosci.* 22 (4), RC210. doi:10.1523/JNEUROSCI.22-04-j0002.2002

Emery, N. J., and Clayton, N. S. (2004). The mentality of crows: convergent evolution of intelligence in corvids and apes. *science* 306 (5703), 1903–1907. doi:10.1126/science.1098410

Emmerton, J., and Delius, J. D. (1980). Wavelength discrimination in the 'visible' and ultraviolet spectrum by pigeons. *J. Comp. Physiology* 141, 47–52. doi:10.1007/BF00611877

Goldsmith, T. H., and Butler, B. K. (2005). Color vision of the budgerigar (*Melopsittacus undulatus*): hue matches, tetrachromacy, and intensity discrimination hue matches, tetrachromacy, and intensity discrimination. *J. Comp. Physiology A* 191, 933–951. doi:10.1007/s00359-005-0024-2

Hahn, L. A., Balakhonov, D., Fongaro, E., Nieder, A., and Rose, J. (2021). Working memory capacity of crows and monkeys arises from similar neuronal computations. *eLife* 10, e72783. doi:10.7554/eLife.72783

Hardman, K. O., Vergauwe, E., and Ricker, T. J. (2017). Categorical working memory representations are used in delayed estimation of continuous colors. *J. Exp. Psychol. Hum. Percept. Perform.* 43 (1), 30–54. doi:10.1037/xhp0000290

Hart, N. S., and Hunt, D. M. (2007). Avian visual pigments: characteristics, spectral tunings and evolution. *Am. Nat.*, 169, 7–26. doi:10.1086/510141

Herrera, G., Zagal, J. C., Diaz, M., Fernández, M. J., Vielma, A., Cure, M., et al. (2008). Spectral sensitivities of photoreceptors and their role in colour discrimination in the green-backed firecrown hummingbird (Sephanoides sephaniodes). *J. Comp. Physiology A* 194, 785–794. doi:10.1007/s00359-008-0349-8

Huth, H. H., and Burkhardt, D. (1972). Der spektrale sehbereich eines violettohr-kolibris. *Naturwissenschaften* 59, 650. doi:10.1007/bf00609559

Hutmacher, F. (2019). Why is there so much more research on vision than on any other sensory modality? *Front. Psychol.* 10, 2246. doi:10.3389/fpsyg.2019.02246

Jacobs, G. H. (2009). Evolution of colour vision in mammals. *Philosophical Trans. R. Soc. B Biol. Sci.* 364 (1531), 2957–2967. doi:10.1098/rstb.2009.0039

Jones, M. P., Pierce Jr, K. E., and Ward, D. (2007). Avian vision: a review of form and function with special consideration to birds of prey special consideration to birds of prey. *J. Exot. pet Med.*, 16(2), 69–87. doi:10.1053/j.jepm.2007.03.012

Kelber, A. (2019). Bird colour vision – from cones to perception. *Curr. Opin. Behav. Sci.* 30, 34–40. doi:10.1016/j.cobeha.2019.05.003

Kelber, A., Vorobyev, M., and Osorio, D. (2003). Animal colour vision: behavioural tests and physiological concepts. *Biol. Rev.*, 78, 81–118. doi:10.1017/s1464793102005985

Kobylkov, D., Mayer, U., Zanon, M., and Vallortigara, G. (2022). Number neurons in the nidopallium of young domestic chicks of young domestic chicks. *Proc. Natl. Acad. Sci.*, 119(32), e2201039119. doi:10.1073/pnas.2201039119

Lefebvre, L., Reader, S. M., and Sol, D. (2004). Brains, innovations and evolution in birds and primates primates. *Brain, Behav. Evol.* 63 (4), 233–246. doi:10.1159/000076784

Malacara, D. (2002). *Color vision and colorimetry: theory and applications*. Bellingham, WA: SPIE Press, 75–101.

Martin, G. R. (2012). Through birds' eyes: insights into avian sensory ecology. *J. Ornithol.* 153 (Suppl. 1), 23–48. doi:10.1007/s10336-011-0771-5

Olsson, P., Lind, O., and Kelber, A. (2015). Bird colour vision: behavioural thresholds reveal receptor noise. *J. Exp. Biol.* 218 (2), 184–193. doi:10.1242/jeb.111187

Osorio, D., and Vorobyev, M. (2008). A review of the evolution of animal colour vision and visual communication signals communication signals. *Vis. Res.* 48 (20), 2042–2051. doi:10.1016/j.visres.2008.06.018

Osorio, D., Vorobyev, M., and Jones, C. D. (1999). Colour vision of domestic chicks. *J. Exp. Biol.* 202 (21), 2951–2959. doi:10.1242/jeb.202.21.2951

Otto, T., and Rose, J. (2024). The open toolbox for behavioral research. *Behav. Res. Methods*, 56(5), 4522–4529. doi:10.3758/s13428-023-02199-x

Panichello, M. F., DePasquale, B., Pillow, J. W., and Buschman, T. J. (2019). Error-correcting dynamics in visual working memory dynamics in visual working memory. *Nat. Commun.*, 10(1), 3366. doi:10.1038/s41467-019-11298-3

Rutz, C., Klump, B. C., Komarczyk, L., Leighton, R., Kramer, J., Wischnewski, S., et al. (2016). Discovery of species-wide tool use in the Hawaiian crow. *Nature* 537 (7620), 403–407. doi:10.1038/nature19103

Rutz, C., and St Clair, J. J. (2012). The evolutionary origins and ecological context of tool use in New Caledonian crows New Caledonian crows. *Behav. Process.* 89 (2), 153–165. doi:10.1016/j.beproc.2011.11.005

Scholtyssek, C., Osorio, D. C., and Baddeley, R. J. (2016). Color generalization across hue and saturation in chicks described by a simple (Bayesian) model saturation in chicks described by a simple (Bayesian) model. *J. Vis.*, 16(10), 8–8. doi:10.1167/16.10.8

Shaw, M., and Fairchild, M. (2002). Evaluating the 1931 CIE color-matching functions. *Color Res. Appl.* 27 (5), 316–329. doi:10.1002/col.10077

Smith, A. C., Buchanan-Smith, H. M., Surridge, A. K., Osorio, D., and Mundy, N. I. (2003). The effect of colour vision status on the detection and selection of fruits by tamarins (Saguinus spp.) of colour vision status on the detection and selection of fruits by tamarins Saguinus spp. *J. Exp. Biol.*, 206(18), 3159–3165. doi:10.1242/jeb.00536

Stockman, A., and Sharpe, L. T. (2000). The spectral sensitivities of the middle- and long-wavelength-sensitive cones derived from measurements in observers of known genotype wavelength-sensitive cones derived from measurements in observers of known genotype. *Vis. Res.*, 40(13), 1711–1737. doi:10.1016/s0042-6989(00)00021-3

Stoddard, M. C., Eyster, H. N., Hogan, B. G., Morris, D. H., Soucy, E. R., and Inouye, D. W. (2020). Wild hummingbirds discriminate nonspectral colors. *Proc. Natl. Acad. Sci. U. S. A.* 117 (26), 15112–15122. doi:10.1073/pnas.1919377117

Veit, L., Hartmann, K., and Nieder, A. (2014). Neuronal correlates of visual working memory in the corvid endbrain. *J. Neurosci.* 34 (23), 7778–7786. doi:10.1523/JNEUROSCI.0612-14.2014

Veit, L., and Nieder, A. (2013). Abstract rule neurons in the endbrain support intelligent behaviour in corvid songbirds corvid songbirds. *Nat. Commun.*, 4(1), 2878. doi:10.1038/ncomms3878

Vernouillet, A., Leonard, K., Katz, J. S., Magnotti, J. F., Wright, A., and Kelly, D. M. (2021). Abstract-concept learning in two species of new world corvids, pinyon jays (Gymnorhinus Cyanocephalus) and California scrub jays (Aphelocoma Californica). *J. Exp. Psychol. Animal Learn. Cognition* 47 (3), 384–392. doi:10.1037/xan0000283

Wagener, L., Loconsole, M., Ditz, H. M., and Nieder, A. (2018). Neurons in the endbrain of numerically naive crows spontaneously encode visual numerosity. *Curr. Biol.* 28 (7), 1090–1094. doi:10.1016/j.cub.2018.02.023

Wasserman, E. A., Kain, A. G., and O'Donoghue, E. M. (2023). Resolving the associative learning paradox by category learning in pigeons. *Curr. Biol.* 33 (6), 1112–1116.e2. doi:10.1016/j.cub.2023.01.024

Wilson, B., Mackintosh, N. J., and Boakes, R. A. (1985). Transfer of relational rules in matching and oddity learning by pigeons and corvids. *Q. J. Exp. Psychol.* 37 (4), 313–332. doi:10.1080/14640748508401173

Wright, A. A. (1972). Psychometric and psychophysical hue discrimination functions for the pigeon. *Vis. Res.* 12, 1447–1464. doi:10.1016/0042-6989(72)90171-x

Xie, H., and Fairchild, M. D. (2023). Representing color as multiple independent scales: brightness versus saturation. *JOSA A* 40 (3), 452–461. doi:10.1364/JOSAA.480040

frontiers | Frontiers in Physiology

TYPE Original Research
PUBLISHED 05 March 2025
DOI 10.3389/fphys.2025.1547661

OPEN ACCESS

EDITED BY
Sandra G. Velleman,
The Ohio State University, United States

REVIEWED BY
Francesca Soglia,
University of Bologna, Italy
Krystyna Pierzchała-Koziec,
University of Agriculture in Krakow, Poland
Colin Guy Scanes,
University of Wisconsin–Milwaukee, United States

*CORRESPONDENCE
Mona Elisabeth Pedersen,
mona.pedersen@nofima.no

RECEIVED 18 December 2024
ACCEPTED 03 February 2025
PUBLISHED 05 March 2025

CITATION
Støle TP, Romaine A, Kleiberg T, Høst V, Lunde M, Hasic A, Lintvedt TA, Sanden KW, Kolset SO, Wold JP, Pisconti A, Rønning SB, Carlson CR and Pedersen ME (2025) Cardiac implications of chicken wooden breast myopathy.
Front. Physiol. 16:1547661.
doi: 10.3389/fphys.2025.1547661

Cardiac implications of chicken wooden breast myopathy

Thea Parsberg Støle[1], Andreas Romaine[1], Thea Kleiberg[2], Vibeke Høst[2], Marianne Lunde[1], Almira Hasic[1], Tiril Aurora Lintvedt[2], Karen Wahlstrøm Sanden[2], Svein O. Kolset[3], Jens Petter Wold[2], Addolorata Pisconti[4], Sissel Beate Rønning[2], Cathrine Rein Carlson[1] and Mona Elisabeth Pedersen[2]*

[1]Institute for Experimental Medical Research, Oslo University Hospital and University of Oslo, Oslo, Norway, [2]Raw Materials and Optimalization, Nofima As, Ås, Norway, [3]Department of Nutrition, Institute of Basic Medical Science, University of Oslo, Oslo, Norway, [4]Department of Biochemistry and Cell Biology, Stony Brook University, Stony Brook, NY, United States

Introduction: Wooden breast disease is a myopathy of the skeletal muscle in chickens of commercial breeding. Although the underlying pathophysiology remains unknown, we and others have previously shown that affected broilers display varying degrees of fibrosis, extracellular matrix (ECM) remodeling, inflammation, and alterations in various molecular signaling pathways. Other myopathy conditions, such as Duchenne muscular dystrophy, also affect the cardiac muscle and are associated with fibrosis and reduced cardiac function. To determine potential cardiac implications of wooden breast disease and identify whether molecular and fibrotic changes were similar to what we have previously found in the breast, we have investigated the hearts of commercial Ross 308 broilers.

Methods: Hearts from male Ross 308 broiler chickens from mildly and severely wooden breast-affected chickens categorized in previous studies were analyzed. Ventricles from the hearts were analyzed by immunoblotting, real-time qPCR, near-infrared spectroscopy, Raman spectroscopy, and Masson`s trichrome histology. RNA sequencing was also conducted to identify the molecular footprint of the mildly and severely wooden breast-affected chickens.

Results: Compared to mildly affected chickens, the severely wooden breast-affected chickens did not show an increase in heart weight, water-binding capacity, or macronutrient composition. The hearts did also not display any differences in fibrosis development, extracellular matrix gene expression, or typical cardiac and inflammatory markers. The severely affected chickens did, however, show a reduction in protein levels of biglycan and fibromodulin, as well as alterations in matrix metalloproteinase 2, Wnt ligands, mTOR signaling, heat shock protein 70, and muscle LIM protein. Functional enrichment analysis of RNA sequencing also suggested a different molecular footprint of biological processes and pathways between the two groups.

Conclusion: Hearts from wooden breast-affected chickens did not display the same fibrotic alterations as those previously found in the breast. Despite few

alterations detected in the markers and signaling molecules tested, RNA sequencing indicated a different molecular footprint in the hearts of severely compared to mildly wooden breast-affected chickens.

KEYWORDS

wooden breast, myopathy, heart, cardiac, broiler chicken

1 Introduction

Wooden breast disease (WB) is a myopathy of the skeletal breast muscle (*Pectoralis major*) in fast-grown broilers (Sihvo et al., 2014; Mudalal et al., 2015), with incidences reported as high as 96.1% (Tijare et al., 2016). Macroscopically, the condition is characterized by a rigid hardening of the tissue, especially at the caudal end of the breast, leading to a reduction in the physical and chemical quality of the meat (de Almeida Assunção et al., 2020; Xing et al., 2020). Due to the growing demand for poultry meat and an increase in the incidence of WB, the condition leads to huge economic losses in the industry (Kuttappan et al., 2016; Zanetti et al., 2018).

While the underlying pathophysiology of the condition remains to be fully understood, it is thought to be induced by the genetic selection of faster-growing broilers, leading to the development of spontaneous myopathies (Petracci et al., 2015; Forseth et al., 2023). Pairing to the name, WB-affected breasts have been found to display fibrosis and immune cell infiltration, resulting in tough and hardened tissue (Sihvo et al., 2014). RNA sequencing of WB-affected breasts has shown an upregulation of genes involved in intracellular calcium regulation, hypoxia, oxidative stress, fiber-type switching, and cellular repair (Mutryn et al., 2015). Our previous molecular studies also suggests alterations in signaling pathways such as mitogen-activated protein kinases (MAPK), Akt and Wnt, and matrix metalloproteinases (MMPs) and transmembrane syndecan shedding in the affected breasts (Pejšková et al., 2023; Pejšková et al., 2024).

While WB is primarily recognized as a myopathy of the skeletal muscle in broilers, skeletal and cardiac muscle share similarities. Myocytes of the skeletal and cardiac muscles both originate from the mesoderm during embryonic development (Costamagna et al., 2014). Like skeletal myocytes, cardiomyocytes contain sarcomeres which facilitate their contractility. However, while the skeletal muscle is under voluntary control, the cardiac muscle is not. A synchronized and coordinated contraction and relaxation cycle of the myocardium is initiated by electrical simulation from the sinus node, allowing the heart to supply the body's organs with the appropriate oxygen and nutrient supply it requires (Stephenson et al., 2016). As such, an increase and accumulation of extracellular matrix (ECM) proteins leads to the stiffening of the heart, associated with a decline in function, ultimately leading to progressive heart failure (Czubryt and Hale, 2021).

Whether WB disease of the broiler breast muscle is associated with changes also in the cardiac muscle has, to our knowledge, not been investigated before. However, similar molecular alterations, such as an increase in syndecan levels and shedding, are observed in the WB-affected breast, and also in the dysfunctional heart (Strand et al., 2015; Herum et al., 2020; Pejšková et al., 2023). Additionally, other myopathies, such as Duchenne muscular dystrophy and inflammatory myopathies, exhibit a correlation between skeletal muscle and cardiac dysfunction (Posner et al., 2016; Prisco et al., 2020). We therefore hypothesized that the heart may be affected by WB and that similar mechanisms of inflammation and fibrotic development may be present. In this study, we investigated the cardiac implications associated with WB disease of the chicken to identify potential alterations in cardiac structure and fibrosis. We also analyzed molecular changes in the ECM, signaling pathways, cardiac and inflammatory markers, and syndecan gene and protein expression.

2 Materials and methods

2.1 Animal sampling and classification of the chicken hearts

Male Ross 308 broiler chickens (*Gallus gallus*) were fed a diet of wheat/maize pellets *ad libitum*, from the age of 10 days. Chickens were housed in 2.4 × 0.95-m pens covered in wood shavings with 6: 18 h light:dark cycles with gradually reduced temperatures of 28 to 21°C. Upon slaughter at 36 days post-hatching, the atria were removed, and the ventricles were snap-frozen in liquid nitrogen. The hearts were from the same chickens we have previously analyzed the breasts from and were grouped (mild and severe) based on the previous WB classification of the chicken breasts (Pejšková et al., 2023). The classification was based on manual palpitation of the breast, followed by histological analysis where the severe group showed marked fibrosis and collagen infiltration in the breast, whereas the mild group showed few signs (Pejšková et al., 2023). Since all chickens of the Ross308 breed seem to display some signs of skeletal muscle myopathy (Pejšková et al., 2023; Pejšková et al., 2024), we have compared cardiac samples from mildly and severely WB-affected chickens.

2.2 Immunoblotting and blocking peptides

Tissue from the ventricles of mild and severely affected chickens was homogenized with TissueLyser (#85300, Qiagen Nordic, Venlo, Netherlands) in ice cold lysis buffer (20 mM Hepes (pH7.5), 150 mM NaCl, 1 mM EDTA, and 0.5% Triton-X100), supplemented with complete EDTA-free protease inhibitor cocktail (#5056489001, Roche Applied Science, Merck, Darmstadt, Germany) and PhosSTOP (#4906837001, Roche Applied Science, Merck). Homogenates were centrifuged (19 cm rotor diameter) at 14,000 rcf for 10 min at 4°C before supernatants were stored at −80°C. Protein concentrations were determined by using a Micro BCA protein assay kit (#PIER23235, Thermo Fisher Scientific, MA, United States). 40 µg protein was loaded per lane on 26- or 18-well 4%–15% Criterion TGX precast gels (#5671085 and

10.3389/fphys.2025.1547661

TABLE 1 Primary antibodies used for immunoblotting.

Protein name:	Uniprot:	Western blot kDa:	Blocking condition:	Antibody:	Dilution:	Supplier:
Wnt3a	Q2LMP1 WNT3A_CHICK (352aa)	45–55 kDa	1 × Casein	ab28472	1:1,000	Abcam
Wnt7a	Q9DEB8 Q9DEB8_CHICK (349a)	40–50 kDa	5% BSA	ab100792	1:1,000	Abcam
Biglycan	Unidentifiable (369aa)	40 kDa	1 × Casein	sc-27936	1:500	SantaCruz
Fibromodulin	P51887 FMOD_CHICK (380aa)	40 kDa	1 × Casein	sc-33772	1:500	SantaCruz
pSer2448-mTOR	F1NUX4 F1NUX4_CHICK (2521aa)	260 kDa	5% BSA	#2971	1:1,000	Cell Signaling
mTOR				#2983		
HSP70	P08106 HSP70_CHICK (634aa)	70 kDa	1 × Casein	sc-373867	1:500	SantaCruz
Wnt4	P49337 Wnt4_CHICK (351aa)	35 kDa	1 × Casein	ab91226	1:1,000	Abcam
Decorin	P28675 PGS2_CHICK (357aa)	50–75 kDa	1 × Casein	AF1060	1:500	R&D systems
LOX	Q05063 LYOX_CHICK (420aa)	42 kDa	1 × Casein	sc-32409	1:500	SantaCruz
MLP	F1NWZ2 F1NWZ2_CHICK (194aa)	20 kDa	1 × Casein	sc-166930	1:1,000	SantaCruz
pThr180Tyr182-p38 MAPK	A0A1D5PIQ5 A0A1D5PIQ5_CHICK (360aa)	40 kDa	5% BSA	#9211	1:1,000	Cell Signaling
p38 MAPK				ab31828	1:1,000	Abcam
pSer473-Akt	057513 057513_CHICK (480aa)	55 kDa	5% BSA	#9271	1:500	Cell Signaling
Akt				#9272	1:500	Cell Signaling
Syndecan-1	F1NV24 F1NV24_CHICK (308aa)	10–250 kDa	1 × Casein	Custom made (Pejšková et al., 2023)	1:1,000	Genscript
Syndecan-2	Q8JIY0 Q8JIY0_CHICK (201aa)	10–75 kDa	1 × Casein	Custom made (Pejšková et al., 2023)	1:1,000	Genscript
Syndecan-3	P26261 SDC3_CHICK (405aa)	10–150 kDa	1 × Casein	Custom made (Pejšková et al., 2023)	1:1,000	Genscript
Syndecan-4	P49416 SDC4-CHICK (197aa)	15–150 kDa	1 × Casein	Custom made (Pejšková et al., 2023)	1:1,000	Genscript
MMP9	A0A8V0YXL9 A0A8V0YXL9_CHICK (688aa)	80 kDa	1 × Casein	NBP1-57940	1:1,500	Novus Biologicals
MMP2	Q90611 MMP2_CHICK (663aa)	66–72 kDa	1 × Casein	ab181286	1:1,500	Abcam
Cardiac troponin T	P02642 TNNT2_CHICK (302aa)	40 kDa	1 × Casein	MA5-12960	1:500	Invitrogen
GAPDH	P00356 G3P_CHICK (333aa)	35 kDa	1 × Casein	sc-47724	1:500	SantaCruz

#5671084, Bio-Rad, CA, United States) before transferring onto PVDF membranes (#1704157, Bio-Rad, or #0301004001, Merck) using a Trans-Blot Turbo system (Bio-Rad). Membranes were blocked in 1 × casein (#11836170001, Merck) or 5% BSA (#805090, Norsk Labex, Høvik, Norway) for 1 h at room temperature and thereafter incubated with primary antibodies overnight at 4°C. Following incubation, membranes were washed in TBS-T [Tris-buffered saline with 1% Tween-20 (#1610781, Bio-Rad)] for 20 min, followed by three 10-min washes. HRP-conjugated secondary antibodies were then added for 1 h at room temperature before the membranes were washed for 20 min, followed by four 5-min washes in TBS-T. Blots were developed with ECL prime (#RPN2236, Cytiva, MA, United States) and signal was detected using Azure 600 Western blot imaging system (Azure Biosciences, CA, United States). Membranes were stripped for 5–10 min (#PIER21603, Thermo Scientific, CA, United States) before reprobing. Equal loading was confirmed with GAPDH or Revert 700 protein staining (#926-11021, LI-COR Biosciences, NE, United States). A list of primary antibodies, blocking conditions, dilutions, molecular weight detected by immunoblotting, and the Uniprot protein IDs are listed in Table 1.

For the four syndecan proteins, blocking peptides against the antibody epitopes were used to analyze the specificity of bands detected with immunoblotting. Here, custom-made blocking peptides (Genscript, NJ, United States) against chicken syndecan-1-4 were pre-incubated with the respective antibodies before immunoblotting of the membranes. The syndecan antibodies and their corresponding blocking peptides were previously used and epitope mapped in Pejšková et al. (2023).

TABLE 2 Gene target and TaqMan primer assays.

TaqMan® probes	Gene name	Assay ID
Actin Alpha 2	*ACTA2*	Gg03352404_m1
Biglycan	*BGN*	Gg07177841_m1
Collagen type 1	*COL1A1*	Gg07167955_g1
Collagen type 3	*COL3A1*	Gg03325764_m1
Decorin	*DCN*	Gg03355063_m1
Desmin	*DES*	Gg03330588_m1
Eukaryotic translation elongation factor 2	*EEF2*	Gg03339740_m1
Interleukine 1 beta	*IL-1B*	Gg03347157_g1
Lysyl Oxidase	*LOX*	Gg03340182_m1
Lumican	*LUM*	Gg03325844_m1
Matrix metalloproteinase-2	*MMP2*	Gg03365277_m1
Matrix metalloproteinase-9	*MMP9*	Gg03338324_g1
Platelet-derived growth factor receptor beta	*PDGFRB*	Gg07165531_s1
Syndecan-1	*SDC1*	Gg07175697_s1
Syndecan-2	*SDC2*	Gg03345645_m1
Syndecan-3	*SDC3*	Gg03339851_m1
Syndecan-4	*SDC4*	Gg03370419_m1
Transforming growth factor beta 1	*TGFB1*	Gg07156069_g1
Tissue inhibitor of metalloproteinases 2	*TIMP2*	Gg07157666_m1
Toll like receptor 4	*TLR4*	Gg03354643_m1
Tropomyosin beta-chain	*TPM2*	Gg03815778_s1
Troponin T2 cardiac type	*TNNT2*	Gg03371505_m1
Tubulin alfa-1	*TUBA1A*	Gg07162375_m1
Tubulin beta-1	*TUBB1*	Gg03371486_g1

2.2.1 Blocking peptides

Syndecan-1: NGGYQKPHKQE.
Syndecan-2: RKPSSAAYQKAPTK.
Syndecan-3: KQANVTYQKPDKQE.
Syndecan-4: DLGKKPIYKKAPTN.

2.2.2 Antibodies

Secondary HRP-conjugated antibodies were anti-rabbit IgG HRP (N934V, Cytiva, MA, United States) and anti-mouse IgG HRP (NA931V, Cytiva).

2.3 Real-time quantitative PCR

Total RNA was extracted according to the manufacturer's instructions using the RNeasy Midi Kit (#75144, Qiagen, Germany) and lysis with Precellys Lysing Kit (#P000911-LYSKO-A.0, Bertin technologies, Montigny-le-bretonneux, lle-de-France, France); 6,000 rpm 4 × 20 s intervals. cDNA was generated from 2 µg RNA using Taqman Reverse Transcription Reagents (#N8080234, Thermo Fisher Scientific, MA, United States) in a 40 µL reaction volume with random hexamers according to the manufacturer's protocol. RT-qPCR analysis was carried out using TaqMan Gene expression Master Mix (#4369510, Life Technologies, Thermo Fisher Scientific) and the QuantStudio5 (Applied Biosystems, Foster City, CA, United States) PCR System. The amplification protocol was initiated at 50°C for 2 min, followed by denaturation at 95°C for 10 min, then 40 cycles of denaturation at 95°C for 15 s followed by annealing of TaqMan probes and amplification at 60°C for 1 min. RT-qPCR analyses were performed with 3 technical replicates from each sample. The relative gene expression (RQ) was calculated by the comparative $2^{-\Delta Ct}$ method (Schmittgen and Livak, 2008; Bustin et al., 2009). Normalization was performed against the eukaryotic translation elongation factor 2 (*EEF2*) reference gene for each sample, and subsequently related to the average gene expression of the mild samples for each gene analyzed. All TaqMan® primers and probes are listed in Table 2.

2.4 Near-infrared spectroscopy

Near-infrared spectroscopy (NIRS) is an established technique for the rapid detection of WB syndrome in chicken breasts, a method which is also developed for industrial sorting (Wold et al., 2017; Wold et al., 2019). The lower content of protein and the more loosely bound water in the affected muscle can easily be quantified by NIRS. Therefore, it was interesting to evaluate if NIRS can distinguish between heart muscles from mild and severely affected chickens. The handheld instrument MicroNIR PAT-U (VIAVI Solutions Inc., AZ, United States) is based on a 128-pixel InGaAs photodiode array and a linear filter. It collects spectra in the wavelength region 908–1,676 nm. Two LEDs are used for illumination, and an approx. circular area of D = 10 mm was probed with the system. Spectral collections were done in physical contact with the heart sections. Each measurement integrated spectra over 1 s. In the analysis, we used the absorption spectra and spectra normalized by standard normal variate (Barnes et al., 1989) to remove the main effect of the light scattering on the spectra.

2.5 Raman spectroscopy

Raman spectroscopy was used to get an indication of collagen accumulation in the hearts. A MarqMetrix All-in-One (AIO) Raman system covering a Raman shift range of 100–3,250 cm^{-1} was employed. The system was equipped with a 785 nm laser operating at 450 mW power and the sampling optic was a wide area illumination (D = 3 mm) Proximal BallProbe HV stand-off Raman probe (MarqMetrix Inc., WA, United States) operating at a 10 cm working distance. The left ventricle (LV) was scanned under illumination for 25 s three times, using the average spectrum for further analyses. Spectra were baseline corrected, meaning that the broad band signal associated with autofluorescence was removed to retain Raman signals only. The ability of Raman spectroscopy to

characterize different types of collagen structures has been demonstrated in many studies (Rygula et al., 2013; Martinez et al., 2019). More recent work (Monago-Maraña et al., 2021; Lintvedt et al., 2024) has also shown that the quantification of hydroxyproline, as a proxy for collagen, in heterogeneous poultry materials is possible, using appropriate probes with larger laser spot sizes. These studies pointed at unique spectral fingerprints for collagen compared to general proteins by the peak intensity ratios at Raman shifts 827/854 cm^{-1}, 919/936 cm^{-1}, and 1,657/1,678 cm^{-1}. Therefore, these ratios were used as collagen markers in this study.

2.6 Masson's trichrome histology and quantification

The LV was excised, washed in ice-cold PBS, segmented, and snap-frozen in liquid nitrogen. LV segments were embedded in Tissue-Tek®O.C.T.™ compound (Sakura Company, CA, United States) and sectioned into 7 µm using a Cryostar NX70 Cryostat (Thermo Scientific, MA, United States). To quantify collagen, sections were stained with Masson's trichrome stain according to the manufacturer's protocol (Polysciences, PA, United States) with the following modifications: slides were cleared with Histoclear II (National Diagnostics, GA, United States) and mounted using VectaMount Express (Vector Laboratories, CA, United States). Images were captured using a ×20 objective on an AxioScan Z1 (Carl Zeiss, Germany), compositing tiles of the whole LV segment. ImageJ (NIH) was used to remove artifacts and residual pericardial tissue if present, then processed images were exported to Zen 2 (Carl Zeiss, Germany) where colour thresholding was used to measure positive pixel area as a proportion of total pixel area. Analysis was conducted by a researcher blinded for phenotype, and entire LV segments were captured and analysed to avoid selection biases.

2.7 RNA sequencing

RNA was extracted using RNeasy Mini Kit and sent to Novogene for library preparation and sequencing. At Novogene, messenger RNA was purified from total RNA using poly-T oligo-attached magnetic beads. After fragmentation, the first strand cDNA was synthesized using random hexamer primers followed by the second strand cDNA synthesis. The library was ready after the end repair, A-tailing, adapter ligation, size selection, amplification, and purification. The library was checked with Qubit and real-time PCR for quantification and bioanalyzer for size distribution detection. Quantified libraries were pooled and sequenced on an Illumina a Novoseq6000 instrument. Sequencing QC was performed with FastQC v0.12.1 (Andrews, 2010), Trim Galore v0.6.7 (Krueger et al., 2021) [and Cutadapt v3.4 (Martin, 2011)]. Reads were mapped to the GRCg7b version of the *Gallus Gallus* reference genome using STAR v2.7.9a (Dobin et al., 2013). Alignments were converted to BAM format and sorted using samtools v1.17 (Li et al., 2009). Transcript expression was then quantified with Salmon v1.10.1 (Patro et al., 2017), and converted to gene-level counts with Tximport v1.12.0 (Soneson et al., 2015). Differential expression analysis comparing the severe and mild groups was next performed using the nf-core differential abundance pipeline v1.4.0 (WackerO et al., 2023), with read count normalization and statistical analysis performed with DESeq2 v1.34.0 (Love et al., 2014). The results of the differential expression analysis were visualized using the Enhanced Volcano R package v1.20.0.

Gene set enrichment analysis (GSEA) was performed with the ClusterProfiler R package v4.10.1 (Yu et al., 2012; Wu et al., 2021) using the fgsea algorithm (Korotkevich et al., 2016). Log2 fold-change scores were used to rank genes, and the results were visualized with the Enrichplot package v1.22.0 (Wu et al., 2021). Network analysis to find genes with correlated expression levels was performed with WGCNA v.1.72.5 (Langfelder and Horvath, 2008) using normalized and variance-stabilized read counts and a soft-thresholding power value of 10. The genes present in selected modules were then subject to functional overrepresentation analysis (ORA) using ClusterProfiler v4.10.1. For the ORA, the background gene list was defined as the set of genes used in the differential expression analysis that also possessed relevant functional annotations.

2.8 Statistics analysis

Immunoblots are displayed as mean ± SEM and qPCR data are presented as the fold change average relative to the mean of the mildly affected samples. qPCR data of mild and severely affected groups were compared using Welch's t-test due to our observation of a larger spread in the breasts of the same severely affected chickens (Pejšková et al., 2023). Mann-Whitney *U*-tests or student's *t*-tests were used for quantified immunoblots due to non-normal or normal distribution, respectively, analyzed by Shapiro-Wilk testing.

Principal component analysis was used to decompose the NIR spectra into a few principal components to detect the grouping of samples and characterize potential spectral differences between these.

3 Results

3.1 Characterization of hearts from mild and severely wooden breast-affected chickens

We have previously shown that severe versus mild WB-affected breasts display lower water-binding capacity (WHC), and differences in fat deposition (Pejšková et al., 2023). To investigate whether the same differences were present in the hearts of chickens affected by WB, hearts from the same broilers were grouped into the same classifications as the breasts (Pejšková et al., 2023). We first assessed differences in the total heart weight. Heart weight was not altered between mild and severe groups, indicating no difference in hypertrophy between the two groups (Figure 1A). Similarly, WHC did not differ between the hearts of mild and severely WB-affected chickens (Figure 1B). Near-infrared spectroscopy (NIR) revealed that there were no differences in water, protein or fat deposition in the hearts between the groups (Figure 1C). Principle component analysis (PCA) confirmed that, compared to the chicken breast (Pejšková et al., 2023), mild and severely affected groups did not

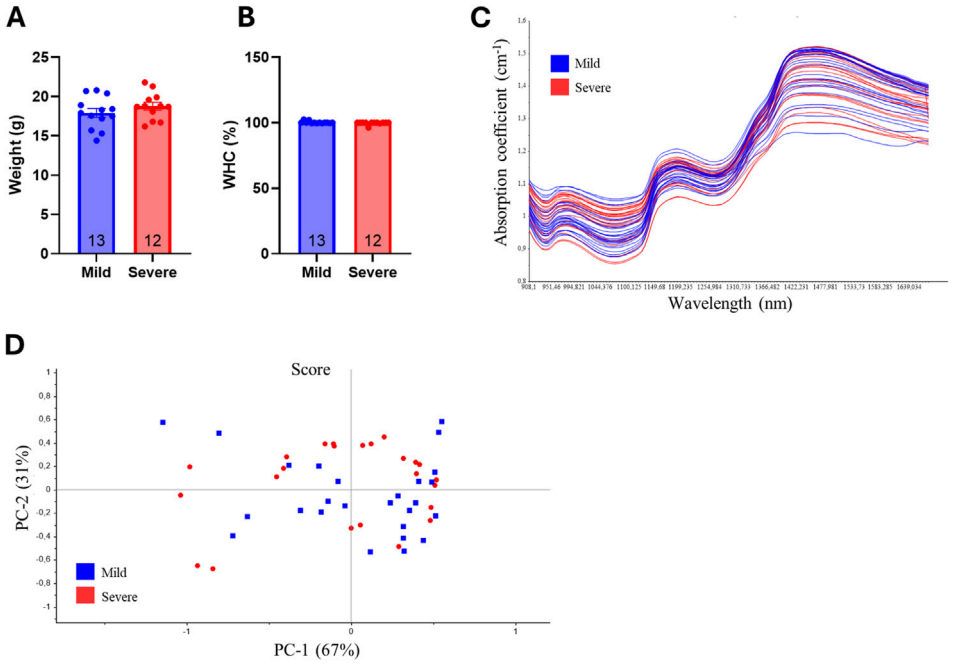

FIGURE 1
No significant differences in heart weight, water binding, protein, or fat deposition were observed between the hearts of mildly and severely WB-affected chickens. Ross 308 chicken heart **(A)** weight and **(B)** water binding capacity between mild and severely affected wooden-breast hearts (n = 12–13). Data are presented as mean ± SEM. Comparison between mild and affected groups was assessed with Welch`s testing **(C)** Near-infrared spectroscopy and **(D)** principal component analysis of chicken heart samples. Blue, mildly affected; red, severely affected (n = 12).

display distinct chemical or physical differences (Figure 1D). Altogether, compared to breasts from broilers with severe versus mild WB, hearts from the same animals did not display statistically significant differences in weight, WHC, or fat and protein deposition.

3.2 Wooden breast disease severity was not associated with cardiac fibrosis

One of the hallmarks of WB is the development of fibrosis and changes in the organization of collagen, contributing to the stiffening of the tissue (Sihvo et al., 2014; Sanden et al., 2021). To examine whether WB was also associated with cardiac fibrosis, left ventricle (LV) sections were stained with Masson's trichrome to identify myocardial tissue (pink) and collagen (blue). Visually, prominent collagen deposition was only observed around and within the larger coronary vessels, with circumferentially aligned fibers present in the tunica media (Figures 2A, B; arrows). The percentage of collagen (blue) in the total area was subsequently quantified, revealing no significant differences in fibrosis in LV tissue between the groups (Figure 2C). Further analysis of collagen accumulation in the hearts with Raman spectroscopy revealed no significant differences in collagen intensity ratios at 827/854 cm^{-1} (Figure 2D), 919/936 cm^{-1} (Figure 2E), or 1,657/1,678 cm^{-1} (Figure 2F), suggesting the levels and distribution of collagen were similar between the groups. Overall, while we and others have previously identified marked changes in fibrosis and collagen organization in WB-affected breasts (Sanden et al., 2021; Pejšková et al., 2023), the same alterations were not present in the heart.

3.3 Few alterations in extracellular matrix constituents were observed in the hearts of wooden breast-affected chickens

The lack of fibrosis in the chicken hearts suggests that the overall extracellular matrix (ECM) in the left ventricle is unaffected by WB, independent of the severity. To further analyze the composition of the ECM, several extracellular matrix proteins, cross-linking proteins, and MMPs were analyzed. The mRNA levels of collagen 1A1, collagen 3A1, decorin, lumican, LOX and biglycan were not altered between hearts from mild and severe WB-affected chickens (Figures 3A–F). Consistently, the protein levels of decorin, and LOX were also not altered between groups (Figures 3G, H). The levels of biglycan and fibromodulin were, however, reduced in the hearts of severe versus mildly WB-affected chickens (Figures 3I, J). Although the mRNA levels of the MMPs, MMP2 and MMP9, were not altered (Figures 3K, L), the protein levels of MMP2, but not MMP9, was increased in the hearts of severe WB-affected chickens (Figures 3M, N). The mRNA level of tissue inhibitor of metalloproteinase 2 (TIMP2) was decreased (Figure 3O).

Altogether, although few alterations were detected in the hearts between the two groups, levels of bigylcan, fibromodulin, MMP2 and TIMP2 appeared to be altered.

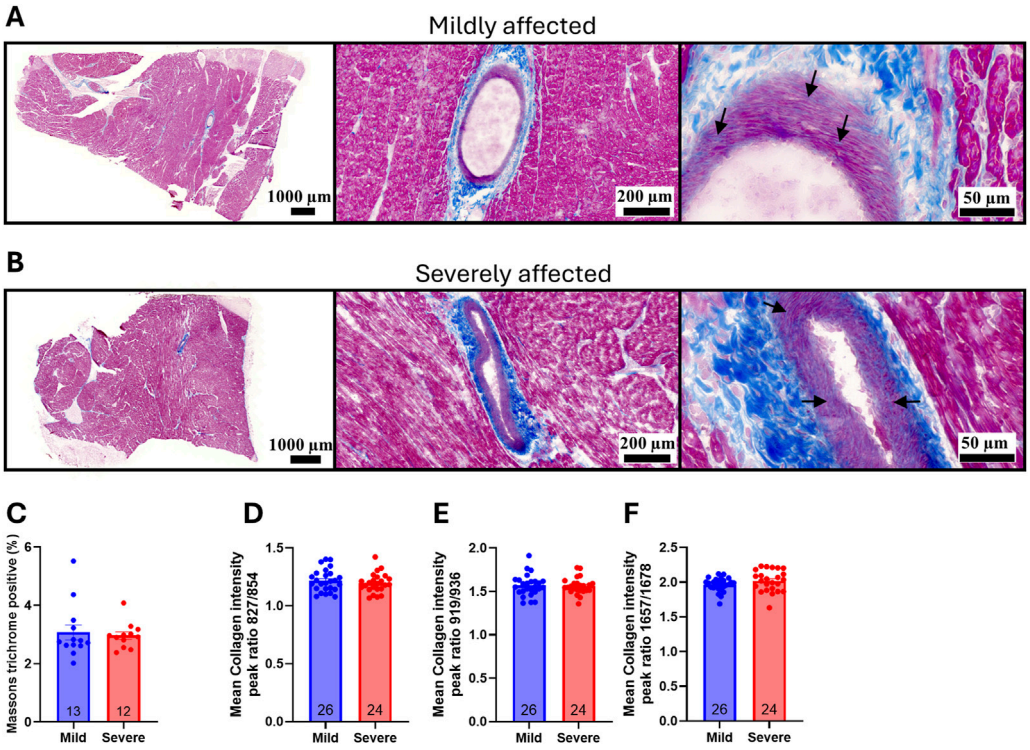

FIGURE 2
WB disease severity was not associated with cardiac fibrosis. Representative Masson`s trichrome staining of **(A)** mild and **(B)** severely affected Ross 308 chicken left ventricles (n = 12–13). Arrows point to collagen deposition in the tunica media **(C)** Quantification of percentage collagen in the total area of the left ventricle (n = 12–13). Raman spectroscopy collagen markers by peak intensity ratios at **(D)** 827/854 cm^{-1} **(E)** 919/936 cm^{-1}, or **(F)** 1,657/1,678 cm^{-1} (n = 12–13, samples run in duplicates). Data are presented as mean ± SEM. Comparison between mild and affected groups was assessed with a Mann-Whitney *U*-test or Welch's t-test.

3.4 Syndecan gene expression and protein levels were not altered between hearts from mildly and severely wooden breast-affected chickens

Syndecans have previously been found to be altered in cardiac fibrosis [reviewed in (Lunde et al., 2016)]. Since we have previously found the syndecans to be differentially regulated between the mild and severely WB-affected groups (Pejšková et al., 2023), we investigated the gene expression and protein levels of the syndecans in the hearts of the same broilers. Compared to the chicken breast where syndecan-2 mRNA expression was decreased and syndecan-4 expression was increased in severely affected WB breasts (Pejšková et al., 2023), no differences were observed in the gene expression levels of syndecan-1-4 in the hearts between groups (Figures 4A–D). To investigate potential alterations in the protein and shedding levels of the syndecans, the heart lysates were immunoblotted for the syndecans using custom-made antibodies against the chicken cytoplasmic domains (Pejšková et al., 2023). As expected, we detected multiple syndecan-positive bands (Figures 4E–H). The specificity of these bands was verified by epitope blocking experiments (Supplementary Figures 1A–D), revealing specificity of bands at ~10–250+ kDa for syndecan-1, ~10–75 kDa for syndecan-2, ~10–150 kDa for syndecan-3 and ~15–150 kDa for syndecan-4 (Figures 4E–H). The core proteins of the chicken syndecans are relatively small where syndecan-1 is 308 amino acids (aa) in length, syndecan-2 is 201 aa, syndecan-3 is 405 aa, and syndecan-4 is 197 aa. The smaller molecular weight fragments (<20 kDa) observed in syndecan-1-4 are likely the cytoplasmic tail and transmembrane domain of the syndecans after extracellular shedding. We also observed multiple higher molecular weight bands which are likely SDS-resistant homo- or hetero-oligomers of the syndecans. We did, however, not observe significant differences in the levels of the different syndecan forms between hearts from mild and severely WB-affected chickens (Figures 4E–H).

3.5 Alterations in Wnt and mTOR signaling, HSP70, and MLP

To assess similarities between the breast and the heart of severely versus mildly WB-affected chickens, we next analyzed various signaling pathways that we have previously found altered (Pejšková et al., 2023). The protein level of the Wnt signaling ligand Wnt3a was reduced in the hearts of the severely WB-affected chickens (Figure 5A), while the levels of Wnt4 were increased (Figure 5B). Levels of Wnt7a remained unaltered between the groups (Figure 5C). We have previously found increased levels of both Wnt4 and Wnt7a in the severely WB-affected chickens (Pejšková et al., 2023). Furthermore, the mammalian target of rapamycin (mTOR) signaling also appeared

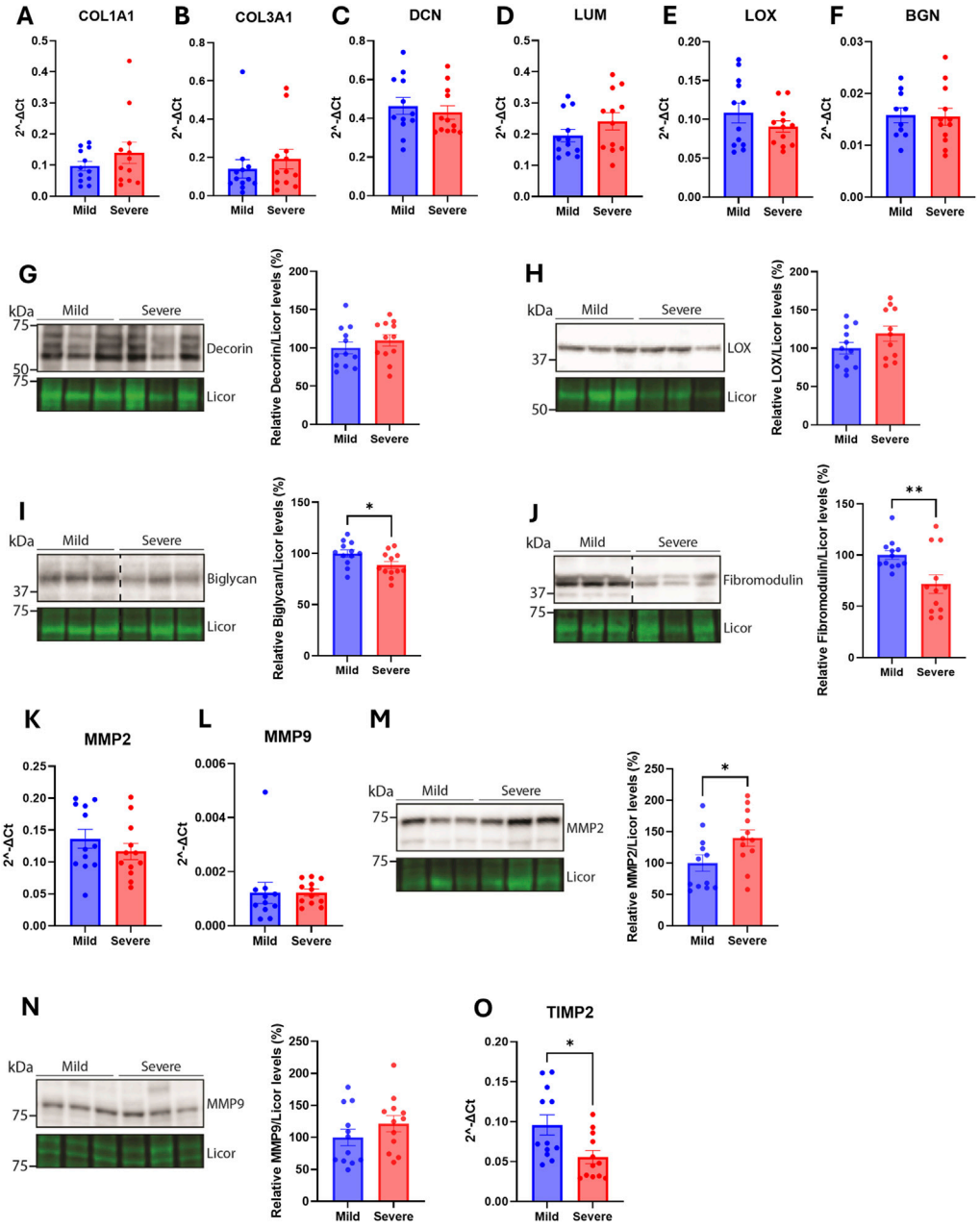

FIGURE 3
Few alterations in extracellular matrix constituents were observed in the hearts WB-affected chickens. Gene expression by RT-qPCR of **(A)** collagen type 1 α1 **(B)** collagen type 3 α1 **(C)** decorin **(D)** lumican **(E)** LOX, and **(F)** biglycan in hearts of mild and severely affected chicken (n = 12). Immunoblotting of **(G)** decorin **(H)** LOX **(I)** biglycan, and **(J)** fibromodulin in hearts of mild and severely affected chickens (n = 11–12). Gene expression by RT-qPCR of **(K)** MMP2, and **(L)** MMP9. Immunoblotting of **(M)** MMP2 and **(N)** MMP9 in hearts of mild and severely affected chickens (n = 12) **(O)** Gene expression by RT-qPCR of TIMP2 in hearts of mild and severely affected chickens (n = 12). RT-qPCR data are presented as the fold change average relative to the mean of the mildly affected samples and immunoblots are presented as mean ± SEM. Licor was used to show equal loading in **(G–J, M, N)** (lower panels). Differences between groups were assessed with either Welch's t-tests, Mann-Whitney *U* tests, or student's *t*-tests.

to be altered in the hearts of severe WB-affected chickens. Whereas both the pSer2448-mTOR and total mTOR levels were reduced, the pSer2448-mTOR/mTOR level was increased (Figure 5D).

The heat shock protein HSP70, known to be increased in the blood of chickens upon heat stimulation (Greene et al., 2024), was also reduced in the hearts of severely WB-affected chickens (Figure 5E). HSP70 is also located in the mitochondria where it acts as an important chaperone of the import, folding, and assembly of proteins in the mitochondria (Herrmann et al., 1994). The small muscle LIM protein (MLP), known for its crucial role in cardiac and skeletal function [reviewed in (Vafiadaki et al., 2015)] was elevated in the hearts of severe WB-affected chickens (Figure 5F). Other signaling pathways, such as Akt and p38 mitogen-activated kinase (MAPK) phosphorylation and total protein levels, and markers of cardiomyocyte contractile health such as cardiac troponin T, were not altered between the WB-affected groups (Supplementary Figures

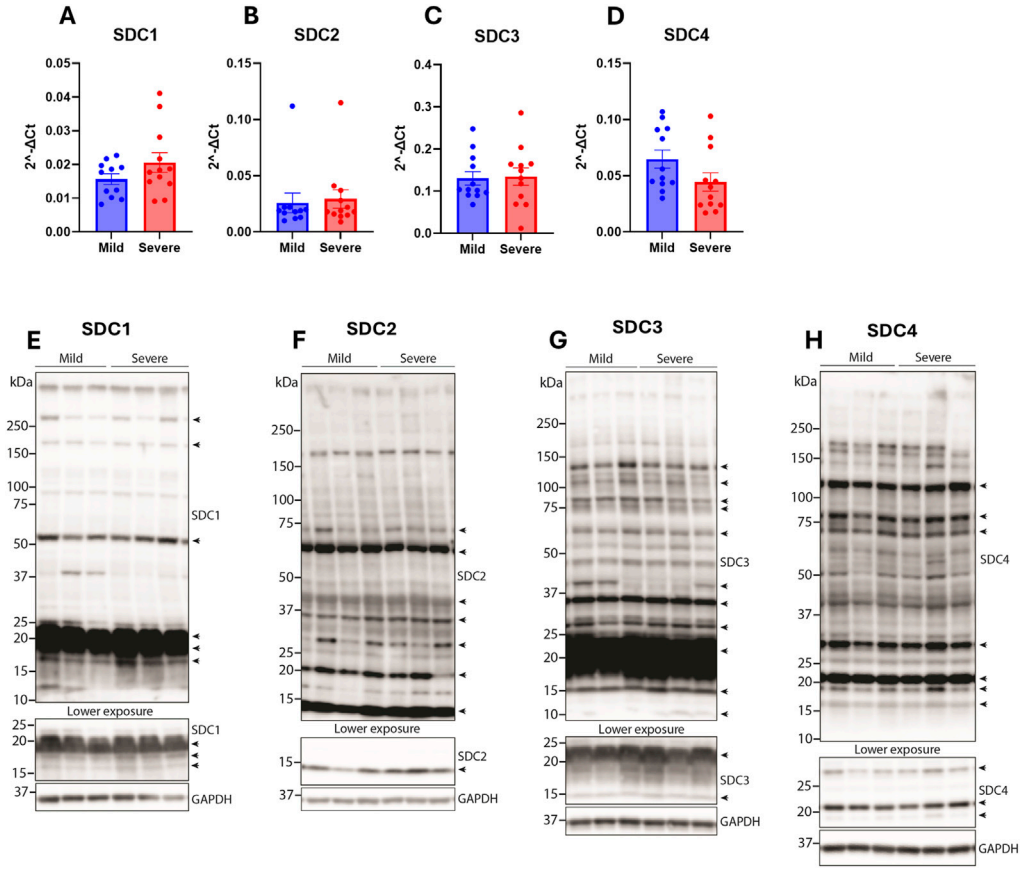

FIGURE 4
Syndecan gene and protein expression were not altered between hearts from mildly and severely WB-affected chickens. Gene expression of **(A)** syndecan-1 **(B)** syndecan-2 **(C)** syndecan-3, and **(D)** syndecan-4 in the hearts from mild and severely affected chickens was assessed by RT-qPCR (n = 12). Data are presented as the fold change average relative to the mean of the mildly affected samples. Differences between groups were assessed by Welch`s t-tests. Immunoblotting of **(E)** syndecan-1 **(F)** syndecan-2 **(G)** syndecan-3, and **(H)** syndecan-4 in the hearts from mild and severely affected chickens (n = 12). Syndecan-specific bands are annotated with arrows on the right (n = 3). Specificity of bands is shown in Supplementary Figures 1A–D. GAPDH was used to verify equal protein loading (40 µg).

2A–C). We also analyzed the expression of known markers of inflammation, the cytoskeleton, myofibroblast, and fibrosis-triggering genes. No differences were observed in interleukin-1β (IL-1β), toll-like receptor 4 (TLR4), tubulin α1 (TUBA1A), tubulin β1 (TUBB1), desmin (DES), β-tropomyosin (TPM2), cardiac troponin T (TNNT2), platelet-derived growth factor receptor β (PDGFRb), α-actin (ACTA2), or transforming growth factor β1 (TGFB1) gene expression between hearts of the mildly and severely WB-affected chickens (Supplementary Figures 3A–J).

3.6 Functional enrichment of RNA sequencing

Finally, since few alterations were found in the macronutrient composition of the hearts, fibrosis, ECM gene expression and protein levels, and classic disease-associated cardiac markers, we performed RNA sequencing to identify potential alterations between hearts from mildly and severely WB-affected chickens. The number of differentially regulated genes between the two groups was minimal, further confirming the absence of a strong pathological signature in the hearts of WB-affected chickens.

However, functional gene set enrichment analysis (GSEA) of the global changes in gene expression between mildly and severely affected chickens, identified an interesting trend: Functions associated with inflammation and acute phase response were enriched with a positive Normalized Enrichment Score (NES) in severely WB-affected chickens, while functions associated with cell proliferation and metabolism were enriched with a negative NES (Figures 6A–C).

4 Discussion

In the present study, we have investigated the histological and molecular alterations in the hearts of mildly and severely WB-affected chickens. While we have previously found alterations in ECM remodeling, fibrosis development, syndecan expression and shedding, and various signaling pathways in severely affected chicken breasts (Pejšková et al., 2023), the hearts from the same

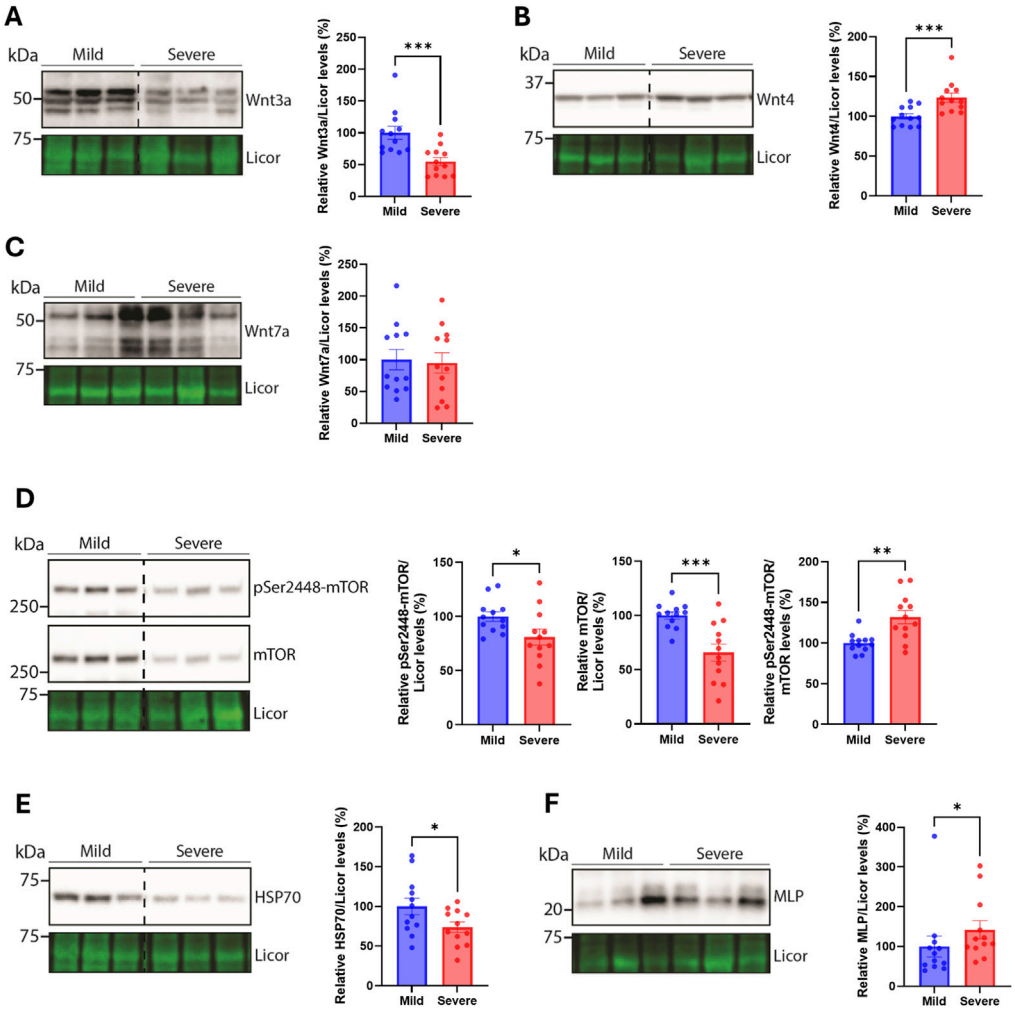

FIGURE 5
Alterations in Wnt and mTOR signaling, HSP70, and MLP. Immunoblotting of **(A)** Wnt3a **(B)** Wnt4 **(C)** Wnt7a **(D)** pSer2448-mTOR and mTOR **(E)** HSP70, and **(F)** MLP in hearts from mild and severely affected chicken hearts (n = 12). Licor was used to show equal loading (lower panels). Immunoblots are presented as mean ± SEM. Differences between groups were assessed with Mann-Whitney *U*-tests or student's *t*-tests.

chickens did not display changes to the same extent. Although we observed a reduction in biglycan and fibromodulin, an increase in MMP2, and alterations in Wnt ligands, mTOR, HSP70, and MLP, few differences in total heart weight, nutritional composition, fibrosis, ECM, or cardiac and inflammatory markers were detected. However, functional enrichment analysis of RNA sequencing of the hearts suggests a different molecular footprint between the groups.

WHC, NIR, and PCA analyses were conducted to analyze macronutrient composition for a larger overview of the hearts between severity groups. Previous studies of WB-affected breasts have shown a decrease in protein content and water binding, but an increase in fat and collagen deposition in severely affected samples (Soglia et al., 2016; Wold et al., 2017; Pejšková et al., 2023). However, the hearts from severely WB-affected chickens did not display alterations in their macronutrient composition compared to samples from mildly affected chickens. Fat accumulation in the heart is known to initiate an inflammatory response, the production of reactive oxygen species, and a decline in mitochondrial function, which can harm the heart's function (Guzzardi and Iozzo, 2011). Consistently with no fat or collagen deposition, we did not detect changes in the gene expression levels of markers associated with inflammation, such as IL-1β, TLR4, or TGFβ.

Hypertrophy of the heart is often associated with fibrotic development and remodeling of the ECM of the myocardium in mammalian disease (Li et al., 2018). Progressive fibrotic remodeling is linked to a decline in cardiac function, an increased risk of arrhythmias, and eventually heart failure (de Jong et al., 2011; Travers et al., 2016; Park et al., 2019). Based on the histological appearance, fibrosis can be categorized into three subtypes: replacement, vascular, or interstitial fibrosis. In the chicken breast, fibrosis as a result of WB disease seems to be mainly interstitial fibrosis, where an increase in ECM proteins expands the space between the myocytes (Che et al., 2022). However, the infiltrative interstitial fibrosis observed in the breast muscle of WB chickens (Soglia et al., 2016) was not evident in the myocardial tissue of mildly and severely affected chickens in this study. We did, however, observe pronounced fibrillar collagen fiber formation within the tunica media of the coronary arteries in both groups. These fibers were circumferentially aligned, a pattern more

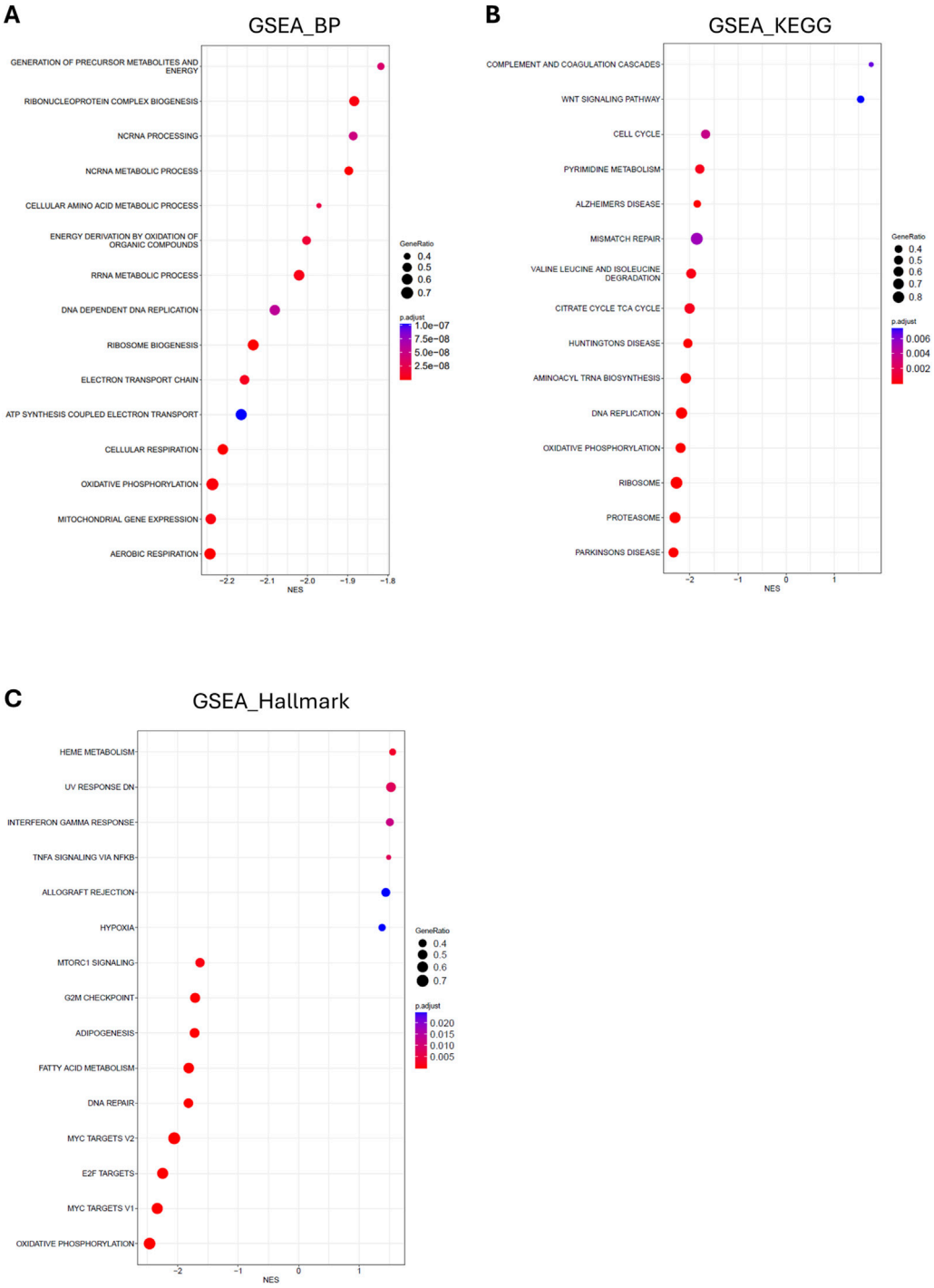

FIGURE 6
Functional enrichment of RNA sequencing of hearts from mild and severely WB-affected chicken. Bubble plot of gene set enrichment analysis of the top 15 altered **(A)** gene ontology biological processes **(B)** KEGG pathways, and **(C)** Hallmark pathways between hearts from mild and severely WB-affected chickens. Dot size indicates the number of genes in each given function. Dot color indicates the p-adjust for each given function as reported in the indicated scale. The X-axis shows the normalized enrichment score (NES) of the differentially expressed processes and pathways in hearts from severe versus mild WB-affected chickens.

commonly observed in arteries during physiological aging (Jadidi et al., 2021) and associated with increased arterial wall stiffness. Given the lack of fibrotic development and other indicators of pathological cardiac remodeling, the pronounced but organized collagen fiber deposition within the coronary vessel may indicate an adaptive development of stabilizing fibers within the heart. Indeed, the radically accelerated growth rate of commercial broilers compared to earlier unselected strains has resulted in larger body mass with a relative smaller heart mass (Harash et al., 2019). It could be postulated that this adds additional

strain on the vasculature of these chickens, including the aorta itself, which may require additional structural support in the form of stabilizing fibrillar collagens in the tunica media, which we observed in our study.

Furthermore, we analyzed Wnt and mTOR signaling, due to our previous findings of dysregulated Wnt and Akt/mTOR in the severely affected breasts of the same broilers (Pejšková et al., 2023). In the heart, Wnt ligands Wnt3a and Wnt4 were decreased and increased, respectively, suggesting the heart of severely versus mildly WB-affected chickens also have altered Wnt signaling. Wnt signaling is important for many embryonic processes such as cell proliferation, spatial tissue patterning and differentiation (Foulquier et al., 2018). In the adult heart, an upregulation in the gene expression of Wnt ligands has been observed after myocardial infarction in mice (Aisagbonhi et al., 2011), and activation of the signaling pathway has been found to promote fibrosis development upon cardiac injury and repair [Reviewed in (Deb, 2014; Pahnke et al., 2016)].

mTOR signaling, on the other hand, is required for hypertrophy development, and its inhibition or deletion leads to a lack of compensatory and pathological hypertrophy, inhibition of protein synthesis, and cardiac dysfunction (Sciarretta et al., 2014). We observed lower levels of pSer2448-mTOR and total mTOR levels, which may indicate that the hearts of severely WB-affected chickens are less able to respond or cope with increased stressors, such as changes in cardiac demand due to an increase in skeletal muscle growth.

The reduction in HSP70 we observed may also suggest that the hearts of severely WB-affected chickens are less robust in coping with prolonged stressors. HSP70 protects the heart from ischemia-reperfusion injury (Song et al., 2020). HSP70 has also been found to trigger hypertrophy and fibrosis (Liu et al., 2019), which we did not observe in the hearts included in our study.

The muscle-specific protein MLP was increased in the hearts of severe WB-affected chickens. MLP has previously been found to be important for chicken satellite cell differentiation, and chicken myofiber composition (Han et al., 2019; Shan et al., 2023). In humans, MLP levels increase in the failing heart (Boateng et al., 2007). Altogether, an increase in MLP levels in the hearts of severe WB-affected chickens may suggest these hearts are more prone to dysfunction later in development.

Lastly, we performed RNA sequencing of hearts from chickens affected by mild and severe WB disease. The finding via GSEA analysis that metabolic functions, especially those related to mitochondrial function, are downregulated, is consistent with our previous findings in skeletal muscle (Pejšková et al., 2023). Also consistent with the early stages of developing heart disease, we observed an increase in inflammatory functions. Altogether, these data suggest that, while at the phenotypic and molecular levels little to no difference is observable between mildly and severely affected chickens, the global transcriptomic landscape appears to be laying the molecular foundation for the development of heart disease.

An important factor to consider in interpreting the presented results is the lack of comparison to a healthy control. However, all chickens of the Ross308 breed seem to display some signs of skeletal muscle myopathy (Pejšková et al., 2023; Pejšková et al., 2024), making the use of a healthy control group difficult. Our study compared cardiac samples from severely affected chickens to those from mildly affected chickens. As such, it is not possible to differentiate whether no changes were present in the heart between the groups, or whether changes were present to the same extent independent of severity. A comparative analysis against another breed, such as the more slow-growing Hubbard JA787 broiler line with a lower mortality rate when bred under commercial conditions, may be necessary to answer such questions (Forseth et al., 2024).

Another alternative is the age at which the broilers were harvested. The chickens used in this study were 36 days post-hatching, which may be too young for cardiac fibrotic remodeling and molecular changes to be present. It is possible that the accelerated growth rate of the skeletal muscle, inducing pathological hypertrophy and fibrotic remodeling, outstrips cardiac growth. This is also evident in Duchenne muscular dystrophy where patients normally develop clinical symptoms of weakness and fatigue in the skeletal muscle of the legs at 3–5 years of age. These patients subsequently develop alterations in their cardiac function at approximately 9–10 years of age (Meyers and Townsend, 2019).

To conclude, we have in this study investigated alterations in the hearts of Ross 308 broiler chickens with mild and severe WB disease. Although few alterations were found in the macro composition of the hearts between the two groups, deeper molecular analysis and RNA sequencing suggest that the molecular footprint does differ depending on WB severity. Such differences may become more prominent with age, perhaps leading to cardiac dysfunction.

Data availability statement

The data presented in the study are deposited in the European Nucleotide Archive (ENA) repository, accession number PRJEB85439.

Ethics statement

Ethical approval was not required for the study involving animals in accordance with the local legislation and institutional requirements because the tissue used was extracted from already slaughtered chickens (Ross 308 breed, NMBU, Norway). Chickens used were in line with common regulatory roles of food production and therefore REC and NSD approval is not required. Complying with Norwegian law and regulations concerning animals for experimental use, ethical approval is not necessary when samples are obtained from slaughtered animals or non-experimental agriculture and aquaculture. This was confirmed by direct communication with the Norwegian Food Safety Authority (Mattilsynet).

Author contributions

TS: Data curation, Formal Analysis, Investigation, Methodology, Software, Validation, Visualization, Writing–original draft,

Writing–review and editing. AR: Data curation, Formal Analysis, Investigation, Methodology, Software, Writing–original draft, Writing–review and editing, Validation, Visualization. TK: Formal Analysis, Investigation, Methodology, Writing–review and editing, Visualization. VH: Methodology, Writing–review and editing. ML: Data curation, Investigation, Methodology, Writing–review and editing, Validation. AH: Investigation, Methodology, Writing–review and editing. TL: Investigation, Methodology, Visualization, Writing–review and editing. KS: Investigation, Methodology, Visualization, Writing–review and editing. SK: Writing–review and editing, Funding acquisition, Resources. JW: Writing–review and editing. AP: Writing–original draft, Data curation, Formal Analysis, Investigation, Methodology, Software, Validation, Visualization. SR: Conceptualization, Supervision, Writing–review and editing, Funding acquisition. CC: Conceptualization, Funding acquisition, Methodology, Project administration, Resources, Supervision, Writing–original draft, Writing–review and editing. MP: Conceptualization, Funding acquisition, Project administration, Supervision, Writing–review and editing.

Funding

The author(s) declare that financial support was received for the research, authorship, and/or publication of this article. This work was supported by a grant from the Research Council of Norway (NFR 323939).

Conflict of interest

The authors declare that the research was conducted in the absence of any commercial or financial relationships that could be construed as a potential conflict of interest.

Generative AI statement

The author(s) declare that no Generative AI was used in the creation of this manuscript.

Publisher's note

Supplementary material

The Supplementary Material for this article can be found online at: https://www.frontiersin.org/articles/10.3389/fphys.2025.1547661/full#supplementary-material

References

Aisagbonhi, O., Rai, M., Ryzhov, S., Atria, N., Feoktistov, I., and Hatzopoulos, A. K. (2011). Experimental myocardial infarction triggers canonical Wnt signaling and endothelial-to-mesenchymal transition. *Dis. Models and Mech.* 4 (4), 469–483. doi:10.1242/dmm.006510

Andrews, S. (2010). *FastQC: a quality control tool for high throughput sequence data*. Cambridge, United Kingdom.

Barnes, R. J., Dhanoa, M. S., and Lister, S. J. (1989). Standard normal variate transformation and de-trending of near-infrared diffuse reflectance spectra. *Appl. Spectrosc.* 43 (5), 772–777. doi:10.1366/0003702894202201

Boateng, S. Y., Belin, R. J., Geenen, D. L., Margulies, K. B., Martin, J. L., Hoshijima, M., et al. (2007). Cardiac dysfunction and heart failure are associated with abnormalities in the subcellular distribution and amounts of oligomeric muscle LIM protein. *Am. J. Physiology-Heart Circulatory Physiology* 292 (1), H259–H269. doi:10.1152/ajpheart.00766.2006

Bustin, S. A., Benes, V., Garson, J. A., Hellemans, J., Huggett, J., Kubista, M., et al. (2009). The MIQE guidelines: minimum information for publication of quantitative real-time PCR experiments. *Clin. Chem.* 55 (4), 611–622. doi:10.1373/clinchem.2008.112797

Che, S., Wang, C., Iverson, M., Varga, C., Barbut, S., Bienzle, D., et al. (2022). Characteristics of broiler chicken breast myopathies (spaghetti meat, woody breast, white striping) in Ontario, Canada. *Poult. Sci.* 101 (4), 101747. doi:10.1016/j.psj.2022.101747

Costamagna, D., Quattrocelli, M., Duelen, R., Sahakyan, V., Perini, I., Palazzolo, G., et al. (2014). Fate choice of post-natal mesoderm progenitors: skeletal versus cardiac muscle plasticity. *Cell. Mol. Life Sci.* 71 (4), 615–627. doi:10.1007/s00018-013-1445-7

Czubryt, M. P., and Hale, T. M. (2021). Cardiac fibrosis: pathobiology and therapeutic targets. *Cell. Signal.* 85, 110066. doi:10.1016/j.cellsig.2021.110066

de Almeida Assunção, A. S., Garcia, R. G., Komiyama, C. M., de Sena Gandra, É. R., de Souza, J. R., dos Santos, W., et al. (2020). Wooden breast myopathy on broiler breast fillets affects quality and consumer preference. *Trop. Animal Health Prod.* 52 (6), 3555–3565. doi:10.1007/s11250-020-02392-6

Deb, A. (2014). Cell-cell interaction in the heart via Wnt/β-catenin pathway after cardiac injury. *Cardiovasc. Res.* 102 (2), 214–223. doi:10.1093/cvr/cvu054

de Jong, S., van Veen, T. A., van Rijen, H. V., and de Bakker, J. M. (2011). Fibrosis and cardiac arrhythmias. *J. Cardiovasc. Pharmacol.* 57 (6), 630–638. doi:10.1097/FJC.0b013e318207a35f

Dobin, A., Davis, C. A., Schlesinger, F., Drenkow, J., Zaleski, C., Jha, S., et al. (2013). STAR: ultrafast universal RNA-seq aligner. *Bioinformatics* 29 (1), 15–21. doi:10.1093/bioinformatics/bts635

Forseth, M., Moe, R. O., Kittelsen, K., Skjerve, E., and Toftaker, I. (2023). Comparison of carcass condemnation causes in two broiler hybrids differing in growth rates. *Sci. Rep.* 13 (1), 4195. doi:10.1038/s41598-023-31422-0

Forseth, M., Moe, R. O., Kittelsen, K., and Toftaker, I. (2024). Mortality risk on farm and during transport: a comparison of 2 broiler hybrids with different growth rates. *Poult. Sci.* 103 (3), 103395. doi:10.1016/j.psj.2023.103395

Foulquier, S., Daskalopoulos, E. P., Lluri, G., Hermans, K. C. M., Deb, A., and Blankesteijn, W. M. (2018). WNT signaling in cardiac and vascular disease. *Pharmacol. Rev.* 70 (1), 68–141. doi:10.1124/pr.117.013896

Greene, E. S., Tabler, T., Bottje, W. G., Orlowski, S., and Dridi, S. (2024). Effect of heat stress on the expression of circulating cyto(chemo)kine and inflammatory markers in broiler chickens selected for high- or low-water efficiency. *Front. Bioscience-Landmark* 29 (10), 359. doi:10.31083/j.fbl2910359

Guzzardi, M. A., and Iozzo, P. (2011). Fatty heart, cardiac damage, and inflammation. *Rev. Diabet. Stud.* 8 (3), 403–417. doi:10.1900/rds.2011.8.403

Han, S., Cui, C., Wang, Y., He, H., Liu, Z., Shen, X., et al. (2019). Knockdown of CSRP3 inhibits differentiation of chicken satellite cells by promoting TGF-β/Smad3 signaling. *Gene* 707, 36–43. doi:10.1016/j.gene.2019.03.064

Harash, G., Richardson, K. C., Alshamy, Z., Hünigen, H., Hafez, H. M., Plendl, J., et al. (2019). Heart ventricular histology and microvasculature together with aortic histology and elastic lamellar structure: a comparison of a novel dual-purpose to a broiler chicken line. *PLOS ONE* 14 (3), e0214158. doi:10.1371/journal.pone.0214158

Herrmann, J. M., Stuart, R. A., Craig, E. A., and Neupert, W. (1994). Mitochondrial heat shock protein 70, a molecular chaperone for proteins encoded by mitochondrial DNA. *J. Cell Biol.* 127 (4), 893–902. doi:10.1083/jcb.127.4.893

Herum, K. M., Romaine, A., Wang, A., Melleby, A. O., Strand, M. E., Pacheco, J., et al. (2020). Syndecan-4 protects the heart from the profibrotic effects of thrombin-cleaved osteopontin. *J. Am. Heart Assoc.* 9 (3), e013518. doi:10.1161/jaha.119.013518

Jadidi, M., Razian, S. A., Anttila, E., Doan, T., Adamson, J., Pipinos, M., et al. (2021). Comparison of morphometric, structural, mechanical, and physiologic characteristics of human superficial femoral and popliteal arteries. *Acta Biomater.* 121, 431–443. doi:10.1016/j.actbio.2020.11.025

Korotkevich, G., Sukhov, V., Budin, N., Shpak, B., Artyomov, M., and Sergushichev, A. (2016). Fast gene set enrichment analysis. *bioRxiv*. doi:10.1101/060012

Krueger, F., James, F. O., Ewels, P. A., Afyounian, E., and Schuster-Boeckler, B. (2021). *FelixKrueger/TrimGalore: v0.6.7 - DOI via zenodo*.

Kuttappan, V. A., Hargis, B. M., and Owens, C. M. (2016). White striping and woody breast myopathies in the modern poultry industry: a review. *Poult. Sci.* 95 (11), 2724–2733. doi:10.3382/ps/pew216

Langfelder, P., and Horvath, S. (2008). WGCNA: an R package for weighted correlation network analysis. *BMC Bioinforma.* 9 (1), 559. doi:10.1186/1471-2105-9-559

Li, H., Handsaker, B., Wysoker, A., Fennell, T., Ruan, J., Homer, N., et al. (2009). The sequence alignment/map format and SAMtools. *Bioinformatics* 25 (16), 2078–2079. doi:10.1093/bioinformatics/btp352

Li, L., Zhao, Q., and Kong, W. (2018). Extracellular matrix remodeling and cardiac fibrosis. *Matrix Biol.* 68-69, 490–506. doi:10.1016/j.matbio.2018.01.013

Lintvedt, T. A., Andersen, P. V., Afseth, N. K., and Wold, J. P. (2024). In-line Raman spectroscopy for characterization of an industrial poultry raw material stream. *Talanta* 266, 125079. doi:10.1016/j.talanta.2023.125079

Liu, P., Bao, H. Y., Jin, C. C., Zhou, J. C., Hua, F., Li, K., et al. (2019). Targeting extracellular heat shock protein 70 ameliorates doxorubicin-induced heart failure through resolution of toll-like receptor 2–mediated myocardial inflammation. *J. Am. Heart Assoc.* 8 (20), e012338. doi:10.1161/JAHA.119.012338

Love, M. I., Huber, W., and Anders, S. (2014). Moderated estimation of fold change and dispersion for RNA-seq data with DESeq2. *Genome Biol.* 15 (12), 550. doi:10.1186/s13059-014-0550-8

Lunde, I. G., Herum, K. M., Carlson, C. C., and Christensen, G. (2016). Syndecans in heart fibrosis. *Cell Tissue Res.* 365 (3), 539–552. doi:10.1007/s00441-016-2454-2

Martin, M. (2011). Cutadapt removes adapter sequences from high-throughput sequencing reads. *EMBnet. J.* 17 (1), 10. doi:10.14806/ej.17.1.200

Martinez, M. G., Bullock, A. J., MacNeil, S., and Rehman, I. U. (2019). Characterisation of structural changes in collagen with Raman spectroscopy. *Appl. Spectrosc. Rev.* 54 (6), 509–542. doi:10.1080/05704928.2018.1506799

Meyers, T. A., and Townsend, D. (2019). Cardiac pathophysiology and the future of cardiac therapies in Duchenne muscular dystrophy. *Int. J. Mol. Sci.* 20 (17), 4098. doi:10.3390/ijms20174098

Monago-Maraña, O., Wold, J. P., Rødbotten, R., Dankel, K. R., and Afseth, N. K. (2021). Raman, near-infrared and fluorescence spectroscopy for determination of collagen content in ground meat and poultry by-products. *LWT* 140, 110592. doi:10.1016/j.lwt.2020.110592

Mudalal, S., Lorenzi, M., Soglia, F., Cavani, C., and Petracci, M. (2015). Implications of white striping and wooden breast abnormalities on quality traits of raw and marinated chicken meat. *Animal* 9 (4), 728–734. doi:10.1017/S175173111400295X

Mutryn, M. F., Brannick, E. M., Fu, W., Lee, W. R., and Abasht, B. (2015). Characterization of a novel chicken muscle disorder through differential gene expression and pathway analysis using RNA-sequencing. *BMC Genomics* 16 (1), 399. doi:10.1186/s12864-015-1623-0

Pahnke, A., Conant, G., Huyer, L. D., Zhao, Y., Feric, N., and Radisic, M. (2016). The role of Wnt regulation in heart development, cardiac repair and disease: a tissue engineering perspective. *Biochem. Biophysical Res. Commun.* 473 (3), 698–703. doi:10.1016/j.bbrc.2015.11.060

Park, S., Nguyen, N. B., Pezhouman, A., and Ardehali, R. (2019). Cardiac fibrosis: potential therapeutic targets. *Transl. Res.* 209, 121–137. doi:10.1016/j.trsl.2019.03.001

Patro, R., Duggal, G., Love, M. I., Irizarry, R. A., and Kingsford, C. (2017). Salmon provides fast and bias-aware quantification of transcript expression. *Nat. Methods* 14 (4), 417–419. doi:10.1038/nmeth.4197

Pejšková, L., Pisconti, A., Lunde, M., Ho, K. Y., Solberg, N. T., Koga, S., et al. (2024). Wooden breast myopathy is characterized by satellite cell dysfunction and syndecan-4 shedding. *Front. Physiology* 15, 1513311. doi:10.3389/fphys.2024.1513311

Pejšková, L., Rønning, S. B., Kent, M. P., Solberg, N. T., Høst, V., Thu-Hien, T., et al. (2023). Characterization of wooden breast myopathy: a focus on syndecans and ECM remodeling. *Front. Physiology* 14, 1301804. doi:10.3389/fphys.2023.1301804

Petracci, M., Mudalal, S., Soglia, F., and Cavani, C. (2015). Meat quality in fast-growing broiler chickens. *World's Poult. Sci. J.* 71 (2), 363–374. doi:10.1017/S0043933915000367

Posner, A. D., Soslow, J. H., Burnette, W. B., Bian, A., Shintani, A., Sawyer, D. B., et al. (2016). The correlation of skeletal and cardiac muscle dysfunction in Duchenne muscular dystrophy. *J. Neuromuscul. Dis.* 3 (1), 91–99. doi:10.3233/jnd-150132

Prisco, F., Papparella, S., and Paciello, O. (2020). The correlation between cardiac and skeletal muscle pathology in animal models of idiopathic inflammatory myopathies. *Acta Myol.* 39 (4), 313–319. doi:10.36185/2532-1900-035

Rygula, A., Majzner, K., Marzec, K. M., Kaczor, A., Pilarczyk, M., and Baranska, M. (2013). Raman spectroscopy of proteins: a review. *J. Raman Spectrosc.* 44 (8), 1061–1076. doi:10.1002/jrs.4335

Sanden, K. W., Böcker, U., Ofstad, R., Pedersen, M. E., Høst, V., Afseth, N. K., et al. (2021). Characterization of collagen structure in normal, wooden breast and spaghetti meat chicken fillets by FTIR microspectroscopy and histology. *Foods* 10 (3), 548. doi:10.3390/foods10030548

Schmittgen, T. D., and Livak, K. J. (2008). Analyzing real-time PCR data by the comparative C(T) method. *Nat. Protoc.* 3 (6), 1101–1108. doi:10.1038/nprot.2008.73

Sciarretta, S., Volpe, M., and Sadoshima, J. (2014). Mammalian target of rapamycin signaling in cardiac physiology and disease. *Circulation Res.* 114 (3), 549–564. doi:10.1161/circresaha.114.302022

Shan, Y.-j., Ji, G.-g., Zhang, M., Liu, Y.-f., Tu, Y.-j., Ju, X.-j., et al. (2023). Use of transcriptome sequencing to explore the effect of CSRP3 on chicken myoblasts. *J. Integr. Agric.* 22 (4), 1159–1171. doi:10.1016/j.jia.2022.08.067

Sihvo, H.-K., Immonen, K., and Puolanne, E. (2014). Myodegeneration with fibrosis and regeneration in the pectoralis major muscle of broilers. *Veterinary Pathol.* 51 (3), 619–623. doi:10.1177/0300985813497488

Soglia, F., Mudalal, S., Babini, E., Di Nunzio, M., Mazzoni, M., Sirri, F., et al. (2016). Histology, composition, and quality traits of chicken Pectoralis major muscle affected by wooden breast abnormality. *Poult. Sci.* 95 (3), 651–659. doi:10.3382/ps/pev353

Soneson, C., Love, M. I., and Robinson, M. D. (2015). Differential analyses for RNA-seq: transcript-level estimates improve gene-level inferences. *F1000Research* 4, 1521. doi:10.12688/f1000research.7563.2

Song, N., Ma, J., Meng, X. W., Liu, H., Wang, H., Song, S. Y., et al. (2020). Heat shock protein 70 protects the heart from ischemia/reperfusion injury through inhibition of p38 MAPK signaling. *Oxidative Med. Cell. Longev.* 2020, 3908641. doi:10.1155/2020/3908641

Stephenson, R. S., Agger, P., Lunkenheimer, P. P., Zhao, J., Smerup, M., Niederer, P., et al. (2016). The functional architecture of skeletal compared to cardiac musculature: myocyte orientation, lamellar unit morphology, and the helical ventricular myocardial band. *Clin. Anat.* 29 (3), 316–332. doi:10.1002/ca.22661

Strand, M. E., Aronsen, J. M., Braathen, B., Sjaastad, I., Kvaløy, H., Tønnessen, T., et al. (2015). Shedding of syndecan-4 promotes immune cell recruitment and mitigates cardiac dysfunction after lipopolysaccharide challenge in mice. *J. Mol. Cell. Cardiol.* 88, 133–144. doi:10.1016/j.yjmcc.2015.10.003

Tijare, V. V., Yang, F. L., Kuttappan, V. A., Alvarado, C. Z., Coon, C. N., and Owens, C. M. (2016). Meat quality of broiler breast fillets with white striping and woody breast muscle myopathies. *Poult. Sci.* 95 (9), 2167–2173. doi:10.3382/ps/pew129

Travers, J. G., Kamal, F. A., Robbins, J., Yutzey, K. E., and Blaxall, B. C. (2016). Cardiac fibrosis: the fibroblast awakens. *Circulation Res.* 118 (6), 1021–1040. doi:10.1161/CIRCRESAHA.115.306565

Vafiadaki, E., Arvanitis, D. A., and Sanoudou, D. (2015). Muscle LIM Protein: Master regulator of cardiac and skeletal muscle functions. *Gene* 566 (1), 1–7. doi:10.1016/j.gene.2015.04.077

WackerO, Manning, J., Zoufir, A., nf-core bot, Peltzer, A., Domínguez, C. T., et al. (2023). *nf-core/differentialabundance: v1.4.0 - 2023-11-27 (1.4.0)*. Geneva, Switzerland: Zenodo. doi:10.5281/zenodo.10209675

Wold, J. P., Måge, I., Løvland, A., Sanden, K. W., and Ofstad, R. (2019). Near-infrared spectroscopy detects woody breast syndrome in chicken fillets by the markers protein content and degree of water binding. *Poult. Sci.* 98 (1), 480–490. doi:10.3382/ps/pey351

Wold, J. P., Veiseth-Kent, E., Høst, V., and Løvland, A. (2017). Rapid on-line detection and grading of wooden breast myopathy in chicken fillets by near-infrared spectroscopy. *PLOS ONE* 12 (3), e0173384. doi:10.1371/journal.pone.0173384

Wu, T., Hu, E., Xu, S., Chen, M., Guo, P., Dai, Z., et al. (2021). clusterProfiler 4.0: a universal enrichment tool for interpreting omics data. *innovation* 2 (3), 100141. doi:10.1016/j.xinn.2021.100141

Xing, T., Zhao, X., Zhang, L., Li, J. L., Zhou, G. H., Xu, X. L., et al. (2020). Characteristics and incidence of broiler chicken wooden breast meat under commercial conditions in China. *Poult. Sci.* 99 (1), 620–628. doi:10.3382/ps/pez560

Yu, G., Wang, L. G., Han, Y., and He, Q. Y. (2012). clusterProfiler: an R package for comparing biological themes among gene clusters. *Omics* 16 (5), 284–287. doi:10.1089/omi.2011.0118

Zanetti, M. A., Tedesco, D. C., Schneider, T., Teixeira, S. T. F., Daroit, L., Pilotto, F., et al. (2018). Economic losses associated with wooden breast and white striping in broilers. *Semina Ciências Agrárias* 39 (2), 887–892. doi:10.5433/1679-0359.2018v39n2p887

frontiers | Frontiers in Physiology

TYPE Original Research
PUBLISHED 19 March 2025
DOI 10.3389/fphys.2025.1549585

OPEN ACCESS

EDITED BY
Sandra G. Velleman,
The Ohio State University, United States

REVIEWED BY
Colin Guy Scanes,
University of Wisconsin–Milwaukee, United States
Jiahui Xu,
University of California, Irvine, United States

*CORRESPONDENCE
Pranav Kumar Seth,
pranavseth93@gmail.com
Henrik Mouritsen,
henrik.mouritsen@uol.de

†These authors have contributed equally to this work and share first authorship

RECEIVED 21 December 2024
ACCEPTED 25 February 2025
PUBLISHED 19 March 2025

CITATION
Seth PK, Heyers D, Satish B, Mendoza E, Haase K, Borowsky L, Musielak I, Koch K-W, Feederle R, Scharff C, Dedek K and Mouritsen H (2025) AAV-mediated transduction of songbird retina.
Front. Physiol. 16:1549585.
doi: 10.3389/fphys.2025.1549585

AAV-mediated transduction of songbird retina

Pranav Kumar Seth[1,2*†], Dominik Heyers[1,3†], Baladev Satish[1†], Ezequiel Mendoza[4], Katrin Haase[1], Lisa Borowsky[1], Isabelle Musielak[1], Karl-Wilhelm Koch[3,5], Regina Feederle[6], Constance Scharff[4], Karin Dedek[1,3] and Henrik Mouritsen[1,3*]

[1]Neurosensorics Group/Animal Navigation, Institute of Biology and Environmental Sciences, Carl on Ossietzky University of Oldenburg, Oldenburg, Germany, [2]Sussex Neuroscience, School of Life Sciences, University of Sussex, Brighton, United Kingdom, [3]Research Centre for Neurosensory Science, Carl von Ossietzky University of Oldenburg, Oldenburg, Germany, [4]Institut für Biologie, Freie Universität Berlin, Berlin, Germany, [5]Department of Neuroscience, Biochemistry Group, University of Oldenburg, Oldenburg, Germany, [6]Monoclonal Antibody Core Facility, Helmholtz Zentrum München, German Research Center for Environmental Health, Neuherberg, Germany

Introduction: Genetic manipulation of murine retinal tissue through ocular administration of adeno-associated viruses (AAVs) has become a standard technique to investigate a multitude of mechanisms underlying retinal physiology. Resultantly, developments of recombinant viral vectors with improved transduction efficiency and further methodological improvements have mostly focused on murine tissue, whereas AAVs successfully targeting avian retinae have remained scarce.

Methodology: Using a custom-designed injection setup, we identified a viral serotype with the capability to successfully induce widespread transduction of the bird retina.

Results: Intravitreal administration of an AAV type 2/9 encoding for enhanced green fluorescent protein (EGFP) in night-migratory European robins (*Erithacus rubecula*) resulted in transduction coverages of up to 60% within retinal tissue. Subsequent immunohistochemical analyses revealed that the AAV2/9-EGFP serotype almost exclusively targeted photoreceptors: rods, various single cones (UV, blue, green, and red cones), and both (accessory and principal) members of double cones.

Discussion: The consistently high and photoreceptor-specific transduction efficiency makes the AAV2/9 serotype a powerful tool for carrying out genetic manipulations in avian retinal photoreceptors, thus opening a wealth of opportunities to investigate physiological aspects underlying retinal processing in birds, such as physiological recordings and/or post-transductional behavioural readouts for future vision-related research.

KEYWORDS

AAV, avian retina, photoreceptors, intravitreal injection, European robin, opsin

Introduction

Adeno-associated virus (AAV) vectors are small, single-stranded DNA viruses displaying high transduction efficiency and tropism towards a wide range of host cells (Bennett et al., 1994; Jomary et al., 1994; Li et al., 1994). Their limited capability to induce immune responses has turned them into viable gene therapy tools (Atchison et al., 1965; Balakrishnan and Jayandharan; Ronzitti et al., 2020) for the investigation and treatment of retinal disorders (Buch et al., 2008; Stieger et al., 2011; Ong et al., 2019), such as, e.g., retinal degeneration and/or photoreceptor dystrophies (Ali et al., 2000; Schlichtenbrede et al., 2003; Isiegas et al., 2016; Ziccardi et al., 2019; Bacci et al., 2022).

Over the last 2 decades, mice have turned into the standard model system for retinal viral transduction experiments. Consequently, the continuously ongoing development of recombinant viral vectors with improved transduction efficiency has mostly targeted the murine visual system. In contrast, avian tissue appears to be particularly resistant to transduction using commonly available viral tools (Ahmadiantehrani and London, 2017). Resultantly, only few recombinant viral vector types have proven capable of transducing retinal tissue in birds (Scott and Lois, 2005; Harpavat and Cepko, 2006; Williams et al., 2006; Verrier et al., 2011; Vergara and Canto-Soler, 2012; Waldner et al., 2019).

Moreover, anatomical characteristics specific to birds appear to be disadvantageous to common ocular injection routes, further impeding successful transductions: the subretinal injection method, which targets the space between the photoreceptors and the retinal pigment epithelium (RPE) (Mühlfriedel et al., 2013; Park et al., 2015; Yiu et al., 2020), causes temporary focal detachment of the retina at the injection site (Cebulla et al., 2012; Waldner et al., 2019), leading to the formation of a "suspension bubble". The subretinal space between the photoreceptors and the retinal pigment epithelium in birds is considerably smaller than in mice, thus, in addition to causing potential harm to retinal tissue within the bubble, it restricts the transduction in bird retinae to the near vicinity of the "suspension bubble" (Waldner et al., 2019).

Similarly, the suprachoroidal injection route, where the space between the sclera and the choroid is targeted for viral injections (Kansara et al., 2020; Yiu et al., 2020), is methodologically challenging in birds, since the vast majority of the avian eye remains hidden in the eye socket with only parts of the sclera being visible. This leaves the intravitreal injection route as the most feasible injection method in birds, where the viral suspension is directly injected into the vitreous chamber of the eye (Giove et al., 2010). This, however, has mainly resulted in low transduction efficiency in avian retinae with the currently available genetic tools (Waldner et al., 2019).

It is surprising that in the continuous development of new genetic tools and methodological improvements for retinal research in birds has been largely neglected over the last years. In particular because birds appear to be exceptionally well suited as model systems for vision-based research: (1) avian eyes occupy a major proportion of the head (Burton, 2008); (2) related visual brain parts occupy up to 50% of the total cranial capacity in certain bird species (Waldvogel, 1990; reviewed in Seifert et al., 2020); (3) the number of retinofugal fibers in birds outclasses that of man by a factor of 2.5 (Güntürkün et al., 1993); (4) several physiological aspects of avian vision, e.g., acuity, luminance detection and/or color discrimination easily surpass that of most mammals (Jones et al., 2007; Niu et al., 2022); (5) in contrast to the rod-dominated mouse retina (Jeon et al., 1998), many avian retinae contain foveae, i.e., areas of high cone photoreceptor density, also found in humans and other primates (Haverkamp et al., 2021). Here, we used the long-distance night-migratory European robin as a study species because its retina contains a light-dependent magnetic compass (Chetverikova et al., 2022; Günther et al., 2018; Wiltschko et al., 1993; Xu et al., 2021; Zapka et al., 2009). Moreover, its retina has recently been morphologically characterized using electron microscopy (Günther et al., 2024; 2025) and immunohistochemistry (Günther et al., 2018; Chetverikova et al., 2022; Balaji et al., 2023). These findings provide a good foundation for electrophysiological studies, which are currently rare (but see Rotov et al., 2022). Finding AAV serotypes that work in the European robin will therefore be a step forward in both the study of magnetoreception and the functional analysis of avian retinal circuits.

Materials and methods

AAV production

The generation of the plasmid was performed as described in Balaji et al. (2023). We used an AAV 2/9 serotype carrying a strong ubiquitous CAG/CAAG promoter and the enhanced green fluorescent protein (EGFP) as the fluorescent reporter. Its titer (CAG: 3.97×10^{12} VG/mL; (Balaji et al., 2023); CAAG: 1.77×10^{12} VG/mL) was quantified via genomic qPCR by the Viral Core Facility of Charité–Universitätsmedizin Berlin, Germany.

Custom-designed ocular injection apparatus

For carrying out the intravitreal injections, we used a custom-designed ocular injection apparatus, consisting of a placement slab, an angular injection unit and attached gas anesthesia delivery extensions (Figure 1A). The apparatus has been designed and constructed to meet the requirements of intravitreal injections in small passerines. The device was made with Poly Vinyl Chloride (PVC) and covered with Perbunan® which prevents unwanted loss of heat from the bird. The placement slab at the bottom was designed to provide stability to the above angular injection unit as well as resistance against sudden movements during the ocular injections (Figure 1C). The angular injection unit contained two beak holders placed on opposite sides to immobilize the bird on either side and to access both eyes easily during the injections.

The isoflurane gas used as an anaesthetic was provided to the birds with the help of a tube connecting the anesthesia device to an inlet in the beak holder. The outlet of the beak holder was connected with a suction pipe to remove excess anesthetic gas. Circular knobs attached to the beak holders enabled a movement along the antero-posterior axis to assist fixation of the bird's head. A PVC block on either side was placed horizontally next to the beak holders to position the bird's body on its side in a natural resting position while being anesthetized. The four corners of the ground

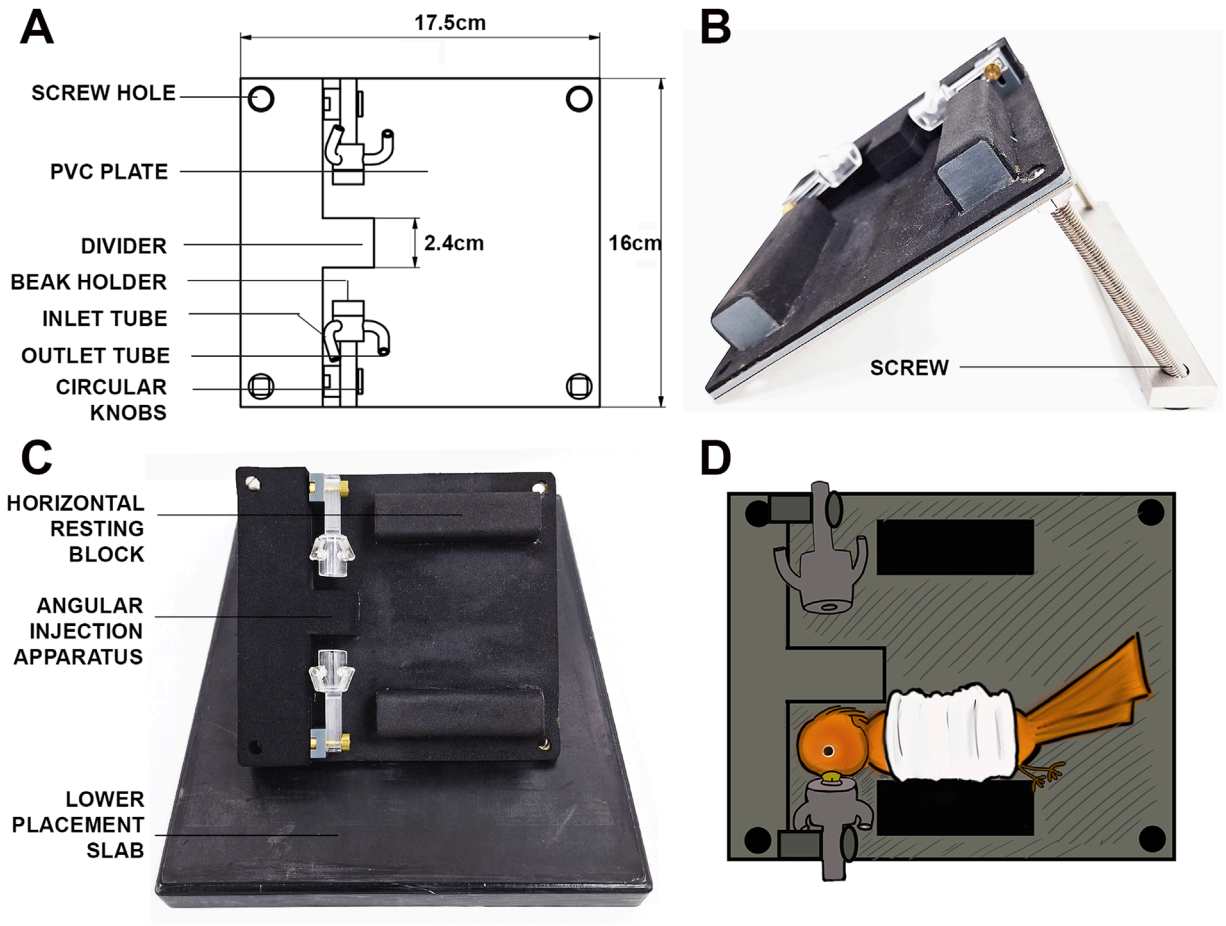

FIGURE 1
Custom-made ocular injection apparatus for intravitreal injections in birds. **(A)** Scheme of the angular injection apparatus, with the two beak holders attached to the PVC plate, and the inlet/outlet tubes attached to the beak holder. **(B)** Side view of the angular injection plate, depicting the beak holders, the inlet/outlet tubes and the metal screws for angular adjustment. **(C)** Front view of the angular injection plate, placed on top of the lower placement slab. **(D)** Schematic depiction of the placement of the experimental bird in the injection apparatus. Note the second beak holder in D can be used to inject the contralateral eye of the bird if need arises.

plate had screw holes to enable the adjustment of the angle of the injection unit to the ground, using two long screws at a time. In our case, an angle of approximately 30° between the angular injection unit and the lower placement slab proved optimal for intravitreal injections (Figure 1B).

Intravitreal injection protocol

Before each surgery, a single adult European robin was food-deprived for 2 h and fully anesthetized using Isoflurane CP® gas anesthesia (1 mL/mL; cp-pharma, Burgdorf, Germany) dissolved in oxygen; (2%–3% volume at initial stages of anesthesia, ~1.5% volume throughout the surgery) directed through the beak holder. Meloxicam (Metacam®, Boehringer Ingelheim, Ingelheim, Germany; 0.2 mL/kg body weight dissolved in 0.9% NaCl) was administered intramuscularly for post-surgical analgesia. The bird was wrapped with a bandage cloth to prevent wing movement and placed in the custom-designed injection apparatus (Figure 1D). The anaesthetized bird´s head was carefully fixed by inserting the beak into the beak holder, and its eye lid was temporarily pulled back to get an unobstructed view of the eye. Additional local anaesthesia to the cornea was provided using Oxibuprocaine-hydrochloride. Upon locating the sclera-cornea junction at the dorso-temporal side of the eye with a stereoscope (Leica M400E, Wetzlar, Germany), a 27G needle was used to puncture the sclera, avoiding nearby blood capillaries from getting ruptured. This puncture was subsequently used as an entry point for the Hamilton syringe attached to a blunt 33G needle (VWR International GmbH, Germany), carrying the AAV2/9 viral suspension.

To minimize any unintentional damage to the bird's vision, we carefully avoided the lens by using an insertion angle of ~60°–70° relative to the eye's coronal axis (Figure 2). Afterwards, the Hamilton syringe was inserted down to the fundus, and 10–20 µL of viral suspension was injected close to the retinal surface with an approximate speed of ~1 µL/s. The syringe was held in place for at least 10 s after the injection in order to prevent reflux and to ensure dispersion of the viral suspension and carefully retracted afterwards. Post-surgery, the bird was taken out of the injection apparatus and transferred onto a warming plate for quick recovery. Each bird

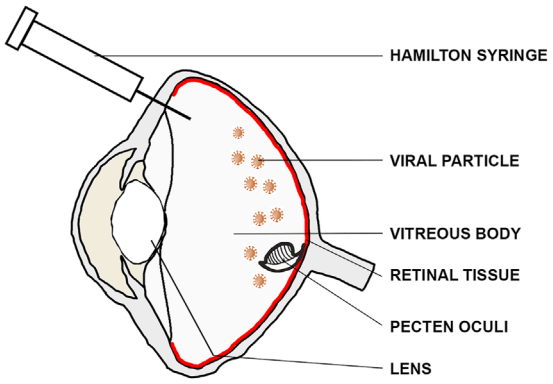

FIGURE 2
Intravitreal injection route. For intravitreal injections, the lens was bypassed using an insertion angle of ~60–70° relative to the eye's coronal axis to inject the viral suspension (brown) close to the retinal surface (red).

was monitored until it recovered from anesthesia and returned to its home cage upon gaining full consciousness. We provided post-surgical analgesia (Meloxicam administered intramuscularly; 0.2 mL/kg body weight dissolved in 0.9% NaCl) for up to 72 h post-surgery to minimize any signs of discomfort resulting from the surgery. For legal and ethical reasons, we did not perform vehicle-only controls as we had a strictly limited number of wild caught birds available. However, in order to validate the general functionality of the virus, we only injected one eye with the virus, while leaving the contralateral one as a negative control for subsequent immunostainings.

Tissue processing

In line with previous studies on virus-mediated transduction of retinal tissue (Waldner et al., 2019; Nieuwenhuis et al., 2023), we let the AAV2/9 suspension reside inside the injected eye for 21–25 days, following which the birds were sacrificed by decapitation and the injected eye was dissected from the skull. The anterior part of the eye was removed along its coronal axis using a sharp razor blade and the vitreous body was carefully taken out. The eye cup was fixed using 4% paraformaldehyde [PFA dissolved in 0.1 M phosphate buffered saline, pH 7.6 (PBS)] for 30 min. Subsequently, the eye cups were washed three times in PBS for 15 min each and cryoprotected in a graded series of sucrose solutions (10%, 20%, 30% dissolved in 0.1 M PBS) overnight. If necessary, the eyecups were stored in 30% sucrose solution at −20°C until they were subjected to immunohistochemistry.

Immunohistochemistry

Retinal tissue was cryosectioned on a freezing microtome (Leica CM 1860; Wetzlar, Germany) into serial cross sections with a thickness of 30 µm and placed onto microscope slides (epredia, Superfrost Plus Adhesion slides, Fisher Scientific, Waltham, MA, United States). For EGFP immunohistochemistry, the slides were briefly dried on a warming plate and washed twice with 0.1 M PBS for 15 min. Unspecific binding sites were blocked using 5% donkey serum (Sigma-Aldrich, Burlington, MA, United States) and 0.3%–0.5% Triton X-100 (Carl Roth, Germany) dissolved in 0.1 M PBS for 1–2 h. The slides were subsequently incubated overnight with a goat anti-GFP antibody (diluted 1:500 in blocking solution; 600-101-215; RRID: AB_218182; Rockland, Pottstown, PA, United States) together with one of the opsin antibodies listed in Table 1 at 4°C to assess the type of transduced photoreceptors. On the following day, slides were washed thrice for 10–15 min each in 0.1 M PBS. The retinal slices were subsequently incubated with appropriate secondary antibodies (Alexa Fluor 488-conjugated (anti goat) for EGFP; Alexa 568-conjugated (anti mouse) for rhodopsin; Alexa647-conjugated (anti guinea pig) for red opsin; Alexa 568-conjugated (anti mouse) for green opsin; Alexa 568 (anti rat) for blue opsin; Alexa 568 (anti rabbit) for UV opsin; dilution 1:500, Thermo Fisher Scientific, Waltham, MA, United States) for 2 h. The slices were washed thrice with PBS for 10–15 min and mounted with Vectashield mounting medium (containing nuclear DAPI stain; BIOZOL, Germany).

Image acquisition, processing, and quantification

Retinal sections were imaged with a confocal laser scanning microscope (Leica TCS SP8, Leica Microsystems, Wetzlar, Germany), using a HC PL APO 40x/1.3 or HC PL APO 63x/1.4 oil immersion objective. We used the "Navigator" software (LAS X Life Science, Wetzlar, Germany) to image retinal sections from each transduced eye. Twelve to fourteen retinal sections across the entire eye cup were used to determine the transduction efficiency in each transduced eye. Each section was individually analyzed as follows: 1) We normalized the intensity using the *Contrast Enhancement* tool (0.2%) in Fiji (Schindelin et al., 2012). 2) Both the transduced area and the total retina area on each section were individually marked using the *Freehand* tool. 3) The *Measure* tool was used to obtain the respective area sizes, and the fraction of transduced area was calculated for each individual section. To estimate the transduction efficiency per total retina, we used spline extrapolation to predict the values of the slides interjacent to the analyzed ones. We then averaged all values to calculate the fraction of transduced retina area. Figures 3C, D, G, H display the series of multiple Z-stack images (0.27 µm step size) merged into a maximum projection image. High-resolution scans of EGFP-labeled photoreceptors were normalized in Fiji using the *Contrast Enhancement* function.

Results

Transduction coverage of european robin retina

Intravitreal ocular injection of AAV2/9 successfully transduced retinal tissue of European robins (Figures 3A–H). The transduced area ranged from 10% to 60% of the total retinal surface (Figure 3I), resulting in an overall mean transduction coverage of ~35 ± 17% across nine individuals, which we considered

TABLE 1 Opsin antibodies used in this study.

Opsin antibody	Clone/company/catalogu number	Host species	Dilution	Immunogen sequence
Rhodopsin	Clone 1D4/Cell essentials/ab5417	Mouse	1:500	Detailed sequence not provided by the manufacturer
Red opsin	Karl W. Koch lab/Davids Biotechnologies	Guinea pig	1:1,000	SRYWPHGLKTSCGPDVFSGSSDP GVQSYMVSI
Green opsin	OPSG2 clone 26G5/Helmholtz Munich	Mouse	1:500	GPDYYTHNPDFH
Blue opsin[a]	OPSB clone 2D6/Helmholtz Munich	Rat	1:5	MHPPRPTTDLPEDF
UV opsin (Opsin, blue)	Millipore/AB5407	Rabbit	1:500	Recombinant human blue opsin

[a]BLUE opsin (OPSB) (Günther et al., 2018).

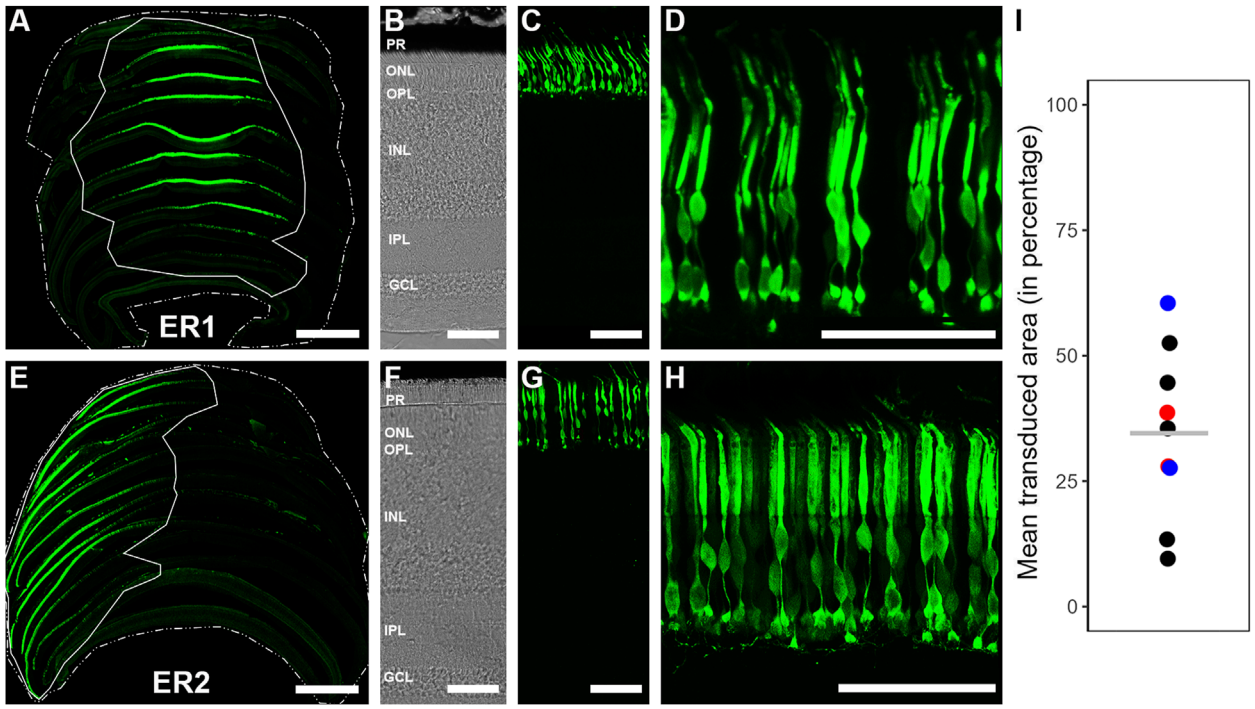

FIGURE 3
EGFP transduction within European robin retinae following intravitreal injection of AAV2/9-CAG-EGFP/AAV2/9-CAAG-EGFP. **(A, E)** 2-D reconstruction and determination of the transduction extent on two exemplary retinae, using single retinal sections placed in their respective order, displaying mean retinal transduction coverages of ~28% (ER1) and ~39% (ER2), respectively. Scale: 1 mm. **(B, F)** Transmission images of European robin retinae ER1 and ER2, respectively, depicting the retinal stratification used for anatomical orientation. Scale: 50 µm. **(C, G)** Vertical sections of European robin retinae ER1 and ER2 depicting the transduction success exclusive to the photoreceptor layer in most cases. Scale: 50 µm. **(D, H)** Zoomed-in images of the photoreceptor layer from European robin retinae ER1 and ER2, proving successful transduction of photoreceptors. Scale: 50 µm. **(I)** Mean transduced area (in %) of all transduced retinae. ER1 (~28%) and ER2 (~39%) are depicted by red circles, black circles depict the other retinal transductions using AAV2/9-CAG-EGFP; blue circles depict two cases where AAV2/9-CAAG-EGFP was used. Note the very similar transduction efficiency irrespective of the promotor type. The overall mean transduction coverage of 35% ± 17% (n = 9) is represented by a grey horizontal line.

consistent enough to act as a "proof of principle" for the effectiveness of the viral serotype. We observed heterogenous transduction densities of EGFP expressing neurons, with the highest numbers usually being proximal to the injection site and a gradual decrease with distance. Figures 3A, E display two exemplary 2-D reconstructions, demonstrating the retinal surface transduction coverage and its regional variability. As expected, in the non-transduced control eyes, no EGFP signal was observed, thereby validating the general functionality of the virus (data not shown).

10.3389/fphys.2025.1549585

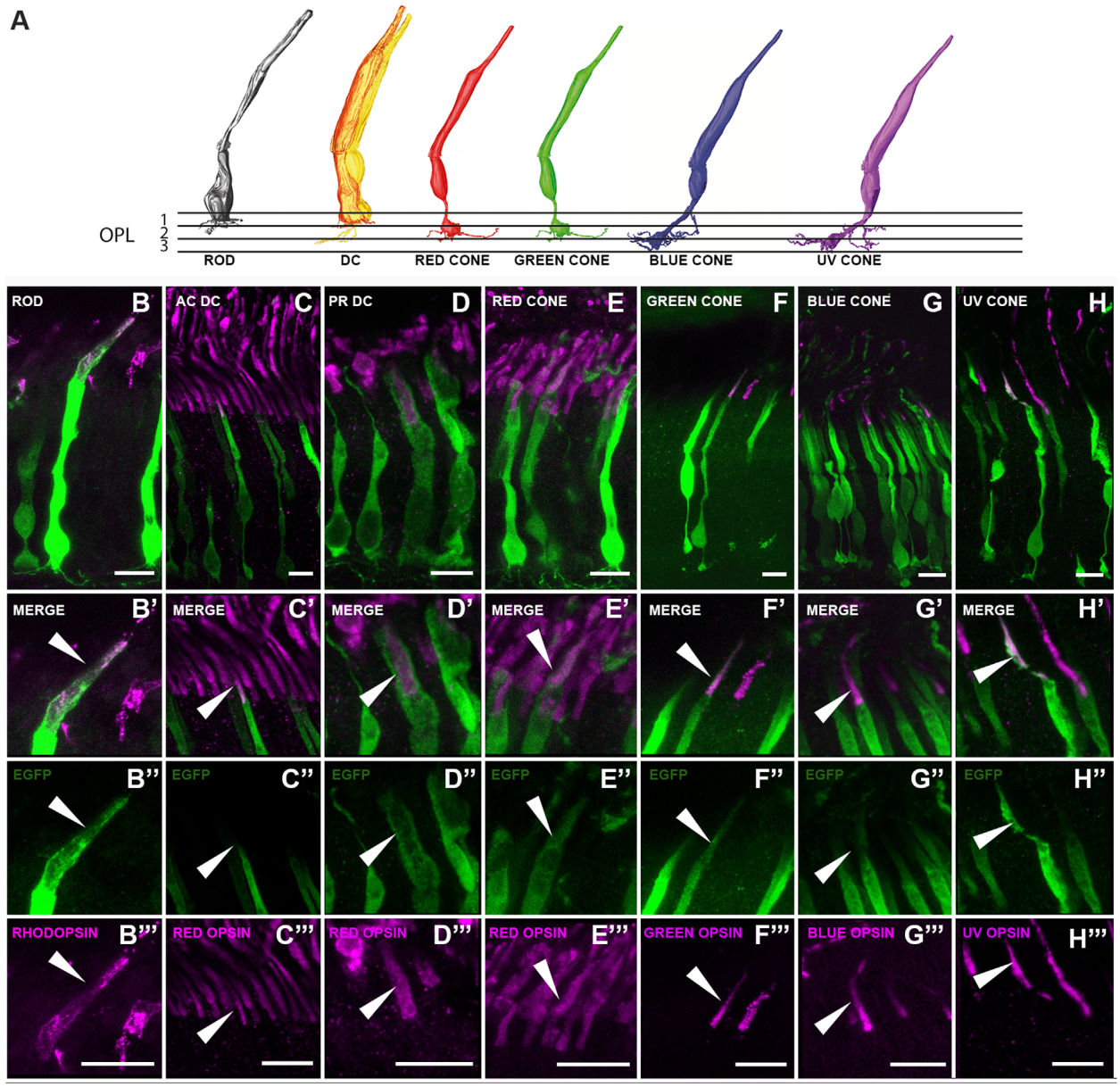

FIGURE 4
Characterization of the EGFP expressing photoreceptor types within the transduced European robin retinae. **(A)** 3-D reconstruction images based on chicken ssmSEM data (Günther et al., 2021; Günther et al., 2024) depicting the morphology of photoreceptors in the avian retina. Please note that the ssmSEM dataset could not distinguish between red-green and blue-UV cones which are presumed to have a very similar shape (Günther et al., 2021). **(B–H)** Images showing EGFP expressing photoreceptors and their outer segment localization with rhodopsin (for rods), red opsin (for accessory (AC) and principal (PR) member of double cones and red cones), green opsin (for green cones), blue opsin (for blue cones) and UV opsin (for UV cones) respectively. **(B′–H′)** Zoomed-in images showing the specific outer segment localization of the EGFP and the respective opsin. **(B″–H″)** EGFP expression in the outer segments. **(B‴–H‴)** Corresponding opsin expression. Arrowheads indicate areas of colocalization. Scale: 10 µm.

Types of transduced neurons in the European robin retina

We enhanced the endogenous EGFP signal with an EGFP antibody to identify the type and detailed morphology of the transduced neurons. The vast majority of EGFP reporter gene expression was found in the photoreceptor layer (Figures 3C, D, G, H). Only in very few cases, we observed EGFP expressing Müller cells, potentially resulting from occasional disruption of the inner limiting membrane (ILM) formed by Müller cell endfeet during the viral injections.

To further characterize the photoreceptor types transduced by the ocular injections, immunostainings were carried out using various opsin antibodies (Table 1; Figures 4B–H, B'–H', B"–H", B'"–H'"). AAV2/9-EGFP targeted all photoreceptor types, i.e., rods, principal and accessory members of double cones, and the four types of single cones (red, green, blue and UV) (Figure 4). Their overall morphology largely resembled the ssmSEM-based

reconstructions of chicken photoreceptors (Günther et al., 2021; Günther et al., 2024) (Figure 4A), thereby validating their morphology in the European robin: rods possessed a stout cell body and terminal with long telodendria; the accessory member of double cones was characterized by a thinner cell body with a distinct brush-like synaptic terminal located far more distal than all other terminals; the principal member of the double cones has a very broad shape and rather thick outer segment; the four single cones (red, green, blue and UV) were observed to have a thin cell body and bulb like terminal endings.

In addition to using a ubiquitous CAG promoter for seven specimens, two additional ocular injections were performed using a CAAG promoter. Both promoters resulted in a very similar high retinal transduction efficiency and variability (see blue dots in Figure 3I), thereby validating the effectiveness of the used serotype irrespective of the promoter.

Discussion

In contrast to both the subretinal (Barker et al., 2009; Watanabe et al., 2013; Petit et al., 2017) and intravitreal route of injection (Giove et al., 2010; Reid et al., 2017), which have proven successful in transducing considerable amounts of retinal tissue in murine model systems, only the intravitreal route, due to its less invasiveness, appears feasible in avian model systems. However, so far, the intravitreal route has not yielded efficient and widespread transduction of retinal tissue in birds (Waldner et al., 2019). This could have been caused by the large relative volume of the vitreous chamber in birds and the much thicker nerve fiber layer in avian eyes, which may act as a barrier for successful transductions. The main reason, however, might have been the lack of appropriate AAV serotypes capable of successfully transducing the retina. In this study, the AAV2/9 serotype proved successful in transducing European robin retinal tissue, reaching widespread transduction coverages of ~35 ± 17% of the total retinal surface (Figure 3I) across seven individuals. Bearing in mind that volumetric calculations indicate that European robin´s eyes are approximately 20 times larger than mouse eyes, increasing the injected volume and/or titer concentration could potentially improve the transduction efficiency even further.

In this "proof of principle" study, transduction efficiency varied between 10% and 60%. Potential reasons for this variability include 1) different amounts of viral suspension, ranging between 10 and 20 µL, 2) occasional efflux of viral suspension during injection, and 3) variable virus titers (ranging between ~2-4 × 10^{12}). Since it is well documented that a certain concentration of viruses is required to induce transduction (Giove et al., 2010; Reid et al., 2017; Waldner et al., 2019), these variations may have impacted the transduction efficiency.

Given the observed variability, future studies investigating functional aspects effects of genetic manipulations using the AAV2/9 serotype as a vehicle will require a more thorough quantitative assessment of transduction efficiency, e.g., by Western blots and/or RT-qPCR.

Avian AAVs (A3Vs) have been used for intravitreal injections in birds, but showed limited transduction efficiency (Waldner et al., 2019). In search for a suitable AAV capable to successfully transduce retinal tissue of European robins, a thorough literature survey revealed that, in contrast to AAV5 and AAV8, both AAV2 and AAV9 displayed a highly specific tropism towards various retinal cell types in mice (Lee et al., 2018). Pseudotyping, i.e., a recombinant AAV containing the structural and enzymatic component from one AAV "wrapped" in the capsid component from another, can further increase the tropism towards certain host cells. Here, we used AAV2/9-CAG-EGFP and AAV2/9-CAAG-EGFP for intravitreal delivery in the European robin retina. This serotype was chosen as it can transfect a broad range of retinal cell types, including photoreceptors and its progenitors (Allocca et al., 2007) in other vertebrate species (Watanabe et al., 2013).

We can only speculate on why AAV2/9 outperformed A3Vs in intravitreal injections in the avian retina. The vitreoretinal junction (inner limiting membrane, ILM) is a serotype specific barrier for naturally occurring AAVs in mice (Dalkara et al., 2009). It contains AAV binding sites, which create a diffusion barrier for AAV particles that arrive from the intravitreal side (Khabou et al., 2016). Thus, one potential explanation could be that the avian ILM contains more binding sites for avian AAVs (A3V) than for non-avian AAV2/9 particles, leading to the larger transduction efficiency of AAV2/9 in the avian retina. However, differences in virus titer, injection routine, or study species may also play a role.

Demonstrating the connectivity between photoreceptors and bipolar cells (Günther et al., 2021; Balaji et al., 2023; Günther et al., 2024) or horizontal cells (Günther et al., 2025) and successfully enabling photoreceptor-specific gene delivery to the European robin retina, might only be the first of many steps towards a plethora of investigations on the morphology, biochemistry and physiology of the avian retina using the AAV2/9 serotype. This is of particular importance, since birds, as mentioned before, have some of the most high-performing eyes amongst vertebrates, but so far, we have lacked the necessary tools to genetically manipulate them. Its proven functionality in European robins makes AAV 2/9 particularly well suited for studying the proposed light dependent, radical pair based magnetoreception mechanism (Hore and Mouritsen, 2016; Mouritsen, 2018; Mouritsen, 2022). This elusive sense (Zapka et al., 2009; Hore and Mouritsen, 2016; Wu et al., 2020; Wang et al., 2021; Xu et al., 2021; Görtemaker et al., 2022) is likely to be based on magnetically sensitive reactions inside the cryptochrome 4 protein (Xu et al., 2021; Chetverikova et al., 2022) located in the outer segments of double cones and long wavelength single cones (Günther et al., 2018). We are convinced that the AAV 2/9 serotype, which we identified here, will be instrumental to explore the physiology of European robin photoreceptors and the role of double cones in magnetoreception.

Data availability statement

The datasets presented in this study can be found in online repositories. The names of the repository/repositories and accession number(s) can be found below: https://www.addgene.org/29778/, Addgene plasmid #29778. The original dataset of this study will be made available from the corresponding author upon request, without undue reservation. Anti-Green opsin antibody can be

obtained from Monoclonal Antibody Core Facility at Helmholtz Center Munich.

Ethics statement

The animal study was approved by the Animal Care and Use Committees of the Niedersächsisches Landesamt für Verbraucherschutz und Lebensmittelsicherheit (LAVES, Oldenburg, Germany, Az.: 33.9-42502-04-17/2566). The study was conducted in accordance with the local legislation and institutional requirements.

Author contributions

PS: Conceptualization, Data curation, Formal Analysis, Investigation, Methodology, Validation, Visualization, Writing–original draft, Writing–review and editing. DH: Conceptualization, Data curation, Formal Analysis, Funding acquisition, Investigation, Methodology, Supervision, Validation, Visualization, Writing–original draft, Writing–review and editing. BS: Formal Analysis, Investigation, Methodology, Visualization, Writing–original draft, Writing–review and editing. EM: Methodology, Resources, Writing–review and editing. KH: Methodology, Writing–review and editing. LB: Methodology, Writing–review and editing. IM: Methodology, Writing–review and editing. K-WK: Funding acquisition, Methodology, Resources, Writing–review and editing. RF: Methodology, Resources, Writing–review and editing. CS: Methodology, Resources, Writing–review and editing. KD: Conceptualization, Funding acquisition, Methodology, Supervision, Writing–review and editing. HM: Conceptualization, Funding acquisition, Supervision, Writing–review and editing.

Funding

The author(s) declare that financial support was received for the research and/or publication of this article. This work was generously funded by Deutsche Forschungsgemeinschaft (RTG 1885/2 "Molecular Basis of Sensory Biology") to KD and HM, employing PS; SFB 1372 (project number: 395940726) "Magnetoreception and Navigation in Vertebrates" given to HM, KD, K-WK and DH, employing BS, KH and IM, the European Research Council under the European Union's Horizon 2020 research and innovation program, grant agreement no. 810002 (Synergy Grant: "QuantumBirds") to HM, employing PS.

Acknowledgments

The authors warmly thank Anja Günther for providing electron microscopy reconstructions, Angelika Einwich for helping in validating the specificity of the green opsin antibody, Irina Fomins, Leonie Lovis Pfeiffer, and Ursula Kobalz for their expert technical assistance and Tobias Woldt for helpful comments on the manuscript. We thank Loren Looger, Kimberly Ritola and Sarada Viswanathan for providing their AAV serotypes and John Neidhardt and Sebastian Swirski for giving us valuable scientific input at early stages of this project. The authors thankfully acknowledge the Fluorescence Microscopy Service Unit of the University of Oldenburg (Imaging Core Facility) for the use of the imaging facilities, the university's animal facility for keeping birds, the university's mechanical workshop for building top quality equipment, and the Viral Core Facility of Charité - Universitätsmedizin Berlin for providing the viruses.

Conflict of interest

The authors declare that the research was conducted in the absence of any commercial or financial relationships that could be construed as a potential conflict of interest.

The author(s) declared that they were an editorial board member of Frontiers, at the time of submission. This had no impact on the peer review process and the final decision.

Generative AI statement

The author(s) declare that no Generative AI was used in the creation of this manuscript.

Publisher's note

References

Ahmadiantehrani, S., and London, S. E. (2017). A reliable and flexible gene manipulation strategy in posthatch zebra finch brain. *Sci. Rep.* 7 (1), 43244. doi:10.1038/srep43244

Ali, R. R., Sarra, G. M., Stephens, C., Alwis, M. D., Bainbridge, J. W., Munro, P. M., et al. (2000). Restoration of photoreceptor ultrastructure and function in retinal degeneration slow mice by gene therapy. *Nat. Genet.* 25 (3), 306–310. doi:10.1038/77068

Allocca, M., Mussolino, C., Garcia-Hoyos, M., Sanges, D., Iodice, C., Petrillo, M., et al. (2007). Novel adeno-associated virus serotypes efficiently transduce murine photoreceptors. *J. Virol.* 81 (20), 11372–11380. doi:10.1128/jvi.01327-07

Atchison, R. W., Casto, B. C., and Hammon, W. M. (1965). Adenovirus-associated defective virus particles. *Science* 149 (3685), 754–756. doi:10.1126/science.149.3685.754

Bacci, G. M., Becherucci, V., Marziali, E., Sodi, A., Bambi, F., and Caputo, R. (2022). Treatment of inherited retinal dystrophies with somatic cell therapy medicinal product: a review. *Life* 12 (5), 708. doi:10.3390/life12050708

Balaji, V., Haverkamp, S., Seth, P. K., Günther, A., Mendoza, E., Schmidt, J., et al. (2023). Immunohistochemical characterization of bipolar cells in four distantly related avian species. *J. Comp. Neurology* 531 (4), 561–581. doi:10.1002/cne.25443

Balakrishnan, B., and Jayandharan, R. (2014). Basic biology of adeno-associated virus (AAV) vectors used in gene therapy. *Curr. Gene. Ther.* 14 (2), 86–100. doi:10.2174/1566523214666140302193709

Barker, S. E., Broderick, C. A., Robbie, S. J., Duran, Y., Natkunarajah, M., Buch, P., et al. (2009). Subretinal delivery of adeno-associated virus serotype 2 results in minimal immune responses that allow repeat vector administration in immunocompetent mice. *J. Gene. Med.* 11 (6), 486–497. doi:10.1002/jgm.1327

Bennett, J., Wilson, J., Sun, D., Forbes, B., and Maguire, A. (1994). Adenovirus vector-mediated *in vivo* gene transfer into adult murine retina. *Investigative Ophthalmol. and Vis. Sci.* 35 (5), 2535–2542.

Buch, P. K., Bainbridge, J. W., and Ali, R. R. (2008). AAV-mediated gene therapy for retinal disorders: from mouse to man. *Gene. Ther.* 15 (11), 849–857. doi:10.1038/gt.2008.66

Burton, R. F. (2008). The scaling of eye size in adult birds: relationship to brain, head and body sizes. *Vis. Res.* 48 (22), 2345–2351. doi:10.1016/j.visres.2008.08.001

Cebulla, C. M., Zelinka, C. P., Scott, M. A., Lubow, M., Bingham, A., Rasiah, S., et al. (2012). A chick model of retinal detachment: cone rich and novel. *PLoS. One.* 7 (9), e44257. doi:10.1371/journal.pone.0044257

Chetverikova, R., Dautaj, G., Schwigon, L., Dedek, K., and Mouritsen, H. (2022). Double cones in the avian retina form an oriented mosaic which might facilitate magnetoreception and/or polarized light sensing. *J. R. Soc. Interface* 19 (189), 20210877. doi:10.1098/rsif.2021.0877

Dalkara, D., Kolstad, K. D., Caporale, N., Visel, M., Klimczak, R. R., Schaffer, D. V., et al. (2009). Inner limiting membrane barriers to AAV-mediated retinal transduction from the vitreous. *Mol. Ther.* 17(12):2096–2102. doi:10.1038/mt.2009.181

Giove, T. J., Sena-Esteves, M., and Eldred, W. D. (2010). Transduction of the inner mouse retina using AAVrh8 and AAVrh10 via intravitreal injection. *Exp. Eye Res.* 91 (5), 652–659. doi:10.1016/j.exer.2010.08.011

Görtemaker, K., Yee, C., Bartölke, R., Behrmann, H., Voß, J. O., Schmidt, J., et al. (2022). Direct interaction of avian cryptochrome 4 with a cone specific G-protein. *Cells* 11 (13), 2043. doi:10.3390/cells11132043

Günther, A., Balaji, V., Leberecht, B., Forst, J. J., Rotov, A. Y., Woldt, T., et al. (2025). Morphology and connectivity of retinal horizontal cells in two avian species. *Front. Cell. Neurosci.* 19. doi:10.3389/fncel.2025.1558605

Günther, A., Dedek, K., Haverkamp, S., Irsen, S., Briggman, K. L., and Mouritsen, H. (2021). Double cones and the diverse connectivity of photoreceptors and bipolar cells in an avian retina. *J. Neurosci.* 41 (23), 5015–5028. doi:10.1523/JNEUROSCI.2495-20.2021

Günther, A., Einwich, A., Sjulstok, E., Feederle, R., Bolte, P., Koch, K. W., et al. (2018). Double-cone localization and seasonal expression pattern suggest a role in magnetoreception for European robin cryptochrome 4. *Curr. Biol.* 28 (2), 211–223. doi:10.1016/j.cub.2017.12.003

Günther, A., Haverkamp, S., Irsen, S., Watkins, P. V., Dedek, K., Mouritsen, H., et al. (2024). Species–specific circuitry of double cone photoreceptors in two avian retinas. *Commun. Biol.* 7 (1), 992. doi:10.1038/s42003-024-06697-2

Güntürkün, O., Miceli, D., and Watanabe, M. (1993). *Anatomy of the avian thalamofugal pathway*. Cambridge: MIT Press.

Harpavat, S., and Cepko, C. L. (2006). RCAS-RNAi: a loss-of-function method for the developing chick retina. *Bmc. Dev. Biol.* 6, 2–7. doi:10.1186/1471-213X-6-2

Haverkamp, S., Albert, L., Balaji, V., Němec, P., and Dedek, K. (2021). Expression of cell markers and transcription factors in the avian retina compared with that in the marmoset retina. *J. Comp. Neurol.* 529 (12), 3171–3193. doi:10.1002/cne.25154

Hore, P. J., and Mouritsen, H. (2016). The radical-pair mechanism of magnetoreception. *Annu. Rev. Biophys.* 45 (1), 299–344. doi:10.1146/annurev-biophys-032116-094545

Isiegas, C., Marinich-Madzarevich, J. A., Marchena, M., Ruiz, J. M., Cano, M. J., de la Villa, P., et al. (2016). Intravitreal injection of proinsulin-loaded microspheres delays photoreceptor cell death and vision loss in the rd10 mouse model of retinitis pigmentosa. *Invest. Ophthalmol. Vis. Sci.* 57 (8), 3610–3618. doi:10.1167/iovs.16-19300

Jeon, C. J., Strettoi, E., and Masland, R. H. (1998). The major cell populations of the mouse retina. *J. Neurosci.* 18 (21), 8936–8946. doi:10.1523/JNEUROSCI.18-21-08936.1998

Jomary, C., Piper, T. A., Dickson, G., Couture, L. A., Smith, A. E., Neal, M. J., et al. (1994). Adenovirus-mediated gene transfer to murine retinal cells *in vitro* and *in vivo*. *Febs. Lett.* 347 (2-3), 117–122. doi:10.1016/0014-5793(94)00512-5

Jones, M. P., Pierce Jr, K. E., and Ward, D. (2007). Avian vision: a review of form and function with special consideration to birds of prey. *J. Exot. Pet. Med.* 16 (2), 69–87. doi:10.1053/j.jepm.2007.03.012

Kansara, V., Muya, L., Wan, C. R., and Ciulla, T. A. (2020). Suprachoroidal delivery of viral and nonviral gene therapy for retinal diseases. *J. Ocul. Pharmacol. Ther.* 36 (6), 384–392. doi:10.1089/jop.2019.0126

Khabou, H., Desrosiers, M., Winckle, C., Fouquet, S., Auregan, G., Bemelmans, A.-P., et al. (2016). Insight into the mechanisms of enhanced retinal transduction by the engineered AAV2 capsid variant -7m8. *Biotechnol. Bioeng.* 113(12):2712–2724. doi:10.1002/bit.26031

Lee, S. H., Yang, J. Y., Madrakhimov, S., Park, H. Y., Park, K., and Park, T. K. (2018). Adeno-associated viral vector 2 and 9 transduction is enhanced in streptozotocin-induced diabetic mouse retina. *Mol. Ther. Methods Clin. Dev.* 13, 55–66. doi:10.1016/j.omtm.2018.11.008

Li, T., Adamian, M., Roof, D. J., Berson, E. L., Dryja, T. P., Roessler, B. J., et al. (1994). *In vivo* transfer of a reporter gene to the retina mediated by an adenoviral vector. *Invest. Ophthalmol. Vis. Sci.* 35 (5), 2543–2549.

Mouritsen, H. (2018). Long-distance navigation and magnetoreception in migratory animals. *Nature* 558 (7708), 50–59. doi:10.1038/s41586-018-0176-1

Mouritsen, H. (2022). "Magnetoreception in birds and its use for long-distance migration," in *Sturkie's avian physiology* (Academic Press), 233–256. doi:10.1016/B978-0-12-819770-7.00040-2

Mühlfriedel, R., Michalakis, S., Garrido, M. G., Biel, M., and Seeliger, M. W. (2013). Optimized technique for subretinal injections in mice. *Methods. Mol. Biol.* 935, 343–349. doi:10.1007/978-1-62703-080-9_24

Nieuwenhuis, B., Laperrousaz, E., Tribble, J. R., Verhaagen, J., Fawcett, J. W., Martin, K. R., et al. (2023). Improving adeno-associated viral (AAV) vector-mediated transgene expression in retinal ganglion cells: comparison of five promoters. *Gene Ther.* 30(6):503–519. doi:10.1038/s41434-022-00380-z

Niu, X., Jiang, Z., Peng, Y., Huang, S., Wang, Z., and Shi, L. (2022). Visual cognition of birds and its underlying neural mechanism: a review. *Avian. Res.* 13, 100023. doi:10.1016/j.avrs.2022.100023

Ong, T., Pennesi, M. E., Birch, D. G., Lam, B. L., and Tsang, S. H. (2019). Adeno-associated viral gene therapy for inherited retinal disease. *Pharm. Res.* 36 (2), 34. doi:10.1007/s11095-018-2564-5

Park, S. W., Kim, J. H., Park, W. J., and Kim, J. H. (2015). Limbal approach-subretinal injection of viral vectors for gene therapy in mice retinal pigment epithelium. *J. Vis. Exp.* 102, 53030. doi:10.3791/53030

Petit, L., Ma, S., Cheng, S. Y., Gao, G., and Punzo, C. (2017). Rod outer segment development influences AAV-mediated photoreceptor transduction after subretinal injection. *Hum. Gene. Ther.* 28 (6), 464–481. doi:10.1089/hum.2017.020

Reid, C. A., Ertel, K. J., and Lipinski, D. M. (2017). Improvement of photoreceptor targeting via intravitreal delivery in mouse and human retina using combinatory rAAV2 capsid mutant vectors. *Invest. Ophthalmol. Vis. Sci.* 58 (14), 6429–6439. doi:10.1167/iovs.17-22281

Ronzitti, G., Gross, D. A., and Mingozzi, F. (2020). Human immune responses to adeno-associated virus (AAV) vectors. *Front. Immunol.* 11, 670. doi:10.3389/fimmu.2020.00670

Rotov, A. Y., Goriachenkov, A. A., Cherbunin, R. V., Firsov, M. L., Chernetsov, N., and Astakhova, L. A. (2022). Magnetoreceptory function of European robin retina: electrophysiological and morphological non-homogeneity. *Cells*. 11(19):3056. doi:10.3390/cells11193056

Schindelin, J., Arganda-Carreras, I., Frise, E., Kaynig, V., Longair, M., Pietzsch, T., et al. (2012). Fiji: an open-source platform for biological-image analysis. *Nat. Methods.* 9 (7), 676–682. doi:10.1038/nmeth.2019

Schlichtenbrede, F. C., MacNeil, A., Bainbridge, J. W. B., Tschernutter, M., Thrasher, A. J., Smith, A. J., et al. (2003). Intraocular gene delivery of ciliary neurotrophic factor results in significant loss of retinal function in normal mice and in the Prph2Rd2/Rd2 model of retinal degeneration. *Gene. Ther.* 10 (6), 523–527. doi:10.1038/sj.gt.3301929

Scott, B. B., and Lois, C. (2005). Generation of tissue-specific transgenic birds with lentiviral vectors. *Proc. Natl. Acad. Sci. USA.* 102 (45), 16443–16447. doi:10.1073/pnas.0508437102

Seifert, M., Baden, T., and Osorio, D. (2020). The retinal basis of vision in chicken. *Semin. Cell Dev. Biol.* 106, 106–115. doi:10.1016/j.semcdb.2020.03.011

Stieger, K., Cronin, T., Bennett, J., and Rolling, F. (2011). Adeno-associated virus mediated gene therapy for retinal degenerative diseases. *Methods. Mol. Biol.* 807, 179–218. doi:10.1007/978-1-61779-370-7_8

Vergara, M. N., and Canto-Soler, M. V. (2012). Rediscovering the chick embryo as a model to study retinal development. *Neural. Dev.* 7, 22–19. doi:10.1186/1749-8104-7-22

Verrier, J. D., Madorsky, I., Coggin, W. E., Geesey, M., Hochman, M., Walling, E., et al. (2011). Bicistronic lentiviruses containing a viral 2A cleavage sequence reliably co-express two proteins and restore vision to an animal model of LCA1. *PloS. One.* 6 (5), e20553. doi:10.1371/journal.pone.0020553

Waldner, D. M., Visser, F., Fischer, A. J., Bech-Hansen, N. T., and Stell, W. K. (2019). Avian adeno-associated viral transduction of the postembryonic chicken retina. *Transl. Vis. Sci. Technol.* 8(4), 1–1. doi:10.1167/tvst.8.4.1

Waldvogel, J. A. (1990). The bird's eye view. *Am. Sci.* 78 (4), 342–353.

Wang, X., Jiang, B., Gu, L., Chen, Y., Mora, M., Zhu, M., et al. (2021). A photoregulatory mechanism of the circadian clock in Arabidopsis. *Nat. Plants* 7 (10), 1397–1408. doi:10.1038/s41477-021-01002-z

Watanabe, S., Sanuki, R., Ueno, S., Koyasu, T., Hasegawa, T., and Furukawa, T. (2013). Tropisms of AAV for subretinal delivery to the neonatal mouse retina and its application for *in vivo* rescue of developmental photoreceptor disorders. *PloS. One.* 8 (1), e54146. doi:10.1371/journal.pone.0054146

Williams, M. L., Coleman, J. E., Haire, S. E., Aleman, T. S., Cideciyan, A. V., Sokal, I., et al. (2006). Lentiviral expression of retinal guanylate cyclase-1 (RetGC1) restores vision in an avian model of childhood blindness. *PLoS Med.* 3 (6), e201. doi:10.1371/journal.pmed.0030201

Wiltschko, W., Munro, U., Ford, H., and Wiltschko, R. (1993). Red light disrupts magnetic orientation of migratory birds. *Nature* 364, 525–527. doi:10.1038/364525a0

Wu, H., Scholten, A., Einwich, A., Mouritsen, H., and Koch, K. W. (2020). Protein-protein interaction of the putative magnetoreceptor cryptochrome 4 expressed in the avian retina. *Sci. Rep.* 10 (1), 7364. doi:10.1038/s41598-020-64429-y

Xu, J., Jarocha, L. E., Zollitsch, T., Konowalczyk, M., Henbest, K. B., Richert, S., et al. (2021). Magnetic sensitivity of cryptochrome 4 from a migratory songbird. *Nature* 594 (7864), 535–540. doi:10.1038/s41586-021-03618-9

Yiu, G., Chung, S. H., Mollhoff, I. N., Nguyen, U. T., Thomasy, S. M., Yoo, J., et al. (2020). Suprachoroidal and subretinal injections of AAV using transscleral microneedles for retinal gene delivery in nonhuman primates. *Mol. Ther. Methods. Clin. Dev.* 16, 179–191. doi:10.1016/j.omtm.2020.01.002

Zapka, M., Heyers, D., Hein, C. M., Engels, S., Schneider, N.-L., Hans, J., et al. (2009). Visual but not trigeminal mediation of magnetic compass information in a migratory bird. *Nature* 461 (7268), 1274–1277. doi:10.1038/nature08528

Ziccardi, L., Cordeddu, V., Gaddini, L., Matteucci, A., Parravano, M., Malchiodi-Albedi, F., et al. (2019). Gene therapy in retinal dystrophies. *Int. J. Mol. Sci.* 20 (22), 5722. doi:10.3390/ijms20225722

frontiers | Frontiers in Physiology

TYPE Original Research
PUBLISHED 21 March 2025
DOI 10.3389/fphys.2025.1534385

OPEN ACCESS

EDITED BY
Sandra G. Velleman,
The Ohio State University, United States

REVIEWED BY
Mahmoud Madkour,
National Research Centre, Egypt
Colin Guy Scanes,
University of Wisconsin–Milwaukee,
United States

*CORRESPONDENCE
Kenneth E. Anderson,
✉ kanderso@ncsu.edu

RECEIVED 25 November 2024
ACCEPTED 18 February 2025
PUBLISHED 21 March 2025

CITATION
Harding KL, Boot E, Evans JO, Shah SB, Malheiros RD and Anderson KE (2025) Determining how different ventilation shutdown plus methods change the electroencephalography, blood chemistry, corticosterone, and heat shock protein 70 of laying hens.
Front. Physiol. 16:1534385.
doi: 10.3389/fphys.2025.1534385

Determining how different ventilation shutdown plus methods change the electroencephalography, blood chemistry, corticosterone, and heat shock protein 70 of laying hens

Kari L. Harding[1], Emmillie Boot[1], Jackson O. Evans[2], Sanjay B. Shah[2], Ramon D. Malheiros[1] and Kenneth E. Anderson[1]*

[1]Prestage Department of Poultry Science, North Carolina State University, Raleigh, NC, United States, [2]Biological and Agricultural Engineering, North Carolina State University, Raleigh, NC, United States

The poultry industry faces a major impediment in dealing with highly pathogenic avian influenza (HPAI). Large outbreaks have resulted in depletion of available resources needed for desired depopulation methods, leading to the need for alternative methods. This study was conducted to explore alternative ventilation shutdown procedures and how they affect laying hens throughout the process. Three treatments evaluated were ventilation shutdown plus heat (VSDH), ventilation shutdown plus heat and relative humidity (VSDHRh), and ventilation shutdown plus carbon dioxide ($VSDCO_2$). There were two phases used: one phase was used to study treatment effects on the hens' EEG responses from beginning to time of death and how laying hens behaved. Phase 2 examined how these treatments affected hen blood chemistry and HSP70 during the process. $VSDCO_2$ had a significantly quicker time of death ($P = 0.0003$), and VSDH and VSDHRh were not different. There were no differences in pre- or post-corticosterone levels in Phase 1; however, there was a trend ($P = 0.07$) toward significance in the post corticosterone levels. Heat shock protein 70 (HSP70) levels were higher ($P = 0.0001$) in the $VSDCO_2$ treatment, which could be due to the protein upregulation to prevent apoptosis. In Phase 2, VSDH corticosterone had a significantly greater treatment effect compared to VSDHRh and $VSDCO_2$. corticosterone levels were significantly greater than those of VSDHRh. There were no significant treatment effects in Phase 2 for HSP70 expression; however, the sequence was significant, with the HSP70 being significantly greater at 75% to the average time of death than at 100% to the average time of death. Overall, VSDHRh could be a good alternative for the industry to use to rapidly depopulate laying hen facilities. However,

more research on this treatment and more in-depth stress parameters measured needs to be conducted to fully determine how it affects laying hens.

KEYWORDS

depopulation, physiology, relative humidity, highly pathogenic avian influenza, laying hen

1 Introduction

Highly pathogenic avian influenza (HPAI) is an infectious disease that has become a major concern for the poultry industry. Beginning in 2014 and carrying over into 2015, the poultry industry experienced a major outbreak of HPAI. This outbreak resulted in the loss of roughly 45 million birds, mostly laying hens or pullets (Greene, 2015). Currently an outbreak of HPAI that was first reported in 2022 and is ongoing has led to 96.91 million birds being depopulated. Of these flocks, 496 have been commercial and 655 have been backyard flocks (USDA, 2024). According to the American Veterinary Medical Association (AVMA), depopulation is defined as "methods by which large numbers of animals must be destroyed quickly and efficiently with as much consideration given to the welfare of animals as practicable, given extenuating circumstances" (AVMA, 2019). Current preferred depopulation methods for floor-reared poultry include use of water-based expanding foam, captive bolt guns, and water-based foam nozzles. Cage-housed laying hens have permitted methods such as CO_2 kill carts, CO_2 injection throughout the entire house, and partial-house gassing. The injection of CO_2 for whole-house or partial-house is a preferred method for floor-reared poultry as well. Under constrained circumstances, some of the following methods are permitted for floor-reared poultry: (VSD) plus (hyperthermia), controlled demolition, and exsanguination, and for caged-house poultry, use of compressed air foam, captive bolt guns, and VSD+ are some of the permitted methods. While all of these methods are successful, the preferred methods are most often quicker methods of depopulation compared to the permitted methods for both housing systems. Ventilation shutdown alone is not permitted for either of these poultry housing types, and therefore was not used for this study. The challenge that was identified from the outbreaks was that multi-tiered housing systems such as conventional or colony cages and aviaries, along with high-rise houses, provided hindrances to some of the preferred depopulation methods. In both outbreaks, supplies, namely, CO_2, were rapidly depleted or not available, resulting in an increase in the suffering of affected birds and leading to the potential for a greater spread of the virus. This led to the need for development of alternative depopulation methods to decrease the potential for a greater spread of the disease and to mitigate bird suffering and biosecurity risks. Eberle-Krish et al. (2018) evaluated ventilation shutdown plus CO_2 ($VSDCO_2$) and ventilation shutdown plus heat (VSDH) vs ventilation shutdown (VSD). They reported that $VSDCO_2$ was more rapid than all other treatments, followed by VSDH, both with 100% mortality compared to VSD alone, which did not meet the 100% mortality standard. Other research studies have found that including high relative humidity levels with heat reduces the time it takes for total depopulation (Zhao et al., 2019). Another study looking at the addition of steam showed that all treatments using steam were significantly faster to observe the first hen death and complete mortality compared to ventilation shutdown plus heat alone (Mendoza and Williams, 2024). There is very limited research evaluating how laying hen electroencephalograms (EEGs) change throughout any of the VSD processes. One study evaluated the EEGs of laying hens during application of whole-house CO_2. The results in individual birds indicated the changes between normal, transitional, suppressed, and isoelectric EEG phases. The results reported that out of ten laying hens, nine exhibited a decrease in EEG amplitude at each of the phases (Mckeegan et al., 2011). Another trial utilized EEGs to determine time to unconsciousness and brain death in broilers, layers, turkeys, and ducks. It was reported that turkeys reached time to brain death faster when water-based foam was used, compared to layers and ducks in which they reach brain death sooner with use of CO_2 gas (Benson et al., 2012). While these studies have observed what one method looks like for laying hens, there are no known studies that have compared EEG signals of laying hens across treatments. There is currently no research comparing the different ventilation shutdown plus methods for their effects on laying hen blood physiology and behaviors either.

2 Materials and methods

All research procedures involving animals in these trials were approved by the North Carolina State University Institutional Animal Care and Use Committee (IACUC # 21-310). This study was conducted in the Bird Wing of the Prestage Department of Poultry Science at North Carolina State University. Throughout the study, all animals were monitored by veterinarians and animal welfare specialists employed by the university.

Both Phase 1 and Phase 2 experiments described below were conducted in four chambers that were housed in a windowless, temperature-controlled room. The chambers were made with Plexiglass® with fittings that allowed for CO_2 sampling using external meters to collect data and for the injection of gas or humidity. The temperature and relative humidity for each chamber was recorded using Aranet sensors (Aranet, Riga, Latvia; model: SKU: TDSPT8U2; accuracy: ±0.3°C and ±2%). These sensors recorded every minute with the base placed approximately 4 cm (0.04 m) from the top of each chamber and the sensor reaching bird eye level when standing. Three sides, top, and bottom were

Abbreviations: HPAI, highly pathogenic avian influenza; VSD+, ventilation shutdown plus; VSDH, ventilation shutdown plus heat; VSDHRh, ventilation shutdown plus relative humidity; $VSDCO_2$ ventilation shutdown plus carbon dioxide; CO2, carbon dioxide; mV, millivolts; EEG, electroencephalographic; Hz, hertz; TOD, time of death; HSP70, heat shock protein 70; Rh, relative humidity; min, minutes.

10.3389/fphys.2025.1534385

TABLE 1 Description of the ventilation shutdown alternative treatments for the trial.

Treatment	Treatment code	Description
Ventilation shutdown plus heat	VSDH	Ventilation is turned off, all inlets and exhausts are sealed, and heat is added
Ventilation shutdown plus heat and relative humidity	VDSHRh	Ventilation is turned off, air inlets and exhausts are sealed, and both heat and humidity are injected into the chambers with the target of ~99% Rh
Ventilation shutdown plus carbon dioxide	$VSDCO_2$	Ventilation is turned off, air inlets and exhausts are sealed, and CO_2 is injected into the chamber to reach 30% concentration

TABLE 2 Description of the behaviors[a] analyzed and reported every 2 min as hens underwent treatment.

Behavior	Description
Conscious	
Headshake	Rapid shaking or lateral movement of the head
Mandibulation	Repetitive tasting movement with the beak
Standing	Legs extended, fully upright
Wing flapping	A bout of continuous, rapid wing flapping
Crouch	Legs are folded under the bird with the body positioned on top
Unconscious	
Panting	Deeper than normal expiration through an open mouth generally accompanied by movements of the tongue and beak
Respiratory disruption	Deep, open beak breathing with prolonged inspiration or prolonged open beak gasping, or both, combined with difficulty inhaling
Loss of posture	Loss of balance or posture or both (lateral recumbency

[a]Behaviors based on definitions by Hurnik et al. (1995).

TABLE 3 Calculated sampling times in minutes of removal times to determine changes in blood chemistry and HSP70[c] over time.

Sequence[a]	0	25%	50%	75%	100%
Treatment[b]	Minutes				
VSDH	0	14	28	42	56
VSDHRh	0	12	24	36	48
$VSDCO_2$	0	6	12	18	24

[a]Sequence is baselines = 0, 25 is 25% to average TOD, 50 is 50% to average TOD, 75 is 75% to average TOD, and 100 is average TOD.
[b]VSDH, ventilation shutdown plus heat; VSDHRh, ventilation shutdown plus heat and relative humidity; $VSDCO_2$ = ventilation shutdown plus carbon dioxide.
[c]HSP70, heat shock protein 70.

covered with 2.5 cm of the closed cell insulation board, with only the front panel uncovered to all the hens to be observed. The chamber size was 1.68 ft. (0.51 m) × 1.68 ft. (0.51 m) × 1.68 ft. (0.51 m) equating to the space volume per hen in a typical caged layer facility. The room containing the chambers was maintained at 26°C to prevent heat loss to the environment. In each chamber, a 100-W incandescent light bulb built into the chamber was used as the heat source for the heat treatments described in Table 1. This allowed for temperatures to reach 40°C, which was chosen based on the Department of Environment, Food, and Rural Affairs (DEFRA, 2009). All chambers were equipped with raised 1 in. × 2 in. (0.305 m × 0.610 m) welded wire floors to mimic cages floors and to allow the hens to maintain posture. A total of three treatments were analyzed in both Phase 1 and Phase 2, and they included ventilation shutdown plus heat (VSDH), ventilation shutdown plus heat and relative humidity (VSDHRh), and ventilation shutdown plus CO_2 ($VSDCO_2$). Phase 1 had four replicates per treatment, totaling 12 white commercial laying hens that were approximately 69 weeks of age. These hens were maintained in the Bird Wing at North Carolina State University and were randomly assigned to the treatments. These hens were housed individually, in conventional cages with no additional treatments or procedures for at least 1 week prior to trial initiation. Treatment hens were removed, and blood was obtained from the brachial vein to obtain a baseline level of blood chemistry and corticosterone levels prior to treatment. Core body temperatures for each hen were evaluated using a SuperMeter® (Stamford, CT, United States; Model: HHM290) before and after treatment. The brain electrical output was measured in millivolts (mV) by using an electroencephalogram (EEG). Individual electrodes were insulated, except at the tips, and were attached to the pre-amplifier (AD Instruments, Colorado Springs, CO, United States), which transfers the EEG signals to a laptop-based recording that was continuously monitored. Prior to electrode placement, the birds were hobbled, which allowed them to stand and walk, but prevented them from scratching their heads and pulling out the electrodes. Hobbling was conducted using a rubber band that was placed on the shanks and above the dewclaws. The electrode tips were 32-gauge needles attached to the insulated wire and were inserted subcutaneously. Electrode colors are of three types: red, black, and green. The red electrode was placed on one side of the hen's cranium, and the black electrode was placed on the other side. The green electrode, also known as the ground, was inserted between the wattles in the

TABLE 4 Genes and their genetic sequences (forward and reverse) utilized for gene expression.

Gene	Primer	Directional sequence	Sequence
Beta actin	b-Actin	Forward	GTCCACCTTCCAGCAGATGT
		Reverse	ATAAAGCCATGCCAATCTCG
Heat shock protein	HSP70	Forward	GCGGAGCGAGTGGCTGACTG
		Reverse	CGGTTCCCCTGGTCGTTGGC

TABLE 5 Start and end temperature, relative humidity, and CO_2 levels for each treatment.

Treatment[a]	Start chamber temperature	Start chamber relative humidity	Start CO_2	End chamber temperature	End chamber relative humidity	End CO_2
	(°C)	(%)	(ppm)	(°C)	(%)	(ppm)
VSDH	31.59^{ab}	44.35	0.19	44.05^{a}	61.63^{b}	1.79^{b}
VSDHRh	32.40^{a}	45.00	0.17	43.63^{a}	91.08^{a}	1.28^{b}
$VSDCO_2$	28.05^{b}	52.88	0.24	29.49^{b}	64.70^{b}	22.73^{a}
Std. Dev	1.60	1.82	0.05	0.46	3.92	0.52
P-value	0.0249	0.2002	0.504	<0.0001	<0.0001	<0.0001

[a]VSDH, ventilation shutdown plus heat; VSDHRh, ventilation shutdown plus heat and relative humidity; $VSDCO_2$, ventilation shutdown plus carbon dioxide.

TABLE 6 Pre- and post-core body temperatures and time of death of hens subjected to each treatment.

Treatment[a]	Hen body weight	Core body temperature (°C)		Time of death
	(kg)	Pre (°C)	Post (°C)	(Minutes)
VSDH	1.81	40.20	45.33^{a}	54.50^{a}
VSDHRh	1.88	40.98	45.48^{a}	45.75^{a}
$VSDCO_2$	1.72	39.43	40.98^{b}	24.50^{b}
Std. Dev	0.09	0.93	1.37	1.00
P-value	0.4270	0.0961	0.0003	0.0003

[a]VSDH, ventilation shutdown plus heat; VSDHRh, ventilation shutdown plus heat and relative humidity; $VSDCO_2$, ventilation shutdown plus carbon dioxide.

lower mandible near the neck. Each electrode tip was secured in its place on the head by using surgical adhesive by employing the catheter taping method. These three leads were then taped together and wound under the wing scapular joint, reducing the probability of the bird getting tangled up and pulling the leads out. Once electrodes were placed, the bird was placed into a chamber with the included treatment.

The start time was determined at the point the chamber was sealed, and the EEG was plugged into the pre-amplifier. The EEG data were recorded at a standard frequency band of 10–50 Hertz (Hz) and sampled at 100 Hz/channel. The EEG was recorded until time of death was called by a veterinarian. Each hen's behaviors were monitored throughout the treatment and recorded in real time every 2 min by a trained observer. To keep up with these 2-min checks, timers were utilized. Behaviors that were observed and their descriptors are described in Table 2 based on definitions by Hurnik et al. (1995). The CO_2 concentrations were measured with two 0%–100% CO_2 monitors (CO_2 Meter, Inc., Ormond Beach, FL; model: CM-0003; accuracy: ±70 ppm ± 5% of measured value). These were also recorded on minute intervals as well. Once time of death (TOD) was called for each hen, they were removed from the treatment chamber, with blood being collected by severing the hepatic artery and collecting blood samples from the body cavity within 5 min of TOD. Blood was collected in BD Vacutainer tubes containing lithium heparin to prevent clotting. Approximately 0.1 mL of heparinized blood was then placed on the

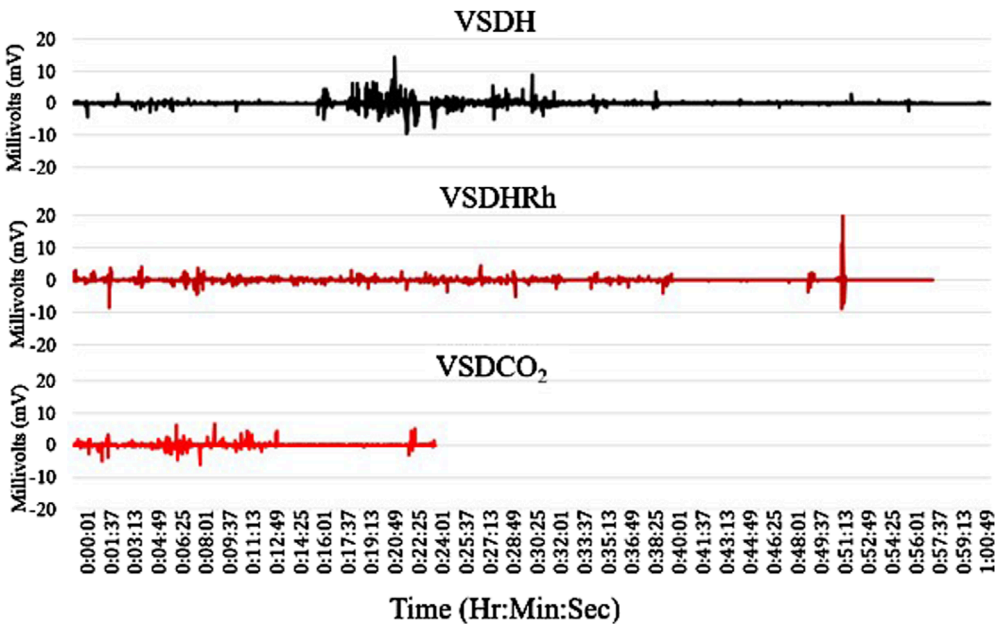

FIGURE 1
Composite electroencephalograms (EEGs) of the four birds per each treatment for VSDH, VSDHRh, and VSDCO2 from initiation to time of death (TOD). VSDH, ventilation shutdown plus heat; VSDHRh, ventilation shutdown plus heat and relative humidity; $VSDCO_2$, ventilation shutdown plus carbon dioxide.

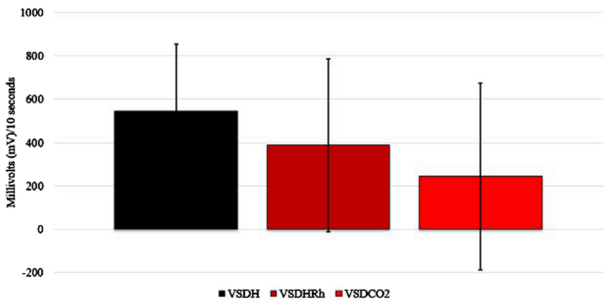

FIGURE 2
Integral area under the electroencephalogram (EEG) graph calculated of the transformed composite EEGs for VSDH, VSDHRh, and $VSDCO_2$ through TOD using the trapezoid method. VSDH, ventilation shutdown plus heat; VSDHRh, ventilation shutdown plus heat and relative humidity; $VSDCO_2$, ventilation shutdown plus carbon dioxide.

i-STAT® diagnostic system using CG8+ cartridges (Abbott Park, IL, United States; Model: 03P8825) for blood chemistry analysis. Birds were then necropsied with the brain being collected and placed into RNA*later*® (Thermo Fisher Scientific, Waltham, MA: Catalog #AM7021) solution. This tube was placed in a refrigerator at 4°C for 24 h and afterward moved to a −20° freezer.

Phase 2 of this trial specifically compared the three treatments with respect to physiological changes (blood chemistry and gene expression) over four time points. Ten ~69-week-old hens were used for each treatment with two replications per treatment, totaling 30 hens. The TOD for the birds in Phase 1 was averaged for each treatment. The average TOD was then quartered, giving a total of four-time intervals, plus one baseline bird that never entered the chamber. The calculated time points to remove the birds are shown in Table 3. This allowed for the evaluation of the hens at the physiological progression over time. At each calculated removal time point, the hen was removed from the chamber, and her blood was collected for blood chemistry and corticosterone analyses within 60 s. The hen was restrained on its side and allowed to bleed via the brachial vein. Between 1.5 and 2 mL of the sample blood was collected using a 3-mL syringe and then transferred to a BD Vacutainer tube with lithium heparin. Then, a 0.1 mL sample of the heparinized blood was placed in the *i*-STAT® diagnostic system using CG8+ cartridges for blood chemistry analysis. The remaining blood was gently shaken to prevent clotting. The blood was then centrifuged and the plasma supernatant collected and frozen at −20°C for future corticosterone analysis. The hen was then euthanized by a trained individual via cervical dislocation, and the brain tissue was collected and placed in RNA*later*® and refrigerated at 4°C for 24 h then moved to a −20°C freezer for later gene expression analysis.

Plasma corticosterone levels for Phase 1 and Phase 2 were collected by using an ELISA corticosterone kit following the manufacturer's guidelines. Corticosterone concentrations were determined by a standard curve as nanograms of corticosterone per milliliter of plasma with each sample run in duplicates. The kit was validated using known standards for each plate run, plotting the values, and adding a best fit line. Values were deemed acceptable with an R^2 value of ≥0.90 (Cayman Chemical Company, Item: 501320, Ann Arbor MI, United States). For brain samples from Phase 1 and Phase 2, an approximately 1-cm sample of the brain was taken to isolate RNA. These samples were placed in homogenization vials with screw caps, and 1 mL of TRI Reagent™ solution was added

10.3389/fphys.2025.1534385

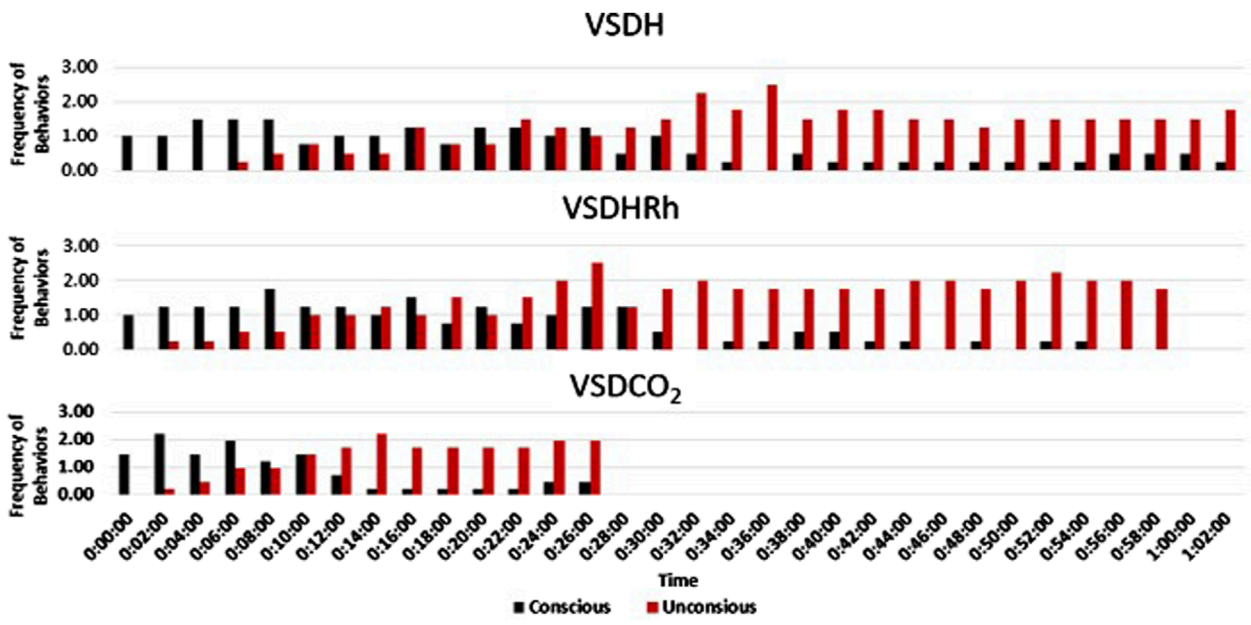

FIGURE 3
Frequency of conscious (voluntary) and unconscious (involuntary) behavioral responses for VSDH, VSDHRh, and $VSDCO_2$ through to time of death. VSDH, ventilation shutdown plus heat; VSDHRh, ventilation shutdown plus heat and relative humidity; $VSDCO_2$, ventilation shutdown plus carbon dioxide. Unconscious behaviors were determined when the electroencephalogram (EEG) readings were below 0.01 millivolts.

TABLE 7 Effect of ventilation shutdown treatment groups on strength of the electroencephalographic waves (mV).

Treatment[a]	Percent EEG time within each mV range[b]			
	0–0.01 mV	0.01–0.03 mV	0.03–0.05 mV	>0.05 mV
	(%)	(%)	(%)	(%)
VSDH	34.76	16.65	4.96	43.63
VSDHRh	45.72	14.69	5.02	34.57
$VSDCO_2$	49.68	6.09	5.94	38.28
Std. Dev	17.92	2.90	2.27	17.45
P-value	0.8333	0.0655	0.9426	0.9347

[a]VSDH, ventilation shutdown plus heat; VSDHRh, ventilation shutdown plus heat and relative humidity; $VSDCO_2$, ventilation shutdown plus carbon dioxide.
[b]Percent EEG time within each mV range explain how long birds were unconscious (0–0.01 mV) and when they were experiencing higher neural activity, which are greater in >0.05 mV and how they vary between the two levels.

to each sample. Each sample was then homogenized using a bead-beater for 20 s and then allowed to incubate at room temperature for 5 min. Then, 200 µL of chloroform was administered to each sample and then vortexed for approximately 10 s. The sample was allowed to sit at room temperature for 2 min and then centrifuged for 20 min at 13,000 × g. Completion of the RNA isolation was performed using an RNeasy kit (QIAGEN, Hilden Germany) according to the manufacturer's guidelines. RNA levels were quantified using the NanoDrop 2000 (Thermo Fisher Scientific-Waltham, MA) to ensure the correct RNA dilutions were obtained. The ideal RNA concentration was between 100 and 1,000 ng/µL, and these were utilized due to ease of pipetting in downstream applications. The RNA was then transcribed into cDNA for qPCR by utilizing a high-capacity cDNA synthesis kit (Applied Biosystems Waltham, Massachusetts, United States). The qPCR was completed on each sample in triplicate. All wells contained 2.5 ng of samples, 500 nM of gene specific forward and reverse primers (Table 4), and 2X power SYBR green master mix (Applied Biosystems Waltham, Massachusetts, United States), and RNase-Free H_2O was added to finalize the volume to 20 µL. The qPCR was performed on the Applied Biosystems StepOnePlus real-time PCR system. Results were normalized to the expression of the basic housekeeping gene, beta actin. The reciprocal was taken for ease of interpretation. The formula used for this is as follows: 1/(target gene cycle threshold/beta actin cycle threshold). All data were then converted to the reciprocal cycle thresholds or CT^{-1}. ΔΔCT was then calculated by first

10.3389/fphys.2025.1534385

TABLE 8 Pearson linear correlation coefficient associated with behavior observations as they relate to the EEG[d] strength.

Treatment[a]	Conscious[b]	Confidence interval			Behavior
	>0.01 mV	Lower 95%	Upper 95%	P-value	N =
VSDH	0.13	2.32	2.35	0.0001	112
VSDHRh	0.00	−0.04	−0.05	0.91	95
$VSDCO_2$	0.05	0.78	0.75	0.11	52
Treatment	Unconscious[c]	Confidence interval			Behavior
	<0.01 mV	Lower 95%	Upper 95%	P-value	N =
VSDH	0.01	2.32	2.35	0.0002	112
VSDHRh	0.00	−0.04	−0.05	0.93	95
$VSDCO_2$	0.04	0.78	0.75	0.18	52

[a]VSDH, ventilation shutdown plus heat; VSDHRh, ventilation shutdown plus heat and relative humidity; $VSDCO_2$, ventilation shutdown plus carbon dioxide.
[b]Conscious behaviors were defined as voluntary behaviors.
[c]Unconscious behaviors were defined as involuntary and were determined when the EEG readings dropped below 0.01 mV.
[d]EEG, electroencephalogram.

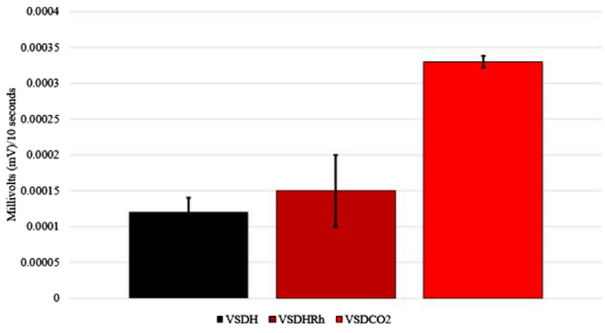

FIGURE 4
Slopes of the transformed electroencephalogram (EEG) readings of laying hens undergoing different methods of ventilation shutdown. VSDH, ventilation shutdown plus heat; VSDHRh, ventilation shutdown plus heat and relative humidity; $VSDCO_2$, ventilation shutdown plus carbon dioxide.

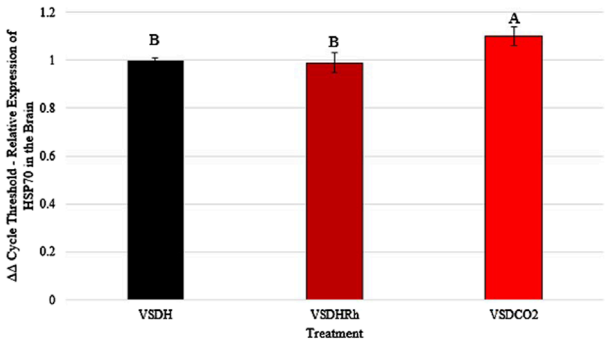

FIGURE 5
*Heat shock protein 70 (HSP70) levels of laying hens exposed to different methods of ventilation shutdown. VSDH, ventilation shutdown plus heat; VSDHRh, ventilation shutdown plus heat and relative humidity; $VSDCO_2$, ventilation shutdown plus carbon dioxide. A, B — different uppercase letters denote significant differences $P < 0.05$. *Depicts parameters with a power of analysis of >0.80.

averaging each treatment CT^{-1}, and VSDH was set to be the control. The average for VSDH was then subtracted from each CT^{-1} to obtain the ΔCT. Because VSDH was used as the control, the ΔΔCT values are the same as the ΔCT values. Each of these values were put into the following equation: $2^{-\Delta\Delta CT}$.

3 Statistical analysis

A one-way ANOVA was used to evaluate the treatment differences in Phase 1, and a two-way ANOVA was used to evaluate if there were any treatment, sequence, or interaction effects between the two in Phase 2. Significant differences were accepted with $\alpha \leq 0.05$, and if there were any differences observed, a Tukey's HSD was utilized for pairwise comparisons. The EEG data were transformed by taking the absolute value of the integral, allowing for the mitigation of the baseline noise, which was relative to the baseline at each 10-s interval, which was conducted using the following equation:

$$\left| \int F(t)dt \right|$$

A hyperbolic arcsine function was used on each value to emphasize the lower millivolt (mV) readings. These transformed EEG data were then analyzed with GLM with full factorial effects of CO_2, heat, and heat and humidity fit to each of several response variables. The transformed EEG data used the integral area under the curve that was calculated using the trapezoid method using an NPARM analysis. Behavior data were summarized as a frequency of behaviors that the hens performed as conscious (voluntary) or unconscious (involuntary) behaviors, overlaid with

10.3389/fphys.2025.1534385

TABLE 9 Comparison of baseline blood chemistry levels in laying hens before undergoing treatment.

Treatment[a]	VSDH	VSDHRh	$VSDCO_2$	Std. Dev	P-value
pH	7.44	7.40	7.43	0.09	0.5151
pCO_2(mmHg)	32.70	36.45	32.70	6.21	0.1297
pO_2(mmHg)	59.00	71.60	63.24	22.09	0.3450
BEecf (mmol/L)	−2.13	−2.10	−3.40	3.17	0.5929
HCO_3(mmol/L)	22.05	22.45	20.93	2.39	0.3349
TCO_2(mmol/L)	23.13	23.50	22.00	2.31	0.3546
sO_2(%)	90.63	91.40	92.61	1.58	0.4892
Na (mmol/L)	137.13[c]	142.80[b]	147.90[a]	1.60	<0.0001
K (mmol/L)	4.15[b]	4.92[a]	3.68[b]	0.40	<0.0001
iCa (mmol/L)	2.44[a]	1.54[b]	1.48[b]	0.13	<0.0001
Glucose (mg/dL)	231.00	217.70	221.60	8.60	0.1758
Hct (% PCV)	20.88[b]	23.90[b]	23.90[b]	1.66	0.0098
Hb (g/dL)	7.10[b]	8.12[a]	8.13[a]	0.56	0.0097

[a]VSDH, ventilation shutdown plus heat; VSDHRh, ventilation shutdown plus heat and relative humidity; $VSDCO_2$, ventilation shutdown plus carbon dioxide. pCO_2, partial pressure of CO_2; pO_2, partial pressure of O_2; BEecf, base excess in extracellular fluid; HCO_3, bicarbonate; TCO_2, total CO_2.

TABLE 10 Changes in laying hen blood chemistry when depopulated using VSDH, VSDHRh, or $VSDCO_2$.

Treatment[a]	VSDH	VSDHRh	$VSDCO_2$	Std. Dev	P-value
pH	7.12	7.20	7.18	0.31	0.89
pCO_2 (mmHg)	61.70	45.55	75.25	39.73	0.50
pO_2 (mmHg)	44.50	62.75	54.75	11.18	0.48
BEecf (mmol/L)	−11.50	−11.50	−4.67	5.67	0.10
HCO_3 (mmol/L)	17.95	16.40	21.77	2.24	0.13
TCO_2 (mmol/L)	20.00	17.75	23.00	1.73	0.23
sO_2 (%)	63.25	73.50	84.00	11.53	0.33
Na (mmol/L)	142.25	139.50	142.75	2.50	0.47
K (mmol/L)	8.75	9.00	6.88	2.45	0.13
iCa (mmol/L)	1.56	1.80	1.57	0.20	0.63
Glucose (mg/dL)	262.75	324.00	265.75	54.54	0.21
Hct (% PCV)	22.50	22.50	24.25	0.96	0.65
Hb (g/dL)	7.65	7.65	8.25	0.33	0.66

[a]VSDH, ventilation shutdown plus heat; VSDHRh, ventilation shutdown plus heat and relative humidity; $VSDCO_2$, ventilation shutdown plus carbon dioxide. pCO_2, partial pressure of CO_2; pO_2, partial pressure of O_2; BEecf, base excess in extracellular fluid; HCO_3, bicarbonate; TCO_2, total CO_2.

TABLE 11 Changes in laying hen corticosterone by treatment before using VSDH, VSDHRh, or $VSDCO_2$ and after.

	Treatment[a]	VSDH	VSDHRh	$VSDCO_2$	Std. Dev	P-value
Pre	Corticosterone (ng/mL)	0.06	0.06	0.05	0.01	0.64
Post		0.11	0.10	0.12	0.001	0.07

[a]VSDH, ventilation shutdown plus heat; VSDHRh, ventilation shutdown plus heat and relative humidity; $VSDCO_2$, ventilation shutdown plus carbon dioxide.

summarized EEG brain activity over the same time intervals. The correlation analysis examined the relationship between the VSDH, VSDHRh, VSDCO2, laying hen EEGs and the behavior profiles. Electroencephalogram activity and conscious and unconscious behaviors was analyzed using Pearson Linear Correlation Analysis in SAS JMP-PRO® 12.2.0 (SAS Institute, 1989).

4 Results and discussion

Table 5 shows the starting and ending chamber temperatures along with relative humidity for each treatment as well as start and end CO_2 levels. There were no significant differences between starting relative humidity or starting CO_2 values of the chamber. There was a significant difference in the start chamber temperature, with the VSDHRh being significantly higher than the starting chamber temperature in the $VSDCO_2$ due to the heating of the outside room for both VSDH and VSDHRh and not the $VSDCO_2$ treatment. There was a significantly lower end chamber temperature for $VSDCO_2$ compared to the other two treatments. This is because this is the only treatment that does not have heat supplemented. The ending relative humidity percentage was significantly greater in the VSDHRh compared to the other two treatments due to addition of humidity. The ending CO_2 levels were significantly greater in $VSDCO_2$, whereas the other two treatments were not different from one another. Table 6 depicts that while there were no significant differences in the pre-core body temperature of hens among the treatments, there was a significantly lower post-core body temperature in the $VSDCO_2$. This again, is due to there being no additional heat being supplemented to this treatment, and the mode of death was hypoxia rather than hyperthermia.

The TOD in minutes is reported in Table 6, and the $VSDCO_2$ treatment has a significantly shorter time of death at 24.50 min than the other two treatments analyzed. This was expected based on previous studies (Eberle-Krish et al., 2018). Results from the composite EEG for all treatments are shown in Figure 1. These results indicate that hens did go unconscious in the later stages of these methods, with sporadic spikes in the EEG mV intensity. This agrees with those results found by Mckeegan et al. (2011) which observed relatively consistent changes over time within the laying hen EEGs. This study also reported that the EEG signal was heavily affected soon after CO_2 was injected, which was observed in this study. Figure 2 depicts the integral area under the electroencephalographic (EEG) composite graph for VSDH, VSDHRh, and $VSDCO_2$ to TOD using the trapezoidal method. The area under the graph of these transformed EEGs was not different among the three treatments. This was unexpected because the TOD for the $VSDCO_2$ treatment was significantly shorter. These results could be because the brainwave activity was variable and relatively high throughout the initial time for all the methods. Figure 3 depicts the frequency of voluntary and involuntary behavioral responses from beginning to time of death. There were no significant differences between the behaviors of the birds undergoing their respective treatments. There were no significant differences in the strength of the EEGs compared to all other treatments, as shown in Table 7. This indicates that even though the EEGs shown in Figure 1 had different patterns of mV strength, there was no difference in the percentages of the mV strengths between the methods. This is supported by the area under the EEG graphs shown in Figure 2, which indicates there are no differences between the depopulation methods compared in this work. There were significant shifts in conscious and unconscious behavior observed, as shown in Figure 3. At the midpoint of each depopulation method, the shift from conscious to unconscious behaviors was dramatic and consistent. This appears to correspond with Wang et al. (2016) observations, where a decline in neuron function in hyperthermia conditions above normal core body temperature was observed. Table 8 illustrates that based on the behavior observations as they relate to the EEG wave strength, there is a poor correlation between hen behaviors and EEG wave strength. VSDH was significant for both conscious and unconscious behaviors, as shown in Table 8. Figure 4 depicts the slope of the transformed EEG reading for each treatment. There was no significant difference between them, showing that there was no difference in magnitude over the course of each treatment when compared to one another.

Heat shock protein 70 (HSP70) levels were significantly upregulated in the $VSDCO_2$ treatment compared to the other two treatments (Figure 5). HSP70 ensures correct protein folding and prevents apoptosis. This gene is heavily upregulated during stress but can be upregulated to make adjustments biologically (Hassan et al., 2019). The elevated levels observed in the $VSDCO_2$ treatment could have just been a biological adjustment or could have been a response to the reaction to the CO_2 injection, which is an irritant that could cause bird stress. However, more research should be conducted on this to pinpoint exactly why this occurred. Table 9 shows the baseline blood chemistry parameters for each treatment with only significant differences in sodium, potassium, and ionized calcium. This could be due to the stress of handling and new environment. No blood chemistry parameters in Phase 1 were significantly different among the treatments, as shown in Table 10. Table 11 depicts the corticosterone levels of hens subjected to different treatments before they entered the chamber, and after TOD was called and they were removed from the chamber. There were no significant differences observed between treatments for either pre or post treatment; however, there was a trend (P = 0.07) for laying hen corticosterone after chamber removal; therefore, there could have potentially been differences observed with a larger sample size.

Phase 2 looked at how these treatments affected the hens over time by removing the hens at specific time points. Due to the small

10.3389/fphys.2025.1534385

TABLE 12 Treatment, sequence, and their interaction effects on laying hen HSP70 levels.

Treatment[b]		ΔΔCT
VSDH		1.00 ± 0.03
VSDHRh		1.00 ± 0.06
$VSDCO_2$		1.04 ± 0.06
P-value		0.1274
Sequence[ac]		
0%		1.00 ± 0.02[ab]
25%		1.00 ± 0.004[ab]
50%		1.01 ± 0.02[ab]
75%		1.07 + 0.08[a]
100%		0.99 ± 0.99[b]
P-value		0.0378
TrtXSequence[a]		
VSDH	0%	1.00
	25%	1.00
	50%	1.00
	75%	1.00
	100%	1.00
VSDHRh	0%	1.01
	25%	1.01
	50%	1.00
	75%	1.06
	100%	0.93
$VSDCO_2$	0%	0.98
	25%	1.00
	50%	1.02
	75%	1.15
	100%	1.06
P-value		0.1324

[a]Sequence is baseline = 0, 25 is 25% to average TOD, 50 is 50% to average TOD, 75 is 75% to average TOD, and 100 is average TOD.
[b]VSDH, ventilation shutdown plus heat; VSDHRh, ventilation shutdown plus heat and relative humidity; $VSDCO_2$, ventilation shutdown plus carbon dioxide.
[c]Depicts parameters with a power of analysis of >0.80.

sample size in this phase, a power of analysis was conducted with parameters with a power greater than 0.80 being labeled. There were no significant treatment or interaction effects with the HSP70 levels for Phase 2 as shown in Table 12. There was, however, a significant sequence effect. The 75% to average TOD was significantly greater than that of the 100% to average TOD. This was thought to be due to the HSP70 being overwhelmed with the misfolded proteins and apoptosis, which resulted in the downregulation of the HSP70 gene at the 100% average time of death. Table 13 depicts the treatment, sequence, and interaction of each on laying hen corticosterone before and after the trial. There were no treatment, sequence, or interaction effects on the pre-corticosterone levels. There also were no sequence or interaction effects on the post-corticosterone levels. A significant treatment effect was observed with VSDH having greater levels at 0.16 ng/mL than all treatments, with $VSDCO_2$ at 0.12 ng/mL being significantly greater than VSDHRh at 0.06 ng/mL. The higher levels of corticosterone in VSDH align with higher levels that are observed in heat stress when compared to hens that are not (Li et al., 2020). Tables 14, 15 depict the baseline blood chemistry for Phase 2 laying hens before they were subjected to their respective treatments. The effects of treatment, sequence, and the interaction as it pertains to blood chemistry parameters from Phase 2 are shown in Tables 16, 17. There is currently no research on how ventilation shutdown plus (hyperthermia) or $VSDCO_2$ affects blood chemistry. There were no treatment or sequence effects observed for pH, pCO_2, pO_2, BEecf, HCO_3, TCO_2, Na, K, iCa, and Hct. Some heat stress studies have reported no changes in blood pH (Barret et al., 2019). Other studies reported that they did see increases in blood pH (Koelkebeck and Odom, 1994). There were, however, sequence effects for sO_2, which dropped significantly at 25% to average TOD; however, they recovered and did not drop again. This could be due to potential increased respiration due to a new environment and the noises at the beginning of the trial. Glucose had a significant sequence effect as well, with both 75% and 100% to average TOD calculated were significantly greater compared to that of the baseline. There were no differences between the other two time points. Koelkebeck and Odom, 1995 also reported there was no change in plasma glucose when laying hens were subjected to heat stress and high CO_2 exposure. Other studies reported that when increasing the environmental temperature for chicks to 40°C for 2 h resulted in no significant impact on blood glucose levels (Bogin et al., 1981). This agrees with our findings of no significant changes in the blood glucose levels when analyzing treatment effects. The significant increase in glucose for the final two points in the sequence could be due to the body increasing energy availability during the treatments overall. There were no significant interaction effects in either Na, glucose, Hct, sO_2, pO_2, HCO_3, or TCO_2. There was a significant interaction in pH with $VSDCO_2$ becoming significantly lower with the 100% TOD having a pH of 7.04. This was expected due to the acidic environment inhalation of CO_2 creates in blood. In turn, this resulted in a significantly higher pCO_2 level in the blood stream at 88.90, which was higher than both 75% and 100% to average TOD in VSDHRh and higher than 75% average TOD in VSDH. The BEecf parameter was significantly lower in the 100% average

10.3389/fphys.2025.1534385

TABLE 13 Effects of treatment, sequence, and their interaction on laying hen corticosterone pre and post treatment.

Treatment[bc]		Corticosterone (ng/mL)	
		Pre[c]	Post[c]
VSDH		0.27 ± 0.05[a-]	0.16 ± 0.02[a]
VSDHRh		0.03 ± 0.01[b]	0.06 ± 0.02[c]
$VSDCO_2$		0.10 ± 0.08[ab]	0.12 ± 0.04[b]
P-value		<0.0001	<0.0001
Sequence[a]			
0%		0.10 ± 0.09	0.10 ± 0.09
25%		0.11 ± 0.10	0.10 ± 0.05
50%		0.17 ± 0.15	0.12 ± 0.04
75%		0.16 ± 0.14	0.12 ± 0.04
100%		0.12 ± 0.12	0.13 ± 0.03
P-value		0.1546	0.3508
TrtXSequence[a]			
VSDH	0%	0.20 ± 0.02	0.20 ± 0.02
	25%	0.24 ± 0.01	0.15 ± 0.003
	50%	0.31 ± 0.06	0.15 ± 0.003
	75%	0.32 ± 0.01	0.14 ± 0.0005
	100%	0.28 ± 0.01	0.15 ± 0.004
VSDHRh	0%	0.03 ± 0.001	0.03 ± 0.002
	25%	0.04 ± 0.02	0.05 ± 0.004
	50%	0.03 ± 0.02	0.06 ± 0.005
	75%	0.03 ± 0.02	0.06 ± 0.001
	100%	0.05 ± 0.008	0.09 ± 0.03
$VSDCO_2$	0%	0.08 ± 0.08	0.08 ± 0.08
	25%	0.06 ± 0.02	0.09 ± 0.05
	50%	0.16 ± 0.15	0.14 ± 0.002
	75%	0.14 ± 0.08	0.14 ± 0.01
	100%	0.04 ± 0.02	0.15 ± 0.003
P-value		0.5077	0.0618

[a]Sequence is baseline = 0, 25 is 25% to average TOD, 50 is 50% to average TOD, 75 is 75% to average TOD, and 100 is average TOD.
[b]VSDH, ventilation shutdown plus heat; VSDHRh, ventilation shutdown plus heat and relative humidity; $VSDCO_2$, ventilation shutdown plus carbon dioxide.
[c]Depicts parameters with a power of analysis of >0.80.

10.3389/fphys.2025.1534385

TABLE 14 Baseline blood chemistry values of laying hens before undergoing treatment.

Trt[b]	Seq[a] (%)	pH	pCO_2 (mmHg)	pO_2[c] (mmHg)	BEecf (mmol/L)	HCO_3 (mmol/L)	TCO_2 (mmol/L)
VSDH		7.34 ± 0.08	48.20 ± 9.38	63.80 ± 9.06	0.10 ± 2.63	25.82 ± 2.18	27.40 ± 2.36
VSDHRh		7.40 ± 0.05	36.30 ± 4.86	64.21 ± 14.33	−2.20 ± 2.82	22.72 ± 2.31	23.80 ± 2.20
$VSDCO_2$		7.39 ± 0.05	42.32 ± 5.46	54.70 ± 20.62	0.90 ± 3.53	25.76 ± 3.16	26.80 ± 3.20
P-value		0.3836	0.1461	0.4517	0.3743	0.2151	0.1773
Sequence[a]							
0%		7.43 ± 0.05	37.73 ± 3.98	92.83 ± 41.13	0.67 ± 2.53	25.02 ± 1.93	26.17 ± 2.00
25%		7.33 ± 0.06	43.68 ± 8.22	88.17 ± 36.63	−3.50 ± 2.94	22.63 ± 2.83	23.83 ± 2.93
50%		7.36 ± 0.04	45.40 ± 8.22	98.00 ± 37.95	−0.33 ± 3.67	25.30 ± 3.75	26.67 ± 4.04
75%		7.38 ± 0.10	44.27 ± 12.71	78.00 ± 24.17	0.83 ± 2.93	26.00 ± 3.11	27.33 ± 3.41
100%		7.40 ± 0.06	40.28 ± 6.17	74.00 ± 22.59	0.33 ± 3.20	24.88 ± 2.43	26.00 ± 2.43
P-value		0.5055	0.7820	0.6357	0.4174	0.5623	0.5512
TrtXSequence							
VSDH	0	7.37 ± 0.004	40.20 ± 3.57	62.50 ± 2.12	−2.00 ± 3.11	23.35 ± 0.21	24.50 ± 0.71
	25	7.29 ± 0.01	51.55 ± 6.15	66.50 ± 2.12	−1.50 ± 3.53	24.95 ± 3,075	26.50 ± 3.54
	50	7.32 ± 0.09	52.60 ± 9.33	56.00 ± 4.24	1.00 ± 1.41	27.20 ± 0.14	29.00 ± 0.71
	75	7.32 ± 0.11	53.80 ± 16.69	65.50 ± 13.44	1.00 ± 2.69	27.15 ± 1.91	29.00 ± 2.83
	100	7.40 ± 0.14	42.85 ± 11.24	68.50 ± 20.51	2.00 ± 4.24	26.45 ± 1.91	28.00 ± 1.41
VSDHRh	0	7.47 ± 0.09	33.60 ± 7.35	63.21 ± 37.38	1.00 ± 2.12	24.60 ± 0.35	26.00 ± 0.71
	25	7.35 ± 0.04	34.20 ± 2.83	61.33 ± 8.49	−2.00 ± 4.95	19.00 ± 3.89	20.00 ± 4.24
	50	7.37 ± 0.03	34.80 ± 2.26	59.56 ± 33.44	−1.50 ± 2.45	20.20 ± 0.21	21.00 ± 0.46
	75	7.43 ± 0.08	37.30 ± 7.28	67.98 ± 40.31	2.50 ± 2.97	24.70 ± 1.27	26.00 ± 1.41
	100	7.40 ± 0.03	41.60 ± 4.10	64.01 ± 16.97	1.50 ± 1.54	25.10 ± 0.57	26.00 ± 0.71
$VSDCO_2$	0	7.45 ± 0.03	39.40 ± 3.68	60.00 ± 12.73	3.00 ± 4.95	27.10 ± 4.17	28.00 ± 4.24
	25	7.33 ± 0.07	45.30 ± 7.36	59.00 ± 1.41	2.00 ± 1.41	23.95 ± 0.21	25.00 ± 1.31
	50	7.37 ± 0.02	48.80 ± 8.13	58.32 ± 37.48	3.00 ± 2.83	28.50 ± 3.61	30.00 ± 4.24
	75	7.40 ± 0.07	41.70 ± 2.26	53.50 ± 0.71	1.50 ± 6.36	26.15 ± 5.59	27.00 ± 5.66
	100	7.41 ± 0.01	36.40 ± 0.49	53.00 ± 38.18	−1.00 ± 2.82	23.10 ± 1.84	24.00 ± 1.41
P-value		0.9975	0.7820	0.1288	0.7682	0.6596	0.5897

[a]Seq is baseline = 0, 25 is 25% to average TOD, 50 is 50% to average TOD, 75 is 75% to average TOD, and 100 is average TOD.

[b]VSDH, ventilation shutdown plus heat; VSDHRh, ventilation shutdown plus heat and relative humidity; $VSDCO_2$, ventilation shutdown plus carbon dioxide.

[c]Depicts parameters with a power of analysis of >0.80.

pCO_2, partial pressure of CO_2; pO_2, partial pressure of O_2; BEecf, base excess in extracellular fluid; HCO_3, bicarbonate; TCO_2, total CO_2.

10.3389/fphys.2025.1534385

TABLE 15 Baseline blood chemistry levels of laying hens before undergoing treatments.

Trt[c]		Na (mmol/L)	K[b] (mmol/L)	iCa[b] (mmol/L)	Glucose (mg/dL)	Hct (% PCV)	sO_2[b] (%)
VSDH		132.90 ± 4.67	4.99 ± 0.97	2.37 ± 0.29	232.00 ± 3.14	20.50 ± 0.93	89.40 ± 3.70[b]
VSDHRh		143.20 ± 20.57	4.44 ± 0.53	2.50 ± 0.18	248.60 ± 14.56	29.20 ± 10.30	99.20 ± 2.20[a]
$VSDCO_2$		130.50 ± 14.06	5.03 ± 0.66	2.50 ± 0.21	233.10 ± 11.46	20.00 ± 6.45	85.40 ± 7.86[b]
P-value		0.0949	0.5350	0.5931	0.0645	0.0750	0.0035
Seq[a]							
0%		130.00 ± 12.92	4.80 ± 0.40	2.50 ± 0.26	238.33 ± 5.89	18.67 ± 3.02	95.17 ± 5.05
25%		143.33 ± 16.76	4.67 ± 0.31	2.40 ± 0.25	248.00 ± 18.07	28.67 ± 9.33	92.33 ± 5.43
50%		137.00 ± 16.08	4.93 ± 0.44	2.50 ± 0.14	251.00 ± 14.29	24.67 ± 8.59	85.00 ± 11.08
75%		136.83 ± 18.94	5.07 ± 1.63	2.38 ± 0.31	224.33 ± 16.77	25.67 ± 7.11	92.00 ± 2.12
100%		130.50 ± 8.08	4.63 ± 0.27	2.50 ± 0.17	227.83 ± 15.46	18.50 ± 2.35	92.17 ± 5.99
P-value		0.2580	0.9524	0.9292	0.0611	0.1839	0.1302
TrtXSequence							
VSDH	0	135.00 ± 2.83	4.70 ± 0.14	2.50 ± 1.22	243.00 ± 1.41	19.00 ± 1.41	91.50 ± 0.71
	25	137.50 ± 0.71	4.75 ± 0.21	2.19 ± 0.44	238.50 ± 12.02	23.50 ± 3.54	90.00 ± 1.41
	50	131.00 ± 4.24	4.80 ± 0.28	2.50 ± 0.23	250.00 ± 9.19	19.00 ± 2.82	85.00 ± 4.95
	75	130.50 ± 9.19	4.20 ± 2.12	2.14 ± 0.52	207.00 ± 8.49	21.50 ± 3.53	90.00 ± 1.41
	100	130.50 ± 3.53	4.50 ± 0.42	2.50 ± 1.12	221.50 ± 3.55	19.50 ± 2.12	90.50 ± 9.19
VSDHRh	0	130.00 ± 19.80	4.80 ± 0.42	2.50 ± 0.33	231.00 ± 1.22	22.00 ± 4.95	100.00 ± 1.41
	25	164.00 ± 35.33	4.30 ± 0.42	2.50 ± 0.09	274.00 ± 23.33	41.00 ± 18.38	99.00 ± 1.55
	50	151.00 ± 24.75	5.10 ± 0.42	2.48 ± 0.14	263.00 ± 5.66	37.00 ± 15.56	100.00 ± 2.83
	75	134.00 ± 24.04	3.30 ± 0.25	2.46 ± 0.30	231.00 ± 7.07	29.00 ± 0.33	99.00 ± 4.24
	100	137.00 ± 12.73	4.70 ± 0.88	2.50 ± 0.16	244.00 ± 4.95	17.00 ± 1.41	98.00 ± 1.41
$VSDCO_2$	0	125.00 ± 6.36	4.90 ± 0.71	2.15 ± 0.38	241.00 ± 0.71	15.00 ± 0.41	94.00 ± 5.66
	25	128.50 ± 4.95	4.95 ± 0.35	2.50 ± 0.44	231.50 ± 14.85	21.50 ± 6.36	88.00 ± 2.83
	50	129.00 ± 16.97	4.90 ± 0.64	2.46 ± 0.23	240.00 ± 12.02	18.00 ± 2.12	70.00 ± 19.09
	75	146.00 ± 16.97	5.70 ± 0.57	2.50 ± 0.73	235.00 ± 14.14	26.50 ± 12.02	87.00 ± 1.41
	100	124.00 ± 5.66	4.70 ± 0.35	2.50 ± 0.29	218.00 ± 21.92	19.00 ± 2.83	88.00 ± 7.07
P-value		0.2111	0.6838	0.9680	0.1736	0.5017	0.3398

[a]Seq is baseline = 0, 25 is 25% to average TOD, 50 is 50% to average TOD, 75 is 75% to average TOD, and 100 is average TOD.
[b]Depicts parameters with a power of analysis of >0.80.
[c]VSDH, ventilation shutdown plus heat; VSDHRh, ventilation shutdown plus heat and relative humidity; $VSDCO_2$, ventilation shutdown plus carbon dioxide.
Hemoglobin (Hb g/dL) data were not recorded by the *i*-STAT® diagnostic system for this parameter.

10.3389/fphys.2025.1534385

TABLE 16 Changes in the blood chemistry of laying hens overtime when depopulated using VSDH (hyperthemic method), VSDHRh (hyperthermic method), or $VSDCO_2$.

Trt[b]	Seq[a] (%)	pH[c]	pCO_2 (mmHg)	pO_2[c] (mmHg)	BEecf[c] (mmol/L)	HCO_3 (mmol/L)	TCO_2 (mmol/L)
VSDH		7.37 ± 0.14	40.20 ± 8.58	62.50 ± 9.20	−2.00 ± 3.72	23.35 ± 2.16	24.50 ± 2.08
VSDHRh		7.41 ± 0.14	38.80 ± 9.23	59.29 ± 13.45	−0.50 ± 3.72	24.35 ± 2.56	25.50 ± 2.63
$VSDCO_2$		7.42 ± 0.18	36.80 ± 29.96	61.00 ± 10.71	−0.50 ± 4.20	24.15 ± 3.75	25.00 ± 3.91
P-value		0.8255	0.9801	0.8635	0.8453	0.9210	0.9340
Sequence[a]							
0%		7.40 ± 0.05	38.60 ± 3.98	65.61 ± 47.13	−1.00 ± 2.53	23.95 ± 1.93	25.00 ± 2.00
25%		7.41 ± 0.08	40.53 ± 11.10	56.50 ± 5.79	1.67 ± 4.58	25.70 ± 4.18	26.83 ± 4.26
50%		7.51 ± 0.12	30.85 ± 10.39	54.67 ± 6.82	0.33 ± 4.68	23.27 ± 4.09	24.33 ± 4.18
75%		7.52 ± 0.28	36.82 ± 30.74	51.83 ± 8.94	1.67 ± 3.82	24.20 ± 3.20	25.33 ± 3.88
100%		7.48 ± 0.36	42.72 ± 44.25	41.33 ± 11.79	−2.22 ± 6.22	22.46 ± 2.61	23.50 ± 2.12
P-value		0.0796	0.7903	0.5641	0.5895	0.3696	0.3748
TrtXSequence							
VSDH	0	7.37 ± 0.004^{bcd}	40.20 ± 2.45^{ab}	62.50 ± 2.12	−2.00 ± 3.2^{bcde}	23.35 ± 0.21	24.50 ± 0.71
	25	7.50 ± 0.07^{abcd}	34.45 ± 0.07^{ab}	40.00 ± 11.31	4.00 ± 5.65^{ab}	27.10 ± 4.38	28.00 ± 4.24
	50	7.64 ± 0.03^{abc}	25.25 ± 2.62^{ab}	46.50 ± 6.36	5.00 ± 1.41^{a}	25.40 ± 1.70	26.00 ± 1.41
	75	7.73 ± 0.08^{a}	19.00 ± 2.55^{b}	45.00 ± 4.24	5.50 ± 2.12^{a}	25.00 ± 1.13	25.50 ± 0.71
	100	7.68 ± 0.05^{ab}	21.30 ± 0.85^{ab}	48.00 ± 1.41	5.00 ± 2.83^{a}	24.95 ± 2.05	25.50 ± 2.12
VSDHRh	0	7.41 ± 0.08^{abcd}	38.80 ± 7.35^{ab}	62.50 ± 47.38	−0.50 ± 2.1^{abcd}	24.35 ± 0.35	25.50 ± 0.71
	25	7.42 ± 0.02^{abcd}	33.00 ± 3.54^{ab}	42.00 ± 1.41	−3.00 ± 4.24^{cde}	21.45 ± 3.46	22.50 ± 3.54
	50	7.50 ± 0.09^{abcd}	23.75 ± 3.75^{ab}	52.00 ± 7.07	−4.50 ± 2.12^{de}	18.50 ± 0.99	19.50 ± 0.71
	75	7.67 ± 0.01^{ab}	18.40 ± 2.69^{b}	55.00 ± 4.24	1.50 ± 2.12^{abcd}	21.40 ± 2.40	22.00 ± 2.83
	100	7.72 ± 0.01^{a}	17.95 ± 0.35^{b}	53.50 ± 16.26	4.00 ± 0.04^{ab}	23.35 ± 0.21	24.00 ± 1.02
$VSDCO_2$	0	7.42 ± 0.03^{abcd}	36.80 ± 3.68^{ab}	61.00 ± 12.73	−0.50 ± 4.9^{abcd}	24.15 ± 4.17	25.00 ± 4.24
	25	7.33 ± 0.05^{cde}	54.15 ± 6.72^{ab}	40.00 ± 5.66	2.50 ± 0.71^{abc}	28.55 ± 0.07	30.00 ± 0.04
	50	7.38 ± 0.007^{bcd}	43.55 ± 5.73^{ab}	46.50 ± 5.66	0.50 ± 3.54^{abcd}	25.90 ± 3.39	27.50 ± 3.53
	75	7.18 ± 0.10^{de}	73.05 ± 27.79^{ab}	45.00 ± 1.41	−2.00 ± 2.8^{bcde}	26.20 ± 4.38	28.50 ± 4.95
	100	7.04 ± 0.24^{e}	88.90 ± 58.12^{a}	48.00 ± 1.41	−9.00 ± 1.34^{e}	19.10 ± 4.54	21.00 ± 4.35
P-value		0.0002	0.0235	0.3450	0.0226	0.1634	0.1953

[a]Seq is baseline = 0, 25 is 25% to average TOD, 50 is 50% to average TOD, 75 is 75% to average TOD, and 100 is average TOD.
[b]VSDH, ventilation shutdown plus heat; VSDHRh, ventilation shutdown plus heat and relative humidity; $VSDCO_2$, ventilation shutdown plus carbon dioxide.
[c]Depicts parameters with a power of analysis of >0.80.
pCO_2, partial pressure of CO_2; pO_2, partial pressure of O_2; BEecf, base excess in extracellular fluid; HCO_3, bicarbonate; TCO_2, total CO_2.

TABLE 17 Blood chemistry change of laying hens overtime when depopulated using VSDH (hyperthemic method), VSDHRh (hyperthermic method), or $VSDCO_2$.

Trt[c]		Na (mmol/L)	K[b] (mmol/L)	iCa[b] (mmol/L)	Glucose (mg/dL)	Hct (% PCV)	sO_2 (%)
VSDH		135.00 ± 5.74	4.70 ± 0.70	2.50 ± 0.24	243.00 ± 19.61	19.00 ± 0.72	91.50 ± 6.78
VSDHRh		116.00 ± 18.56	4.50 ± 0.37	2.27 ± 0.37	231.00 ± 41.81	18.50 ± 7.43	99.00 ± 7.90
$VSDCO_2$		120.50 ± 10.50	4.40 ± 1.65	2.23 ± 0.17	241.50 ± 31.67	15.00 ± 5.16	90.00 ± 8.53
P-value		0.3788	0.9195	0.3062	0.8694	0.7564	0.2594
Seq[a]							
0%		123.83 ± 12.92	4.53 ± 0.40	2.33 ± 0.26	238.50 ± 3.02[b]	17.50 ± 1.02	93.50 ± 5.05[a]
25%		134.67 ± 16.84	4.65 ± 0.92	2.45 ± 0.12	270.67 ± 38.27[ab]	21.00 ± 8.92	77.00 ± 8.27[b]
50%		129.67 ± 6.31	4.77 ± 0.59	2.33 ± 0.28	276.33 ± 20.30[ab]	16.50 ± 3.21	89.67 ± 1.70[a]
75%		129.33 ± 18.10	4.48 ± 0.55	2.23 ± 0.43	288.17 ± 28.85[a]	22.83 ± 5.92	90.50 ± 5.68[a]
100%		128.33 ± 6.09	5.77 ± 1.98	2.20 ± 0.40	291.17 ± 40.99[a]	16.83 ± 2.23	91.83 ± 2.97[a]
P-value		0.7567	0.0581	0.3062	0.0152	0.3341	0.0013
TrtXSequence							
VSDH	0	135.00 ± 2.82	4.70 ± 0.14[b]	2.50 ± 0.54[a]	243.00 ± 11.41	19.00 ± 0.49	91.50 ± 0.71
	25	138.50 ± 2.12	5.15 ± 1.63[b]	2.50 ± 2.10[a]	265.50 ± 23.33	16.50 ± 2.12	80.00 ± 12.72
	50	129.00 ± 4.24	4.65 ± 0.78[b]	2.50 ± 1.33[a]	277.00 ± 18.38	15.50 ± 0.71	91.00 ± 2.83
	75	126.50 ± 7.77	4.70 ± 0.42[b]	2.50 ± 1.68[a]	255.50 ± 10.61	18.00 ± 4.24	92.00 ± 4.24
	100	131.50 ± 4.95	4.65 ± 0.78[b]	2.50 ± 2.25[a]	248.00 ± 31.11	17.00 ± 2.83	92.50 ± 0.71
VSDHRh	0	116.00 ± 19.79	4.50 ± 0.42[b]	2.27 ± 0.33[abc]	231.00 ± 32.41	18.50 ± 4.95	99.00 ± 1.41
	25	139.00 ± 33.94	4.65 ± 0.78[b]	2.35 ± 0.21[ab]	303.50 ± 54.44	26.00 ± 15.56	78.50 ± 2.12
	50	128.00 ± 12.73	4.45 ± 0.07[b]	2.00 ± 0.19[abc]	280.00 ± 38.18	19.00 ± 3.53	89.50 ± 6.36
	75	117.00 ± 24.04	4.00 ± 1.02[b]	1.70 ± 0.28[bc]	303.50 ± 9.19	27.00 ± 4.58	95.00 ± 1.41
	100	126.50 ± 10.61	4.45 ± 0.07[b]	1.60 ± 0.23[c]	321.00 ± 38.18	17.50 ± 5.65	94.00 ± 4.24
$VSDCO_2$	0	120.50 ± 6.36	4.40 ± 0.71[b]	2.23 ± 0.38[abc]	241.50 ± 0.71	15.00 ± 1.21	90.00 ± 5.66
	25	126.50 ± 7.77	4.15 ± 0.07[b]	2.50 ± 1.23[a]	243.00 ± 8.49	20.50 ± 7.78	72.50 ± 10.61
	50	132.00 ± 1.41	5.20 ± 0.71[ab]	2.50 ± 2.11[a]	272.00 ± 14.14	15.00 ± 2.49	88.50 ± 3.53
	75	144.50 ± 14.85	4.75 ± 0.78[b]	2.50 ± 1.12[a]	305.50 ± 27.58	23.50 ± 7.78	84.50 ± 4.95
	100	127.00 ± 4.24	8.20 ± 1.13[a]	2.50 ± 2.55[a]	304.50 ± 10.61	16.00 ± 1.41	89.00 ± 3.78
P-value		0.7712	0.0182	0.0015	0.1633	0.9152	0.9165

[a]Seq is baseline = 0, 25 is 25% to average TOD, 50 is 50% to average TOD, 75 is 75% to average TOD, and 100 is average TOD.
[b]Depicts parameters with a power of analysis of >0.80.
[c]VSDH, ventilation shutdown plus heat; VSDHRh, ventilation shutdown plus heat and relative humidity; $VSDCO_2$, ventilation shutdown plus carbon dioxide.
Hemoglobin (Hb g/dL) data were not recorded by the *i*-STAT® diagnostic system for this parameter.

TOD for $VSDCO_2$ compared to the final two sequence points for both VSDH and VSDHRh, most likely due to the increased acidic environment caused by the CO_2. There was a significantly greater amount of K in the $VSDCO_2$ treatment at 50% and 100% to average TOD compared to all other treatments. This could possibly be due to the K trying to balance the body's acidic environment. There was also an interaction for iCa with VSDHRh having significantly lower levels at 100% average TOD than all other treatment sequences, except for VSDHRh 75% average TOD. This potentially could be due to increased panting by the birds, leading to water loss.

This study was conducted to try to get an understanding of what birds are experiencing throughout different depopulation methods. Due to the nature of this study, the smallest possible sample size that could get approved was utilized. This was to try to get a better understanding of the blood physiology, behaviors, and TOD for laying hens undergoing these treatments. Bird variability could have played a large factor in significance and non-significance. A larger sample size is necessary to allow for a stronger understanding of what exactly is occurring in the laying hen. It would also be beneficial to conduct this study analyzing different parameters to fully understand the stress that the laying hens are undergoing.

5 Conclusion

As HPAI continues to be a major concern for the poultry industry, it is important to know the methods used for emergency depopulation and how they affect the laying hen. This study examined how three treatments, VSDH, VSDHRh, and $VSDCO_2$, were compared with respect to laying hen TOD, blood physiology, and behaviors. $VSDCO_2$ had a significantly shorter TOD than the other two treatments. While the VSDH and VSDHRh treatments were not significantly different, VSDHRh had a time reduction of 16%. There also were no significant differences associated with the hens' EEGs nor their behaviors. There were significantly greater levels of HSP70 production in $VSDCO_2$ compared to the other two treatments. Overall, this study demonstrated that while $VSDCO_2$ may have significantly quicker TOD, in the event that there are limited supplies, both VSDH and VSDHRh may be available as alternatives to depopulate laying hen houses. Having multiple alternative methods that have met the guidelines as defined in the Red Book (USDA-APHIS, 2017), like VSDH and VSDHRh, may allow for the reduction in the spread of HPAI. The approval for use comes from the AVMA Depopulation Guidelines; however, the USDA makes the final decision on which methods will be administered depending on different factors such as bird type and housing type. Future research with these treatments may potentially provide a better understanding of laying hen stress and could measure respiratory rate, internal body temperature measurements, thyroid hormones like T3 and T4, and adrenocorticotropic hormone (ACTH) levels.

Data availability statement

The original contributions presented in the study are included in the article/Supplementary Material; further inquiries can be directed to the corresponding author.

Ethics statement

The animal study was approved by the North Carolina State University Institutional Animal Care and Use Committee (IACUC # 21-310). The study was conducted in accordance with the local legislation and institutional requirements.

Author contributions

KH: conceptualization, data curation, investigation, methodology, writing–original draft, and writing–review and editing. EB: data curation, investigation, methodology, and writing–review and editing. JE: data curation, investigation, methodology, software, and writing–review and editing. SS: conceptualization, data curation, funding acquisition, investigation, methodology, software, supervision, and writing–review and editing. RM: conceptualization, data curation, funding acquisition, investigation, methodology, supervision, and writing–review and editing. KA: conceptualization, data curation, funding acquisition, investigation, methodology, project administration, supervision, and writing–review and editing.

Funding

The author(s) declare that financial support was received for the research, authorship, and/or publication of this article. The authors would like to thank U.S. Poultry & Egg Association for funding this project (Project F99).

Acknowledgments

The authors would like the thank staff at Prestage Department of Poultry Science-North Carolina State University for all of their help throughout the study.

Conflict of interest

The authors declare that the research was conducted in the absence of any commercial or financial relationships that could be construed as a potential conflict of interest.

Generative AI statement

The author(s) declare that no Generative AI was used in the creation of this manuscript.

Publisher's note

References

American Veterinary Medical Association (2019). AVMA guidelines for the depopulation of animals: 2019 edition. Available at: https://www.avma.org/resources-tools/avma-policies/avma-guidelines-depopulation-animals (Accessed June 17, 2024).

Barret, N. W., Rowland, K., Schmidt, C. J., Lamont, S. J., Rothschild, M. F., Ashwell, C. M., et al. (2019). Effects of acute and chronic heat stress on the performance, egg quality, body temperature, and blood gas parameters of laying hens. *Poult. Sci.* 98, 6684–6692. doi:10.3382/ps/pez541

Benson, E. R., Aplhin, R. L., Rankin, M. K., and Caputo, M. P. (2012). Mass emergency water-based foam depopulation of poultry. *BioOne Compl* 56, 891–896. doi:10.1637/10160-040912-Reg.1

Bogin, E., Weisman, Y., and Friedman, Y. (1981). The effect of heat stress on the levels of certain blood constituents in chickens. *Refuah Vet.* 38, 98–104.

Department of Environment, Food, and Rural Affairs (DEFRA). (2009). Guidelines for killing poultry using ventilation shutdown (VSD).

Eberle-Krish, K. N., Martin, M. P., Malheiros, R. D., Shah, S. B., Livingston, K. A., and Anderson, K. E. (2018). Evaluation of ventilation shutdown in a multi-level caged system. *J. App. Poult. Res.* 27, 555–563. doi:10.3382/japr/pfy036

Greene, J. L. (2015). Congressional research service, update on the highly-pathogenic avian influenza outbreak of 2014-2015. Available at: http://sgp.fas.org/crs/misc/R44114 (Accessed June 17, 2024).

Hassan, F., Nawaz, A., Rehman, M. S., Ali, M. A., Dilshad, S. M. R., and Yang, C. (2019). Prospects of HSP70 as a genetic marker for thermo-tolerance and immuno-modulation in animals under climate change scenario. *Anim. Nutr.* 5, 340–350. doi:10.1016/j.aninu.2019.06.005

Hurnik, J. F., Webster, A. B., and Siegal, P. B. (1995). *Dictionary of farm animal behavior*. Second Edition. Ames: Iowa State University Press.

Koelkebeck, K. W., and Odom, T. W. (1994). Laying hen responses to acute heat stress and carbon dioxide supplementation: I. Blood gas changes and plasma lactate accumulation. *Comp. Biochem. Physiol.* 107A, 603–606. doi:10.1016/0300-9629(94)90358-1

Koelkebeck, K. W., and Odom, T. W. (1995). Laying hen responses to acute heat stress and carbon dioxide supplementation: II. Changes in plasma enzymes, metabolites, and electrolytes. *Comp. Biochem. Physiol.* 112A, 119–122. doi:10.1016/0300-9629(95)00081-H

Li, G. M., Liu, L. P., Yin, B., Liu, Y. Y., Dong, W. W., Gong, S., et al. (2020). Heat stress decreases egg production of laying hens by inducing apoptosis of follicular cells via activating the FasL/fas and TNF-α systems. *Poult. Sci.* 99, 6084–6093. doi:10.1016/j.psj.2020.07.024

Mckeegan, D. E. F., Sparks, N. H. C., Sandilands, V., Demmers, T. G. M., Boulcott, P., and Wathers, C. M. (2011). Physiological responses of laying hens during whole-house killing with carbon dioxide. *Br. Poult. Sci.* 52, 645–657. doi:10.1080/00071668.2011.640307

Mendoza, A. V., and Williams, Z. (2024). Can steam be usable as a "plus" for ventilation shutdown? *J. Appl. Poult. Res.* 33, 100381. doi:10.1016/j.japr.2023.100381

United States Department of Agriculture (2024). Confirmations of highly pathogenic avian influenza in commercial and backyard flocks. Available at: https://www.aphis.usda.gov/livestock-poultry-disease/avian/avian-influenza/hpai-detections/commercial-backyard-flocks (Accessed June 17, 2024).

United States Department of Agriculture Animal and Plant Health Inspection Service (2017). Foreign animal disease preparedness and response plan: highly pathogenic avian influenza response plan. *Red Book*. Available at: https://www.aphis.usda.gov/animal_health/emergency_management/downloads/hpai_response_plan.pdf (Accessed June 18, 2024).

Wang, H., Kim, M., Normoyle, K. P., and Llano, D. (2016). Thermal regulation of the brain – an anatomical and physiological review for clinical neuroscientists. *Front. Neurosci.* 9, 528. doi:10.3389/fnins.2015.00528

Zhao, Y., Xin, H., and Li, L. (2019). Modelling and validating the indoor environment and supplemental heat requirement during ventilation shutdown (VSD) for rapid depopulation of hens and turkeys. *Biosyst. Eng.* 184, 130–141. doi:10.1016/j.biosystemseng.2019.06.014

frontiers | Frontiers in Physiology

TYPE Review
PUBLISHED 15 April 2025
DOI 10.3389/fphys.2025.1562569

OPEN ACCESS

EDITED BY
Colin Guy Scanes,
University of Wisconsin–Milwaukee,
United States

REVIEWED BY
Masaki Shirai,
Central Research Institute of Electric Power Industry (CRIEPI), Japan
Dominik Heyers,
University of Oldenburg, Germany

*CORRESPONDENCE
Nikita Chernetsov,
nikita.chernetsov@gmail.com

RECEIVED 17 January 2025
ACCEPTED 27 March 2025
PUBLISHED 15 April 2025

CITATION
Chernetsov N and Utvenko G (2025) Do first-time avian migrants know where they are going: the clock-and-compass concept today.
Front. Physiol. 16:1562569.
doi: 10.3389/fphys.2025.1562569

Do first-time avian migrants know where they are going: the clock-and-compass concept today

Nikita Chernetsov[1,2]* and Gleb Utvenko[3]

[1]Ornithology Lab, Zoological Institute of the Russian Academy of Sciences, St. Petersburg, Russia, [2]Department of Vertebrate Zoology, St. Petersburg State University, St. Petersburg, Russia, [3]Biological Station Rybachy, Zoological Institute of the Russian Academy of Sciences, St. Petersburg, Russia

What if your life depended on finding a place you've never been—without a GPS device, a guide, or any way of knowing where to go? For young songbirds, this is the reality of their first migration. While this once puzzled researchers studying bird migration, advances in the field have since uncovered that many songbirds rely on an inherited genetic program to guide their remarkable solo journeys. Today, the most widely accepted theory explaining how young birds of species that migrate solitary and do not follow experienced conspecifics find their way to wintering grounds is the 'clock-and-compass' concept. According to this concept, naïve migrants follow a certain compass direction for a pre-defined period. In the simplest case, when the program runs out, they find themselves in their species-specific non-breeding range. However, recent research suggests that this process might be significantly more complex. New data indicate that first-time migrants may not have a complete map but rather a system of beacons. This system could be based, for example, on geomagnetic cues or other cues that help first-year birds navigate their location along the migration route. To date, a significant body of evidence has been gathered to revise the classic 'clock and compass' program. It is likely that first-time migrants of many species (although perhaps not all) are capable of varying degrees of location control based on innate information. The question of what data sources they use and how precise their control remains open for further investigation.

KEYWORDS

animal navigation and orientation, bird migration, genetics of behavior, endogenous programs, clock-and-compass concept, vector navigation, innate beacons, innate component magnetic map

Introduction

Billions of birds annually migrate between their breeding and non-breeding areas (Hahn et al., 2009). Most importantly, many of them show site fidelity to their natal and former breeding sites, and to non-breeding areas (Sokolov, 1997). The degree of spatial accuracy varies between species, is difficult to study, and is a subject of ongoing debate, but there is little doubt that most birds return to the areas that are small compared to the range of their migratory movements, and those that do not return and show nomadic behaviour do so for a reason and not because they fail to navigate.

More than 60 years ago, Gustav Kramer suggested the map and compass concept, which initially referred to homing pigeons but is applicable to all animals that move beyond their usual home ranges. According to this concept, to reach a certain goal located beyond the sensory perception range, a traveling animal (e.g., a migrating bird) needs (i) a positioning system (map), i.e., a mental representation of space at the scale it intends to travel, and (ii) a compass system that allows it to select and maintain a certain compass direction of travel (Kramer, 1953). It means that the question 'how migrating animals find their way' actually consists of two closely related but independent questions: What is the physical and sensory basis of the positioning system (map), and what is the physical and sensory basis of the compass system. Both these questions are a subject of active research, and in recent decades, significant progress has been made in both fields, even though important open questions remain (Mouritsen, 2018; Wiltschko and Wiltschko, 2023).

The map and compass concept leaves open the question of how juvenile migrants perform their maiden travel, when they migrate to the areas they have never been before. In some species, social interactions play an important role, with first-time migrants closely watching and following experienced conspecifics, related or unrelated ones (Chernetsov et al., 2004; Mueller et al., 2013; Loonstra et al., 2023; Fugate et al., 2024). However, individuals of many species migrate solitary, often at night, and without much interaction with conspecifics. It has been suggested that such species follow an innate spatio-temporal programme that has been termed a 'clock-and-compass' programme (Gwinner and Wiltschko, 1978) but would be more appropriately called calendar-and-compass programme.

Simplified, a young birds' migration can be represented as a sequence of steps: begin migration at a certain age, head towards α and fly in that direction for d_1 days, then change course to β and maintain it for d_2 days, and so on. After several iterations, juvenile migrants reach their population-specific winter quarters (Figure 1). The change of migratory direction in a certain area is called *Zugknick* (from German, bend of migratory path). An obvious question is whether such a rather rough spatio-temporal programme is sufficient to perform migration to the population-specific wintering area. Weather events may delay migration, e.g., because of a protracted period of opposing winds, or a storm may blow the migrants off course. Obviously, such a programme is insufficient for pinpoint navigation, when migrants successfully reach a goal with linear size several orders of magnitude smaller than the range of migratory journey (several kilometres vs thousands of kilometres). This situation is typical of return migration when migrants get back to the areas where they have bred before or to their natal areas, showing breeding or natal site fidelity, or philopatry (Sokolov, 1981). However, also during first outward migration when first-winter individuals should reach their population-specific non-breeding area, with much more relaxed requirements for navigation accuracy (Cresswell, 2014), it is still not obvious that spatiotemporal programme without compensation for accidental movements off course would be sufficient, when the population-specific area is smaller than e.g., the whole of sub-Saharan Africa (Sokolov et al., 2024).

These considerations triggered hypotheses that assumed some kind of awareness of where migrating birds are currently located during the first migratory journey. These hypotheses received some support from experimental data.

Clock-and-compass concept

The study of the concept of clocks and compass in young migrating birds through their physical displacement from their migration route (Figure 2) is important for understanding the mechanisms of navigation and orientation that these birds use during their long migrations. In this context, the compass is responsible for orientation, meaning the direction of movement relative to external factors such as the Earth's magnetic field, the position of the sun, or the moving stars. The compass helps them understand which direction they need to fly. The question is whether birds following this inherited compass direction realize where they are currently, e.g., when they are displaced from the migratory route, e.g., by a storm or by the experimenter. This question is equivalent to the question whether they have some kind of a map.

Before the concept of clocks and compasses emerged, Rüppell (1944) displaced 507 hooded crows *Corvus cornix* 750 km west during their spring migration. The birds were transported from the Courish Spit on the southeastern Baltic coast to Flensburg in northern Germany, which is located north of their usual wintering sites. Ring recoveries showed that neither young nor adult birds compensated for the displacement. Instead, they settled parallel to the breeding range of the undisturbed individuals. The lack of compensation in hooded crows in this experiment was consistent with the clock-and-compass mechanism.

Subsequently, between 1948 and 1957, Perdeck (1958), Perdeck (1964), Perdeck (1967) conducted similar experiments, capturing 11,247 common starlings *Sturnus vulgaris* in the Netherlands and transporting them to Switzerland by airplane. According to the recoveries of the displaced birds, adult birds were able to correct their migration route and flew to the northwest towards their population-specific winter quarters in northwestern France and southern England, demonstrating their ability for navigation, meaning they used both the compass and the map. At the same time, young birds continued migrating to the southwest and remained for the winter in southern France and Spain, showing only the ability for orientation, that is, the use of the compass but not the map.

Based on these data, A. Perdek was one of the first researchers to suggest that young migrants follow a spatio-temporal program, while adults possess a bicoordinate map that allows them to correct for natural or artificial displacements. How important the studies by Perdeck remain to this day, is clearly illustrated by the recent publication of a re-analysis of his data (Pot et al., 2024). It showed that even though starlings are social and keep in groups outside of their breeding season, Perdeck's results cannot be explained by his displaced birds joining the flocks of local conspecifics and following them.

Similar results were obtained by Kasper Thorup and co-authors in North America while studying the migration of white-crowned sparrows *Zonotrichia leucophrys* (Thorup et al., 2007). The researchers transported the birds from the northwest to the

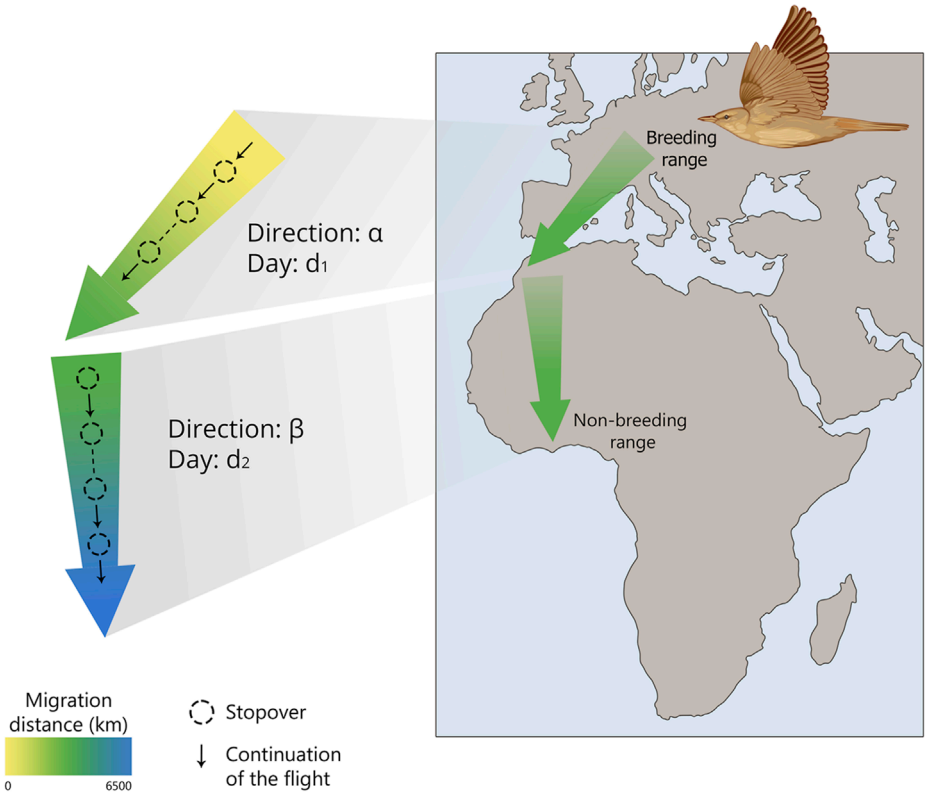

FIGURE 1
Schematic representation of the "Clock and Compass" concept in naïve migratory birds, showing how they navigate from their breeding grounds to their wintering areas using an internal timekeeping mechanism and directional cues.

northeast of the United States (a physical displacement of 3,700 km) and used radio transmitters to track their movements after release. The authors found that birds that had already migrated were able to compensate for the longitude displacement, whereas young birds were did not do so (Figure 3).

Another example of age-related difference in migratory paths is demonstrated by streaked shearwaters *Calonectris leucomelas*. Shearwaters use a wind- and wave-based flight pattern, known as dynamic soaring, to extract energy for highly efficient travel over oceans, and therefore are generally reluctant to fly over land. However, whereas experienced adults circumvented the landmass of Japanese islands during their post-breeding migration towards the southwestern Pacific, juveniles flew across the landmass of Honshu Island, i.e., across most inhospitable terrain, apparently relying on an inherited compass direction (Yoda et al., 2017; Yoda et al., 2021).

The existence of a spatio-temporal program in birds was also confirmed in laboratory tests. Gwinner and Wiltschko (1978) showed that hand-reared garden warblers *Sylvia borin* from Germany followed an innate sequence of orientation behaviors when tested in circular arenas, which corresponds to the flight directions of their free-living counterparts. Garden warblers followed this sequence of predisposed flights in a specific compass direction, with their duration and timing being controlled by endogenous circannual rhythms. As a result, they reach the population-specific winter quarters.

Furthermore, studies show that the spatio-temporal program is inherited and manifested in an intermediate form in first-generation hybrids with respect to both timing (for example, the duration of migration restlessness in blackcaps *Sylvia atricapilla*; Berthold and Querner, 1981; Berthold, 1988) and direction of migration (for example, studies on blackcaps (Figure 4), European robins *Erithacus rubecula*, blackbirds *Turdus merula*, and song sparrows *Melospiza melodia*; Helbig, 1991; Berthold and Helbig, 1992; Berthold et al., 1992). However, willow warblers *Phylloscopus trochilus* from central Sweden where two subspecies migrating towards the southwest and southeast intergrade, do not show an intermediate direction but migrate in either one or the other direction (Sokolovskis et al., 2023). Thus, the initial hypothesis of inherited migration direction was based on data about intermediate migration direction in hybrids, but further research has shown that the situation can be quite different [see a recent review by Caballero-López and Bensch (2024)].

It has been shown that naïve songbirds, tested in Emlen funnels, exhibit innate seasonal spring orientation under laboratory conditions, despite never having undertaken their first migration and having spent the winter in the aviary (Figure 5; Zolotareva et al., 2021; Wynn et al., 2023).

Despite considerable advancements in molecular genetics and the development of research techniques over the past decade, the molecular mechanisms underlying migratory behavior in birds remain largely unexplained. While researchers have made

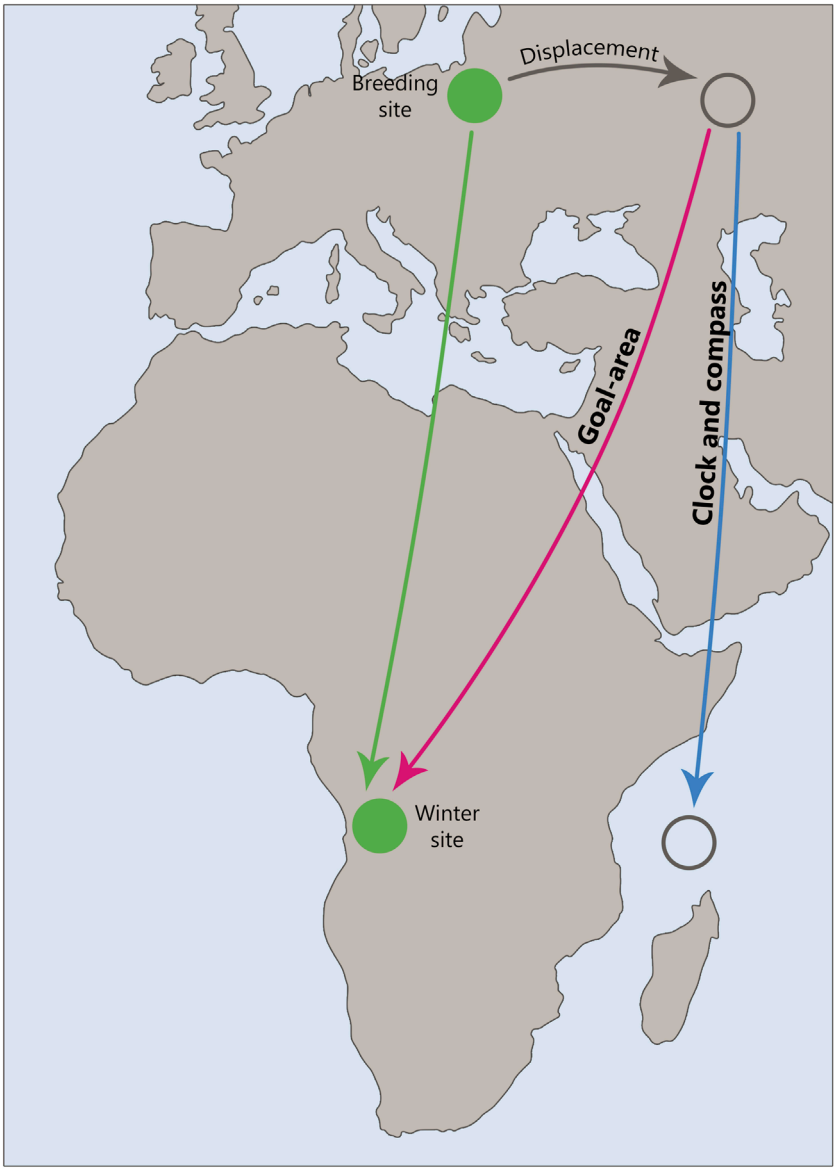

FIGURE 2
Schematic representation of a displacement experiment, illustrating the potential outcomes predicted by the "Clock and Compass" and "Goal-area Navigation" hypotheses. The diagram highlights the differences in navigational strategies and the resulting trajectories or goal areas in response to displacement.

notable strides in identifying genetic markers associated with migration, the specific genes and molecular pathways that regulate the complex processes of orientation, navigation, and migration timing are still not fully understood. Recent studies are beginning to shed light on this issue, revealing the role of specific genes (Bingman and Ewry, 2020; Chernetsov, 2023). One such gene is VPS13A, identified as a key element associated with the selection of wintering regions in songbirds such as the golden-winged warbler *Vermivora chrysoptera* and the blue-winged warbler *V. cyanoptera*. These species, which hybridize in the wild, have different migratory routes: blue-winged warblers winter in northern South America, while golden-winged warblers winter in both Central and South America (Toews et al., 2019). Variations in the VPS13A gene are closely linked to the selection of wintering regions and migratory direction. However, the role of this gene in birds is not yet fully understood, but it is hypothesized that it may influence energy turnover during migration. In addition, studies show that the VPS13A gene plays an important role in adaptation to different wintering conditions, allowing birds to successfully travel long distances and survive in various climatic zones. Although the link between this gene and migration has been established, the molecular mechanisms through which it influences bird behavior remain unclear. This discovery highlights the complexity of the interplay between genetic, physiological, and environmental factors influencing migration and necessitates further investigation.

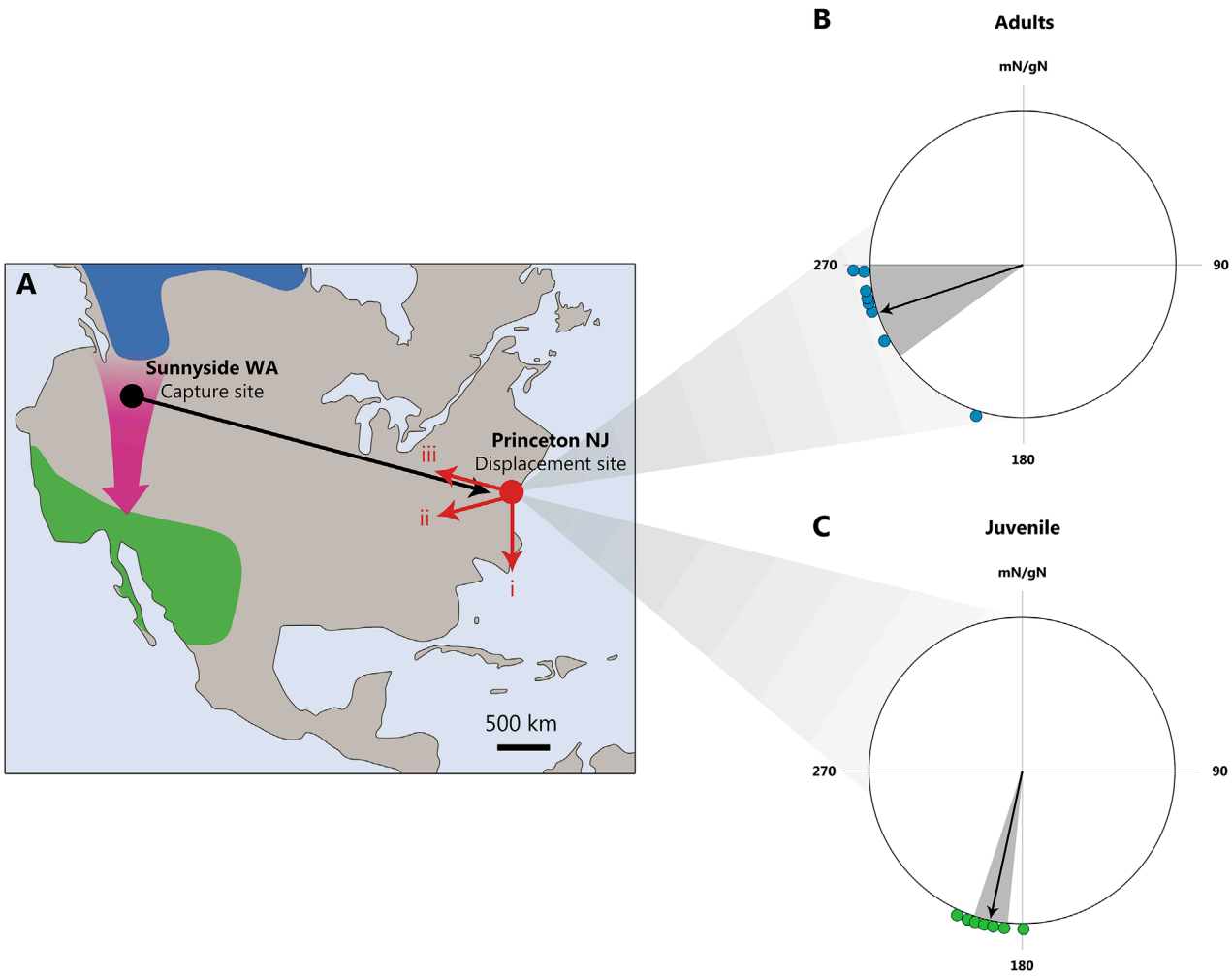

FIGURE 3
The displacement of white-crowned sparrows *Zonotrichia leucophrys* from Sunnyside, WA, to Princeton, NJ. **(A)** Map illustrating possible migration routes after release at Princeton: (1) continuation along the normal migration direction, (2) course correction toward the wintering area, and (3) return to the capture site. The breeding area is shown in blue, the wintering area in green, and the normal migration route with a purple arrow. **(B, C)**: Radio tracking data collected from small aircraft reveal that only adult, and not juvenile, long-distance migrating white-crowned sparrows were able to rapidly recognize and correct for a continent-wide displacement of 3,700 km. For both groups, only positions >25 km from the release site are included in the analysis. **(B)** Directions from the release site to the last observed positions for adults (blue). The mean direction = 252° ± 18°, r = 0.931 (Z = 6.94, N = 8, P < 0.001, Rayleigh test). One adult exhibited a southerly orientation, likely due to initial drift in strong northwesterly winds. **(C)** Directions from the release site to the last observed positions for juveniles (red). The mean direction = 192° ± 6°, r = 0.99 (Z = 8.82, N = 9, P < 0.001, Rayleigh test). Mean directions (black arrows) and 95% confidence intervals (gray area) are shown for adults and juveniles, respectively. mN/gN, magnetic North/geographical North. This figure is based on the results of Thorup et al. (2007).

A recent study conducted by Sokolovskis et al. (2023) revealed the genetic basis of autumn migration direction in willow warblers *P. trochilus*, marking a significant breakthrough in the study of orientation and navigation. In Scandinavia, two willow warbler subspecies breed: *P. trochilus* from southern Scandinavia and the Baltic coast, which winter in western tropical Africa and migrate towards the southwest, and *P. t. acredula*, nesting in northern Scandinavia and migrating south-southeast to winter in eastern Africa. These subspecies differ in size, plumage coloration, and genetic markers (Zhao et al., 2020; Caballero-López et al., 2022).

Intrigued by this phenomenon, researchers discovered that the direction of migration in these birds is primarily determined by a combination of two genes: MARB-a and InvP-Ch1, with MARB-a suppressing the effect of InvP-Ch1 through epistatic mechanisms. This discovery is particularly important because it has shown that the migratory behavior of hybrids in the geographical regions where these subspecies overlap is inherited in such a way that their migration direction aligns with the parental populations' migration patterns (Figure 6; Sokolovskis et al., 2023).

These findings have supported the hypothesis that the direction of bird migration can be inherited through complex polygenic mechanisms, suggesting that the spatio-temporal migration program can indeed be transmitted from generation to generation. However, the data also indicate that the mechanisms of inheriting migratory behavior may be species-specific. In some cases, hybrids inherit the migratory routes characteristic of their parental

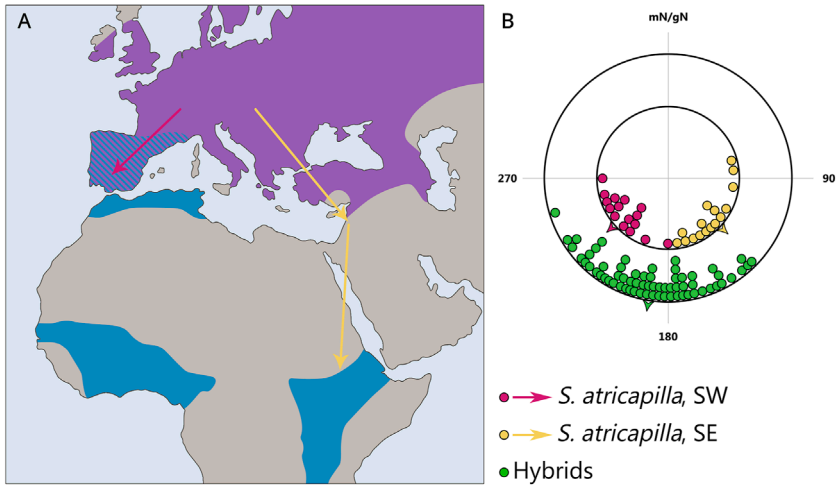

FIGURE 4
Inheritance of migratory direction in blackcaps *Sylvia atricapilla*: directional choices of hand-raised birds from SE- and SW-migrating populations during early autumn migration. **(A)** Map illustrating the breeding (violet) and primary overwintering (blue) areas of the blackcap. Arrows indicate the general autumn migration routes of the central European populations: southwest (yellow) and southeast (purple). **(B)** Directional choices of hand-raised blackcaps during the early and late parts of the autumn migration season. The inner circle represents the parental generation; purple dots indicate birds from the west Germany, and yellow dots represent birds from eastern Austria. The outer circle (green dots) shows the F1 generation. Arrowheads indicate the group mean migration directions. mN/gN, magnetic North/geographical North. This figure is based on the results of Helbig, (1991).

populations, while in others, they choose an intermediate direction, highlighting the diversity of genetic mechanisms underlying such behavior.

Criticism of the clock-and-compass concept

At the moment, the 'clock-and-compass' concept is more or less the accepted mainstream of how migration proceeds in naïve migrants (Able and Bingman, 1987; Berthold, 1996; Åkesson and Helm, 2020). Avian migrants that strongly rely on social interactions may differ in this respect (Chernetsov et al., 2004; Mueller et al., 2013; Loonstra et al., 2023; Sokolovskis et al., 2024), but species whose migratory behavior does not strongly depend on social learning mechanisms are believed to follow a spatiotemporal program or clock-and-compass approach.

However, as often happens, after a mainstream view settles in, some ugly facts start to emerge that do not exactly fit in the pattern. In contrast to the "clock-and-compass" model, which explains bird orientation through the use of internal biological clocks and compass mechanisms, the concept of "navigation by goal area" suggests that migratory routes are determined by genetically encoded information about the geographic coordinates of destinations or stopover sites. This idea places inherited spatial targeting, rather than orientation based on directions or temporal parameters, at the core of migratory behavior, allowing birds to reach specific points regardless of their starting location. Rabøl (1978) analyzed recoveries of three passerine species in Europe and proposed the hypothesis that it is the geographic coordinates of wintering or stopover sites that are inherited. This approach challenges the traditional paradigm and highlights the need to reconsider established views on the nature of migration.

Further experiments conducted by Jørgen Rabøl over several decades demonstrated that young birds possess the ability to detect deviations from their route and, under certain conditions, adjust their course. These studies, based on artificial displacement of various bird species from their natural migratory paths, led to significant discoveries. Rabøl showed that migratory mechanisms include complex components that cannot be fully explained solely by the "clock-and-compass" model (Rabøl, 1969; Rabøl, 1970; Rabøl, 1972; Rabøl, 1975; Rabøl, 1981; Rabøl, 1985; Rabøl, 1993; Rabøl, 1994; Rabøl, 1995). He also argued that the results of Perdeck's classic experiment conducted on a short-distance migrant (the starling) cannot be entirely extrapolated to long-distance migrants with more complex routes. Moreover, this author claimed that the results by Gwinner and Wiltschko (1978) may be interpreted differently (Rabøl, 1985). Data published several years after the original study, regarding migration routes in the Gibraltar area (Hilgerloh, 1989) and West Africa (Gatter, 1987a; Gatter, 1987b), suggest that the course change for most Palaearctic migrants occurs differently than what E. Gwinner and W. Wiltschko proposed for garden warblers. Apparently, the change in direction from a southwest to a southeast-east course does not occur after crossing the desert belt, but much later, along the northern coast of the Gulf of Guinea.

Studies have shown that migratory restlessness, typical of birds during the preparation for long flights, can be suppressed under experimental conditions. This is achieved by providing birds with unlimited food after a fasting period simulating the depletion of energy reserves during flight (Biebach, 1985; Gwinner et al., 1985; Gwinner et al., 1988). This scenario mimics natural conditions where birds reach suitable stopover sites, such as desert oases, to replenish their fat reserves. Notably, migratory restlessness disappears long before the birds achieve high fat levels and body mass. This suggests that the process of replenishing energy resources itself may serve as a

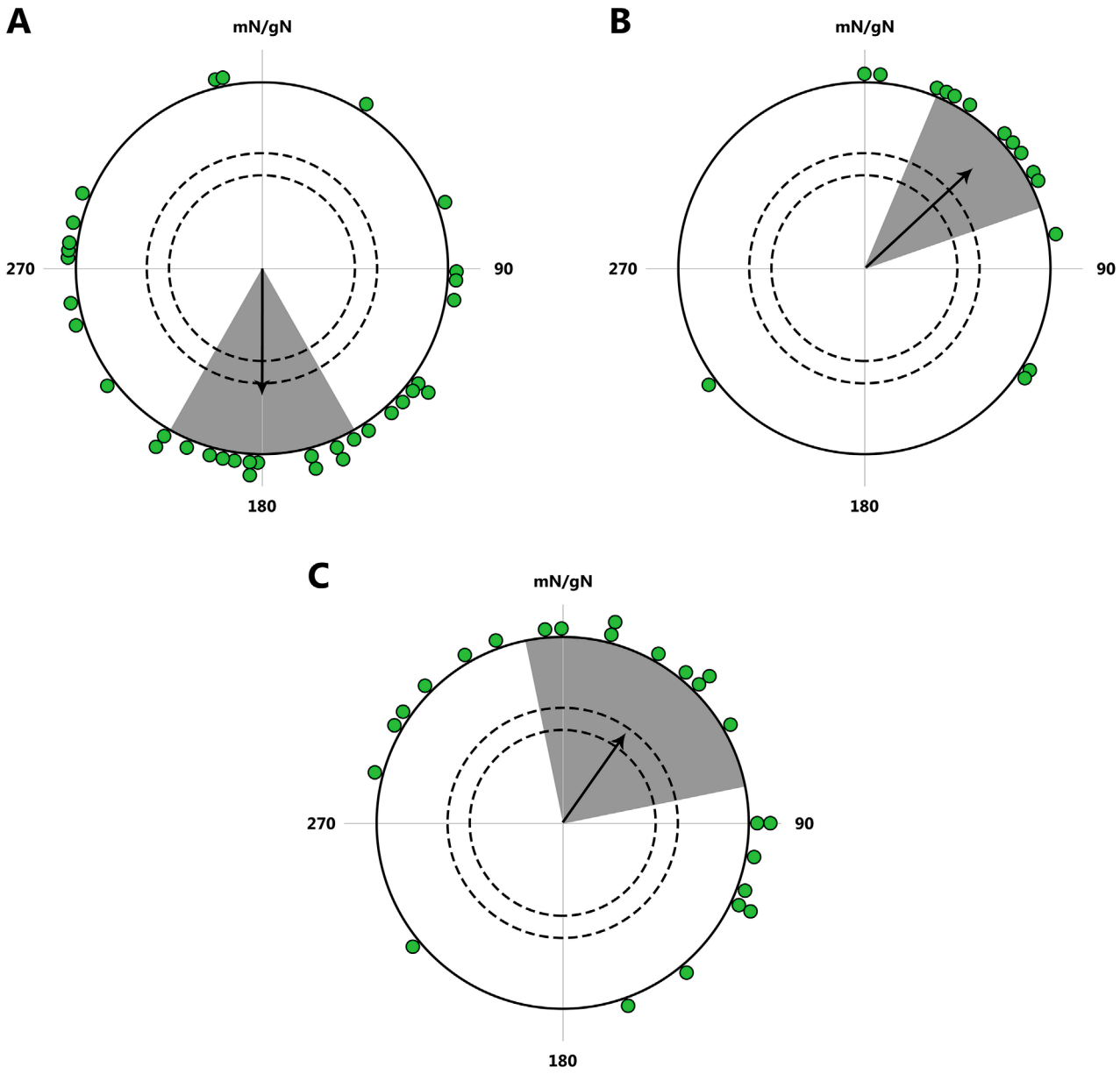

FIGURE 5
Orientation of naïve birds in Emlen funnels. **(A, B)**: Results obtained from juvenile pied flycatchers *Ficedula hypoleuca*. **(A)** Birds from 3 days of age were kept indoors without access to natural celestial cues, hand-fed, and tested in Emlen funnels in the fall, in a natural magnetic field and without access to stars. N = 35, mean direction 178° (r = 0.42, P = 0.002), 95% confidence interval (CI): 148°–209°. **(B)** Birds were kept indoors all winter without access to natural celestial cues prior to spring experiments were tested in Emlen funnels in the spring, in a natural magnetic field and without access to stars. N = 16, mean direction 47° (r = 0.70, P≪0.001), 95% CI: 23°–70°. **(C)** Results from juvenile Eurasian blackcaps *Sylvia atricapilla*. Birds were tested in Emlen funnels in the spring. N = 24, mean direction 35.4° (r = 0.395, P = 0.022), 95% CI: 352°–80.4°. The dots at the periphery of the circle represent the mean heading of a single bird, the arrow represents the group orientation mean vector (circle radius represents a vector length r = 1); the gray areas indicate the 95% CI; the inner and outer dashed circles indicate the required length of r for significance levels of 5% and 1% according to the Rayleigh test, respectively. mN/gN, magnetic North/geographical North. This figure is based on the results of Zolotareva et al., (2021); Wynn et al., (2023).

signal for the temporary cessation of migratory behavior. Even when the total duration of such interruptions accounts for a significant proportion (25%–30%) of the autumn migration season, this does not lead to a proportional extension of the migration period. The migration season is not prolonged by the time spent at stopovers, despite the considerable time investment (Gwinner et al., 1992; Bairlein and Gwinner, 1994; Gwinner, 1996). If a similar situation occurs under natural conditions, and the duration of migration is indeed determined solely by an innate spatiotemporal program, some individuals may complete their migration prematurely, for instance, ending up in the middle of the Sahara. The consequences would most likely have been fatal.

Numerous studies on the impact of weather conditions on migration have confirmed that factors such as wind strength and

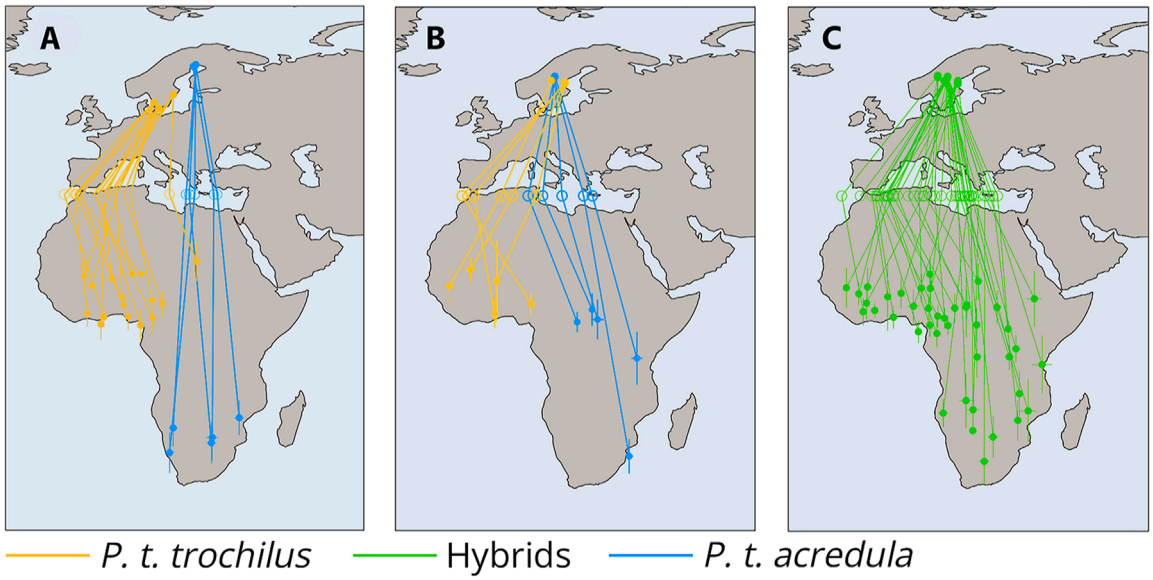

FIGURE 6
Migration routes and genetic differentiation of *P. t. acredula*, *P. t. trochilus* and hybrids across the Mediterranean Divid. **(A)** Tracks of allopatric *acredula* (N = 5) in blue and *trochilus* (N = 16) in orange. **(B)** Tracks of genetically defined acredula in blue (birds with the MARB-a allele and homozygous for *acredula* alleles on invP-Ch1 and invP-Ch5, N = 5) and genetically defined *trochilus* in orange (birds lacking the MARB-a allele and homozygous for *trochilus* alleles on invP-Ch1 and invP-Ch5, N = 5). **(C)** Tracks of birds from the migratory divide with hybrid genotypes (N = 41). Hollow circles in **(A–C)** indicate estimated longitudes where birds crossed latitude 35°N (Mediterranean Sea). The lines connect individuals to their respective breeding sites, Mediterranean crossing points, and primary wintering sites. Whiskers around locations in Africa in **(A–C)** represent standard deviations in longitude and latitude from the main winter site. This figure is based on the results of Sokolovskis et al., (2023).

direction significantly influence the migratory behavior of birds (Alerstam, 1978; Richardson, 1978; Richardson, 1990; Alerstam and Lindström, 1990; Åkesson, 1993a). In particular, unfavorable wind conditions can substantially increase energy expenditure and cause birds to deviate from their course. If young individuals during their first migration are unable to adjust their position and rely solely on innate directional knowledge and a temporal program, they risk failing to compensate for deviations and perishing.

Some published data suggest that at least in certain migratory bird species, young individuals undertaking their first migration possess if not a detailed navigational map, but at least a system of beacons enabling them to determine their position along the migration route at any given moment (Fransson et al., 2001; Thorup and Rabøl, 2007; Gschweng et al., 2008; Thorup et al., 2011; 2020). Very impressive in this respect are the circumpolar movements of juvenile Northern giant petrels *Macronectes halli* that are difficult to explain without assuming some kind of innate map (de Grissac et al., 2016).

Young individuals of some bird species indeed possess innate orientation abilities and elements of a navigational map. First-autumn Eleonora's falcons *Falco eleonorae*, which migrate separately from adult birds, demonstrate rather complex species-specific migration routes. Their trajectories also exhibit individual characteristics, indicating a combination of innate mechanisms and environmental adaptations (Gschweng et al., 2008). The persistence with which juvenile falcons try to cross the Mozambique Channel and reach their species-specific winter quarters in Madagascar suggests that they have some innate knowledge of a landmass behind the water that they should reach.

Young common cuckoos *Cuculus canorus* also demonstrate the ability to compensate for deviations from their migration route. In a recent study common cuckoos were displaced 1800 km east from their original location on the Baltic coast to Kazan (Tatarstan, Russia; Thorup et al., 2020). The results suggested that young cuckoos were able to return to their species-specific migration route after such a displacement (Figure 7). The findings of this study are particularly interesting because it was previously believed that such corrective reactions were characteristic only of experienced birds. It suggests that their migratory behavior is based not only on an innate temporal program but also on genetically programmed spatial landmarks that ensure high accuracy in reaching necessary destinations, even with significant deviations.

Thorup and co-authors showed that young common whitethroats *Curruca communis*, garden warblers, and willow warblers are capable of compensating for shifts in their autumn migration route by more than 1,000 km (Figure 8). This was confirmed both under experimental conditions and through observations of birds that experienced natural displacement due to winds from Scandinavia to Faroe Islands (Thorup et al., 2011).

Thus, in our view, the concept of 'clock and compass' in young migrants requires further clarification. It is possible that what is involved is not a detailed map, but a system of beacons based on geomagnetic or other information, which allows first-year migrants to control their position along the migration route, at least to some extent.

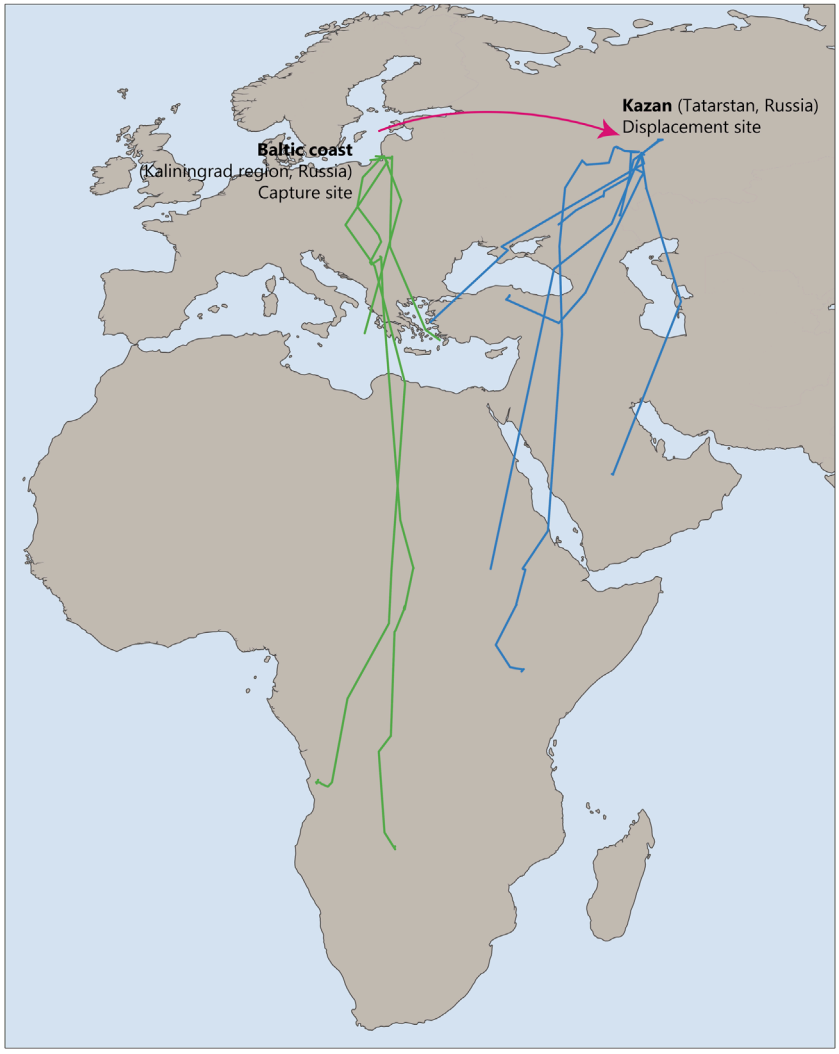

FIGURE 7
Tracks of control naïve common cuckoos migrating through Baltic coast, Kaliningrad region, Russia, during autumn (green) and experimental birds displaced to Kazan, Russia (blue). This figure is based on the results of Thorup et al., (2020).

Experiments suggesting the role of magnetic conditions

One of the first dataset that suggested that some first-time migrants need additional non-social information for successful autumn migration and cannot complete it in the basis of innate spatiotemporal program alone came from a study in pied flycatchers *Ficedula hypoleuca* (Beck and Wiltschko, 1988). An earlier study by Gwinner and Wiltschko (1978) demonstrated that garden warblers followed an inborne sequence of directions in captivity without any external stimuli that would suggest that they actually move along their migratory path. However, pied flycatchers studied by Beck and Wiltschko (1988) needed to experience the characteristics of the magnetic field encountered *en route*, in southern Iberian Peninsula and in northern Africa, to display the seasonally appropriate orientation in round arenas. The experiments in garden warblers and pied flycatchers were performed by the members of the same research group, which strengthened the belief that their different outcomes were due to the genuine between-species variation in migratory program, and not to methodological issues.

Another very influential study was published more than a decade later and involved thrush nightingales *Luscinia luscinia* (Fransson et al., 2001; Figures 9A, B). The authors showed that first-time migrants exposed to the magnetic field of northern Egypt, i.e., in front of the major ecological barrier (the Sahara desert), gained significantly more fuel than birds maintained in the magnetic conditions of their capture site (central Sweden). Apparently, thrush nightingales preparing to cross a major barrier need more fuel because refueling opportunities in the desert were extremely limited to non-existent (Biebach, 1990). First-time migrants did not have any prior experience of the magnetic conditions typical of the northern edge of the barrier and could only rely on some innate knowledge when to start serious fueling. Being fat is not without costs for birds, because fatter (i.e., heavier) individuals have less maneuverable flight and are less able to avoid predation (Kullberg et al., 2003; 2007). Even if we keep in mind that the effects

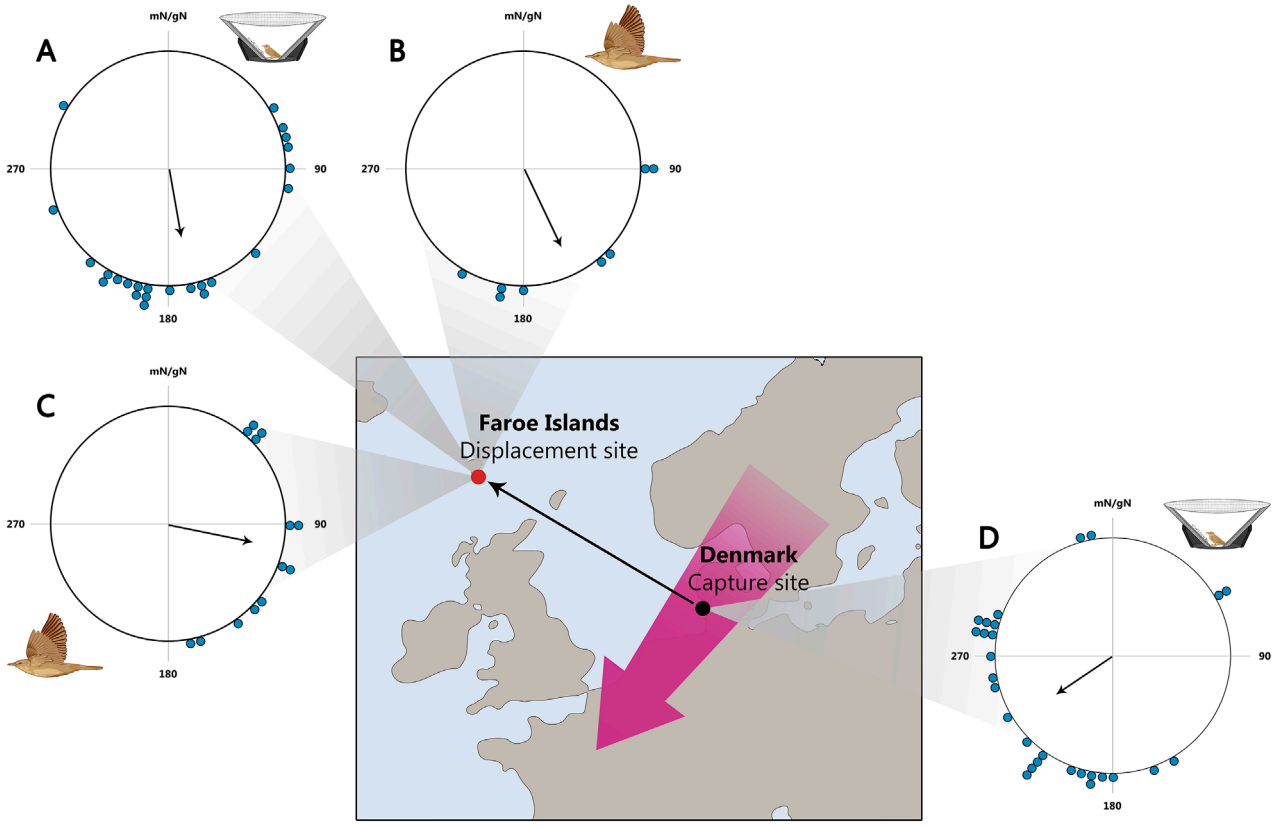

FIGURE 8
Orientation of naïve birds displaced to the Faroe Islands. **(A–C)**: Orientation on the Faroe Islands. **(A)** Tested in Emlen funnels of birds displaced from Denmark to the Faroe Islands. **(B)** Vanishing bearings of birds caught on the Faroe Islands. **(C)**: Vanishing bearings of birds translocated from Denmark to the Faroe Islands. **(D)** Orientation in Emlen funnels of birds caught and tested in Denmark. Map of Northwest Europe showing the location of the Faroe Islands (red dot) and the main migration through Northwest Europe (purple arrow). The 1,100 km displacement from Denmark (black dot) to The Faroes is shown by the thin arrow. In circular diagrams, the orientation of individual birds is marked on the periphery of the circle and the mean sample orientation is shown as a black arrow starting in the circle centre and with its length relative to the radius corresponding to the length of the mean vector r. mN/gN, magnetic North/geographical North. All sample orientations differ significant from random according to the Rayleigh test ($P < 0.05$). This figure is based on the results of Thorup et al., (2011).

of extra fat only start to show when fuel load exceeds ca. 30% of lean mass (Chernetsov, 2012), they are still significant for long-distance flights necessary to cross ecological barriers like the Sahara, the Gulf of Mexico or Central Asian deserts (Bairlein, 1985; Biebach, 1990; Dolnik, 1990; Smolinsky et al., 2013).

Most interestingly, a similar study in northern wheatears *Oenanthe oenanthe* found the opposite effect of simulated magnetic conditions *en route* on fattening (Bulte et al., 2017; Figures 9A, C). Northern wheatears kept in the magnetic conditions that simulated their movement from northern Europe across southwestern Europe to western Africa gained significantly less fuel (not more, as thrush nightingales did) and showed much less nocturnal restlessness than their conspecifics maintained in the magnetic conditions of northwestern Germany. The authors interpreted their results in the sense that wheatears that 'remained' in northwestern Germany realized that their perceived position did not fit the position they should occupy in the given season (they were lagging behind their innate temporal schedule) and therefore fueled more and showed more restlessness (were 'flying' more) than birds under 'normal' conditions (the ones that 'moved' as expected).

However, the Fransson et al. (2001) study was replicated. The same research group conducted a similar experiment with the design that included two trials, with 8 birds each (Kullberg et al., 2003). In the early trial (around August 5 ± 2 days) and the late trial (around August 19 ± 2 days) young thrush nightingales captured during the early stage of autumn migration in southeastern Sweden and subjected to magnetic treatment simulating their movement to northern Egypt, accumulated more fuel than birds in the control group. However, in the late trial, regardless of magnetic treatment, the birds had greater fuel reserves, and no difference was observed between the control and experimental groups, unlike in the early trial. The authors suggested that the significance of endogenous and ecological factors for individual birds varies depending on the season and geographical location. As birds approach natural barriers, ecological signals may outweigh the endogenous temporal program and act independently. In the end of the season, being under stricter time constraints, the birds always increase their fuel reserves, which neutralizes the effect of magnetic treatment.

Another study providing evidence for the existence of innate reference points along birds' migration routes was conducted by

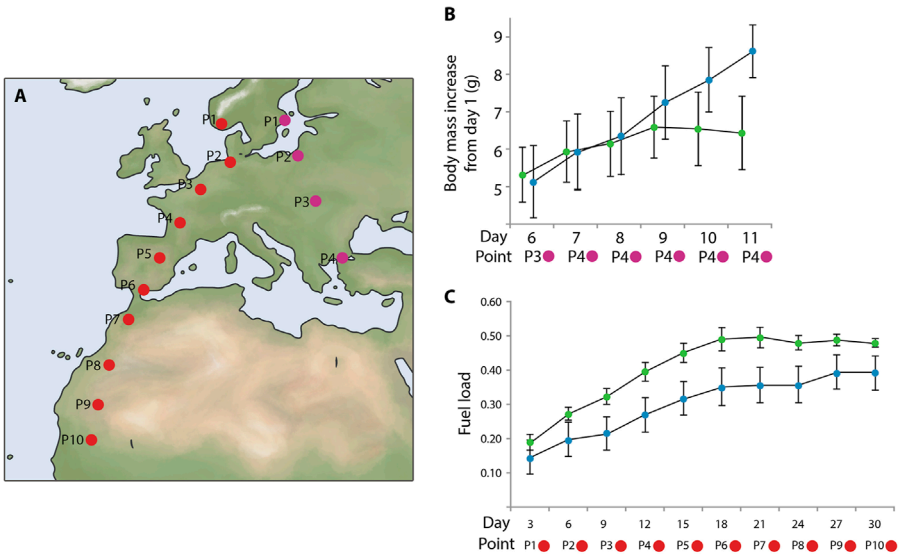

FIGURE 9
Effect of magnetic-field simulation on migratory refuelling in naïve birds. **(A)** Map showing the geographical locations of the dots used for magnetic simulations for the experimental groups: purple dots–thrush nightingales *Luscinia luscinia*; red dots–northern wheatears *Oenanthe oenanthe*. **(B)** Experimental data from thrush nightingales. Average body mass increase during the experiment: the magnetic field experienced by experimental birds was altered to simulate the conditions of four localities throughout the experiment. Experimental birds were kept in the magnetic field of northern Egypt from day 7 until the end of the experiment on day 11, when all birds were released back into the wild. Green dots: birds consistently exposed to the magnetic field of Sweden. Blue dots: experimental birds exposed to a magnetic field simulating progress along the migratory route. The x-axis represents the days, and the y-axis shows the average body mass increase (g). Error bars represent the standard error. Data for days prior to day 6 are not provided by the authors. **(C)** Experimental data from northern wheatears. Average fuel load, defined as: (body mass - lean body mass)/lean body mass) per 3-day period. Green dots: birds consistently exposed to the magnetic field of northern Germany. Blue dots: experimental birds exposed to a magnetic field simulating progress along the migratory route. The x-axis shows the 3-day periods, and the y-axis shows the average change in fuel load per 3-day period. Error bars represent the standard error. On both graphs, the x-axis shows the days when measurements were taken, as well as the specific points where the experimental birds were located at different times. These points correspond to real geographical areas along the migration route, where the birds might encounter certain magnetic field conditions, such as changes in intensity or direction. For each of these points, similar magnetic field conditions were virtually simulated during the experiment. The points located below the graphs represent these locations on the map, clearly linking the results to actual geographical locations and helping to visualize how the data relates to the birds' true migration route. This figure is based on the results of Fransson et al., (2001); Bulte et al., (2017).

Wiltschko and Wiltschko (1992). The study suggests that birds do not perceive the polarity of the magnetic field (the direction of the field vector), but rather the inclination (the angle between the field lines and the horizontal plane). In this context, particular interest lies in bird species that cross the magnetic equator during migration, where the magnetic field lines run parallel to the Earth's surface at the magnetic equator, creating an angle of 0° (horizontal magnetic field). In such a situation, distinguishing between the directions 'toward the equator' and 'toward the pole' becomes impossible (Schwarze et al., 2016). When one such species, the garden warbler, was subjected to laboratory conditions simulating the crossing of the magnetic equator during their autumn migration, 2 days of exposure to a horizontal magnetic field caused a change in their direction from 'towards the equator' to 'towards the pole', acting as a trigger for significant changes in their migratory behavior (Figure 10). However, a recent experiment with marsh warblers *Acrocephalus palustris* and spotted flycatchers *Muscicapa striata* (Utvenko et al., 2025) did not reveal a shift in orientation direction after exposure to a horizontal magnetic field, suggesting species-specific variation in response to this stimulus.

Robert Beason's research on bobolinks *Dolichonyx oryzivorus* that breed in central North America and winter in central and western South America, yields valuable data. In his experiments, the birds were tested in a planetarium, where a static star map was shown to them. During the trials, the birds were exposed to a series of alternating artificial magnetic fields that simulated the natural magnetic conditions of the migration route across the equator into the Southern Hemisphere. Despite this, the bobolinks continued to orient southward throughout the experiment. This suggests that the horizontal magnetic field at the equator, possibly in combination with stellar signals, helped them switch from 'towards the equator' to 'towards the pole' orientation during migration (Beason, 1987; Beason, 1989; Beason, 1992). However, the design of the experiment does not allow for a definitive determination of whether the birds used the magnetic field for orientation. It is possible that they ignored the magnetic field and relied on the star compass they had developed, orienting by the stars displayed in the planetarium.

Despite the significant body of research on the ability of songbirds to perceive the magnetic field (Wynn and Liedvogel, 2023), our understanding of when, where, and how young migrating birds first use magnetic signals to make decisions about migration and orientation in the natural environment remains incomplete. The data obtained from experiments are fragmentary, collected across different bird species, and often not independently verified by research groups other than the authors of the original studies. Independent replication of these experiments in other

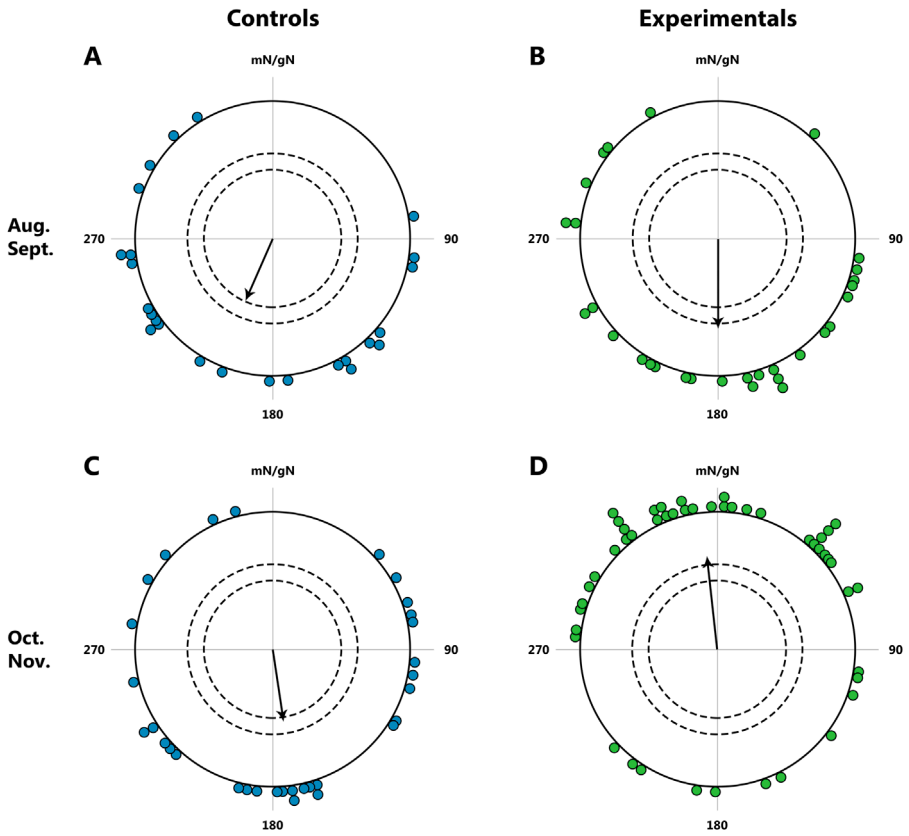

FIGURE 10
Orientation of garden warblers *Sylvia borin* during autumn migration; tests in the natural geomagnetic field. **(A, B)**: Tests in August and September. Controls (blue dot): N = 25, mean direction 204°, r = 0.43; Experimentals (green dot): N = 30, mean direction 180°, r = 0.44. **(C, D)**: Tests in October and November; beginning on October 1, the experimental birds were exposed to a horizontal magnetic field for 2 days. Controls (blue dot): N = 32, mean direction 169°, r = 0.33; Experimentals (green dot): N = 50, mean direction 353°, r = 0.40. The dots at the periphery of the circle represent the mean heading of a single bird, the arrow represents the group orientation mean vector (circle radius represents a vector length r = 1); the inner and outer dashed circles indicate the required length of r for significance levels of 5% and 1% according to the Rayleigh test, respectively. mN/gN, magnetic North/geographical North. This figure is based on the results of Wiltschko and Wiltschko, (1992).

trans-equatorial migrant species could significantly strengthen the empirical foundation of the research. Furthermore, such studies could shed light on the question of whether there is an innate mechanism that helps young birds in their first year of life to know their position on the migration route.

The role of photoperiod during the first migration

One of the key factors regulating migration is the photoperiod, which acts as a synchronizer of circannual rhythms and significantly influences the timing of migration (Berthold, 1996; Gwinner, 1996). For example, birds that hatch later in the breeding season and are exposed to shorter day lengths show an accelerated completion of molt and begin migration at an earlier age (Berthold, 1988; Gwinner, 1986; Gwinner, 1989). In contrast, the lengthening days stimulate earlier spring migration and winter molt (Farner and Gwinner, 1980; Gwinner, 1996; Dawson et al., 2001; Rani et al., 2005).

In experiments with long-tailed tits *Aegithalos caudatus*, short daylength stimulated increased locomotor activity, which in the wild would allow the birds to leave northern areas more quickly in the case of delays (Bojarinova and Babushkina, 2015). Studies of closely related chats from three regions, namely, African stonechats *Saxicola axillaris* from East Africa, European stonechats *S. rubicola* from Central Europe, and Siberian stonechats *S. maura* from Siberia raised under naturally varying day lengths, yielded similar results (Helm et al., 2005). Chicks reared under shorter photoperiods, simulating late hatching in late summer, compensated by undergoing accelerated postjuvenile development in ways specific to their populations. Late-hatched individuals from all populations were able largely to catch up with those that hatched earlier, advancing their autumn migratory restlessness (*Zugunruhe*) by 0.9 days for each additional day of later hatching. This genetically programmed compensatory mechanism, supported by field observations of wild individuals, enabled the stonechats to achieve a high degree of synchrony within the population, counteracting the effects of delayed hatching. Similar advancement in migratory restlessness for later-hatched chicks was also observed in birds breeding at low latitudes, such as yellow-green vireos *Vireo flavoviridis* (Styrsky et al., 2004).

Ring recovery analyses in both long- and short-distance migrants have shown that migration speed tends to increase later in the season, with birds migrating later in the season traveling faster than those that depart earlier (Ellegren, 1993; Fransson, 1995; Bensch and Nielsen, 1999; Bojarinova et al., 2008; Bojarinova and Babushkina, 2010; Babushkina and Bojarinova, 2011).

The role of stars during the first migration

Despite the fact that the star compass is not innate (Emlen, 1967a; Emlen, 1967b), the role of stars in the first migration of birds has been confirmed by a series of experiments conducted under cloudy conditions and with visible starry skies. These experiments indicate the ability of birds to detect and respond to positional changes (compensating for displacement). For instance, in circular arena experiments under the starry sky, birds adjusted for positional shifts, whereas in cloudy weather, their orientation remained unchanged or even reversed (Thorup and Rabøl, 2007). This suggests the possible involvement of stars in detecting positional changes. The role of celestial cues is further emphasized by research conducted under planetarium skies (Beason, 1992).

It is also possible that young birds use stars as beacons during migrations. They could learn and adapt their star compass to specific migration conditions, which could affect their ability to re-route and navigate new geographic environments. Experimental results indicate that the star compass can develop in spring, even after the first migration (Zolotareva et al., 2021). This suggests that the sensitive period for learning it does not end at a specific age. However, the question remains: how flexible is this learning process, and can it continue during migration itself? Can birds re-learn their star compass during migration in response to new conditions?

If so, during migration, birds might observe the starry sky during stopovers for refueling along their route. For example, marsh warblers spend a considerable period in Kenya (Åkesson, 1993b), where they might hypothetically study new for them equatorial star patterns that help them migrate across the magnetic equator. Forming a fully operational star compass may require 2–3 weeks (Michalik et al., 2014; Zolotareva et al., 2021). This highlights the birds' remarkable ability to quickly learn and adapt to new conditions. The formation and calibration of the star compass are particularly crucial for crossing the magnetic equator, where the inclination magnetic compass malfunctions and becomes ambiguous. The star compass knowledge acquired during a stopover in Kenya enables birds to adapt to changing conditions and confidently continue their migration, guided by celestial cues. This plays a decisive role in the successful completion of their journey.

Conclusion

The data described above suggest that, in addition to a clock (or calendar) and a compass, inexperienced migrants may possess an innate understanding of the magnetic and/or photoperiodic conditions they are expected to encounter during the typical "on-schedule" passage of their autumn migration route. This innate knowledge may enable them to adjust their migratory behavior in the event of deviations from this schedule. Furthermore, birds may recognize changing conditions during migration, learn from them, and use additional information to adjust their migration routes.

We suggest that the data currently available warrant a revision of the clock and compass concept. It seems that young individuals of many migratory species are aware of their position along the migration route with varying degrees of accuracy. Below, we present our speculations on how young birds undertaking their first autumn migration from the Northern Hemisphere to the Southern Hemisphere might employ a variety of navigation mechanisms, which change depending on the stage of their journey.

At the initial stage, when leaving their birthplace, birds rely on cues learned during natal dispersal. These cues may include odors remembered from their native area (Gagliardo, 2013) and visual features of the landscape, such as characteristic contours of the terrain or water bodies.

The innate magnetic compass and the star compass, if learned and established, allow birds to choose the general direction of migration. As birds move further away from their native territory, they begin to use additional mechanisms. Among these, genetically encoded navigation beacons related to Earth's magnetic field parameters may play a significant role. Changes in magnetic inclination or intensity before major ecological barriers can serve as landmarks, helping birds refine their path (Fransson et al., 2001; Bulte et al., 2017). Additionally, some species may have an innate ability to reorient upon encountering the horizontal magnetic field of the equator, where the magnetic field lines become nearly parallel to Earth's surface (Wiltschko and Wiltschko, 1992).

It is interesting to hypothesize that birds engaged in trans-equatorial migration, upon stopping near the equator, are able to retrain their star compass, adapting it to the stellar patterns of the Southern Hemisphere. This could allow them to continue their journey through the magnetic equator where the magnetic compass becomes ineffective (Schwarze et al., 2016). However, this hypothesis requires further research, as there is currently insufficient evidence to confirm that birds can adapt their star compass in response to hemisphere shifts.

In the final phase of migration, as birds approach their wintering grounds, they begin to rely again on innate landmarks. Genetic patterns may guide them to specific habitats suitable for wintering. Throughout migration, birds can track the number of days spent in particular areas, enabling them to align their movement with their internal biological clocks and adjust their speed based on their current location. This ability, known as the "clock and compass" concept, complements their suite of navigation strategies, ensuring a successful completion of their first journey. Such a complex set of mechanisms allows young birds to cover vast distances and reach the Southern Hemisphere despite their lack of experience.

Further research should focus on the sources of information they rely on and the precision of this control.

Author contributions

NC: Conceptualization, Funding acquisition, Supervision, Writing – original draft, Writing – review and editing. GU: Visualization, Writing – original draft, Writing – review and editing.

Funding

The author(s) declare that financial support was received for the research and/or publication of this article. Financial support for this study was made available by the Russian Science Foundation (grant No. 24-14-00085 to NC).

Acknowledgments

The authors are most grateful to Kasper Thorup and Kristaps Sokolovskis who kindly provided vector files with their data. It helped us a lot to draw figures illustrating their important findings.

Conflict of interest

The authors declare that the research was conducted in the absence of any commercial or financial relationships that could be construed as a potential conflict of interest.

The author(s) declared that they were an editorial board member of Frontiers, at the time of submission. This had no impact on the peer review process and the final decision.

Generative AI statement

The author(s) declare that no Generative AI was used in the creation of this manuscript.

Publisher's note

References

Able, K. P., and Bingman, V. P. (1987). The development of orientation and navigation behavior in birds. *Q. Rev. Biol.* 62, 1–29. doi:10.1086/415265

Åkesson, S. (1993a). Coastal migration and wind drift compensation in nocturnal passerine migrants. *Ornis Scand.* 24, 87–94. doi:10.2307/3676357

Åkesson, S. (1993b). Effect of geomagnetic field on orientation of the marsh warbler, *Acrocephalus palustris*, in Sweden and Kenya. *Anim. Behav.* 46, 1157–1167. doi:10.1006/anbe.1993.1305

Åkesson, S., and Helm, B. (2020). Endogenous programs and flexibility in bird migration. *Front. Ecol. Evol.* 8, 78. doi:10.3389/fevo.2020.00078

Alerstam, T. (1978). Analysis and a theory of visible bird migration. *Oikos* 30, 273–349. doi:10.2307/3543483

Alerstam, T., and Lindström, Å. (1990). "Optimal bird migration: the relative importance of time, energy, and safety," in *Bird migration*. Editor E. Gwinner (Berlin: Springer), 331–351. doi:10.1007/978-3-642-74542-3_22

Babushkina, O., and Bojarinova, J. (2011). Photoperiodically regulated cycle of locomotory activity and fat reserves during migration seasons in the irruptive bird species, the long-tailed tit *Aegithalos c. caudatus*. *J. Avian Biol.* 42, 169–177. doi:10.1111/j.1600-048X.2010.05149.x

Bairlein, F. (1985). Body weights and fat deposition of Palaearctic passerine migrants in the central Sahara. *Oecologia* 66, 141–146. doi:10.1007/BF00378566

Bairlein, F., and Gwinner, E. (1994). Nutritional mechanisms and temporal control of migratory energy accumulation in birds. *Annu. Rev. Nutr.* 14, 187–215. doi:10.1146/annurev.nu.14.070194.001155

Beason, R. C. (1987). Interaction of visual and non-visual cues during migratory orientation by the bobolink (*Dolichonyx oryzivorus*). *J. Ornithol.* 128, 317–324. doi:10.1007/BF01640301

Beason, R. C. (1989). Use of an inclination compass during migratory orientation by the bobolink (*Dolichonyx oryzivorus*). *Ethology* 81, 291–299. doi:10.1111/j.1439-0310.1989.tb00775.x

Beason, R. C. (1992). You can get there from here: responses to simulated magnetic equator crossing by the bobolink (*Dolichonyx oryzivorus*). *Ethology* 91, 75–80. doi:10.1111/j.1439-0310.1992.tb00852.x

Beck, W., and Wiltschko, W. (1988). Magnetic factors control the migratory direction of pied flycatchers (*Ficedula hypoleuca* Pallas). *Acta XIX Congr. Int. Ornithol.* 2, 1955–1962.

Bensch, S., and Nielsen, B. (1999). Autumn migration speed of juvenile reed and sedge warblers in relation to date and fat loads. *Condor* 101, 153–156. doi:10.2307/1370456

Berthold, P. (1988). Evolutionary aspects of migratory behavior in European warblers. *J. Evol. Biol.* 1, 195–209. doi:10.1046/j.1420-9101.1998.1030195.x

Berthold, P. (1996). *Control of bird migration*. Springer Science and Business Media.

Berthold, P., and Helbig, A. J. (1992). The genetics of bird migration: stimulus, timing, and direction. *Ibis* 134, 35–40. doi:10.1111/j.1474-919X.1992.tb04731.x

Berthold, P., Helbig, A. J., Mohr, G., and Querner, U. (1992). Rapid microevolution of migratory behaviour in a wild bird species. *Nature* 360, 668–670. doi:10.1038/360668a0

Berthold, P., and Querner, U. (1981). Genetic basis of migratory behavior in European warblers. *Science* 212, 77–79. doi:10.1126/science.212.4490.77

Biebach, H. (1985). Sahara stopover in migratory flycatchers: fat and food affect the time program. *Experientia* 41, 695–697. doi:10.1007/BF02007727

Biebach, H. (1990). "Strategies of trans-Sahara migrants," in *Bird migration: physiology and ecophysiology* (Springer), 352–367.

Bingman, V. P., and Ewry, E. M. (2020). On a search for a neurogenomics of cognitive processes supporting avian migration and navigation. *Integr. Comp. Biol.* 60, 967–975. doi:10.1093/icb/icaa040

Bojarinova, J., and Babushkina, O. (2010). Are ecological differences of irruptive bird species from typical migrants real? (The example of the Long-tailed Tit *Aegithalos c. caudatus*). *Russ. J. Ecol.* 41, 422–427. doi:10.1134/S1067413610050103

Bojarinova, J., and Babushkina, O. (2015). Photoperiodic conditions affect the level of locomotory activity during autumn migration in the long-tailed Tit (*Aegithalos c. caudatus*). *Auk* 132, 370–379. doi:10.1642/auk-14-155.1

Bojarinova, J., Ilves, A., Chernetsov, N., and Leivits, A. (2008). Body mass, moult and migration speed of the Goldcrest Regulus regulus in relation to the timing of migration at different sites of the migration route. *Ornis Fenn.* 85, 55–65.

Bulte, M., Heyers, D., Mouritsen, H., and Bairlein, F. (2017). Geomagnetic information modulates nocturnal migratory restlessness but not fueling in a long distance migratory songbird. *J. Avian Biol.* 48, 75–82. doi:10.1111/jav.01285

Caballero-López, V., and Bensch, S. (2024). The regulatory basis of migratory behaviour in birds: different paths to similar outcomes. *J. Avian Biol.*, e03238. doi:10.1111/jav.03238

Caballero-López, V., Lundberg, M., Sokolovskis, K., and Bensch, S. (2022). Transposable elements mark a repeat-rich region associated with migratory phenotypes of willow warblers (*Phylloscopus trochilus*). *Mol. Ecol.* 31, 1128–1141. doi:10.1111/mec.16292

Chernetsov, N. (2012). *Passerine migration: stopovers and flight*. Springer Science and Business Media.

Chernetsov, N. (2023). Bird migration research today: some achievements and new challenges. *Proc. Zool. Inst. RAS* 327, 607–622. doi:10.31610/trudyzin/2023.327.4.607

Chernetsov, N., Berthold, P., and Querner, U. (2004). Migratory orientation of first-year white storks (*Ciconia ciconia*): inherited information and social interactions. *J. Exp. Biol.* 207, 937–943. doi:10.1242/jeb.00853

Cresswell, W. (2014). Migratory connectivity of Palaearctic–African migratory birds and their responses to environmental change: the serial residency hypothesis. *Ibis* 156, 493–510. doi:10.1111/ibi.12168

Dawson, A., King, V. M., Bentley, G. E., and Ball, G. F. (2001). Photoperiodic control of seasonality in birds. *J. Biol. Rhythms* 16, 365–380. doi:10.1177/074873001129002079

de Grissac, S., Börger, L., Guitteaud, A., and Weimerskirch, H. (2016). Contrasting movement strategies among juvenile albatrosses and petrels. *Sci. Rep.* 6, 26103. doi:10.1038/srep26103

Dolnik, V. (1990). "Bird migration across arid and mountainous regions of Middle Asia and Kasakhstan," in *Bird migration* (Berlin, Heidelberg: Springer), 368–386. doi:10.1007/978-3-642-74542-3_24

Ellegren, H. (1993). Speed of migration and migratory flight lengths of passerine birds ringed during autumn migration in Sweden. *Ornis Scand.* 24, 220–228. doi:10.2307/3676737

Emlen, S. T. (1967a). Migratory orientation in the indigo bunting, *Passerina cyanea*. Part I: evidence for use of celestial cues. *Auk* 84, 309–342. doi:10.2307/4083084

Emlen, S. T. (1967b). Migratory orientation in the indigo bunting, *Passerina cyanea*. Part II: mechanism of celestial orientation. *Auk* 84, 463–489. doi:10.2307/4083330

Farner, D. S., and Gwinner, E. (1980). "Photoperiodicity, circannual and reproductive cycles," in *Avian endocrinology* (Academic Press), 331–366.

Fransson, T. (1995). Timing and speed of migration in North and West European populations of Sylvia warblers. *J. Avian Biol.* 26, 39–48. doi:10.2307/3677211

Fransson, T., Jakobsson, S., Johansson, P., Kullberg, C., Lind, J., and Vallin, A. (2001). Magnetic cues trigger extensive refuelling. *Nature* 414, 35–36. doi:10.1038/35102115

Fugate, J., Wallace, C., Aikens, E. O., Jesmer, B., and Kauffman, M. (2024). Origin stories: how does learned migratory behaviour arise in populations? *Biol. Rev.* 100, 996–1014. doi:10.1111/brv.13171

Gagliardo, A. (2013). Forty years of olfactory navigation in birds. *J. Exp. Biol.* 216, 2165–2171. doi:10.1242/jeb.070250

Gatter, W. (1987a). Zugverhalten und Überwinterung von paläarktischen Vögeln in Liberia (Westafrika). *Verh. Ornithol. Ges. Bayern* 24, 479–508.

Gatter, W. (1987b). Vogelzug in Westafrika: Beobachtungen und Hypothesen zu Zugstrategien und Wanderrouten. *Vogelwarte* 34, 80–92.

Gschweng, M., Kalko, E. K., Querner, U., Fiedler, W., and Berthold, P. (2008). All across Africa: highly individual migration routes of Eleonora's falcon. *Proc. R. Soc. B Biol. Sci.* 275, 2887–2896. doi:10.1098/rspb.2008.0575

Gwinner, E. (1986). Circannual rhythms in the control of avian migrations. *Adv. Study Behav.* 16, 191–228. doi:10.1016/S0065-3454(08)60191-6

Gwinner, E. (1989). Photoperiod as a modifying and limiting factor in the expression of avian circannual rhythms. *J. Biol. Rhythms* 4, 125–138. doi:10.1177/074873048900400210

Gwinner, E. (1996). Circadian and circannual programmes in avian migration. *J. Exp. Biol.* 199, 39–48. doi:10.1242/jeb.199.1.39

Gwinner, E., Biebach, H., and v Kries, I. (1985). Food availability affects migratory restlessness in caged garden warblers (*Sylvia borin*). *Naturwissenschaften* 72, 51–52. doi:10.1007/BF00405336

Gwinner, E., Schwabl, H., and Schwabl-Benzinger, I. (1988). Effects of food-deprivation on migratory restlessness and diurnal activity in the garden warbler *Sylvia borin*. *Oecologia* 77, 321–326. doi:10.1007/BF00378037

Gwinner, E., Schwabl, H., and Schwabl-Benzinger, I. (1992). The migratory time program of the Garden Warbler: is there compensation for interruptions? *Ornis Scand.* 23, 264–270. doi:10.2307/3676648

Gwinner, E., and Wiltschko, W. (1978). Endogenously controlled changes in migratory direction of the Garden Warbler *Sylvia borin*. *J. Comp. Physiol. A* 125, 267–273. doi:10.1007/bf00656605

Hahn, S., Bauer, S., and Liechti, F. (2009). The natural link between Europe and Africa – 2.1 billion birds on migration. *Oikos* 118, 624–626. doi:10.1111/j.1600-0706.2008.17309.x

Helbig, A. J. (1991). Inheritance of migratory direction in a bird species: a cross-breeding experiment with SE-and SW-migrating blackcaps (*Sylvia atricapilla*). *Behav. Ecol. Sociobiol.* 28, 9–12. doi:10.1007/BF00172133

Helm, B., Gwinner, E., and Trost, L. (2005). Flexible seasonal timing and migratory behavior: results from Stonechat breeding programs. *Ann. N. Y. Acad. Sci.* 1046, 216–227. doi:10.1196/annals.1343.019

Hilgerloh, G. (1989). Autumn migration of trans-Saharan migrating passerines in the Straits of Gibraltar. *Auk* 106, 233–239.

Kramer, G. (1953). Wird die Sonnenhöhe bei der Heimfindeorientierung verwertet? *J. für Ornithol.* 94, 201–219. doi:10.1007/bf01922508BF01922508

Kullberg, C., Henshaw, I., Jakobsson, S., Johansson, P., and Fransson, T. (2007). Fuelling decisions in migratory birds: geomagnetic cues override the seasonal effect. *Proc. R. Soc. B Biol. Sci.* 274, 2145–2151. doi:10.1098/rspb.2007.0554

Kullberg, C., Lind, J., Fransson, T., Jakobsson, S., and Vallin, A. (2003). Magnetic cues and time of season affect fuel deposition in migratory thrush nightingales (*Luscinia luscinia*). *Proc. R. Soc. B* 270, 373–378. doi:10.1098/rspb.2002.2273

Loonstra, A. J., Verhoeven, M. A., Both, C., and Piersma, T. (2023). Translocation of shorebird siblings shows intraspecific variation in migration routines to arise after fledging. *Curr. Biol.* 33, 2535–2540.e3. doi:10.1016/j.cub.2023.05.014

Michalik, A., Alert, B., Engels, S., Lefeldt, N., and Mouritsen, H. (2014). Star compass learning: how long does it take? *J. Ornithol.* 155, 225–234. doi:10.1007/s10336-013-1004-x

Mouritsen, H. (2018). Long-distance navigation and magnetoreceptor in migratory animals. *Nature* 558, 50–59. doi:10.1038/s41586-018-0176-1

Mueller, T., O'Hara, R. B., Converse, S. J., Urbanek, R. P., and Fagan, W. F. (2013). Social learning of migratory performance. *Science* 341, 999–1002. doi:10.1126/science.1237139

Perdeck, A. C. (1958). Two types of orientation in migrating starlings, *Sturnus vulgaris* L., and chaffinches, *Fringilla coelebs* L., as revealed by displacement experiments. *Ardea* 46, 194–202.

Perdeck, A. C. (1964). An experiment on the ending of autumn migration in starlings. *Ardea* 52, 133–139.

Perdeck, A. C. (1967). Orientation of starlings after displacement to Spain. *Ardea* 55, 194–202.

Pot, M. T., Visser, M. E., Helm, B., von Rönn, J. A., and van der Jeugd, H. P. (2024). Revisiting Perdeck's massive avian migration experiments debunks alternative social interpretations. *Biol. Lett.* 20, 20240217. doi:10.1098/rsbl.2024.0217

Rabøl, J. (1969). Orientation of autumn migrating garden warblers (*Sylvia borin*) after displacement from western Denmark (blåvand) to eastern Sweden (ottenby). A preliminary experiment. *Dan. Orn. Foren. Tidsskr.* 63, 93–104.

Rabøl, J. (1972). Displacement experiments with night-migrating passerines (1970)1. *Z. Tierpsychol* 30, 14–25. doi:10.1111/j.1439-0310.1972.tb00840.x

Rabøl, J. (1975). The orientation of night-migrating passerines without the directional influence of the starry sky and/or the earth magnetic field. *Z. Tierpsychol.* 38, 251–266.

Rabøl, J. (1981). The orientation of Robins *Erithacus rubecula* after displacement from Denmark to Canary Islands, autumn 1978. *Ornis Scand.* 12, 89–98. doi:10.2307/3676032

Rabøl, J. (1985). The moving goal area and the orientation system of migrant birds. *Dan. Orn. Foren. Tidsskr.* 79, 29–42.

Rabøl, J. (1993). The orientation systems of long-distance passerine migrants displaced in autumn from Denmark to Kenya. *Ornis Scand.* 24, 183–196. doi:10.2307/3676734

Rabøl, J. (1994). Compensatory orientation in Pied Flycatchers *Ficedula hypoleuca* following a geographical displacement. *Dan. Orn. Foren. Tidsskr.* 88, 171–182.

Rabøl, J. (1995). Compensatory orientation in juvenile garden warblers, *Sylvia borin*, and redstarts, *Phoenicurus phoenicurus*, following a geographical displacement. *Dan. Orn. Foren. Tidsskr.* 89, 61–65.

Rabøl, J., and Rabol, J. (1970). Displacement and phaseshift experiments with night-migrating passerines. *Ornis Scand.* 1, 27–43. doi:10.2307/3676332

Rabøl, J., and Rabol, J. (1978). One-direction orientation versus goal area navigation in migratory birds. *Oikos* 30, 216–223. doi:10.2307/3543481

Rani, S., Singh, S., Misra, M., Malik, S., Singh, B. P., and Kumar, V. (2005). Daily light regulates seasonal responses in the migratory male redheaded bunting (*Emberiza bruniceps*). *J. Exp. Zool.* 303, 541–550. doi:10.1002/jez.a.187

Richardson, W. J. (1978). Timing and amount of bird migration in relation to weather: a review. *Oikos* 30, 224–272. doi:10.2307/3543482

Richardson, W. J. (1990). "Timing of bird migration in relation to weather: updated review," in *Bird migration* (Berlin, Heidelberg: Springer), 78–101. doi:10.1007/978-3-642-74542-3_6

Rüppell, W. (1944). Versuche über Heimfinden ziehender Nebelkrähen nach Verfrachtung: Versuche zur Ortstreue und Fernorientierung der Vögel XI. *J. Ornithol.* 92, 106–132. doi:10.1007/BF02086330

Schwarze, S., Steenken, F., Thiele, N., Kobylkov, D., Lefeldt, N., Dreyer, D., et al. (2016). Migratory blackcaps can use their magnetic compass at 5 degrees inclination, but are completely random at 0 degrees inclination. *Sci. Rep.* 6, 33805. doi:10.1038/srep33805

Smolinsky, J. A., Diehl, R. H., Radzio, T. A., Delaney, D. K., and Moore, F. R. (2013). Factors influencing the movement biology of migrant songbirds confronted with an ecological barrier. *Behav. Ecol. Sociobiol.* 67, 2041–2051. doi:10.1007/s00265-013-1614-6

Sokolov, L. V. (1981). The sensitive period in the process of formation of the connections with the place of future nesting in the chaffinch (*Fringilla coelebs*) at the Kurische Nehrung. *Zool. Zhurn.* 60, 887–894. (in Russian).

Sokolov, L. V. (1997). *Philopatry of migratory birds*. Harwood Academic Press.

Sokolov, L., Sinelschikova, A. Y., and Markovets, M. Y. (2024). The first satellite tracking data on the migration of the common cuckoo *Cuculus canorus* (Cuculiformes, Cuculidae) from Southern Siberia (Khakassia, Russia). *Proc. Zool. Inst. RAS* 328, 374–378. doi:10.31610/trudyzin/2024.328.3.374

Sokolovskis, K., Lundberg, M., Åkesson, S., Willemoes, M., Zhao, T., Caballero-Lopez, V., et al. (2023). Migration direction in a songbird explained by two loci. *Nat. Commun.* 14, 165. doi:10.1038/s41467-023-35788-7

Sokolovskis, K., Piironen, A., and Laaksonen, T. (2024). Translocation experiment of taiga bean geese *Anser fabalis* provides evidence for oblique social learning of moult migration. *J. Avian Biol.*, e03263. doi:10.1111/jav.03263

Styrsky, J. D., Berthold, P., and Robinson, W. D. (2004). Endogenous control of migration and calendar effects in an intratropical migrant, the yellow–green vireo. *Anim. Behav.* 67, 1141–1149. doi:10.1016/j.anbehav.2003.07.012

Thorup, K., Bisson, I. A., Bowlin, M. S., Holland, R. A., Wingfield, J. C., Ramenofsky, M., et al. (2007). Evidence for a navigational map stretching across the continental US in a migratory songbird. *Proc. Natl. Acad. Sci. U.S.A.* 104, 18115–18119. doi:10.1073/pnas.0704734104

Thorup, K., Ortvad, T. E., Rabøl, J., Holland, R. A., Tøttrup, A. P., and Wikelski, M. (2011). Juvenile songbirds compensate for displacement to oceanic islands during autumn migration. *PLoS One* 6, e17903. doi:10.1371/journal.pone.0017903

Thorup, K., and Rabøl, J. (2007). Compensatory behaviour after displacement in migratory birds: a meta-analysis of cage experiments. *Behav. Ecol. Sociobiol.* 61, 825–841. doi:10.1007/s00265-006-0306-x

Thorup, K., Vega, M. L., Snell, K. R. S., Lubkovskaia, R., Willemoes, M., Sjöberg, S., et al. (2020). Flying on their own wings: young and adult cuckoos respond similarly to long-distance displacement during migration. *Sci. Rep.* 10, 7698. doi:10.1038/s41598-020-64230-x

Toews, D. P., Taylor, S. A., Streby, H. M., Kramer, G. R., and Lovette, I. J. (2019). Selection on VPS13A linked to migration in a songbird. *Proc. Natl. Acad. Sci. U.S.A.* 116, 18272–18274. doi:10.1073/pnas.1909186116

Utvenko, G., Gorvat, P., Grebenkova, A., Pakhomov, A., and Chernetsov, N. (2025). Magnetic orientation of marsh warblers (*Acrocephalus palustris*) and spotted flycatchers (*Muscicapa striata*) after simulated crossing of the magnetic equator. *J. Exp. Biol.* 228, jeb248169. doi:10.1242/jeb.248169

Wiltschko, R., and Wiltschko, W. (2023). Animal navigation: how animals use environmental factors to find their way. *Eur. Phys. J. Spec. Top.* 232, 237–252. doi:10.1140/epjs/s11734-022-00610-w

Wiltschko, W., and Wiltschko, R. (1992). Migratory orientation: magnetic compass orientation of garden warblers (*Sylvia borin*) after a simulated crossing of the magnetic equator. *Ethology* 91, 70–74. doi:10.1111/j.1439-0310.1992.tb00851.x

Wynn, J., Leberecht, B., Liedvogel, M., Burnus, L., Chetverikova, R., Döge, S., et al. (2023). Naive songbirds show seasonally appropriate spring orientation in the laboratory despite having never completed first migration. *Biol. Lett.* 19, 20220478. doi:10.1098/rsbl.2022.0478

Wynn, J., and Liedvogel, M. (2023). Lost: on what level should we aim to understand animal navigation? *J. Exp. Biol.* 226, jeb245441. doi:10.1242/jeb.245441

Yoda, K., Okumura, M., Suzuki, H., Matsumoto, S., Koyama, S., and Yamamoto, M. (2021). Annual variations in the migration routes and survival of pelagic seabirds over mountain ranges. *Ecology* 102, e03297. doi:10.1002/ecy.3297

Yoda, K., Yamamoto, T., Suzuki, H., Matsumoto, S., Müller, M., and Yamamoto, M. (2017). Compass orientation drives naïve pelagic seabirds to cross mountain ranges. *Curr. Biol.* 27, R1152–R1153. doi:10.1016/j.cub.2017.09.009

Zhao, T., Ilieva, M., Larson, K., Lundberg, M., Neto, J. M., Sokolovskis, K., et al. (2020). Autumn migration direction of juvenile willow warblers (*Phylloscopus t. trochilus* and *P. t. acredula*) and their hybrids assessed by qPCR SNP genotyping. *Mov. Ecol.* 8, 22. doi:10.1186/s40462-020-00209-7

Zolotareva, A., Utvenko, G., Romanova, N., Pakhomov, A., and Chernetsov, N. (2021). Ontogeny of the star compass in birds: pied flycatchers (*Ficedula hypoleuca*) can establish the star compass in spring. *J. Exp. Biol.* 224, jeb237875. doi:10.1242/jeb.237875

frontiers | Frontiers in Physiology

TYPE Original Research
PUBLISHED 17 June 2025
DOI 10.3389/fphys.2025.1583958

OPEN ACCESS

EDITED BY
Sandra G Velleman,
The Ohio State University, United States

REVIEWED BY
Krystyna Pierzchała-Koziec,
University of Agriculture in Krakow, Poland
Birendra Mishra,
University of Hawaii at Manoa, United States

*CORRESPONDENCE
Elizabeth Gilbert,
egilbert@vt.edu

RECEIVED 26 February 2025
ACCEPTED 05 May 2025
PUBLISHED 17 June 2025

CITATION
Vaughan R, Sulaiman U, Flynn A, Biase F, Meiri N, Liu D, Siegel P, Cline M and Gilbert E (2025) Embryonic thermal conditioning and post-hatch heat challenge alter hypothalamic expression of genes related to appetite, thermoregulation, and stress modulation in broiler chicks.
Front. Physiol. 16:1583958.
doi: 10.3389/fphys.2025.1583958

Embryonic thermal conditioning and post-hatch heat challenge alter hypothalamic expression of genes related to appetite, thermoregulation, and stress modulation in broiler chicks

Reagan Vaughan[1], Usman Sulaiman[2], Annalise Flynn[2], Fernando Biase[2], Noam Meiri[3], Dongmin Liu[1], Paul Siegel[2], Mark Cline[4] and Elizabeth Gilbert[4]*

[1]Department of Human Nutrition, Foods, and Exercise, Virginia Polytechnic Institute and State University, Blacksburg, VA, United States, [2]School of Animal Sciences, Virginia Polytechnic Institute and State University, Blacksburg, VA, United States, [3]Institute of Animal Science, Agricultural Research Organization, Volcani Center, Rishon Leziyyon, Israel, [4]School of Neuroscience, Virginia Polytechnic Institute and State University, Blacksburg, VA, United States

The objective of this study was to determine the effects of an acute heat challenge on day 4 post-hatch on the transcriptome of several brain nuclei associated with thermal regulation, stress, and appetite. These included the paraventricular nucleus (PVN) of the hypothalamus, the pre-optic anterior/hypothalamic area (POAH), and the nucleus of the hippocampal commissure (nCPa), in broilers that were subjected to either control incubation conditions or embryonic heat conditioning (EHC). Nuclei were collected at three timepoints relative to the start of heat challenge (0, 2, and 12 h). Total RNA was isolated, and RNA-sequencing was performed. Transcript abundance was quantified, differentially expressed genes (DEGs) were identified, and Gene Ontology analyses were performed. In the nCPa, 469 DEGs were identified across the three timepoints. There were 0 DEGs at hour 0, 2 at hour 2, and 467 at hour 12. Gene Ontology analysis of nCPa samples at hour 12 revealed enrichment in five biological processes, namely, mitochondrial electron transport, mitochondrial respiratory chain complex 1 assembly, synaptic vesicle lumen acidification, protein export from the nucleus, and aerobic respiration. Most of these genes were downregulated, suggesting reduced activity in these processes in EHC chicks. In the POAH, a total of 18 DEGs were identified, with 0, 18, and 0 at hour 0, 2, and 12, respectively. Fewer differences were observed in the PVN, with only four DEGs identified. All four were upregulated in the EHC group, with two involved in hypothalamic thermal responses: vasoactive intestinal peptide transporter 1 (VIPR1) and caprin family member 2 (CAPRIN2). In the nCPa, no differences were detected between hour 2 and hour 0; however, the comparison between hour 12 and hour 2 yielded 9 DEGs. All except one were downregulated at hour 12. The hour 12 vs. hour 0 comparison revealed 49 DEGs, of which 24 were downregulated at hour 12. The results revealed pathways associated with energy metabolism were altered in response to EHC, with most differences in the nCPa. Surprisingly, the fewest differences were observed in the PVN. The findings highlight potential target regions, such as the nCPa, and

metabolic pathways that may help better understand how EHC affects stress responses and energy homeostasis later in life.

KEYWORDS

embryonic heat conditioning, heat stress, hypothalamus, transcriptome, broiler chicks

1 Introduction

High ambient temperatures are a major environmental factor in the agriculture industry, accounting for annual losses of over $2.36 billion, including $165 million in the poultry industry alone (Nawab et al., 2018). Due to the increases in climate change and the rising global warming crisis, this monetary loss is likely to increase in the coming years, having detrimental effects on the poultry industry and causing a potential food crisis for the growing population. Poultry is the second-highest meat type consumed in the world, following pork. Broiler chicken consumption reached 37.0 million metric tons (mmt) in 1998 and has exponentially increased to 138 mmt by 2022, coinciding with the global population surpassing 8 billion (Dawson, 2023).

Broiler chickens are vulnerable to heat stress due to their selection for high body weight over time. Selection programs have pushed to increase growth, feed-to-gain ratio, and breast muscle size (Reed et al., 2022). Because of these high growth rates, insulation of feathers, and the lack of sweat glands in poultry, heat stress is particularly detrimental in broilers (Rosenberg et al., 2020). These changes have decreased their tolerance to heat, and the impacts of heat stress on broilers account for many physiological issues associated with an increase in the stress response, weight loss, and decreased food intake. These changes often lead to a decrease in meat/carcass production and have resulted in mortalities because of prolonged heat exposure.

In previous studies, we demonstrated that embryonic heat conditioning (EHC) makes chicks more stress-resilient later in life and is associated with improved growth performance, but we have only started to elucidate the underlying molecular mechanisms (Rosenberg et al, 2020; 2022). The use of EHC has shown that animals exposed to thermal stress during the critical part of development display resistance to high temperatures (Labunskay and Meiri, 2006). The hypothalamus is implicated in these effects due to its role in maintaining homeostasis. It integrates central and peripheral signals to modulate endocrine and autonomic output related to the regulation of temperature, appetite, thirst, and other survival-related functions. However, there is little understanding of which hypothalamic nuclei are responsible for the adaptations associated with EHC.

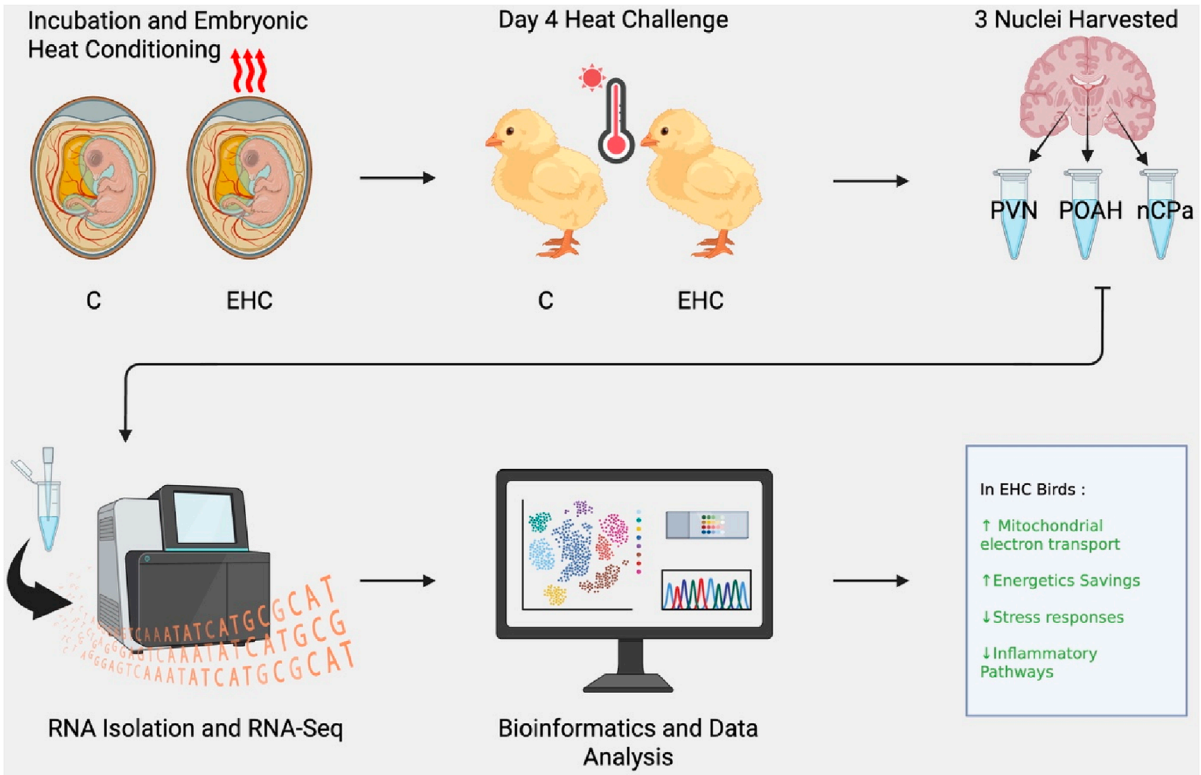

GRAPHICAL ABSTRACT

Aside from the agricultural applications, chicks are an ideal model for EHC due to the embryonic environment post-oviposition, allowing for the manipulation of the embryo's environment. Specific hypothalamic regions of interest are the paraventricular nucleus (PVN), hippocampal commissure (nCPa), and pre-optic anterior hypothalamic area (POAH). Thermoregulation in mammals and avian species (Rothhaas and Chung, 2021) is mediated by the POAH, which is responsible for the innate temperature response and adjusting energy expenditure based on external factors. Heat initiates the stress response, and the POAH projects onto other hypothalamic nuclei associated with stress response, such as the PVN and the dorsomedial hypothalamus (Rothhaas and Chung, 2021; Bohler et al., 2021). The POAH is also responsible for monitoring and integrating temperature alterations from the periphery to maintain homeostasis (Tan and Knight, 2018; Kisliouk et al., 2024). Heat also has intrinsic effects on the response to the stressor in chicks. The initiation of the stress response is through the expression of the corticotropin-releasing factor or hormone (CRF or CRH, respectively). CRF regulates the hypothalamic–pituitary–adrenal (HPA) axis during the stress response and is a potent anorexigenic factor. The nCPa and PVN are both integral in the expression of CRH and for mediating responses to the stressor. The nCPa is essential for the stress response by containing CRH neurons and expressing CRF prior to the PVN, which is understood to maintain and modulate stress in the HPA axis (Kadhim et al., 2019). The PVN, in conjunction with mediating the stressor response, is also essential for modulating feeding behavior and appetite regulation. The PVN regulates water intake and controls food intake by receiving signals from other brain nuclei, with emphasis on neuropeptide Y (NPY) receptors (orexigenic) and melanocortin ligands (anorexigenic) such as pro-opiomelanocortin (POMC) and alpha-melanocyte stimulating hormone (a-MSH) (Yousefvand and Hamidi, 2019). The PVN is intrinsically an anorexigenic center and promotes decreases in appetite due to its population of melanocortin receptors and CRF neurons. Ghrelin stimulates CRF neurons located on the PVN, resulting in decreased food intake (Yousefvand and Hamidi, 2019).

The present study was designed to employ nucleus punch biopsy isolation and RNA sequencing to identify differentially expressed genes and their associated pathways in the nCPa, POAH, and PVN in the control and EHC incubation groups. To help elucidate the effects of EHC on stress resilience, we collected samples from chicks exposed to a heat stress paradigm on day 4 post-hatch. We hypothesized that the identified genes would be related to metabolic and thermoregulatory pathways.

2 Materials and methods

2.1 Animals

All experimental protocols were approved by the Institutional Animal Care and Use Committee (IACUC) at Virginia Tech. Hubbard x Cobb-500 eggs (*Gallus gallus)* were obtained from a nearby commercial hatchery (same source and flock breeder age as in our previous studies (Sulaiman et al., 2024; Beck et al., 2024)). Upon arrival, eggs were kept at 26.6°C for 12 h and were then randomly divided into the control and EHC groups. These groups were placed in two separate incubators (Rite Farm Products Pro-1056) and labeled as control and EHC, respectively. Both groups from embryonic day (ED) 0–7 were incubated at 37.5°C and 80% relative humidity. The eggs in the control group continued to be incubated at 37.5°C and 80% relative humidity until hatching on ED 21. The EHC group was separated from the control group on ED 7 and introduced to an increased temperature of 39.5°C and 80% relative humidity for 12 h per day (07:30–19:30) and 37.5°C for the remainder of the 24 h until ED 16. The EHC group was then maintained at 37.5°C for the remaining 5 days until hatching. On ED 18.5, all eggs were subjected to candling. Infertile eggs and dead embryos were removed from the study. Eggs with viable embryos were transferred to a common hatching incubator (Rite Farm Products Pro-264) and maintained within their separate groups (separate enclosed trays to prevent mixing of treatments) at 36.9°C and 50% relative humidity for 18 h. The temperature was gradually decreased to 35°C until the hatch was collected. Chicks were arbitrarily divided into group cages based on treatment in preparation for the acute day 4 post-hatch heat challenge. The relative room temperature was 30°C, with *ad libitum* access to feed and water and 24 h continuous light exposure, similar to our previous studies (Sulaiman et al., 2024; Beck et al., 2024).

2.2 Acute heat challenge

On day 4 post-hatch, control and EHC groups were subjected to an acute heat challenge at 36°C. The temperature of 36°C was carefully selected based on preliminary trials designed to induce observable behavioral indicators of heat stress, such as panting and wing spreading while avoiding more severe physiological responses. Punch samples were collected at three timepoints: 0 h (before heat challenge; baseline), 2 h, and 12 h from the start of the increased temperature. Within these three timepoints, 10 chicks were randomly collected and euthanized from the control and EHC groups (20 total) for each timepoint. Chicks were individually weighed, euthanized by decapitation, and sexed *via* gonad identification.

2.3 Punch biopsy collection

Three hypothalamic nuclei, namely, the PVN, POAH, and nCPa, were collected from each bird (n = 60), yielding a total of 180 samples. Brains were perfused with 1.5 mL of RNA stabilizing solution *via* the carotid artery based on methods used by Bohler et al. (2020). Immediately after perfusion, brains were processed into tissue blocks, mounted on chucks with OCT embedding medium, and sectioned at −15°C in a cryostat. Brain sections were cut at a thickness of 500 µm, and biopsies were collected based on anatomical landmarks described in the stereotaxic atlas by Kuenzel and Masson (1988). The nCPa was the most rostral, referring to 8.2 mm in the stereotaxic atlas. The POAH was next at 7.8 mm, and the PVN was collected at 6.8 mm. Punches were collected using disposable 1-mm biopsy punch instruments (Integra Lifesciences Corp, Princeton, NJ). Anatomy and biopsy collection were confirmed using a digitized stereotaxic atlas, with photos of tissue sections overlaid on the atlas; the methods were further

described by Bohler et al. (2020). After collection, the punches were immediately submerged in 1.5 mL microcentrifuge tubes containing RNA lysis buffer (Norgen Biotek, Thorold, ON, Canada) and 1% beta-mercaptoethanol (Calbiochem, San Diego, CA, United States). The tubes were vortexed, snap-frozen in liquid nitrogen, and stored at −80°C until RNA isolation was performed.

2.4 Total RNA extraction, cDNA synthesis, and real-time quantitative PCR

Total RNA was isolated using the Total RNA Purification Micro Kit (Norgen Biotek, Thorold, ON, Canada), according to the manufacturer's instructions. Samples were thawed to room temperature (3 min) and vortexed for 30 s. An amount of 100 µL of 70% molecular-biology-grade ethanol was added to the lysate, and then steps were performed according to the kit's instructions. Purity and concentration of the total RNA were analyzed at 260/280/230 ng/µL using the NanoPhotometer Pearl Spectrophotometer (Implen, Westlake Village, CA, United States), according to the manufacturer's instructions. The High-Capacity cDNA Reverse Transcription Kit (Applied Biosystems, Carlsbad, CA, United States) was used to synthesize the first-strand complementary DNA (cDNA) from 100 ng of total RNA in 20 µL reactions, according to the manufacturer's protocol. Reactions were performed under the following conditions: 25°C for 10 min, 37°C for 120 min, and 85°C for 5 min. Primers (Table 1) for RT-qPCR were designed using Primer Express software (Applied Biosystems, Carlsbad, CA, United States), following the manufacturer's instructions. RT-PCRs were performed in duplicate using 10 µL reaction volumes, each containing 5 µL of Fast SYBR Green Master Mix (Applied Biosystems, Carlsbad, CA, United States). PCR was performed as follows: at 95°C for 20 s, followed by 40 cycles at 90°C for 3 s, and at 60°C for 30 s. A dissociation step at 95°C for 15 s, 60°C for 1 min, 95°C for 15 s, and 60°C for 15 s was performed at the end of each PCR to ensure amplicon specificity. PCR data were analyzed using JMP Pro 16 (SAS Institute Inc., Cary, NC) with the ΔΔCT method, with β-actin as the reference gene, and the calibrator sample of each nucleus was the average of the control chicks per group. The statistical model included the effect of treatment (EHC vs control), timepoints (0, 2, and 12 h), and the interactions between them.

2.5 Selection of chick samples for RNA-sequencing and production of sequencing data

Selection of samples was based on concentrations (ng/µL) and the ability to use the three nuclei samples from the same bird. A total of 72 samples were submitted to the Genomic Sequencing Center at Virginia Tech (Blacksburg, VA, United States). The 72 samples were collected from 24 total chicks (three samples per chick, n = 8 chicks per timepoint). All the 72 samples were split to account for 36 EHC and 36 control samples. Among the selected chicks, 12 were male and 12 were female; however, sex did not prove to be significantly different. NanoDrop concentrations from the Pearl Spectrophotometer ranged from 4.8 ng/µL to 29.2 ng/µL with an average of 13.5 ng/µL. Each sample submitted was strictly between 16 and 18 µL. The integrity of RNA was verified using High Sensitivity RNA ScreenTape Assays for TapeStation (Agilent).

2.6 RNA-seq library preparation

RNA samples were converted into a strand-specific library using Illumina Stranded Total RNA Prep, Ligation with Ribo-Zero Plus Sample Prep Kit (Illumina, 20040529) for subsequent cluster generation and sequencing on Illumina's NovaSeq 6000. The libraries were enriched by 13 cycles of PCR, quality-checked using Agilent TapeStation, and quantitated by qPCR. Individually indexed cDNA libraries were pooled and sequenced on a NovaSeq 6000 S2 (200 cycle, PE) using Illumina NovaSeq Control Software (version 1.8.0.). Binary base call (BCL) files were converted to FASTQ files, and adapters were trimmed and demultiplexed using bcl2fastq Conversion Software. The FASTQ files were provided by the Genomic Sequencing Center for further analysis.

2.7 RNA-seq alignment, processing of sequences, and gene quantification

First, adapters were removed from the sequences using Trimmomatic (v 0.39), retaining only those with a length of ≥100 nucleotides and an average quality score ≥30. We aligned the reads to the chicken genome (galgal1) using HISAT2 (v 2.2.1) (Kim et al., 2019). Next, we used SAMtools (v 1.10) (Li et al., 2009) to retain the reads with one match to the genome, followed by removing duplicates using bammarkduplicates from biobambam2 (v 2.0.95) (Tischler and Leonard, 2014). Samples with 90% or greater alignment accuracy were used for counting.

featureCounts (v 2.0.1) (Liao et al., 2014) was used to count reads according to the ensemble annotation (Gallus_gallus.bGalGal1.mat.broiler.GRCg7b.110.gtf). We quantified counts per million (CPM) and fragments per kilobase per million (FPKM) using the functions "cpm" or "rpkm" from the "edgeR" package (McCarthy et al., 2012; Robinson et al., 2010). We also calculated transcript per million using the formula presented by Li and Dewey (2011). We retained genes annotated as long non-coding RNA (lncRNA), protein-coding, and pseudogenes (Robinson et al., 2010). Genes were only used for further analysis if the CPM and FPKM were >1 in at least four samples. This approach was adopted to reduce the number of genes with low expression and, thus, prone to producing confounding results (Bourgon et al., 2010).

2.8 Analysis of differential transcript abundance

Transcript abundance between samples from each group was compared using the R packages "edgeR" (McCarthy et al., 2012; McCarthy and Smyth, 2012), with the quasi-likelihood test and "DEseq2" (Love et al., 2014), using the Wald and likelihood tests. We also added sex as a fixed effect in the model. The nominal *p*-values of both tests were corrected for multiple hypothesis testing using the

TABLE 1 Primers used for real-time PCR.

Gene	Sequences (forward/reverse)	Accession no.
β-Actin	GTCCACCGCAAATGCTTCTAA/TGCGCATTTATGGGTTTTGTT	NM_205,518.2
NPY	CATGCAGGGCACCATGAG/CAGCGACAAGGCGAAAGTC	NM_205,473.2
CRH	TCAGCACCAGAGCCATCACA/GCTCTATAAAAATAAAGAGGTGACATCAGA	NM_001123031.1
POMC	GCCAGACCCCGCTGATG/CTTGTAGGCGCTTTTGACGAT	NM_001398117.1
CCK	GGAAGGAAGGGAAGGAGGAA/GAGGAGCACGCAGATGCA	NM_001001741.2
UCN3	GGGCCTTCCGTCTCTACAATG/GGTGAGGGCCGTGTTGAG	XM_001231710.6
TRH	GCAGAAAATCACAATGCCATCTAT/CACCAGACAAGGTCAGGCAAA	NM_001030383.2
HSP90	GCAGCAGCTGAAGGAATTTGA/GGAAGCTCTAAGCCCTCTTTTGT	NM_001109785.2

Abbreviations: NPY, neuropeptide Y; CRF, corticotropin-releasing factor; POMC, proopiomelanocortin; CCK, cholecystokinin; UCN3, urocortin-3; TRH, thyrotropin-releasing hormone; HSP90, heat shock protein 90.

false discovery rate (FDR) method (Benjamini and Hochberg, 1995). Differential transcript abundance was assumed when FDR ≤0.1 for both tests and the |Log fold change (logFC)| > 1.

2.9 Enrichment of Gene Ontology

Tests for enrichment of Gene Ontology (GO) categories were carried out using the "goseq" package (Young et al., 2010) in R software. In all tests, we used the genes whose transcript abundances were estimated for the samples being tested as the background. The nominal *p*-value was adjusted for multiple hypothesis testing by controlling the familywise error rate following the method proposed by Holm (1979) using the function "p.adjust" from the "stats" R package. Significance was acknowledged when FWER ≤0.1.

3 Results

3.1 RNA-seq analysis

From RNA sequencing, a total of 25,067,562 fragment sequence reads were obtained, and an average of 4,217,491 pairs of reads per sample were mapped to the chicken genome (Hillier et al., 2004). There were 17,584 total genes identified, with 3,403 being lncRNA, 14,160 being protein-coding, and 21 being pseudogenes. Among these genes, there were a total of 491 DEGs across the nCPa, POAH, and PVN when comparing EHC vs control (C) at different timepoints. The principal component analysis (Figure 1) visualizes our dataset separated by timepoints into three graphs. Within these graphs, EHC samples are represented in red and control is represented in blue. The nuclei are differentiated by shape, with POAH as squares, PVN as circles, and nCPa as triangles. There was no explicit separation of chicks based on treatment or tissue when all 17,584 genes were included for a principal component analysis.

3.2 Differential gene expression in EHC chicks relative to control

3.2.1 DEGs identified in the nCPa

For the three different nuclei assessed, there was variation in the numbers and types of differentially expressed genes (DEGs) for EHC chicks vs. control at the different timepoints in the heat challenge. In the nCPa, there were a total of 469 DEGs identified across all three timepoints. There were 0 DEGs identified at hour 0. At hour 2, in the nCPa, there were 2 DEGs, namely, keratin 13 and phosphoserine aminotransferase 1, both of which were downregulated in the EHC group (Table 2). With only 2 DEGs in hour 2 in nCPa EHC chicks, we investigated the functions of these genes individually rather than performing an enrichment analysis.

Hour 12 nCPa tissues yielded a total of 467 DEGs. We selected the 10 highest upregulated and 10 lowest downregulated genes for tabular display (Table 3). Because of the large number of DEGs, we performed an enrichment of GO test on the hour 12 nCPa sample data. On completing the GO enrichment, 24 genes were considered significantly enriched with a FWER ≤0.1. Among these, five biological processes were enriched, namely, mitochondrial electron transport, mitochondrial respiratory chain complex 1 assembly, synaptic vesicle lumen acidification, protein export from nucleus, and aerobic respiration (Table 4). Twenty one out of the 24 genes were downregulated, suggesting that these biological processes were less functional/depleted in EHC chicks.

3.2.2 DEGs identified in the POAH

In the POAH, a total of 18 DEGs were identified after performing edgeR and DEseq2 tests. Similar to the nCPa, at hour 0, there were 0 DEGs identified between treatment groups. At hour 2, there were 18 DEGs (Table 5). These genes were investigated individually as there were not enough genes to perform a robust enrichment analysis. All but one gene were upregulated (BEND3), 17 genes were protein-coding, and 1(ENSGALG00010004520) was lncRNA. GO enrichment was not performed. At hour 12, no DEGs were identified.

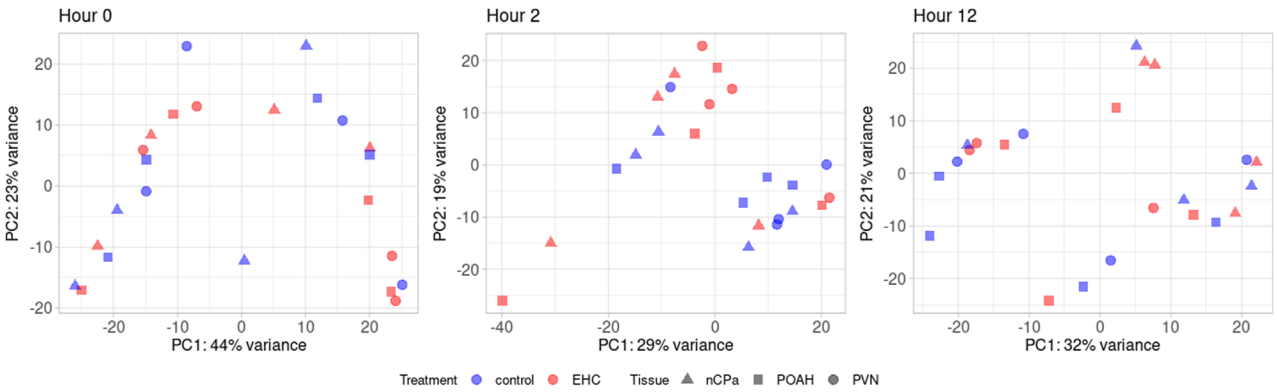

FIGURE 1
Principal component analysis using 17,584 quantified genes. Among these are the nCPa (n = 4/treatment/timepoint), POAH (n = 4/treatment/timepoint), and PVN (n = 4/treatment/timepoint) tissues from EHC (n = 12/timepoint) and control (n = 12/timepoint).

TABLE 2 DEGs in EHC chicks at hour 2 in nCPa nuclei[a].

Direction	Ensembl id	Name	Description	logFC	P-value	FDR
Downregulated	ENSGALG00010022872	KRT13	Keratin 13	−4.43240	2.14E-06	0.03771
Downregulated	ENSGALG00010015533	PSAT1	Phosphoserine aminotransferase 1	−0.96427	1.06E-05	0.09292

Abbreviations: KRT13, keratin 13; PSAT1, phosphoserine aminotransferase 1.
[a]All results were determined with FDR <0.1.

3.2.3 DEGs identified in the PVN

Fewer differences were observed in the PVN than in the nCPa and POAH, with only four DEGs identified (Table 6). Four of these were different at hour 2. At hour 0 and 12, there were no DEGs. The four genes that were differentially expressed were upregulated in the EHC group. Among these four, two are associated with hypothalamic responses: vasoactive intestinal peptide receptor 1 (VIPR1) and caprin family member 2 (CAPRIN2) Bárez-López et al., 2022). Of the other two, one gene encodes a factor involved in mitochondrial calcium uptake (MICU1) and the other encodes an actin-binding protein, Kaptin (KPTN).

3.3 Differential gene expression relative to 0-, 2-, and 12-h timepoints irrespective of EHC vs control

The differences described in Section 3.2 were detected by comparing the two treatment groups, EHC and control. We also completed analyses that determined the effect of timepoints in the heat challenge, irrespective of treatment. Timepoint comparisons were made as follows: hour 12 relative to hour 2 (12 vs 2), hour 2 vs hour 0, and hour 12 vs hour 0 within tissue. There were no DEGs identified in the POAH or PVN.

No differences were detected in the nCPa for hour 2 vs hour 0; however, the comparison between hour 12 and hour 2 yielded 9 DEGs (Table 7). All genes, except for ubiquitin-associated protein 2-like (UBAP2L), were downregulated at hour 12 relative to hour 2.

In the nCPa, the hour 12 vs hour 0 comparison revealed 49 DEGs (Table 8). Of these genes, 16 were upregulated and 24 genes were downregulated at hour 12. After individually investigating each DEG, it was observed that these genes were classified as protein-coding or lncRNA and that to our knowledge, no existing literature links these genes to either hypothalamic regulation or control.

4 Discussion

Studies have demonstrated that EHC has had positive effects on thermotolerance in chick embryos and broiler chicks (Piestun et al., 2013). Heat shock proteins (HSPs) were measured and found to increase simultaneously with thermotolerance development, suggesting that HSPs are essential for survival and provide protective mechanisms (Amaz et al, 2024a; 2024b). Although differences were also observed in the gut and adipose tissue, metabolism-related effects in the brain are unknown (Sulaiman et al., 2024; Beck et al., 2024). Previous studies have also shown that EHC increases the expression of anti-inflammatory genes in the hypothalamus (Rosenberg et al., 2020; Rosenberg et al., 2022). The objective of this study was to identify differences in the transcriptomes of the nCPa, POAH, and PVN resulting from embryonic heat conditioning and in response to a post-hatch heat challenge (which we anticipated would accentuate changes related to effects of EHC on thermotolerance). The heat challenge was introduced on day 4 post-hatch to align with our previous studies on appetite regulation and metabolism, which were also conducted on day 4 post-hatch to

10.3389/fphys.2025.1583958

TABLE 3 Ten most upregulated and 10 most downregulated DEGs in EHC at hour 12 in nCPa tissue[a].

Direction	Ensembl ID	Name	Description	logFC	P-value	FDR
Upregulated	ENSGALG00010000384			0.97207	1.76E-08	5.72E-05
Upregulated	ENSGALG00010005981	AREL1	Apoptosis-resistant E3 ubiquitin protein ligase 1	0.81544	4.16E-07	5.62E-04
Upregulated	ENSGALG00010023442	STK25	Serine/threonine kinase 25	0.42320	7.56E-06	0.00415
Upregulated	ENSGALG00010017973	PKD1	Polycystin 1, transient receptor potential channel interacting	0.70729	1.46E-05	0.00677,265
Upregulated	ENSGALG00010016544	ADCY9	Adenylate cyclase 9	0.47785	2.03E-05	0.00791,217
Upregulated	ENSGALG00010020608	CAPZB	Capping actin protein of muscle Z-line beta subunit	0.52601	2.17E-05	0.00795,085
Upregulated	ENSGALG00010013908	TBC1D20	TBC1 domain family member 20	0.46503	3.07E-05	0.00967,321
Upregulated	ENSGALG00010018022	XPO6	Exportin 6	0.46862	3.20E-05	0.00971,448
Upregulated	ENSGALG00010026900			0.68841	3.67E-05	0.01046038
Upregulated	ENSGALG00010028151	DOCK3	Dedicator of cytokinesis 3	0.71350	3.67E-05	0.01046038
Downregulated	ENSGALG00010008407	GNAI1	G protein subunit alpha i1	−1.38534	1.57E-10	2.05E-06
Downregulated	ENSGALG00010023910	RNF7	Ring finger protein 7	−1.15010	2.33E-10	2.05E-06
Downregulated	ENSGALG00010007903	PSMA2	Proteasome subunit alpha 2	−1.09620	8.55E-09	5.01E-05
Downregulated	ENSGALG00010021639	SCG5	Secretogranin V	−1.91617	1.44E-08	5.72E-05
Downregulated	ENSGALG00010016240	EIF4A2	Eukaryotic translation initiation factor 4A2	−0.66176	1.95E-08	5.72E-05
Downregulated	ENSGALG00010014967	HNRNPH1	Heterogeneous nuclear ribonucleoprotein H1	−1.01498	4.32E-08	1.08E-04
Downregulated	ENSGALG00010024777			−2.48793	5.93E-08	1.30E-04
Downregulated	ENSGALG00010001738	PUDP	Pseudouridine 5′-phosphatase	−1.00633	1.34E-07	2.60E-04
Downregulated	ENSGALG00010000011	ND2	NADH dehydrogenase subunit 2	−3.19799	1.52E-07	2.60E-04
Downregulated	ENSGALG00010000022	ATP8	ATP synthase F0 subunit 8	−2.74138	1.63E-07	2.60E-04

Apoptosis-resistant E3 ubiquitin protein ligase 1 (AREL1), serine/threonine kinase 25 (STK25), polycystin 1, transient receptor potential channel interacting (PKD1), adenylate cyclase 9 (ADCY9), capping actin protein of muscle Z-line beta subunit (CAPZB), TBC1 domain family member 20 (TBC1D20), exportin 6 (XPO6), dedicator of cytokinesis 3 (DOCK3), G protein subunit alpha i1 (GNAI1), ring finger protein 7 (RNF7), proteasome subunit alpha 2 (PSMA2), secretogranin V (SCG5), eukaryotic translation initiation factor 4A2 (EIF4A2), heterogeneous nuclear ribonucleoprotein H1 (HNRNPH1), pseudouridine 5′-phosphatase (PUDP), NADH dehydrogenase subunit 2 (ND2), and ATP synthase F0 subunit 8 (ATP8). Abbreviations are not provided for unannotated genes.

[a]All DE results were determined with FDR <0.1.

facilitate free-hand intracerebroventricular injections (Bohler et al., 2020; Sulaiman et al., 2024; Beck et al., 2024). Chicks were observed to be panting, a primary indication of heat expenditure and stress. Additionally, we hypothesized that EHC is associated with epigenetic changes, as previously demonstrated by Rosenberg et al. (2020). As chick age increases, environmental factors have the potential to "mute" epigenetic programming that occurs during embryonic development. We hypothesize that these epigenetic changes will lead to persistent effects on gene expression and transcriptional regulation. Accordingly, our design included hour 0 as a baseline to capture the effects of the EHC on gene expression and the heat stress timepoints to measure the effects of EHC on transcriptional regulatory effects that are not manifested without an external stressor.

RNA-seq analysis suggests that EHC influenced gene expression, with a total of 491 DEGs across tissues, with most localized in the nCPa. Almost no DEGs were detected in the PVN, in which we hypothesized that stress-related factors might be affected. In all tissues, no DEGs were identified at hour 0, suggesting that in the absence of a stressor, gene expression profiles were similar in control and EHC chicks. At hour 2 of the heat challenge, a few DEGs were detected in all three tissues, suggesting that although the heat exposure revealed differences in transcriptional regulation that were not apparent in the absence of a stressor, relatively few genes were affected (4 in PVN, 18 in POAH, and 2 in the nCPa). Although there were no DEGs detected in the PVN or POAH at hour 12, 467 DEGs were identified in the nCPa, suggesting that this region was more susceptible to the effects of heat challenge on transcriptional

TABLE 4 DEGs after Gene Ontology enrichment and biological process category; FWER ≤0.1.

Ensembl gene ID	Gene name	Overrepresented p-value	Number DE in category	Total number in category	Biological process	FWER	Fold enrichment	Fold change
ENSGALG00010000011	ND2	7.03E-10	10	23	Mitochondrial electron transport, NADH to ubiquitone	6.12E-08	14.90296	−3.19799
ENSGALG00010000029	ND4	7.03E-10	10	23	Mitochondrial electron transport, NADH to ubiquitone	6.12E-08	14.90296	−2.84102
ENSGALG00010000037	ND6	7.03E-10	10	23	Mitochondrial electron transport, NADH to ubiquitone	6.12E-08	14.90296	−2.17901
ENSGALG00010000007	ND1	7.03E-10	10	23	Mitochondrial electron transport, NADH to ubiquitone	6.12E-08	14.90296	−2.01385
ENSGALG00010000033	ND5	7.03E-10	10	23	Mitochondrial electron transport, NADH to ubiquitone	6.12E-08	14.90296	−1.75243
ENSGALG00010003358	DNAJC15	7.03E-10	10	23	Mitochondrial electron transport, NADH to ubiquitone	6.12E-08	14.90296	−1.35734
ENSGALG00010000026	ND3	7.03E-10	10	23	Mitochondrial electron transport, NADH to ubiquitone	6.12E-08	14.90296	−1.34728
ENSGALG00010008731	NDUFB9	7.03E-10	10	23	Mitochondrial electron transport, NADH to ubiquitone	6.12E-08	14.90296	−1.12493
ENSGALG00010028036	NDUFS7	7.03E-10	10	23	Mitochondrial electron transport, NADH to ubiquitone	6.12E-08	14.90296	−1.12090
ENSGALG00010007555	NDUFS6	7.03E-10	10	23	Mitochondrial electron transport, NADH to ubiquitone	6.12E-08	14.90296	−1.04794
ENSGALG00010000011	ND2	1.70E-07	11	43	Mitochondrial respiratory chain complex I assembly	1.46E-05	8.76848	−3.19799
ENSGALG00010000029	ND4	1.70E-07	11	43	Mitochondrial respiratory chain complex I assembly	1.46E-05	8.76848	−2.84102

(Continued on the following page)

10.3389/fphys.2025.1583958

TABLE 4 (*Continued*) DEGs after Gene Ontology enrichment and biological process category; FWER ≤0.1.

Ensembl gene ID	Gene name	Overrepresented p-value	Number DE in category	Total number in category	Biological process	FWER	Fold enrichment	Fold change
ENSGALG00010000037	ND6	1.70E-07	11	43	Mitochondrial respiratory chain complex I assembly	1.46E-05	8.76848	−2.17901
ENSGALG00010000007	ND1	1.70E-07	11	43	Mitochondrial respiratory chain complex I assembly	1.46E-05	8.76848	−2.01385
ENSGALG00010000033	ND5	1.70E-07	11	43	Mitochondrial respiratory chain complex I assembly	1.46E-05	8.76848	−1.75243
ENSGALG00010018137	NDUFB5	1.70E-07	11	43	Mitochondrial respiratory chain complex I assembly	1.46E-05	8.76848	−1.35734
ENSGALG00010017738	NDUFS5	1.70E-07	11	43	Mitochondrial respiratory chain complex I assembly	1.46E-05	8.76848	−1.34728
ENSGALG00010008731	NDUFB9	1.70E-07	11	43	Mitochondrial respiratory chain complex I assembly	1.46E-05	8.76848	−1.12493
ENSGALG00010028036	NDUFS7	1.70E-07	11	43	Mitochondrial respiratory chain complex I assembly	1.46E-05	8.76848	−1.12090
ENSGALG00010004123	NDUFAF4	1.70E-07	11	43	Mitochondrial respiratory chain complex I assembly	1.46E-05	8.76848	−0.61710
ENSGALG00010024338	NDUFA9	1.70E-07	11	43	Mitochondrial respiratory chain complex I assembly	1.46E-05	8.76848	−0.37826
ENSGALG00010010906	ATP6V1C1	1.85E-04	4	8	Synaptic vesicle lumen acidification	0.01570	17.13840	−1.19382
ENSGALG00010004370	ATP6V1H	1.85E-04	4	8	Synaptic vesicle lumen acidification	0.01570	17.13840	−0.86649
ENSGALG00010028896	ATP6V1G1	1.85E-04	4	8	Synaptic vesicle lumen acidification	0.01570	17.13840	−0.72372
ENSGALG00010020015	ATP6V1D	1.85E-04	4	8	Synaptic vesicle lumen acidification	0.01570	17.13840	−0.60052
ENSGALG00010010262	HSPA9	9.57E-04	5	22	Protein export from nucleus	0.08035	7.79018	−0.53047

(Continued on the following page)

10.3389/fphys.2025.1583958

TABLE 4 (*Continued*) DEGs after Gene Ontology enrichment and biological process category; FWER ≤0.1.

Ensembl gene ID	Gene name	Overrepresented p-value	Number DE in category	Total number in category	Biological process	FWER	Fold enrichment	Fold change
ENSGALG00010028137	NUP214	9.57E-04	5	22	Protein export from nucleus	0.08035	7.79018	0.46482
ENSGALG00010018022	XPO6	9.57E-04	5	22	Protein export from nucleus	0.08035	7.79018	0.46862
ENSGALG00010020305	XPO7	9.57E-04	5	22	Protein export from nucleus	0.08035	7.79018	0.49686
ENSGALG00010017973	PKD1	9.57E-04	5	22	Protein export from nucleus	0.08035	7.79018	0.70729
ENSGALG00010000029	ND4	1.03E-03	4	14	Aerobic respiration	0.08582	9.79337	−2.84102
ENSGALG00010000007	ND1	1.03E-03	4	14	Aerobic respiration	0.08582	9.79337	−2.01385
ENSGALG00010000017	COX1	1.03E-03	4	14	Aerobic respiration	0.08582	9.79337	−1.27152
ENSGALG00010022937	BLOC1S1	1.03E-03	4	14	Aerobic respiration	0.08582	9.79337	−1.1705

10.3389/fphys.2025.1583958

10.3389/fphys.2025.1583958

TABLE 5 Differentially expressed genes in the EHC group vs control group at hour 2 in the POAH[a].

Direction	Ensembl ID	Name	Description	logFC	P-value	FDR
Upregulated	ENSGALG00010004520			1.85130	1.28E-05	0.06251
Upregulated	ENSGALG00010003429			1.94931	1.34E-05	0.06251
Upregulated	ENSGALG00010017487	C1QTNF8	C1q and TNF-related 8	5.44959	1.78E-05	0.06251
Upregulated	ENSGALG00010003395			1.86689	1.80E-05	0.06251
Upregulated	ENSGALG00010029651	CHAD		5.30853	3.09E-05	0.06251
Upregulated	ENSGALG00010003346			1.75279	3.33E-05	0.06251
Upregulated	ENSGALG00010022764	MFAP5	Microfibril-associated protein 5	2.54772	3.50E-05	0.06251
Upregulated	ENSGALG00010003368			1.87428	3.59E-05	0.06251
Upregulated	ENSGALG00010011181			1.37643	3.62E-05	0.06251
Upregulated	ENSGALG00010003377			1.78224	3.80E-05	0.06251
Upregulated	ENSGALG00010012092	OC3	Osteocalcin-like protein OC3	6.42273	3.91E-05	0.06251
Upregulated	ENSGALG00010003408			1.74615	5.20E-05	0.07613
Upregulated	ENSGALG00010029387	SERPINF1	Serpin family F member 1	3.53737	8.04E-05	0.09889
Upregulated	ENSGALG00010012083	MGP	Matrix Gla protein	6.29646	8.60E-05	0.09889
Downregulated	ENSGALG00010012529	BEND3	BEN domain containing 3	−0.67962	8.73E-05	0.09889
Upregulated	ENSGALG00010029270	TIMP2	TIMP metallopeptidase inhibitor 2	1.01350	9.49E-05	0.09889
Upregulated	ENSGALG00010003202	FAM46A	Family with sequence similarity 46 member A	1.57178	9.70E-05	0.09889
Upregulated	ENSGALG00010000651			4.04485	1.01E-04	0.09889

Microfibril-associated protein 5 (MFAP5), osteocalcin-like protein OC3 (OC3), serpin family F member 1 (SERPINF1), matrix Gla protein (MGP), BEN domain containing 3 (BEND3), TIMP metallopeptidase inhibitor 2 (TIMP2), and family with sequence similarity 46 member A (FAM46A). Abbreviations are not provided for unannotated genes.
[a]All DE results were determined with FDR <0.1. C1q and TNF-related 8 (C1QTNF8).

TABLE 6 Differentially expressed genes in EHC vs control chicks at hour 2 in the paraventricular nucleus[a].

Direction	Ensembl ID	Name	Description	logFC	P-value	FDR
Upregulated	ENSGALG00010027363	VIPR1	Vasoactive intestinal peptide receptor 1	1.64135	3.77E-06	0.06319
Upregulated	ENSGALG00010010774	KPTN	Kaptin, actin-binding protein	2.40213	1.01E-05	0.06319
Upregulated	ENSGALG00010021481	MICU1	Mitochondrial calcium uptake 1	0.84260	1.08E-05	0.06319
Upregulated	ENSGALG00010012072	CAPRIN2	Caprin family member 2	1.31568	2.16E-05	0.09515

Vasoactive intestinal peptide receptor 1 (VIPR1), Kaptin, actin binding protein (KPTN), mitochondrial calcium uptake 1 (MICU1), and caprin family member 2 (CAPRIN2).
[a]All DE results were determined with FDR <0.1.

regulation and that the 2 h of heat exposure was not sufficient for transcriptional changes to be revealed. It was also interesting to note that the few DEGs detected in the POAH and PVN at hour 2 were more highly expressed in the EHC group than in the control group, whereas in the nCPa, most DEGs identified at hour 2 and those highlighted by the enrichment analysis at hour 12 were downregulated by EHC. This suggests that the associated pathways might have reduced activity during heat stress in chicks that were subjected to EHC. Additionally, the nCPa was the only nucleus in which effects were observed with time during the heat stress, with most occurring at 12 h. This implies that this region is more responsive to the effects of acute heat stress than the POAH or PVN.

10.3389/fphys.2025.1583958

TABLE 7 DEGs identified at hour 12 relative to those identified at hour 2 in the nCPa[a].

Direction	Ensembl ID	Name	Description	logFC	P-value	FDR
Downregulated	ENSGALG00010014243	HIGD2A		−1.32130	4.20E-06	0.05620
Downregulated	ENSGALG00010016502	YIPF5	Yip1 domain family member 5	−0.60054	6.39E-06	0.05620
Downregulated	ENSGALG00010019810	ZFAND6	Zinc finger AN1-type containing 6	−0.68436	1.28E-05	0.05747
Upregulated	ENSGALG00010027867	UBAP2L	Ubiquitin-associated protein 2 like	0.56530	1.31E-05	0.05747
Downregulated	ENSGALG00010011991	CSNK1A1	Casein kinase 1 alpha 1	−0.43456	1.79E-05	0.06285
Downregulated	ENSGALG00010027359			−1.03567	3.02E-05	0.08838
Downregulated	ENSGALG00010028459	MCL1	BCL2 family apoptosis regulator	−0.50885	4.68E-05	0.09720
Downregulated	ENSGALG00010027617			−0.43455	4.72E-05	0.09720
Downregulated	ENSGALG00010028823	GFI1B	Growth factor independent 1B transcriptional repressor	−3.11826	4.98E-05	0.09720

Yip1 domain family member 5 (YIPF5), zinc finger AN1-type containing 6 (ZFAND6), ubiquitin-associated protein 2 like (UBAP2L), casein kinase 1 alpha 1 (CSNK1A1), BCL2 family apoptosis regulator (MCL1), and growth factor independent 1B transcriptional repressor (GFI18). Abbreviations are not provided for unannotated genes.
[a]All DE results were determined with FDR <0.1.

All differentially expressed genes in the EHC group relative to the control group were individually investigated, exception for those identified at hour 12 in the nCPa, where only the top 10 upregulated and 10 downregulated genes were further analyzed and discussed below. At hour 2 in the nCPa, two genes were differentially expressed. Keratin 13 (KRT13) is involved in the maintenance of mucosal stratified squamous epithelial cells (Kalabusheva et al., 2023), and phosphoserine aminotransferase 1 (PSAT1) is related to high feed efficiency in Iranian native turkeys (Pezeshkian et al, 2022a; 2022b). However, both genes were downregulated, suggesting a decreased level of expression in EHC. If these pathways are less active in EHC chicks, it might indicate an energy-saving mechanism that enhances their efficiency in coping with the energetic demands of heat dissipation during heat stress.

4.1 Identification and physiological relevance of DEGs in the nCPa

Of the top 10 upregulated and 10 downregulated DEGs at hour 12 in the nCPa, two genes had a correlation with muscle and body weight. Secretogranin V (SCG5) expression in congenic mice was correlated with decreased body weight (Farber et al., 2008). SCG5 was downregulated in our RNA-seq analysis. Body weight was measured, and there were no significant differences between groups; however, this downregulation could suggest that EHC chicks may have sustained body weight through the entire growth period more than the control group when presented with heat stress. This could propose future studies where EHC chicks are kept through maturation and heat-challenged at a later period. Eukaryotic translation initiation factor 4A2 (EIF4A2) was also downregulated in EHC chicks. EIF4A2 is correlated with the formation and development of muscle tissue in swine; however, the underlying regulatory processes are still unknown (Wang et al., 2007). To our knowledge, no existing literature reports SCG5 or EIF4A2 being investigated in chick models. There were also genes identified related to inhibiting apoptosis, metabolic genes, and immune response. Apoptosis-resistant E3 ubiquitin protein ligase 1 (AREL1) inhibits apoptosis (Jo et al., 2021), which may prolong cell life in EHC chicks. Upregulated genes related to metabolism include ATP synthase F0 subunit 8 (ATP8), NADH dehydrogenase subunit 2 (ND2), and adenylate cyclase 9 (ADCY9). ATP8 encodes mitochondrial gene expression, which is important for providing energy to be used by the cell. In a study analyzing phytase supplementation and its effects on broiler growth, meat quality, and muscle myopathies such as woody breast syndrome, ATP8 was upregulated, indicating abundant intracellular ATP (Walk et al., 2024). For EHC chicks, ATP8 was downregulated, which may suggest less ATP synthesis and energy conservation at the cellular level. ND2 was also downregulated in EHC chicks. ND2 is a component of the NADH dehydrogenase complex, which is responsible for catalyzing NADH to ubiquinone and facilitating proton pumping out of the mitochondrial matrix (Čermáková et al., 2021). In a normal homeostatic state, the downregulation of ND2 would be considered a problem due to lack of catalyzation; however, downregulated ND2 in EHC chicks may imply energy-conserving properties. Genes related to inflammation and immune response include TBC1 domain family member 20 (TBC1D20), exportin 6 (XPO6), and proteasome subunit alpha 2 (PSMA2). TBC1D20 expression mediates autophagy in mice and was upregulated in EHC chicks (Sidjanin et al., 2016). With autophagy being important for removing damaged proteins and organelles at the cellular level, it can be assumed that TBC1D20 maintains cellular health and homeostasis in EHC chicks. Upregulated XPO6 showed the activation of the NF-kB inflammatory response signaling pathway in pulmonary monocytes in mice (Wu et al., 2024) and was upregulated in EHC chicks. This could suggest cellular protection from the NF-kB inflammatory response being activated in EHC. PSMA2 was the only downregulated gene associated with inflammation and the immune response. In a study with PSMA2 knockdown,

10.3389/fphys.2025.1583958

TABLE 8 DEGs at hour 12 vs hour 0 in the nCP[a].

Direction	Ensembl ID	Name	Description	logFC	P-value	FDR
Downregulated	ENSGALG00010024651	PSMD3	Proteasome 26S subunit, non-ATPase 3	−0.68594	2.15E-06	0.02871
Downregulated	ENSGALG00010012032			−1.28093	3.27E-06	0.02871
Downregulated	ENSGALG00010014243	HIGD2A		−1.27669	5.64E-06	0.03307
Downregulated	ENSGALG00010006120	MOGS	Mannosyl-oligosaccharide glucosidase	−1.00933	8.47E-06	0.03723
Downregulated	ENSGALG00010011531	MTDH	Metadherin	−0.44060	1.52E-05	0.05334
Downregulated	ENSGALG00010020476	TMEM132A	Transmembrane protein 132A	−0.53498	1.98E-05	0.05796
Downregulated	ENSGALG00010021416	PLEKHH3	Pleckstrin homology, MyTH4, and FERM domain containing H3	−0.78872	3.03E-05	0.06675
Downregulated	ENSGALG00010028008	NTMT1	N-terminal Xaa-Pro-Lys N-methyltransferase 1	−0.53559	3.89E-05	0.06675
Downregulated	ENSGALG00010006065	WDR54	WD repeat domain 54	−0.68781	5.49E-05	0.06675
Upregulated	ENSGALG00010024961	LSM12	LSM12 homolog	0.66363	6.03E-05	0.06675
Downregulated	ENSGALG00010019064	DPY19L1		−0.60439	6.30E-05	0.06675
Upregulated	ENSGALG00010010126			1.77888	6.44E-05	0.06675
Downregulated	ENSGALG00010014278	G3BP1	G3BP stress granule assembly factor 1	−0.48920	6.73E-05	0.06675
Downregulated	ENSGALG00010008172	SNTB2	Syntrophin beta 2	−1.04640	7.09E-05	0.06675
Downregulated	ENSGALG00010015299	GALE	UDP-galactose-4-epimerase	−0.64200	7.17E-05	0.06675
Downregulated	ENSGALG00010024635			−0.86725	7.43E-05	0.06675
Downregulated	ENSGALG00010027617			−0.41535	7.81E-05	0.06675
Downregulated	ENSGALG00010025323	KLHDC8A	Kelch domain containing 8A	−0.48698	8.10E-05	0.06675
Downregulated	ENSGALG00010002792			−0.64896	8.28E-05	0.06675
Upregulated	ENSGALG00010001837	TAB3	TGF-beta activated kinase 1 (MAP3K7) binding protein 3	0.34290	8.42E-05	0.06675
Downregulated	ENSGALG00010018482	C10orf2	Twinkle mtDNA helicase	−0.89467	8.67E-05	0.06675
Upregulated	ENSGALG00010002185			0.94745	9.03E-05	0.06675
Downregulated	ENSGALG00010018951	YKT6	YKT6 v-SNARE homolog (*S. cerevisiae*)	−0.71108	9.11E-05	0.06675
Upregulated	ENSGALG00010001744			0.94319	1.12E-04	0.07224
Upregulated	ENSGALG00010029333			0.59066	1.24E-04	0.07224
Upregulated	ENSGALG00010029624	RASL10B	RAS-like family 10 member B	0.61430	1.33E-04	0.07224
Downregulated	ENSGALG00010022034			−0.69617	1.33E-04	0.07224
Upregulated	ENSGALG00010000022	ATP8	ATP synthase F0 subunit 8	2.64221	1.39E-04	0.07224
Downregulated	ENSGALG00010022513	NDUFAF1	NADH: ubiquinone oxidoreductase complex assembly factor 1	−0.41088	1.40E-04	0.07224
Downregulated	ENSGALG00010027359			−0.90077	1.45E-04	0.07224
Upregulated	ENSGALG00010000011	ND2	NADH dehydrogenase subunit 2	3.16881	1.53E-04	0.07224
Downregulated	ENSGALG00010004991	FAM133B	Family with sequence similarity 133 member B	−0.40436	1.62E-04	0.07224

(Continued on the following page)

TABLE 8 (*Continued*) DEGs at hour 12 vs hour 0 in the nCP[a].

Direction	Ensembl ID	Name	Description	logFC	P-value	FDR
Downregulated	ENSGALG00010019042	PEX6	Peroxisomal biogenesis factor 6	−0.43292	1.62E-04	0.07224
Downregulated	ENSGALG00010023482	SOGA1	Suppressor of glucose, autophagy associated 1	−0.42100	1.66E-04	0.07224
Upregulated	ENSGALG00010000020	COX2	Cytochrome c oxidase subunit II	1.06082	1.73E-04	0.07224
Upregulated	ENSGALG00010000033	ND5	NADH dehydrogenase subunit 5	1.68731	1.75E-04	0.07224
Upregulated	ENSGALG00010000026	ND3	NADH dehydrogenase subunit 3	1.56277	1.77E-04	0.07224
Downregulated	ENSGALG00010020451			−0.63924	2.09E-04	0.07952
Downregulated	ENSGALG00010020970	C6H10orf76	Armadillo-like helical domain containing 3	−0.46178	2.17E-04	0.07952
Downregulated	ENSGALG00010018044	INTS11	Integrator complex subunit 11	−1.44967	2.22E-04	0.07952
Upregulated	ENSGALG00010000023	ATP6	ATP synthase F0 subunit 6	2.29204	2.29E-04	0.08025
Downregulated	ENSGALG00010008010	CERK	Ceramide kinase	−0.56402	2.36E-04	0.08025
Upregulated	ENSGALG00010000029	ND4	NADH dehydrogenase subunit 4	2.66278	2.37E-04	0.08025
Downregulated	ENSGALG00010027533	WDR18	WD repeat domain 18	−0.76318	2.69E-04	0.08749
Downregulated	ENSGALG00010028129	CYB561D2	Cytochrome b561 family member D2	−0.81944	2.84E-04	0.08908
Downregulated	ENSGALG00010013402	MARCKS	Myristoylated alanine rich protein kinase C substrate	−0.52691	3.04E-04	0.09188
Downregulated	ENSGALG00010029763	GEMIN4	Gem nuclear organelle associated protein 4	−0.50494	3.08E-04	0.09188
Upregulated	ENSGALG00010010111	CNOT4	CCR4-NOT transcription complex subunit 4	0.38662	3.21E-04	0.09254
Upregulated	ENSGALG00010000034	CYTB	Cytochrome b	1.99713	3.27E-04	0.09272

Proteasome 26S subunit, non-ATPase 3 (PSMD3), mannosyl-oligosaccharide glucosidase (MOGS), metadherin (MTDH), transmembrane protein 132A (TMEM132A), pleckstrin homology, MyTH4, and FERM domain containing H3 (PLEKHH3), N-terminal Xaa-Pro-Lys N-methyltransferase 1 (NTMT1), WD repeat domain 54 (WDR54), LSM12 homolog (LSM12), G3BP stress granule assembly factor 1 (G3BP1), syntrophin beta 2 (SNTB2), UDP-galactose-4-epimerase (GALE), kelch domain containing 8A (KLHDC8A), TGF-beta activated kinase 1 (MAP3K7) binding protein 3 (TAB3), twinkle mtDNA helicase (C10orf2), YKT6 v-SNARE homolog (*S. cerevisiae*) (YKT6), RAS like family 10 member B (RASL10B), ATP synthase F0 subunit 8 (ATP8), NADH: ubiquinone oxidoreductase complex assembly factor 1 (NDUFAF1), NADH dehydrogenase subunit 2 (ND2), family with sequence similarity 133 member B (FAM133B), peroxisomal biogenesis factor 6 (PEX6), suppressor of glucose, autophagy associated 1 (SOGA1), cytochrome c oxidase subunit II (COX2), NADH dehydrogenase subunit 5 (ND5), NADH dehydrogenase subunit 3 (ND3), armadillo like helical domain containing 3 (C6H10orf76), integrator complex subunit 11 (INTS11), ATP synthase F0 subunit 6 (ATP6), ceramide kinase (CERK), NADH dehydrogenase subunit 4 (ND4), WD repeat domain 18 (WDR18), cytochrome b561 family member D2 (CYB561D2), myristoylated alanine rich protein kinase C substrate (MARCKS), gem nuclear organelle associated protein 4 (GEMIN4), CCR4-NOT transcription complex subunit 4 (CNOT4), and cytochrome b (CYTB). Abbreviations are not provided for unannotated genes.
[a]All DE results were determined with FDR <0.1.

dysregulation of signaling pathways involving the immune system and signal transduction was widely affected (Rashid et al., 2023). With PSMA2 being downregulated in EHC, this means that pathways involving signaling transduction and cellular health are lower than those in the controls. This could suggest that the signaling pathways involving PSMA2 are being energetically conserved in EHC chicks; however, additional research is needed to confirm this hypothesis.

4.2 Identification and physiological relevance of DEGs in the POAH

The POAH exhibited one downregulated and 17 upregulated DEGs, all at hour 2 of the heat challenge, and none had any effect on appetite, thermotolerance, or stress regions. In addition, none of those nine genes had an associated gene name or description as they are not annotated in the genome. This suggests future avenues of research to understand the pathways and actions of these unidentified genes. Although the DEGs in this group did not appear to cluster into a specific function or pathway, some relevant roles are noted. The C1q and TNF-related 8 (C1QTNF8) is an inflammation-related factor, and immune cross-tolerance was shown to be a consequence of EHC (Rosenberg et al., 2020; 2021; 2022) Microfibril-associated protein 5 (MFAP5) is downregulated during adipogenesis in patients with femoral head necrosis (Zhang et al., 2023). Although this study was carried out in humans, the adipogenic properties of MFAP5 could be translatable to the chicks in our study. MFAP5 was upregulated in the EHC group, and this could suggest adipocyte formation is reduced in EHC chicks compared to controls, potentially indicating thermoregulatory mechanisms mediated by the POAH.

Serpin family F member 1 (SERPINF1) was also upregulated in EHC. SERPINF1 was found to be anti-angiogenic and prevents new blood vessels from forming in triple-negative breast cancer (Maiti et al., 2019). Relevance to EHC could be speculated by promoting centralized thermoregulation through decreasing new blood vessel formation in the body of the EHC chicks. The only downregulated gene, BEN domain containing 3 (BEND3), has not been shown, to our knowledge, to have direct biological functions. However, it is essential in transcriptional repression and actively binds with heterochromatin in the nucleus, making it an essential binding protein (Shiheido and Shimizu, 2015). Overall, the genes noted are indicative of EHC potentially improving thermotolerance, which aligns with the mechanistic action of the POAH.

4.3 Identification and physiological relevance of DEGs in the PVN

The PVN produced four DEGs specifically at hour 2. Two of them stand out as factors that may play a role in hypothalamic regulation of the water and salt balance. They are vasoactive intestinal peptide receptor 1 (VIPR1) and caprin family member 2 (CAPRIN2), both of which were upregulated in EHC chicks. Signaling through VIPR1 has previously been demonstrated to decrease food intake in mice, and Yu et al. (2008) showed that mice treated with a VPAC1 (alias of VIPR1) agonist also showed inhibited food intake. In addition, VPAC1 also delayed development and reduced weight in mice (Fabricius et al., 2011). Although food intake was not measured in our study, the effects of decreased food intake in mice could be translated to EHC chicks being more energetically efficient during heat stress and maintaining their body weight during this stress, thus providing more energy to protect and maintain homeostasis in their visceral organs. The endogenous ligand for VPAC1, vasoactive intestinal peptide, is involved in smooth muscle relaxation, hormone release, and water and mineral movement in the gut. CAPRIN2 is vastly increased in the nucleus and cytoplasm of arginine vasopressin (AVP) neurons during dehydration in rats (Bárez-López et al., 2022) and may affect thermotolerance due to its water-regulating properties. It is tempting to speculate that *via* the PVN, the expression of these factors may regulate salt and water retention during heat stress. In endotherms, body temperature and water balance are strongly associated, and in chickens, evaporative heat loss can be facilitated through increased panting during heat stress (also making them susceptible to alkalosis).

4.4 Identification and physiological relevance of DEGs with timepoint interactions

Although there were only DEGs at timepoint interactions at hour 12, these observed time effects were also of importance. We chose to analyze timepoint interactions to compare the different hours of heat exposure on the tissues themselves, without treatment being compared. While we anticipated more DEGs across tissues other than the nCPa, these data provided insights on gene expression as the heat challenge progressed. Hour 12 vs 2 yielded nine genes, and upon further investigation, two were of importance. Ubiquitin-associated protein 2 like (UBAP2L), when triggered by stress, plays a role in processing body (PB) formation and PB interaction with stress granules (Riggs et al., 2024). Because UBAP2L was upregulated at hour 12 relative to that at hour 2, this suggests that a prolonged stress cascade from the heat challenge increased the expression. BCL2 family apoptosis regulator (BCL1) is anti-apoptotic, and the BCL2 family plays a role in inhibiting mitophagy, which are both essential in regulating reactive oxygen species (ROS) (Su et al., 2023). ROS production can be stimulated during heat stress by causing oxidative stress, so it is plausible that because BCL1 was downregulated, heat stress at hour 12 vs. 2 caused increased production of ROS throughout the heat challenge.

Moving into hour 12 vs. hour 0, there were 49 DEGs between these timepoints. With a greater number of genes becoming activated as time progressed, the heat challenge can be noted as a dynamic process. This result is expected as hour 0 was set as the baseline for the heat challenge and hour 2 and 12 were collected afterward to measure any resulting differences. Of the 49 genes, 13 had no title or name association, showing that they are not annotated in the chicken genome. The remaining genes were investigated, and genes discussed below were associated with cellular metabolism and/or stress regulation and had relevance to changes associated with heat.

Metabolic genes include mannosyl-oligosaccharide glucosidase (MOGS), metadherin (MTDH), UDP-galactose-4-epimerase (GALE), twinkle mtDNA helicase (C10orf2), ATP synthase F0 subunit 8 (ATP8) and subunit 6 (ATP6), suppressor of glucose, autophagy-associated 1 (SOGA1), NADH dehydrogenase subunit 5 (ND5), subunit 3 (ND3), and subunit 4 (ND4), CCR4-NOT transcription subunit 4 (CNOT4), and cytochrome B. Each of these genes had regulatory effects in most phases of cellular metabolism. In particular, genes related to ATP and NADH regulation were present, where ATP8 was upregulated and increased intracellular ATP abundance (Walk et al., 2024), and ATP6 was also upregulated, which has been shown to facilitate the flow of protons across the mitochondrial membrane and drive ATP synthesis for energy production. ATP6 was shown to be decreased when lipopolysaccharide-induced intestinal oxidative stress is present. This suggests that chicks at 12 h had reduced oxidative stress, thus upregulating the gene. ND3, ND4, and ND5 were also all upregulated, and all of these are involved in the mitochondrial electron transport chain. This implies that at hour 12, cellular function was not disrupted at the mitochondrial level. In addition, C10orf2 has been shown to cause mitochondrial DNA depletion syndrome in infants (Remtulla et al., 2019) and was found to be downregulated in chicks at hour 12. To further support the idea of mitochondrial preservation, the CNOT4 complex, which regulates RNA metabolism (Collart, 2016), was also upregulated at hour 12. CYTB was upregulated at hour 12 and affects energy metabolism through oxidative phosphorylation. In a study carried out on sheep, CYTB increased thermodynamic stability and energy metabolism (Pal et al., 2019). Moreover, some cellular metabolism genes were also downregulated, such as MOGS and MTDH. MTDH regulates vascular endothelial growth factor expression *via* the PI3/AKT pathway, and the PI3/AKT pathway is also responsible for cell metabolism and growth (Zhu et al., 2015). MOGS was also a surprising gene to be downregulated, given its important role in

cellular metabolism. A previous study showed that the knockdown of MOGS led to increased proliferation and differentiation of Schwann cells (Zhang et al., 2022). Schwann cells play an active role in forming the myelin sheath, which covers the axon and facilitates faster nerve signal transmission (Zhang et al., 2022). GALE at 12 h was downregulated, so processes were muted. The overexpression of GALE increases gluconeogenesis, and it is an enzyme that converts galactose to glucose (Zhu et al., 2017). The downregulation of these genes could be because of a variety of factors; however, at hour 12, genes had prolonged expression, causing them to decrease over time. SOGA1 was also downregulated at hour 12. However, SOGA1 promotes AMPK, which further upregulates PDK4, which is a protein that decreases glucose metabolism. Therefore, SOGA1 being downregulated at hour 12 could promote glucose metabolism (Wei et al., 2023).

There were two stress-associated genes that were also found in 12 vs 0, which are the gem nuclear organelle associated protein 4 (GEMIN4) and G3BP stress granule assembly factor 1(G3BP1). Both these genes were downregulated at hour 12 and have important effects on stress responses. G3BP1 is an RNA binding protein associated with the assembly of stress granules following a stimulus (Martin et al., 2013). Downregulation could be due to an expression plateau, where G3BP1 had higher expression at time 0, and as the heat challenge progressed, there was a decline in expression. Another noteworthy gene was GEMIN4, which functions as a novel co-regulator of the mineralocorticoid receptor (MR) and actually decreases MR activity (Yang et al., 2015). MRs are responsible for mediating the action of aldosterone and cortisol, which are widely changed due to stress.

With timepoint interactions being irrespective of treatment, it is worth speculating whether or not EHC had a strong influence on these DEGs. Regardless, most of the genes described were of benefit to the physiological and molecular health of the chicks. Given that 12 h is a substantial amount of time, we expected to observe many genes downregulated and/or a cessation of metabolic processes to come to a halt because of the prolonged stress that heat imposes on the body. However, these data show that cellular resiliency is much more of a theme than anticipated.

The punch biopsy isolation of individual nuclei afforded superior anatomical resolution in parsing out effects of gene expression that were region-specific. These regions were selected based on previous work (Kuenzel and van Tienhoven, 1982; Bohler et al., 2020). CRH is a major neuron projected onto the PVN from the nCPa for mediating the stressor response; however, our results did not contain any notable levels of CRF being expressed in the nCPa or PVN. Other genes that were expected to be differentially expressed were HSPs, adrenocorticotropic hormone (ACTH), a stress modulator, appetite-regulating factors such as NPY, and melanocortin ligands such as POMC and a-MSH. Within our RT-PCR data, which are provided as supplementary tables, NPY, CRF, POMC, CCK, UCN3, TRH, and HSP90 mRNA abundance was measured in each of the nuclei. RT-PCR was measured before RNA-seq genome annotation. In the PVN, CRF was significant between control and EHC. In addition, there was significance in timepoint differences for NPY, POMC, UCN3, and TRH. HSP90 also displayed significant differences for timepoint–treatment interactions. For the POAH, CRF was also significant between control and EHC; POMC was significant for treatment, timepoint, and treatment–timepoint interactions, and HSP90 was significant between treatments. It is especially relevant that the RT-PCR data for the nCPa had the least amount of differences—with only NPY showing statistical significance between timepoints. Considering that the nCPa was the highest-yielding tissue for DEGs in the RNA-seq analysis, this difference in expression from RNA-seq to RT-PCR was intriguing. It is also important to note that these were not identified as differentially expressed. Additionally, genes tested with RT-PCR could not be found in any of the RNA-seq raw data. Reasons for this could be because of the large number of genes in the genome and that RT-PCR is a targeted assay.

Previous studies have shown that chicks on day 4 have differences in stress- and appetite-related gene expression in both the PVN and nCPa, particularly in brain-derived neurotrophic factor (BDNF) and CRF. However, it is important to note that in the experiment performed by Bohler et al. (2020), chicks were intracerebroventricularly injected with either NPY, astressin, a-MSH—direct regulators of appetite—or CRH, which directly affects stress modulation (Bohler et al., 2020). Although feed intake was not measured in this study, it is also possible that decreased feed intake in both groups could have reduced the differential expression related to appetite-regulating genes. When chicks experience hyperthermia, production aspects such as growth and reproduction decrease to maintain organ homeostasis (Moraes et al., 2003; Wolfenson et al., 1981). Thus, heat exposure also decreases feed consumption to reduce thermogenic effects on metabolization and nutrient partitioning (Mckee et al., 1997). This may explain why no appetite-regulating genes were found to be differentially expressed during the heat challenge.

To conclude, EHC has been credited with reducing the severity of heat stress on hypothalamic responses, and further research is needed to determine whether the identified DEGs play a direct role in heat stress tolerance in chicks. Additionally, some of these studies were conducted in non-chick models and may involve mammalian models where respiration is different (active vs positive) from that in avians, which means that physiological and molecular responses may differ. Future research could explore whether the duration of heat exposure influences gene expression (e.g., longer exposure periods), whether age affects these responses, and whether reduced feed intake contributes to muted hypothalamic activity. Combined with previous literature on EHC, our transcriptomic analysis suggests that the gene expression profile of the hypothalamus and the different nuclei resembles patterns that align with remediated stress in EHC chicks. This study enhances our understanding of the molecular mechanisms underlying DEG expression in response to high ambient temperatures.

Data availability statement

The data presented in the study are deposited in the GEO repository, accession number GSE298648.

Ethics statement

The animal study was approved by the Virginia Tech Institutional Animal Care and Use Committee. The study was

conducted in accordance with the local legislation and institutional requirements.

Author contributions

RV: data curation, formal analysis, investigation, writing – original draft, and writing – review and editing. US: investigation, methodology, and writing – review and editing. AF: formal analysis, investigation, and writing – review and editing. FB: data curation, formal analysis, methodology, resources, writing – original draft, and writing – review and editing. NM: conceptualization, funding acquisition, methodology, and writing – review and editing. DL: investigation and writing – review and editing. PS: formal analysis, investigation, methodology, validation, and writing – review and editing. MC: conceptualization, funding acquisition, investigation, project administration, resources, supervision, and writing – review and editing. EG: conceptualization, funding acquisition, investigation, project administration, supervision, and writing – review and editing.

Funding

The author(s) declare that financial support was received for the research and/or publication of this article. This research was funded by The John Lee Pratt Endowment at Virginia Tech and NSF-BSF award #2041923. Sequencing was performed at the *Genomics Sequencing Center*, which is part of the *Fralin Life Science Institute at Virginia Tech.* , 540-231-1229

Conflict of interest

The authors declare that the research was conducted in the absence of any commercial or financial relationships that could be construed as a potential conflict of interest.

Generative AI statement

The author(s) declare that no Generative AI was used in the creation of this manuscript.

Publisher's note

Supplementary material

The Supplementary Material for this article can be found online at: https://www.frontiersin.org/articles/10.3389/fphys.2025.1583958/full#supplementary-material

References

Amaz, S. A., Chaudhary, A., Mahato, P. L., Jha, R., and Mishra, B. (2024b). Pre-hatch thermal manipulation of embryos and post-hatch baicalein supplementation mitigated heat stress in broiler chickens. *J. animal Sci. Biotechnol.* 15 (1), 8. doi:10.1186/s40104-023-00966-6

Amaz, S. A., Shahid, M. A. H., Chaudhary, A., Jha, R., and Mishra, B. (2024a). Embryonic thermal manipulation reduces hatch time, increases hatchability, thermotolerance, and liver metabolism in broiler embryos. *Poult. Sci.* 103 (4), 103527. doi:10.1016/j.psj.2024.103527

Bárez-López, S., Konopacka, A., Cross, S. J., Greenwood, M., Skarveli, M., Murphy, D., et al. (2022). Transcriptional and post-transcriptional regulation of oxytocin and vasopressin gene expression by CREB3L1 and CAPRIN2. *Neuroendocrinology* 112 (11), 1058–1077. doi:10.1159/000522088

Beck, D. L., Gilbert, E. R., and Cline, M. A. (2024). Embryonic thermal challenge is associated with increased stressor resiliency later in life: molecular and morphological mechanisms in the small intestine. *Comp. Biochem. Physiol. A Mol. Integr. Physiol.* 297, 111724. doi:10.1016/j.cbpa.2024.111724

Benjamini, Y., and Hochberg, Y. (1995). Controlling the false discovery rate: a practical and powerful approach to multiple testing. *J. R. Stat. Soc. Ser. B Stat. Methodol.* 57 (1), 289–300. doi:10.1111/j.2517-6161.1995.tb02031.x

Bohler, M., Gilbert, E. R., and Cline, M. A. (2020). Reduced food intake during exposure to high ambient temperatures is associated with molecular changes in the nucleus of the hippocampal commissure and the paraventricular and arcuate hypothalamic nuclei. *Gen. Comp. Endocrinol.* 298, 113576. doi:10.1016/j.ygcen.2020.113576

Bohler, M. W., Chowdhury, V. S., Cline, M. A., and Gilbert, E. R. (2021). Heat stress responses in birds: a review of the neural components. *Biol. (Basel)* 10 (11), 1095. doi:10.3390/biology10111095

Bourgon, R., Gentleman, R., and Huber, W. (2010). Independent filtering increases detection power for high-throughput experiments. *Proc. Natl. Acad. Sci. U. S. A.* 107 (21), 9546–9551. doi:10.1073/pnas.0914005107

Čermáková, P., Maďarová, A., Baráth, P., Bellová, J., Yurchenko, V., and Horváth, A. (2021). Differences in mitochondrial NADH dehydrogenase activities in trypanosomatids. *Parasitology* 148 (10), 1161–1170. doi:10.1017/S0031182020002425

Collart, M. A. (2016). The Ccr4-Not complex is a key regulator of eukaryotic gene expression. *Wiley Interdiscip. Rev. RNA* 7 (4), 438–454. doi:10.1002/wrna.1332

Dawson, M. (2023). Global poultry meat production reaches 138 million tons. WATTPoultry.com. Available online at: https://www.wattagnet.com/broilers-turkeys/article/15536618/global-poultry-meat-production-reaches-138-million-tons (Accessed July, 2024).

Fabricius, D., Karacay, B., Shutt, D., Leverich, W., Schafer, B., Takle, E., et al. (2011). Characterization of intestinal and pancreatic dysfunction in VPAC1-null mutant mouse. *Pancreas* 40 (6), 861–871. doi:10.1097/mpa.0b013e318214c783

Farber, C. R., Chitwood, J., Lee, S.-N., Verdugo, R. A., Islas-Trejo, A., Rincon, G., et al. (2008). Overexpression of SCG5 increases enzymatic activity of PCSK2 and is inversely correlated with body weight in congenic mice. *BMC Genet.* 9 (1), 34. doi:10.1186/1471-2156-9-34

Hillier, L. W., Miller, W., Birney, E., Warren, W., Hardison, R. C., Ponting, C. P., et al. (2004). Sequence and comparative analysis of the chicken genome provide unique perspectives on vertebrate evolution. *Nature* 432 (7018), 695–716. doi:10.1038/nature03154

Holm, S. (1979). A simple sequentially rejective multiple test procedure. *Scand. J. Statistics* 6 (2), 65–70.

Jo, Y., Kim, B., and Shin, D. (2021). AREL1 E3 ubiquitin ligase inhibits TNF-induced necroptosis via the ubiquitination of MTX2. *Exp. Ther. Med.* 22, 1195. doi:10.3892/etm.2021.10629

Kadhim, H. J., Kang, S. W., and Kuenzel, W. J. (2019). Differential and temporal expression of corticotropin releasing hormone and its receptors in the nucleus of the hippocampal commissure and paraventricular nucleus during the stress response in chickens (*Gallus gallus*). *Brain Res.* 1714, 1–7. doi:10.1016/j.brainres.2019.02.018

Kalabusheva, E. P., Shtompel, A. S., Rippa, A. L., Ulianov, S. V., Razin, S. V., and Vorotelyak, E. A. (2023). A kaleidoscope of keratin gene expression and the mosaic of its regulatory mechanisms. *Int. J. Mol. Sci.* 24 (6), 5603. doi:10.3390/ijms24065603

Kim, D., Paggi, J. M., Park, C., Bennett, C., and Salzberg, S. L. (2019). Graph-based genome alignment and genotyping with HISAT2 and HISAT-genotype. *Nat. Biotechnol.* 37 (8), 907–915. doi:10.1038/s41587-019-0201-4

Kisliouk, T., Ravi, P. M., Rosenberg, T., and Meiri, N. (2024). Embryonic manipulations shape life-long, heritable stress responses through complex epigenetic mechanisms: a review. *Front. Neurosci.* 18, 1435065. doi:10.3389/fnins.2024.1435065

Kuenzel, W. J., and Masson, M. (1988). A stereotaxic atlas of the brain of the chick (*Gallus domesticus*). Poultry Science Faculty Publications and Presentations. Available online at: https://scholarworks.uark.edu/poscpub/1 (Accessed August, 2024).

Kuenzel, W. J., and van Tienhoven, A. (1982). Nomenclature and location of avian hypothalamic nuclei and associated circumventricular organs. *J. Comp. Neurol.* 206 (3), 293–313. doi:10.1002/cne.902060309

Labunskay, G., and Meiri, N. (2006). R-Ras3/(M-Ras) is involved in thermal adaptation in the critical period of thermal control establishment. *J. Neurobiol.*66, 56–70. doi:10.1002/neu.20191

Li, B., and Dewey, C. N. (2011). RSEM: accurate transcript quantification from RNA-seq data with or without a reference genome. *BMC Bioinforma.* 12 (1), 323. doi:10.1186/1471-2105-12-323

Li, H., Handsaker, B., Wysoker, A., Fennell, T., Ruan, J., Homer, N., et al. (2009). The sequence alignment/map format and SAMtools. *Bioinforma. Oxf. Engl.* 25 (16), 2078–2079. doi:10.1093/bioinformatics/btp352

Liao, Y., Smyth, G. K., and Shi, W. (2014). featureCounts: an efficient general purpose program for assigning sequence reads to genomic features. *Bioinforma. Oxf. Engl.* 30 (7), 923–930. doi:10.1093/bioinformatics/btt656

Love, M. I., Huber, W., and Anders, S. (2014). Moderated estimation of fold change and dispersion for RNA-seq data with Deseq2. *Genome Biol.* 15, 550. doi:10.1186/s13059-014-0550-8

Maiti, A., Qi, Q., Peng, X., Yan, L., Takabe, K., and Hait, N. C. (2019). Class I histone deacetylase inhibitor suppresses vasculogenic mimicry by enhancing the expression of tumor suppressor and anti-angiogenesis genes in aggressive human TNBC cells. *Int. J. Oncol.* 55 (1), 116–130. doi:10.3892/ijo.2019.4796

Martin, S., Zekri, L., Metz, A., Maurice, T., Chebli, K., Vignes, M., et al. (2013). Deficiency of G3BP1, the stress granules assembly factor, results in abnormal synaptic plasticity and calcium homeostasis in neurons. *J. Neurochem.*, 125(2), 175–184. doi:10.1111/jnc.12189

McCarthy, D. J., Chen, Y., and Smyth, G. K. (2012). Differential expression analysis of multifactor RNA-Seq experiments with respect to biological variation. *Nucleic Acids Res.* 40 (10), 4288–4297. doi:10.1093/nar/gks042

McKee, J., Harrison, P., and Riskowski, G. (1997). Effects of supplemental ascorbic acid on the energy conversion of broiler chicks during heat stress and feed withdrawal. *Poult. Sci.* 76 (9), 1278–1286. doi:10.1093/ps/76.9.1278

Moraes, V. M. B., Malheiros, R. D., Bruggeman, V., Collin, A., Tona, K., Van As, P., et al. (2003). Effect of thermal conditioning during embryonic development on aspects of physiological responses of broilers to heat stress. *J. Therm. Biol.* 28(2), 133–140. doi:10.1016/S0306-4565(02)00049-9

Nawab, A., Ibtisham, F., Li, G., Kieser, B., Wu, J., Liu, W., et al. (2018). Heat stress in poultry production: mitigation strategies to overcome the future challenges facing the Global Poultry Industry. *J. Therm. Biol.* 78, 131–139. doi:10.1016/j.jtherbio.2018.08.010

Pal, A., Pal, A., Banerjee, S., Batabyal, S., and Chatterjee, P. N. (2019). Mutation in Cytochrome B gene causes debility and adverse effects on health of sheep. *Mitochondrion* 46, 393–404. doi:10.1016/j.mito.2018.10.003

Pezeshkian, Z., Mirhoseini, S., Ghovvati, S., and Ebrahimie, E. (2022a). Expression of serine biosynthesis pathway genes in breast muscles of Iranian native turkeys with divergent feed efficiency. *J. Appl. Anim. Sci.* 14 (3), 427–437. doi:10.22067/ijasr.2022.74768.1061

Pezeshkian, Z., Mirhoseini, S. Z., Ghovvati, S., and Ebrahimie, E. (2022b). Transcriptome analysis of breast muscle reveals pathways related to protein deposition in high feed efficiency of native turkeys. *Animals* 12 (10), 1240. doi:10.3390/ani12101240

Piestun, Y., Druyan, S., Brake, J., and Yahav, S. (2013). Thermal treatments prior to and during the beginning of incubation affect phenotypic characteristics of broiler chickens posthatching. *Poult. Sci.* 92 (4), 882–889. doi:10.3382/ps.2012-02568

Rashid, M. U., Lorzadeh, S., Gao, A., Ghavami, S., and Coombs, K. M. (2023). PSMA2 knockdown impacts expression of proteins involved in immune and cellular stress responses in human lung cells. *Biochim. Biophys. Acta Mol. Basis Dis.* 1869 (2), 166617. doi:10.1016/j.bbadis.2022.166617

Reed, K. M., Mendoza, K. M., Strasburg, G. M., and Velleman, S. G. (2022). Transcriptome response of proliferating muscle satellite cells to thermal challenge in commercial Turkey. *Front. Physiol.* 13, 970243. doi:10.3389/fphys.2022.970243

Remtulla, S., Emilie Nguyen, C. T., Prasad, C., and Campbell, C. (2019). Twinkle-associated mitochondrial DNA depletion. *Pediatr. Neurol.* 90, 61–65. doi:10.1016/j.pediatrneurol.2018.08.007

Riggs, C. L., Kedersha, N., Amarsanaa, M., Zubair, S. N., Ivanov, P., and Anderson, P. (2024). UBAP2L contributes to formation of P-bodies and modulates their association with stress granules. *J. Cell Biol.* 223 (10), e202307146. doi:10.1083/jcb.202307146

Robinson, M. D., McCarthy, D. J., and Smyth, G. K. (2010). edgeR: a Bioconductor package for differential expression analysis of digital gene expression data. *Bioinforma. Oxf. Engl.* 26 (1), 139–140. doi:10.1093/bioinformatics/btp616

Rosenberg, T., Kisliouk, T., Ben-Nun, O., Cramer, T., and Meiri, N. (2021). Cross-tolerance: embryonic heat conditioning induces inflammatory resilience by affecting different layers of epigenetic mechanisms regulating *IL6* expression later in life. *Epigenetics* 16 (2), 228–241. doi:10.1080/15592294.2020.1795596

Rosenberg, T., Kisliouk, T., Cramer, T., Shinder, D., Druyan, S., and Meiri, N. (2020). Embryonic heat conditioning induces TET-dependent cross-tolerance to hypothalamic inflammation later in life. *Front. Genet.* 11, 767. doi:10.3389/fgene.2020.00767

Rosenberg, T., Marco, A., Kisliouk, T., Haron, A., Shinder, D., Druyan, S., et al. (2022). Embryonic heat conditioning in chicks induces transgenerational heat/immunological resilience via methylation on regulatory elements. *Faseb J.* 36 (7), e22406. doi:10.1096/fj.202101948R

Rothhaas, R., and Chung, S. (2021). Role of the preoptic area in sleep and thermoregulation. *Front. Neurosci.* 15, 664781. [Review]. doi:10.3389/fnins.2021.664781

Shiheido, H., and Shimizu, J. (2015). Basic amino acid residues located in the N-terminal region of BEND3 are essential for its nuclear localization. *Biochem. Biophys. Res. Commun.* 457 (4), 589–594. doi:10.1016/j.bbrc.2015.01.029

Sidjanin, D. J., Park, A. K., Ronchetti, A., Martins, J., and Jackson, W. T. (2016). TBC1D20 mediates autophagy as a key regulator of autophagosome maturation. *Autophagy* 12 (10), 1759–1775. doi:10.1080/15548627.2016.1199300

Su, L., Zhang, J., Gomez, H., Kellum, J. A., and Peng, Z. (2023). Mitochondria ROS and mitophagy in acute kidney injury. *Autophagy* 19 (2), 401–414. doi:10.1080/15548627.2022.2084862

Sulaiman, U., Vaughan, R. S., Siegel, P., Liu, D., Gilbert, E. R., and Cline, M. A. (2024). Embryonic heat conditioning increases lipolytic gene expression in broiler chicks at day 4 post-hatch. *Front. Physiol.* 15, 1445569. doi:10.3389/fphys.2024.1445569

Tan, C. L., and Knight, Z. A. (2018). Regulation of body temperature by the nervous system. *Neuron* 98 (1), 31–48. doi:10.1016/j.neuron.2018.02.022

Tischler, G., and Leonard, S. (2014). biobambam: tools for read pair collation based algorithms on BAM files. *Source Code Biol. Med.* 9, 13. doi:10.1186/1751-0473-9-13

Walk, C. L., Mullenix, G. J., Maynard, C. W., Greene, E. S., Maynard, C., Ward, N., et al. (2024). Novel 4th-generation phytase improves broiler growth performance and reduces woody breast severity through modulation of muscle glucose uptake and metabolism. *Front. Physiol.* 15, 1376628. doi:10.3389/fphys.2024.1376628

Wang, H., Wang, H., Zhu, Z., Yang, S., and Li, K. (2007). Molecular cloning, mapping, and expression analysis of the EIF4A2 gene in pig. *Biochem. Genet.* 45 (1-2), 51–62. doi:10.1007/s10528-006-9065-7

Wei, W., Zhang, Z. Y., Shi, B., Cai, Y., Zhang, H. S., Sun, C. L., et al. (2023). METTL16 promotes glycolytic metabolism reprogramming and colorectal cancer progression. *J. Exp. Clin. Cancer Res.* 42 (1), 151. doi:10.1186/s13046-023-02732-y

Wolfenson, D., Frei, Y. F., Snapir, N., and Berman, A. (1981). Heat stress effects on capillary blood flow and its redistribution in the laying hen. *Pflugers Archiv Eur. J. Physiol.* 390 (1), 86–93. doi:10.1007/BF00582717

Wu, Y., Gou, Y., Wang, T., Li, P., Li, Y., Lu, X., et al. (2024). Exportin XPO6 upregulation activates the TLR2/MyD88/NF-κB signaling by facilitating TLR2 mRNA nuclear export in COPD pulmonary monocytes. *Int. Immunopharmacol.* 135, 112310. doi:10.1016/j.intimp.2024.112310

Yang, J., Fuller, P. J., Morgan, J., Shibata, H., Clyne, C. D., and Young, M. J. (2015). GEMIN4 functions as a coregulator of the mineralocorticoid receptor. *J. Mol. Endocrinol.* 54 (2), 149–160. doi:10.1530/jme-14-0078

Young, M. D., Wakefield, M. J., Smyth, G. K., and Oshlack, A. (2010). Gene ontology analysis for RNA-seq: accounting for selection bias. *Genome Biol.* 11 (2), R14. doi:10.1186/gb-2010-11-2-r14

Yousefvand, S., and Hamidi, F. (2019). Role of paraventricular nucleus in regulation of feeding behaviour and the design of intranuclear neuronal pathway communications. *Int. J. Peptide Res. Ther.* 26 (3), 1231–1242. doi:10.1007/s10989-019-09928-x

Yu, R. J., Zhang, L., Yi, T. H., Xie, S. S., and Dai, Y. (2008). *In vivo* anti-obesity effect of the agonist for receptor VPAC1. *Sheng Li Xue Bao* 60 (6), 751–758.

Zhang, T., Li, H., Sun, S., Zhou, W., Zhang, T., Yu, Y., et al. (2023). Microfibrillar-associated protein 5 suppresses adipogenesis by inhibiting essential coactivator of PPARγ. *Sci. Rep.* 13 (1), 5589. doi:10.1038/s41598-023-32868-y

Zhang, Y., Yang, M., Shen, Y., Yi, S., and Wang, X. (2022). Metabolism-related MOGS gene is dysregulated after peripheral nerve injury and negatively regulates schwann cell plasticity. *J. Mol. Neurosci.* 72 (6), 1402–1412. doi:10.1007/s12031-022-02024-8

Zhu, G. C., Yu, C. Y., She, L., Tan, H. L., Li, G., Ren, S. L., et al. (2015). Metadherin regulation of vascular endothelial growth factor expression is dependent upon the PI3K/Akt pathway in squamous cell carcinoma of the head and neck. *Med. Baltim.* 94 (6), e502. doi:10.1097/md.0000000000000502

Zhu, Y., Zhao, S., Deng, Y., Gordillo, R., Ghaben, A. L., Shao, M., et al. (2017). Hepatic GALE regulates whole-body glucose homeostasis by modulating Tff3 expression. *Diabetes* 66 (11), 2789–2799. doi:10.2337/db17-0323

frontiers | Frontiers in Physiology

TYPE Original Research
PUBLISHED 03 September 2025
DOI 10.3389/fphys.2025.1627516

OPEN ACCESS

EDITED BY
Sandra G. Velleman,
The Ohio State University, United States

REVIEWED BY
Jamie M. Cornelius,
Oregon State University, United States
Colin Guy Scanes,
University of Wisconsin–Milwaukee,
United States

*CORRESPONDENCE
D. Singh,
devrajsingh23@uky.edu

RECEIVED 12 May 2025
ACCEPTED 12 August 2025
PUBLISHED 03 September 2025

CITATION
Singh D, Fudickar AM and Ketterson ED (2025) Seasonal divergence in reproductive timing on the verge of spring: comparing hypothalamic transcriptome of two seasonally sympatric North American songbird populations. *Front. Physiol.* 16:1627516. doi: 10.3389/fphys.2025.1627516

Seasonal divergence in reproductive timing on the verge of spring: comparing hypothalamic transcriptome of two seasonally sympatric North American songbird populations

Devraj Singh[1]*, Adam M. Fudickar[2,3] and Ellen D. Ketterson[2,3]

[1]Biology Department, University of Kentucky, Lexington, KY, United States, [2]Biology Department, Indiana University, Bloomington, IN, United States, [3]Environmental Resilience Institute, Indiana University Bloomington, Bloomington, IN, United States

Every year as spring approaches and day length increases, many birds begin to reproduce, an annual expression of seasonal phenology that requires physiological preparation. In species distributed over a broad geographic range, populations that breed at higher latitudes are often migratory and delay reproduction until later in the year as compared to those breeding at lower latitudes. Dark-eyed Juncos serve as an excellent model for understanding the timing mechanisms regulating population-level variation in seasonal reproductive responses. We compared two seasonally sympatric dark-eyed junco populations in early spring. One migrates (*Junco hyemalis hyemalis*) and breeds in Alaska and Canada, while the other remains resident (*Junco hyemalis carolinensis*) and breeds in the Appalachian Mountains of Virginia USA. These populations exhibit different photoperiodic responses to the same environment with respect to activation of the HPG axis, leading to earlier gonadal recrudescence in the resident population. We caught co-wintering sympatric male migrant (n = 6) and resident (n = 7) juncos from the field in March and collected the hypothalamic tissues. We also collected blood samples to determine circulating testosterone and a wing feather to determine stable isotope ratios (δ^2H) as estimate of breeding latitude. We found three differentially expressed genes, among which gonadotropin releasing hormone 1 (GnRH1) showed significantly higher expression in early breeding residents as compared to migrant juncos. The δ^2H showed a positive linear correlation with testosterone levels and GnRH1 mRNA, providing strong evidence for latitudinal variation in breeding phenology. This study provides insight into the underlying neuroendocrine response giving rise to a population-level difference in the timing of reproduction observed in a seasonally sympatric (co-wintering) population of resident and migrant juncos.

KEYWORDS

seasonal reproduction, stable hydrogen isotope, migration, dark-eyed junco, hypothalamus, gnrh1

Introduction

Seasonal animals have evolved different timing strategies to match their recurring physiology of migration and reproduction to the environment (Ketterson and Greives, 2025). Annual changes in day length (photoperiod) are a primary entraining cue for endogenous clocks to synchronize with the environment. Avian populations that live in sympatry during the non-breeding state from winter to early spring may differ in whether or not they migrate. If they do, then they may breed at different locations in spring and summer, thus becoming allopatric (Fudickar et al., 2016; Ramenofsky et al., 2017; Wanamaker et al., 2020). One such species is the dark-eyed junco, which is distributed over a broad geographic range. In the junco, closely related populations winter in sympatry but differ in when they breed and whether they migrate. This pattern of sympatry in winter and allochrony in breeding makes the dark-eyed junco a powerful model to investigate the neuroendocrine basis of differences in the timing of reproduction because they pass through an overwintering period together and start to differ in their behavioral and physiological responses to similar environmental cues as spring approaches.

Use of hydrogen isotope signatures in the movement ecology of birds is a common tool in practice to predict breeding latitude (Fudickar et al., 2016; Wanamaker et al., 2020; Singh et al., 2021). Birds incorporate isotope signatures through their diet or nearby water bodies (Cormie et al., 1994; Langin et al., 2007). The local isotopic signature is incorporated into the growing feather during the post breeding molt. Because feathers are epidermal growths that are metabolically inactive, they later reflect the local isotopic signature from the geographical location where they were grown (Hobson, 1999). Stable isotopes such as hydrogen vary geographically and are used to estimate the breeding location and location of feather growth (Hobson, 2005; Powell and Hobson, 2006; Girvan et al., 2007; Maggini et al., 2016). In the case of the junco, migrant and resident populations can be distinguished during winter by the lighter hydrogen stable isotope values in migrants as compared to the heavier values found in residents.

Songbirds undergo seasonal recrudescence in their reproductive processes, primarily regulated by hypothalamic GnRH neurons (Li et al., 1994; Stevenson et al., 2009). In the temperate zone, birds initiate their gonadal development in response to increasing day lengths during early spring. However, the time of reproductive response varies depending on breeding latitude. The seasonal reproductive response is induced primarily through the interaction of increasing day length with the hypothalamic-pituitary-gonadal (HPG) axis (Li et al., 1994; Cho et al., 1998). After the winter solstice, the photoperiod starts to increase, which stimulates the HPG on reaching a population-specific threshold level of photoperiod (Wanamaker et al., 2020; Singh et al., 2021). The annual change in day length varies with latitude, such that birds breeding at higher latitudes often require longer days to initiate gonadal recrudescence than birds breeding at lower latitudes (Dawson, 2013; Fudickar et al., 2016; Singh et al., 2021). The birds breeding at lower latitudes recrudesce gonads earlier, stay in the stimulatory phase for a longer period, and terminate breeding later than high latitude birds that have a short breeding period (Singh et al., 2021).

In studies done on populations that overwinter in sympatry and breed at different locations, the higher latitude breeding birds have to accommodate an additional life-history event of spring migration that delays their reproduction (Greives et al., 2016; Fudickar et al., 2016; Ramenofsky et al., 2017). This process of spring migratory preparedness involves seasonal pre-migratory fattening, increase in food intake, and an increase in metabolic activity in flight muscles and liver in phenology and behavior (Sharma et al., 2022; Fudickar et al., 2016; Singh et al., 2018). There is also a striking shift in the locomotor activity of migratory birds, switching from only day activity to nighttime activity (Gwinner and Czeschlik, 1978; Berthold, 1996; Singh et al., 2015; Singh and Kumar, 2017; Singh et al., 2018). These changes in behavior and physiology associated with seasonal induction of reproduction and migration are potentially an outcome of some key RNA molecules changing their expression in the hypothalamus in response to changes in spring day length and other timing cues (Singh et al., 2015; Mishra et al., 2016; Johnston et al., 2016). The hypothalamus along with the pituitary, is a key neural center that synthesizes and releases neuropeptides and hormones critical to the regulation of seasonal reproductive and migratory processes. A key step in the induction of the gonad recrudescence is initiated by release of gonadotropin releasing hormone 1 (GnRH1) from the hypothalamus followed by its binding to the pituitary gonadotroph to stimulate release of luteinizing hormone (LH) and follicle-stimulating hormone (FSH) (Li et al., 1994). Investigating molecules involved in gonad growth, production of sex steroids, energy homeostasis and metabolism may help advance our understanding of differences in the reproductive timing of songbirds breeding at different latitudes.

The Dark-eyed junco provides a powerful model system for investigating the neuroendocrine mechanisms that underlie variation in reproductive and migratory timing. In early spring, populations of juncos that differ in whether they migrate are found living together in the same environment (Greives et al., 2016; Wanamaker et al., 2020). As spring progresses, the locally breeding population undergoes gonadal recrudescence, while the migratory population delays recrudescence to prepare to migrate. In a common garden study on resident and migrant juncos held in captivity, neuroendocrine tissues collected during the reproductive divergence state revealed differential patterns of gene and protein expression between residents and migrants (Fudickar et al., 2016; Bauer et al., 2018; Singh et al., 2020). However, a comprehensive account of the transcriptome associated with divergent state physiology in neuroendocrine tissue is needed to better understand the underlying mechanisms regulating early spring-induced phenologies.

The objective of this study was to discover key transcripts in the hypothalamus tissue of free-living juncos on the verge of divergence in early spring. Prior studies (Fudicker et al., 2016) conducted on captives provided insight into the mechanisms through which population-level seasonal divergence is set in a controlled indoor condition, including differentially expressed genes in muscle, blood, and hypothalamus. The present study asks how the populations differ in their hypothalamic gene expression when sampled directly from their natural environment during the time of seasonal divergence.

The following hypothesis to understand how neuroendocrine response will determine the timing of reproduction in junco populations on the verge of divergence: 1) We predicted to find

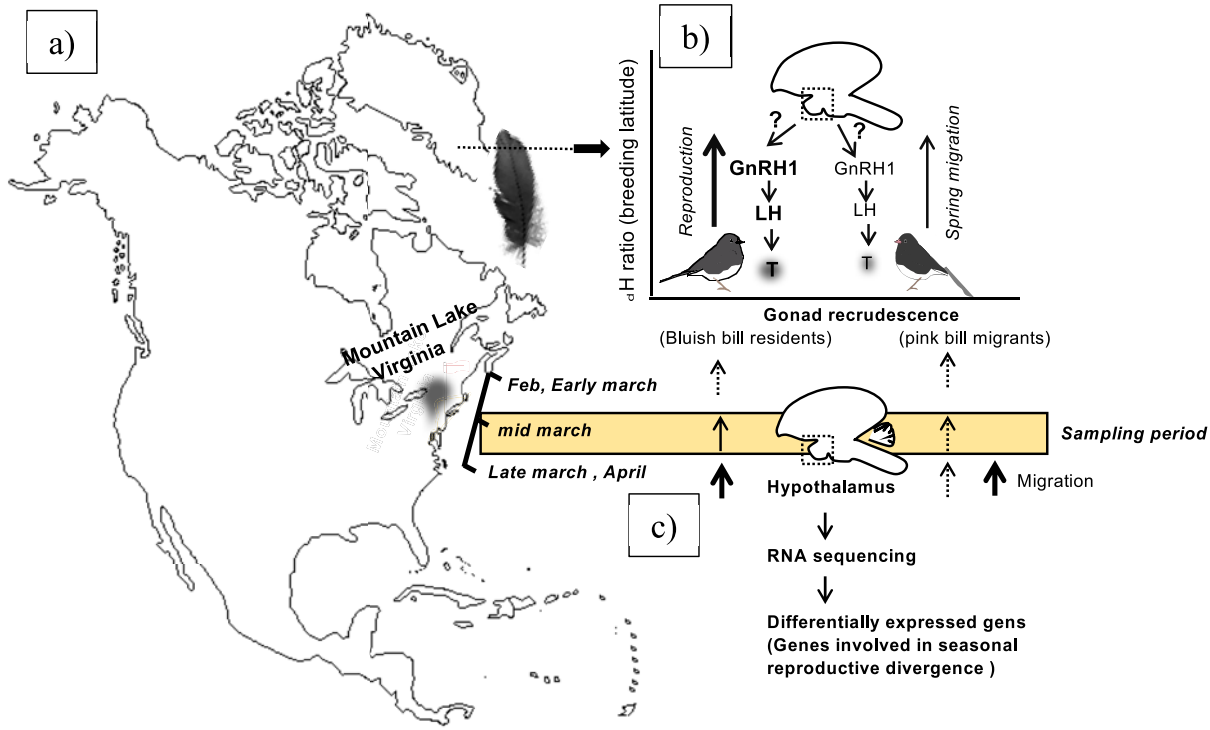

FIGURE 1
Schematic showing the wintering ground location of sympatric resident (*J. h. carolinesis*; bluish bill) and migrant (*J. h. hyemalis*; pink bill based on IUCN, 2019) dark-eyed juncos on the North America map **(a,b)**. The right upper schematic figure shows early spring difference in gonad development between early breeding resident juncos compared to migrants when captured on their wintering ground **(b)**. The lower right schematic figure shows the flow-chart outline steps of RNA sequencing, differentially expressed genes (DEGs) analysis **(c)**.

differences in the plasma testosterone levels as a physiological measure of gonadal recrudescence. 2) We predicted to see the differences in the key hypothalamic transcripts associated with the latitude of breeding. 3) We predicted to see differential expression of hypothalamic transcripts associated with migratory preparedness. To test these hypotheses, we sampled sympatric resident/migrant birds that breed at different latitudes and flock together during early spring with a pre-notion of individual variation in response to constantly changing natural day length and climatic conditions.

Materials and methods

The study system

The dark-eyed junco subspecies live in sympatry and flock together at Mountain Lake Biological Station (MLBS), Virginia, from early fall to spring and start to diverge as soon as the photoperiod starts increasing (Figures 1a,b). In the wintering ground, the resident and migrant juncos are identified by their beak color. The migrants are pink-billed, and residents have blue-billed resident birds that breed at MLBS (Greives et al., 2016; Fudickar et al., 2016). The migrant juncos start to prepare for departure to the North as day length increases. Whereas resident juncos start showing gonadal recrudescence (Figure 1).

Body mass and Fat score

After taking the bird out of the mist net, we visually estimated subcutaneous fat score (0–5) deposition in the furcular and abdominal regions, as follows: no fat present (0), trace amounts of fat in the furcular region (1), trace amounts of fat in the abdominal region (2), half full in both furcular and abdomen area (3), full in both the areas (4), bulging in both the areas (5). Body mass was measured using a Pesola Spring scale (0–50 g), tared to zero with a small piece of sock used to carry the bird for body mass measurement.

Capture and tissue collection

We captured six migrants and seven resident male dark-eyed juncos using mist nets from state road 714, Giles County Virginia at Mountain Lake Biological Station (MLBS; 37.37 0N, 80.52 0W). Migrants (J. h hyemalis) and residents (J. h carolinensis) were identified using bill coloration, plumage, and wing cord (Ketterson and Nolan, 1976). Birds were caught from 13 to 20 March 2017 during spring initiation at MLBS (11.72 ± 0.1 h of average day length and −1 to −4 °C average daily temperature). Juncos were euthanized using isoflurane within 5 min from the time they were caught in the mist net. Before euthanizing, 100 µL of blood was collected by puncturing the wing vein for baseline testosterone hormone measurement. After the capture of the birds, the brain and testes were immediately dissected within 5 min, and tissues were flash-frozen on dry ice and stored at −80 °C until further processing of tissues. Scientific collecting permits were issued by the Virginia

Department of Game and Inland Fisheries (permit # 052971). All methods were approved under a protocol (# 15-026-17) by the Indiana University Institutional Animal Care and Use Committee.

The hypothalamic area was dissected from the whole brain under the cryostat (Leica Biosystems CM1850, Buffalo Grove, IL, United States) maintained at −20 °C using a modified protocol adapted from Ashley et al. (2014). The frozen brain was sliced on the rostral caudal position until we saw the tractus septomesencephalicus (TrSM) as a landmark for the beginning of the hypothalamus. We sliced 30 µm thick sections and punched directly above the optic chiasma using a sterile 3 mm-diameter biopsy punch (Thermo Fisher Scientific, Integra™ 3332; Cat no. 12-460-406). All the tissue punches starting from TrSM to the end of the infundibular nuclear complex (INc) as a posterior landmark for the hypothalamus were collected in a sterile 1.5 mL eppendorf tube kept in cryostat throughout brain punching (Singh and Kumar, 2017; Mishra et al., 2016; Singh et al., 2023).

Stable hydrogen isotope analyses

The distal most secondary feather from each individual was collected and stored in the coin envelopes and transported to the Indiana University, Bloomington. All feathers were cleaned using a chloroform: methanol in a 2:1 ratio to remove any external contaminants. A small fraction from the tip of the feather was cut, weighed to approximately 0.5 mg, placed in a 3 × 5 mm silver capsule, and shipped to a laboratory located in the US Geological Survey in Denver, CO, to analyze the hydrogen isotope (δ^2H) values. Hydrogen isotope ratios were measured using established methods of mass spectrometry (Wunder et al., 2012; Fudickar et al., 2016; Singh et al., 2021; Wanamaker et al., 2020). The non-exchangeable δ^2H values were reported in parts per mil notation (‰) with respect to VSMOW (Vienna Standard Mean Oceanic Water) using Caribou (−157‰) and Kudu (−35.3‰) standards. We used δ^2H values to estimate the latitude and photoperiod where each bird spent the breeding, molting season and incorporated local δ^2H signatures in the growing feathers (Singh et al., 2021). To estimate the latitude and photoperiod for each corresponding δ^2H value, we obtained North America hydrogen isotope ratios for August month precipitation (δ^2H_p) from the OPIC 3.2 database (Bowen, 2020). For each bird, we found all feather δ^2H values in the North America compatible to δ^2H precipitation values (for detailed methods see Singh et al., 2021). The δ^2H values were used as a continuous variable against all the physiological, hormone measures, and expressed transcripts.

Testosterone ELISA

We measured circulating baseline testosterone levels in blood plasma by puncturing the wing vein and collecting blood into heparinized capillary tubes. The blood samples were stored at 4 °C and plasma was extracted by centrifuging blood samples at 3000 rpm for 15 min at room temperature. The plasma was separated using a Hamilton syringe and stored at −20 °C until assayed to measure testosterone. The plasma samples were thawed on ice, and 20 µL of plasma from each individual was aliquoted in glass tubes. Hormone was extracted using diethyl-ether mixed by agitating and incubation at room temperature for 20 min. After incubation, all tubes were snap frozen and the supernatant was immediately transferred to a fresh tube. This procedure was repeated three times to extract the hormone, and finally the tube was dried using high pressure liquid nitrogen. Assay buffer (250 µL) was added to each tube, and 100 µL of extracted hormone was used in duplicate wells to run the testosterone assay. Plasma testosterone was measured using high sensitivity testosterone ELISA kit (Enzo ADI-900-176) as per manufacturer's protocol. All samples were placed on one plate, testosterone ELISA with intra-assay coefficient variability of 0.6% ± 0.06 (mean ± SE) and sensitivity of 2.6 pg/mL.

Measurement of gene expression

RNA extraction and sequencing

A total of 13 brains (6 migrant and 7 resident juncos) hypothalamii were punched and homogenized in RLT buffer containing 1% 2-Mercaptoethanol (BME) on ice. Total RNA was extracted with AllPrep DNA/ RNA Universal kit (Qiagen, Cat. # 80224) according to manufacturer protocol. RNA concentration and Integrity (RIN; Schroeder et al., 2006) were determined on Agilent 2200 TapeStation system. Total RNA was submitted to the Center for Genomics and Bioinformatics at Indiana University for subsequent RNA quality check, RNA library preparation and Illumina Nexseq 500 (43 nucleotides, paired end reads).

Quality filtering and mapping

The paired-end reads were de-multiplexed using bcl2fastq version v2.20.0.422 and about 28.5 million reads, with a raw read length of 43 nucleotides were assigned to each library. Raw reads were adapter trimmed and quality filtered using Trimmomatic version 0.33 (Bolger et al., 2014) requiring a minimum base quality score of 20 averaged across a sliding window of 3 bases. Reads shorter than 20 bases post trimming were discarded. Trimmed reads were mapped to the dark-eyed junco draft genome assembly sequence using the RNA-Seq read aligner STAR version 2.5.3a (Dobin et al., 2013).

Differential gene expression analysis

The transcriptome was annotated against functionally annotated regions defining the potentially transcribed elements on the dark eye junco draft genome assembly homologous to protein sequences from zebra finch (*Taeniopygia guttata, version 3.2.4*), a Passeriformes species phylogenetically closer to junco, were identified and annotated using BLASTX (Pruitt et al., 2009). Counts for read pairs aligning uniquely to each of the annotated transcribed elements were generated using feature Counts version 1.6.3 (Liao et al., 2014) and were used to identify the potentially significantly differentially expressed regions between migrant and resident birds at 5% FDR using the Bioconductor R package DESeq2 version 1.12.3 (Love et al., 2014).

Statistical Analysis

All analysis was done using R (version 3.2.0). Differences in mean hydrogen isotope ratio and T levels were calculated using a non-parametric Student's t-test (Mann-Whitney U test) between subpopulation means. We used the Pearson correlation method to

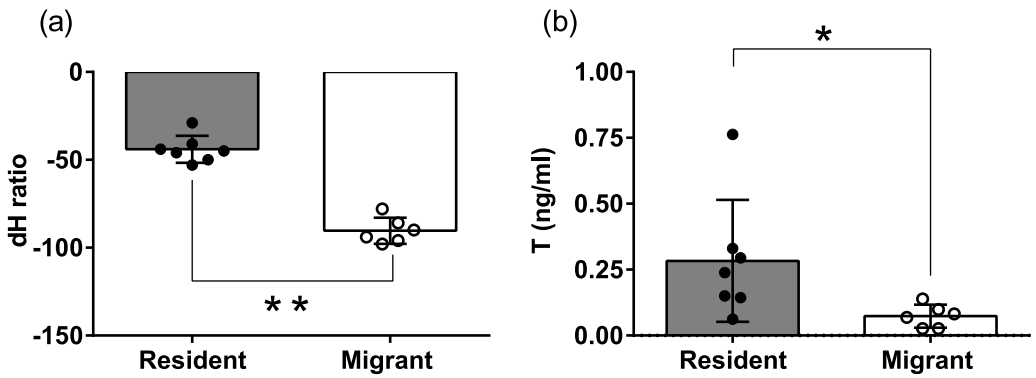

FIGURE 2
Scatter bar graph plot of feather hydrogen isotope (δ^2H) value **(a)**, Plasma testosterone levels (ng/mL) **(b)**. Residents shown in the brown color bar, solid circles represent individual values. Migrants shown in white color bar, hollow circles represent individual values. An asterisk (*) on the line connecting the bars indicates a significant difference between groups ($p < 0.05$, Mann-Whitney U test). For statistical significance, alpha was set at 0.05.

identify any significant correlation between hydrogen isotope ratios, testosterone levels, and normalized Differentially expressed gene expression values. For statistical significance, alpha was set at 0.05. The Benjamini–Hochberg procedure with a failed discovery rate of 5% was used to correct for multiple tests (Waite et al., 2006).

Results

Differences in seasonal phenotypes on the verge of spring

Every year from fall to early spring, dark-eyed junco subspecies are sympatric and flock together at Mountain Lake Biological Station (MLBS), Virginia (Figures 1a,b). The pink-billed migrants arrive in the beginning of fall and depart to the north as spring approaches. Whereas blue-billed resident birds live year-round and breed at MLBS. In early spring, the migrants start preparing for migration. By the time resident juncos start showing gonadal recrudescence, the migrants are departing for their breeding ground. (Figure 1). The residents breeding and growing feathers at lower latitude had heavier δ^2H than migrants (Mann-Whitney U test, $p = 0.0012$, Figure 2a). Also, there were significantly higher blood testosterone levels in resident as compared to migratory birds (Mann-Whitney U test, $p = 0.014$, Figure 2b). We did not find any significant difference in the body weight or subcutaneous fat scores of migrant and resident birds.

Differentially expressed genes

A total of 11,454 expressed sequenced tags (ESTs) were found after mapping to the dark-eyed junco draft genome assembly homologous to protein sequences from zebra finch (*Taeniopygia guttata*) as summarized in Supplementary Table S1. Further, we found three DEGs (FDR <0.05; Figure 3; Supplementary Table S1). Among the three DEGs, only one, gene macrophage mannose receptor 1-like (MMR1), was downregulated in resident birds (FDR = 0.0135; Figure 3a). Unlike MMR1, uncharacterized protein C21orf58 homolog (C7H21orf58; FDR = 0.0135; Figure 3b), gonadotropin releasing hormone 1 (GnRH1; FDR = 0.0216; Figure 3c) were upregulated in resident birds.

DEGs correlation with δ^2H isotope and plasma testosterone levels

Macrophage mannose receptor 1 (MMR1) expression level showed a significant negative correlation to both δ^2H isotope values ($r^2 = 0.7724$, $p < 0.0001$) and T levels ($r^2 = 0.4574$, $p = 0.011$; Figures 4a,b). In contrast, GnRH1 showed a positive correlation to both δ^2H ($r^2 = 0.4692$, $p = 0.0098$) and T levels ($r^2 = 0.3693$, $p = 0.0276$; Figures 4c,d), indicating latitudinal differences in the HPG axis activation in anticipation to spring.

Discussion

We compared the early spring transcriptome of neuroendocrine tissues (hypothalamus) derived from two populations of free-living dark-eyed juncos that reside in the same non-breeding location but differ in timing of reproduction and whether or not they migrate. We identified only three differentially expressed genes (GnRH 1, MMR1, C7H21orf58) in the resident and migrant junco hypothalamic tissue transcriptome in early spring. The most relevant gene to this study was GnRH1 encoding transcript, which was expressed at higher levels in early breeding residents than in migrant breeding at higher latitudes. A critical step in the hypothalamic-gonadal axis (HPG) induction is the release of GnRH1 that binds to gonadotrophic cells in the anterior pituitary to release luteinizing hormone (LH) and follicle-stimulating hormone (FSH) that goes in the circulation and binds to the gonads to release sex hormones (Cho et al., 1998). In addition to the differentially expressed genes (DEGs), we also found higher The hydrogen Prior research on this system using transcriptomics, proteomics, and quantification of specific target genes has shown variation in gene expression in tissues related to this phase lag in the timing of reproduction in migrants as

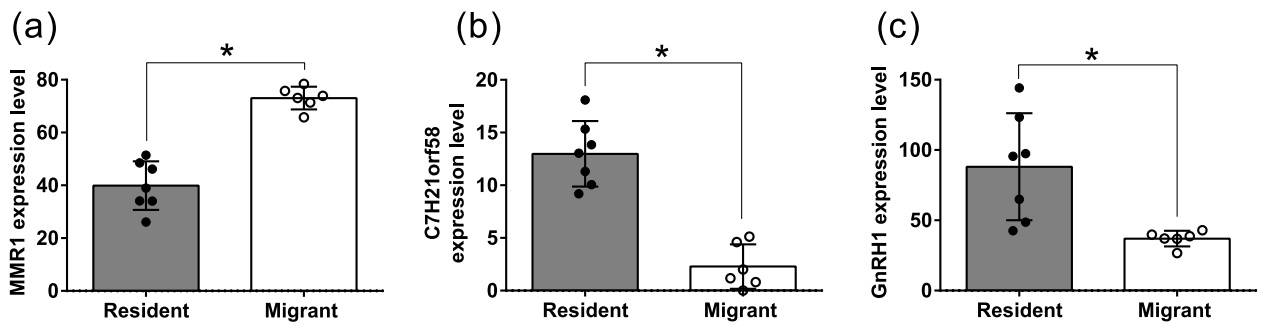

FIGURE 3
Transcriptome-wide differential gene expression (DGE). Box plot of significantly differentially expressed genes **(a–c)** in resident (solid circles) and migrant (hollow circles) hypothalamic transcriptome comparison. Each box plot represents the normalized expression value of transcripts. The false discovery rate multiple correction test was used to determine the significant change. For significance, the alpha was set at 0.05.

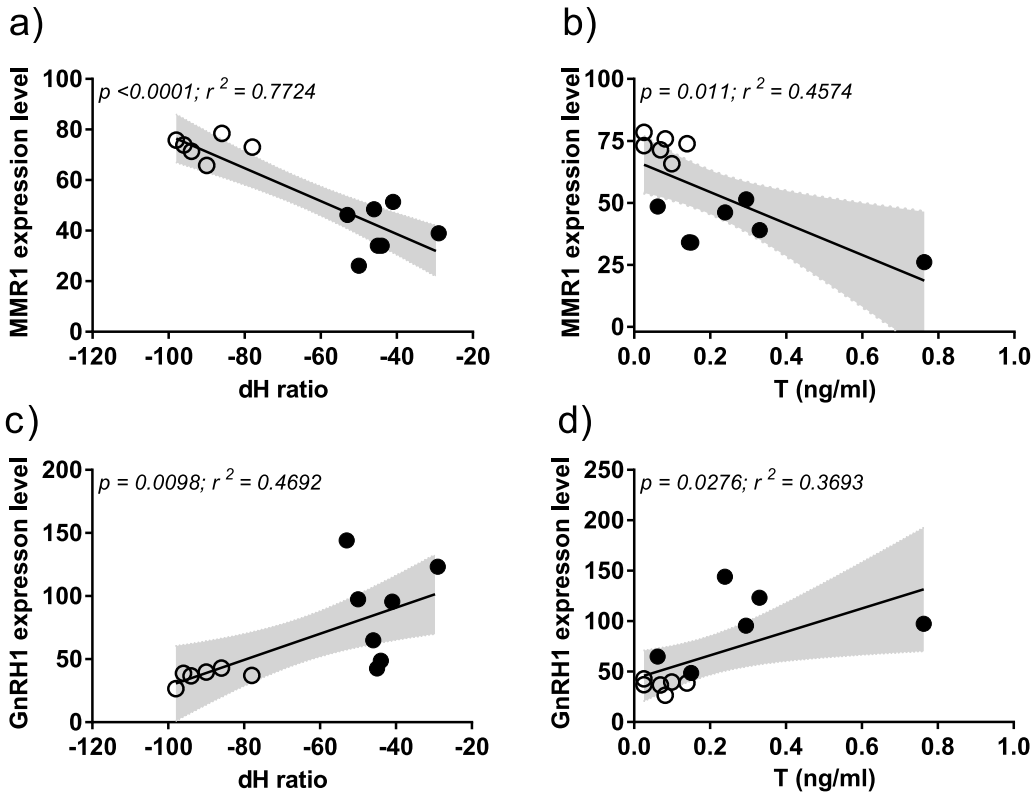

FIGURE 4
Correlation of DEGs with feather hydrogen isotope ratio (δ^2H) and testosterone levels (T) in resident (solid circle) and migrant (hollow circles) juncos. X-axis represents the δ^2H isotope values **(a–c)**, T levels in ng/mL **(b,d)**. Y-axis represents the normalized gene expression values **(a–d)**. Pearson's correlation was used to determine the statistical significance; the alpha was set at 0.05. The positive and negative slope of regression line defines the direction of correlation between normalized gene expression levels, δ^2H and T levels.

compared to residents, including muscle, blood, and hypothalamus (Fudicker et al., 2016; Bauer et al., 2018; Singh et al., 2020). But to our knowledge, no other study has quantified gene expression in the hypothalamic-pituitary complex of two closely related sympatric populations of birds living in the wild during their divergence in reproductive timing and migratory preparedness under the same photoperiod and weather conditions in the wintering ground.

Latitude of origin is related to the timing of gonad recrudescence

Populations of dark eyed junco are distributed across different latitudes in North America and vary widely in their phenotypic (body size, feather color, eye color) and migratory behavior as well as their reproductive phenologies (Nolan et al., 2002). Those breeding at higher latitudes are more likely to be migratory, and in spring,

these higher latitude birds increase body fattening in preparation for migration. Juncos breeding at lower latitudes are more likely to be resident, and these non -migratory birds start to grow their gonads earlier in the year in response to the increase in early spring daylengths (Rogers et al., 1993; Fudickar et al., 2016). After autumn migration, high and low latitude populations typically overwinter together in sympatry.

Feather stable hydrogen isotope ratios have been used as a proxy for breeding latitude in movement ecology studies (Rubenstein et al., 2002; Hobson, 2003; Maggini et al., 2016). Because juncos molt their feathers late in the breeding season before they migrate, analysis of feather hydrogen isotope (δ^2H) ratios in sympatric dark-eyed juncos during the non-breeding season can provide an estimate of their breeding latitudes (Fudickar et al., 2016; Singh et al., 2021; Wanamaker et al., 2020). Birds with lighter hydrogen isotope ratios likely breed at higher latitudes and those with heavier hydrogen isotope ratios likely breed at lower latitudes (Fudickar et al., 2016; Singh et al., 2021).

Several studies on junco populations have used feather hydrogen isotope ratios to show the latitudinal cline in spring preparedness of reproductive processes on the overwintering ground (Fudickar et al., 2016; Kimmitt et al., 2019; Wanamaker et al., 2020). These studies comparing overwintering resident and migrant junco populations from two separate locations, Virginia and Colorado, indicate that lower latitude juncos begin to grow their gonads earlier, thus on shorter days, than high latitude juncos (Fudickar et al., 2016; Wanamaker et al., 2020). This difference is likely related to the difference in the threshold photoperiod required to stimulate the neuroendocrine system regulating reproduction (Singh et al., 2021).

Temperate birds preparing to reproduce sense the change in day length and begin to rise in circulating testosterone, but activation of the hypothalamic-pituitary-gonad axis precedes that. Populations breeding at higher latitudes need relatively longer critical photoperiod than lower latitude birds to activate their HPG axis, grow gonads, and increase the circulating testosterone levels (Singh et al., 2021). Several field and captive studies in junco populations show co-variation between hydrogen isotope ratios and elevation of circulating testosterone levels in response to external GnRH 1 challenge, suggesting a latitudinal cline in reproductive timing (Fudickar et al., 2016; Greives et al., 2016; Wanamaker et al., 2020; Singh et al., 2021). In our study, we found higher variability in circulating baseline testosterone and GnRH-1 transcript in resident juncos, suggesting a plausible effect of non-photic cues, such as food availability and exposure to predators, regulating the pace of reproductive maturity among resident birds (Jacobs and Wingfield, 2000; Chmura et al., 2019).

Latitude of origin is related to early spring hypothalamic GnRH 1 mRNA expression

In spring temperate-zone birds induce their gonads to grow in response to increasing day length. As noted, birds breeding at higher latitudes typically delay gonadal recrudescence until the days are longer because they migrate prior to reproducing (Dawson and Goldsmith, 1983; Silverin et al., 1993; Dawson, 2013; Greives et al., 2016). This additional spring migratory phenology in migratory populations breeding at higher latitudes delays the activation of the HPG axis and uses all energy in preparing for the migratory process.

The preoptic area (POA), a key regulatory nucleus located in the hypothalamus, has neuronal populations that synthesize and release a neuropeptide, gonadotropin-releasing hormone (GnRH1). Transition from short to long day lengths is known to induce GnRH1 release from the hypothalamus that in turn stimulates the release of luteinizing hormone (LH) from gonadotroph cells in the anterior pituitary (Dawson et al., 1985; Dawson and Goldsmith, 1997; Millar, 2005). Increased levels of LH coming to the systemic blood circulation further stimulate gonadal recrudescence and synthesis of testosterone, a gonadal steroid (Wingfield and Farner, 1993; Norris, 2007). Based on the studies on seasonal breeding songbirds, GnRH1 is the most critical top hierarchical molecule in stimulation of HPG axis with its elevation eventually leading to gonadal recrudescence.

In many avian species, levels of hypothalamic GnRH1 have been shown to be elevated significantly in the breeding season as compared to the non-breeding season (Dawson, 2013; Bauer et al., 2018). Significant seasonal changes in the abundance of hypothalamic GnRH1 transcript/peptide have been found in several songbird species, such as house sparrow (*Passer domesticus;* Hahn and Ball, 1995; Stevenson and MacDougall-Shackleton, 2005), American tree sparrow (*Spizella arborea*; Reinert and Wilson, 1996), house finches (*Carpodacus mexicanus*; Cho et al., 1998); dark-eyed juncos (*Junco hyemalis*; Deviche et al., 2006; Greives et al., 2016; Fudickar et al., 2016) and rufous-winged sparrows (*Aimophila carpolis*; Small et al., 2008).

A prior study comparing captive resident and migrant juncos in a common garden demonstrated differential response of the HPG axis to the same day lengths despite exposure to similar photoperiod, food, and temperature in captive condition. At a given early spring day length, resident juncos showed higher GnRH mRNA expression levels than migrant juncos, providing evidence for difference in the HPG axis activation in individuals originating from different latitudes (Bauer et al., 2018).

In our study, the hypothalamic transcriptome data collected from early spring free-living overwintering junco populations showed higher GnRH mRNA expression in resident compared to migrant juncos. This indicates stimulation of GnRH neurons leading to earlier recrudescence in low-latitude residents as compared to high-latitude migratory juncos. The higher GnRH1 transcript levels in resident junco than migrants could be involved in earlier activation of the hypothalamic gonadal axis in residents than in migrant juncos. Thus, differential GnRH1 synthesis in junco populations experiencing similar environmental conditions suggests difference in the photic sensitivity of the neuroendocrine machinery regulating the timing of reproduction in junco populations breeding at different latitudes.

In a similar study of the neuroendocrine tissue proteome of resident and migrant junco populations collected in early spring showed key proteins involved in GnRH 1 transcription, translation, and post-translational modification, stability, and synthesis (Singh et al., 2020). In addition, a proteome study on the juncos reported on here showed differential expression of Vasoactive Intestinal Peptide (VIP), a key neuropeptide

molecule that has been implicated in the photoperiodic reproductive response and as a synchronizer of key circadian pacemaker cells in both birds and mammals (Singh et al., 2020; Rastogi et al., 2014).

Research on female phenology as compared to males is lacking. A study comparing female junco populations in Virginia showed similar trends of higher expression of key reproductive genes in the ovary and ovary mass in resident juncos than high-latitude migrants (Kimmitt et al., 2019). Future work should focus on investigating the role of GnRH1 and other key genes discussed above in the seasonal divergence of reproductive timing, comparing sex and population-level differences in both free-living and captive conditions.

In addition to GnRH 1, we found two more genes differentially expressed in the hypothalamus of resident and migrant juncos. Macrophage mannose receptor 1-like (MMR1), which encodes a glycan-binding protein expressed in macrophages, was downregulated in resident juncos. The MMR1 role has been studied in several biological processes that include the regulation of circulating reproductive hormone levels, homeostasis, innate immune response, and neuroinflammation (Cummings, 2022). The protein encoded from Mannose receptor gene is involved in the clearance of circulating Luteinizing hormone (LH) from the bloodstream which could lead to a decrease in the circulating testosterone levels (Cummings, 2022). Though in our study, we found a negative correlation of MMR1 transcripts level with testosterone levels. But given the low sample size and high variability in resident testosterone levels, we would avoid deriving any mechanistic relationship between MMR1 transcript levels regulating circulating testosterone levels. Another gene, C21orf58 homolog (C7H21orf58), which is an uncharacterized protein, showed higher transcript levels in resident birds. Not much is known about the function of the C7H21orf58 gene and its role in regulating the seasonal phenologies of birds.

Conclusion

Based on transcriptomic differences in neuroendocrine tissue and circulating levels of testosterone, along with stable hydrogen isotope data revealing breeding latitude, we conclude that the HPG axis is activated earlier in the year in resident juncos that breed at lower latitudes as compared to migrant juncos that breed at higher latitudes. Future studies should focus on locating the neuronal cell bodies of GnRH 1 peptide and comparing its expression in winter non-breeding state and early spring divergent state when residents prepare to breed, while migrants prepare to migrate and delay breeding until they reach a higher latitude. In addition, future studies should extend to include other life-history states, the non-breeding wintering state, and the breeding phase at different latitudes.

The data presented in this study show the latitudinal effect on the timing of reproduction mediated via early activation of the HPG axis in birds that breed and develop at lower latitudes compared to higher latitude birds that breed in extreme long photoperiod. It will be interesting to explore the stimulation of the HPG axis at population-specific threshold photoperiod, where lower latitude resident juncos need relatively shorter photoperiod to induce gonads, and higher latitude migrants wait until they reach a critical photoperiod.

Data availability statement

The sequencing data are available in the NCBI Gene Expression Omnibus repository and are accessible through the GEO accession number # GSE305857.

Ethics statement

The animal study was approved by Virginia Department of Game and Inland Fisheries (permit # 052971)/ (# 15-026-17) Indiana University Institutional Animal Care and Use Committee. The study was conducted in accordance with the local legislation and institutional requirements.

Author contributions

DS: Conceptualization, Data curation, Formal Analysis, Investigation, Methodology, Validation, Visualization, Writing – original draft, Writing – review and editing. AF: Conceptualization, Data curation, Funding acquisition, Project administration, Resources, Writing – review and editing. EK: Conceptualization, Funding acquisition, Project administration, Resources, Supervision, Writing – review and editing.

Funding

The author(s) declare that financial support was received for the research and/or publication of this article. The funds were provided by National Science Foundation (IOS- 1856423) and, Indiana University Faculty Research Support Program, (FRSP, account number # 2224640) to AMF and EDK. DS received pilot grants from Neuroscience Research priority Area (NRPA) and Advancing Innovative Research pilot grant from college of arts and sciences University of Kentucky.

Conflict of interest

The authors declare that the research was conducted in the absence of any commercial or financial relationships that could be construed as a potential conflict of interest.

The author(s) declared that they were an editorial board member of Frontiers, at the time of submission. This had no impact on the peer review process and the final decision.

Generative AI statement

The author(s) declare that no Generative AI was used in the creation of this manuscript.

Any alternative text (alt text) provided alongside figures in this article has been generated by Frontiers with the support of

artificial intelligence and reasonable efforts have been made to ensure accuracy, including review by the authors wherever possible. If you identify any issues, please contact us.

Publisher's note

All claims expressed in this article are solely those of the authors and do not necessarily represent those of their affiliated organizations, or those of the publisher, the editors and the reviewers. Any product that may be evaluated in this article, or claim that may be made by its manufacturer, is not guaranteed or endorsed by the publisher.

Supplementary material

The Supplementary Material for this article can be found online at: https://www.frontiersin.org/articles/10.3389/fphys.2025.1627516/full#supplementary-material

References

Ashley, N. T., Ubuka, T., Schwabl, I., Goymann, W., Salli, B. M., Bentley, G. E., et al. (2014). Revealing a circadian clock in captive arctic-breeding songbirds, Lapland longspurs (*Calcarius lapponicus*), under constant illumination. *J. Biol. Rhythms* 29, 456–469. doi:10.1177/0748730414552323

Bauer, C. M., Fudickar, A. M., Anderson-Buckingham, S., Abolins-Abols, M., Atwell, J. W., Ketterson, E. D., et al. (2018). Seasonally sympatric but allochronic: differential expression of hypothalamic genes in a songbird during gonadal development. *Proc. R. Soc. B* 285, 20181735. doi:10.1098/rspb.2018.1735

Berthold, P. (1996). *Control of bird migration*. London, UK: Chapman and Hall.

Bolger, A. M., Lohse, M., and Usadel, B. (2014). Trimmomatic: a flexible trimmer for illumina sequence data. *Bioinformatics*, btu170.

Bowen, G. J. (2020). Gridded maps of the isotopic composition of meteoric waters. Available online at: http://www.waterisotopes.org.

Chmura, H. E., Wingfield, J. C., and Hahn, T. P. (2019). Non-photic environmental cues and avian reproduction in an era of global change. *J. Avian Biol.*, e02.

Cho, R. N., Hahn, T. P., MacDougall-Shackleton, S., and Ball, G. F. (1998). Seasonal variation in brain GnRH in free-living breeding and photorefractory house finches (*Carpodacus mexicanus*). *Gen. Comp. Endocrinol.* 109, 244–250. doi:10.1006/gcen.1997.7027

Cormie, A., Scwarcz, H., and Gary, J. (1994). Relation between hydrogen isotopic ratios of bone collagen and rain. *Geochim. Cosmochim.* 58, 819–830.

Cummings, R. D. (2022). The mannose receptor ligands and the macrophage glycome. *Curr. Opin. Struct. Biol.* 75, 102394. doi:10.1016/j.sbi.2022.102394

Dawson, A. (2013). The effect of latitude on photoperiodic control of gonadal maturation, regression and molt in birds. *Gen. Comp. Endocrinol.* 190, 129–133. doi:10.1016/j.ygcen.2013.05.017

Dawson, A., and Goldsmith, A. R. (1983). Plasma prolactin and gonadotrophins during gonadal development and the onset of photorefractoriness in male and female starlings (*Sturnus vulgaris*) on artificial photoperiods. *J. Endocrinol.* 97, 253–260. doi:10.1677/joe.0.0970253

Dawson, A., and Goldsmith, A. R. (1997). Changes in gonadotrophin-releasing hormone (GnRH-I) in the pre-optic area and median eminence of starlings (*Sturnus vulgaris*) during the recovery of photosensitivity and during photostimulation. *J. Reprod. Fertil.* 111, 1–6. doi:10.1530/jrf.0.1110001

Dawson, A., Follett, B. K., Goldsmith, A. R., and Nicholls, T. J. (1985). Hypothalamic gonadotrophin-releasing hormone and pituitary and plasma FSH and prolactin during photostimulation and photorefractoriness in intact and thyroidectomized starlings (*Sturnus vulgaris*). *J. Endocrinol.* 105, 71–77. doi:10.1677/joe.0.1050071

Deviche, P., Martin, R. K., Small, T., and Sharp, P. J. (2006). Testosterone induces testicular development but reduces GnRH-I fiber density in the brain of the house finch, Carpodacus mexicanus. *General Comp. Endocrinol.* 147 (2), 167–174. doi:10.1016/j.ygcen.2005.12.024

Dobin, A., Davis, C. A., Schlesinger, F., Drenkow, J., Zaleski, C., Jha, S., et al. (2013). STAR: ultrafast universal RNA-seq aligner. *Bioinformatics* 29 (1), 15–21. doi:10.1093/bioinformatics/bts635

Fudickar, A. M., Greives, T. J., Atwell, J. W., Stricker, C. A., and Ketterson, E. D. (2016). Reproductive allochrony in seasonally sympatric populations maintained by differential response to photoperiod: implications for population divergence and response to climate change. *Am. Nat.* 187, 436–446. doi:10.1086/685296

Girvan, M. K., Jones, J., Norris, D. R., Barg, J. J., Kyser, T. K., and Robertson, R. J. (2007). Long-distance dispersal patterns of Male cerulean warblers (dendroica cerulea) measured by stable-hydrogen isotopes. *Avian Conserv. Ecol.* 2, 3. doi:10.5751/ace-00173-020203

Greives, T. J., Fudickar, A. M., Atwell, J. W., Meddle, S. L., and Ketterson, E. D. (2016). Early spring sex differences in luteinizing hormone response to gonadotropin releasing hormone in co-occurring resident and migrant dark-eyed juncos (*Junco hyemalis*). *General Comp. Endocrinol.* 236, 17–23. doi:10.1016/j.ygcen.2016.06.031

Gwinner, E., and Czeschlik, D. (1978). On the significance of spring migratory restlessness in caged birds. *Oikos* 30, 364–332. doi:10.2307/3543485

Hahn, T. P., and Ball, G. F. (1995). Changes in brain GnRH associated with photorefractoriness in house sparrows (*Passer domesticus*). *General Comp. Endocrinol.* 99 (3), 349–363. doi:10.1006/gcen.1995.1119

Hobson, K. A. (1999). Tracing origins and migration of wildlife using stable isotopes: a review. *Oecologia* 120, 314–326. doi:10.1007/s004420050865

Hobson, K. A. (2003). Making migratory connections with stable isotopes. In: *Avian migration*. Editor P. Berthold, E. Gwinner, and E. Sonnenschein. Berlin, Heidelberg: Springer, 379–391. doi:10.1007/978-3-662-05957-9_27

Hobson, K. A. (2005). Stable isotopes and the determination of avian migratory connectivity and seasonal interactions. *Auk* 122, 1037–1048. doi:10.1093/auk/122.4.1037

Jacobs, J. D., and Wingfield, J. C. (2000). Endocrine control of life-cycle stages: a constraint on response to the environment? *Condor* 102, 35–51. doi:10.1093/condor/102.1.35

Johnston, R. A., Paxton, K. L., Moore, F. R., Wayne, R. K., and Smith, T. B. (2016). Seasonal gene expression in a migratory songbird. *Mol. Ecol.* 25, 5680–5691. doi:10.1111/mec.13879

Ketterson, E. D., and Greives, T. J. (2025). Mechanisms matching timing to resources: comparisons of closely related seasonally sympatric, migratory and non-migratory populations. *J. Avian Biol.* 2025, e03380. doi:10.1002/jav.03380

Ketterson, E. D., and Nolan, Jr V. (1976). Geographic variation and its climatic correlates in the sex ratio of eastern-wintering dark-eyed juncos (Junco hyemalis hyemalis). *Ecology* 57, 679–693. doi:10.2307/1936182

Kimmitt, A. A., Hardman, J. W., Stricker, C. A., and Ketterson, E. D. (2019). Migratory strategy explains differences in timing of female reproductive development in seasonally sympatric songbirds. *Funct. Ecol.* 33, 1651–1662. doi:10.1111/1365-2435.13386

Langin, K., Reudink, M. W., Marra, P. P., Norris, D. R., Kyser, T. K., and Ratcliffe, L. M. (2007). Hydrogen isotopic variation in migratory bird tissues of known origin: implications for geographic assignment. *Oecologia* 152, 449–457. doi:10.1007/s00442-007-0669-3

Li, Q., Tamarkin, L., Levantine, P., and Ottinger, M. (1994). Estradiol and androgen modulate chicken luteinizing hormone-releasing hormone-I release *in vitro*. *Biol. Reprod.* 51, 896–903. doi:10.1095/biolreprod51.5.896

Liao, Y., Smyth, G. K., and Shi, W. (2014). featureCounts: an efficient general purpose program for assigning sequence reads to genomic features. *Bioinformatics* 30 (7), 923–930. doi:10.1093/bioinformatics/btt656

Love, M. I., Huber, W., and Anders, S. (2014). Moderated estimation of fold change and dispersion for RNA-seq data with DESeq2. *Genome Biol.* 15, 550. doi:10.1186/s13059-014-0550-8

Maggini, I., Metzger, B., Voss, M., Voigt, C. C., and Bairlein, F. (2016). Morphometrics and stable isotopes differentiate wintering populations of a migratory bird. *Mov. Ecol.* 4, 20. doi:10.1186/s40462-016-0085-6

Millar, R. P. (2005). GnRHs and GnRH receptors. *Anim. Reprod. Sci.* 88, 5–28. doi:10.1016/j.anireprosci.2005.05.032

Mishra, I., Singh, D., and Kumar, V. (2016). Daily expression of genes coding for neurotransmitters in central and peripheral tissues of redheaded bunting: implication for circadian regulation of physiology in songbirds. *Chronobiology Int.* 33 (3), 280–292. doi:10.3109/07420528.2016.1139587

Nolan, Jr., V., Ketterson, E. D., Cristol, D. A., Rogers, C. M., Clotfelter, E. D., Titus, R. C., et al. (2002). "Dark-eyed Junco (*Junco hyemalis*)," in *The birds of North America online*. Editor A. Poole (Ithaca, NY: Cornell Lab of Ornithology). Available online at: http://bna.birds.cornell.edu/bna.

Norris, D. O. (2007). *Vertebrate endocrinology*. 4th edn. Burlington, MA: Academic Press.

Powell, L. A., and Hobson, K. A (2006). Enriched feather hydrogen isotope values for Wood Thrushes sampled in Georgia, USA, during the breeding season: implications for quantifying dispersal. *Can. J. Zool.* 84 (9), 1331–1338. doi:10.1139/z06-114

Pruitt, K. D., Tatusova, T., Klimke, W., and Maglott, D. R. (2009). NCBI reference sequences: current status, policy and new initiatives. *Nucleic Acids Res.* 37, D32–D36. doi:10.1093/nar/gkn721

Ramenofsky, M., Campion, A. W., Pérez, J. H., Krause, J. S., and Németh, Z. (2017). Behavioral and physiological traits of migrant and resident white crowned sparrows: a common garden approach. *J. Exp. Biol.* 220, 1330–1340. doi:10.1242/jeb.148171

Rastogi, A., Kumari, Y., Rani, S., and Kumar, V. (2014). Neural correlates of migration: activation of hypothalamic clock (s) in and out of migratory state in the blackheaded bunting (emberiza melanocephala). *PLoS One* 8 (10), e70065. doi:10.1371/journal.pone.0070065

Reinert, B. D., and Wilson, F. E. (1996). Thyroid dysfunction and thyroxine dependent programming of photoinduced ovarian growth in American tree sparrows (Spizella arborea). *General Comp. Endocrinol.* 103 (1), 71–81. doi:10.1006/gcen.1996.0095

Rogers, C. M., Nolan, V., and Ketterson, E. D. (1993). Geographic variation in winter fat of dark-eyed juncos: displacement to a common environment. *Ecology* 74, 1183–1190. doi:10.2307/1940488

Rubenstein, D. R., Chamberlain, C. P., Holmes, R. T., Ayres, M. P., Waldbauer, J. R., Graves, G. R., et al. (2002). Linking breeding and wintering ranges of a migratory songbird using stable isotopes. *Science* 295, 1062–1065. doi:10.1126/science.1067124

Schroeder, A., Mueller, O., Stocker, S., Salowsky, R., Leiber, M., Gassmann, M., et al. (2006). The RIN: an RNA integrity number for assigning integrity values to RNA measurements. *BMC Mol. Biol.* 31 (7), 3. doi:10.1186/1471-2199-7-3

Sharma, A., Das, S., Singh, D., Rani, S., and Kumar, V. (2022). Differences in transcription regulation of diurnal metabolic support to physiologically contrasting seasonal life-history states in migratory songbirds. *J. Ornithol.* 163 (1), 199–212. doi:10.1007/s10336-021-01926-5

Silverin, B., Massa, R., and Stokkan, K. A. (1993). Photoperiodic adaptation to breeding at different latitudes in great tits. *Gen. Comp. Endocrinol.* 90, 14–22. doi:10.1006/gcen.1993.1055

Singh, D., and Kumar, V. (2017). Extra-hypothalamic brain clocks in songbirds: photoperiodic state dependent clock gene oscillations in night-migratory blackheaded buntings, emberiza melanocephala. *J. Photochem. Photobiol. B Biol.* 169, 13–20. doi:10.1016/j.jphotobiol.2017.02.016

Singh, D., Trivedi, A. K., Rani, S., Panda, S., and Kumar, V. (2015). Circadian timing in central and peripheral tissues in a migratory songbird: dependence on annual life-history states. *FASEB J.* 29 (10), 4248–4255. doi:10.1096/fj.15-275339

Singh, D., Swarup, V., Le, H., and Kumar, V. (2018). Transcriptional signatures in liver reveal metabolic adaptations to seasons in migratory blackheaded buntings. *Front. physiology* 9, 1568. doi:10.3389/fphys.2018.01568

Singh, D., Fudickar, A., Smiley, T., and Ketterson, E. D. (2020). *Comparative proteomics reveals molecular correlates of population-level variation in reproductive timing in a North American songbird*. Authorea Preprints.

Singh, D., Reed, S. M., Kimmitt, A. A., Alford, K. A., Stricker, C. A., Polly, P. D., et al. (2021). Breeding at higher latitude is associated with higher photoperiodic threshold and delayed reproductive development in a songbird. *Hormones Behav.* 128, 104907. doi:10.1016/j.yhbeh.2020.104907

Singh, O., Singh, D., Mitra, S., Kumar, A., Lechan, R. M., and Singru, P. S. (2023). TRH and NPY interact to regulate dynamic changes in energy balance in the Male zebra finch. *Endocrinology* 164 (3), bqac195. doi:10.1210/endocr/bqac195

Small, T. W., Sharp, P. J., Bentley, G. E., Millar, R. P., Tsutsui, K., Mura, E., et al. (2008). Photoperiod-independent hypothalamic regulation of luteinizing hormone secretion in a free-living sonoran desert bird, the rufous-winged sparrow *(aimophila carpalis). Brain behav evol. Brain Behav. Evol.* 71 (2), 127–142. doi:10.1159/000111459

Stevenson, T. J., and MacDougall-Shackleton, S. A. (2005). Season-and age related variation in neural cGnRH-I and cGnRH-II immunoreactivity in house sparrows (Passer domesticus). *General Comp.* 143 (1), 33–39. doi:10.1016/j.ygcen.2005.02.019

Stevenson, T. J., Bernard, D. J., and Ball, G. F. (2009). Photoperiodic condition is associated with region-specific expression of GNRH1 mRNA in the preoptic area of the male starling (Sturnus vulgaris). *Biol. Reproduction* 81 (4), 674–680. doi:10.1095/biolreprod.109.076794

Waite, T. A., Campbell, L. G., and Biology, O. (2006). Controlling the false discovery rate and increasing statistical power in ecological studies. *Ecoscience* 13, 439–442. doi:10.2980/1195-6860(2006)13[439:ctfdra]2.0.co;2

Wanamaker, S. M., Singh, D., Byrd, A. J., Smiley, T. M., and Ketterson, E. D. (2020). Local adaptation from afar: migratory bird populations diverge in the initiation of reproductive timing while wintering in sympatry. *Biol. Lett.* 16 (10), 20200493. doi:10.1098/rsbl.2020.0493

Wingfield, J. C., and Farner, D. S. (1993). "Endocrinology of reproduction in wild species," in *Avian biology*. Editors D. S. Farner, J. King, and K. Parkes (New York: Press), Vol. 9, 163–327.

Wunder, M. B., Jehl, J. R., and Stricker, C. A. (2012). The early bird gets the shrimp: confronting assumptions of isotopic equilibrium and homogeneity in a wild bird population. *J. Animal Ecol.* 81, 1223–1232. doi:10.1111/j.1365-2656.2012.01998.x

Frontiers in Physiology

Understanding how an organism's components work together to maintain a healthy state

The second most-cited physiology journal, promoting a multidisciplinary approach to the physiology of living systems - from the subcellular and molecular domains to the intact organism and its interaction with the environment.

Discover the latest Research Topics

See more →

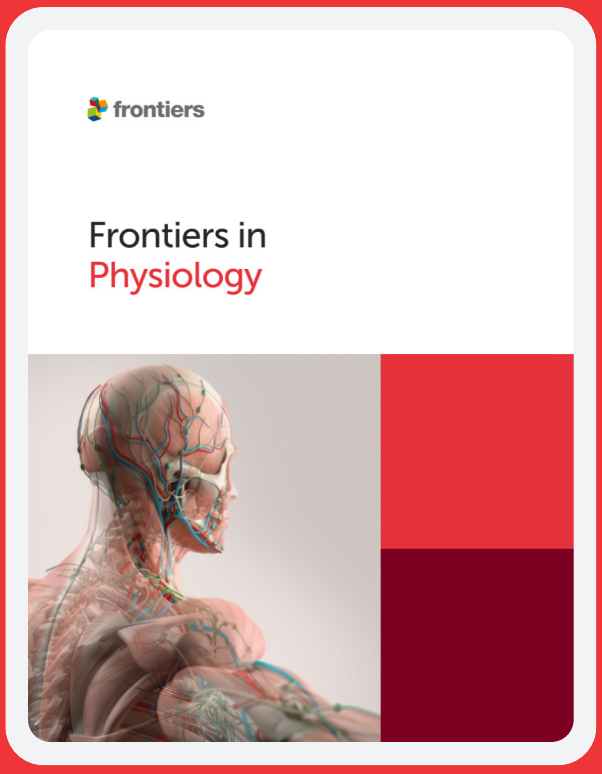

Frontiers

Avenue du Tribunal-Fédéral 34
1005 Lausanne, Switzerland
frontiersin.org

Contact us

+41 (0)21 510 17 00
frontiersin.org/about/contact